# Facies, Paleogeography, and Carbonate Precipitation on the Archean (2520 Ma) Campbellrand-Malmani Carbonate Platform, Transvaal Supergroup, South Africa

by

**Dawn Yvonne Sumner**

B.S., Geology
California Institute of Technology, 1989

Submitted to the Department of Earth, Atmospheric and Planetary Sciences
in Partial Fulfillment of the Requirements for the Degree of

**Doctor of Philosophy**

at the Massachusetts Institute of Technology
September, 1995



Signature of Author _____

Department of Earth, Atmospheric and Planetary Sciences
September, 1995

Certified by _____

John P. Grotzinger
Thesis Supervisor

Accepted by _____

Thomas H. Jordan
Department Head

**Facies, Paleogeography, and Carbonate Precipitation on the Archean (2520 Ma) Campbellrand-Malmani Carbonate Platform, Transvaal Supergroup, South Africa**

by

**Dawn Yvonne Sumner**

Submitted to the Department of Earth, Atmospheric and Planetary Sciences in Partial Fulfillment of the Requirements for the Degree of Doctor of Philosophy at the Massachusetts Institute of Technology, September, 1995.

The 2520 Ma Campbellrand and Malmani subgroups contain a >1 km-thick carbonate platform that is preserved over 190,000 $km^2$ on the Kaapvaal Craton, South Africa. Carbonate rocks are preserved from basinal to supratidal depositional environments allowing detailed analysis of depositional facies and evaluation of the modes and mechanisms of carbonate precipitation. Results document that the *in situ* precipitation of carbonate on the sea floor was an important rock-forming process in deposition of the platform. Precipitation of both aragonite and calcite crusts on the sea floor was common in supratidal to above wave-base subtidal depositional environments. Up to 50 cm-diameter fans of fibrous aragonite (preserved as calcite) grew directly on the sea floor, as well as forming cm-thick crusts on stromatolites. Herringbone calcite (a new calcite cement morphology described here) precipitation was very abundant in deep subtidal depositional environments composing more than 15% of the rock in a 40 m-thick interval preserved for 140 x 50 km. It is associated with deep subtidal microbialites that are encased in precipitated carbonate. The microbialites have complex morphologies that are defined by the geometrical arrangement of three components: 1) fine laminae interpreted as the remnants of microbial mats; 2) two dimensional, vertically oriented supports also interpreted as microbial in origin; and 3) voids filled with calcite cements. Calcite preferentially precipitated on the supports over the well developed mats, suggesting that the mat inhibited nucleation of calcite.

Changes in carbonate textures through time, such as a decline in herringbone calcite and thick beds of precipitated carbonate, suggest that an inhibitor to calcite precipitation, possibly ferrous iron, may have caused the herringbone calcite microtexture, promoted the *in situ* precipitation of thick beds of carbonate on the sea floor, and inhibited micrite precipitation in Archean oceans. An increase in ferrous iron concentration with depth in the oceans also may have caused the observed transition from limestone to siderite precipitates with depth by increasing siderite saturation.

Thesis Advisor: John P. Grotzinger, Associate Professor of Geology

## ACKNOWLEDGEMENTS

Thanks to Prof. John Grotzinger for:
the opportunity to work on the Campbellrand-Malmani platform carbonates and the money to do so.
the freedom to follow my scientific curiosity and allowing my interests to shape the direction of this research.
innumerable discussions that helped me develop the ideas presented here and helped me mature as a scientist.
encouraging participation in other research projects including the modeling of giant ooids, constraining the age of the Campbellrand-Malmani platform, evaluating the potential of Pb-Pb dating of carbonates, and field work in various Archean greenstone belts.
actively promoting my work to the geologic community at large.

Thanks to Prof. Sam Bowring for:
showing me the importance of knowing the limits as well as the implications of data.
supporting research leading the age constraints for the Campbellrand-Malmani platform and the evaluation of Pb-Pb dating of carbonates.
his support of my work.

Thanks to Prof. Nic Beukes for extensive field support in South Africa, his geological insights, and his outstanding hospitality. My greetings go to Marni, Thys, Jackie, Brian, Tiki, and Mrs. Beukes.

Thanks to my committee members, Professors Andy Knoll, Noel James, John Southard, and John Grotzinger, for their insightful comments and for being available in the same week in the middle of the field season.

Thanks to Dr. Drew Coleman for reading and bleeding on various manuscripts, and for his help with lab work.

Thanks to Prof. Fred Read for his hospitality during a brief visit to Porterfield build-up, Virginia.

Thanks to Professors Hans Hofmann, Bruce Simonson, and Henry Chafetz for insightful discussions and their interest in my research.

Thanks to Prof. Philip Sandberg for getting me started on the petrography of carbonate cements.

Thanks to Drs. Jack Farmer and David DesMarais for insights into modern microbial mats.

Thanks to Linda Kah for insightful discussions and for being my roommate at various conferences.

Thanks to my field assistants Esmé van Achterbergh, Jennifer Kleck, Beverly Saylor, and Ray Bambha.

Thanks to all the professors who have taught my geology classes, especially Bob Sharp who taught me more about geology on his 3 day field trips than I learned in many classes.

Thanks to Prof. Paul Hoffman, Prof. Tony Prave, and Hu Guowei for an enlightening 7 weeks in Namibia that helped me place my research into a wider context and helped me appreciate Archean carbonates even more.

Thanks to the following organizations for financial support:
National Science Foundation Graduate Fellowship
Gretchen L. Blechsmidt Research Grant, Geological Society of America
Student Research Funds, E.A.P.S., M.I.T.
NASA Grant #NAGW-2795 to John P. Grotzinger
NSF Grant #EAR-9058199 to John P. Grotzinger

Thanks to Shell Minerals, South Africa; Goldfields; and the Geological Survey of South Africa for access to core.

Thanks to the numerous farmers who allowed access to outcrop on their farms and for their hospitality.

Thanks to Ray Bambha for his loyal friendship, his belief in my scientific abilities, and his unwavering support of my career.
Thanks to Bill Sumner, my father, for his encouragement to pursue my goals, his belief in my ability to do anything I want, and his advise on how to live and enjoy life.
Thanks to Margaret Carver, my mother, for her encouragement to pursue a career in science, her pride and support of my accomplishments, and for her understanding of the give and take of pursuing both career success and personal happiness.
Thanks to Ted Sumner, my brother, for being just that: a fantastic brother who supports, challenges, irritates, surprises, and, most importantly, loves his sister.
Thanks to Uncle Paul and Aunt Mary Sumner for essential supplies (i.e. pizza) and for promoting interest in my work at the Sumner Seismic Laboratory.
Thanks to Martha House for her friendship and for dragging me away from my work for delicious dinners and much needed breaks.
Thanks to Shane Pelechaty, Beverly Saylor, and Jen Carlson for their scientific insights, enjoyable company, and encouragement.
Thanks to Mark Simons for his friendship and for interesting conversations.
Thanks to fellow graduate students Gunter, Gretchen, Anke, Meg, Jim, Nancy, CJ, David, Mousumi, Helen, Audrey for their company, encouragement, and support.
Thanks to former fellow graduate students Drs. Dave McCormick, Cathy Summa, Roy Adams, Paula Washbush, David Applegate, Erchie Wang, Peter Kaufman, and Martha House who have all demonstrated that the thesis goal is obtainable.
Thanks to Scott Adams, Dilbert, Dogbert, and coworkers for comic relief. Join Dogbert's ruling class at /www.unitedmedia.com/comics/dilbert/

This thesis is dedicated to the people of South Africa who
showed me the importance of human dignity and
gave me hope for humanity in spite of all of our shortcomings.

# BIOGRAPHICAL SKETCH

**Dawn Y. Sumner**
Born: 4 December 1966
Seattle, Washington
To: Margaret Susan (VanSkike) Sumner
and William Quintin Sumner

***Education***

| | |
|---|---|
| 1989-1995 | Department of Earth, Atmospheric, and Planetary Sciences, Massachusetts Institute of Technology: Ph.D. 9/95, Geology. |
| 1985-1989 | Division of Geological Sciences, California Institute of Technology: B.S. with Honor 6/89, Geology. |
| 1984-1985 | Ellensburg High School, Ellensburg, Washington: High School Diploma with Honor. |
| 1981-1984 | White Swan High School, White Swan, Washington. |

***Awards***

| | |
|---|---|
| 1989-1992 | National Science Foundation Graduate Fellowship |
| 1991 | Gretchen L. Blechsmidt Research Grant, Geological Society of America |
| 1988-1989 | Carnation Scholarship Merit Award |
| 1988 | George W. Green Memorial Prize |
| 1987-1988 | Chevron Undergraduate Scholarship |

***Research Experience***

**Thesis Research:**

| | |
|---|---|
| 1989-present | Analysis of the 2520 Ma Campbellrand-Malmani carbonate platform, Transvaal Supergroup, South Africa, through field characterization of stratigraphic and facies relationships, and carbonate petrography. (with Prof. J. Grotzinger) |
| 1989-present | Petrographic and geochemical characterization of herringbone calcite, a newly recognized morphology of marine cement, and investigations into the chemical significance of its stratigraphic distribution. (with Prof. J. Grotzinger; results in review) |
| 1992-1994 | Dating of volcanic ash zircons in the Campbellrand-Malmani platform and evaluation of the effects of diagenesis on the Pb-isotopic composition of carbonate minerals. (with Prof. S. Bowring; results in press) |

**Other Research:**

| | |
|---|---|
| 1993-present | *Archean Carbonates:* Field descriptions of the Late Archean Cheshire Formation (Belingwe Greenstone Belt) and Huntsman Limestone (Bulawayo Succession), Zimbabwe, and comparisons to Campbellrand-Malmani platform facies. (with Prof. J. Grotzinger) |
| 1994 | *Neoproterozoic Otavi Group, Namibia:* Stratigraphic analysis and structural mapping of carbonates, diamictites, and siliciclastic sediments in the ~700-600 Ma Otavi Group. (with Profs. P. Hoffman and A. Prave) |
| 1992 | *Origin of Ooids:* Numerical modeling of physical processes affecting ooid size. (with Prof. J. Grotzinger; results published) |
| 1990-1991 | *Lithospheric Strength:* Analytical model estimates of lithospheric strength during deposition of the Late Archean Witwatersrand Basin, South Africa. (with Prof. L. Royden) |
| 1987-1989 | *Paleomagnetic Studies:* Paleomagnetic field tests to determine 1) the paleolatitude of Neoproterozoic glacial sediments, and 2) the depositional oxidation state of iron in a Paleoproterozoic iron formation, South Africa. (with Prof. J. Kirschvink) |
| 1988 | *Climate Modeling:* Sensitivity of an atmospheric general circulation model to large changes in atmospheric carbon dioxide and albedo, reflecting possible Neoproterozoic glacial conditions. (with Dr. D. Crisp and Prof. Y. Yung) |

1986 *Environmental Geology:* Evaluation of the 1986 Draft Environmental Impact Statement for redisposal of radioactive waste at Hanford Nuclear Reservation, Washington. (with State Representative J. Unsoeld)

***Publications***

**Papers:**

Sumner, Dawn Y. and John P. Grotzinger, in review. Was the carbonate saturation state of Archean seawater related to oxygen concentration? Submitted to Geology, 6/95.

Sumner, Dawn Y. and John P. Grotzinger, in review. Herringbone calcite. Submitted to Journal of Sedimentary Research, 12/94.

Sumner, Dawn Y. and Samuel A. Bowring, in press. U-Pb geochronologic constraints on deposition of the Campbellrand Subgroup, Transvaal Supergroup, South Africa. Precambrian Research.

Sumner, Dawn Y. and John P. Grotzinger, 1993. Numerical modeling of ooid size and the problem of Neoproterozoic giant ooids. Journal of Sedimentary Petrology, v. 63, p. 974-982.

**Abstracts:**

Sumner, Dawn Y. and John P. Grotzinger, in press. Archean carbonates and supersaturated sea water. SEPM Congress on Sedimentary Geology, 8/95.

Sumner, Dawn Y. and John P. Grotzinger, 1994. Archean microbialites and carbonate precipitation. Death Valley International Stromatolite Symposium, Laughlin, Nevada, 15-17 October 1994, Abstracts (ed. S. M. Awramik), p. 75.

Sumner, Dawn Y. and John P. Grotzinger, 1994. Microbial mats and carbonate precipitation: Nucleation and inhibitory effects in the 2.52 Ga Gamohaan Fm., South Africa. GAC/MAC Annual Meeting, Program with Abstracts, v. 19, p. A108.

Sumner, Dawn Y. and John P. Grotzinger, 1994. Herringbone cement: A new marine calcite morphology. GAC/MAC Annual Meeting, Program with Abstracts, v. 19, p. A108.

Sumner, Dawn Y., John P. Grotzinger, and Nicolas J. Beukes, 1993. Mat growth and carbonate precipitation in conoform stromatolites, 2.52 Ga Gamohaan Formation, South Africa. GSA Annual Meeting, Abstracts, v. 25, p. A357.

Sumner, Dawn Y. and John P. Grotzinger, 1992. Herringbone cement: a new marine cement morphology. GSA Annual Meeting, Abstracts, v. 24, p. A105.

Sumner, Dawn Y. , Nicolas J. Beukes, and John P. Grotzinger, 1991. Evidence for widespread precipitation of aragonite and calcite in the construction of the ~2.5 Ga Campbellrand-Malmani carbonate platform, South Africa. GSA Annual Meeting, Abstracts, v. 23, p. A65.

Sumner, Dawn Y., Nicolas J. Beukes, and John P. Grotzinger, 1991. Massive marine cementation of the Archean Campbellrand-Malmani carbonate platform, South Africa. GAC/MAC Annual Meeting, Program with Abstracts, v. 16, p. A120.

Sumner, D. Y., J. L. Kirschvink, and B. N. Runnegar, 1987. Soft-sediment paleomagnetic field test of late Precambrian glaciogenic sediments. AGU Fall Meeting Abstracts, v. 68, p. 1251.

Grotzinger, John P., Dawn Y. Sumner, and Nic J. Beukes, 1993. Archean carbonate sedimentation in an active extensional basin, Belingwe Greenstone Belt, Zimbabwe. GSA Annual Meeting, Abstracts, v. 25, p. A64.

# Table of Contents

**Chapter 3: Deep Subtidal Microbialites**



**Chapter 4: Lithofacies and Stratigraphy of the Gamohaan and Frisco Formations**

**Chapter 5: Herringbone Calcite**



**Chapter 6: Carbonate Chemistry and Archean Seawater**

## FIGURES

# CHAPTER 1: INTRODUCTION

Carbonate rocks record complex interactions among biological, chemical, and physical processes in the oceans. They contain some of the best macroscopic evidence for the presence and evolution of life (e.g. Buick, et al., 1981; Kazmierczak, et al., 1985; Walter and Heys, 1985), their primary mineralogy reflects the carbonate saturation state of seawater (e.g. Grotzinger and Read, 1983; Sandberg, 1985; Wilkinson and Given, 1986), and they contain trace elements that can be used to constrain processes such at the balance between sea floor hydrothermal activity and weathering of old crust (Veizer and Compston, 1976; Veizer, 1989; Asmerom, et al., 1991). Understanding the causes and dynamics of the deposition of carbonate rocks can lead to a better understanding of carbon cycling through time and its implications for long term variations in atmospheric $CO_2$.

Two very important questions in studies of Archean carbonates are: 1) What chemical processes controlled carbonate deposition, and 2) What was the role of biological processes in mediating carbonate precipitation? Significant chemical changes have occurred on the surface of Earth through time. One of the most significant has been the rise in free oxygen beginning about 2.1 Ga (e.g. Cloud, 1972; Garrels, et al., 1973; Holland, 1984). Since oxygen is reactive, it influences many surficial geochemical processes including atmospheric chemical reactions, weathering, ion transport in water, and cycling of elements within the oceans (e.g. Berkner and Marshall, 1965; Cloud, 1972; Garrels, et al., 1973; Holland, 1984; Kasting, 1987, 1991). Archean oceans and atmosphere contained very little free oxygen suggesting that a number of chemical processes may have been significantly different than those in younger oceans. Since carbonate precipitation depends on a variety of these processes, changes in environmental chemistry may be reflected in the modes and mechanisms of carbonate precipitation.

The presence and evolution of microbial life also affected carbonate precipitation. Stromatolites are generally considered to be among the best evidence of life on the early Earth, and various interpretations of early microbial evolution, particularly of photosynthesis, have been based on the presence of stromatolites in Archean carbonates (e.g. papers and references in Schopf, 1983; Buick, 1992). Unfortunately, critical evaluations of the role of microbes in stromatolite formation are rare, and use of the term "stromatolite" can be misleading. Stromatolites are almost universally defined as laminated, relief-forming structures of biogenic, specifically microbial, origin (e.g. Monty, 1973; Semikhatov, et al., 1979; Krumbein, 1983). Laminated, relief-forming structures are easy to identify in the field and

are usually called stromatolites even though a biogenic origin can be demonstrated only rarely based on field data (Semikhatov, et al., 1979; Buick, et al., 1981; Lowe, 1994). A biogenic origin is implied, however, by the use of the term "stromatolite", and the application of a non-genetic field term implicitly leads to the genetic interpretation of a biological origin. In most cases, laminated, relief-forming structures in carbonate are biologically influenced, and no problems arise. However, when biological interpretations are based on the presence and morphology of "stromatolites", it becomes very important to explicitly address the biogenicity of the structures (Buick, et al., 1981; Walter, 1983; Lowe, 1994). The reinterpretation of some of the oldest stromatolites, previously regarded as biogenic, as various abiotically formed structures illustrates the importance, and the difficulty, of demonstrating a biological influence (Lowe, 1994, 1995; Buick, et al., 1995). In the case of many of the structures described by Lowe (1994), the evidence conclusively supports neither abiotic nor biotic interpretations, and poor preservation and structural ambiguity make a definitive interpretation unlikely.

Even where evidence of ancient microbial communities is preserved, it is difficult to distinguish between the effects of environmental and biological chemistry due to the complexity of of interactions between them. A wide range of biological processes affect carbonate precipitation: Calcification in and on organisms can be the result of enzymatic calcification of skeletons, biologically induced changes in environmental chemistry that result in precipitation, or physio-chemical precipitation due to the saturation state of the environment (e.g. Westbroek and de Jong, 1982; Leadbeater and Riding, 1986; Lowenstam and Weiner, 1989; Simkiss and Wilbur, 1989; Riding, 1991). Sometimes the role of biological processes is clear. For example, the process of macroscopic calcification resulting in bones and shells is controlled biologically by specialized enzymes that can precipitate carbonate in undersaturated environments or by molecular frameworks that regulate the location and morphology of precipitation (e.g. Degens, 1979; Lowenstam and Weiner, 1989; Simkiss and Wilbur, 1989; Weiner, et al., 1982 and references therein). In contrast, carbonate coatings on bacteria and cyanobacteria result from a complex interaction of biotic and abiotic processes, and cellular controls on precipitation, if present, are not obvious (e.g. Lowenstam and Weiner, 1982, 1989; Simkiss and Wilbur, 1989; Pentecost, 1991). Various metabolic processes (such as $CO_2$-fixing reactions, nitrate reduction, sulfate reduction, and release on ammonia) can induce precipitation if they cause the local extracellular solubility product to be exceeded (e.g. Simkiss and Wilbur, 1989; Thompson and Ferris, 1990; Buczynski and Chafetz, 1991; Pentecost, 1991). Microbial communities may also enhance or inhibit the nucleation of minerals on their cell walls or the gelatinous coating excreted by mats (e.g. Jain, 1988), but no detailed studies have been performed on the role of these

factors in affecting nucleation of carbonate on bacterial or cyanobacterial sheaths (Pentecost, 1991). The difficulty of distinguishing biological influences are magnified when attempts are made to evaluate the role of microbes in the precipitation of ancient carbonate deposits since the processes that formed the rock are no longer active and have to be inferred from preserved morphological and compositional attributes. In some cases, it is possible to address the problem by comparing the composition of the rock containing the microbial communities to that of the surrounding environment. For example, some stromatolites that are surrounded by siliciclastic detritus consist predominantly of carbonate suggesting a precipitated origin for the carbonate (Horodyski, 1976; Fairchild, 1991; Serebryakov and Semikhatov, 1974; Hoffman, 1976). However, unless the surrounding sediment is free of precipitated carbonate, the biological role could be the exclusion of detrital sediment rather than the inducement of carbonate precipitation. In most precipitated stromatolites, it is extremely difficult if not impossible, to distinguish between precipitates formed primarily by biological processes and those due to abiotic precipitation.

Many of the questions about the role of microbial communities in carbonate precipitation as well as abiotic chemical affects on the modes and mechanisms of carbonate precipitation can be addressed with careful observations of rocks from the 2520 Ma (Sumner and Bowring, in press; Appendix A) Campbellrand and Malmani Subgroups, Transvaal Supergroup, South Africa, which contain the oldest extensively preserved carbonate platform known. The Campbellrand-Malmani carbonate platform covers 190,000 $km^2$ and probably originally covered the entire Kaapvaal Craton, >600,000 $km^2$ (Beukes, 1987). The platform is over 1 km thick in the predominantly peritidal Malmani Subgroup and in the predominantly shallow subtidal Campbellrand Subgroup (Button, 1973; Beukes, 1987). Approximately 500 $km^2$ of basinal sediments equivalent to the platform also are preserved. These basinal equivalents are only about 500 m thick (Beukes, 1987). The outstanding petrographic preservation of rocks representing a wide range of depositional environments in the Campbellrand-Malmani carbonate platform provides a unique opportunity to study the modes and mechanisms of Archean carbonate precipitation in a well constrained stratigraphic framework.

### *Previous Work*

The earliest studies of the Transvaal Supergroup concentrated on mineral prospecting (e.g. Brown, 1896; Thord-Gray, 1905; Dessauer, 1909; Kupferburger, 1927). Young (1928, 1932, 1933, 1934, 1940, 1943, 1945) was one of the first workers to report on sedimentary structures in the carbonates of the Campbellrand Subgroup. He initially described stromatolites from section BT as unusual deformation structures, but later as stromatolites.

He was also one of the first to point out the similarities between carbonates near Johannesburg and in the northern Cape Province (Young, 1933).

The first comprehensive stratigraphic studies began in the 1970's with limited work by Visser and Grobler (1972) in the Cape Province, and thorough studies by Truswell and Eriksson (1972, 1973), Eriksson (1972, 1977), Eriksson and Truswell (1974), and Button (1973) in the Transvaal Province that established the regional stratigraphy of the Malmani Subgroup and depositional environments for many of the lithofacies. The stratigraphy of the Campbellrand Subgroup was not established until the work of Beukes (1980, 1987) who also provided excellent interpretations of depositional environments. Beukes (1980, 1987) identified basinal deposits south of the Griquatown Fault Zone and proposed ramp to rimmed platform geometry for the Campbellrand Subgroup. Thus, by the mid 1980's, the depositional environments of the Campbellrand-Malmani carbonate platform were established as predominantly peritidal in the Transvaal Province with deeper platform margin and basinal deposition in the Cape Province.

Since initial work by Beukes (1980, 1987), various reinterpretations of basin geometry and depositional environments have been proposed. In particular, Altermann and Herbig (1991) suggested a peritidal origin for laminated rhythmites interpreted by Beukes (1980, 1987) as basinal, and Hälbich, et al. (1992) interpreted the transition from carbonate to iron-formation deposition at the top of the platform as a change from marine to lacustrine depositional environments as opposed to a deepening-upward, entirely marine transition (Beukes, 1980, 1983, 1984, 1987; Klein and Beukes, 1989; Beukes, et al., 1990). Clendenin, et al. (1988a and b) propose that subsidence of the Campbellrand-Malmani basin was due to earlier rifting represented by the Ventersdorp Supergroup, and that it was and intracratonic basin with a depositional axis trending north-south between exposures of the Malmani and of the Campbellrand subgroups.

### *Methods*

This thesis extends previous work by compiling stratigraphic data for the entire Campbellrand-Malmani platform and by specifically addressing the modes and mechanisms of carbonate precipitation in Archean carbonates. Stratigraphic sections (Appendix B) were measured using a Jacobs staff with an attached level and sight. Cores were measured using a combination of depths marked on the core and direct thickness measurements. Core thicknesses were corrected for apparent dip of the core in cross sections, but the actual measured thicknesses are presented in Appendix B along with core dips. The detail of measured sections and cores varied according to the purpose of the data, and the detail included in Appendix B generally reflects the original detail of measurement. In a few

cases, sections were simplified in Appendix B because the more detailed data were not used. Petrographic data includes detailed descriptions of rock fabrics in the field, polished slabs, and thin sections. Standard microscopic (including optical, cathodoluminescence, and UV reflected light), etching, and staining techniques were used in the laboratory.

## THESIS OUTLINE

The results of this study are divided into five chapters. Chapter 2 contains descriptions of the geological setting of the Campbellrand-Malmani platform, stratigraphic and facies characteristics that establish depositional environments, evidence that Archean seawater was supersaturated with respect to aragonite, and evidence for abiotic precipitation of carbonate minerals. Chapter 3 is a description of deep subtidal microbialites which demonstrate that microbial communities were capable of complex morphological constructions in late Archean time. Geometric relationships between mats and enclosing calcite cements suggest that the mats inhibited carbonate precipitation. Chapter 4 establishes stratigraphic relationships for the various microbialite lithofacies assemblages in the Gamohaan and Frisco formations at the top of the Campbellrand-Malmani platform. Stratigraphic data document that subtidal carbonate deposition was dominated by the precipitation of calcite crusts directly on the sea floor, sometimes as laterally continuous beds of herringbone calcite, a new morphology of marine cement. Chapter 5 provides a petrographic description of herringbone calcite and proposes a growth model for herringbone calcite that requires the presence of an inhibitor to calcite precipitation. Chapter 6 argues that the inhibitor was $Fe^{2+}$ and that $Fe^{2+}$ also helped maintain the high calcium carbonate saturation state of Archean seawater and was the cause of a change from limestone to siderite-facies banded iron-formation deposition with depth in Archean oceans.

## REFERENCES


Altermann, W. and H. C. Herbig, 1991. Tidal flat deposits of the Lower Proterozoic Campbell Group along the southwestern margin of the Kaapvaal Craton, Northern Cape Province, South Africa. Journal of African Earth Sciences, v. 13, p. 415-435.

Asmerom, Y., S. B. Jacobsen, A. H. Knoll, N. J. Butterfield and K. Swett, 1991. Strontium isotopic variations of Neoproterozoic seawater: Implications for crustal evolution. Geochimica et Cosmochimica Acta, v. 55, p. 2883-2894.

Berkner, L. V. and L. C. Marshall, 1965. On the origin and rise of oxygen concentration in the Earth's atmosphere. Journal of the Atmospheric Sciences, v. 22, p. 225-261.

Beukes, N. J., 1980. Stratigrafie en litofasies van die Campbellrand-subgrop van die Proterofitiese Ghaapgroep, noord-Kaapland. Transactions of the Geological Society of South Africa, v. 83, p. 141-170.

Beukes, N. J., 1983. Paleoenvirnomental setting of iron-formations in the depositional basin of the Transvaal Supergroup, South Africa in Iron-formation: Facts and problems (A. F. Trendall and R. C. Morris, eds.). Elsevier, Amsterdam. p. 131-198.

Beukes, N. J., 1984. Sedimentology of the Kuruman and Griquatown iron formations, Transvaal Supergroup,

Griqualand West, South Africa. Precambrian Research, v. 24, p. 47-84.
Beukes, N. J., 1987. Facies relations, depositional environments and diagenesis in a major early Proterozoic stromatolitic carbonate platform to basinal sequence, Campbellrand Subgroup, Transvaal Supergroup, southern Africa. Sedimentary Geology, v. 54, p. 1-46.
Beukes, N. J., C. Klein, A. J. Kaufman and J. M. Hayes, 1990. Carbonate petrography, kerogen distribution, and carbon and oxygen isotope variations in an Early Proterozoic transition from limestone to iron-formation deposition, Transvaal Supergroup, South Africa. Economic Geology, v. 85, p. 663-689.
Brown, N., 1896. The succession of the rocks in the Pilgrim's Rest Goldfield. Transactions of the Geological Society of South Africa, v. 2, p. 3-4.
Buick, R., 1992. The antiquity of oxygenic photosynthesis: Evidence from stromatolites in sulphate-deficient Archean lakes. Science, v. 255, p. 74-77.
Buick, R., J. S. R. Dunlop and D. I. Groves, 1981. Stromatolite recognition in ancient rocks: An appraisal of irregularly laminated structures in an Early Archaean chert-barite unit from North Pole, Western Australia. Alcheringa, v. 5, p. 161-181.
Buick, R., D. I. Groves and J. S. R. Dunlop, 1995. Abiological origin of described stromatolites older than 3.2 Ga - Comment. Geology, v. 23, p. 191.
Button, A., 1973. The stratigraphic history of the Malmani dolomite in the eastern and north-eastern Transvaal. Transactions of the Geological Society of South Africa, v. 76, p. 229-247.
Clendenin, C. W., E. G. Charlesworth and S. Maske, 1988a. An early Proterozoic three-stage rift system, Kaapvaal Craton, South Africa. Tectonophysics, v. 145, p. 73-86.
Clendenin, C. W., E. G. Charlesworth and S. Maske, 1988b. Tectonic style and mechanism of early Proterozoic successor basin development, southern Africa. Tectonophysics, v. 156, p. 275-291.
Cloud, P., 1972. A working model of the primitive Earth. American Journal of Science, v. 272, p. 537-548.
Dessauer, V., 1909. Some shales in and observations on, the Dolomite of Pilgrim's Rest. Transactions of the Geological Society of South Africa, v. 12, p. 78-81.
Eriksson, K. A., 1972. Cyclic sedimentation in the Malmani Dolomite, Potchefstroom Synclinorium. Transactions of the Geological Society of South Africa, v. 75, p. 85-97.
Eriksson, K. A., 1977. Tidal flat and subtidal sedimentation in the 2250 M.Y. Malmani dolomite, Transvaal, South Africa. Sedimentary Geology, v. 18, p. 223-244.
Eriksson, K. A. and J. F. Truswell, 1974. Stratotypes from the Malmani Subgroup northwest of Johannesburg, South Africa. Transactions of the Geological Society of South Africa, v. 77, p. 211-222.
Garrels, R. M., E. A. J. Perry and F. T. Mackenzie, 1973. Genesis of Precambrian iron-formations and the development of atmospheric oxygen. Economic Geology, v. 68, p. 1173-1179.
Grotzinger, J. P. and J. F. Read, 1983. Evidence for primary aragonite precipitation, lower Proterozoic (1.9 Ga) dolomite, Wopmay orogen, northwest Canada. Geology, v. 11, p. 710-713.
Hälbich, I. W., D. Lamprecht, W. Altermann and U. E. Horstmann, 1992. A carbonate-banded iron formation transition in the Early Protorezoicum of South Africa. Journal of African Earth Sciences, v. 15, p. 217-236.
Holland, H. D., 1984. The Chemical Evolution of the Atmosphere and Oceans. Princeton University Press, Princeton. 582 p.
Kasting, J. F., 1987. Theoretical constraints on oxygen and carbon dioxide concentrations in the Precambrian atmosphere. Precambrian Research, v. 34, p. 205-229.
Kasting, J. F., 1991. Box models for the evolution of atmospheric oxygen: an update. Palaeogeography, Palaeoclimatology , Palaeoecololgy , v. 97, p. 125-131.
Kazmierczak, J., V. Ittekot and E. T. Degens, 1985. Biocalcification through time: Environmental challenge and cellular response. Paläontologische Zeitschrift, v. 59, p. 15-33.
Klein, C. and N. J. Beukes, 1989. Geochemistry and sedimentology of a facies transition from limestone to iron-formation deposition in the Early Proterozoic Transvaal Supergroup, South Africa. Economic Geology, v. 84, p. 1733-1742.
Krumbein, W. E., 1983. Stromatolites — The challenge of a term in space and time. Precambrian Research, v. 20, p. 493-531.
Kupferburger, W., 1927. The fluorospar, lead and zinc deposits of the western Transvaal. Transactions of the Geological Society of South Africa, v. 30, p. 5-56.
Lowe, D. R., 1994. Abiological origin of described stromatolites older than 3.2 Ga. Geology, v. 22, p. 287-

390.
Lowe, D. R., 1995. Abiological origin of described stromatolites older than 3.2 Ga - Reply. Geology, v. 23, p. 191-192.
Monty, C. L. V., 1973. Precambrian background and Phanerozoic history of stromatolitic communities, an overview. Annales de la Société Géologique de Belgique, v. 96, p. 585-624.
Sandberg, P. A., 1985. Nonskeletal aragonite and pCO2 in the Phanerozoic and Proterozoic in The carbon cycle and atmospheric CO2: Natural variations Archean to Present (E. T. Sundquist and W. S. Broecker, eds.). American Geophysical Union, Washington. Geophysical Monograph 32, p. 585-594.
Schopf, J. W., 1983, Earth's Earliest Biosphere: Its origin and evolution: Princeton, Princeton University Press, 544 p.
Semikhatov, M. A., C. D. Gebelein, P. Cloud, S. M. Awramik and W. C. Benmore, 1979. Stromatolite morphogenesis—progress and problems. Canadian Journal of Earth Science, v. 16, p. 992-1015.
Sumner, D. Y. and S. A. Bowring, in press. U-Pb geochronologic constraints on deposition of the Campbellrand Subgroup, Transvaal Supergroup, South Africa. Precambrian Research.
Thord-Gray, I., 1905. Notes on the geology of the Lydenburg gold fields. Transactions of the Geological Society of South Africa, v. 8, p. 66-78.
Truswell, J. F. and K. A. Eriksson, 1972. The morphology of stromatolites from the Transvaal Dolomite north-west of Johannesburg, South Africa. Transactions of the Geological Society of South Africa, v. 75, p. 99-110.
Truswell, J. F. and K. A. Eriksson, 1973. Stromatolitic associations and their palaeo-environmental significance: A re-appraisal of a lower Proterozoic locality from the northern Cape Province, South Africa. Sedimentary Geology, v. 10, p. 1-23.
Veizer, J., 1989. Strontium isotopes in seawater through time. Annual Reviews of Earth and Planetary Science, v. 17, p. 141-167.
Veizer, J. and W. Compston, 1976. 87Sr/86Sr in Precambrian carbonates as an index of crustal evolution. Geochemica et Cosmochemica Acta, v. 40, p. 905-914.
Visser, J. and N. J. Grobler, 1972. The transition beds at the base of the Dolomite Series in the northern Cape Province. Transactions of the Geological Society of South Africa, v. 75, p. 265-274.
Walter, M. R., 1983. Archean stromatolites: Evidence of the Earth's earliest benthos *in* Earth's Earliest Biosphere: Its origin and evolution (J. W. Schopf, ed.). Princeton University Press, Princeton. p. 187-213.
Walter, M. R. and G. R. Heys, 1985. Links between the rise of the metazoa and the decline of stromatolites. Precambrian Research, v. 29, p. 149-174.
Wilkinson, B. W. and R. K. Given, 1986. Secular variation in abiotic marine carbonates: Constraints on Phanerozoic atmospheric carbon dioxide contents and oceanic Mg/Ca ratios. Journal of Geology, v. 94, p. 321-333.
Young, R. B., 1928. Pressure phenomena in the dolomitic limestones of the Campbell Rand Series in Griqualand West. Transactions of the Geological Society of South Africa, v. 31, p. 157-165.
Young, R. B., 1932. The occurrence of stromatolitic or algal limestones in the Campbell Rand Series, Griqualand West. Transactions of the Geological Society of South Africa, v. 35, p. 29-36.
Young, R. B., 1933. Conditions of deposition at the Dolomite basin. Transactions of the Geological Society of South Africa, v. 36, p. 121-135.
Young, R. B., 1934. A comparison of certain stromatolitic rock in the Dolomite basin of South Africa with modern algal sediments in the Bahamas. Transactions of the Geological Society of South Africa, v. 37, p. 153-162.
Young, R. B., 1940. Further notes on algal structures in the Dolomite Series. Transactions of the Geological Society of South Africa, v. 43, p. 17-22.
Young, R. B., 1943. The domical-columnar structures and other minor deformations in the Dolomite Series. Transactions of the Geological Society of South Africa, v. 46, p. 91-104.
Young, R. B., 1945. Nodular bodies in the Dolomite Series. Transactions of the Geological Society of South Africa, v. 48, p. 43-50.

# CHAPTER 2: FACIES AND STRATIGRAPHY OF THE CAMPBELLRAND-MALMANI CARBONATE PLATFORM


## ABSTRACT

The 2520 Ma Campbellrand and Malmani subgroups are a more than 1 km thick carbonate platform that is preserved over 190,000 $km^2$ on the Kaapvaal craton, South Africa. Carbonate sediments deposited in depositional environments ranging from basinal to supratidal are grouped into 7 assemblages: 1) subtidal to supratidal grainstone-dominated lithofacies; 2) supratidal to upper intertidal lithofacies; 3) shallow subtidal to lower intertidal columnar stromatolite-dominated lithofacies; 4) lagoonal lithofacies; 5) subtidal giant stromatolite lithofacies; 6) deep subtidal microbialite lithofacies; and 7) slope and basinal lithofacies. Precipitation of aragonite and calcite crusts on the sea floor was common in supratidal to deep subtidal depositional environments. Fans of aragonite pseudomorphs grew directly on the sea floor and reached diameters of over 50 cm.

The Campbellrand-Malmani carbonate platform developed from a ramp to a rimmed platform early in deposition and seven sequences are recognizable. A major transgression in the middle of the platform resulted in deep water iron-formation deposition on the platform margin and subtidal giant stromatolites across the interior of the platform. Shallow platformal deposition continued above this transgression until deposition of the Gamohaan and Frisco formations, the uppermost units in the platform. These two formations are transgressive deposits that grade upward into the overlying deep water iron-formations. The geometry of the platform and the regional subsidence patterns are inconsistent with deposition on either a passively subsiding margin or a foreland basin. Rather, the Kaapvaal craton seems to have subsided uniformly, on average, during deposition of the carbonate platform.


## INTRODUCTION

Carbonate rocks record complex interactions among biological, chemical, and physical processes in the oceans. In addition to providing abundant data on the evolution of marine organisms, carbonates can be used to constrain secular variations in ocean chemistry (e.g. Sandberg, 1985a; Wilkinson and Given, 1986; Grotzinger and Kasting,1993). The balance between biological and abiotic processes has changed with the evolution of new organisms and changes in ocean chemistry. For example, prior to the evolution of carbonate secreting organisms near the Neoproterozoic-Cambrian boundary, carbonate precipitation may have occurred abiotically, depending exclusively on ocean chemistry, been con-

trolled by microbial processes, or been due to a combination of abiotic and biological influences (e.g. Westbroek and de Jong, 1982; Leadbeater and Riding, 1986; Lowenstam and Weiner, 1989; Simkiss and Wilbur, 1989; Riding, 1991). The dramatic change in the mode of carbonate precipitation due to the evolution of carbonate secreting organisms affected the texture of carbonate rocks as well as the dynamics of carbonate deposition. Similarly, microbial evolution and secular variations in ocean chemistry within Precambrian time affected the textures in Precambrian carbonates. The modes and mechanisms of Archean carbonate deposition are particularly interesting because of their potential to provide constraints on the early evolution of life and the chemistry of the early oceans.

Most Archean carbonates are preserved as relatively thin build-ups covering areas of less than a few hundred square kilometers (see review in Grotzinger, 1989; Hofmann and Masson, 1994; Hofmann, et al., 1985). Only a few depositional environments are preserved in any given occurrence limiting the potential for development of stratigraphic constraints on depositional environments and for detailed studies of lateral facies transitions. Two exceptions are the latest Archean Wittenoom Formation and Carawine Dolomite, Hamersley Basin, Australia (Simonson, et al., 1993) and the Campbellrand-Malmani carbonate platform, Transvaal Supergroup, South Africa. Preservation of the Campbellrand-Malmani carbonate platform is more extensive than that of the Hamersley carbonates and the Campbellrand-Malmani platform contains a more continuous range of depositional environments. In addition, petrographic textures are exceedingly well preserved. Thus, the Campbellrand-Malmani platform provides a unique opportunity to develop facies models for Archean carbonates in a well constrained stratigraphic framework. The constraints placed on facies distributions developed on this platform can be used to extend understanding of depositional environments in less extensively preserved carbonates.

## GEOLOGIC SETTING

The 2520 Ma (Sumner and Bowring, in press; Appendix A) Campbellrand-Malmani platform was deposited on the Kaapvaal craton which contains an extensive record of Archean to Paleoproterozoic platform sedimentation (Figure 2-1). Archean basement of the Kaapvaal craton consists of granitoids, gneisses, and greenstone belts older than 3.0 Ga (Tankard, et al., 1982). The oldest sediments deposited after stabilization of the Kaapvaal craton consists of the 3074±6 Ma (Armstrong, et al., 1991) siliciclastic and volcanic Dominion Group and partially correlative Nsuzi Group (Beukes and Cairncross, 1991). These sediments mark a change in preservation style on the craton since they lack the structural disruption and metamorphism of the older greenstone sediments. The Dominion and Nsuzi groups are

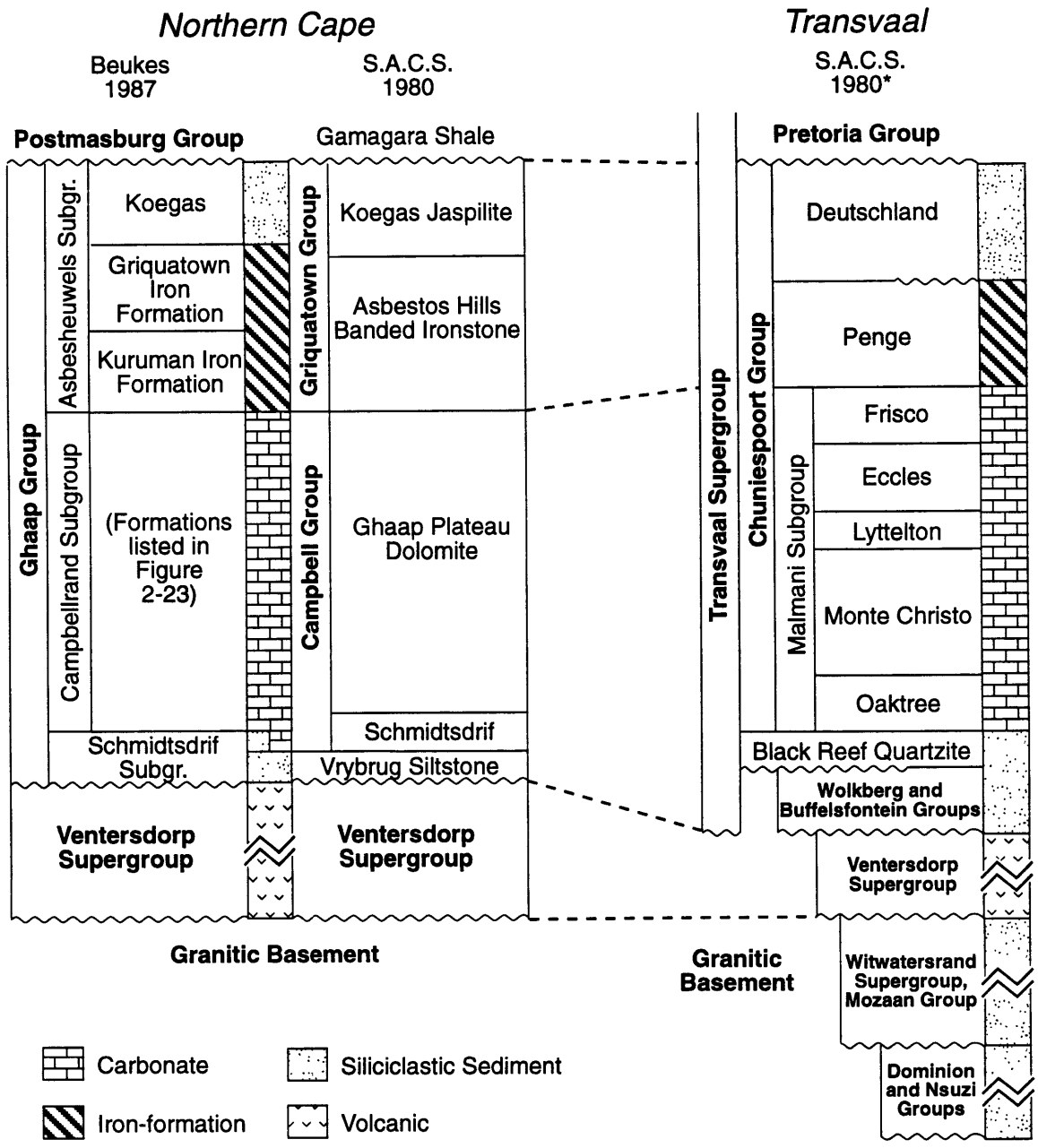


Figure 2-1: Stratigraphy and nomenclature of Archean sediments in the Transvaal and Cape provinces.

folded and unconformably overlain by the Witwatersrand Supergroup and Mozaan Group, respectively (Figure 2-1), which consist of fluvial to shallow marine siliciclastic sediments (Beukes and Cairncross, 1991). Detrital zircons from the Witwatersrand Supergroup range in age from 3.33-2.89 Ga (Barton, et al., 1989; Robb, et al., 1990). The tectonic environment during deposition of Witwatersrand Supergroup and the Mozaan Group is somewhat controversial with interpretations suggesting that they formed in foreland and rift basins respectively (e.g. Burke, et al., 1985b; Burke, et al., 1986; Winter, 1987). However, recent stratigraphic data indicate that deposition extended beyond the preserved margins on the basins with few significant facies changes suggesting passive margin or continental seaway deposition (Beukes and Cairncross, 1991). Although the Witwatersrand and Mozaan groups probably were deposited across much of the Kaapvaal craton, they are only preserved in limited basins, demonstrating differential subsidence or tectonic activity on the Kaapvaal craton.

The Witwatersrand Supergroup is unconformably overlain by the ~2720 Ma Ventersdorp Supergroup (Armstrong, et al., 1986; see Appendix A; Figure 2-1), a succession of volcanic rocks, featuring extensive flood basalts, and other sedimentary rocks. The Ventersdorp Supergroup is interpreted to have formed in a rift resulting from collision between the Kaapvaal and Zimbabwe cratons (Clendenin, et al., 1988a and b; Burke, et al., 1985a). The two cratons are sutured along the Limpopo belt (Figure 2-2), a several hundred kilometer wide metamorphic province. This belt contains multiple structural and metamorphic events, and a variety of ages have been obtained reflecting different events (Kamber, et al., 1995, and references therein). Most data suggest that tectonic activity was concentrated from 2.65 to 2.7 Ga (Barton and van Reenen, 1992; Barton, et al., 1992; Kamber, et al., 1995). Age constraints are consistent with suturing of the two cratons prior to 2.6 Ga, and before deposition of the Campbellrand-Malmani carbonate platform.

The Transvaal Supergroup unconformably overlies the Ventersdorp Supergroup and older granitic-greenstone basement (Figure 2-1; Button, 1973a; Tyler, 1979; Clendenin, et al., 1991). The base of the Transvaal Supergroup in the Transvaal Province is marked by 0-2 km of quartz arenite and shale forming the Wolkberg Group, Buffelsfontein Group, and correlatives. Isopach maps reveal large thickness variations across the Transvaal Province related to paleotopography and differential subsidence (Beukes, 1983a). The Wolkberg and Buffelsfontein groups are overlain by the fluvial to shallow marine Black Reef Quartzite. In the Cape Province, the base of the Transvaal Supergroup is marked by the mixed siliciclastic and carbonate rocks of the Schmidtsdrif Subgroup. The Schmidtsdrif Subgroup and Black Reef Quartzite are the oldest deposits that are preserved over much of the Kaapvaal craton and not in isolated, structurally controlled basins. The Schmidtsdrif Sub-

group and Black Reef Quartzite grade conformably into the carbonate platform of the Campbellrand and Malmani subgroups respectively (Figure 2-1; Beukes, 1977, 1983a).

The Campbellrand-Malmani carbonate platform covers 190,000 $km^2$ (Figure 2-2) and probably originally covered the entire Kaapvaal craton, >600,000 $km^2$ (Beukes, 1987). The platform is over 1 km thick in the predominantly peritidal Malmani Subgroup and in the predominantly shallow subtidal Campbellrand Subgroup (Button, 1973b; Beukes, 1987). Approximately 500 $km^2$ of basinal sediments equivalent to the platform sediments are preserved near Prieska (Figure 2-2) and are only about 500 m thick (Beukes, 1987).

The Kuruman Iron Formation conformably overlies the Campbellrand Subgroup (Figure 2-1) and consists of deep water, microbanded iron formation and grades upward into the Griquatown Iron Formation which consists of various clastic-textured iron formation lithotypes deposited in a shallow epeiric sea or a fresh water lake (Beukes, 1984). The Penge Iron Formation in the Transvaal Province is correlative with and lithologically similar to the Kuruman Iron Formation and also formed on a stable shelf below wave base (Beukes, 1973). The Penge Iron Formation is overlain by a mixed carbonate and siliciclastic unit, the Duitschland Formation, whereas the Griquatown Iron Formation is overlain by remnants of a siliciclastic delta, the Koegas Formation. The Duitschland and Koegas formations are probably correlative (Beukes, 1983b).

An unconformity developed after deposition of the Deutschland and Koegas formations, but before deposition of the overlying the Pretoria and Postmasburg groups (Figure 2-1). This unconformity removed at least 2 km of underlying sediment in the southeastern Transvaal Province where sediments overlying the unconformity rest directly on basement (Button, 1973b; Eriksson and Truswell, 1974). In the northern extreme of outcrop in the Transvaal Province and the western edge of the Kaapvaal craton in the Cape Province, the Deutschland and Koegas formations were folded prior to deposition of the Pretoria and Postmasburg groups (Button, 1976; Beukes and Smit, 1987). Age determinations of 2.0-2.3 Ga for the Pretoria and Postmasburg groups (Burger and Coertze, 1975; Hunter and Hamilton, 1978; Walraven, et al., 1990) suggest a significant stratigraphic break at this unconformity and that the overlying sediments were part of a separate phase of basin evolution.

The Pretoria and Postmasburg groups consist of siliciclastic, carbonate, and volcanic sediments deposited in a range of marine, lacustrine, and glacial depositional environments (Button and Vos, 1977; Stear, 1977). Towards the end of Pretoria and Postmasburg deposition, the ~2060 Ma (Walraven, et al., 1990) Bushveld Complex intruded the Transvaal Supergroup.

### *Preservation*

The Campbellrand-Malmani carbonate platform is extremely well preserved. Structural disruption of preserved strata is limited to gentle warping over most of the craton. Structural disruption is limited to locally steeper dips around the Bushveld Complex and to intense folding and faulting in the Kheis Belt and Dooringberg Fault Zone coincident with the western boundary of the Kaapvaal craton (Figure 2-2; Stowe, 1986; Beukes and Smit, 1987). The present limits of preserved strata are related to post depositional erosion and do not reflect the extent and shape of the original depositional basin. Metamorphic alteration has been limited with most outcrops below greenschist facies metamorphism (Button, 1973b; Miyano and Beukes, 1984). Locally, amphibole is present due to Bushveld contact metamorphism in the Malmani Subgroup, and supergene alteration during late fluid flow produced local Pb-Zn, fluorite, and gold deposits in both the Malmani and Campbellrand subgroups (e.g. Martini, 1976; Clay, 1986; Duane, et al., 1991). Early, fabric retentive dolomite replaced most of the Malmani Subgroup, particularly peritidal facies which are also associated with chert replacement (Button, 1973b; Eriksson, et al., 1975, 1976). However, significant amounts of the Campbellrand Subgroup still consist of limestone (Beukes, 1987).

## LITHOFACIES

Preserved lithofacies in the Campbellrand-Malmani platform range from basinal to supratidal (Figure 2-3), and contain varying amounts of clastic and precipitated carbonate. Lithofacies are grouped into assemblages representing different depositional environments.

### *Grainstone-dominated Lithofacies Assemblage*

Carbonate Sand

Beds of carbonate sand range in thickness from 1 mm to >1 m, but average 1-30 cm thick. Often, they are replaced by sucrosic dolomite. Wave, interference, climbing, and current ripples are common (Figure 2-4), and rare beds contain hummocky cross stratification and low angle truncations or trough cross stratification. No stratification suggesting bedforms over a few decimeters tall is preserved, although thick intervals of massive dolomite interpreted as grainstones based on sparse hints of cross stratification could have been deposited by larger bedforms. Primary grain sizes varied from silt-sized to very coarse, and sorting is difficult to determine due to extensive recrystallization. Packstones are present as well, but appear to be less common. The range in cross stratification styles suggests deposition in environments ranging from shallow subtidal to supratidal (Figure 2-3).

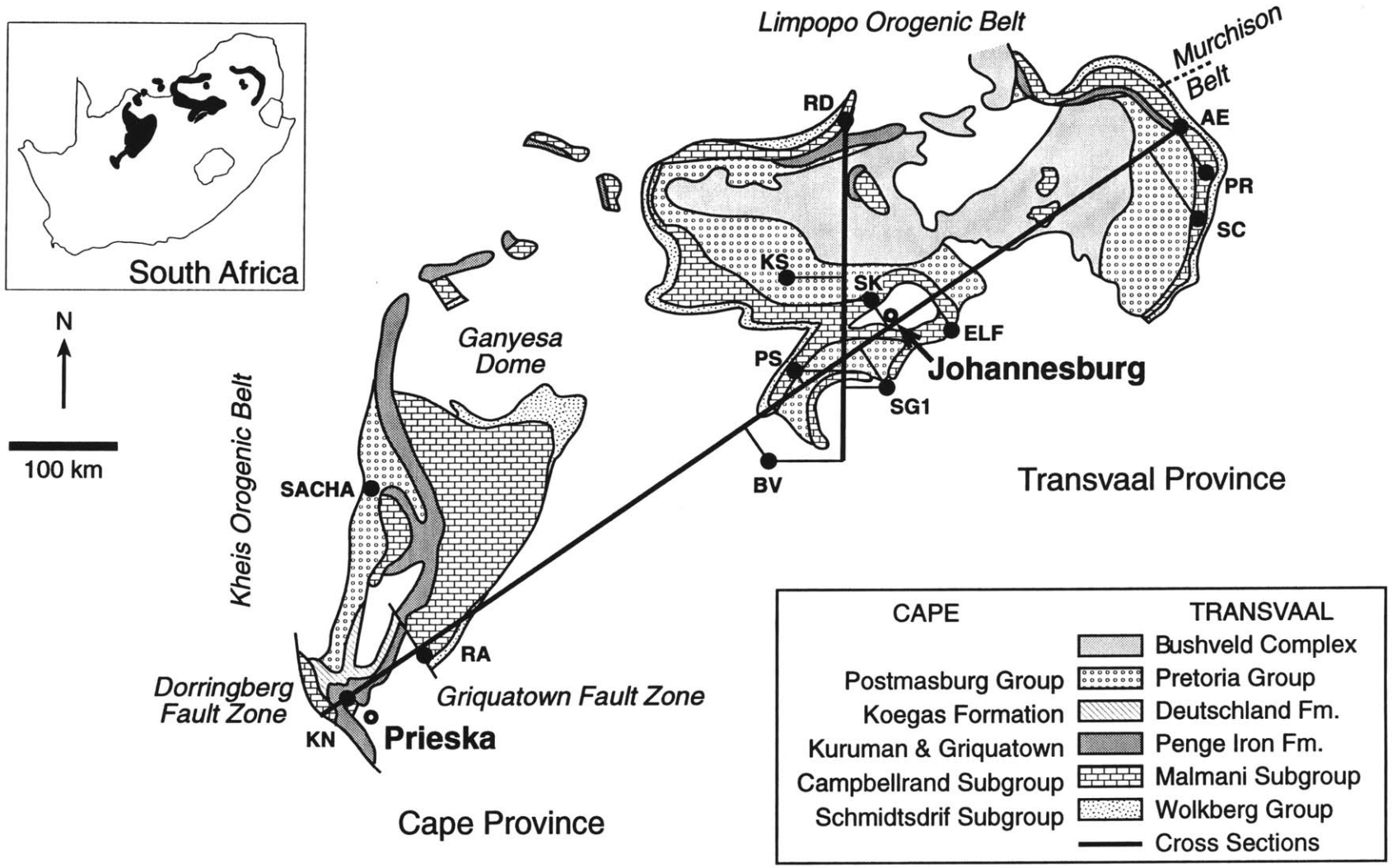


Figure 2-2: Outcrop map of the lower Transvaal Supergroup.

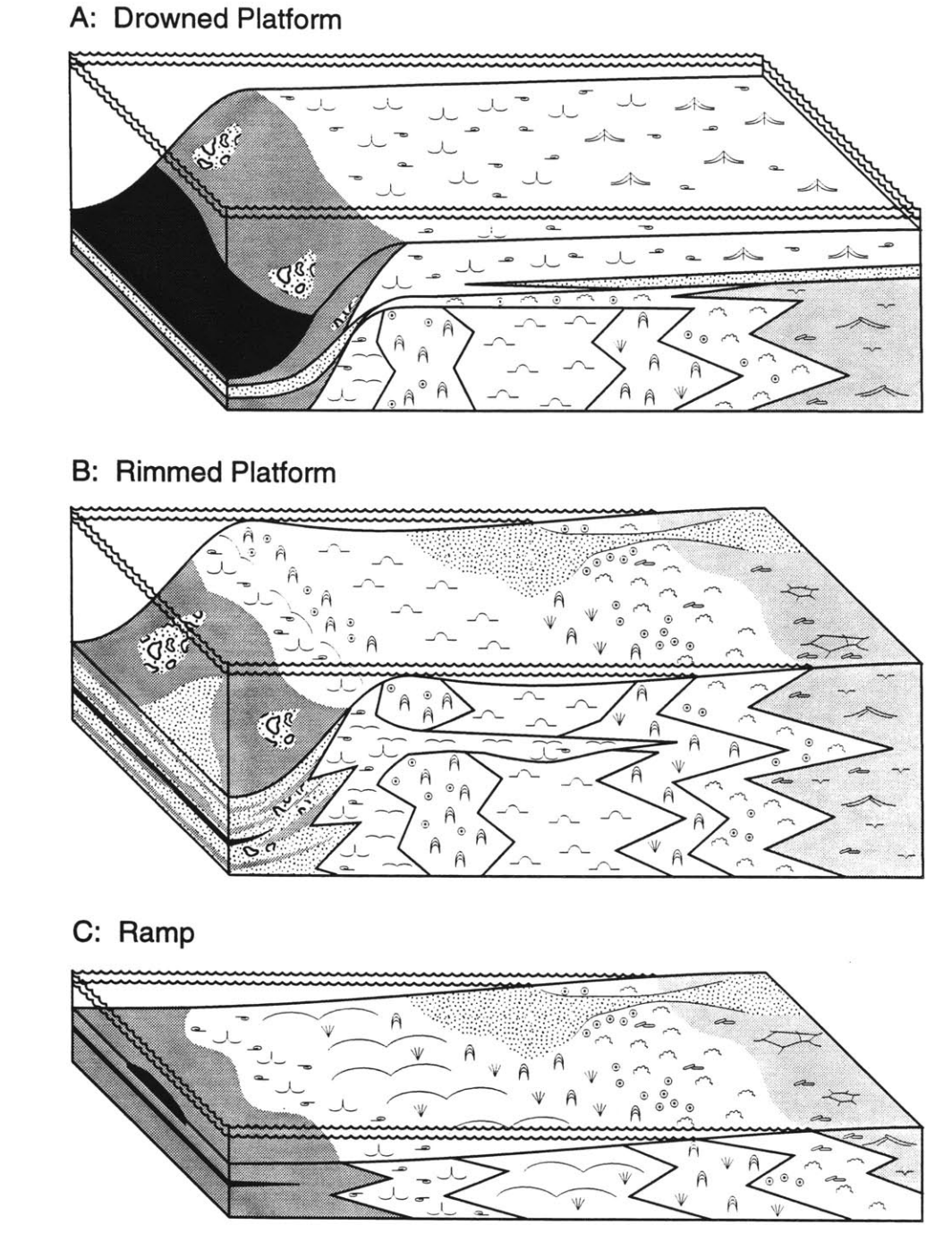


Figure 2-3: Block diagrams illustrating the distribution of lithofacies for different platform geometries

Oolite

In addition to forming oolite beds, ooids are extremely common mixed with non-oolitic sand and in lenses and troughs associated with stromatolites. Oolites compose up to about 80% of the grainstone-dominated lithofacies assemblage in the eastern Transvaal Province and are less common elsewhere in the platform. Many beds and lenses of oolite are either normally or inversely graded. Inversely graded beds commonly range in grain size from very fine to 3 mm-diameter ooids (Figure 2-5). The inverse grading is interpreted as the result of a single influx of ooid nuclei that were coated and progressively buried as they grew leaving only larger and larger ooids at the sediment-water interface to continue growing (see Sumner and Grotzinger, 1993). Wave and interference ripples are present in oolite beds that are not graded. Large-scale cross stratification is not observed. Oolites are interpreted to have formed on the tidal flats and in quiet shallow subtidal depositional environments. The absence of large-scale cross-stratification suggests that shoals did not form.

Wavy Laminated Dolomite

Wavy laminated, light gray rocks contain centimeter-thick laminae that are defined by diffuse orange bands. Sedimentary structures are rare, but beds pinch and swell over topographic highs and lows, suggesting that this facies predominantly consists of clastic carbonate. The absence of sedimentary structures could be due to fine grain-sizes and a low energy environment or to fabric loss during dolomitization. It is commonly associated with carbonate sands and stromatolites that suggest tidal flat depositional environments in the interior of the platform.

**Interpretation of Lithofacies Assemblage**

Grainstone, including oolites, and wavy laminated sediments are common in several lithofacies assemblages. They also form the dominant lithofacies in some regions. The variety of cross stratification styles in these areas suggests depositional environments ranging from shallow subtidal to supratidal for the grainstone-dominated lithofacies assemblage. Interbeds of other lithofacies, particularly stromatolites, support diverse depositional environments for the grainstone-dominated lithofacies assemblage.

### *Quartz Sand and Siliciclastic Shales*

Very rare quartz sands, siltstones, and siliciclastic shales are present. The quartzites are fine- to coarse-grained and are chemically and physically mature. Cross stratification consists of small-scale trough cross bedding, wave and current ripples, and low angle truncations. Shales and siltstones usually are poorly exposed, and sedimentary structures are

hard to identify. Rare current-rippled grainstones are interbedded with some shales, and Button (1973b) reports some ripples in siltstones. Cross stratification suggests shallow subtidal to supratidal depositional environments. Quartzites, siltstones, and siliciclastic shales commonly overly sequence boundaries, consistent with shallow depositional environments.

### *Supratidal to Shallow Intertidal Lithofacies Assemblage*

Micrite

Less than 15% of the supratidal to shallow intertidal lithofacies assemblage consists of light gray micrite which is present in <30 cm thick beds and lenses, and is sometimes finely interbedded with silt to sand-sized carbonate. Commonly, micrite is replaced by chert. Occasional mud cracks are present, particularly in thinner beds. Intraclasts consisting of reworked mud chips are common. Micrite beds and lenses are interpreted as carbonate mud that settled from suspension. They are present only in association with other facies that suggest shallow depositional environments.

Intraclast Breccias

Dolomite intraclasts are very common as single clasts between stromatolites, in lenses of breccia, and in ≤1 m-thick breccia beds. Clasts are platy to equant and range in size from a few millimeters to >70 cm long. They commonly contain textures similar to associated stromatolites or micritic layers. Imbricated clasts with a carbonate sand matrix are common. Occasionally, clasts form rosettes (Figure 2-6), and rare decimeter to meter-long platy clasts form jumbled piles. Many clasts associated with colloform stromatolites are coated with laminae identical to that in the stromatolites, and clasts sometimes act as nuclei for new domes.

The diverse geometry of breccias suggest that clasts represent locally brecciated carbonates that were reworked during high energy events. Brecciation probably was caused by diverse processes such as storm scouring, desiccation cracking, karstic fracturing, and tepee growth (e.g. Assereto and Kendall, 1977; Plummer and Gostin, 1981; Laznicka, 1988; Tucker and Wright, 1990; Sami and James, 1994). Rosette geometries of some clasts suggests wave or tidal reworking (Eriksson, 1977).

Chert Breccias

Unstratified breccias consisting of jumbled chert blocks up to meters in diameter are developed along regionally continuous unconformities. They are unstratified and commonly have a shale matrix. These breccias are interpreted as residual blocks left over from extensive dissolution and erosion of underlying carbonate units (Button, 1973b; Eriksson

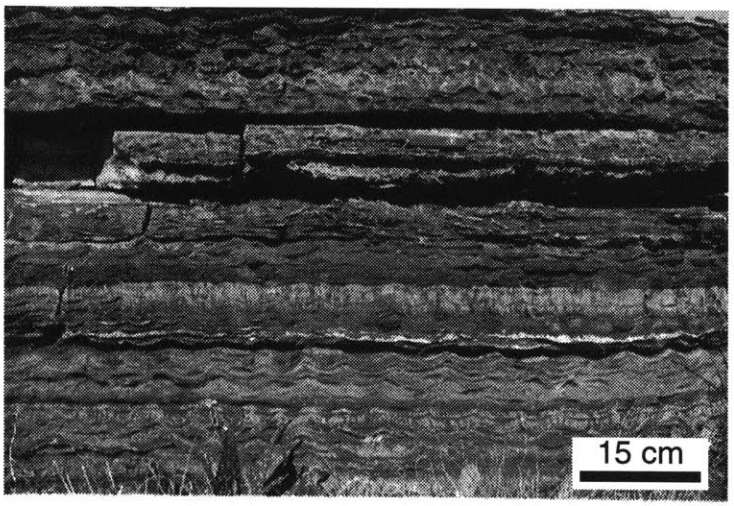


Figure 2-4: Wave rippled sand with rare cemented or microbially bound layers.

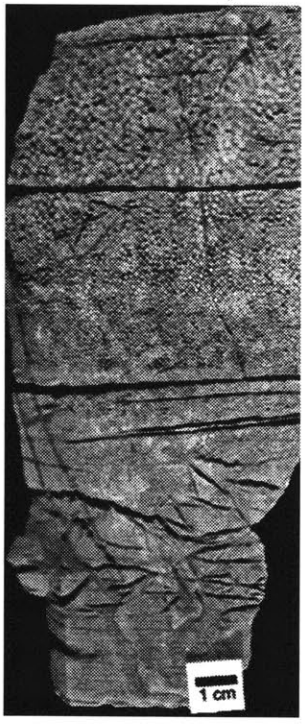


Figure 2-5: Inversely graded ooids lacking cross stratification.

and Truswell, 1974). The chert blocks remained because they were resistant to both chemical and physical weathering.

Stromatolites

Stromatolites commonly are present as laterally linked domes with diameters of 50-100 cm and up to 40 cm of synoptic relief. Many domes are composite and contain smaller secondary domes that range from <1 to 10 cm in diameter. They grew along flat to irregular bedding surfaces, including intraclasts (Figure 2-7). Commonly, domes are truncated by erosion surfaces overlain by breccias and grainstones.

Domes contain four styles of lamination: bumpy colloform, smooth colloform, peaked, and smooth deformed laminae. Bumpy colloform laminae (Figure 2-7A) consist of pairs of ≤0.1 mm-thick, dark red-orange lamellae and ≤0.5 mm-thick light orange lamellae. Both lamellae are constant thickness along laminae in the domes, but the lighter laminae thin into troughs between domes. Laminae dome over mm-scale irregularities on the larger stromatolites producing composite domes with occasional overhanging sides. In some cases, these irregularities are propagated for several centimeters whereas in others, they flatten out. Millimeter-thick layers of herringbone calcite occasionally are present within layers of bumpy colloform laminae. Smooth colloform laminae (Figure 2-7B) also consist of 0.1 mm-thick dark red-orange lamellae and 0.5 mm-thick, light orange lamellae. Commonly, laminae are truncated at the edges of domes, and lighter color lamellae occasionally thicken and thin across domes. Smooth colloform laminae also form overhanging composite domes on stromatolites, but they lack the mm-scale topographic irregularities. Occasionally, smooth colloform laminae are intercalated with abundant pods and lenses of grainstone. Peaked laminae (Figure 2-7C) consist of 0.1 mm-thick ,dark red-orange lamellae and 1.0 mm-thick light orange lamellae that are often replaced by chert. They form peaks (5 mm-wide and 10 mm-high) with high inheritance. Peaked laminae do not form composite domes although they coat intraclasts. Layers of peaked laminae commonly thicken into troughs, usually with an increase in the number of laminae. Smooth, deformed laminae (Figure 2-8) are composed of 0.2-1.0 mm-thick pairs of gray and light orange lamellae that thin on the sides of domes where they are inclined up to 80°. Lamellae do not form composite domes. Lenses of cross-stratified grainstone less than 10 mm thick are common between flat-lying laminae. Broken and folded lamellae are common in the interiors of domes, and overlying laminae seal the microfaults demonstrating that deformation occurred during growth of the dome. Commonly, deformation is accompanied by dewatering structures similar to sand volcanoes (Figure 2-8; Collinson and Thompson, 1989). In many cases, folding or microfaulting of the laminae resulted in disaggregation of light orange lamellae, whereas

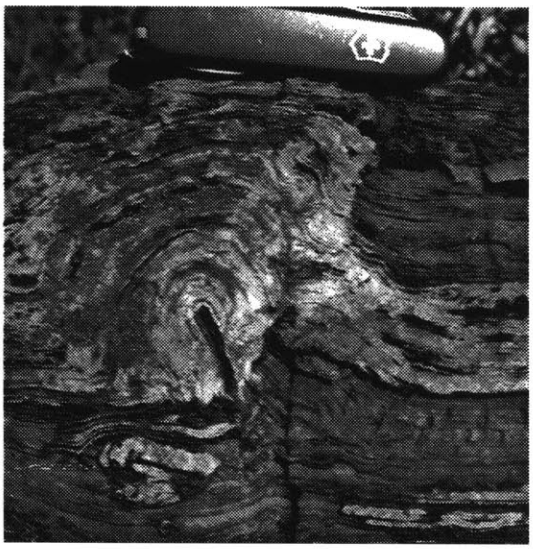

Figure 2-6: Smooth colloform laminae coating a small breccia clast.

gray lamellae maintained their integrity.

In addition to forming domal stromatolites, red and light orange lamellae are present in pseudoencapsulated structures that grew in current-rippled grainstones with abundant interbedded layers of bumpy to smooth colloform laminae (Figure 2-9). The structures nucleated as domes on small clasts and developed overhanging sides which gives an encapsulated appearance in most cross sections. Light orange lamellae thicken towards the downstream side (defined by associated current ripples) giving rise to elongation of up to four times the height. Their upper surfaces have streamlined profiles, and lower surfaces contain irregularly folded laminae. Laminae are overturned and underlie older laminae on the downstream side suggesting that the structures rotated during growth.

Bumpy colloform laminae also grew downwards from the bottom of platy intraclasts as linked mini-domes, 1-8 mm in diameter (Figure 2-7B). Laminae in the mini-domes pinch out around the edge of the clast and are absent from the top. The character of the laminae is identical to that in composite domal stromatolites with bumpy colloform laminae, although much of it is replaced by chert. Similar mini-domes also grew upright above the clast.

Interpretation

Three origins for the various lamellae are possible: unbound micritic sediment, microbially bound micritic sediment or precipitated microcrystalline carbonate, or crusts of precipitated microcrystalline carbonate. Dark red lamellae are interpreted as dense crusts of microcrystalline carbonate that precipitated in place due to their continuity, even thickness, and presence in mini-domes hanging downward from the undersides of clasts. Also, they are not associated with soft sediment deformation suggesting they were originally well lithified. Light orange lamellae also are laterally continuous and present in mini-domes, suggesting a precipitated origin. However, they also are associated with lenses of sediment and some light lamellae are deformed suggesting that they consist predominantly of micrite or loosely aggregated precipitated microcrystalline carbonate. Thus, light orange lamellae have a range of compositions and are interpreted as *in situ* precipitated microcrystalline carbonate in bumpy colloform laminae, tightly bound micrite or deformable microcrystalline carbonate crusts in smooth colloform laminae, peaked laminae, and pseudoencapsulated structures, and poorly bound micrite in domes with soft-sediment deformation. Gray layers in domes with deformation features are interpreted as firmly bound micrite or precipitated microcrystalline carbonate in microbial mats since they were more laterally cohesive than light lamellae in the same dome, but still deformable.

Composite domal stromatolites contain laterally continuous laminae that isopachously coat small and large clasts (Figures 2-6 and 2-7). They are interpreted as consisting pre-

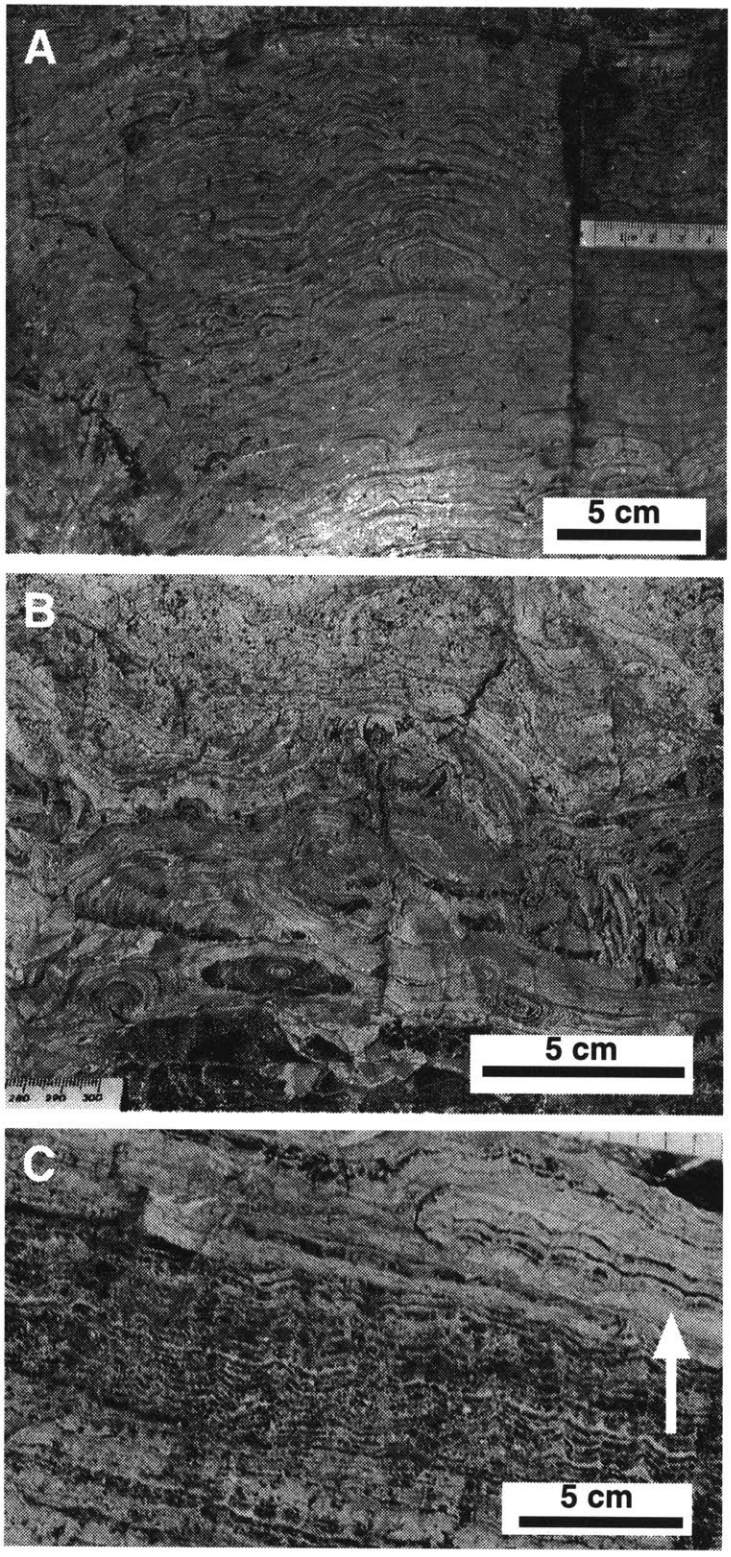


Figure 2-7: A) Composite domal stromatolites consisting of bumpy colloform laminae. B) Composite domal stromatolites consisting of smooth colloform laminae. C) Peaked laminae in a domal stromatolites. An overturned clast containing peaked laminae (arrow) is coated by peaked laminae.

dominantly of precipitated carbonate, formed either as the primary sediment or as syn-sedimentary cement. Composite domes with bumpy colloform laminae contain less sediment than those with smooth colloform laminae. Peaked laminae within domes were deposited during times of higher sediment incorporation into the domes as demonstrated by the thickening of these layers into troughs. Early lithification is demonstrated by the presence of rip-up clasts containing peaked laminae, and the coating of vertical clast sides by peaked laminae demonstrates a significant component of either microbial binding or *in situ* precipitation (Figure 2-7C). Folding of light lamellae in pseudoencapsulated structures and soft-sediment deformation in domes with smooth, non-colloform laminae demonstrate poor lithification. The presence of 80° slopes on the sides of these domes suggests the presence of a microbial mat. Neither micritic sediment nor precipitated microcrystalline carbonate would retain such steep slopes without the binding action of a microbial mat and still be soft enough to deform during dewatering of the underlying sediments. The origin of the carbonate, i.e. whether it is trapped-and-bound or precipitated within a mat as microcrystalline carbonate, is uncertain.

Crystal Fans

Layers of radiating crystal pseudomorphs, 3-30 cm-thick, are preserved in chert and occasionally dolomite. These pseudomorphs nucleated as botryoids on the sea floor and grew upward in a radiating fan-like pattern (Figure 2-10). Where botryoids nucleated close together, growth of neighboring botryoids interfered, and only the most upright crystals continued growth, thus creating a fringe of crystals oriented perpendicular to bedding. Preservation of crystal fans in the supratidal to shallow intertidal lithofacies assemblage is too poor to allow direct identification of precursor mineralogy, but similar crystal pseudomorphs, interpreted as neomorphosed aragonite, are common in intertidal to shallow subtidal deposits of the Campbellrand-Malmani platform.

Flat Laminae with Vertically Oriented Crystals

Beds of flat-lying, <1 mm-thick laminae commonly contain pseudomorphs of crystals that were elongate perpendicular to bedding. Occasionally, hints of fibrous crystals extend through multiple laminae (Eriksson, 1977; Button, 1973b). These fibrous crystal traces are always oriented perpendicular to bedding, and are similar to the dolomitized crystal fans, but with laminated sediment between elongate crystals. This lithofacies probably originally consisted of upward growing aragonite crystals around which fine-grained carbonate was deposited.

Evaporite Pseudomorphs

Rare, 1 cm cubic pseudomorphs are present in micrite layers (Figure 2-11A). They

Figure 2-8: Internal deformation of smooth laminae in a decimeter-diameter domal stromatolite. Scale has millimeter gradations.

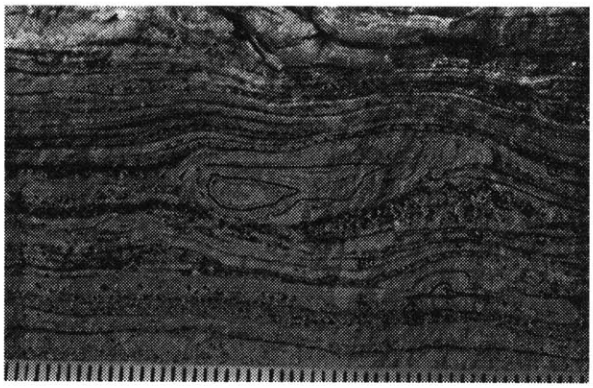

Figure 2-9: Pseudoencapsulated structures. Selected laminae are outlined with pen. Current ripples above and below this layer indicate sediment transport from left to right. Scale has millimeter gradations.

consist of chert or void-filling dolomite cement. The cubic geometry of the pseudomorphs suggests they replace halite crystals that grew displacively in micrite much like those observed in modern salt pans (Lowenstein and Hardie, 1985).

In addition, three layers of possible pseudomorphs after another evaporite mineral were observed, each about 3 cm thick (Figure 2-11B). The layers consist of continuous rows of 1 cm-wide chert columns with peaked tops. Preservation was insufficient to allow identification of primary growth morphology and it is unclear whether or not they represent pseudomorphs after an evaporite mineral or another type of sedimentary structure. Similar structures from the late Archean Carawine Dolomite, Australia, were interpreted as gypsum pseudomorphs (Simonson, et al., 1993), and they are roughly similar in morphology to better preserved younger gypsum pseudomorphs (e.g. Lowenstein, 1988). However, all the chert columns are oriented vertically in the Campbellrand-Malmani pseudomorphs, whereas gypsum crystals growing upward into still water tend to be variably inclined (Lowenstein, 1988), so a gypsum pseudomorph interpretation is questionable.

Other Structures

Tepees are developed in association with many of the above lithofacies and are up to 1 m high (Button, 1973b; Eriksson and Truswell, 1974; Eriksson, 1977).

Channels are up to 50 cm deep and commonly are filled with breccias and colloform stromatolites.

**Interpretation of Lithofacies Assemblage**

Sedimentary structures, including erosional channels, stromatolites, wave and interference ripples, abundant imbricated intraclasts, mud cracks, tepee structures, and rare evaporite pseudomorphs, support a shallow intertidal to supratidal depositional environment for this lithofacies assemblage. In addition, composite domes such as those described here have previously been interpreted as shallow intertidal to supratidal stromatolites (e.g. Grey and Thorne, 1985; Hoffman, 1988).

***Columnar Stromatolite-dominated Lithofacies Assemblage***

Stromatolites

Columnar stromatolites of various morphology are preserved in limestones and dolostones. They form beds up to several meters thick beds as well as isolated bioherms up to 1 m in diameter. Bioherms commonly are developed on unconformities and are overlain by grainstones. Individual stromatolites, usually 1-20 cm in diameter, show a variety of branching patterns and wall structures. Many of the columnar stromatolites at section BT

Figure 2-10: Poorly preserved aragonite fan pseudomorphs in chert from the supratidal to upper intertidal lithofacies assemblage.

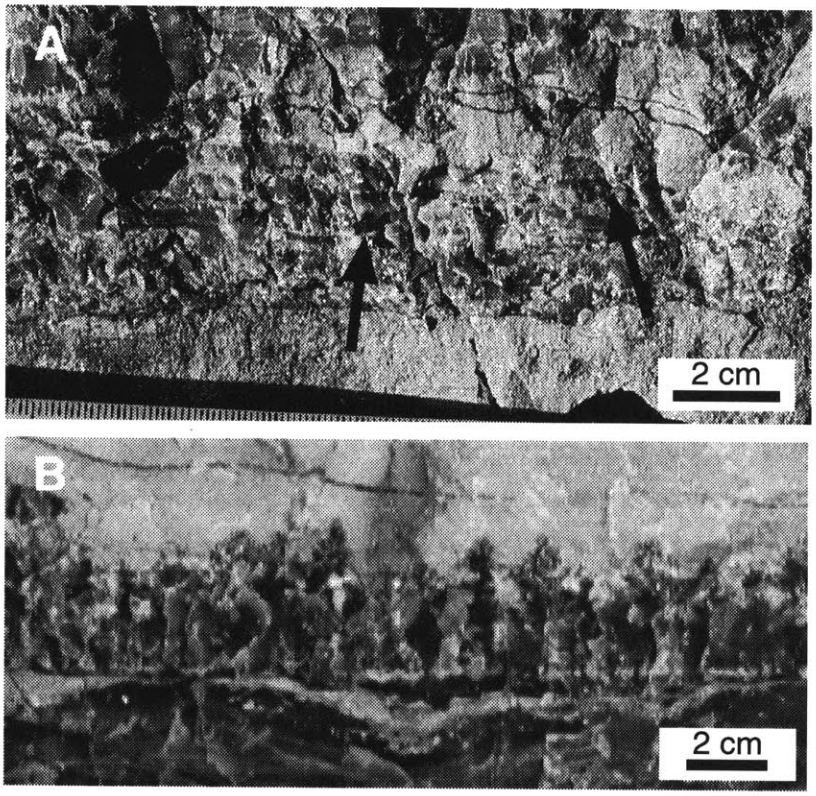


Figure 2-11: A) Halite casts replaced by chert (arrows). B) Chert-replaced structures that may also be pseudomorphs after another evaporite mineral.

were classified as belonging to the groups *Topinamboura, Radiatina, Katernia, Pilbaria, Tibia,* and *Sapinia* (Bertrand-Sarfati and Eriksson, 1977), and similar morphologies are present in the columnar stromatolites-dominated lithofacies assemblage throughout the platform. The microtexture of most of these stromatolites consists of vertically oriented elongate crystals and fine, filmy laminae defined by organic inclusions. The crystals are optically oriented and are consistent with a precipitated calcite or Mg-calcite origin. Rare columns have a herringbone calcite microtexture (Figure 2-12A). Commonly, the columns are associated with fringes and botryoids of aragonite pseudomorphs (see following section for petrographic criteria; Figure 2-12).

Rare irregular decimeter-scale domal stromatolites are preserved in dolomite. These domes contain cm-thick laminae that pinch and swell and are truncated along abundant micro-unconformities. They have low inheritance. Lenses of grainstone are common between and within domes. The pinching, swelling, and truncation of laminae as well as the abundance of associated grainstone suggest that these domes formed by trapping-and-binding of (coarse-grained) sediment rather than precipitation.

Crystal Fans

Crystal fan pseudomorphs grew off the sides of columnar stromatolites and upward from bedding planes (Figure 2-12). They consist of bundles of fibrous crystals that grew upward in a radial pattern from a single point and reach heights of over 50 cm. Commonly, they are draped by sediment and form domes geometrically similar to stromatolites (Figure 2-13). Rare fan layers contain no clastic carbonate and void space between fans is filled with herringbone calcite and other precipitated carbonate. Neighboring fans commonly intersected each other as they grew, and the most inclined bundles of crystals abut each other. Occasionally, shelter porosity is present below rare crystal bundles that grew at small angles to bedding. The exclusively upward growth of fans, their presence in beds lacking detrital carbonate, and the presence of shelter porosity all suggests that the fans grew directly on the sea floor and not as diagenetic crystals within the sediment.

The bundles of fibrous crystals in fans are replaced by calcite. Inclusions in the calcite suggest primary fibrous crystal growth and flat, irregular crystal terminations. Preserved inclusions and trace elemental distributions (as observed with cathodoluminescence) occasionally preserve the morphology of the original fibrous crystals extremely well (Figure 2-14). Rare pseudohexagonal cross sections of fiber bundles are also preserved. The secondary calcite mosaic consists of optically unoriented, elongate crystals that crosscut primary crystal boundaries. The combination of fibrous crystal habit, pseudo hexagonal cross sections, and the characteristics of the replacing mosaic suggest an aragonitic precur-

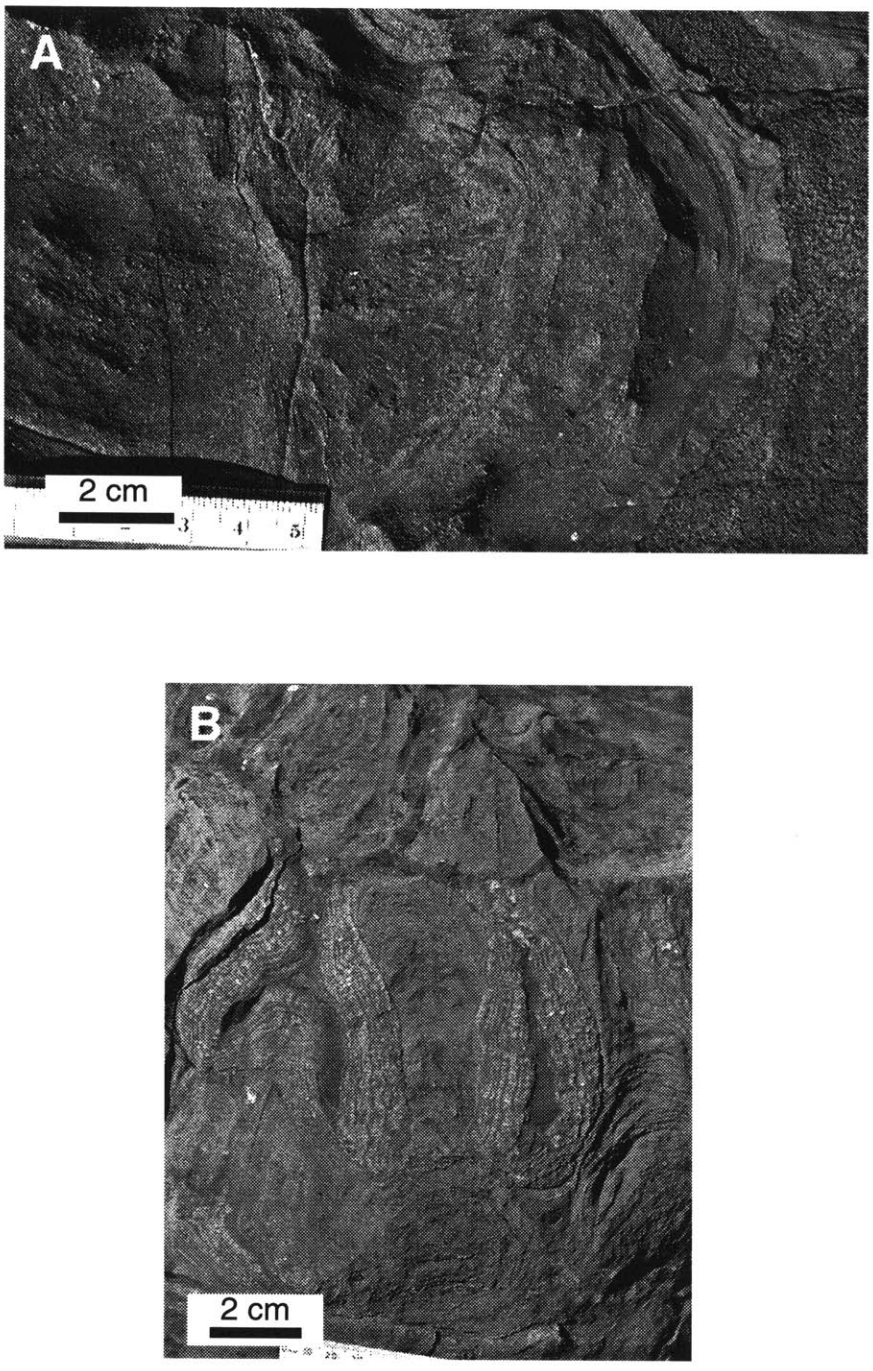


Figure 2-12: A) Plan view of columnar stromatolite with a herringbone calcite microtexture, an aragonite fan pseudomorph, and a thick coating of herringbone calcite. Coarse sediment filled troughs between stromatolites (far right). B) Vertical section of a bulbous stromatolite with cm-thick aragonite crusts.

sor (Sandberg, 1985b). These crystal fans have previously been interpreted as gypsum pseudomorphs (Bertrand-Sarfati, 1976), but the outstanding preservation of original fibrous crystal morphologies is inconsistent with gypsum crystals replaced by calcite and the primary crystal morphologies are inconsistent with gypsum precipitation (Lowenstein, 1988).

Clastic Carbonate

Oolites and carbonate sand form lenses and thin beds containing wave ripple, current ripple, and low-angle cross stratification. Commonly, they are present in troughs between columnar stromatolites and fill topography created by stromatolite beds and bioherms. One bed of ≤3 mm-diameter oncolites contains 20 cm-high dunes with wavelengths of 100 cm (Truswell and Eriksson, 1973).

Platy breccias are common overlying unconformities. They are usually imbricated and contain a grainstone matrix, but occasionally, they form edgewise rosettes in channels. Rare siliciclastic shales also overlie unconformities near the base of the platform.

**Interpretation of Lithofacies Assemblage**

The columnar stromatolite-dominated lithofacies assemblage consists mainly of precipitated columnar stromatolites with abundant oolites and grainstones, and lesser aragonite fan pseudomorphs and trapped-and-bound stromatolites. These facies are interbedded on a meter-scale and no obvious cyclicity was observed although shales and grainstones preferentially overly unconformities. Abundant unconformities also are associated with truncated stromatolites (Figure 2-15) and platy breccias. The abundance of unconformities, rare channeling, the ripple, small dune, and low angle cross stratification in grainstones, and the 1 meter synoptic relief of bioherms suggest a lower intertidal to shallow subtidal depositional environment for the columnar stromatolite-dominated lithofacies assemblage.

***Lagoonal Lithofacies Assemblage***

The fenestral laminite lithofacies consists of dark, finely laminated, 5 mm-thick layers of calcite that alternate with 5 mm-thick white spary calcite layers to form meter-thick beds of limestone (Figure 2-16). Both dark and white layers of calcite are laterally discontinuous and abundant erosional truncation of laminae is apparent. Rare breccias with <1 cm diameter clasts are associated with some of the truncation surfaces. White layers are coarsely crystalline and crystals appear to have grown inward from the top and bottom of the layers. Fine laminae in dark layers are defined by organic inclusions. These laminae may have been produced by microbial mats based on the abundance of organic inclusions (Beukes, 1987). White layers are probably laminoid fenestrae filled with early cements

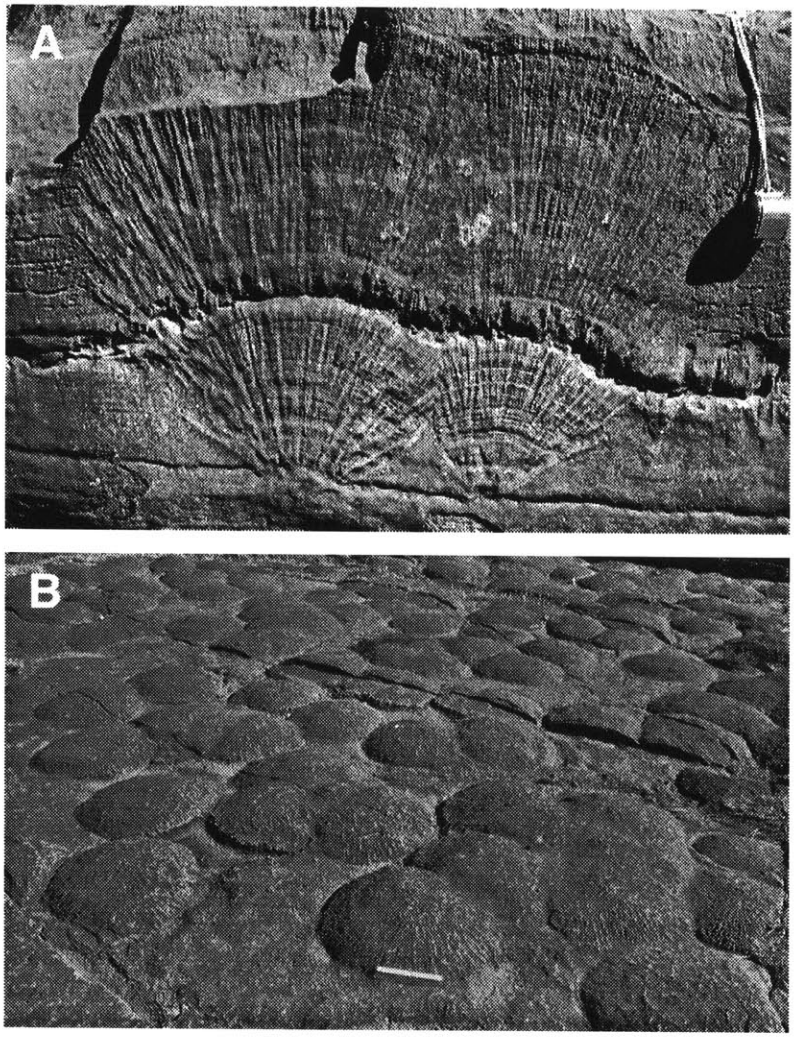


Figure 2-13: A) Vertical section of large aragonite fan pseudomorphs. The blades of the fans are draped by sediment. Hand lens is 2 cm across. B) Domes formed by large fans like those in A draped by sediment. Their growth is consistent with a purely abiotic origin. Scale is 15 cm long.

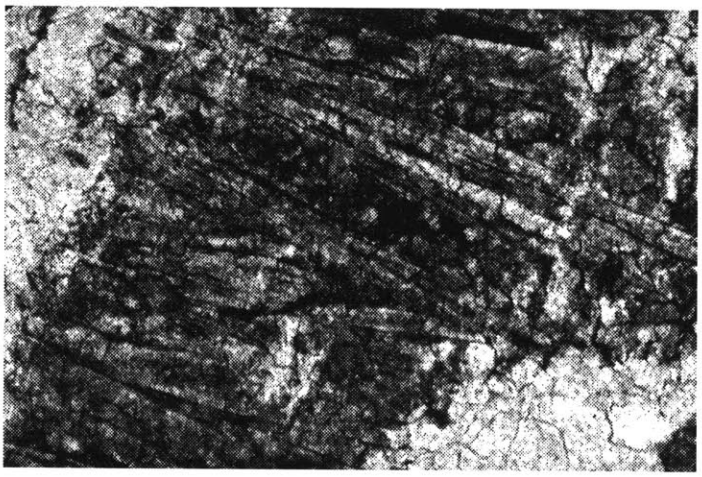

Figure 2-14: Thin section in plane polarized light showing fibrous textures in aragonite pseudomorphs. This thin section comes from the aragonite coatings on stromatolites in Figure 2-12B.

(Beukes, 1987).

Light gray ≤10 cm-diameter domes are interbedded with the fenestral laminite lithofacies (Figure 2-16). Typically, these domes formed 5-10 cm-thick beds, but beds up to 1.5 m-thick are present. Domes are laterally linked and hemispherical. They nucleated on planar surfaces and grew upward with isopachous laminae, a few mm-thick, coating the initial dome. Domes are then truncated by an erosional surface and new domes formed or the domes are overlain by fenestral laminite rocks. The domes are composed of coarsely crystalline calcite with a rare crystal elongation perpendicular to lamination. The isopachous geometry of the domes and the crystal elongation are consistent with a precipitated origin, with or without the presence of a microbial mat. The absence of organic inclusions in the domes, in contrast to well defined organic laminae in the fenestral lithofacies, suggests that well developed mats may not have been present on the domes.

**Interpretation of Lithofacies Assemblage**

The fenestral laminite lithofacies alternates with the isopachous dome lithofacies on a decimeter to meter scale. Occasionally, several meter-thick intervals of fenestral laminite lithofacies contain very poorly developed isopachous domes, and the two lithofacies are gradational into each other. The interbedding of these two lithofacies appears to be cyclic in some areas with cycles based by an erosional surface overlain by isopachous domes and then fenestral laminite laminae. The lack of a third facies makes it difficult to establish whether these are true cycles or random alternation of facies.

The abundance of small truncation surfaces and the lack of cross stratification and channeling suggest a shallow subtidal depositional environment with little agitation. The stratigraphic position of these lithofacies platformward of a rimmed platform consisting of the columnar stromatolite-dominated lithofacies assemblage suggests a lagoonal depositional environment (Beukes, 1987).

### *Giant Stromatolite Lithofacies Assemblage*

Giant, elongate mound stromatolites range from 2 to 10 meters wide and from 5 to >45 meters long (Figure 2-17; Truswell and Eriksson, 1972, 1973; Eriksson, 1977; Eriksson and Truswell, 1974; Button, 1973b; Beukes, 1987; Eriksson, et al., 1976). Synoptic relief ranges from 30 to 200 cm. The mounds contain either small columnar stromatolites with fine laminae or smooth to peaked laminae (herein called Boetsap-style lamination after section BT where it is best exposed) associated with aragonite pseudomorph fans and lacking columnar stromatolites.

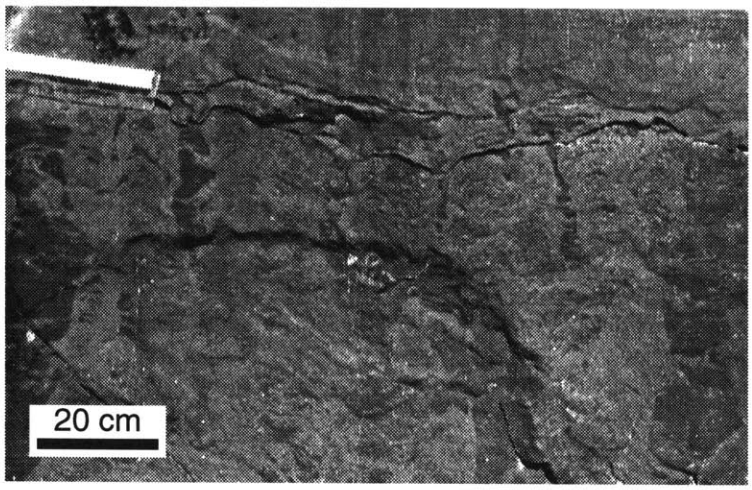


Figure 2-15: Columnar stromatolites truncated by an erosional surface (at the level of the scale). The unconformity is overlain by grainstone.

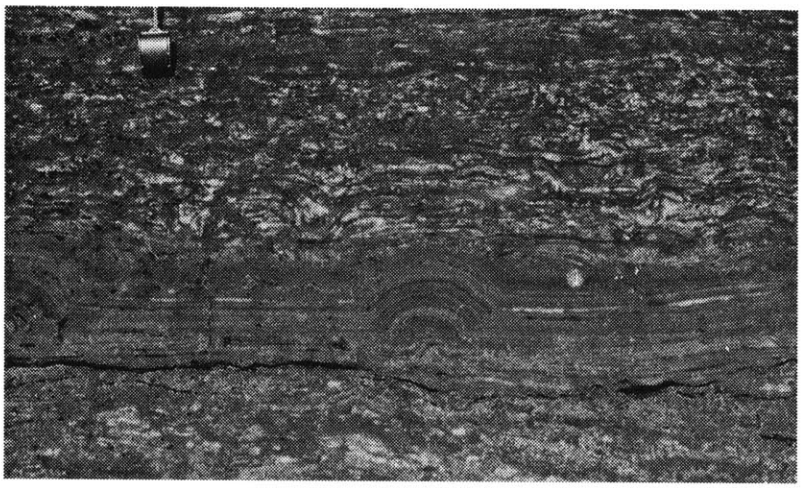

Figure 2-16: Fenestral stratiform lithofacies with a thin layer of isopachous domes. Hand lens is 2 cm wide.

Columnar Stromatolites

Small columnar stromatolites are 1-5 cm in diameter and have convex to rectangular laminae with various branching patterns. Some of them are classified as belonging to the groups *Radiatina* and *Katernia* (Bertrand-Sarfati and Eriksson, 1977). These stromatolites contain both optically oriented crystals, particularly on the walls of columns, and silt-sized clastic grains, including rare quartz silt (Bertrand-Sarfati and Eriksson, 1977), suggesting a combined precipitated and trapped-and-bound origin for the stromatolites.

Boetsap-style Lamination

The Boetsap-style lamination consists of red-brown microcrystalline carbonate laminae, lighter red-brown finely crystalline laminae, dark gray finely crystalline layers, and coarse sparry layers (Figure 2-18). Red-brown microcrystalline carbonate laminae consist of dolomite, and range from 1 to 3 mm thick along a single lamina. Commonly, upper surfaces are peaked, possibly rippled. They occasionally contain a vertical fabric suggestive of very fine, vertically oriented aragonite pseudomorphs. Red-brown microcrystalline carbonate laminae make up about 50% of a bed classified as containing the Boetsap-style lamination. Red-brown, finely crystalline laminae also consist of dolomite and are uniformly <1 mm thick. Occasionally, laminae are up to 3 mm thick in more coarsely crystalline layers. A fine, vertical fabric rarely is present. Red-brown, finely crystalline laminae grade laterally into dark gray, finely crystalline laminae that consist of limestone. Gray, finely crystalline laminae also are uniformly <1 mm in thickness and tend to be thinner than red-brown, finely crystalline laminae. A vertical fabric is visible in thicker laminae, and occasionally projects through microcrystalline carbonate and finely crystalline laminae in a fan-like geometry (Figure 2-18). Red-brown and gray finely-crystalline laminae make up about 50% of layers with the Boetsap-style lamination. Coarse sparry laminae consist of dolomite and vary laterally in thickness, occasionally pinching out. They are up to 1 cm thick and contain ripples. Coarse sparry laminae do not contain a vertically oriented fabric and make up <1% of laminae. Rare patches of herringbone calcite also are preserved in rocks with the Boetsap-style lamination.

Red-brown microcrystalline carbonate layers are interpreted as a combination of dolomitized fine-grained clastic carbonate with a small proportion of neomorphosed aragonite represented by the vertically oriented fabric. Both red-brown and gray finely crystalline laminae are interpreted as variably altered precipitated laminae. The optically unoriented calcite or dolomite crystal mosaic that replaces the vertical crystal fibers suggests an original aragonitic mineralogy, whereas the rare presence of herringbone calcite suggests Mg-calcite precipitation. Preservation is too poor to allow definitive identification for all of the

Figure 2-17: Giant stromatolite mounds that are more than 45 m long and 10 m wide from Boetsap (BT).

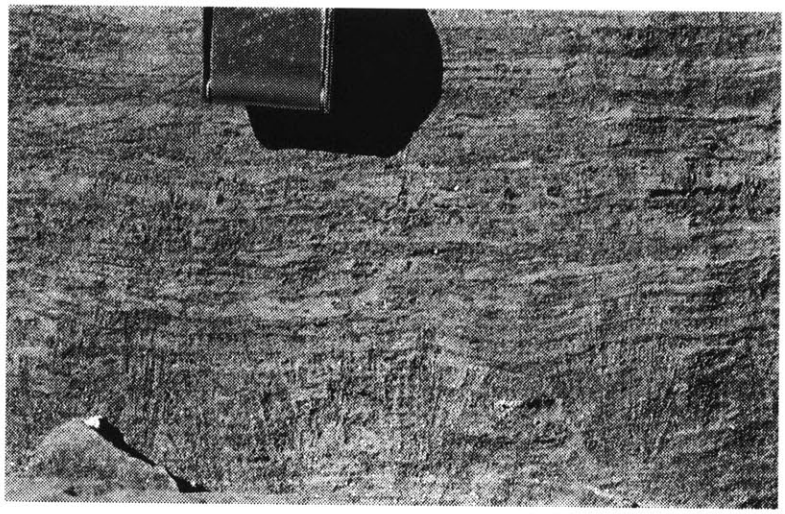

Figure 2-18: The Boetsap-style lamination with abundant vertically elongate pseudomorphs that extend from the base to the top of the photograph. A fan-like geometry is developed at the base. Hand lens is 2 cm wide.

laminae, but evidence suggests that both aragonite and Mg-calcite were present. Coarse, sparry laminae are interpreted as recrystallized clastic carbonate deposited from tractional currents.

Crystal Fans

Isolated and layers of crystal fans are present within the giant mound stromatolites. These fans have the same characteristics as those in the columnar stromatolite-dominated assemblage, including crystallographic characteristics suggesting an aragonitic primary mineralogy. These fans have been previously interpreted as domal stromatolites with a radiating internal fabric (Truswell and Eriksson, 1973; Eriksson, 1977). The presence of aragonite fan pseudomorphs and the vertical fabric in the Boetsap-style laminae suggest abundant precipitation of aragonite in well-agitated subtidal environments.

**Interpretation of Lithofacies Assemblage**

Giant elongate mounds stromatolites are common in Precambrian carbonate platforms, and above wave-base, open marine subtidal depositional environments for them have been well established (e.g. Truswell and Eriksson, 1973; Eriksson and Truswell, 1974; Button, 1973b; Hoffman, 1969; Grotzinger, 1986, 1988; Pelechaty and Grotzinger, 1988). Characterization of the giant mound stromatolite lithofacies assemblage and its stratigraphic distribution in the Campbellrand-Malmani platform supports this interpretation. Thus, the aragonite pseudomorph fans within the giant stromatolite mounds precipitated from open marine waters.

### *Deep Subtidal Microbialite Lithofacies Assemblage*

Microbialites of the Gamohaan and Frisco Formations

Thick sections of the Gamohaan and Frisco formations consist exclusively of microbialites encased in calcite that precipitated *in situ* (Figure 2-20A; Chapter 4). These microbialites consist of three components (Chapter 3): filmy laminae interpreted as the remnants of microbial mats, supports interpreted as non-mat microbial growth structures, and calcite-filled primary voids. The filmy laminae are commonly draped over the supports creating complex microbial structures with abundant voids. These structures are classified into six end-member microbialite morphologies: planar laminae, rolled-up laminae, tented microbialites, cuspate microbialites, irregular columnar microbialites, and plumose structures (Chapter 3). Beds of herringbone calcite also are present. Four microbialite assemblages are defined in Chapter 4: 1) the bedded cuspate microbialite assemblage, 2) the planar-laminae assemblage, 3) the irregular columnar microbialite assemblage, and 4) the

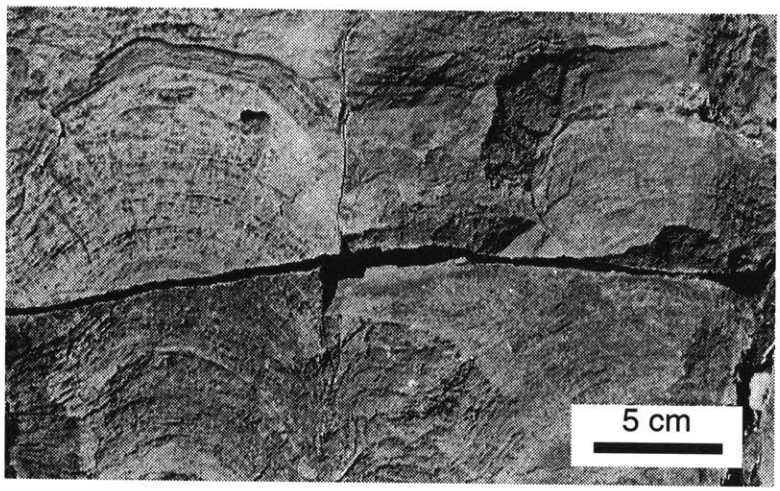


Figure 2-19: Dolomitized fans in a giant stromatolite. The internal fibrous texture is variably preserved.

rolled-up laminae assemblage. These assemblages are grouped into a single deep subtidal lithofacies assemblage for the purposes of this chapter.

Net-like Microbialites

Similar microbialites also are present as centimeter to decimeter-thick beds with grainstone caps (Figure 2-20B). These microbialites are coarsely dolomitized and carbonate cement textures were either not developed or not preserved, but filmy laminae and supports are present. The filmy laminae are draped over the supports creating a very open, net-like fabric similar to that of cuspate microbialites in the Gamohaan and Frisco formations (Chapter 3). The net-like microbialites overly sharp surfaces and grade upward into stratiform stromatolites with irregular laminae, overlain by coarsely laminated dolomite that occasionally contains poorly preserved cross stratification. The coarsely laminated dolomite is capped by a sharp surface on which the next microbialites grew.

The thicknesses and textures of 352 beds of net-like microbialites were logged in core SACHA to look for systematic transitions from net-like microbialites to stratiform stromatolites and carbonate sand suggests cyclic deposition. Analyses of bed thickness, net-like microbialite thickness, and clastic carbonate thickness demonstrate that there are no rhythmic changes in bed thickness or composition within the interval measured (Figure 2-21). Thus, deposition is interpreted to have been a result of non-cyclic facies stacking.

**Interpretation of Lithofacies Assemblage**

The delicate morphology of the microbialites (Chapter 3), the lack of evidence for scouring, and the absence of clastic carbonate all suggest a deep subtidal, sub-wave base depositional environment for the microbialite assemblages in the Gamohaan and Frisco formations. Net-like microbialite beds were deposited in wedges on the top of the Campbellrand-Malmani platform between facies tracts consisting of the giant stromatolite lithofacies assemblage, and are also interpreted as low-energy subtidal deposits with variable clastic carbonate influx. Thus, the microbialites are grouped into a single deep subtidal microbialite lithofacies assemblage.

### *Slope and Basinal Lithofacies Assemblage*

Rhythmites

Rhythmites consists of sucrosic dolomite to dolomitic limestone in 5 cm massive beds separated by cm-thick finely laminated layers (Beukes, 1987). Commonly, beds are nodular, although they are brecciated occasionally. Graded interbeds are present, and rarely, they are capped by rippled grainstones. Occasional interbeds contain crinkled, probably

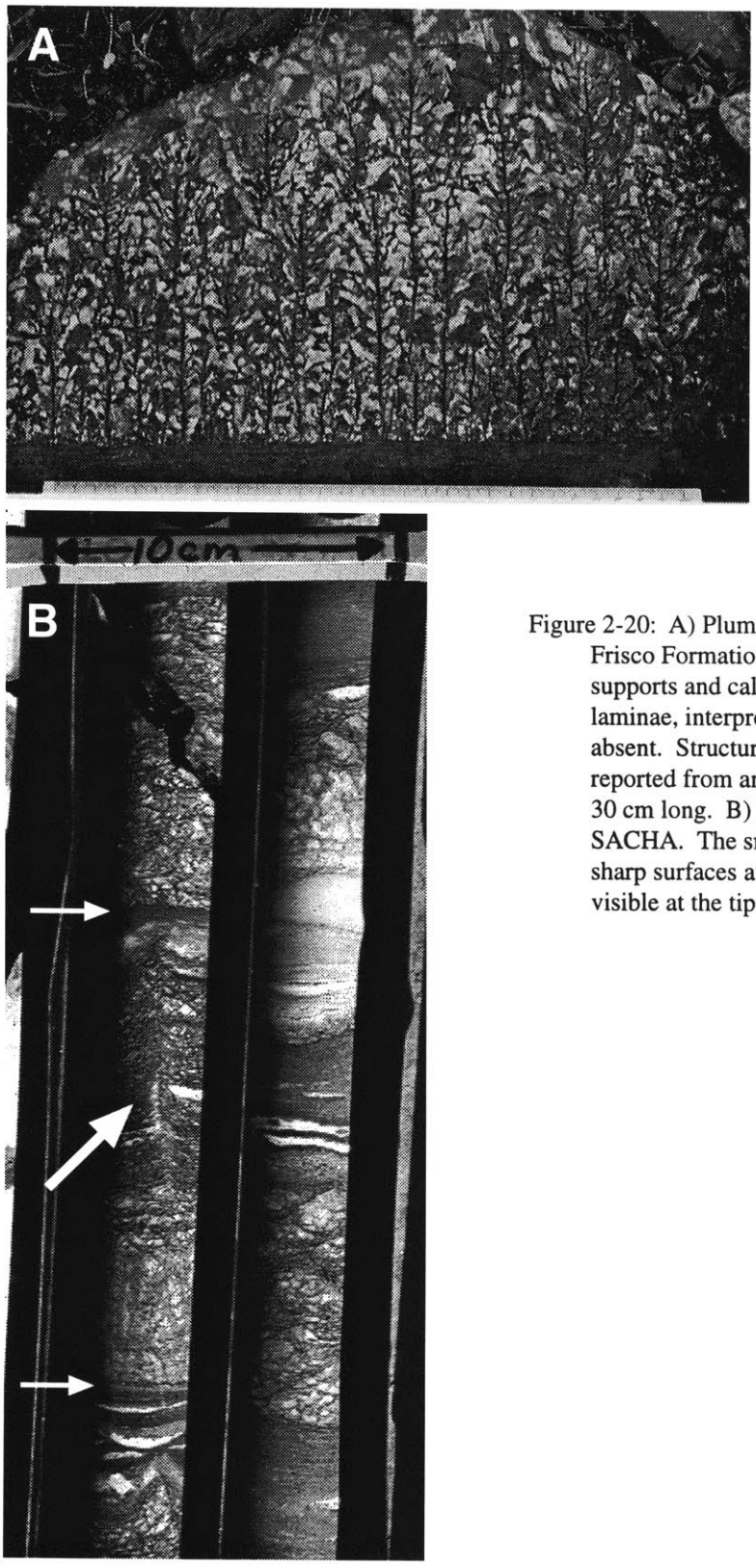


Figure 2-20: A) Plumose microbialites from the Frisco Formation consisting of exclusively supports and calcite-filled primary voids. Filmy laminae, interpreted as microbial mat, are absent. Structures of this type have not been reported from any other deposits. The scale is 30 cm long. B) Net-like microbialites from core SACHA. The small white arrows indicate the sharp surfaces at the bases of beds. A support is visible at the tip of the large white arrow.

microbial, laminae (Beukes, 1987; Simonson, et al., 1993). This lithofacies is typical of peri-platform ooze and distal carbonate turbidites in slope to basinal environments (McIlreath and James, 1979; Cook and Mullins, 1983; Beukes, 1987).

Chert and Dolostone Breccia

Sedimentary breccias with chert and dolostone clasts and matrix are common along the slope margin. Clasts range in size from <1 mm to decimeter-scale and are both platy and equidimensional. The breccias usually are poorly sorted, and the matrix is unlaminated. They form lenticular beds and commonly are associated with soft sediment deformation. The lack of sorting, the lack of grading, their tabular geometry, and their association with soft sediment deformation are consistent with deposition from debris flows along the platform margin (Hubert, et al., 1977; McIlreath and James, 1979; Cook and Mullins, 1983).

Other Lithofacies

Carbonaceous shales are finely laminated and are associated with siderite-rich iron-formation, rare pyrite nodules, chert pods, and rolled-up microbial mat (Beukes, 1987; Chapter 4). They are interbedded with both the deep subtidal microbialite lithofacies assemblage and iron-formation, suggesting deeper depositional environments than the deep subtidal microbialite lithofacies (Beukes, 1987; Chapter 4).

Iron-formation in basinal deposits of the Campbellrand-Malmani platform consists of finely laminated siderite beds or finely laminated chert with abundant iron oxides (jasper; Beukes, 1983b, 1987). Iron-formation is interbedded with carbonaceous shales, slope breccias, and carbonate rhythmites.

Tuffaceous beds are 5-40 cm thick and have graded bases and cross stratified tops (Figure 2-22; Beukes, 1987). Rare carbonate clasts and volcanic spherules are present at the bases of some beds. The tuffaceous sediment is dark green to black in color and occasionally is replaced by carbonate.

**Interpretation of Lithofacies Assemblage**

The interbedding of these five lithofacies, each of which independently suggests deep water sedimentation, strongly supports a basinal depositional environment for this lithofacies assemblage, as concluded by Beukes (1980, 1987). However, Altermann and Herbig (1991) interpret these lithofacies as peritidal. The differences in sedimentary structures and composition between clearly identified peritidal lithofacies described above and the lithofacies described here strongly support a basinal, rather than a peritidal, interpretation.

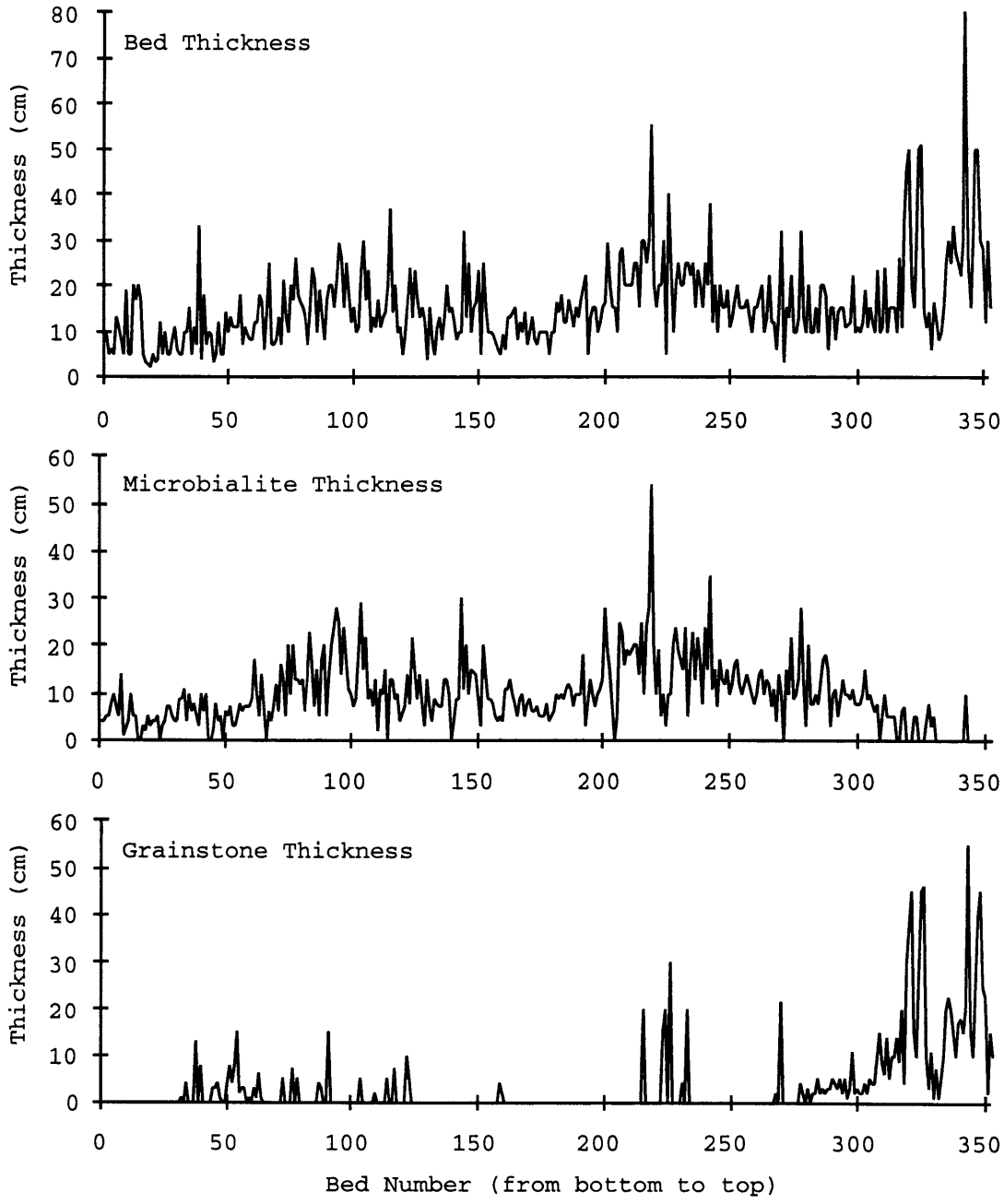


Figure 2-21: Plots of the thicknesses of net-like microbialite beds, microbialite thickness, and grainstone thicknesses compiled from core SACHA in the Fairfield Formation. No systematic changes are apparent besides an increase in grainstones at the top of the section.

## STRATIGRAPHY

The Transvaal Supergroup contains numerous sequences that are separated by unconformities of varying temporal significance. The Campbellrand-Malmani carbonate platform is contained within a supersequence defined by craton-wide unconformities. The lower unconformity developed after deposition of the Wolkberg Group and equivalent units, and is overlain by the Black Reef Quartzite which grades upward into the Campbellrand-Malmani carbonate platform. The upper unconformity developed after deposition of iron-formations and siliciclastic sediments above the Campbellrand-Malmani platform. Within the Campbellrand-Malmani platform, seven sequences have been identified based on regional facies patterns and the development of unconformities. This section describes the general stratigraphic development of the supersequence containing the Campbellrand-Malmani platform and the stratigraphic development of the platform, including a new correlation between the Campbellrand and Malmani subgroups.

### Stratigraphic Data

Stratigraphic data for the regional stratigraphy of units other than the Campbellrand and Malmani subgroups have been taken from the literature. New stratigraphic data for the Campbellrand and Malmani subgroups, presented in Appendix B, was combined with sections from the literature. These data have been compiled into two cross sections of the platform, one from north to south through the Malmani Subgroup and one from southwest to northeast extending from the eastern Transvaal Province to the southwest corner of outcrop (Figure 2-23). The stratigraphy of the Campbellrand Subgroup is based on Beukes (1980, 1987) with minor modifications.

The stratigraphy of the Malmani Subgroup is based on a compilation of sections and core logs from Eriksson (1972), Button (1973b), Eriksson and Truswell (1974), Clendenin (1989), and Appendix B. Correlations using raw stratigraphic thickness and using smoothed stratigraphic thicknesses in the Johannesburg area are both presented (Figure 2-23). Much of the data from the Johannesburg area consists of composite sections from several areas or core. For cores, no mention of corrections for the dip of sediments were reported in logs taken from the literature. The thickest sections from the Johannesburg area are composite sections and uncorrected cores, and units in these sections are uniformly thicker with no single unit in any of the sections accounting for increased thicknesses. Thus, it is reasonable to interpret the differences in thickness from the Johannesburg area as inaccurate estimates of true thicknesses. However, differences in thickness reflecting tectonic activity cannot be ruled out. Eriksson (1977) proposed uplift in the Johannesburg area during car-

bonate deposition based on facies distributions, but the cross sections presented here do not confirm this interpretation. Apparent differences between facies from section to section could be due to differences in the emphases and experience of the various authors. The large scale stratigraphy and depositional environment interpretations are consistent between workers, however, and is considered reliable, even though the distribution of facies changes and the role of local structure is uncertain.

### *Underlying Siliciclastic Sediments*

The Wolkberg Group and its correlatives, the Buffelsfontein, Wachteenbeetje, and Groblersdal groups, are the lowest strata of the Transvaal Supergroup in the Transvaal Province (Button, 1973a; Tyler, 1979; Hartzer, 1989; Clendenin, et al., 1991). They consist predominantly of fluvial to deltaic siliciclastic sediments and lesser volcanics, and unconformably overlie older sediments and volcanics as well as Archean granite-greenstone basement. The Wolkberg and equivalent sediments are up to 2 km thick near section AE, section RD, and the Crocodile River Fragment and pinch out to the north and south due to erosion prior to deposition of the Black Reef Formation (Button, 1973a; Tyler, 1979; Clendenin, 1989; Clendenin, et al., 1991). The similarities in stratigraphy across the Transvaal Province suggest regional development of the fluvial plain (Collinson and Lewin, 1983). Paleocurrents in the Wolkberg Group demonstrate transport from the north, north of the Murchison Greenstone Belt, and from the east and northeast south of the Murchison Greenstone Belt (Button, 1973a). Paleocurrents from the Buffelsfontein Group show south to southeast-directed sediment transport. The predominance of southerly current indicators suggests that deposition occurred south of the preserved outcrop areas and that the current outcrop pattern reflects differential subsidence of the Kaapvaal craton, and not the depositional geometry of the basin.

The Wolkberg and correlative groups are overlain by the Black Reef Quartzite, the basal unit of the Transvaal Supergroup. Deposition of the Black Reef Quartzite extended beyond the preserved limits of the underlying sediments, often overlying Archean basement. Button (1973a) and Tyler (1979) report that the Wolkberg Group and Buffelsfontein Group, respectively, are conformably overlain by the Black Reef Quartzite in the centers of preserved depositional areas, but are truncated by an unconformity at the base of the Black Reef Quartzite to the south. Clendenin et al. (1991) however, interpret the contact between the Wolkberg Group and the Black Reef Quartzite as higher in the section than Button and unconformable everywhere, and Hartzer (1989) reports an unconformable contact in the Crocodile River Fragment. If the contact between the two is unconformable, deposition of the Wolkberg Group may not be genetically related to deposition of the overlying Black

Figure 2-22: Tuffaceous turbidites from the basinal lithofacies assemblage at KN. A pod of carbonate breccia is present below the hammer. The hammer is 35 cm long.

Figure 2-23: Cross sections of the Campbellrand-Malmani carbonate platform. The scale bars are for both sections with facies patterns. Sources of data: KN: field section; RA: field section from RA and log of core SD1; GC: field check of facies, thicknesses from Beukes (1987) below Kamden Member; GG: field check of facies, thicknesses Beukes (1987) above Kamden Member; BV: core log from Bothaville after Clendenin (1989); PS: core log from Potchefstroom after Clendenin (1989); KS: core log from Koster after Clendenin (1989); GP: composite section from Potchefstroom to Johannesburg after Eriksson (1972) (Not marked on map); SG: log of core SG1 shown corrected for 20° dip in core; SK: composite field section after Eriksson and Truswell (1974); ELF: log of core corrected for 15° dip; SC: field section; PR: section at Pilgrims Rest after Clendenin (1989); AE: field section with thickness of Frisco Formation from Button (1973b).

→

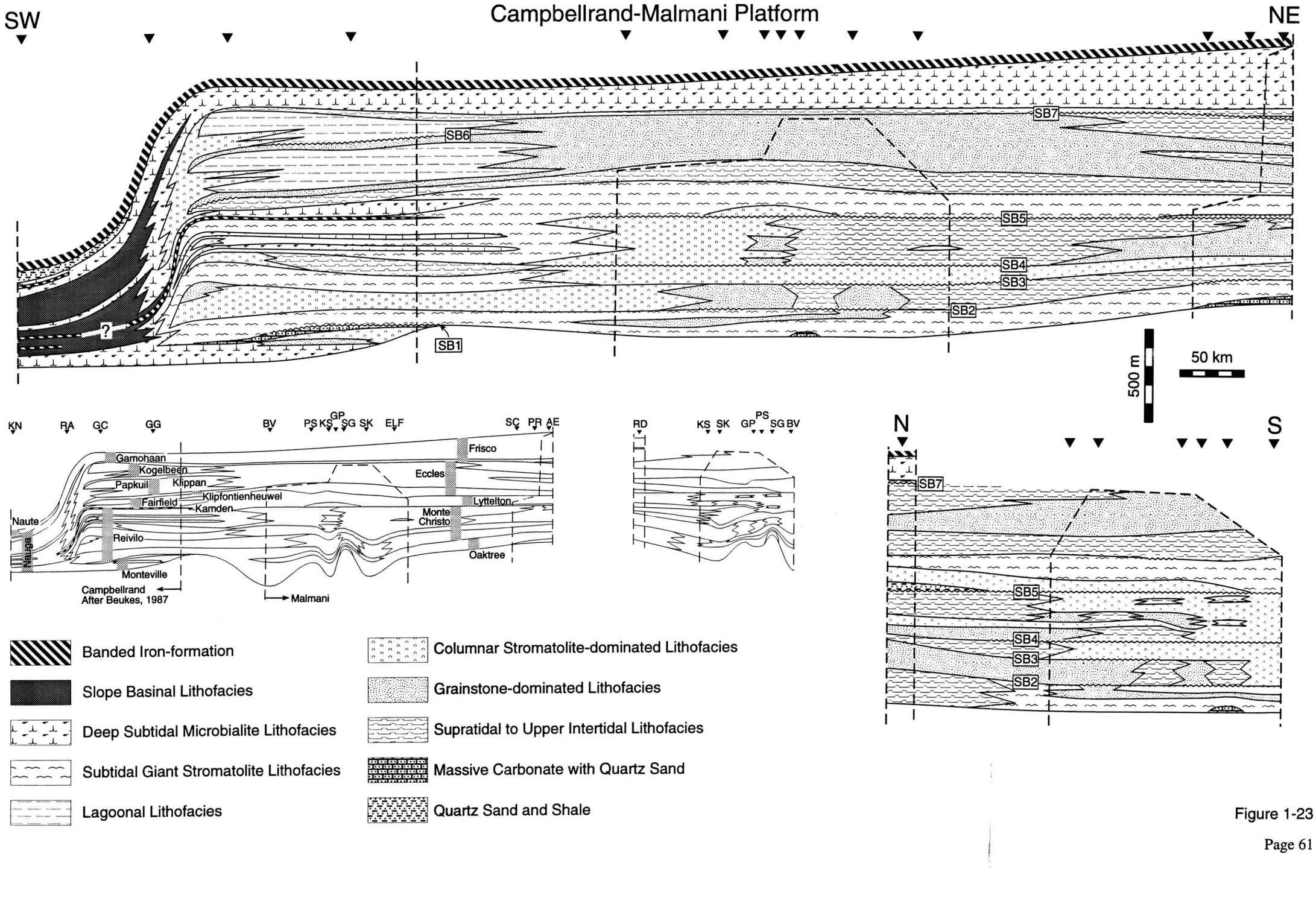
SW
Campbellrand-Malmani Platform
NE
SB1
SB2
SB3
SB4
SB5
SB6
SB7
?
50 km
500 m
KN RA GC GG BV PS KS GP SG SK ELF SC PR AE
Gamohaan
Kogelbeen
Papkuil
Klippan
Fairfield
Klipfontienheuwel
Kamden
Naute
Reivilo
Nauga
Monteville
Frisco
Eccles
Lyttelton
Monte Christo
Oaktree
Campbellrand
After Beukes, 1987
Malmani
RD KS SK GP PS SG BV
N
S
Banded Iron-formation
Slope Basinal Lithofacies
Deep Subtidal Microbialite Lithofacies
Subtidal Giant Stromatolite Lithofacies
Lagoonal Lithofacies
Columnar Stromatolite-dominated Lithofacies
Grainstone-dominated Lithofacies
Supratidal to Upper Intertidal Lithofacies
Massive Carbonate with Quartz Sand
Quartz Sand and Shale

Figure 1-23

Reef Quartzite and Malmani Subgroup (Clendenin, et al., 1991). The extensive truncation of the Wolkberg and Buffelsfontein groups in the south prior to Black Reef Quartzite deposition suggests that an unconformable contact is likely. In addition, rocks above this contact are flat-lying and preserved regionally in contrast to older sediments on the Kaapvaal craton which are preserved only locally. Thus, the unconformity between the Black Reef Quartzite and the underlying Wolkberg Group and equivalents is interpreted as a sequence boundary defining the base of the supersequence containing the Campbellrand-Malmani platform.

The Black Reef Quartzite is a fluvial to shallow marine unit ranging from 1 m thick in the southeast to 30 m (Clendenin, et al., 1991) or >500 m (Button, 1973a) thick over the Murchison Greenstone Belt, depending on how the boundaries of the unit are defined, and 60 m near RD (Tyler, 1979). Near Johannesburg, the Black Reef Quartzite is 24 m thick and consists of quartzite with 2 horizons of dolomite (Eriksson and Truswell, 1974). Eriksson and Truswell (1974) suggest that the dolomite horizons represent the remains of a much thicker carbonate unit. The Black Reef Quartzite grades upward into the thick carbonate sequence of the Malmani Subgroup.

In the northern Cape Province, the base of the Transvaal Supergroup (also called the Griqualand West Supergroup) consists of the Schmidtsdrif Subgroup. At the base, the Vryburg Formation lies unconformably over the Ventersdorp Supergroup and consists of feldspathic arenites, quartz arenites, quartz wackes, argillites, and lesser carbonates and lavas (Beukes, 1979, 1983a). Most of the detritus was sourced from the north, but an additional source from south of the present day Dooringberg Fault Zone is indicated by sand lenses near section KN (Beukes, 1983a). A thin carbonate succession developed in the Schmidtsdrif Subgroup and consists of ooids, calcarenites, and stromatolites with minor argillites. It pinches out over The Ganyesa dome (Figure 2-2). The Schmidtsdrif Subgroup is overlain conformably by the Monteville Formation, the basal formation of the Campbellrand Subgroup. The Schmidtsdrif Subgroup may be a distal equivalent of the Wolkberg Group, the Black Reef Quartzite, or a combination of the two (Beukes, 1983b).

### *Stratigraphy of the Campbellrand and Malmani Subgroups*

The basal unit of the Campbellrand-Malmani platform in the northern Cape Province is the Monteville Formation (0-200 m thick; Figure 2-23) which pinches out from south to north (Beukes, 1987). The top of the formation consists of an exposure surface with a 1-30 m-thick unit of mature coarse quartz sand mixed in a carbonate grainstone. In contrast, the basal formation in the Transvaal Province, the Oaktree Formation, contains quartz sand reworked from the underlying the Black Reef Quartzite, but no continuous

quartz sands are present above the base of the formation (Button, 1973a). The next regional quartzite is 300 m farther up in the Malmani Subgroup at the base of the Lyttelton Formation. The absence of quartzite in the Oaktree Formation and the presence of dolomite horizons in the Black Reef Quartzite near Johannesburg (Eriksson and Truswell, 1974) suggest that the top of the Monteville Formation is correlative with the base of the Oaktree Formation in the Transvaal Province.

The exposure surface at the top of the Monteville Formation represents a sequence boundary (SB1), above which the entire platform was flooded, and siliciclastic sedimentation was shut off (Figure 2-23). In the Campbellrand Subgroup, the Reivilo Formation overlies SB1. The Reivilo Formation (560-900 m thick) correlates with the Oaktree (90-200 m thick) and overlying Monte Christo (400-500 m thick) formations in the Malmani Subgroup. Several sequences are developed in these formations. The lowest one is based by rocks of the giant stromatolite lithofacies assemblage and shallows upward into shallow subtidal to supratidal lithofacies. It develops from a ramp at the base to a rimmed platform and is capped by a sequence boundary (SB2). SB2 and the next overlying sequence boundary (SB3) are marked by sporadically developed unconformities and basinward shifts in facies (Figure 2-23). A transgression above SB3 resulted in deposition of subtidal stromatolite mounds in the northern Cape Province and shallow subtidal to intertidal columnar stromatolites in the Johannesburg area and eastern Transvaal Province. Peritidal to supratidal deposition continued in the northern Transvaal Province. These transgressive deposits are overlain by a dramatic basinward shift in facies that resulted in deposition of peritidal facies in the northern Cape Province and a regional unconformity in the central Transvaal Province (SB4; Figure 2-23). This unconformity was not recognized in either the eastern or northern Transvaal Province, but the abundance of detrital carbonate in both areas is consistent with a downward shift in facies.

Above this sequence boundary, intertidal to supratidal deposition resumed in the Transvaal Province, but in the Cape Province, subtidal deposition predominated. In this part of the Reivilo Formation, two transgressive deposits reflect deposition of the subtidal net-like microbialite lithofacies on the platform. These deposits are interpreted as transgressive incursions where the deep subtidal microbialite lithofacies lapped onto the platform. In contrast, Beukes (1987) interpreted them as deep lagoonal deposits. The new interpretation is based on observations from core near the platform margin that suggest that the microbialite facies were deposited continuously over the platform margin (Beukes, pers. comm.). The platform rim did shallow to intertidal water depths between the two microbialite incursions although deposition of subtidal giant stromatolites continued behind the rim. None of these stratigraphic changes have been identified in sections in the Transvaal Prov-

ince (Figure 2-23).

The top of the Monte Christo Formation in the Transvaal Province consists of a regional unconformity (SB5; Figure 2-23) represented by chert breccia overlain by the Blyde River Quartzite (0-10 m thick; Button, 1973b) and correlative shales (Eriksson and Truswell, 1974). The quartzite contains cm-scale trough and hummocky cross stratification at section RD and dcm-scale trough cross bedding in the eastern Transvaal Province (Button, 1973b). The quartzite commonly is overlain by shale, and shale are interbedded with the overlying carbonate. The quartzite thins from north to south suggesting a northerly sediment source (Eriksson, 1977; Button, 1973b). The overlying Lyttelton Formation (120-300 m thick) is composed of the giant stromatolite mound facies; these are the deepest subtidal deposits in the Malmani Subgroup with the exception of carbonates in the Frisco Formation.

In the Campbellrand Subgroup, deep subtidal deposition continued throughout development of the sequence boundary in the Malmani Subgroup. Deposition of a transgressive iron-formation, called the Kamden Member (0-15 m thick), represents the deepest depositional environment on the platform prior to drowning of the platform during Gamohaan time. The absence of an unconformity or a basinward shift in facies in the Campbellrand Subgroup poses a stratigraphic problem since the sequence boundary in the Malmani Subgroup appears to have been widely developed. However, correlation of the Lyttelton Formation and the Kamden Member is reasonable lithostratigraphically (Beukes, 1983b). In addition, exposure in this part of the Campbellrand Subgroup is poor, and thin shifts in facies may not have been recognized. Unfortunately, continued subsidence of the Campbellrand Subgroup during extensive erosion of the Malmani Subgroup is inconsistent with the tectonic behavior during deposition of the rest of the platform. Thus, better stratigraphic control and age constraints are necessary to understand the dynamics of subsidence during deposition of this portion of the platform.

Above the Lyttelton Formation, peritidal deposition resumed after a gradual shallowing upwards. In the Campbellrand Subgroup, facies change abruptly from deep subtidal microbialites of to peritidal colloform stromatolites at the platform margin. Upward in core SACHA, the microbialite lithofacies contains more grainstone and then passes abruptly into 1 meter of coarsely crystalline dolomite with hints of large domes, followed by coarsely crystalline dolomite with hints of breccias and grainstones. This is consistent with either very rapid shallowing due to an abrupt lowering of relative sea level or to the presence of an unrecognized unconformity that removed transitional facies.

Once peritidal depositional environments were established in the Campbellrand Subgroup, a paleogeography characterized by intertidal to shallow subtidal platform rim and a broad intrashelf "lagoon" continued vertically for hundreds of meters. One prograding

unit of intertidal grainstone-rich deposits is capped by a sequence boundary (SB6; Figure 2-23). Contemporaneous deposition in the Malmani Subgroup consists of predominantly peritidal grainstones, including abundant oolites, with few documented regional facies changes.

The base of the Frisco and Gamohaan formations is marked by a sequence boundary (SB7; Figure 2-23) associated with siliciclastic shales in the east (Chapter 4). Above this sequence boundary, peritidal deposits are briefly established and then facies deepen upward into deep subtidal microbialite assemblages (Chapters 3 and 4). The Frisco and Gamohaan formations were deposited during a transgression in which the Campbellrand-Malmani carbonate platform was terminally drowned; deposition of basinal iron-formation (Penge and Kuruman iron-formations) occurred over the entire platform.

During deposition of the relatively shallow platform deposits described above, slope and basinal deposition occurred between sections KN and RA (Figures 2-2 and 2-23). The basinal lithofacies assemblage near section KN lacks breccia, but rhythmites are very common (Beukes, 1987). Near section RA, slope lithofacies dominated with abundant slope breccias, rhythmites, and interbeds of the deep subtidal microbialite lithofacies assemblage. The proportion of shale and iron-formation increase rapidly at the transition to the Naute Shale. Above this 100 m-thick shale, continuous banded iron-formation of the Kuruman Iron Formation was deposited (Beukes, 1980, 1987).

### *Overlying Iron Formations*

The Kuruman Iron Formation conformably overlies the Campbellrand Subgroup and consists of deep water, microbanded iron formation (Beukes, 1984). It shallows upward into the Griquatown Iron Formation which consists of various clastic-textured iron-formation lithotypes deposited in a shallow epeiric sea or a fresh water lake (Beukes, 1983b, 1984). Combined, they are up to 500 m thick over the platform and 1000 m thick over basinal sediments of the underlying carbonates (Beukes, 1983b). They are correlative to the Penge Iron Formation in the Transvaal Province, which is lithologically similar to the Kuruman Iron Formation and also formed on a stable shelf below wave base (Beukes, 1973, 1983b). The Griquatown Iron Formation grades upward into the Koegas Subgroup which consists of chloritic claystone, siltstone and quartz wackes (Beukes, 1983b). Correspondingly, the Penge Iron Formation is overlain by a mixed carbonate and siliciclastic unit, the Deutschland Formation. Thus, deep water deposition over the entire platform was followed by deposition of shallow water iron-formation and siliciclastic deposition, some of which may have occurred in lacustrine rather than marine depositional environments (Beukes, 1983b).

A major unconformity developed after deposition of the Deutschland and Koegas formations, but before deposition of the overlying the Pretoria and Postmasburg groups. As discussed earlier, this unconformity removed at least 2 km of underlying sediment in the southeastern Transvaal Province where it overlies basement (Button, 1973b; Eriksson and Truswell, 1974) and removed the entire Koegas Subgroup north of the Griquatown Fault Zone. The overlying Pretoria and Postmasburg groups represent a much younger depositional era ranging in age from 2.3 to 2.0 Ga (Burger and Coertze, 1975; Hunter and Hamilton, 1978; Walraven, et al., 1990). Thus, the sequence boundary at the base of the Pretoria and Postmasburg groups marks the top of the supersequence containing the Campbellrand-Malmani carbonate platform.

### *Discussion*

The depositional geometry of the Campbellrand-Malmani platform has been described as an intercontinental basin by various authors who have proposed depositional axes within outcrop of the Malmani Subgroup or between the Malmani and Campbellrand subgroups (Eriksson, et al., 1976; Clendenin, et al., 1988a and b; Altermann and Herbig, 1991; Hälbich, et al., 1992). In contrast, Beukes (1980, 1987) proposed deposition of a ramp to rimmed platform with the margin to the southwest. He also proposed that the margin continued northward along what is now the Kheis Belt. The correlations between the two subgroups proposed here, combined with detailed facies analyses supports the interpretation that the Campbellrand-Malmani platform was a ramp to rimmed shelf with a margin passing into basinal deposition along the Griquatown Fault Zone in the far southwest. In addition to supporting this interpretation, cross sections through the Malmani Subgroup suggest shallow depositional environments to the north and northeast with deepening facies to the south and southwest. This implies the presence of a platform margin south of preserved Malmani Subgroup outcrops. The continuation of the margin to the west or north of the preserved area is largely unconstrained. Stratigraphic data from core SACHA suggests that platform deposition continued at least this far west, although the abundance of platform margin-like columnar stromatolites in core SACHA is consistent with deposition near the platform margin (Appendix B).

The tabular geometry of the Campbellrand-Malmani platform is inconsistent with passive margin subsidence following rifting. First, rift related sediments are absent along the preserved platform margin (Beukes, 1977, 1983a). Also, subsidence was fairly uniform across the entire platform. This suggests that accommodation space was created either by long term rise of absolute sea level or subsidence of the entire Kaapvaal craton.

**Platform Drowning**

Uniform subsidence of the platform continued through deposition of the Gamohaan and Frisco formations which both show progressive deepening from peritidal to basinal depositional environments. This drowning of the platform represents a dramatic event since throughout the Campbellrand-Malmani platform, transgressions resulted in deposition of deep subtidal lithofacies over the platform, but carbonate deposition was able to keep up with relative sea level rise. Either eustatic or tectonic processes may have caused the drowning. The behavior of sea level during late Archean time is unconstrained, and it only can be established in the future once the tectonics of the few preserved platform-like deposits are well understood. Thus, it is critical to address possible tectonic components of subsidence on the Kaapvaal craton.

The drowning of the carbonate platform across the entire Kaapvaal craton is roughly contemporaneous with intrusion of the 2514±16 Ma Great Dyke on the Zimbabwe craton (Hamilton, 1977). The Kaapvaal and Zimbabwe cratons were attached along the Limpopo Belt prior to deposition of the Campbellrand-Malmani platform, and tectonic activity to the north of the Gamohaan and Frisco formations is supported by the sourcing of siliciclastic sediment from the north at the base of the Frisco Formation as well as the thickening of volcanic ash beds to the north. The intrusion of the Great Dyke may reflect a change in the tectonic environment of the Kaapvaal and Zimbabwe cratons that resulted in drowning of the Campbellrand-Malmani carbonate platform. However, large intrusions such as the Great Dyke typically are the result of lithospheric heating which causes uplift rather than subsidence (e.g. Lachenbruch and Morgan, 1985).

A second possible explanation for drowning is a change in dynamic topography related to mantle convection. Gurnis (1990) estimates a maximum change in sea level of 150 m can be accounted for by drift of a continent from a dynamic topography low to a high during Phanerozoic time, and Cazenave, et al. (1989) estimate modern dynamic topography due to mantle convection may be as high as 250 m. These changes have long wavelengths and could cause deepening over large areas such as that of the Kaapvaal craton. Changes in dynamically driven flooding are accentuated at convergent margins due to the presence of cold slabs at depth (Gurnis, 1993). Thus, it may be possible that a change in dynamic topography accentuated subsidence of the Kaapvaal craton and contributed to drowning of the Campbellrand-Malmani carbonate platform in combination with a change in tectonic environment, possibly development of a convergent margin.

**Long-term Subsidence and Uplift**

The Black Reef Quartzite is the first unit with preserved shallow dips across the

Kaapvaal craton. Earlier deposits (i.e. the Witwatersrand and Pongola supergroups) show evidence of deposition in an interior seaway, but they are preserved in small, structurally controlled basins (Beukes and Cairncross, 1991). Thus, deposition and preservation of the Black Reef Quartzite and the Schmidtsdrif Subgroup marked a change in tectonics on the Kaapvaal craton. Some similarities in erosional style are present pre- and post deposition of the Campbellrand-Malmani platform, however. In particular, both unconformities that bound the supersequence containing the Campbellrand-Malmani platform rest on lower stratigraphic levels along the southeastern boundary of outcrop. The preservation of the Wolkberg and Buffelsfontein Groups only in the northern Transvaal Province suggests that erosion between the deposition of these fluvial rocks and the overlying Black Reef Quartzite was concentrated along the southern margin of preserved outcrop of the Transvaal Supergroup. A similar relationship is seen at the pre-Pretoria Group unconformity where 2 kilometers of sediment (preserved along the northern boundary of outcrop) are absent in the southeastern Transvaal Province. This erosional pattern contrasts sharply with deposition in the Campbellrand-Malmani platform where sediment sources were to the north and northeast and facies deepen to the south and southwest. Thus, the supersequence-bounding unconformities may have developed as a result of tectonic tilting of the Kaapvaal craton with or without a contemporaneous eustatic sea level influence.

On a smaller scale, the deep subtidal deposition at the top of the Reivilo Formation during exposure at the top of the Monte Christo Formation in the Malmani Subgroup suggests cratonic tilting with the northeastern Transvaal Province uplifted. The progradation of siliciclastic sediments from the northeast suggests that the basin margin was located to the northeast rather than southeast. Above the Reivilo Formation, however, stratigraphic relationships are consistent with uniform subsidence of the craton. Thus, stratigraphic data suggest episodic uplift of different parts of the Kaapvaal craton during deposition of the Transvaal Supergroup, but the tabular geometry of large stratigraphic units suggests uniform subsidence on average. Additional stratigraphic and chronological constraints will help test and refine regional tectonic patterns.

## SUMMARY

Carbonate lithofacies are grouped in depositional assemblages including the grainstone-dominated, supratidal to shallow intertidal, columnar stromatolite-dominated, lagoonal, giant stromatolite, deep subtidal microbialite, and slope and basinal lithofacies assemblages. Aragonite precipitation was abundant in the supratidal to shallow intertidal, the columnar stromatolite-dominated, and giant stromatolite lithofacies assemblages. Cal-

cite precipitation, particularly herringbone calcite, was extremely abundant in the deep subtidal microbialite lithofacies assemblage. The abundance of aragonite and calcite that precipitated as encrustations on the sea floor demonstrate that late Archean seawater was supersaturated with respect to both in shallow depositional environments and to calcite in deep subtidal seawater.

The subsidence and tectonic behavior of the Kaapvaal craton changed between deposition of the Wolkberg Group and the Black Reef Quartzite when uniform subsidence across the platform was developed for deposition of the Campbellrand-Malmani carbonate platform. During deposition of this >1 km-thick carbonate platform, siliciclastic sedimentation was restricted to meter-thick sheets of sediment deposited on unconformities. The siliciclastic sediments thin to the south suggesting sediment sources in the direction of the Limpopo Belt and Zimbabwe craton. The Campbellrand-Malmani platform contains sediments representing depositional environments ranging from basinal to supratidal. Facies relationships suggest that the platform deepened to the south and southwest and that preserved outcrop patterns do not reflect the dimensions of the original basin.

## REFERENCES


Altermann, W. and H. C. Herbig, 1991. Tidal flat deposits of the Lower Proterozoic Campbell Group along the southwestern margin of the Kaapvaal Craton, Northern Cape Province, South Africa. Journal of African Earth Sciences, v. 13, p. 415-435.

Armstrong, R. A., W. Compston, E. A. Retief and N. J. Wilke, 1986, Ages and isotopic evolution of the Ventersdorp volcanics Extended Abstract, Geocongress '86, Geological Society of South Africa, p. 89-92.

Armstrong, R. A., W. Compston, E. A. Retief, I. S. Williams and H. J. Welke, 1991. Zircon ion microprobe studies bearing on the age and evolution of the Witwatersrand triad. Precambrian Research, v. 53, p. 243-266.

Assereto, R. and C. G. S. C. Kendal, 1977. Nature, origin, and classification of peritidal teepee structures and related breccias. Sedimentology, v. 24, p. 153-210.

Barton, E. S., W. Compston, I. S. Williams, J. W. Bristow, D. K. Hallbauer and C. B. Smith, 1989. Provenance ages for the Witwatersrand Supergroup and the Ventersdorp Contact Reef: Constraints from ion microprobe U-Pb ages of detrital zircons. Economic Geology, v. 84, p. 2012-2019.

Barton, J. M. J. and D. D. van Reenen, 1992. When was the Limpopo Orogeny? Precambrian Research, v. 55, p. 7-16.

Barton, J. M., R. Doig, C. B. Smith, F. Bohlender and D. D. vanReenen, 1992. Isotopic and REE characteristics of the intrusive charneonderbite and endrbite geographically associated with the Matok Pluton, Limpopo Belt, southern Africa. Precambrian Research, v. 58, p. 451-467.

Bertrand-Sarfati, J., 1976. Pseudomorphoses de gypse en rosettes dans un calcaire cryptalgo-laminaire du Precambrien inferiur (Systeme du Transvaal, Afrique du Sud). Bulletin de la Societe Geologique de France, v. 18, p. 88-102.

Bertrand-Sarfati, J. and K. A. Eriksson, 1977. Columnar stromatolites from the Early Proterozoic Schmidtsdrift Formation, northern Cape Province, South Africa—Part 1: Systmatic and diagnostic features. Palaeont. Africa, v. 20, p. 1-26.

Beukes, N. J., 1973. Precambrian iron-formations of southern Africa. Economic Geology, v. 68, p. 960-1004.

Beukes, N. J., 1977. Transition from siliciclastic to carbonate sedimentation near the base of the Transvaal Supergroup, northern Cape Province, South Africa. Sedimenary Geology, v. 18, p. 201-221.

Beukes, N. J., 1979. Litostratigrafiese onderverdeling van die Schmidtsdrif-subgroep van die Ghaap-groep in noord-Kaapland. Transactions of the Geological Society of South Africa, v. 82, p. 313-327.

Beukes, N. J., 1980. Stratigrafie en litofasies van die Campbellrand-subgrop van die Proterofitiese Ghaap-groep, noord-Kaapland. Transactions of the Geological Society of South Africa, v. 83, p. 141-170.

Beukes, N. J., 1983a. Ooids and oolites of the Proterophytic Boomplaas Formation, Transvaal Supergroup, Griqualand West, South Africa in Coated Grains (T. M. Peryt, ed.). Springer-Verlag, Berlin. p. 199-214.

Beukes, N. J., 1983b. Paleoenvirnomental setting of iron-formations in the depositional basin of the Transvaal Supergroup, South Africa in Iron-formation: Facts and problems (A. F. Trendall and R. C. Morris, eds.). Elsevier, Amsterdam. p. 131-198.

Beukes, N. J., 1984. Sedimentology of the Kuruman and Griquatown iron formations, Transvaal Supergroup, Griqualand West, South Africa. Precambrian Research, v. 24, p. 47-84.

Beukes, N. J., 1987. Facies relations, depositional environments and diagenesis in a major early Proterozoic stromatolitic carbonate platform to basinal sequence, Campbellrand Subgroup, Transvaal Supergroup, southern Africa. Sedimentary Geology, v. 54, p. 1-46.

Beukes, N. J. and B. Cairncross, 1991. A lithostratigraphic-sedimentological reference profile for the Late Archaean Mozaan Group, Pongola Sequence: application to sequence stratigraphy and correlation with the Witwatersrand Supergroup. South African Journal of Geology, v. 94, p. 44-69.

Beukes, N. J. and C. A. Smit, 1987. New evidence for thrusting in Griqualand West, South Africa: implications for stratigraphy and the age of red beds. South African Journal of Geology, v. 90, p. 378-394.

Burger, A. J. and F. J. Coertze, 1975. Age determinations-April 1972 to March 1974. Annals of the Geological Survey of South Africa, v. 10, p. 135-141.

Burke, K., W. S. F. Kidd and T. Kusky, 1985a. Is the Venterdorp rift system of southern Africa related to a continental collision between the Kaapvaal and Zimbabwe cratons at 2.64 Ga ago? Tectonophysics, v. 115, p. 1-24.

Burke, K., W. S. F. Kidd and T. M. Kusky, 1985b. The Pongola structure of southeastern Africa: the world's oldest preserved rift? Journal of Geodynamics, v. 2, p. 35-49.

Burke, K., W. S. F. Kidd and T. M. Kusky, 1986. Archean foreland basin tectonics in the Witwatersrand, South Africa. Tectonics, v. 5, p. 439-456.

Button, A., 1973a. The depositional history of the Wolkberg proto-basin, Transvaal. Transactions of the Geological Society of South Africa, v. 76, p. 15-25.

Button, A., 1973b. The stratigraphic history of the Malmani dolomite in the eastern and north-eastern Transvaal. Transactions of the Geological Society of South Africa, v. 76, p. 229-247.

Button, A., 1976. Transvaal and Hamersley basins — review of basin development and mineral deposits. Minerals Science Engineering, v. 8, p. 262-293.

Button, A. and R. G. Vos, 1977. Subtidal and intertidal clastic and carbonate sedimentation in a macrotidal environment: an example from the lower Proterozoic of South Africa. Sedimentary Geology, v. 18, p. 175-200.

Cazenave, A., A. Souriau and K. Dominh, 1989. Global coupling of Earth surface topography with hotspots, geoid and mantle heterogeneities. Nature, v. 340, p. 54-57.

Clay, A. N., 1986. The stratigraphy of the Malmani Dolomite Subgroup in the Carletonville area, Transvaal: Genetic implications for lead-zinc mineralization in Mineral Deposits of Southern Africa (C. R. Anhaeusser and S. Maske, eds.). Geological Society of South Africa, p. 853-860.

Clendenin, C. W., 1989. Tectonic Influence on the Evolution of the Early Proterozoic Transvaal Sea, Southern Africa (Doctoral Thesis). University of the Witwatersrand, Johannesburg, 367 pp.

Clendenin, C. W., E. G. Charlesworth and S. Maske, 1988a. An early Proterozoic three-stage rift system, Kaapvaal Craton, South Africa. Tectonophysics, v. 145, p. 73-86.

Clendenin, C. W., E. G. Charlesworth and S. Maske, 1988b. Tectonic style and mechanism of early Proterozoic successor basin development, southern Africa. Tectonophysics, v. 156, p. 275-291.

Clendenin, C. W., G. Henry and E. G. Charlesworth, 1991. Characteristics of and influences on the Black Reef depositional sequence in the eastern Transvaal. South African Journal of Geology, v. 94, p. 321-327.

Collinson, J. D. and J. Lewin, 1983, Modern and Ancient Fluvial Systems: Oxford, UK, Blackwell Scientific Publications, 575 p.

Collinson, J. D. and D. B. Thompson, 1989. Sedimentary Structures. Unwin Hyman, London. 207 p.

Cook, H. E. and H. T. Mullins, 1983. Basin margin in Carbonate Depositional Environments (P. A. Scholle, D. G. Bebout and C. H. Moore, eds.). American Association of Petroleum Geologists, Tulsa, OK. p. 539-618.

Duane, M. J., F. J. Kruger, P. J. Roberts and G. B. Smith, 1991. Pb and Sr isotope and origin of Proterozoic base metal (fluorite) and gold deposits, Transvaal Sequence, South Africa. Economic Geology, v. 86, p. 1491-1505.

Eriksson, K. A., 1972. Cyclic sedimentation in the Malmani Dolomite, Potchefstroom Synclinorium. Transactions of the Geological Society of South Africa, v. 75, p. 85-97.

Eriksson, K. A., 1977. Tidal flat and subtidal sedimentation in the 2250 M.Y. Malmani dolomite, Transvaal, South Africa. Sedimentary Geology, v. 18, p. 223-244.

Eriksson, K. A. and J. F. Truswell, 1974. Stratotypes from the Malmani Subgroup northwest of Johannesburg, South Africa. Transactions of the Geological Society of South Africa, v. 77, p. 211-222.

Eriksson, K. A., T. S. McCarthy and J. F. Truswell, 1975. Limestone formation and dolomitization in a lower Proterozoic succession from South Africa. Journal of Sedimentary Petrology, v. 45, p. 604-614.

Eriksson, K. A., J. F. Truswell and A. Button, 1976. Palaeoenvironmental and geochemical models from an early Proterozoic carbonate succession in South Africa in Stromatolites (M. R. Walter, ed.). Elsevier, Amserdam. p. 635-643.

Grey, K. and A. M. Thorne, 1985. Biostratigraphic significance of stromatolites in upward shallowing sequences of the early Proterozoic Duck Creek Dolomite, Western Australia. Precambrian Research, v. 29, p. 183-206.

Grotzinger, J. P., 1986. Cyclicity and paleoenvironmental dynamics, Rocknest platform, northwest Canada. Geological Society of America Bulletin, v. 97, p. 1208-1231.

Grotzinger, J. P., 1988. Construction of early Proterozoic (1.9 Ga) barrier reef complex, Rocknest Platform, Northwest Territories in Reefs: Canada and Adjacent Areas (H. H. J. Geldsetzer, N. P. James and G. E. Tebbutt, eds.). Canadian Society of Petroleum Geologists, Calgary. Memoir 13, p. 30-37.

Grotzinger, J. P., 1989. Construction of Early Proterozoic (1.9 Ga) barrier reef complex, Rocknest Platform, Northwest Territories *in* Reefs, Canada and Adjacent Area (H. H. J. Geldsetzer, N. P. James and G. E. Tebbutt, eds.). Canadian Society of Petroleum Geologists, Memoir 13, p. 30-37.

Grotzinger, J. P. and J. F. Kasting, 1993. New constraints on Precambrian ocean composition. Journal of Geology, v. 101, p. 235-243.

Gurnis, M., 1990. Bounds on global dynamic topography from Phanerozoic flooding of continental platforms. Nature, v. 344, p. 754-756.

Gurnis, M., 1993. Phanerozoic marine inundation of continents driven by dynamic topography above subducting slabs. Nature, v. 364, p. 589-593.

Hälbich, I. W., D. Lamprecht, W. Altermann and U. E. Horstmann, 1992. A carbonate-banded iron formation transition in the Early Protorezoicum of South Africa. Journal of African Earth Sciences, v. 15, p. 217-236.

Hamilton, J., 1977. Sr isotope and trace element studies of the Great Dyke and Bushveld mafic phase and their relations to Early Proterozoic magma genesis in southern Africa. Journal of Petrology, v. 18, p. 24-52.

Hartzer, F. J., 1989. Stratigraphy, structure, and tectonic evolution of the Crocodile River Fragment. South African Journal of Geology, v. 92, p. 110-124.

Hoffman, P. F., 1969. Proterozoic paleocurrents and depositional history of the East Arm fold belt, Great Slave Lake, Northwest Territories. Canadian Journal of Earth Sciences, v. 6, p. 441-462.

Hoffman, P. F., 1988. Pethei reef complex (1.9 Ga), Great Slave Lake, N. W. T. in Reefs: Canada and Adjacent Areas (H. H. J. Geldsetzer, N. P. James and G. E. Tebbutt, eds.). Canadian Society of Petroleum Geologists, Calgary. Memoir 13, p. 38-48.

Hofmann, H. J. and M. Masson, 1994. Archean stromatolites from Abitibi greenstone belt, Quebec, Canada. Geological Society of America Bulletin, v. 106, p. 424-429.

Hofmann, H. J., P. C. Thurston and H. Wallace, 1985. Archean Stromatolites from Uchi greenstone belt, Northwestern Ontario in Evolution of Archean Supracrustal Sequences (L. D. Ayres, P. C. Thurston, K. D. Card and W. Weber, L. D. Ayres, P. C. Thurston, K. D. Card and W. Weber). Geological Association of Canada Special Paper 28, p. 1125-132.

Hubert, J. K., R. K. Suchecki and R. K. M. Callahan, 1977. The Cowhead Breccia: Sedimentology of the Cambro-Ordovician continental margin, Newfoundland in Deep-Water Carbonate Environments (H. E. Cook and P. Enos, eds.). SEPM, Tulsa. 25, p. 125-154.

Hunter, D. R. and P. J. Hamilton, 1978. The Bushveld Complex in Evolution of the Earth's Crust (D. H. Tarling, eds.). Academic Press, London. p. 107-173.

Kamber, B. S., J. D. Kamers, R. Napier, R. A. Cliff and H. R. Rollinson, 1995. The Triangle Shearzone, Zimbabwe revisited: new data document an important event at 2.0 Ga in the Limpopo Belt. Precambrian Research, v. 70, p. 191-219.

Lachenbruch, A. H. and P. Morgan, 1985. Continental extension, magmatism, and elevation: Formal relations and rules of thumb. Tectonophysics, v. 174, p. 39-62.

Laznicka, P., 1988. Breccias and coarse Fragnentites. Elsevier, Amsterdam. Developments in Economic Geology, 25, 832 p.

Leadbeater, B. S. C. and R. Riding, 1986, editors. Biomineralization in Lower Plants and Animals: Oxford, Clarendon, 401 p.

Lowenstein, T. K., 1988. Origin of depositional cycles in a Permian "saline giant": The Salado (McNutt zone) evaporites of New Mexico and Texas. Geological Society of America Bulletin, v. 100, p. 592-608.

Lowenstein, T. K. and L. A. Hardie, 1985. Criteria for the recognition of salt-pan evaporites. Sedimentology, v. 32, p. 627-644.

Martini, J. E. J., 1976. The fluorite deposits in the Dolomite Series of the Marico District, Transvaal, South Africa. Economic Geology, v. 71, p. 625-635.

McIlreath, I. A. and N. P. James, 1979. Carbonate slopes in Facies Models (R. G. Walker, ed.). Geoscience Canada, Reprint Series 1, p. 133-144.

Miyano, T. and N. J. Beukes, 1984. Phase relations of stilpnomelane, ferri-annite, and riebeckite in very low-grade metamorphosed iron-formations. Transactions of the Geological Society of South Africa, v. 87, p. 111-124.

Pelechaty, S. M. and J. P. Grotzinger, 1988. Stromatolite bioherns of a 1.9 Ga foreland basin carbonate ramp, Beechey Formation, Kilohigok Basin, Northwest Territories in Reefs: Canada and Adjacent Areas (H. H. J. Geldsetzer, N. P. James and G. E. Tebbutt, eds.). Canadian Society of Petroleum Geologists, Calgary. Memoir 13, p. 93-104.

Plummer, P. S. and V. A. Gostin, 1981. Shrinkage cracks: desiccation or synaeresis. Journal of Sedimentary Petrology, v. 51, p. 1147-1156.

Riding, R., 1991, Calcareous Algae and Stromatolites: Berlin, Springer-Verlag, 571 p.

Robb, L. J., D. W. Davis and S. L. Kamo, 1990. U-Pb ages on single detrital zircon grains from the Witwatersrand basin, South Africa: Constraints on the age of sedimentation and on the evolution of granites adjacent to the basin. Journal of Geology, v. 98, p. 311-328.

Sami, T. T. and N. P. James, 1994. Peritidal carbonate platform growth and cyclicity in an early Proterozoic foreland basin, Upper Pethei Group, northwest Canada. Journal of Sedimentary Research, v. B64, p. 111-131.

Sandberg, P. A., 1985a. Nonskeletal aragonite and pCO2 in the Phanerozoic and Proterozoic in The carbon cycle and atmospheric CO2: Natural variations Archean to Present (E. T. Sundquist and W. S. Broecker, eds.). American Geophysical Union, Washington. Geophysical Monograph 32, p. 585-594.

Sandberg, P., 1985b. Aragonite cements and their occurrence in ancient limestone in Carbonate Cements (N. Schneidermann and P. M. Harris, eds.). S.E.P.M. Special Publication No. 36, p. 33-57.

Simkiss, K. and K. M. Wilbur, 1989. Biomineralization: Cell Biology and Mineral Deposition. Academic Press, Inc., San Diego. 338 p.

Simonson, B. M., K. A. Schubel and S. W. Hassler, 1993. Carbonate sedimentology of the early Precambrian Hamersley Group of Western Australia. Precambrian Research, v. 60, p. 287-335.

Stear, W. M., 1977. The stratigraphy and sedimentology of the Pretoria Group at Rooiberg, Transvaal. Transactions of the Geological Society of South Africa, v. 80, p. 53-65.

Stowe, C. W., 1986. Synthesis and interpretation of structures along the north-eastern boundary of the Namaqua tectonic province, South Africa. Transactions of the Geological Society of South Africa, v. 89, p. 185-198.

Sumner, D. Y. and S. A. Bowring, in press. U-Pb geochronologic constraints on deposition of the Campbellrand

Subgroup, Transvaal Supergroup, South Africa. Precambrian Research, v. p.

Sumner, D. Y. and J. P. Grotzinger, 1993. Numerical modeling of ooid size and the problem of Neoproterozoic giant ooids. Journal of Sedimentary Petrology, v. 63, p. 974-982.

Truswell, J. F. and K. A. Eriksson, 1972. The morphology of stromatolites from the Transvaal Dolomite north-west of Johannesburg, South Africa. Transactions of the Geological Society of South Africa, v. 75, p. 99-110.

Truswell, J. F. and K. A. Eriksson, 1973. Stromatolitic associations and their palaeo-environmental significance: A re-appraisal of a lower Proterozoic locality from the northern Cape Province, South Africa. Sedimentary Geology, v. 10, p. 1-23.

Tucker, M. E. and V. P. Wright, 1990. Carbonate Sedimentology. Blackwell Scientific Publications, Oxford. 482 p.

Tyler, N., 1979. The stratigraphy of the early-Proterozoic Buffalo Springs Group in the Thabazimbi area, west-central Transvaal. Transactions of the Geological Society of South Africa, v. 82, p. 215-226.

Walraven, F., R. A. Armstrong and F. J. Kruger, 1990. A chronostratigraphic framework for the north-central Kaapvaal craton, the Bushveld Complex and the Vredefort structure. Tectonophysics, v. 171, p. 23-48.

Westbroek, P. and E. W. de Jong, 1982, Biomineralization and Biological Metal Accumulation: Boston, Reidel Publishing Co., 533 p.

Wilkinson, B. W. and R. K. Given, 1986. Secular variation in abiotic marine carbonates: Constraints on Phanerozoic atmospheric carbon dioxide contents and oceanic Mg/Ca ratios. Journal of Geology, v. 94, p. 321-333.

Winter, H. d. l. R., 1987. A cratonic foreland model for Witwatersrand Basin development in a continental back-arc, plate tectonic setting. Transactions of the Geological Society of South Africa, v. 90, p. 409-427.

# CHAPTER 3: DEEP SUBTIDAL MICROBIALITES


## ABSTRACT

Microbialites in the late Archean Gamohaan and Frisco formations, South Africa, consist of three components: fine, filmy laminae that are interpreted as remnants of microbial mats; irregular surfaces that acted as supports, also interpreted as biological in origin; and cement-filled voids which formed contemporaneously with microbialite growth. The proportions of laminae and supports, disruption of laminae, and abundance of voids vary, and seven end-member morphologies have been defined: planar laminae, rolled-up laminae, tented microbialites, cuspate microbialites, irregular columnar microbialites, plumose structures, and herringbone calcite beds. The complexity of these microbialites suggests that a remarkably diverse set of microbe-substrate interactions had developed by late Archean time. However, most of these structures do not have previously described younger analogs.

Herringbone calcite, a fibrous marine cement, precipitated contemporaneously with microbial growth. It preferentially precipitated on the supports over the mats as demonstrated by the concentration of herringbone calcite near supports, growth banding in herringbone calcite which indicates that calcite nucleated on and grew away from supports but not mat, and the abutment of herringbone calcite coatings against mat attached to supports. These observations suggest that the mat inhibited nucleation of calcite and that calcite precipitation was driven by supersaturation of ambient seawater, not mat-related chemical effects.


## INTRODUCTION

The influence of microbial communities on the morphology and internal texture of stromatolites has been a hotly debated topic at the center of studies of Precambrian carbonates for decades (see discussions in Cloud and Semikhatov, 1969; Walter, 1976; Semikhatov, et al., 1979; and Ginsburg, 1991). Early Soviet workers documented secular variations in stromatolite morphology and internal textures which they generally interpreted as representing the evolution of microbial communities through time (summarized in Semikhatov, 1976). In contrast, many western workers considered stromatolite morphology a function of depositional environment rather than the composition of microbial communities (e.g. Cloud, 1942; Donaldson, 1963; Logan, et al., 1964). More recently, focus has shifted from stromatolite morphology, which is now generally considered a complex function of both biological and environmental processes (e.g. Buick, et al., 1981; Krumbein, 1983; Ginsburg, 1991), to stromatolite microtextures. Due to the complexity of both biotic and abiotic chem-

istry, the specific roles of microbial and environmental processes in shaping stromatolite microtextures also are difficult to distinguish, particularly for stromatolites consisting of carbonate that precipitated in place rather than trapped-and-bound detrital carbonate. Documenting the role of microbial communities in shaping stromatolite microtextures becomes increasingly difficult with increasing age due to the decreasing abundance of well preserved stromatolites. More care must also be taken with increasing age to carefully constrain biological influences since interpretations of the presence of specific biological processes (such as photosynthesis), have significant implications if they were present during the Archean Eon (e.g. Schopf, et al., 1971; Walter, 1983; Buick, 1992). Although Archean stromatolites have been used to support interpretations that photosynthetic communities had evolved, the specific role of microbial communities in the formation of many of the oldest stromatolites is unknown (e.g. Buick, et al., 1981; Lowe, 1994, 1995; Buick, et al., 1995).

Some Archean stromatolites, however, contain a better preserved microbial presence. For example, stromatolites from the 2.6 Ga Bulawayo greenstone belt, Zimbabwe, contain organic inclusions defining remnants of microbial mat (Schopf, et al., 1971; Walter, 1983). Reinvestigation of the Bulawayo locality, including measurement of detailed stratigraphic sections, demonstrates that the stromatolites figured by Schopf, et al. (1971) and Walter (1983) were incorrectly interpreted and that they are cuspate rather than convex columnar stromatolites (Grotzinger and Sumner, in prep.). When viewed correctly, they are similar to stromatolites from the ~2.8 Ga Steeprock Group, Canada (Walter, 1983, described upside down; Grotzinger and Sumner, in prep.), the 2.72 Ga Abitibi greenstone belt, Canada (Hofmann and Masson, 1994), and the 2.52 Ga Campbellrand and Malmani subgroups, South Africa (Beukes, 1980, 1987; Chapters 2 and 4). Besides the stromatolites in the Campbellrand and Malmani subgroups, petrographic preservation of the stromatolites is poor, and outcrops are limited. The cuspate stromatolites in the Campbellrand and Malmani subgroups, however, outcrop within a 1.5 km thick carbonate platform with exposures stretching across 800 km. The outstanding petrographic preservation of the cuspate stromatolites and associated rocks in this platform provides a unique opportunity to critically analyze their morphological variations, growth mechanisms, and interactions with encasing carbonate cements and sediments.

### *Geological Setting*

The well preserved stromatolites and microbialites[1] are found in the 2520 Ma (Sumner

[1] Most fossil microbial structures are classified as stromatolites, thrombolites, or cryptalgalaminated

and Bowring, in press; Appendix A) Gamohaan and Frisco formations and basinward of the underlying carbonate platform margin (Button, 1973; Beukes, 1980, 1987; Chapters 2 and 4). Data presented here are from the Gamohaan and Frisco formations which are exposed over a combined range of 800 km. Structural disruption is minimal as demonstrated by flat-lying beds and lack of cleavage. Metamorphic overprints in the Gamohaan Formation are minimal everywhere with no metamorphic minerals developed, whereas talc and amphibole are developed in parts of the Frisco Formation (Chapter 4). The Gamohaan and Frisco formations were deposited during a transgression that drowned the carbonate platform; stratigraphic data constrains deposition of the microbialites to deep subtidal, sub-wave base environments (Chapters 2 and 4).

## MICROBIALITE MORPHOLOGY

The Gamohaan and Frisco formations contain a wide morphological range of microbialites, all of which can be described in terms of the proportion and geometrical arrangement of three components: fine filmy laminae, supports, and voids filled with carbonate cement (Figure 3-1). Remarkably, little or no carbonate or siliciclastic sediment occurs in these rocks. Filmy laminae consist of planar, draped, and recumbently folded layers that are dark gray to black in hand sample (Figures 3-1, 3-2, and 3-3). Planar or draped laminae are stacked on top of each other forming layers of filmy laminae up to several centimeters thick. Usually, they are oriented horizontally although where they drape off of supports they dip up to 80°. Disrupted laminae can be isoclinally folded and refolded multiple times, and occasionally, they are rolled into balls (Figure 3-3). In thin section, the laminae are defined by pigmentation and micron-scale black inclusions in microcrystalline calcite or dolomite (Figure 3-4). Well preserved laminae are typically 10-20 μm thick, although they can be as thin as 3 μm. In the Frisco Formation, preservation is much poorer and laminae are always ≥20 μm thick.

---

carbonate (Aitken, 1967; Pratt and James, 1982; Kennard and James, 1986). Most workers use the term "stromatolite" for well laminated, relief-forming structures (e.g. Monty, 1973; Semikhatov, et al., 1979; Krumbein, 1983). In contrast, thrombolites are unlaminated, but contain a distinctive clotted texture (Aitken, 1967; Kennard and James, 1986), and the adjective "cryptalgalaminate" applies to "planar-laminated carbonate rocks bearing evidence of algal-mat activity" (Aitken, 1967). Although some of the microbialites in the Gamohaan and Frisco formations are stromatolites or cryptalgalaminated carbonate in the strict sense, many are not regularly laminated and some are unlaminated. None of them contain the clotted microtexture of thrombolites. Since all the Gamohaan and Frisco microbialites do not fit easily into the standard classification of microbial sediments, I call the wide range of microbial structures in the Gamohaan and Frisco formations "microbialites" to avoid the problem of calling some well-laminated structures "stromatolites", but calling other, genetically similar structures "cryptalgalaminates" or "microbialites". This emphasizes the common origins of the microbialites in the Gamohaan and Frisco formations.

Filmy laminae are interpreted as remnants of very finely laminated microbial mat for several reasons (Button, 1973; Beukes, 1980, 1987). First, the laminae are very fine and smooth, even when isoclinally folded and rolled into balls. Individual laminae must therefore have been very flexible and laterally cohesive prior to deposition. These properties are consistent with folding of gelatinous microbial mat laminae, but not with deformation of unconsolidated sediment layers. Second, the filmy laminae are defined by organic inclusions encased in carbonate cements. Since there is no evidence for a mineralogical or grain size variations to define the lamination, a biotic origin for the laminae is likely. Similar laminae are present as "roll-ups" in the 2.6 Ga Wittenoom Formation, Carawine Dolomite, and Lewin Shale of the Hamersley Group, Australia (Simonson, et al., 1985) where they also are interpreted as contorted microbial mats based on their cohesiveness and strength during deformation and on their carbonaceous composition (Simonson, et al., 1985).

The supports are somewhat irregular surfaces that are interconnected in three dimensions (Figure 3-5). In most microbialites, they are oriented vertically (Figure 3-1). Infrequently, they branch outward or even downward beneath overhangs (Figures 3-6 and 3-7). Filmy laminae drape over the supports where both are present, although in samples

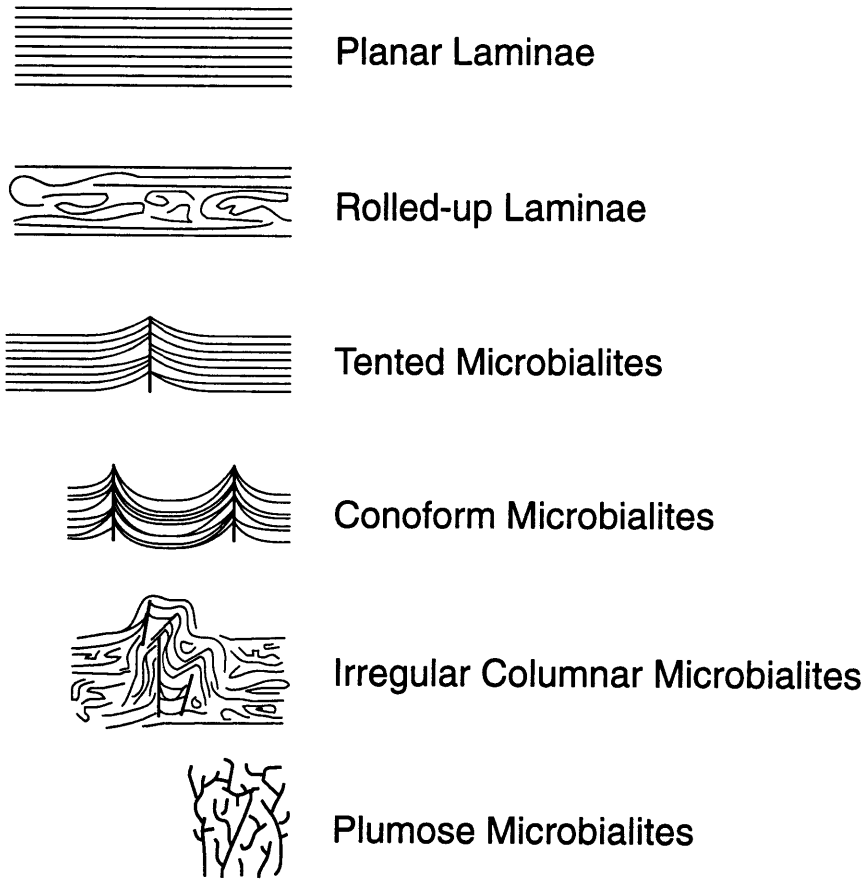


Figure 3-1. Schematic illustrations of the six microbialite end-members. Not to scale.

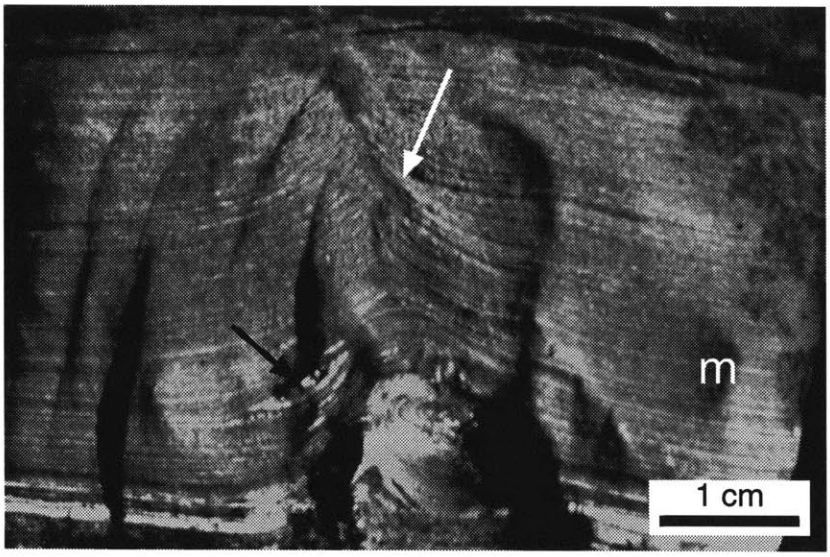


Figure 3-2. Tented microbialite in a bed predominantly consisting of planar laminae (l). The black arrow indicates the central support showing evidence for compaction and the white arrow indicates a cement-filled void.

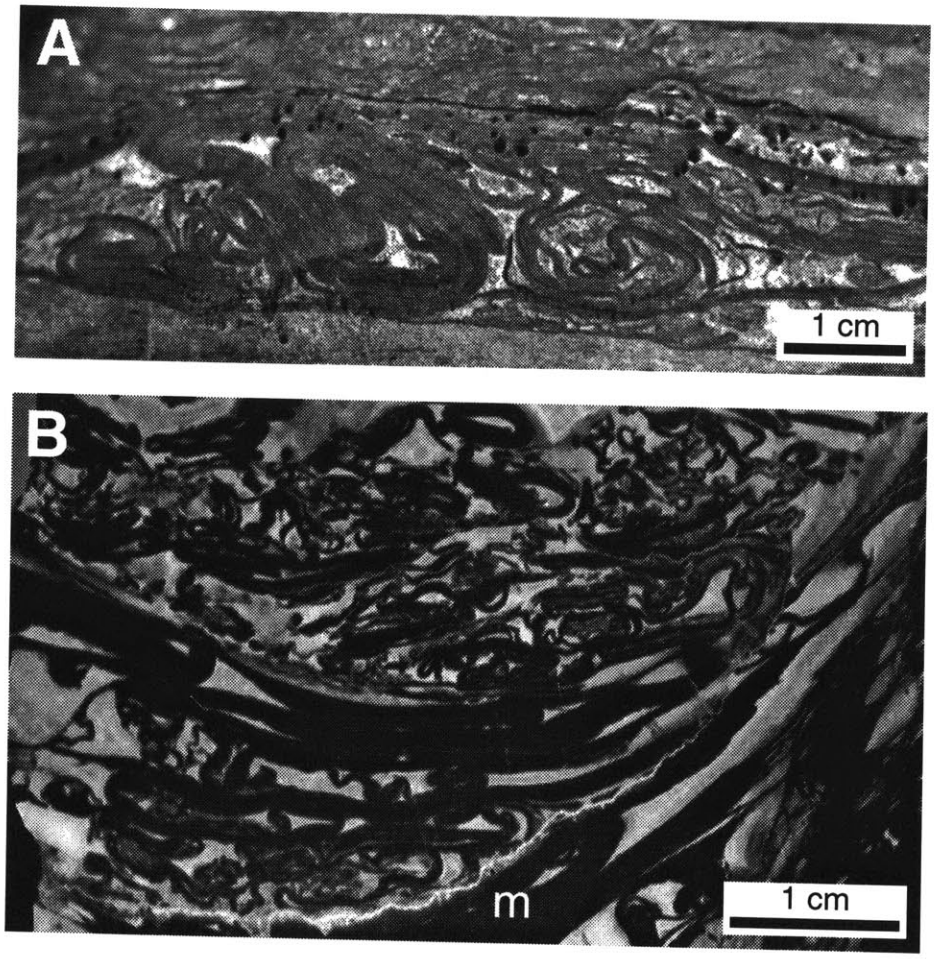


Figure 3-3. Rolled-up laminae. A) Outcrop view illustrating the contorted folding of very fine laminae. The laminae are rolled into balls and often are folded recumbently. Little compaction of the laminae occurred implying early cementation and precipitation of void-filling cements. B) Polished slab showing contorted laminae that both sloughed off a neighboring irregular columnar microbialite. Note the highly contorted character of the mat (black) and the large volume of void-filling cements (white). Cementation was early as demonstrated by the lack of compaction in the roll-ups.

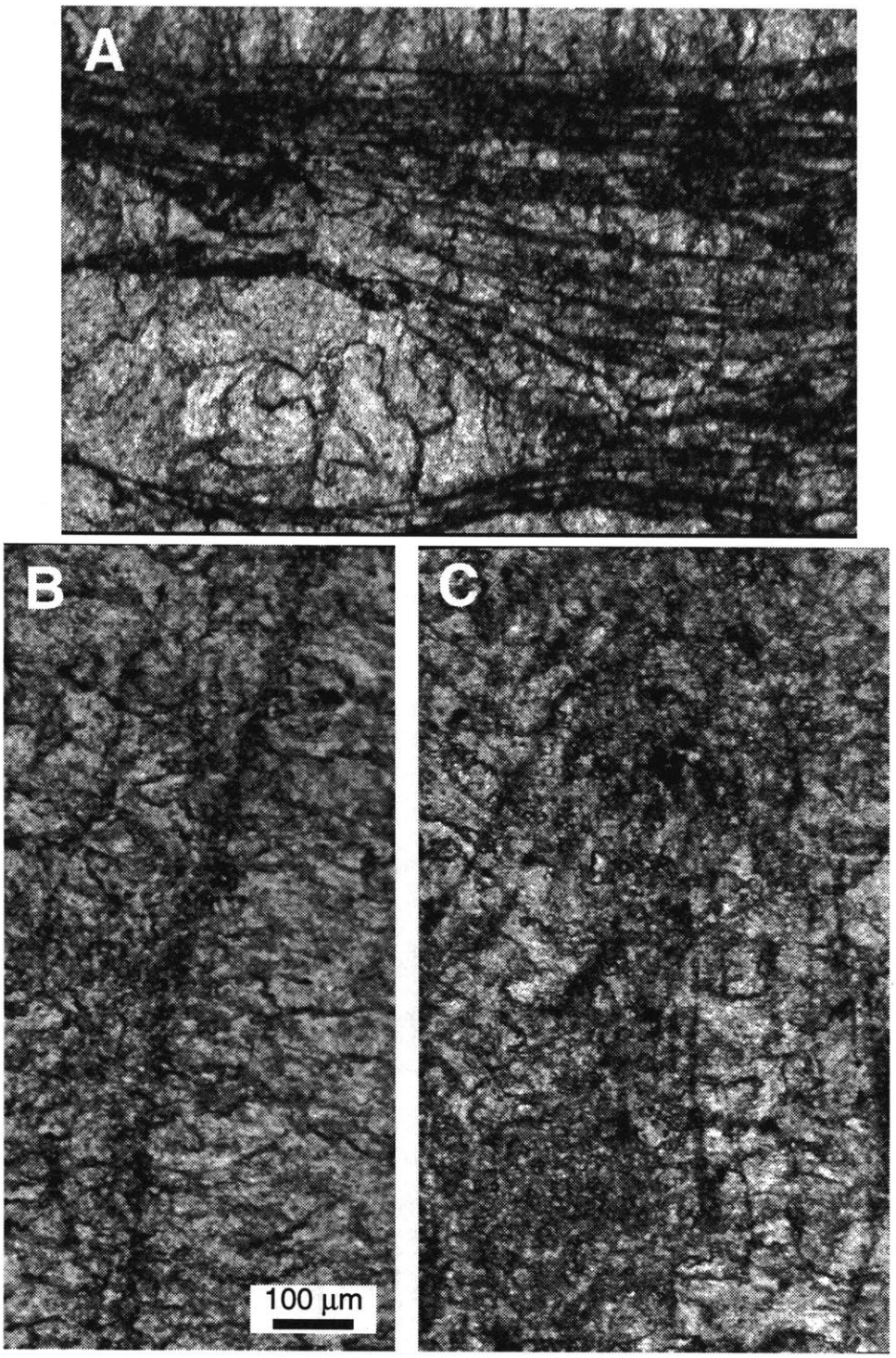


Figure 3-4. A) Thin section of filmy laminae in plane polarized light. B) and C) Thin sections of supports. B is a well preserved, isolated support and C is draped by filmy laminae. All photos are at the same scale.

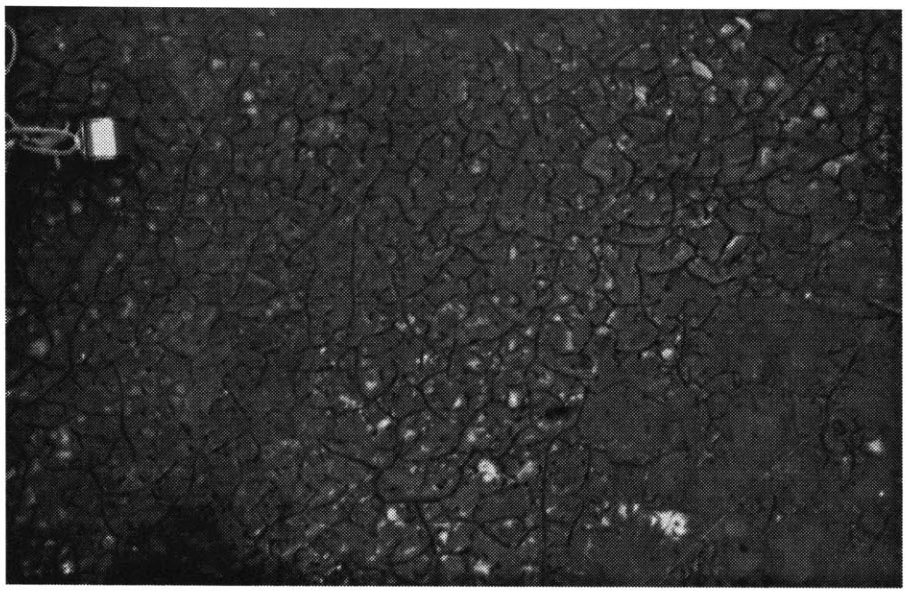

Figure 3-5. Plan view of cuspate microbialites to plumose structures from section EC. Supports are interconnected in a polygonal pattern. Hand lens is 2 cm.

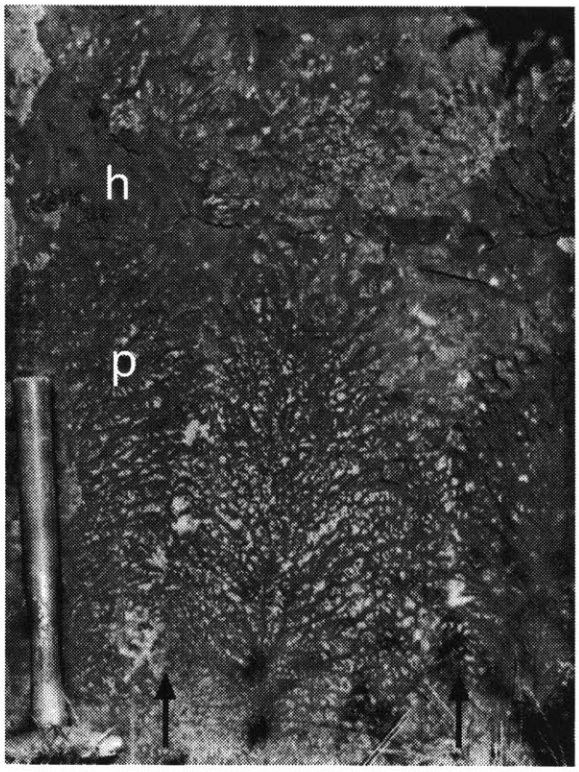


Figure 3-6. Vertical section of plumose structures (p) overlain by a decimeter-scale bed of herringbone calcite (h) and then another layer of plumose structures. These microbialites formed individual structures that grew against each other leaving zones of interfering growth (black arrows). This bed is laterally continuous for at least 140x50 km (see Chapter 3). Hammer is 35 cm long.


Figure 3-7. Vertical section of a plumose structure that grew downward off an overhang consisting of disrupted planar laminae. Note that many of the central supports project and branch downwards with textures similar to those projecting horizontally and upwards.

with abundant branching and downward-growing supports, filmy laminae are rare to absent. Microscopically, supports are defined by zones of diffuse pigmentation and black inclusions in calcite or, more commonly, microcrystalline dolomite, as are the filmy laminae. Most supports are >200 μm wide, although the narrowest supports are only 50 μm wide. Narrow supports consist of a nearly linear zone of inclusions in calcite with well defined margins. Wider supports are often associated with more abundant filmy laminae and consist of clusters of inclusions in dolomite where filmy laminae are attached to the support. All poorly preserved supports also tend to be >200 μm, independent of the abundance of filmy laminae. The genetic interpretation of the supports is discussed after descriptions of the microbialites.

A complex framework with abundant primary voids is created by the branching of supports, draping of filmy laminae over supports, and folding of filmy laminae. These voids are filled with herringbone, bladed, and blocky calcite. Herringbone calcite is a fibrous marine cement with a distinctive light-dark, mm-scale banding which trends approximately perpendicular to the growth direction (Sumner and Grotzinger, in review; Chapter 5). Herringbone calcite precipitated as the first generation of carbonate cement within many voids, particularly those defined by supports draped with filmy laminae and by branching of supports. It is less common in voids created by folding of filmy laminae. Herringbone calcite coatings are followed by columnar and then blocky calcite spar. Columnar and blocky cements occlude porosity in all primary voids. In some microbialites, herringbone calcite layers contain minute fractures filled with spar that appears to be the same generation as the final, void-filling blocky calcite. This suggests that blocky spar precipitation occurred after minor burial compaction of the plumose structures. Interpretation of the origin of the voids also is discussed after descriptions of the microbialites.

Microbialite morphology is influenced by the extent of disruption of the filmy laminae in addition to the proportions of filmy laminae, supports, and voids. Variations in the extent of laminated mat disruption combined with the range in proportions of filmy laminae, supports, and voids lead to the definition of six distinctive end member microbial forms (Figure 3-1): planar laminae, rolled-up laminae, tented microbialites, cuspate microbialites, irregular columnar microbialites, and plumose structures. There are gradational forms between each of these end members forming a full spectrum of microbialites (Figure 3-8). Laterally continuous beds of herringbone calcite which lack both filmy laminae and supports constitute an additional end member of the microbialites.

**Planar Laminae**

Beds of filmy planar laminae are common, and layers of planar laminae are present

in troughs between irregular columnar microbialites. Individual laminae are very smooth and continuous for up to several meters along the outcrop. They are rarely truncated, usually where associated with pods of rolled-up and contorted laminae. They drape over topography on the bedding surface, showing less compaction in lows than over highs. Laminae are typically spaced by 10's of microns, and supports are absent unless tented microbialites are present (Figure 3-2). There are no void-filling cements in undisrupted planar laminae (Figure 3-8).

**Rolled-Up Laminae**

Rolled-up filmy laminae are present as distinct beds, lenses of contorted laminae in predominantly planar-laminated beds, trough-fill between irregular columnar microbialites, and slumps on the sides of irregular columnar microbialites. They consist of planar or draping filmy laminae that were isoclinally to recumbently folded or rolled into balls (Figure 3-3). Voids in the hinges and between fold limbs of the roll-ups are often filled with bladed and blocky calcite cement. Where mat accumulation was slow relative to carbonate precipitation, abundant voids were preserved and filled with cements. Roll-ups were compacted where accumulation rates were high, or precipitation rates were low. The volumetric proportion of void-filling cements in roll-ups ranges from 0- 60% (Figure 3-8). Individual laminae are very closely spaced and are poorly defined in uncemented roll-ups. Supports are absent.

**Tented Microbialites**

Tented microbialites consist of planar filmy laminae that are draped over a single nearly vertically oriented support creating a tent-like morphology (Figure 3-2). Layers of planar laminae are connected to the support at different heights creating inclined elongate voids that are filled with bladed calcite spar. Voids are <1 cm thick and <3 cm long. In tented microbialites lacking voids, some of the supports are folded (Figure 3-2 and 3-9). These folds have low amplitudes and are isoclinal. In one case (Figure 3-9), the top of the support appears folded over.

The spacing of individual laminae in tented microbialites is similar to that in planar laminated beds. Supports are horizontally spaced from 10-50 cm in beds composed of tented microbialites. Isolated tented microbialites are also present in beds of planar laminae and may be spaced meters apart. They are also present in troughs between irregular columnar microbialites. The volumetric proportion of void-filling cements in the tented microbialites is low with a maximum of 15% (Figure 3-8).

**Cuspate Microbialites**

Cuspate microbialites consist of supports draped by filmy laminae much like tented microbialites, but supports are more closely spaced and laminae drape between them (Figure 3-10). Layers of laminae are more widely spaced along the supports creating abundant dish-shaped voids defined by a net-like framework on which both herringbone and bladed calcite precipitated. Usually, supports are oriented vertically and are more abundant at the bases than the tops of cuspate microbialites. Small voids are also more abundant at the base and filmy laminae are more densely spaced at the top (Figure 3-10). In plan view, the base of cuspate microbialites have a densely spaced network pattern, and upward they develop an interconnected polygonal pattern, and then consist of short, disconnected ridges at the top (Figure 3-5 and 3-11). The growth morphology of cuspate microbialites was probably

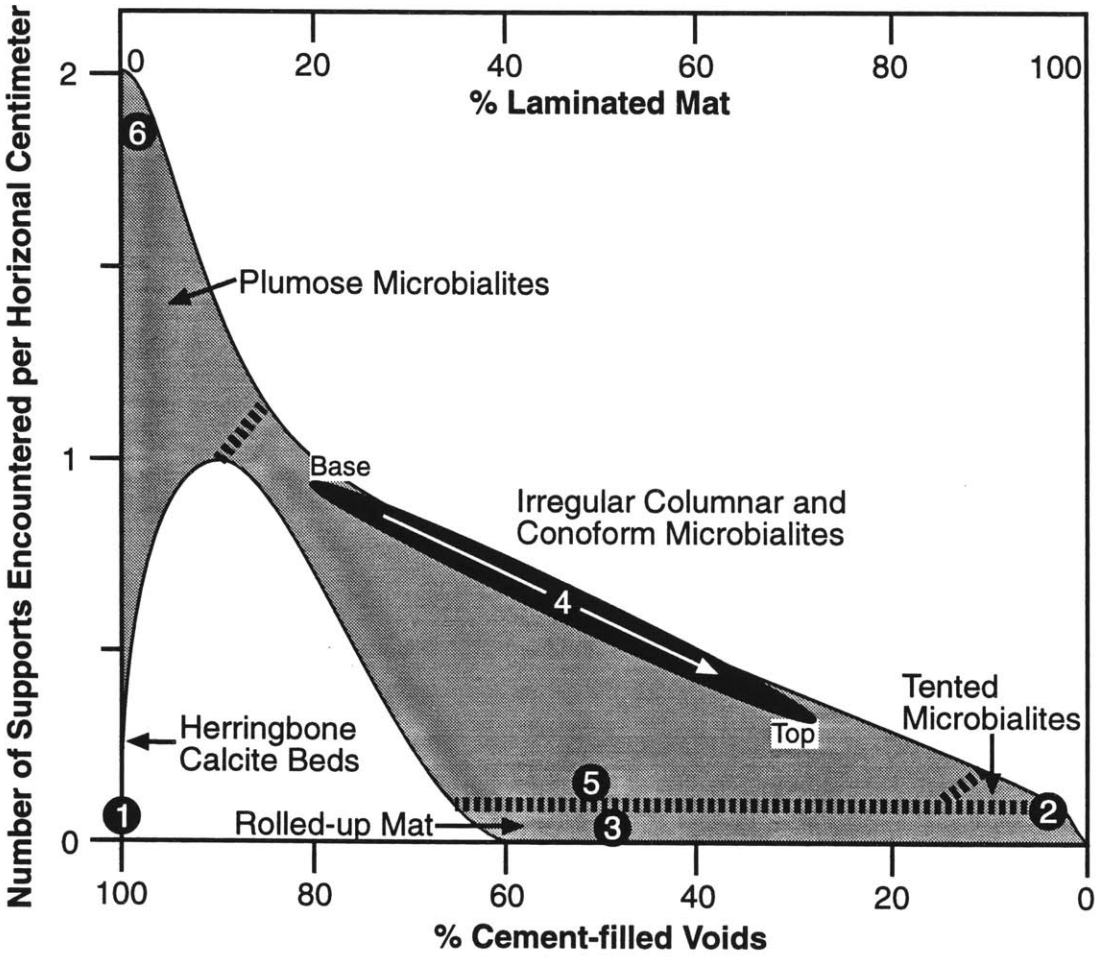


Figure 3-8. Diagram of the proportions of void-filling cements, laminated mat, and supports in the various types of microbialites. The numbers represent the composition of microbialites in the following photographs: 1 : Figure 3-17, 2 : Figure 3-2, 3 : Figure 3-3, 4 : Figure 3-10, 5 : Figure 3-13, and 6 : Figures 3-6 and 3-15.

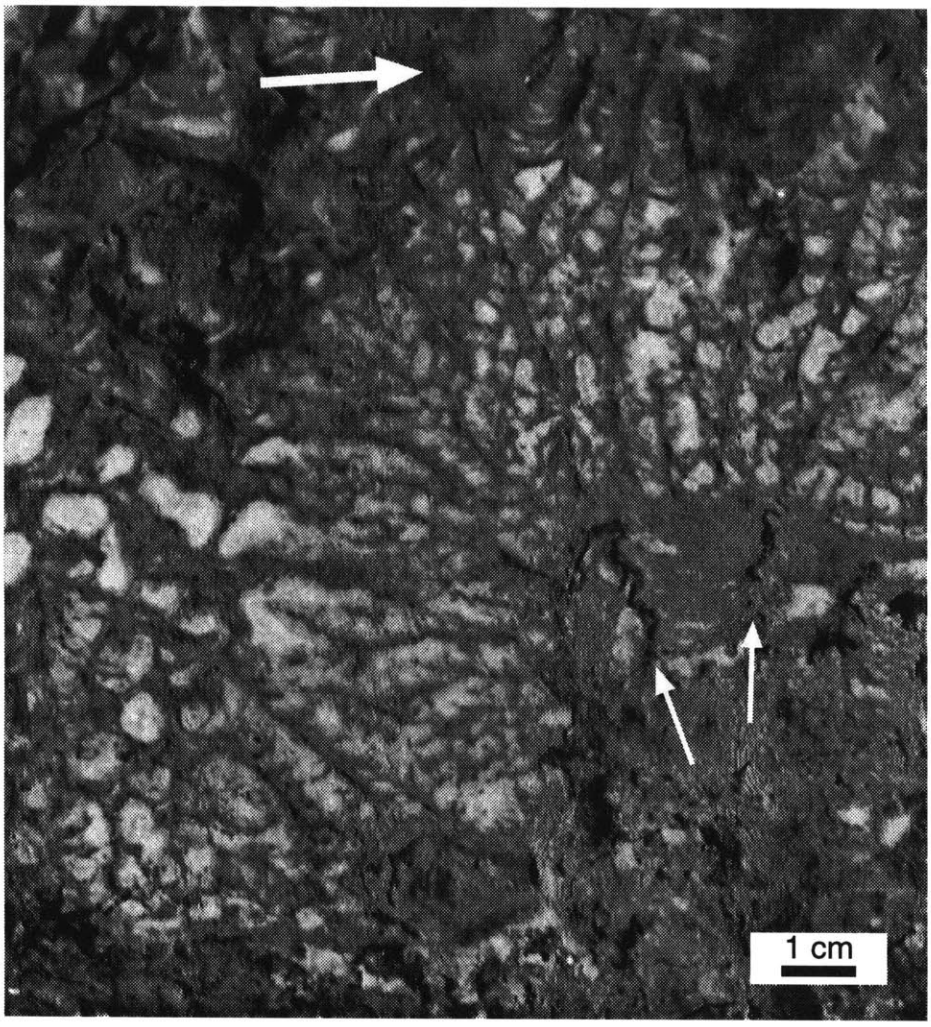


Figure 3-9. Vertical section of a plumose structure growing over a protrusion consisting of a round-topped tented microbialite. Note that the support in the tented microbialite is folded, particularly at the top (small white arrows). The plumose structures grade upward into cuspate microbialites (large white arrow).

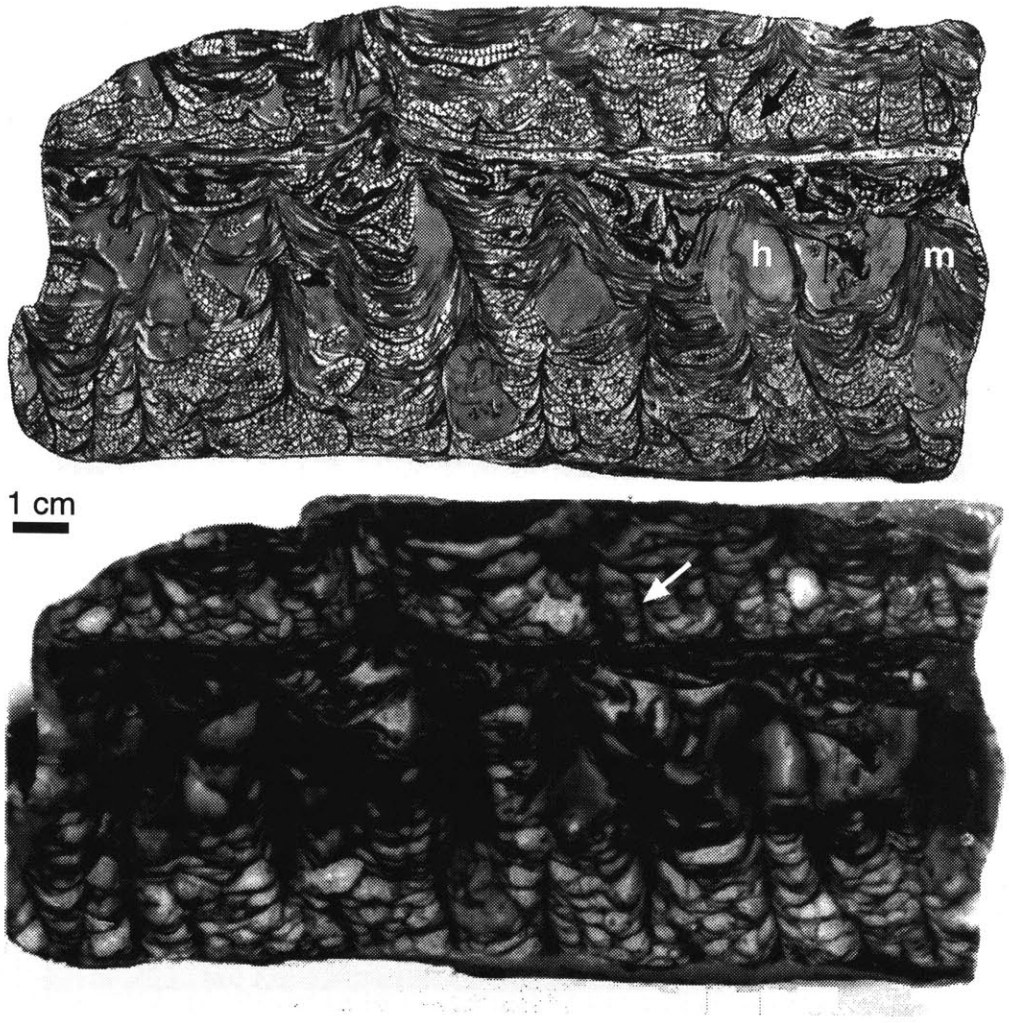


Figure 3-10. Polished slab and tracing showing cuspate microbialites. Herringbone calcite is indicated by "h", filmy laminated mat by "m", void-filling bladed and blocky calcite by a black arrow, and central supports by a white arrow. The texture of the microbialite changes from an open net-like framework at the base to a denser, more laminae-rich structure at the top. Successive layers of cuspate microbialites are separated by thin layers of roll-ups.

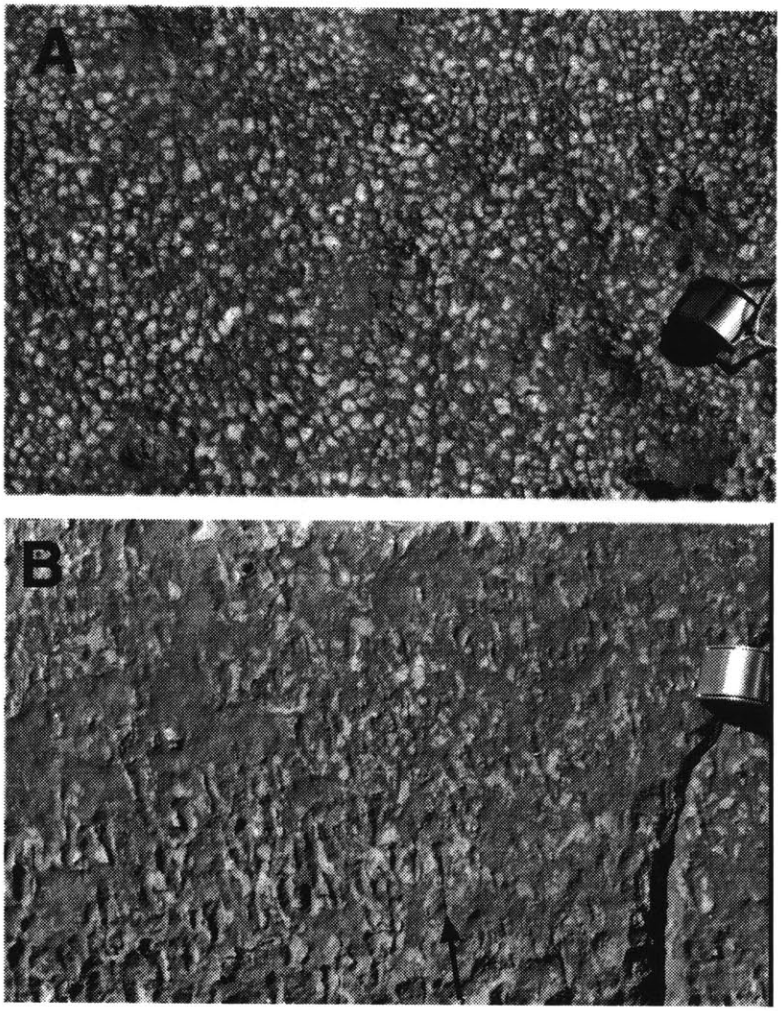


Figure 3-11. Plan views of cuspate microbialites in outcrop. A) View near the base of a bed of cuspate microbialites. The voids (white) separated by filmy laminae and central supports (dark) are equant. B) View near the top of the same bed. The central supports (dark lines) are distinguishable from the laminated mat. They are elongate and oriented in the direction of the black arrow. Voids (white) are less abundant and are also elongate. Hand lens is 2 cm wide.

similar to that proposed for similar microbialites from the Abitibi greenstone belt (Hofmann and Masson, 1994), with small peaks connected by ridges and separated by dish-shaped depressions.

The spacing of individual laminae within a layer of laminae is typically <1 mm, but layers are separated by 1-10 mm. Supports are spaced horizontally from 1-10 cm (Figure 3-8) and are oriented vertically. Void-filling cements often make up 10-90% of the microbialite with an average of 30% of the cement consisting of herringbone calcite (Figure 3-8).

**Irregular Columnar Microbialites**

Irregular columnar microbialites consist of 5-20 cm diameter columns with synoptic relief of 3-20 cm and spacing from 5-30 cm; larger columns are more widely spaced. They contain multiple supports and irregularly distributed filmy laminae (Figures 3-12 and 3-13). Some of the supports radiate outward from the center of the column at oblique angles whereas others are oriented vertically as in cuspate microbialites. The variations in orientation of the supports as well as the discontinuity of filmy laminae give the interiors of columns an irregular, contorted appearance. In plan view, the columns are either circular or similar to spider webs due to radiating supports and draping laminae (Figure 3-14).

Laminae commonly form mm- to cm-thick layers that are separated by voids. The spacing between layers of laminae is 1-10 mm. The spacing of supports is extremely variable; within columns it ranges from 1-10 cm and overall in beds, it mimics the spacing of the columns. Cements commonly form 40-80% of the columnar microbialites with about 50% of the cement consisting of herringbone calcite (Figure 3-8).

Troughs between columns are filled with roll-ups, planar laminae, and cuspate microbialites. Rare tented microbialites also are present. Many of the roll-ups appear to have sloughed off the sides of the columns, although some of them may have grown in the troughs. The intra-column fill contains variable amounts of void-filling cement ranging from 0-50%, and significantly less than the 40-80% in columns. Herringbone calcite is absent from most trough-fill, and in rare cases, some of the sediment in the troughs was uncemented. This sediment shows signs of compaction, leading to the formation of horizontal sheet cracks under well cemented beds that stretched from one column to the next. These cracks are filled with herringbone, bladed, and blocky calcite.

**Plumose Structures**

Plumose structures consist of supports and cement-filled voids with only very rare draping laminae (Figures 3-6, 3-7, 3-9, and 3-15). The supports branch outward forming

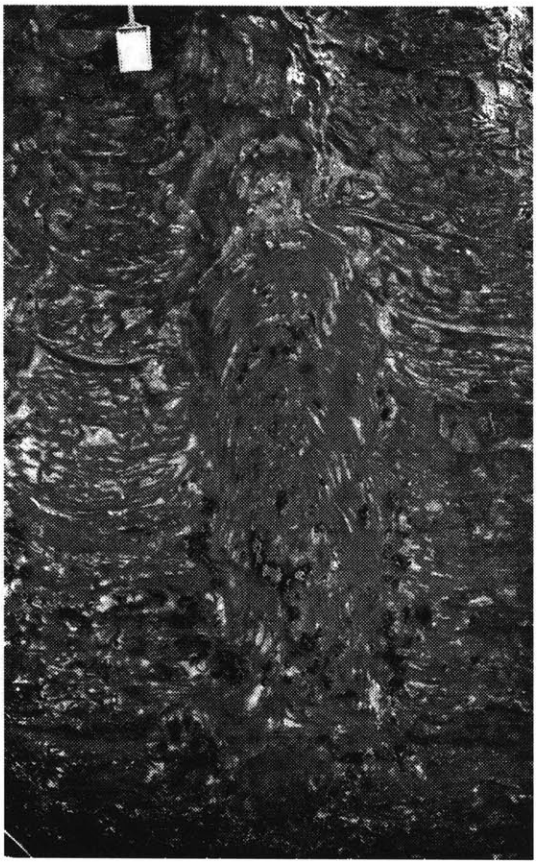

Figure 3-12. Irregular columnar microbialite in outcrop. The irregular columnar microbialite shown here has convex laminae separated by white voids filled with calcite. Columns are separated by thin layers of planar laminae and roll-ups. Hand lens is 2 cm wide.


Figure 3-13. Polished slab and tracing showing irregular columnar microbialites and intervening rolled-up laminae. Herringbone calcite is indicated by "h", filmy laminated mat by "m", secondary chert by "ch", void-filling bladed and blocky calcite by a black arrow, and central supports by a white arrow. Laminae within the column are discontinuous and irregular.

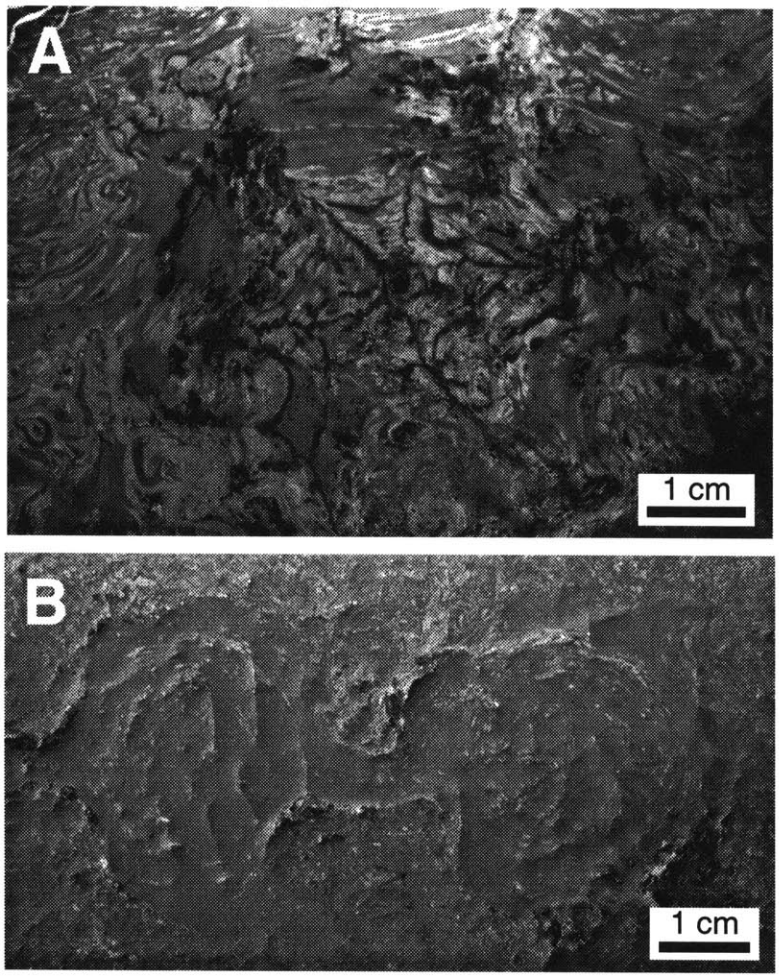


Figure 3-14. Plan views of irregular columnar microbialites. A) Plan view with a spider web-like arrangement of central supports (black) and draping laminae. Roll-ups are present in the troughs around the column and are visible in the upper left. B) Plan view of two columns with a more common circular geometry. Central supports are not visible, but the two columns are connected. Roll-ups surround them.

complex bush-like structures with "branches" defining irregular cm-scale voids mostly filled with herringbone calcite. The supports are surfaces and are interconnected in the third dimension (Figure 3-16). The supports are variously oriented in space with some appearing to have grown downward. In one case, a plumose structure grew downward off an overhanging surface while adjacent plumose structures grew upward (Figure 3-7). There is no difference in morphology between the downward and upward oriented supports.

Supports in plumose structures are spaced from 0.5 to 2 cm both horizontally and vertically. Many of the plumose structures consist of 95% void-filling cement with 80% herringbone calcite (Figure 3-8). Filmy laminae are virtually absent. Nearly horizontal supports are associated with 0.5 cm-thick zones with diffuse black inclusions and pigments that define a coarse lamination parallel to the support. These inclusions are present only below the supports (Figure 3-15).

The growth morphology of plumose structures is very difficult to determine due to the lack of laminae that define growth horizons. Two different growth styles are apparent, however. Plumose structures most often grew in continuous beds of branching supports without the development of individual microbialite structures (Figures 3-7 and 3-9). Occasionally, however, beds are composed of individual plumose structures separated by narrow, cement-filled troughs (Figure 3-6). In these beds, each microbialite is roughly circular or hexagonal in plan view.

**Herringbone Calcite Beds**

Herringbone calcite beds consist of laterally continuous sea floor encrustations which lack filmy laminae and supports (Figures 3-8 and 3-17) and can be up to 40 cm thick. They isopachously coat topography on the underlying bed, and sometimes form dome-like structures that were the direct result of coating an irregular surface with a constant thickness of cement. These are described in Chapter 5 and Sumner and Grotzinger (in review).

### *Variations in Microbialite Morphology*

Although it is possible to define seven end members, there is a continuum between their forms and internal textures (Figure 3-8). For example, planar laminae often are associated with roll-ups and tented microbialites. The differences between these structures are due to the disruption of laminae for the roll-ups and the presence of rare supports in tented microbialites (Figure 3-8). Tented microbialites also form a continuum with cuspate microbialites. As supports become more closely spaced, voids become dish-shaped, and there is a progressive change from tented to cuspate end members. The main difference between cuspate and irregular columnar microbialites is the extent of disruption of filmy


Figure 3-15. Polished slab and tracing showing part of a plumose structure from the bed shown in Figure 3-9. Herringbone calcite is indicated by "h", void-filling blocky calcite by a black arrow, and central supports by a white arrow. Central supports project in a variety of directions including horizontally. Short dashes indicate areas with abundant black inclusions that define a poor lamination parallel to the overlying support. Note that these always occur within herringbone calcite and below the associated support. This sample consists of ~90% herringbone calcite.

laminae, and the change in morphology from conical to rounded laminae shape is accompanied by laminae disruption. Laminae are also more densely spaced in the irregular columnar microbialites and voids are smaller and less regular. The proportions of cement are similar, as is the spacing of supports (Figure 3-8). A transition from cuspate to plumose structures occurs with a decrease in the abundance of filmy laminae accompanied by an increase in the branching of supports and the proportion of herringbone calcite.

Gradational changes from one end member to another can occur upward within a single microbialite bed. The most common gradational changes are between cuspate and irregular columnar microbialites. Microbialites that begin with a regular, cuspate structure often become disrupted upward becoming irregular columnar microbialites (Figure 3-13). Also, plumose structures often pass upward into cuspate microbialites with a continuous increase in the abundance of draping laminae and a loss of supports (Figure 3-9). In other cases, plumose structures grade upward into beds of pure herringbone calcite with a progressive loss of supports without a corresponding increase in draping laminae (Figure 3-6). Cuspate microbialites are sometimes coated with cm-thick beds of herringbone calcite, but the textural change is abrupt rather than gradational.

The abundance of herringbone calcite shows a strong correlation to morphological variations in the microbialites. Planar laminae and tented microbialites contain the fewest voids and contain bladed rather than herringbone calcite cements. Roll-ups contain a highly variable amount of void-filling cement, but herringbone calcite is rare. Cuspate and irregular columnar microbialites contain more cement, particularly herringbone calcite. Plumose structures contain the highest abundance of both cements in general and herringbone calcite in particular, whereas they contain almost no laminated mat. These observations suggest that there is a correlation between slower laminated mat growth and more abundant herringbone calcite precipitation. Slower mat growth probably led to lower accumulation rates, allowing more time for marine cement precipitation prior to burial. Higher proportions of herringbone calcite would be present in slower growing microbialites given a constant rate of carbonate precipitation. For example, very low growth rates of mats and supports could allow the precipitation of thick beds of herringbone calcite. Where microbial growth was slow, herringbone calcite precipitated within the microbial structures. Where mat accumulated quickly, herringbone calcite is absent. In addition, the number of supports increases and the volume of mat decreases with increasing proportions of herringbone calcite. This correlation suggests that supports developed in beds with low accumulation rates relative to beds with abundant mat and less herringbone calcite, assuming that the precipitation rate of herringbone calcite is approximately constant.

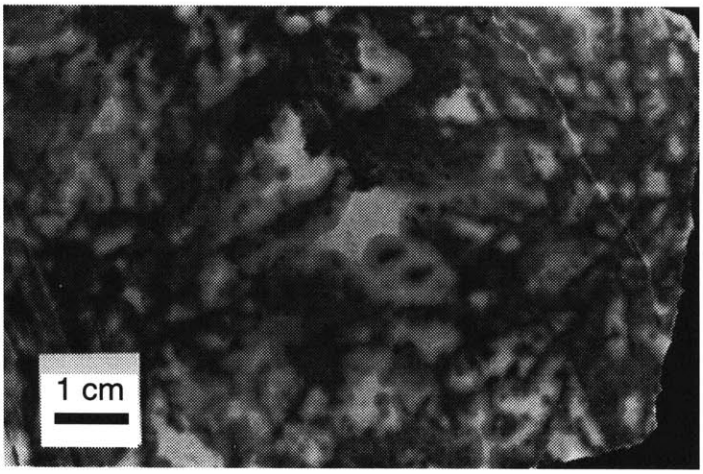


Figure 3-16. Plan view of a plumose structure. Note the branching pattern in the supports is similar to that in vertical sections (compare with Figure 3-15). The dark gray areas are cross sections through the inclusion-rich zones under horizontal supports.

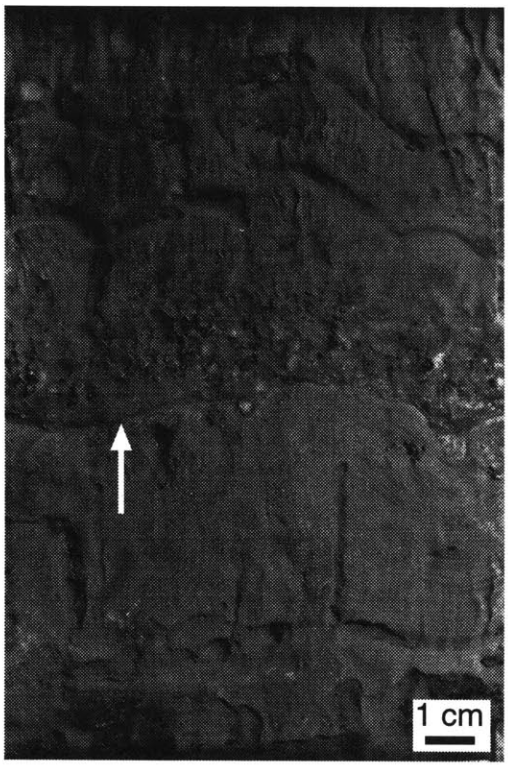


Figure 3-17. A laterally continuous (140 x 50 km) bed of herringbone calcite with a thin layer of plumose structures layer in the middle (white arrow points to base of layer). This is the same bed as shown in Figure 5-3A.

## CONSTRAINTS ON THE ORIGIN OF THE MICROBIALITES

### *Origin of Supports and Voids*

The two components that distinguish the Gamohaan and Frisco microbialites from most previously described examples, particularly those of younger geologic ages, are the supports and cement-filled voids.

### Origin of Supports

Neither biological nor inorganic analogs for the supports are known, but morphological and textural data indirectly favor a biological origin. First, physical processes such as desiccation produce polygonal, interconnected cracks, but do not produce the upward branching patterns seen in supports in plumose structures (Figure 3-7). Escaping gas bubbles would not create the complex upward branching and downward growth of supports. In addition, the supports are surfaces in three dimensions, not linear escape paths, and are thus inconsistent with models of gas escape. Finally, void-filling cements nucleated on the supports and grew inward, implying that the supports are primary growth features and not later desiccation cracks or voids left by escaping gas.

A mineralogical origin for the supports is also questionable. Although plumose structures have a superficial resemblance to dendritic crystal growth patterns and models of diffusion limited aggregation (DLA) in vertical cross-section (Figure 3-18), this resemblance is only superficial. There are several distinct morphological differences which demonstrate that plumose structures are not DLA structures: 1) Individual plumose structures are more closely spaced (Figure 3-6) than true DLA structures (Figure 3-18). 2) Small branches are rare in plumose structures (Figure 3-15) whereas they are very abundant in DLA clusters and dendritic crystals. 3) Voids are common in plumose structures whereas

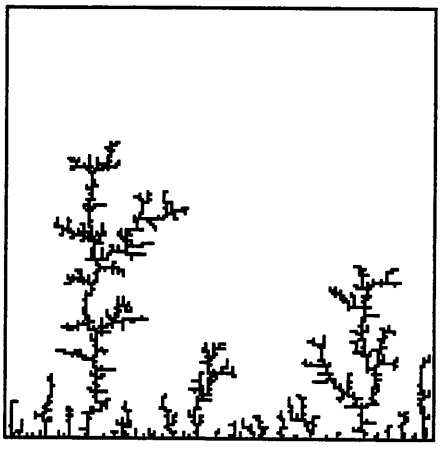

Figure 3-18. Computer generated diffusion-limited aggregation (DLA) structures created by the random nucleation and then walk of 1500 particle. The random walk stopped once the particle encountered another particle of the floor of the model (see Stanley, 1991, for details). Note that the "trees" are more widely spaced than plumose structures, and enclosed voids are very rare.

enclosed spaces are rare in DLA clusters. 4) Voids and supports in plumose structures have characteristics sizes and are not fractally distributed (Seth McGinis, pers. comm.), a defining characteristic of DLA growth (Stanley, 1991). 5) Most importantly, the supports in plumose structures are surfaces in three dimensions, and not branches (Figure 3-16). Three dimensional DLA clusters consist exclusively of branches (Stanley, 1991). Thus, supports in plumose structures are distinct from dendritic growth morphologies. No other crystal precipitation models create morphologies similar to the branching supports or the growth of vertically oriented surfaces connected in a roughly polygonal framework as seen in cuspate microbialites. In addition, the supports of the tented microbialites, which have less contemporaneous cementation than the other morphologies of microbialites, show some indications of folding (Figures 3-2 and 3-9). The folds in the supports are consistent with compaction because supports are thickened in the folds, laminae adjacent to side of supports are thickened, support tops are occasionally folded over, and folded supports occur in microbialites with little evidence for abundant synsedimentary carbonate precipitation. The folds are unlikely to be growth structures because they are never observed in microbialites with more abundant early cementation and this growth pattern is only observed in areas consistent with compaction. Compaction of supports suggests that they were intrinsically soft; although precipitated carbonate gave them their rigid character, it was not necessary for their growth.

The lack of physical and chemical processes that can account for the properties of the supports suggests that they have a biological origin. Organic inclusions define the supports petrographically implying the presence of a microbial community. Although this does not demonstrate a biological origin, given the complex morphologies developed in modern mats (e.g. Walter, et al., 1976; Horodyski, 1977), it is conceivable that the supports could be biologically produced. Thus, although no microbial communities have been described that can provide an analog for the supports, a biological interpretation seems reasonable.

**Origin of Voids**

Most voids probably formed contemporaneously with microbialite growth, either through gas escape or due to the growth morphology of the microbial communities. Many of the voids in the irregular columnar microbialites have ragged edges where laminae are broken, and occasionally the laminae above the voids are compressed (Figure 3-19) suggesting that the upward migration of gas bubbles within the mat created some voids. The irregular folding of laminae at the edges of the voids demonstrates that they were disrupted prior to lithification. Other voids in irregular columnar microbialites and most voids in

cuspate microbialites do not have associated broken laminae or overlying compressed laminae. Instead, they are surrounded by two continuous filmy laminae: one over the top of the void, and a second around the bottom of the void. The laminae pinch together on either side of the void, demonstrating that the void formed between the two laminae. In cuspate microbialites, these voids are usually dish-shaped with their concave surface facing upward (Figure 3-10). The geometry of these voids is less consistent with separation of the laminae due to gas bubbles, because if bubbles formed the voids, the upper surface probably would be convex rather than concave (Figure 3-20). It is possible that gas may first have separated the laminae creating the initial void and then leaked out allowing the laminae to sag to form a concave surface. The edges of successive laminae often are attached to the supports at spaced intervals, however, suggesting that the laminae originally grew separated and that gas bubbles were not necessary to separate laminae. The laminae originally may have grown suspended in water, but attached to the supports; as calcite precipitated on them, they sagged down between the supports creating dish-shaped voids (Figure 3-20). This model suggests that the dish-shaped voids represent constructional features of the microbialites related to the growth habit of the microbial communities. It does not require the action of gas bubbles, but does not exclude them as a mechanism for allowing suspended growth of the laminae.

Most voids in cuspate and irregular columnar microbialites are not consistent with

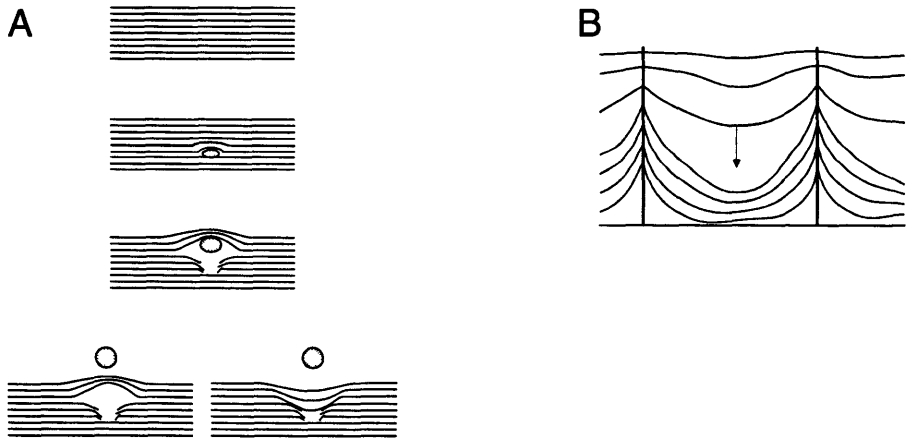


Figure 3-20. A) Illustration of void formation via the creation and escape of gas bubbles. First a bubble forms between mat laminae. It breaks some layers and lifts others. If laminae are cemented before the bubble escapes, the upper laminae remain domed. If the layers are uncemented when the bubble escapes, they collapse. They may become concave after collapse if the mat expanded when it was uplifted by the bubble. B) Laminae could have grown suspended between two supports. As the mat aged, it stretched and collapsed between the supports creating dish-shaped voids. In cuspate microbialites, more mat is present between supports than attached to them suggesting that addition mat grew in concave areas during or after stretching of the initial mat.

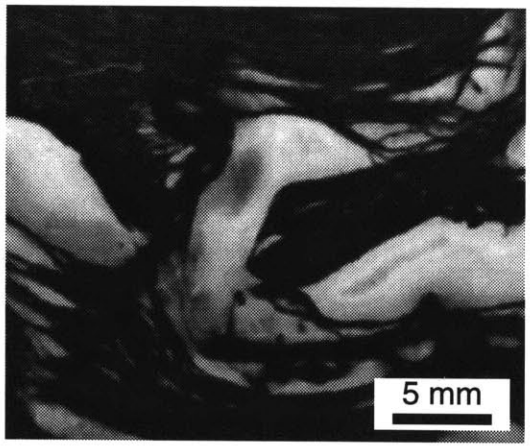


Figure 3-19. Etched polished slab of a void that may have formed during gas escape from the underlying mat. Note the broken layers of mat that hang down the sides of the void and the compressed overlying laminae.

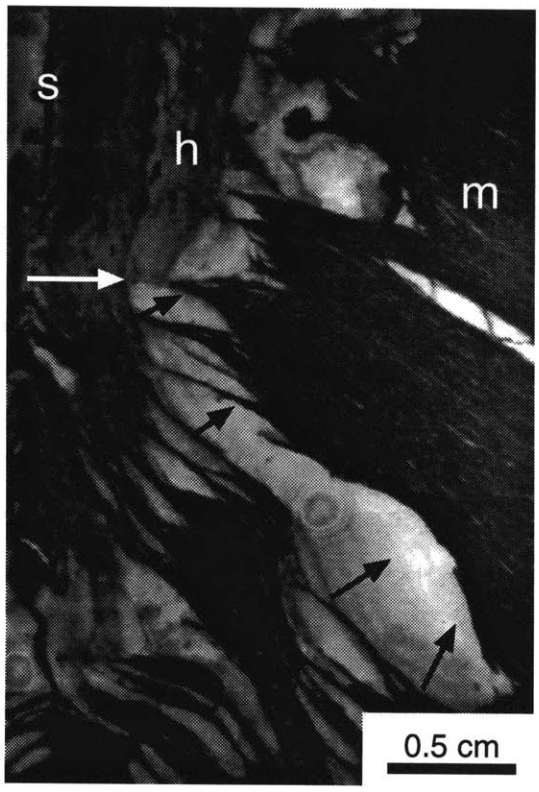


Figure 3-21. Etched polished slab of the edge of an irregular columnar microbialites (to left). Herringbone calcite (h) grew off a central support (s) and some laminated mat (m). Herringbone calcite banding is truncated against some draping laminae (white arrow), although many of the voids are also filled with herringbone calcite. It did not grow as traditional void filling cement, however, and textures indicate that it predominantly grew upward and outward from supports and draping laminated mats (growth directions indicated by black arrows). Small spherical patterns are secondary chert nodules.

formation due to displacement of overlying mat by the force exerted by crystal growth (Maliva, 1989; Saigal and Walton, 1988; Buczynski and Chafetz, 1987). In most voids, crystals grew inward from all edges of the voids, demonstrating that the voids were present prior to cement precipitation and could not have formed due to the pushing apart of laminae by displacive precipitation. In a few voids, however, herringbone calcite grew upward from the lower void surface (Figure 3-21). In this case, it is conceivable that the displacive growth lifted the overlying laminae. Even in most of these voids, however, the final fill is isopachous and crystals grew inward demonstrating the presence of a void. Thus, displacive calcite precipitation is unlikely to have caused most if not all of the voids in cuspate and irregular columnar microbialites.

Voids in plumose structures have a different geometry than those in cuspate and irregular columnar microbialites. They are equant, have irregular outlines, and are defined by the branching of supports (Figure 3-15). The void-filling cements grew inwards from the supports to the centers of the voids, demonstrating that the cements precipitated in voids and not outwards from the center. Much of the first millimeter or so of herringbone calcite void-fill has organic inclusions defining growth horizons suggesting that initial herringbone calcite precipitation was contemporaneous with microbial growth, and that the voids are not diagenetic in origin. The contemporaneous growth of microbial communities and herringbone calcite as well as the void geometry suggest that the voids are a direct result of the growth morphology of the supports and are a primary feature of plumose structures.

### *Potential Analogs and Constraints on Constituent Microbes*

The closest modern analog for the Gamohaan and Frisco microbialites was described by Walter et al. (1976) from silica-precipitating hot springs in Yellowstone National Park, Wyoming. These stromatolites, classified as *Conophyton weedii*, consist of 0.1-10.0 cm high cones with rare spinose projections and radially arranged narrow vertical ridges. Internally, they consist of 1-15 μm laminae with rare 35-60 μm thick "macrolaminae", and "crestal zones" which are 0.5-2.0 mm wide. Walter et al. (1976) propose that the conical morphology was created by *Phormidium tenue* var. *granuliferum* Copeland (a filamentous cyanobacteria with a strong phototactic response), *Chloroflexus aurantiacus* (a filamentous, phototactic bacteria), and rare other bacteria and cyanobacteria. *P. tenue* is more abundant in crestal zones and the tops of cones than in the intervening mat and the reverse is true of *C. aurantiacus*. The differences in their distribution within the microbialites are attributed to the stronger phototactic response of *P. tenue* (Walter, et al., 1976). In laboratory experiments, cones like those in the hot springs were produced by *P. tenue* var. *granuliferum* cultures whereas *Chloroflexus cultures* produced mats with low amplitude


Figure 3-22. Detail of the etched polished slab shown in Figure 3-13. Herringbone calcite (h) preferentially grew off the central support (s) over the laminated mat (m). Herringbone calcite grew outward from the support encasing draping laminae attached to it, but did not coat the laminae away from the support. The mat was present during herringbone calcite precipitation as demonstrated by the truncation of herringbone calcite banding against draping laminae (white arrow). Voids between draping laminated mats near the supports are filled with bladed calcite (white).

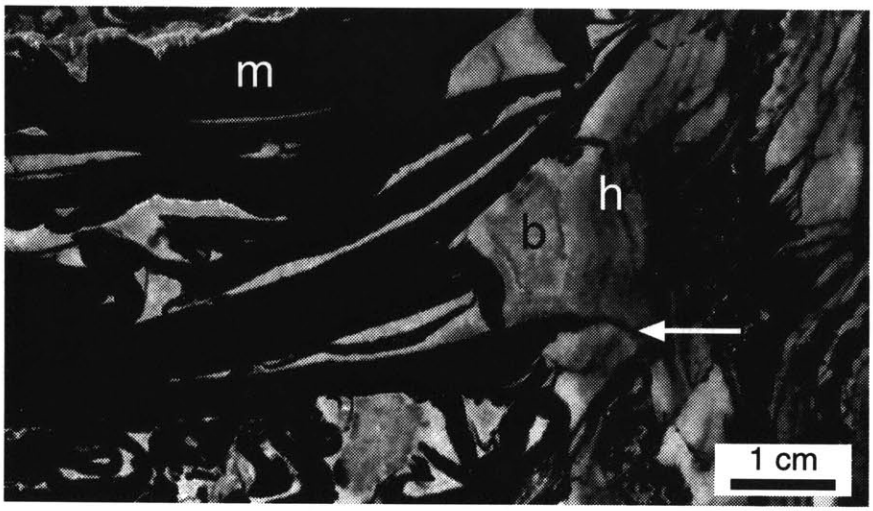


Figure 3-23. Detail of the etched polished slab shown in Figure 3-13. Herringbone calcite (h) preferentially grew off the margin of the irregular columnar microbialite over the laminated mat (m). The laminae were present during growth of the herringbone calcite as demonstrated by the encasing of some mat in the herringbone calcite (white arrow). This mat is coated by only a very thin layer of herringbone calcite and most of the void space is filled with blocky calcite (b).

nodules suggesting that the morphology of the stromatolites is controlled by the specific behavior of *P. tenue* var. *granuliferum* with possible modification by less abundant microbes (Walter, et al., 1976). Mats with similar geometries in Laguna Mormona, Baja California, Mexico, are dominated by various *Lyngbia* species demonstrating that the peaked geometry of mats is not restricted to *P. tenue* (Horodyski, 1977).

*C. weedii* are similar in morphology to the cuspate, irregular columnar, and tented microbialites from the Gamohaan and Frisco formations. For example, ridged cones from figures 12, 15, and 16 of Walter et al. (1976) are similar to the growth morphology of cuspate microbialites from the Gamohaan Formation. Walter et al. (1976) do not report whether or not the deep valleys between ridges become enclosed to form voids as in cuspate microbialites, and none of the photographs show voids. Thin section photographs of *C. weedii* in figures 20-22 of Walter et al. (1976) are vaguely similar to irregular columnar microbialites (Figure 3-13), but again lack well defined voids. Finally, the crestal zone in Figure 19 of Walter et al. (1976) looks similar to the compacted supports in tented microbialites described here (Figures 3-2 and 3-9). Despite these morphological similarities, the analog between *C. weedii* and any of the Gamohaan and Frisco microbialites fails in that the rigid supports, ubiquitous cement-filled voids, and structures analogous to plumose structures are all absent from *C. weedii*.

Previously described conophyton stromatolites also fail to provide an analog for the Gamohaan and Frisco microbialites, because they lack abundant cement-filled voids and are not associated with any structures similar to plumose structures. Conophyton do have crestal zones, but these zones are distinct from supports in the Gamohaan and Frisco microbialites because they are usually millimeters wide, 1-dimensional zones of voids and not 2-dimensional surfaces (Donaldson, 1976; Horodyski, 1976; Bertrand-Sarfati and Moussine-Pouchkine, 1985). In addition, organic debris between conophyton stromatolites does not consist of the long folds of mat typical of the Gamohaan and Frisco microbialites suggesting that the mats forming previously described conophyton were not as laterally cohesive when disrupted.

Despite the lack of analogs, the character of the filmy laminae suggests similarities to microbes in conophyton stromatolites. In particular, the fine, smooth laminae texture suggests that it was composed of filamentous microbes that secreted a gelatinous coating (Walter, et al., 1976; Bertrand-Sarfati, 1976). Filamentous microfossils have been reported in the Gamohaan Formation, but they were found in a chert bed that does not contain macroscopic microbial structures (Klein, et al., 1987). In addition, the fossils are filaments with diameters of 15-25 μm (Klein, et al., 1987), but the lamination in the microbialites is as thin as 3 μm, suggesting that it was formed of ≤3 μm bacteria or cyanobacteria. Thus, the

microfossils reported by Klein et al. (1987) could not have formed the laminated mat. Until more microfossils are found in the Gamohaan and Frisco microbialites, constraints on the constituent microbes must come from morphological evaluation of the microbialites.

An important constraint on microbe behavior is provided by the simultaneous growth of supports and laminated mat. These two features have different characteristics suggesting that they may have been formed by different microbial communities. A difference in microbial composition of the supports and mats is consistent with observations of C. weedii. In particular the more strongly phototactic P. tenue var. granuliferum are more abundant in the peaks of the C. weedii cones whereas C. aurantiacus are preferentially in the valleys between them. Thus, different microbial responses can segregate species of microbes that live in the same environment (Walter, et al., 1976). This provides an analog for the different geometries of the supports and the laminated mat. As discussed earlier, the conical morphology of *C. weedii* may be due to the phototactic behavior of a single cyanobacteria (Walter, et al., 1976). In the Gamohaan and Frisco microbialites, however, draping of laminae over the supports seems to generate the conical morphology. Since some of the supports grew downward from overhangs, the supports probably were not formed by phototactic microbes. If formation of the supports was due to a phototactic response, supports would only grow upward, toward the light. It is possible that a chemotactic response could produce structures similar to those produced by phototactic behavior. If so, the supports could have grown in the direction of bulk solution which contained a necessary nutrient or growth component. Chemotactic behavior may not be able to account for all of the features seen in plumose structures, and further documentation of the morphology of plumose structures is necessary.

If growth of the supports is independent of phototactic responses, the microbialites did not necessarily contain photosynthetic organisms. Simonson, et al. (1985) interpreted similar deposits in the Hamersley basin as chemosynthetic rather than photosynthetic based on stratigraphically inferred water depths of 100's m for their deposition. Although there are no data from the Gamohaan and Frisco formations which demand water depths that would eliminate photosynthetic activity (Chapter 4), it is similarly difficult to discount the possibility that the microbial communities were entirely chemosynthetic.

## ROLE OF MICROBIAL MATS IN CARBONATE PRECIPITATION

The Gamohaan and Frisco microbialites contain abundant *in situ* precipitated carbonate and the remnants of well-developed microbial mats. The geometrical arrangement of the cements, mat, and supports provides the opportunity to address an extremely impor-

tant aspect of microbialite (and stromatolite) growth: the biological or abiotic origin of precipitated carbonate.

### *Mechanisms of Carbonate Precipitation*

Recent advances in our understanding of the role of biological processes in carbonate precipitation have been extensively discussed and summarized in a number of books (Westbroek and de Jong, 1982; Leadbeater and Riding, 1986; Lowenstam and Weiner, 1989; Simkiss and Wilbur, 1989; Riding, 1991). These discussions illustrate the wide range of processes that affect carbonate precipitation and the complexity of interactions between biological and abiotic chemistry. Calcification in and on organisms can be the result of enzymatic calcification of skeletons, biologically induced changes in environmental chemistry that result in precipitation, or physio-chemical precipitation due to the saturation state of the environment. Sometimes the role of biological processes is clear. For example, the process of macroscopic calcification resulting in bones and shells is controlled biologically by specialized enzymes that can precipitate carbonate in undersaturated environments or by molecular frameworks that regulate the location and morphology of precipitation (e.g. Degens, 1979; Weiner, et al., 1982; Lowenstam and Weiner, 1989; Simkiss and Wilbur, 1989 and references therein). In contrast, carbonate coatings on bacteria and cyanobacteria result from a complex interaction of biotic and abiotic processes, and cellular controls on precipitation, if present, are not obvious (e.g. Lowenstam and Weiner, 1982, 1989; Simkiss and Wilbur, 1989; Pentecost, 1991).

Various metabolic processes (such as $CO_2$-fixing reactions, nitrate reduction, sulfate reduction, and release on ammonia) can induce precipitation if they cause the local extracellular solubility product to be exceeded (Simkiss and Wilbur, 1989) as demonstrated by various experiments. For example, cultures of the cyanobacteria *Synechococcus* produced calcite, magnesite, and gypsum precipitates in filtered natural alkaline lake water, whereas sterilized cultures did not (Thompson and Ferris, 1990). In another experiment, cultures inoculated with live bacteria produced abundant aragonite or calcite crystals whereas those inoculated with sterilized bacteria did not yield precipitates (Buczynski and Chafetz, 1991). In some cases, careful observations of natural systems also suggest a biological role in precipitation. For example, some cyanobacteria contain ordered crystals with morphologies inconsistent with abiotic precipitation suggesting a strong biological influence in precipitation (e.g. Pentecost, 1978; Lowenstam and Weiner, 1982). Pentecost (1991) interprets diffuse bands of calcite in the polysaccharide gel produced by colonies of the fresh water cyanobacteria *Rivularia haematites* as a crystallization product of photosynthetically induced $Ca^{2+}$ and $CO_3^{2-}$ gradients in the gel. In contrast, he interprets dense bands produced

during winter lulls in growth as predominantly abiotic precipitates since photosynthetic rates were low (Pentecost, 1991). (Additional evidence for bacterial and cyanobacterial influences on carbonate precipitation can be found in Golubic (1973), Monty (1976), and Fairchild (1991) among others.) Similarly, the abundance of carbonate cements in environments lacking evidence for significant microbial involvement demonstrates that abiotic precipitation also occurs (e.g. Schroeder, 1972; Schmidt, 1977; Kendall, 1985; Ross, 1991 for examples of abiotic marine cementation).

Microbial communities may also enhance or inhibit the nucleation of minerals on their cell walls or the gelatinous coating excreted by mats. In general, cell membranes have complex charge distributions and provide specific binding sites for various ions (e.g. Jain, 1988), but no detailed studies have been performed on the role of these factors in affecting nucleation of carbonate on bacterial or cyanobacterial sheaths (Pentecost, 1991). Theoretically, a specific distribution of bound $Ca^{2+}$ determined by the structures of microbial sheaths could promote the nucleation of calcite (Simkiss and Wilbur, 1989; Pentecost, 1991). In contrast, several organic compounds have been identified that inhibit the nucleation of calcite, including poly(meta)phosphates, phosphonates, phosphate esters, oththophosphates, polyphenols, and a range of polysaccharides (Pentecost, 1991 and references therein). Both cell walls and the gelatinous coatings on mats contain many different polysaccharides (Brock and Madigan, 1988) some of which may inhibit calcite nucleation. Thus, some microbes could have the ability to inhibit nucleation of calcite on their cell walls or on the mat in general.

The difficulty of distinguishing biological influences are magnified when attempts are made to evaluate the role of microbes in the precipitation of ancient carbonate deposits since the processes that formed the rock are no longer active and have to be inferred from preserved morphological and compositional attributes. In some cases, it is possible to address the problem by comparing the composition of the rock containing the microbial communities to that of the surrounding environment. For example, some stromatolites that are surrounded by siliciclastic detritus consist predominantly of carbonate suggesting a precipitated origin for the carbonate (Serebryakov and Semikhatov, 1974; Hoffman, 1976; Horodyski, 1976; Fairchild, 1991). However, unless the surrounding sediment is free of precipitated carbonate, the biological role could be the exclusion of detrital sediment rather than the inducement of carbonate precipitation. In most precipitated stromatolites, it is extremely difficult if not impossible, to distinguish between precipitates formed primarily by biological processes and those due to abiotic precipitation. Thus, few studies have addressed this question without assuming a strong biological influence on carbonate precipitation. However, microbialites in the Gamohaan Formation contain specific cross-cutting

geometries among precipitated carbonate, remnants of microbial mats, and supports that constrain the role of microbial processes in carbonate precipitation.

### *Gamohaan Microbialites*

The correlation between an abundance of herringbone calcite and a lack of mat on the scale of individual microbialite structures and beds of microbialites (see above and Chapter 4) is also seen on the scale of individual laminae and supports: Herringbone calcite preferentially precipitated on supports over laminated mat. Several observations illustrate this difference in calcite precipitation: 1) The proportion of herringbone calcite within an individual microbial structure is higher near supports than in mat-rich areas. Often, herringbone calcite is concentrated within about 5 mm of the support, and no herringbone calcite is present in the mat-rich areas. Other microbialites contain some herringbone calcite in mat-rich areas, but most of it precipitated on the supports (Figure 3-21). 2) Growth banding in herringbone calcite shows that the herringbone calcite nucleated on the supports and grew outward from them. Banding is parallel to the orientation of the support (Figures 3-21 and 3-22). (Herringbone crystal banding rather than growth banding is visible in Figures 3-21 and 3-22, but it is parallel to growth banding at distances of a millimeter and larger; see Chapter 5.) Crystal orientations and optical axis rotations confirm that herringbone calcite grew outward from the supports. 3) Herringbone calcite is often truncated against mat near the supports (Figures 3-21 and 3-22). Where the mat approaches the support, it is perpendicular to herringbone banding. After several bands of herringbone calcite abut the mat, the mat bends upward 90° and runs parallel to herringbone banding. The part of the mat that is oriented parallel to the support and herringbone banding was encased in the herringbone calcite coating. Herringbone calcite did not nucleate on horizontally oriented parts of the mat, however, since crystal textures all indicate that herringbone calcite continued to grow outward and not upward at the mat surface. Sometimes mat cut obliquely across herringbone calcite banding at steep angles (Figure 3-21).

The abundance of herringbone calcite near supports, the support-parallel banding in herringbone calcite, and the abutment of herringbone calcite layers against mat suggest that herringbone calcite preferentially grew off supports rather than mat. Even where mat is surrounded by herringbone calcite, the growth direction of the herringbone calcite coating and the lack of herringbone calcite on mat away from supports suggests that herringbone calcite did not nucleate off of the mat. Rather, it encased mat that was present at a pre-existing precipitation front. In some samples with very high abundance of herringbone calcite, herringbone calcite did grow on mat. It is concentrated on specific surfaces (Figure 3-21) or on the sides of irregular columnar microbialites (Figure 3-23). The precipitation of

herringbone calcite on mats in samples with high percentages of herringbone calcite suggests that in cases where abundant herringbone calcite precipitation was favored, the preference of herringbone calcite to nucleate on supports was overcome and herringbone calcite grew off mat surfaces as well. Herringbone calcite still showed a preference for growth off mat composing the irregular columnar microbialites over growth off better laminated mat in troughs (Figure 3-23).

### *Interpretation*

The preferential precipitation of calcite on supports rather than mats may be due to differences in the ability of the supports and the mats to induce precipitation, or to differences in ability of crystals to nucleate on supports and mat. Herringbone calcite layers coating the supports often are thicker that 5 mm (Figures 3-21 and 3-22). Thus, if the supports induced the precipitation of herringbone calcite through metabolic processes, the processes would have to affect the chemical properties of the surrounding water for several millimeters. In previously reported cases of microbially induced precipitation, calcite nucleation and growth occurred on cell walls (Thompson and Ferris, 1990; Buczynski and Chafetz, 1991), in the gelatinous coating secreted by the microbes (Pentecost, 1991), within the mat (Chafetz and Buczynski, 1992; Knoll, et al., 1993), or in an artificial gel (Buczynski and Chafetz, 1991). The reduced rates of chemical transport in gelatinous media may help maintain the chemical changes caused by the microbes, and microbially-induced precipitation is less likely in surrounding water (Pentecost, 1991). Gelatinous coatings secreted by 100-200 μm-thick microbial communities are rarely several millimeters thick suggesting that it would be difficult for microbes in the supports to induce the precipitation of millimeter-thick layers of herringbone calcite. Despite these difficulties, if microbes in the supports did affect the chemistry of water to the extent that they induced the precipitation, herringbone calcite would have precipitated off both the supports and the mats within the region of modified chemistry *in the absence of calcite nucleation inhibition by the mat.* This is inconsistent with the observation that millimeter thick layers of herringbone calcite abut against and lap onto mat, but did not nucleate on it (Figure 3-22). Thus, the inducement of herringbone calcite precipitation by microbes in the supports is not sufficient to explain the preferential precipitation of herringbone calcite on the supports over the mat.

Calcite nucleation differences on the supports and mats can explain the differences in the location of herringbone calcite precipitation. Two variations are possible: First, calcite nucleation may be promoted by some aspect (metabolic activity, surface charge distribution, or surface molecular structure) of the supports, but not by the mat. In this case, herringbone calcite would require the special characteristics of the supports to nucleate, but

growth would be controlled by abiotic processes. The lack of herringbone calcite coatings on the mat would be due to the lack of enhanced nucleation sites. This interpretation implies that herringbone calcite precipitation would not occur without the presence of the supports. The abundance of herringbone calcite beds lacking microbial textures implies that it precipitated even in the absence of supports. The second variation in nucleation differences is a (metabolic or surficial) inhibition of herringbone calcite nucleation by the mat. In this case, nucleation of herringbone calcite would occur on all surfaces lacking characteristics that specifically inhibited crystal nucleation, and precipitation could be abiotic, although induced precipitation by the supports is not excluded. This interpretation is supported by the large volume of precipitated calcite associated with the microbialites which suggests that herringbone calcite precipitation was a background sedimentary process promoted by the supersaturated state of ambient seawater (Chapter 4). Thus, the inhibition of precipitation by the mat is favored over the enhancement of nucleation by the supports as the most important factor determining the location of herringbone calcite precipitation.

Inhibition of calcite nucleation by the mat during growth is consistent with the observation that mat is often coated by cements. Bladed and blocky calcite nucleated on the mat during very early burial, after the interval of most active mat growth. Thus, nucleation inhibition by the mat could have been reduced by the decay of inhibiting substances or by a change in metabolic processes of the mat after burial. The growth of herringbone calcite on mat may have occurred only on old mat surfaces that had also lost their ability to inhibit calcite nucleation or decomposition enhanced nucleation (e.g. Chafetz and Buczynski, 1992), but no observations have specifically implied this interpretation. Alternatively, the inhibiting effect of the mat may have been too weak to prohibit the nucleation of herringbone calcite under all circumstances. If seawater surrounding the mat was supersaturated enough, nucleation of calcite could have occurred on the mat despite inhibiting effects. This explanation is consistent with the abundance of herringbone calcite on mat in irregular columnar microbialites where the mat is less well laminated than it is in the herringbone calcite-poor troughs. A small difference in the microbial community may have reduced the inhibiting effect in columnar microbialites versus mat in troughs.

## CONCLUSIONS

The Gamohaan and Frisco microbialites formed from finely laminated microbial mat, supports of microbial origin, and predominantly abiotic calcite cements. The biogenic interpretation for both mat and supports suggests that the morphological variations in the microbialites are due to differences in the composition and behavior of the microbial com-

munities. The presence of two contemporaneous yet distinct microbial communities and the morphological intricacy of some of the microbialites suggest that late Archean microbial communities were capable of complex behavior and possibly ecological zonation. The presence of similar microbialites in other Archean carbonates imply that such communities developed prior to 2.7 Ga (Hofmann and Masson, 1994).

Calcite precipitation appears to have played no role in directly determining the morphology of the microbialites. In the absence of supports and mat, herringbone calcite formed planar beds. Microbial communities may have been sensitive to the rate of calcite precipitation, however, and changes in the calcite saturation state of seawater may have influenced the composition of the microbial communities, indirectly affecting microbialite morphology. Mats may have played an important role in the location of herringbone calcite precipitation by inhibiting the nucleation of calcite. The inverse correlation between the abundance of herringbone calcite and the presence of well developed mat at scales ranging from sub-millimeter to regional (see Chapter 4) suggests that conditions promoting the growth of one did not favor growth of the other. This observation contradicts the standard dogma that microbial mats induce carbonate precipitation. Although this may be true in many cases, the mat in the Gamohaan and Frisco formations clearly is inimical to abundant herringbone calcite precipitation. Thus, microbial growth and carbonate precipitation appear to have been decoupled. Microbial communities shaped the microbialites, but depended on abiotic precipitation to preserve them. Without contemporaneous lithification, the delicate microbial structures would not have survived early burial compaction, and without the microbial communities, herringbone calcite would have formed flat-lying beds.

## REFERENCES


Aitken, J. D., 1967. Classification and environmental significance of cryptalgal limestones and dolomites, with illustrations from the Cambrian and Ordovician of southwestern Alberta. Journal of Sedimentary Petrology, v. 37, p. 1163-1178.

Bertrand-Sarfati, J., 1976. An attempt to classify late Precambrian stromatolite microstructures *in* Stromatolites (M. R. Walter, ed.). Developments in Sedimentology, 20, p. 251-259.

Bertrand-Sarfati, J. and A. Moussine-Pouchkine, 1985. Evolution and environmental conditions of *Conophyton-Jacutophyton* associations in the Atar Dolomite (Upper Proterozoic, Mauritania). Precambrian Research, v. 29, p. 207-234.

Beukes, N. J., 1980. Stratigrafie en litofasies van die Campbellrand-subgrop van die Proterofitiese Ghaapgroep, noord-Kaapland. Transactions of the Geological Society of South Africa, v. 83, p. 141-170.

Beukes, N. J., 1987. Facies relations, depositional environments and diagenesis in a major early Proterozoic stromatolitic carbonate platform to basinal sequence, Campbellrand Subgroup, Transvaal Supergroup, southern Africa. Sedimentary Geology, v. 54, p. 1-46.

Brock, T. D. and M. T. Madigan, 1988. Biology of Microorganisms. Prentice Hall, Englewood Cliffs, N.J. 835 p.

Buczynski, C. and H. S. Chafetz, 1987. Siliciclastic grain breakage and displacement due to carbonate crystal growth: an example from the Lueders Formation (Permian) of north-central Texas, U.S.A. Sedi-

mentology, v. 34, p. 837-843.
Buczynski, C. and H. S. Chafetz, 1991. Habit of bacterially induced precipitates of calcium carbonate and the influence of medium viscosity on mineralogy. Journal of Sedimentary Petrology, v. 61, p. 226-233.
Buick, R., 1992. The antiquity of oxygenic photosynthesis: Evidence from stromatolites in sulphate-deficient Archean lakes. Science, v. 255, p. 74-77.
Buick, R., J. S. R. Dunlop and D. I. Groves, 1981. Stromatolite recognition in ancient rocks: An appraisal of irregularly laminated structures in an Early Archaean chert-barite unit from North Pole, Western Australia. Alcheringa, v. 5, p. 161-181.
Buick, R., D. I. Groves and J. S. R. Dunlop, 1995. Abiological origin of described stromatolites older than 3.2 Ga - Comment. Geology, v. 23, p. 191.
Button, A., 1973. The stratigraphic history of the Malmani dolomite in the eastern and north-eastern Transvaal. Transactions of the Geological Society of South Africa, v. 76, p. 229-247.
Chafetz, H. S. and C. Buczynski, 1992. Bacterially induced lithification of microbial mats. Palaios, v. 7, p. 277-293.
Cloud, P. E., 1942. Notes on stromatolites. American Journal of Science, v. 240, p. 363-379.
Degens, E. T., 1979. Why to organisms calcify? Chemical Geology, v. 25, p. 257-269.
Donaldson, J. A., 1976. Paleoecology of Conophyton and associated stromatolites in the Pre-Cambrian Dismal Lakes and Rae Groups, Canada *in* Stromatolites (M. R. Walter, ed.). Developments in Sedimentology, 20, p. 523-534.
Fairchild, I. J., 1991. Origins of carbonate in Neoproterozoic stromatolites and the identification of modern analogues. Precambrian Research, v. 53, p. 281-299.
Ginsburg, R. N., 1991. Controversies about stromatolites: Vices and virtues *in* Controversies in Modern Geology. Academic Presss Limited, p. 25-36.
Golubic, S., 1973. The relationship between bule-green algae and carbonate deposits *in* The Biology of Blue-Green Algae (N. G. Carr and B. A. Whitton, eds.). University of California Press, Berkeley. 9, p. 434-472.
Hoffman, P., 1976. Environmental diversity of middle Precambrian stromatolites *in* Stromatolites (M. R. Walter, eds.). Developments in Sedimentology, 20, p. 599-611.
Hofmann, H. J. and M. Masson, 1994. Archean stromatolites from Abitibi greenstone belt, Quebec, Canada. Geological Society of America Bulletin, v. 106, p. 424-429.
Horodyski, R. J., 1976. Stromatolites from the Middle Proterozoic Altyn Limestone, Belt Supergroup, Glacier National Park, Montana *in* Stromatolites (M. R. Walter, ed.). Developments in Sedimentology, 20, p. 585-597.
Horodyski, R. J., 1977. *Lyngbya* mats at Laguna Mormona, Baja California, Mexico: Comparison with Proterozoic stromatolites. Journal of Sedimentary Petrology, v. 47, p. 1305-1320.
Jain, M. K., 1988. Introduction to Biological Membranes. Wiley & Sons, New York. 423 p.
Kendall, A. C., 1985. Radiaxial fibrous calcite: A reappraisal *in* Carbonate Cements (N. Schneidermann and P. M. Harris, eds.). S.E.P.M., Special Publication No. 36, Tulsa. p. 59-78.
Kennard, J. M. and N. P. James, 1986. Thrombolites and stromatolites: Two distinct types of microbial structures. Palaios, v. 1, p. 492-503.
Klein, C., N. J. Beukes and J. W. Schopf, 1987. Filamentous microfossils in the early Proterozoic Transvaal Supergroup: Their morphology, significance and paleoenvironmental setting. Precambrina Research, v. 36, p. 81-94.
Knoll, A. H., I. J. Fairchild and K. Swett, 1993. Calcified microbes in Neoproterozoic carbonates: Implications for our understanding of the Proterozoic/Cambrian transition. Palaios, v. 8, p. 512-525.
Krumbein, W. E., 1983. Stromatolites — The challenge of a term in space and time. Precambrian Research, v. 20, p. 493-531.
Leadbeater, B. S. C. and R. Riding, 1986, editors. Biomineralization in Lower Plants and Animals: Oxford, Clarendon, 401 p.
Logan, B. W., R. Rezak and R. N. Ginsburg, 1964. Classification and environmental significance of algal stromatolites. Journal of Geology, v. 72, p. 68-83.
Lowe, D. R., 1994. Abiological origin of described stromatolites older than 3.2 Ga. Geology, v. 22, p. 287-390.
Lowe, D. R., 1995. Abiological origin of described stromatolites older than 3.2 Ga - Reply. Geology, v. 23,

p. 191-192.
Lowenstam, H. A. and S. Weiner, 1982. Mineralization by organisms and the evolution of biomineralization *in* Biomineralization and Biological Metal Accumulation (P. Westbroek and E. W. deJong, eds.). Reidel Publishing Co., Boston. p. 191-203.
Lowenstam, H. A. and S. Weiner, 1989. On Biomineralization. Oxford University Press, New York. 324 p.
Maliva, R. G., 1989. Displacive calcite syntaxial overgrowths in open marine limestones. Journal of Sedimentary Petrology, v. 59, p. 379-403.
Monty, C. L. V., 1973. Precambrian background and Phanerozoic history of stromatolitic communities, an overview. Annales de la Société Géologique de Belgique, v. 96, p. 585-624.
Monty, C. L. V., 1976. The origin and development of cryptalgal fabrics *in* Stromatolites, Developments in Sedimentology 20 (M. R. Walter, eds.). Elsevier, Amsterdam. p. 193-250.
Pentecost, A., 1978. Blue-green algae and freshwater carbonate deposits. Proceedings of the Royal Society of London, v. B200, p. 43-61.
Pentecost, A., 1991. Calcification processes in algae and cyanobacteria *in* Calcareous Algae and Stromatolites (R. Riding, eds.). Springer-Verlag, Berlin. p. 3-20.
Pratt, B. R. and N. P. James, 1982. Cryptalgal-metazoan bioherms of Early Ordovician age in the St. George Group, western Newfoundland. Sedimentology, v. 29, p. 543-569.
Riding, R., 1991, Calcareous Algae and Stromatolites: Berlin, Springer-Verlag, 571 p.
Ross, D. J., 1991. Botryoidal high-magnesium calcite marine cements from the Upper Cretaceous of the Mediterranean region. Journal of Sedimentary Petrology, v. 61, p. 349-353.
Saigal, G. C. and E. K. Walton, 1988. On the occurrence of displacive calcite in Lower Old Red Sandstone of Carnoustic, eastern Scotland. Journal of Sedimentary Petrology, v. 58, p. 131-135.
Schmidt, V., 1977. Inorganic and organic reef growth and subsequent diagenesis in the Permian Capitan Reef Complex, Guadalupe Mountains, Texas, New Mexico *in* Uper Guadalupian Facies, Permian Reef Complex, Guadalupe Mountains New Mexico and West Texas: 1977 Field Conference Guidebook (M. E. Hileman and J. J. Mazzullo, eds.). S.E.P.M., Permian Basin Section. Publication 77-16, p. 93-131.
Schopf, J. W., D. Z. Oehler, R. J. Horodyski and K. A. Kvenvolden, 1971. Biogenicity and significance of the oldest known stromatolites. Journal of Paleontology, v. 45, p. 477-485.
Schroeder, J. H., 1972. Fabrics and sequences of submarine carbonate cements in Holocene Bermuda cup reefs. Geologische Rundschau, v. 61, p. 708-730.
Semikhatov, M. A., 1976. Experience in stromatolite studies in the U.S.S.R. *in* Stromatolites (M. R. Walter, eds.). Elsevier, New York. p. 337-358.
Semikhatov, M. A., C. D. Gebelein, P. Cloud, S. M. Awramik and W. C. Benmore, 1979. Stromatolite morphogenesis—progress and problems. Canadian Journal of Earth Science, v. 16, p. 992-1015.
Serebryakov, S. N. and M. A. Semikhatov, 1974. Riphean and recent stromatolites: A comparison. American Journal of Science, v. 274, p. 556-574.
Simkiss, K. and K. M. Wilbur, 1989. Biomineralization: Cell Biology and Mineral Deposition. Academic Press, Inc., San Diego. 338 p.
Simonson, B. M., 1985. Sedimentological constraints on the origins of Precambrian iron-formations. Geological Society of America Bulletin, v. 96, p. 244-252.
Stanley, H. E., 1991. Fractals and multifractals: The interplay of physics and geometry *in* Fractals and Disordered Systems (A. Bunde and S. Havlin, eds.). Springer-Verlag, Berlin. p. 1-49.
Sumner, D. Y. and S. A. Bowring, in press. U-Pb geochronologic constraints on deposition of the Campbellrand Subgroup, Transvaal Supergroup, South Africa. Precambrian Research.
Sumner, D. Y. and J. P. Grotzinger, in review. Herringbone calcite. Journal of Sedimentary Research.
Thompson, J. B. and F. G. Ferris, 1990. Cyanobacterial precipitation of gypsum, calcite, and magnesite from natural alkaline lake water. Geology, v. 18, p. 995-998.
Walter, M. R., 1976, editor. Stromtolites: Amsterdam, Elsevier, 790 p.
Walter, M. R., 1983. Archean stromatolites: Evidence of the Earth's earliest benthos *in* Earth's Earliest Biosphere: Its origin and evolution (J. W. Schopf, ed.). Princeton University Press, Princeton. p. 187-213.
Walter, M. R., J. Bauld and T. D. Brock, 1976. Microbiology and morphogenesis of columnar stromatolites (*Conophyton, Vacerrilla*) from hot springs in Yellowstone National Park *in* Stromatolites (M. R.

Walter, ed.). Elsevier, Amsterdam. p. 273-310.
Weiner, S., W. Traub and H. A. Lowenstam, 1982. Organic matrix in calcified exoskeletons *in* Biomineralization and Biological Metal Accumulation (P. Westbroek and E. W. deJong, eds.). Reidel Publishing Co., Boston. p. 205-224.
Westbroek, P. and E. W. de Jong, 1982, Biomineralization and Biological Metal Accumulation: Boston, Reidel Publishing Co., 533 p.

# CHAPTER 4: LITHOFACIES AND STRATIGRAPHY OF THE GAMOHAAN AND FRISCO FORMATIONS

## ABSTRACT

The correlative ~2520 Ma Gamohaan and Frisco formations represent a partial depositional sequence (TST) whose lower sequence boundary is overlain by carbonate peritidal and subtidal lithofacies that pass upward into very deep subtidal iron-formation at the top. The lithofacies transitions demonstrate that the Gamohaan and Frisco formations were deposited during a transgression that terminated carbonate production, resulting in drowning of the Campbellrand-Malmani platform. Four microbialite assemblages form the bulk of the deep subtidal lithofacies. The microbialites are associated with abundant sea floor-encrusting and void-filling calcite, especially in the Gamohaan Formation, where marine precipitates compose more than 35% of the rocks in 40 m of section. Sea floor-encrusting precipitated beds in this interval are up to 30 cm thick and are laterally continuous for the entire 140 x 50 km of good stratigraphic control. The abundance of precipitated carbonate and the lateral continuity of individual beds demonstrate that deep subtidal seawater was supersaturated with respect to calcite, and carbonate precipitation was controlled by regional chemical gradients as opposed to locally enhanced precipitation.

Basinal equivalents of the Gamohaan and Frisco formations contain interbeds of siderite and oxide facies iron-formation demonstrating that calcite and iron-formation deposition occurred simultaneously in different depositional environments of the platform. The difference in mineral precipitation with depth can be accounted for by a gradient in $Fe^{2+}$ concentration: As the concentration of $Fe^{2+}$ increased with depth due to decreasing oxygen concentration, the water became supersaturated with respect to siderite and undersaturated with respect to calcite.

## INTRODUCTION

The oceans have played a critical role in the cycling of $CO_2$ throughout Earth history (e.g. Des Marais, 1985; Volk and Hoffert, 1985; Marshall, et al., 1988). The deposition of carbonates in shallow marine waters (and in the deep sea after evolution of calcareous plankton) is an important sink for atmospheric $CO_2$. Since the evolution of carbonate secreting organisms, carbonate precipitation has been dominated by the enzymatic excretion of calcite, Mg-calcite, and aragonite. Prior to their evolution, however, carbonate precipitation was either abiotic or induced by extracellular chemical changes. Thus, during Precam-

brian time, the mechanisms of carbonate precipitation and, thus, one of the important controls on atmospheric $CO_2$ was controlled by different chemical processes. Attempts to understand these changes and their effects on ocean chemistry have led to the development of a wide range of models. Many models of Archean seawater are based on processes in modern oceans. For example, Walker (1983) and Holland (1984) propose that the concentrations of dominant cations and anions in seawater have been fairly constant through time, with the exceptions of oxygen and iron. In contrast, Kempe and Degens (1985) propose that oceans prior to ~800 Ma were dominated by bicarbonate rather than chlorine, resulting in a "soda ocean". Their model requires pH of 9 to 11 and low atmospheric $CO_2$. Grotzinger and Kasting (1993) propose less dramatic change with oceans containing approximately the same pH as modern oceans (pH=8.1), higher atmospheric $CO_2$, but an increase in bicarbonate such that $[HCO_3^-]>2[Ca^{2+}]$ in seawater. Sumner and Grotzinger (in review b) propose that $Fe^{2+}$ in seawater allowed maintenance of high saturation states and affected the location of calcite precipitation. Constraints on models such as these can be obtained by careful studies of the field and petrographic relationships in ancient marine sediments.

The Gamohaan and Frisco formations, Transvaal Supergroup, South Africa, provide an excellent opportunity to address several important aspects of Archean ocean chemistry: They contain deposits that reflect deep subtidal carbonate precipitation processes, unaffected by the influx of siliciclastic sediment or carbonate grainstones. In addition, the upward gradation from carbonate to iron-formation deposition provides constraints on changes in seawater chemistry with depth in Archean oceans.

### *Previous Work*

The Gamohaan and Frisco formations are correlative units outcrop over 800 km at the tops of the Campbellrand and Malmani subgroups, respectively, and were deposited during a transgression that resulted in drowning of the carbonate platform (Figures 4-1, 4-2, and 4-3; Chapter 2; Beukes, 1980, 1987). Correlative rocks south of the Griquatown Fault Zone consist of slope lithofacies that are unassigned to a specific formation (core BD2, Figures 4-1 and 4-3), and basinal lithofacies composing part of the Naute Shale or Kuruman Iron Formation (Chapter 2; Beukes, 1987).

In previous studies, the Gamohaan and Frisco formations have been studied separately. Button (1973) presented the basic stratigraphy of the Frisco Formation which he called the Mixed Zone of the Malmani Subgroup. He reported average thicknesses as well as limestone, dolostone, shale, and Fe-rich sediment distributions. A regional unconformity was identified at the base of the Frisco Formation associated with variable development of chert breccia and carbonaceous shale. Ripples, ooids, cross stratification, and edgewise

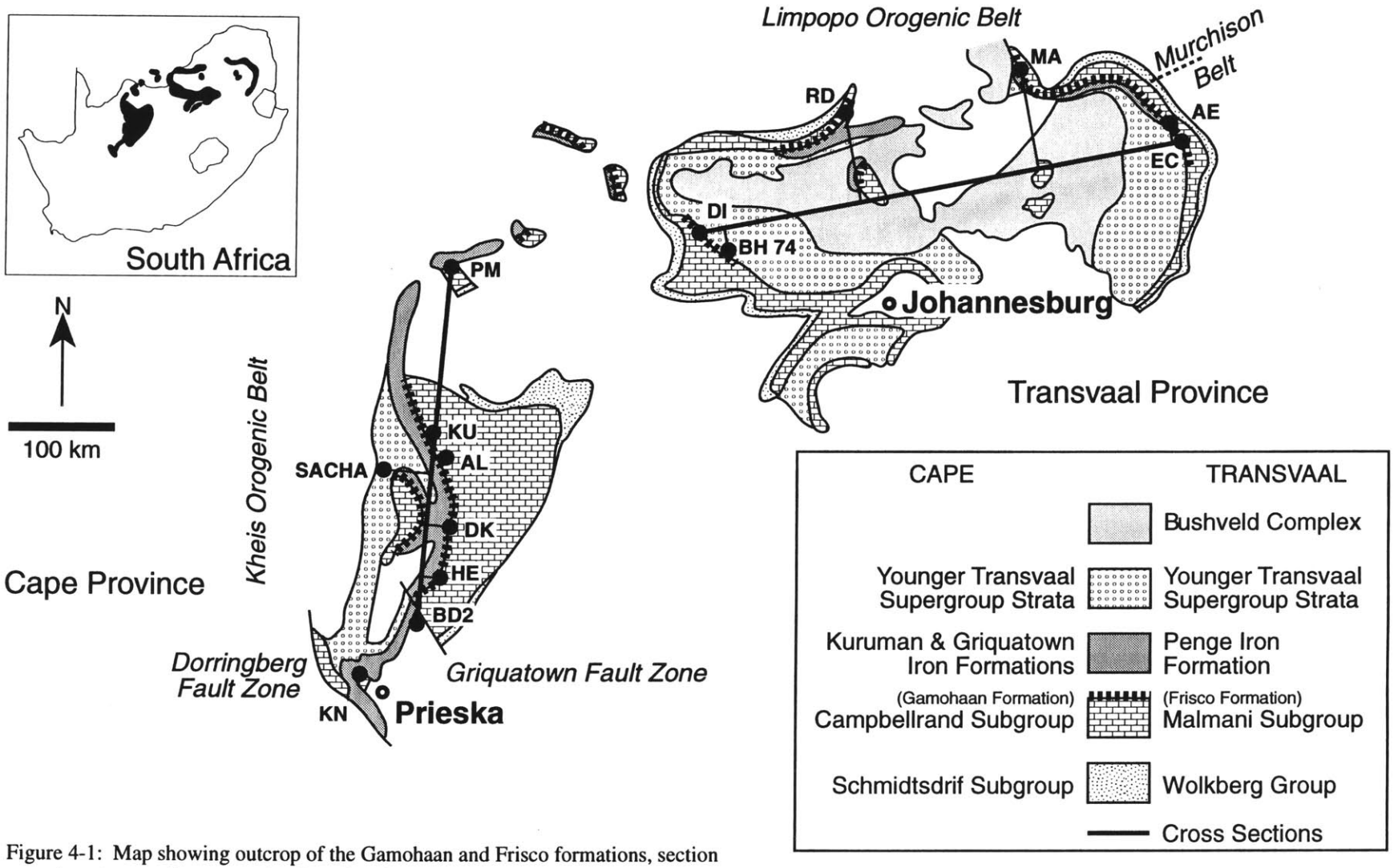


Figure 4-1: Map showing outcrop of the Gamohaan and Frisco formations, section locations, and cross section lines for Figures 4-2 and 4-3. The Crocodile River Fragment is within the Bushveld Complex south of section RD. After Beukes (1983).

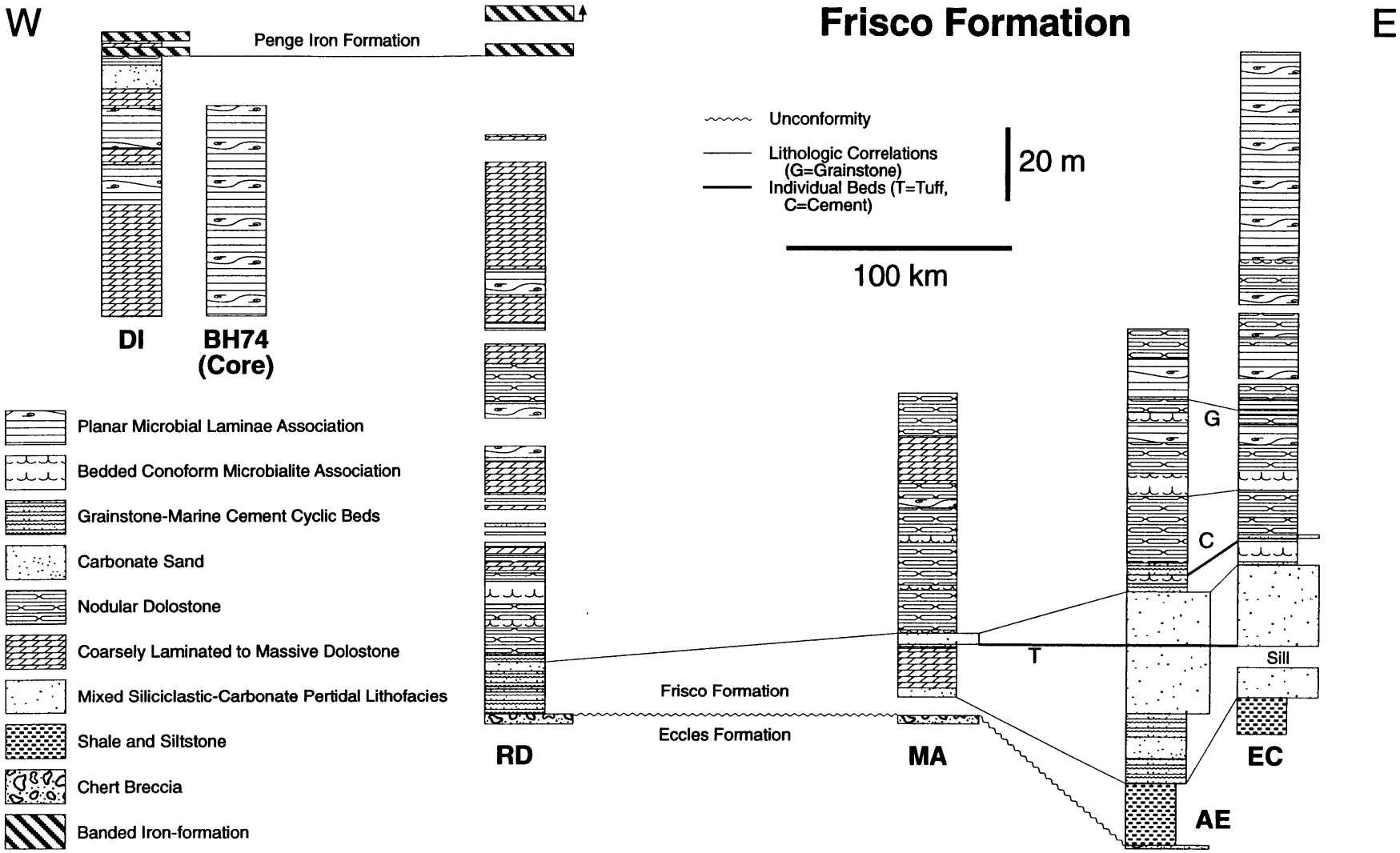


Figure 4-2: Cross section of the Frisco Formation. The cross section datums are a bed of accretionary lapilli ("T"; Figure 4-5) in the east and the base of the Penge Iron Formation in the west. Section line shown in Figure 4-1.

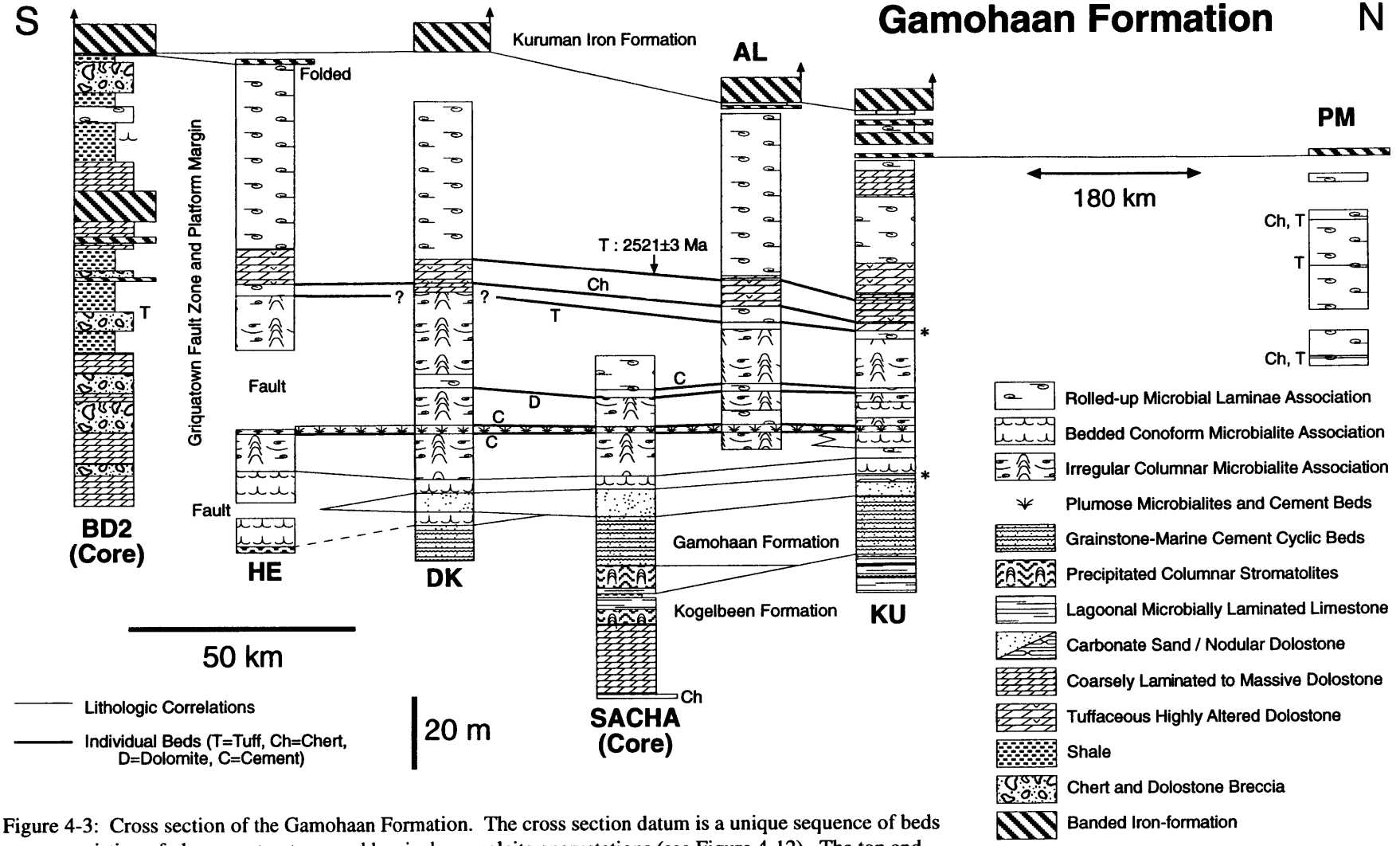


Figure 4-3: Cross section of the Gamohaan Formation. The cross section datum is a unique sequence of beds consisting of plumose structures and herringbone calcite encrustations (see Figure 4-12). The top and bottom of the 40 m used to estimate the proportion of *in situ* precipitated calcite are marked by "*" to the right of section KU. Section line shown in Figure 4-1.

conglomerates were noted near the base of the formation and on this basis, it was inferred that the entire Frisco Formation was deposited in shallow depositional environments (Button, 1973). The transition from carbonate deposition to iron-formation deposition of the overlying Penge Iron Formation is gradational as illustrated by several iron-rich horizons developed within the Frisco Formation (Button, 1976). No other published studies address the regional stratigraphy of the Frisco Formation, although a log of the Frisco Formation was presented by Hartzer (1989) for the highly metamorphosed Crocodile River Fragment, an inlier within the Bushveld Complex (Figure 4-1).

The stratigraphy of the Gamohaan Formation was presented by Beukes (1980, 1987). He interpreted the Gamohaan Formation as a deepening-upward succession that passed gradationally into the Kuruman Iron Formation (Beukes, 1987; Klein and Beukes, 1989; Beukes, et al., 1990). Beukes (1987) also recognized the lateral continuity of lithofacies within the Gamohaan Formation as well as the continuity of single beds for 10's to 100's of kilometers. This work provides a solid framework for more detailed studies of the lithofacies architecture within the Gamohaan Formation. Hälbich, et al. (1992) also studied the transition from the Gamohaan Formation to the Kuruman Iron Formation and concluded that it was characterized by local variations in depositional environment that resulted in discontinuous deposition even in nearby sections. However, they did not correct their stratigraphic sections for tectonic duplication and omission although they discussed the problem throughout their paper and identified several areas with specific problems. On the basis of limited geochemical data, Hälbich, et al. (1992) also suggested that the Gamohaan Formation to Kuruman Iron Formation transition represents a shallowing-upward sequence with increasing fresh water influx, contrary to the conclusions reached here (see also Chapter 2; Beukes, 1987).

## LITHOFACIES

Many lithofacies of the Gamohaan and Frisco formations contain an abundance of calcite that precipitated on the sea floor with cement-like crystallographic textures (herein called "precipitates"; Table 4-1). Many peritidal and subtidal deposits contain laterally continuous beds that consist solely of herringbone calcite (Chapter 5; Sumner and Grotzinger, in review a). Other lithofacies, such as nodular dolostone, coarsely bedded to massive dolostone, shale, and breccias, contain little *in situ* precipitated marine calcite.

### *Microbialite Assemblages*

Microbialites in the Gamohaan and Frisco formations consist of three components

Table 4-1: Summary of Lithofacies Characteristics

| Lithofacies | Sedimentary Structures | "Cement" Textures | Interpreted Water Depth |
|---|---|---|---|
| Bedded Conoform Microbialite Assemblage | Conoform microbialites, rolled-up laminae, plumose microbialites; abundant marine cements | 50%* (5-100%) | Deep subtidal; shallowest microbialite assemblage |
| Planar Laminae Assemblage | Planar laminae, tented microbialites, rolled-up laminae; rare marine cements, abundant microspar | <10% (0-75%) | Deep subtidal |
| Irregular Columnar Microbialite Assemblage | Irregular columnar microbialites, rolled-up laminae, planar laminae, plumose microbialites, herringbone calcite encrustations, conoform microbialites, tented microbialites; abundant marine cements | 30% (0-100%) | Deep subtidal |
| Rolled-up Laminae Assemblage | Beds of rolled-up laminae, planar laminae, shale, conoform microbialites; rare marine cements | <5% (0-30%) | Deep subtidal; deeper than other microbialite assemblages |
| Mixed Siliciclastic-Carbonate Peritidal | Quartz sand, fine-grained volcaniclastic sediment, grainstones, precipitated calcite encrustations, hardgrounds, rare micrite, rare ooids; trough, wave ripple, current ripple, and rare hummocky cross stratification; cycles occasionally present | 5% (0-100%) | Peritidal with exposure surfaces |
| Grainstone-Precipitate Cyclic Beds | 3-10 cm beds based by grainstones, grading upwards into precipitated crusts; scoured surfaces, microbreccia, wave ripples, 3-5 cm bulbous stromatolites, m-scale giant stromatolite mounds | 50% (5-75%) | Low energy intertidal to shallow subtidal |
| Grainstone | Rare climbing ripples, low angle cross stratification, platy microbreccia, soft sediment deformation; dolomitized | 10% (0-75%) | Subtidal |
| Nodular | Elongate dolostone or limestone nodules parallel to bedding; rare rolled-up laminae. | 0% | Subtidal; below wave base |
| Tuffaceous Dolostone | Coarsely laminated dolostone, graded ash beds; concretionary domes | 0% | Diagenetic in origin; deep subtidal sediments originally |
| Chert and Dolostone Breccia | Clasts <0.1 to >20 cm; both clasts and matrix consist of chert, dolomite, and shale; clasts platy or equant, matrix massive | 0% | Platform slope |
| Coarsely Laminated to Massive Dolostone | Coarse lamination rarely preserved | 0% | Diagenetic |
| Shale | Rare ripple cross stratification or early diagenetic calcite concretions, but not both | 0% | Rippled: shallow subtidal to supratidal<br>Concretions: deep subtidal |
| Banded Iron-formation | Finely laminated siderite, chert, hematite, and/or magnetite | 0% | Deep basinal |

*Average percent of facies with preserved precipitated calcite textures. The numbers in parentheses are the minimum and maximum proportions of precipitated carbonate in single beds.

(Chapter 3): filmy laminae interpreted as the remnants of microbial mats, supports interpreted as a non-mat microbial growth structures, and calcite-filled primary voids. The filmy laminae are commonly draped over the supports creating complex microbial structures with abundant voids. These structures are classified into six end member microbialite morphologies: planar laminae, rolled-up laminae, tented microbialites, cuspate microbialites, irregular columnar microbialites, and plumose structures (Chapter 3). Beds of herringbone calcite also are present. The microbialite-rich rocks in the Gamohaan and Frisco formations are classified into four microbialite assemblages: 1) the bedded cuspate microbialite assemblage, 2) the planar-laminae assemblage, 3) the irregular columnar microbialite assemblage, and 4) the rolled-up laminae assemblage.

The *bedded cuspate microbialite assemblage* consists of interbedded cuspate microbialites, rolled-up microbial mat, and plumose structures, all forming 1-10 cm thick beds. Rare cm-thick encrusting herringbone calcite layers are also present. Roll-ups commonly contain abundant void-filling cement and show little evidence for compaction. Plumose structure beds are rare, but are laterally continuous. A high proportion of cements (50%) suggests that calcite precipitation rates were comparable to microbial accumulation rates. The first microbialites to be deposited over peritidal deposits near the base of the Gamohaan and Frisco formations consist of the bedded cuspate microbialite assemblage.

The *planar-laminae assemblage* consists of planar laminae, tented microbialites, and rolled-up laminae with <10% void-filling cements. These components are characterized by few cement-filled voids and abundant laminated mat. The planar-laminae assemblage had higher accumulation rates relative to calcite precipitation than the bedded cuspate microbialite assemblage (Chapter 3). It overlies the bedded cuspate microbialite assemblage in the Frisco Formation.

The *irregular columnar microbialite assemblage* consists of irregular columnar microbialites, trough-filling and bed-forming rolled-up and planar laminae, plumose structures, herringbone calcite beds, cuspate microbialites, and tented microbialites, in order of decreasing abundance. The most prominent beds of this assemblage are decimeter to meter-thick beds of irregular columnar microbialites. The troughs between columns are filled with rolled-up and planar laminae with less abundant tented and cuspate microbialites. Laterally continuous layers of plumose structures rarely are present within these beds. More commonly, they form individual beds like those in the bedded cuspate microbialite assemblage. This assemblage contains abundant precipitated carbonate (30%) and laminated mat. This lithofacies is present above the bedded cuspate microbialite assemblage in the Gamohaan Formation.

The *rolled-up laminae assemblage* consists of centimeter to decimeter-thick beds of

rolled-up and planar laminae with rare interbeds of shale and cuspate microbialites. Rolled-up laminae commonly have less void space preserved than in the other three assemblages and show more evidence for compaction. Interbedded shales are calcareous and carbonaceous, and may represent remnants of uncemented rolled-up and planar mat. This assemblage differs from the planar-laminae assemblage in the presence of shale and more compaction of rolled-up laminae. Void-filling cements are extremely rare (<5%). The rolled-up laminae assemblage is most abundant at the top of the Gamohaan Formation.

**Interpretation**

The delicate morphology of the microbialites (Chapter 3), the lack of evidence for scouring, and the absence of clastic carbonate all suggest a deep subtidal, sub-wave base depositional environment for the microbialite assemblages. This interpretation is supported by their stratigraphic position between intertidal and basinal lithofacies both vertically in the Gamohaan and Frisco formations, and across the platform margin throughout deposition of the underlying Campbellrand-Malmani platform (Chapter 2). The relative water depths of the four assemblages is problematic. The bedded cuspate microbialite assemblage is the first assemblage that transgresses across the platform, and thus may have been deposited in the shallowest subtidal environments. The rolled-up laminae assemblage contains the least marine cement and is interbedded with iron-formation interpreted as very deep subtidal due to its presence in basinal deposits outboard of the platform margin, suggesting the deepest depositional environment of the four assemblages. The planar laminae assemblage and the irregular columnar microbialite assemblage were probably deposited at intermediate depths. The planar laminae assemblage contains more abundant mat than the irregular columnar microbialite assemblage implying it was deposited in environments with higher microbial productivity, but since the two assemblages do not occur together, relative water depths are unknown.

### *Mixed Siliciclastic-Carbonate Peritidal Lithofacies*

This lithofacies consists of interbedded quartzite, fine-grained volcaniclastic debris, dolomitized grainstones, dolomitized marine carbonate precipitates, and rare dolomicrite beds. Quartzite beds commonly contain trough cross stratification and are mixed rarely with tuffaceous sediment. Carbonate grainstones contain current and wave ripples, other cross stratification, and rare ooids. Hardgrounds, herringbone calcite crusts, and grainstone-precipitate cyclic beds (see below) are also developed. At section MA, there are abundant giant ooids reaching a maximum diameter of 18 mm although most are ≤5 mm in diameter (Figure 4-4). The largest ooids are often surrounded by coarsely crystalline dolomite, and

when they became immobile, columnar stromatolites with the same diameter and lamination style grew upward from them (Figure 4-4). Tuffaceous shales are found throughout the lithofacies and rare beds of accretionary lapilli (Figure 4-5) and glass shards are present (Button, 1973), particularly in the northeast.

At section EC, these lithologies are arranged into meter-scale cycles (Appendix 2, Section EC) with basal erosional surfaces overlain by medium to coarse quartzite or dolomite grainstones. Upward in each cycle, the proportion of quartz decreases and carbonate increases. The cycles are capped by hardgrounds and precipitated carbonate encrustations. In other sections, these cycles are developed poorly or outcrop is not sufficient to allow identification. Rocks of the mixed siliciclastic-carbonate peritidal lithofacies are present at the base of the Frisco Formation, particularly in the eastern Transvaal.

**Interpretation**

Each cycle is interpreted to represent a transition from a supratidal-intertidal depositional environment with high sediment influx to an intertidal-shallow subtidal depositional environment with low sediment influx. The giant ooids may have formed in a lagoonal environment, although many of the smaller ooids show evidence for abundant agitation during deposition. The presence of accretionary lapilli, shard-rich ash beds, and tuffaceous shales and siltstones implies that a volcanic center was located near outcrops in the northeast although the lack of volcanic sediment in most of the carbonates indicates that supply of volcanic detritus was sporadic.

### *Grainstone-Precipitate Cyclic Lithofacies*

This lithofacies consists of 3-10 cm dolostone cyclic beds with basal light tan grainstone that grades upward into 75-90% pure precipitated crusts that are reddish brown in color (Figure 4-6) and can be divided into a grainstone-rich subfacies and a precipitate-rich subfacies. Grainstone-rich cyclic beds are usually planar bedded to domical. Where domes are present, they have less than 20 cm of relief, have minimum diameters of 1-10 m, and are highly elongate. Grainstones fill troughs between domes and often lack the precipitated encrustations at the tops of beds. Bases of grainstone-rich beds are scoured. Ripples with internal cross stratification suggesting bi-directional sediment transport are common (Figure 4-6A). The ripple crests propagate almost vertically upward in the bed, and the locations of ripple crests were occasionally inherited from one bed to the next.

Precipitate-rich beds form low domes like those in grainstone-rich beds. Occasionally they also form domes, 0.5-1 m in diameter and with up to 50 cm of relief. Columnar stromatolites, 3-5 cm in diameter, are common in precipitate-rich beds (Figure 4-6B). These

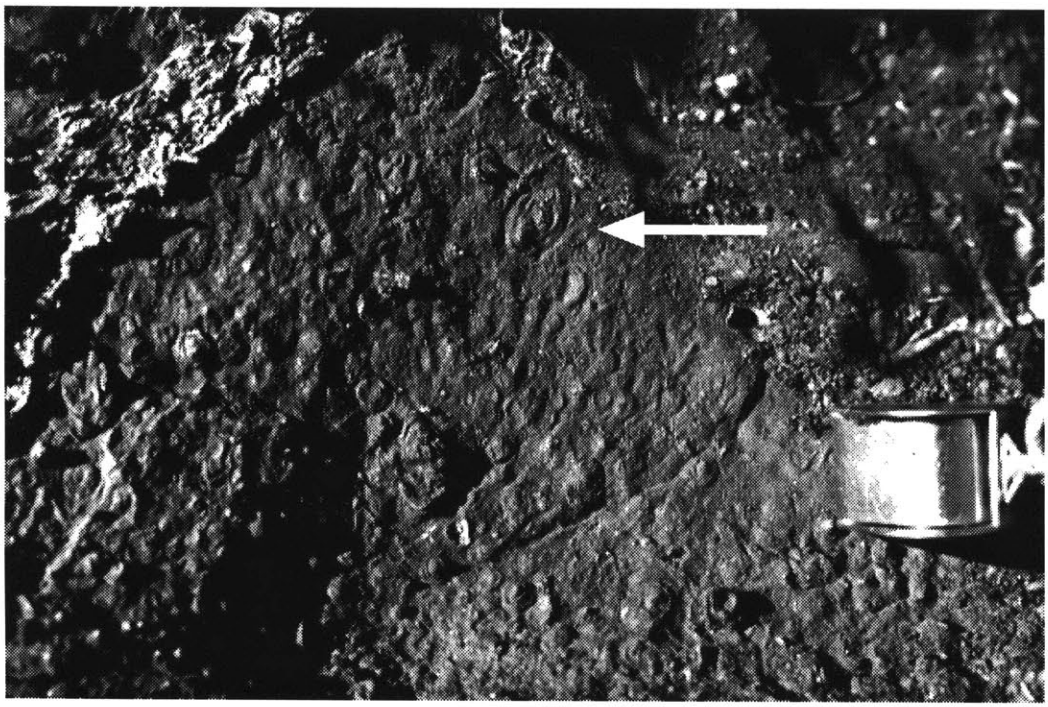

Figure 4-4: Giant ooid growing upward into a small column (arrow). Sample is from the mixed siliciclastic-carbonate peritidal lithofacies at section MA. Hand lens is 2 cm across.

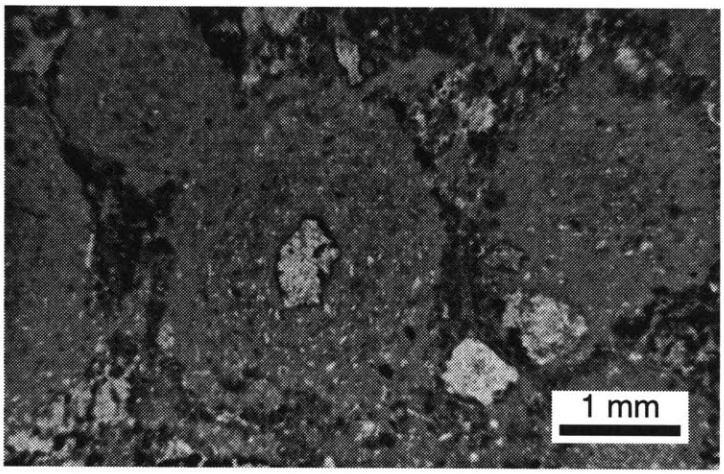


Figure 4-5: Accretionary lapilli from the mixed siliciclastic-carbonate peritidal lithofacies. Light grains are quartz and dark crystals between lapilli are secondary carbonate. Thin section from section AE.

stromatolites are poorly laminated and contain a herringbone calcite microtexture. They nucleated on thin grainstone layers at the base of the beds and widen upward leaving teardrop shaped troughs that are filled with the basal grainstone of the overlying bed. The tops of cycles are sometimes scoured and rarely show dissolutional features such as irregular truncation surfaces. In the Frisco Formation, rare precipitate-rich cyclic beds contain cuspate-like microbialites with central supports (Figure 4-6C). These beds contain the gradation in color from bottom to top and scoured bases like other grainstone-precipitate cyclic beds.

Beds of the grainstone-precipitate cyclic lithofacies are abundant at the base of the Gamohaan Formation and are interbedded with rocks of the mixed siliciclastic-carbonate peritidal lithofacies in the lower Frisco Formation. Grainstone-rich beds are more common at the base of the formations, with the proportion of precipitate-rich beds increasing upward.

**Interpretation**

The presence of bi-directional transport ripples in the grainstone-rich cycles suggests that these cycles were deposited above wave base. The unusual vertical propagation of ripple crests may be due to cementation that immediately followed deposition and locked the ripple crests into place. During the next depositional event, ripples could not migrate freely because the previous crest was immobile. The lack of channeling and erosion in the cycles implies subtidal or low energy intertidal depositional environments. The high relief domes in some precipitate-rich beds suggest subtidal depositional environments. The differences in composition between individual beds probably reflects variability in carbonate sand flux. When sand supply was low, columnar stromatolites formed through the precipitation of carbonate, and when the supply was relatively high, rippled and cross-stratified grainstones were deposited. Carbonate sand influx must have been cyclical as demonstrated by the rhythmic nature of the beds and the consistent gradation within beds from grainstones to precipitated encrustations. The overall supply of carbonate sand was low relative to calcite precipitation rates, however, as demonstrated by the volumetric abundance of carbonate precipitates (50%).

### *Nodular Lithofacies*

The nodular lithofacies consists of light to medium tan or gray dolomitic limestone to limy dolostone forming nodules that are flattened parallel to bedding (Figure 4-7). They are separated by orange, compacted dolomicrite layers with minor shale. The finely crystalline nodules are coarsely laminated and rarely contain primary sedimentary features such

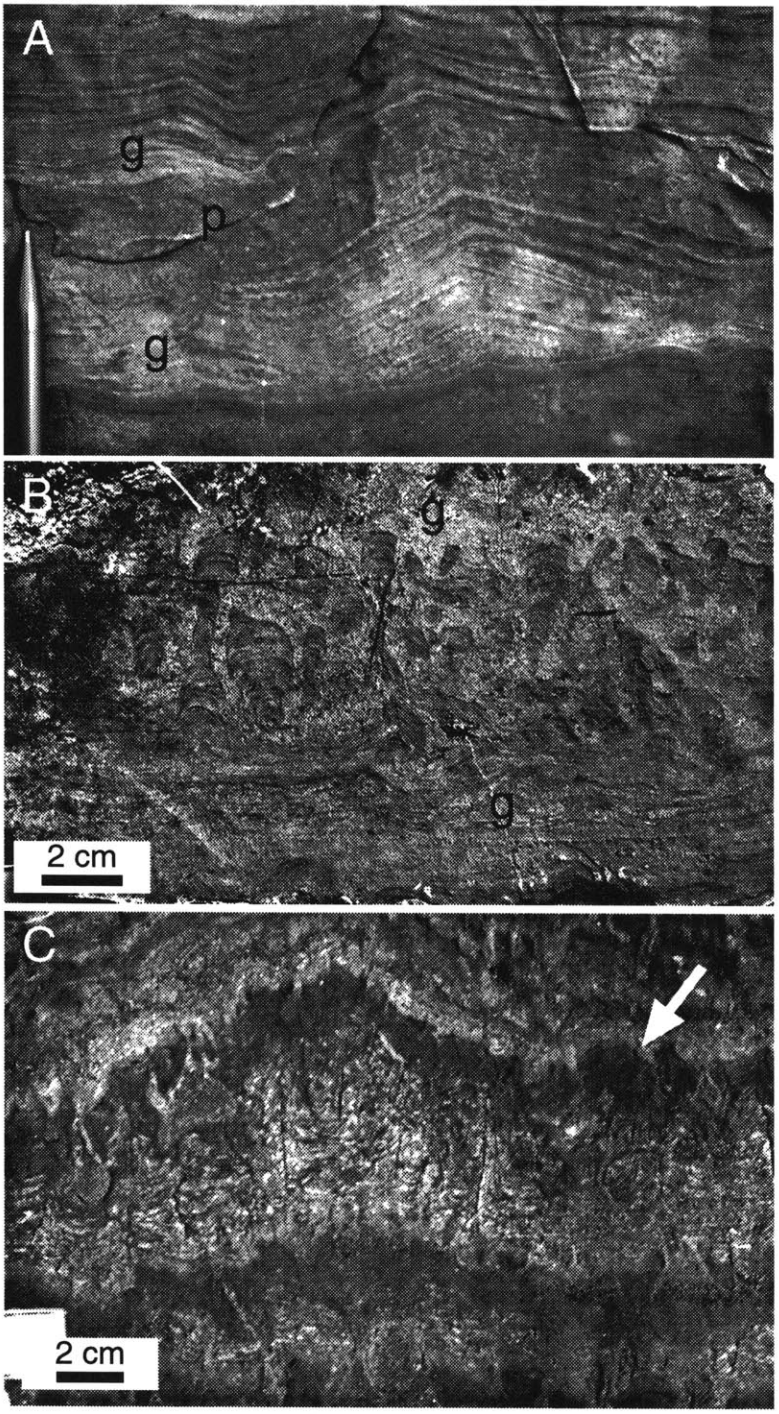


Figure 4-6: Various end members of the grainstone-precipitate cyclic lithofacies. A) A symmetric ripple in a grainstone-rich bed. The base of each bed consists of grainstone (g) that grades upwards into a precipitated crust (p). Note that the peak of the ripple in the middle bed affects the geometry of the overlying bed. Photo from section KU. Mechanical pencil is 0.9 cm wide. B) Columns in a precipitate-rich bed. The columns, which contain a precipitated microtexture, widen upwards and troughs between them are filled with grainstone (g). Photo from section EC. C) Cuspate microbialite-like structures in a precipitate-rich bed. The central supports are closely spaced, but laminae are poorly preserved and each bed is capped by a precipitated crust (arrow). Rare grainstone is present at the base of some beds. Photo from section EC.

as uncompacted rolled-up microbial films. They sometimes pass laterally into thinly bedded layers of rolled-up microbial films or cuspate microbialites. This lithofacies is present in the lower Gamohaan Formation and is abundant throughout the Frisco Formation.

**Interpretation**

Similar nodular limestones and dolostones are present in numerous other carbonates (e.g. Noble and Howells, 1974; Kennedy and Garrison, 1975; Moller and Kvingan, 1988). They are variously interpreted, but many are thought to have formed due to differential cementation during early diagenesis (Mullins, et al., 1980; Moller and Kvingan, 1988). The nodular lithofacies in the Frisco and Gamohaan formations is interpreted as partially cemented carbonate sediment. The nodules formed prior to substantial compaction as demonstrated by the presence of rare uncompacted rolled-up laminae within them and are interpreted as very early diagenetic in origin.

The nodular deposits are interpreted as having formed predominantly below wave base because they are associated with rocks of the planar-laminae assemblage in the Frisco Formation.

### *Grainstone Lithofacies*

Grainstones in the Gamohaan and Frisco formations are dolomitized and retain few primary sedimentary structures. Rare climbing ripples, low angle cross stratification, and platy microbreccia are present in well-cemented grainstones. Poorly cemented grainstones are more abundant and contain abundant evidence of soft-sediment deformation. They are present as isolated beds in the Frisco Formation and in a wedge in the lower Gamohaan Formation.

The depositional environment for the grainstones is difficult to determine due to the paucity of preserved sedimentary structures. The presence of platy breccia and climbing ripples indicates occasional agitation and high deposition rates suggestive of storm activity. These features, combined with the interfingering of the grainstones and deep subtidal microbial lithofacies (Figures 4-2 and 4-3), suggest a subtidal origin for the grainstones.

### *Tuffaceous Dolostone*

This lithofacies consists of 5-20 cm thick beds of coarsely-laminated dolostone and volcaniclastic detritus. Original sedimentary textures were destroyed during diagenesis and only hints of coarsely-laminated beds and rolled-up microbial films are preserved. The deposits are characterized by carbonate domes defined by mm-scale color variations that cross-cut sedimentary layering (Figure 4-8). "Troughs" between domes are filled with finely-

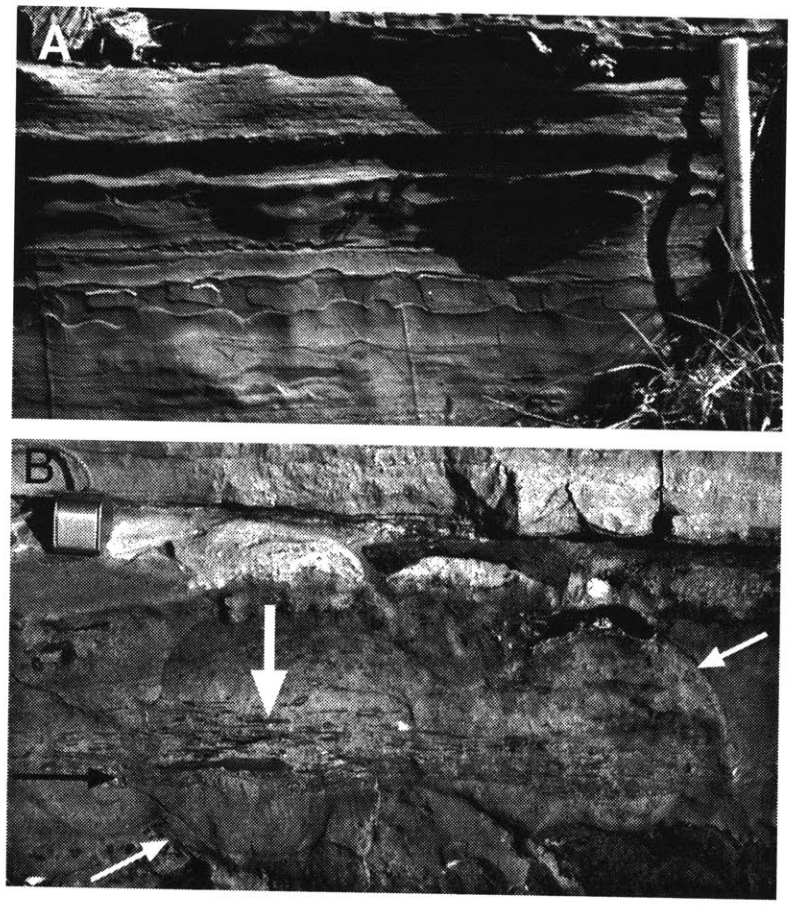


Figure 4-7: Nodular dolostone lithofacies. A) A layer of nodules between continuous beds. Photo from section EC. B) A nodule containing compacted rolled-up laminae (large white arrow). The black arrow indicates bedding orientation, whereas the small white arrows indicate the edges of the nodule. Photo from section KU. Hand lens is 2 cm wide.

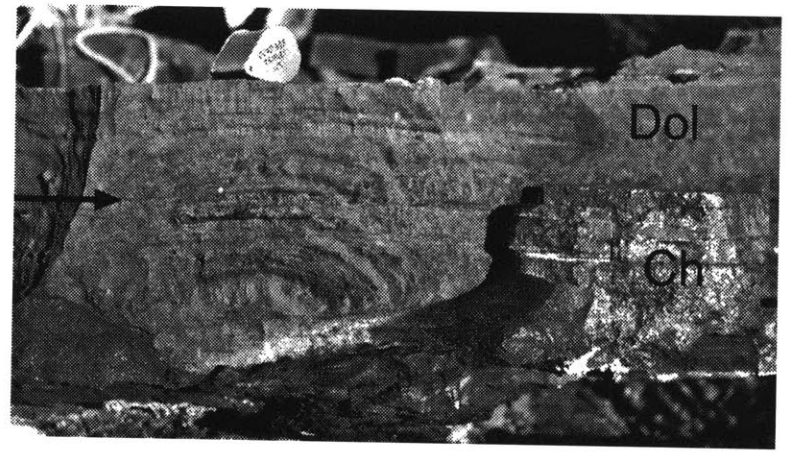


Figure 4-8: Tuffaceous dolostone. Coarsely laminate dolostone (Dol) is partially replaced by impure chert (Ch). Bedding is parallel to the black arrow and a concretionary dome grew below the hand lens. Photo from section KU. Hand lens is 2 cm wide.

laminated dolostone that shows evidence of compaction around the domes. Sometimes this dolomite was replaced with impure chert. These domes are interbedded with volcanic ash-rich beds. Ash beds consist of fine sand to very fine silt-sized volcanic grains, are green to black in color, and outcrop resistantly. Some of the ash beds are graded while others contain more complete Bouma sequences.

**Interpretation**

The cross-cutting relationships between compositional lamination and color changes defining carbonate domes demonstrate that the domes are the result of diagenetic processes. The compaction of laminae between domes suggests that they are early diagenetic concretions that grew upward from the bases of beds rather than in a more conventional, radial pattern. The complex alteration in these deposits may have been influenced by the influx of volcanic ash which was deposited by settling from suspension and from turbidity currents (Sumner and Bowring, in press).

### *Coarsely Laminated to Massive Dolostone*

This lithofacies consists of sucrosic dolomite in 10 cm or thicker beds. Sedimentary structures are rare although a few beds contain remnants of rolled-up laminae. Coarsely laminated dolomite occasionally grades laterally into nodular or planar laminae beds in the Frisco Formation.

Coarsely laminated to massive dolostone is a diagenetic lithofacies that replaced a variety of other rock types preserving few sedimentary structures. It often replaced rolled-up and planar-laminated mat in the Gamohaan and Frisco formations. In core BD2, it may have predominantly replaced grainstones. Massive dolomitization is not stratigraphically controlled whereas coarsely-laminated dolostone is usually present at a given stratigraphic interval.

### *Chert and Dolostone Breccia*

Sedimentary breccias with chert and dolostone clasts and matrix are common in core BD2 (Figure 4-9). Shale clasts and matrix are also present. Clasts range in size from <1 mm to decimeter-scale and are both platy and equidimensional. The breccias are usually poorly sorted and not graded (Figure 4-9). The matrix is unlaminated. Their lateral geometry is unknown since they are only observed in core, but their mixed composition, the lack of sorting, and the lack of grading are consistent with deposition from debris flows. They are most abundant in slope deposits and probably were sourced off the nearby platform margin.

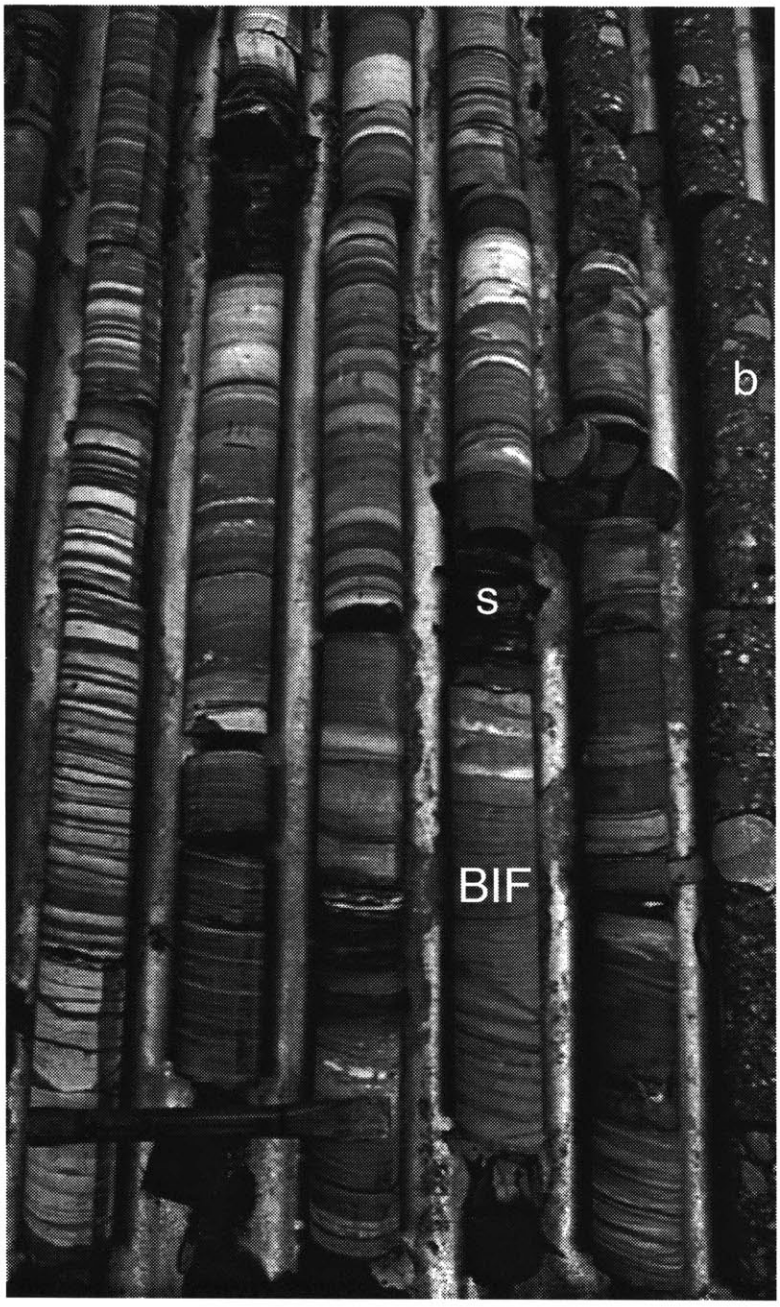


Figure 4-9: Interbedded banded iron formation (BIF), shale (s), and breccia (b) from core BD2. Up is to the right. The chisel is 18 cm long.

A chert breccia with a shale matrix is also present at the base of the Frisco Formation. This chert is a residual deposit from extensive erosion and karsting of the underlying Eccles Formation (Button, 1973).

### *Shale and Siltstone*

In outcrop, shales weather recessively and commonly coincide with Tertiary calcrete development. Shale and siltstone at the base of the Frisco Formation contain rare ripple marks (Button, 1973), but usually lack visible sedimentary features due to poor exposure and shearing along bedding planes. Shales near the top of the Gamohaan and Frisco formations are often associated with pods of calcite that are either nodules of marine cement or concretionary calcite. The shales are well preserved in core BD2 where they are black and carbonaceous, often containing abundant pyrite (Figure 4-9). Calcite pods in similar shales contain uncompacted rolled-up laminated mat (Figure 4-10).

## Interpretation

Shales at the base of the Frisco Formation probably represent the distal tongue of siliciclastic sedimentation. The depositional environment is uncertain due to the scarcity of preserved sedimentary structures, but stratigraphic constraints suggest shallow depositional environments with a sediment source from the east or northeast.

Shales at the top of the Gamohaan and Frisco formations and in core BD2 probably formed from the accumulation of uncemented microbial mat and small amounts of detrital carbonate and siliciclastic mud. They are interpreted as having formed in very deep subtidal environments, predominantly below the depth of significant calcite precipitation, based on their stratigraphic setting and the paucity of precipitated calcite.

### *Banded Iron-Formation*

Banded iron-formation is interbedded with carbonates at the top of the Gamohaan and Frisco formations as well as in core BD2 (Figures 4-2, 4-3, and 4-9). Iron-formation at the top of the Gamohaan and Frisco formations is similar to the overlying Kuruman and Penge iron-formations which consist of hematite, magnetite, and siderite banded chert. Iron-formation in core BD2 is lithologically similar; iron-formation beds developed in predominantly carbonate sediments consist of decimeter-scale siderite-rich chert beds above and below hematite-rich chert beds. Where interbedded with shale in core BD2, iron-formation beds consist of centimeter-scale siderite-chert beds with minor amounts of hematite. Deposition in deep basinal environments is strongly supported by the lateral continuity of mm-thick bands, lack of cross stratification, their stratigraphic setting throughout deposition of


Figure 4-10: Calcareous pod containing rolled-up microbial mat surrounded by carbonaceous shale from core SD1.

the Campbellrand-Malmani platform, and chemical signatures (Chapter 2; Beukes, 1987; Klein and Beukes, 1989; Beukes, et al., 1990).

## REGIONAL STRATIGRAPHY

### *Frisco Formation*

The Frisco Formation crops out along the northern and western margins of the Bushveld Complex (Figure 4-1). To the south, it is truncated by an erosional unconformity developed prior to deposition of the Paleoproterozoic Pretoria Group (Chapter 2), and to the north it is truncated by younger erosion. Metamorphism associated with intrusion of the Bushveld Complex variably affected the Frisco Formation which consists of talc-free, talc-bearing, and amphibole-bearing dolostone with subordinate limestone. All sections were measured in lower-grade, amphibole-free areas. Hydrothermal fluorite and sulfide deposits are common in the northwestern Transvaal Province, but these areas also were avoided except in core BH 74. Much of the formation has been dolomitized, however, and in some cases, sedimentary features are poorly preserved.

The base of the Frisco Formation is defined by a chert breccia with a shale matrix that is developed on the underlying Eccles Formation (Button, 1973). The breccia is overlain by siliciclastic shales and siltstones reaching a maximum of ~17 m thick at section AE (Figure 4-2). This siliciclastic unit thins to about a meter to the northwest and to 10 m to the south before it is truncated by the pre-Pretoria Group unconformity (Button, 1973). It is either not present or not exposed at sections MA and RD, although section MA contains 5 m of cover immediately above the breccia suggesting a lithology with a low weathering profile such as shale. Poor exposure of the shales as well as bedding plane slip make sedimentary features difficult to identify at sections AE and EC, although Button (1973) reports rare ripple marks.

The shale unit is overlain by mixed siliciclastic-carbonate peritidal rocks in the eastern Transvaal Province (Figure 4-2). The mixed siliciclastic-carbonate unit thins to the west where the base of the Frisco Formation consists of grainstone-precipitate cyclic beds with rare grainstones and quartzite beds. The grainstone-precipitate cyclic beds grade upward into microbialites of the bedded cuspate microbialite assemblage and then nodular dolostone. At sections EC and AE, this transition begins with rare cuspate microbialites and rolled-up microbial mat developed within grainstone-precipitate cyclic beds (Figure 4-4C). After about 20 m of interbedded nodular to coarsely-laminated dolostone and bedded cuspate microbialites, interbedded nodular to coarsely-laminated dolostone and microbialites

of the planar-laminae assemblage become predominant in all sections. These lithofacies dominate the rest of the Frisco Formation (Figure 4-2). Thick sequences of diagenetic massive dolostone are also present at sections DI, RD, and MA.

The contact between the Frisco Formation and the overlying Penge Iron Formation is covered or eroded except at section DI. Here, the Penge Iron Formation is preceded by a 10 m sequence of cross-bedded grainstones with rare shales. Sedimentary structures in the grainstone consist of low angle truncations, rare scoured surfaces, and ripples. Rare roll-ups are also present. Immediately above the grainstone, decimeter-thick chert beds are interbedded with coarsely-laminated dolostone. The chert becomes progressively more iron-rich and a bed of finely-laminated chert-oxide iron-formation is present. Four meters above the first chert bed, continuous iron-formation of the Penge Iron Formation was deposited.

**Interpretation**

The breccia at the base of the Frisco Formation is developed over hundreds of kilometers suggesting that it is a major sequence boundary. The lenticular geometry of the overlying shale with greatest thicknesses in the east and over the Murchison Greenstone Belt (Button, 1973; Figures 4-1 and 4-2) suggests that the sediment source was in the east or northeast and subsidence of the trough was reactivated prior to deposition of the Frisco Formation (Chapter 2). In addition, the thinning of siliciclastic beds in the mixed siliciclastic-carbonate peritidal lithofacies to the west and sparse paleocurrent directions from trough crossbedding at section EC also suggest that siliciclastic sediment was transported from east to west, possibly along the axis of the Selati Trough. The microbialite lithofacies represent deepening of the depositional environment upward in the Frisco Formation. The interbedding of coarsely-laminated dolostone and chert with upward-increasing iron concentration in the transition into the Penge Iron Formation indicates that the transition from carbonate to iron-formation deposition was gradational.

### *Gamohaan Formation*

The Gamohaan Formation is exposed in a 50-100 km wide, north-south trending outcrop belt running from section PM in the north to the Griquatown Fault Zone in the south (Figure 4-1). It is exposed on the slopes of ridges capped by the resistant Kuruman Iron Formation. To the east, the Gamohaan Formation is truncated by erosion, and to the west, strata are truncated by the 2.0-2.2 Ga Kheis Orogenic Belt (Beukes and Smit, 1987). The Gamohaan Formation is exceptionally well preserved. Metamorphic alteration was minor with talc present only at section PM. In addition, Miyano and Beukes (1984) ana-

lyzed mineral assemblages in the overlying Kuruman Iron Formation and report maximum regional metamorphic temperatures of <170°C. Much of the Gamohaan Formation consists of limestone, although fabric retentive dolomite is abundant in shallow subtidal deposits at the base, whereas massive dolomitization occurred along rare late faults throughout the formation. The top of the formation contains more late (Fe-rich) dolomite than lower carbonates (Beukes, 1987; Klein and Beukes, 1989). Some karsting of the Gamohaan Formation occurred along the contact with the overlying Kuruman Iron Formation during development of a regional unconformity prior to deposition of the Paleoproterozoic Olifantshoek Group (Van Schalkwyk and Beukes, 1986). Sink holes developed but disruption is local.

The base of the Gamohaan Formation is defined by a gradational change from lagoonal, microbially-laminated lithofacies of the Kogelbeen Formation (Chapter 2) to grainstone-precipitate cyclic rocks (Figure 4-3): Columnar stromatolites are interbedded with the lagoonal microbially-laminated lithofacies for 20 meters, and exhibit an upward increase in the volume of precipitated carbonate. Shallowest water depths are represented by a thin interval of shallow intertidal to supratidal stromatolites associated with a thin shale. Upward, small columnar stromatolites develop into grainstone-precipitate cyclic beds which form a unit approximately 15 m thick. This unit is overlain by massive dolomitized grainstones to the north of core SACHA. To the south, it is overlain by bedded cuspate microbialites. The grainstones thin to the south and form a wedge within the bedded cuspate microbialites that pinches out south of section DK. The unit of bedded cuspate microbialites overlying the grainstone wedge is ~10 m thick and is overlain in turn by ~15 m of the irregular columnar microbialite assemblage (Figure 4-3). This succession is capped by a unique 2 m sequence of beds consisting of plumose structures, herringbone calcite beds, and rolled-up mat which is discussed in detail below. Above these beds, the irregular columnar microbialite assemblage is reestablished with some lateral variations in the north. The top of this ~30 m thick succession is marked by an influx of volcaniclastic sediment. Columnar microbialites become rare, whereas coarsely-laminated dolostone and tuffaceous dolostone increase in abundance. The tuffaceous dolostone unit is variable in both thickness and stratigraphic position relative to a chert and 2 ash beds that mark time horizons (Figure 4-3). Ash beds thin from north to south. Above the tuffaceous unit, the Gamohaan Formation consists of the rolled-up mat assemblage with rare bedded cuspate microbialites. The extent of compaction in the roll-ups and the abundance of shale increase upward to a gradational contact with the Kuruman Iron Formation. The interbedding of iron-formation with beds of roll-ups, coarsely-laminated dolostone, and rare columnar stromatolites is best exposed at section KU, but is also present at section AL. Similar interbedding has been documented in several cores by Klein and Beukes (1989) and Beukes, et al. (1990).

**Interpretation**

The supratidal stromatolites and shale in the transition from the Kogelbeen to Gamohaan formations represents the shallowest unit and may represent the conformity correlative to a sequence boundary. A transgression above this boundary is represented by peritidal-subtidal grainstone-precipitate cyclic beds which are in turn overlain by subtidal microbialites. The pinching of the grainstone wedge to the south suggests a northerly sediment source. Above this wedge, clastic sediment is shut off until the influx of volcanic detritus in the tuffaceous dolostone unit. The thinning of ash beds to the south suggests a northerly volcanic source. Above the tuffaceous dolostone zone, the upward increasing abundance of shale suggests a decrease in carbonate precipitation rates due to increasing water depths. Continued deepening led to a gradational change to banded iron-formation deposition and drowning of the carbonate platform.

### *Basinal Equivalents*

South of the Griquatown Fault Zone, sediments below the Kuruman Iron Formation are dramatically different as demonstrated by core BD2 and section KN (Figures 4-1 and 4-3; Chapter 2; Appendix 2, Sections BD2 and KN). Core BD2 contains 16 m of the Kuruman Iron Formation which is unconformably truncated by overlying Paleozoic Dwyka glacial deposits. Sediments below the iron-formation consist of interbedded shales, dolostone and chert breccia, massive to coarsely-laminated dolostone and limestone, hematite-siderite-chert banded iron formation, and rare rolled-up microbial mat. A single bed of cuspate microbialites and a single 5 cm ash bed are also present. Farther south at section KN, sediments below the base of the Kuruman Iron Formation consist of shales with interbeds of iron-formation (Chapter 2; Beukes, 1987).

**Interpretation**

Breccia textures in core BD2 are consistent with debris flow deposits and the interbedding of breccias and coarsely-laminated dolostone are characteristic of slope deposits (e.g. Cook and Taylor, 1977; Davies, 1977). The presence shale and thin layers of iron-formation are consistent with a deep slope environment (Beukes, 1983; Simonson, et al., 1993). Shale and iron-formation sediments in section KN are consistent with basinal depositional environments where the paucity of carbonate is due to deposition below depths at which *in situ* calcite precipitation was volumetrically significant.

### *Stratigraphic Correlations*

General stratigraphic trends in the Frisco and Gamohaan formations are similar.

The sequence boundary and shale in the Frisco Formation probably correlate with the shallowest lithofacies at the base of the Gamohaan Formation. The presence of siliciclastic detritus only at the base of the Frisco Formation and the thinning of the clastic carbonate wedge from north to south in the Gamohaan Formation supports uplift in the north or northeast, whereas the presence of deep subtidal microbialites below the wedge in the south suggests contemporaneous subsidence in the southwest. The upward deepening suggested by lithofacies changes implies that the Gamohaan and Frisco formations were deposited during a transgression that proceeded from southwest to north or northeast across the platform.

The difference in lithofacies between core BD2 and sections to the north probably is due to antecedent topography inherited from the underlying platform and deeper depositional environments. Topographic gradients were high across the platform margin just north of core BD2 (Chapter 2; Beukes, 1987), so deposition occurred in much deeper water than synchronous sediments to the north of the margin, with high topographic gradients provided a source for downslope breccias and turbidity current deposits. Correlations between core BD2 and the Gamohaan Formation are not possible, but the presence of rare roll-ups and cuspate microbialites suggests that deposition was contemporaneous with the Gamohaan Formation, although similar lithofacies are also present basinward of the platform margin lower in the Campbellrand-Malmani platform (Chapter 2; Beukes, 1987).

Lithologic correlations among the Frisco Formation, the Gamohaan Formation, core BD2, and section KN can be made at the base of the Penge and Kuruman iron-formations. The temporal significance of the correlation is uncertain. Two relationships suggest that iron-formation and carbonate deposition occurred simultaneously in different depositional environments in the Campbellrand-Malmani basin. First, core BD2 contains several layers of iron-formation below the base of the Kuruman Iron Formation. These interbeds were deposited during deposition of the Gamohaan Formation or underlying carbonates. Second, iron-formation and carbonate are interbedded at the top of the Gamohaan and Frisco formations. Based on the fine scale of interbedding and gradational lithofacies changes, the most likely explanation of interbedding is fluctuations in water depth or upwelling pulses of basinal water with a different chemistry rather than chemical change of the overlying water column (Klein and Beukes, 1989; Beukes, et al., 1990). These observations suggest that iron-formation is a deep water lithofacies that was deposited contemporaneously with shallower water carbonates (see also Beukes, 1987; Klein and Beukes, 1989; Beukes, et al., 1990). If this is the case, iron-formation deposition may have begun sooner in basinal environments such as at section KN than in sections deposited at shallower depths on top of the platform. Thus, the lithologic correlation of the base of the Kuruman and Penge iron-

formations could be time transgressive.

Absolute water depths for deposition of the Gamohaan and Frisco formations are poorly constrained. The bases of the formations contain abundant features suggesting intertidal depositional environments. Depths for deposition of the upper parts of the formations, however, are much more difficult to determine. The lack of scouring and the delicate nature of the microbialites suggest that they were deposited below storm wave base, but do not provide absolute depth estimates. Although, Klein, et al. (1987) estimate water depths of 40-45 m for a chert bed a few 10's of meters below the transition to iron formation deposition at the top of the Gamohaan Formation, their estimate is based on the interpreted presence of photosynthetic cyanobacteria. Simonson, et al. (1993) interpret similar microbial lithofacies of the Hamersley Basin, Australia, as chemosynthetic and deposited in 100's m water depth based on stratigraphic considerations. Thus, the presence of the microbialites may not require deposition within the photic zone. Maximum water depths of 700 m are estimated by Klein and Beukes (1989) for basinal sediments equivalent to the Campbellrand-Malmani platform based on the relative thickness of basinal and platform sediments using corrections for progressive compaction of shales. These basinal sediments contain rare beds of microbialites similar to those in the Gamohaan Formation. Thus, water depths may have reached hundreds of meters during deposition of the Gamohaan and Frisco formations, although much shallower depths cannot be ruled out.

## DISCUSSION

### *Deep Subtidal Seawater Chemistry*

The abundance of calcite precipitated and the lateral continuity of individual beds in the Gamohaan Formation have important implications for processes controlling carbonate precipitation in late Archean oceans. To quantitatively document the abundance of calcite that precipitated *in situ* as sea floor encrustations and in voids, a detailed survey was conducted at section KU. For each bed ≥5 cm thick, the sedimentary texture, proportions of microcrystalline carbonate, carbonate sand, and *in situ* precipitated carbonate, and the ratio of herringbone calcite to other precipitated textures were recorded (Figure 4-11). These estimates represent minimum proportions because only the percent of the rock that contained preserved crystallographic evidence for a precipitated origin or visible grains was recorded. For example, recrystallized carbonate that did not contain direct crystallographic evidence of a precipitated origin was not included in the estimates, even where a genetic interpretation could be justified. Thus, totals of the proportions of all primary components

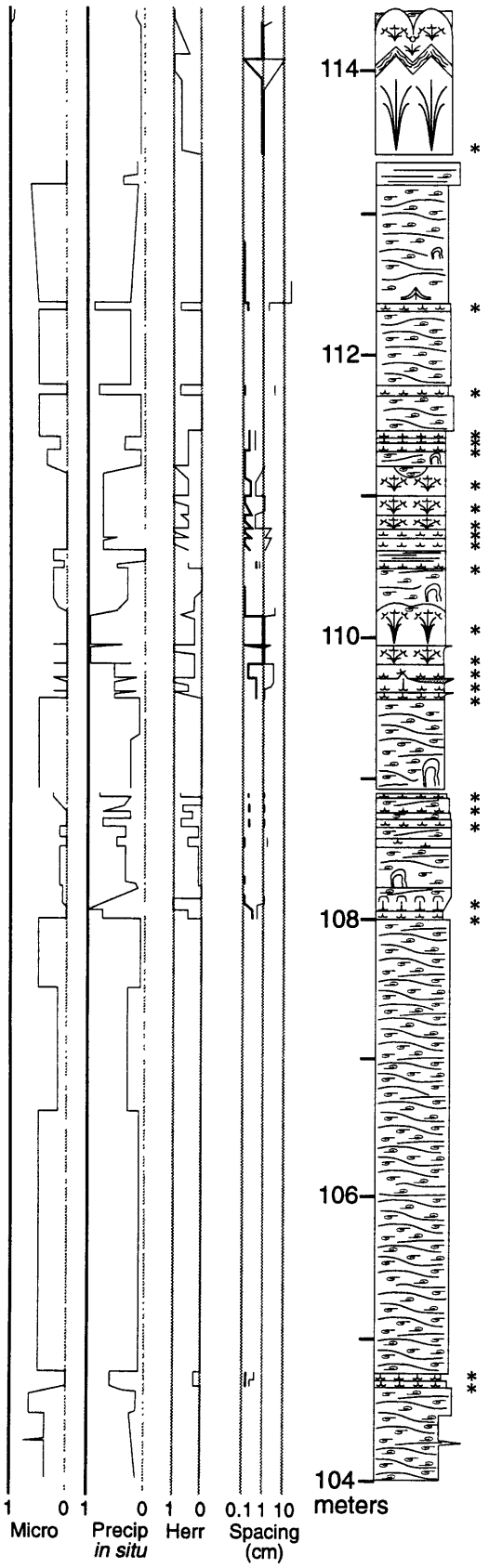


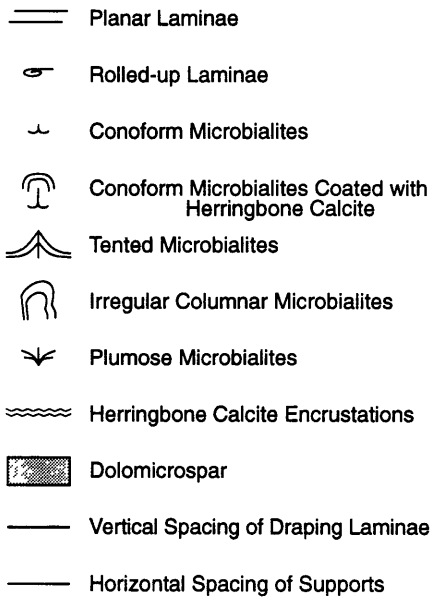


Figure 4-11: Sample stratigraphic column of the Gamohaan Formation from section KU#2 showing textural descriptions of microbialites and proportions of various carbonate components. The "Micro" column represents the proportion of microcrystalline carbonate in each bed. Similarly, the "Precip *in situ*" column represents the proportion of the rock with calcite cement-like textures. The "Herr" column is the proportion of the *in situ* precipitated rock that contains a herringbone calcite microtexture. The "Spacing" column is a measure of the vertical and horizontal dimensions of voids and reflects microbialite morphology (see Chapter 3). The proportion of carbonate sand is negligible in this part of the section and is not shown. The total proportion of each component was calculated by multiplying bed thickness by the proportion of the texture in the bed. For herringbone calcite, bed thickness was multiplied by both the proportion of total precipitated calcite and the proportion of the calcite that consists of herringbone calcite. These products were summed for the entire section and divided by the total thickness to obtain average compositions. The plumose beds at 114 m are shown in Figure 4-12. Beds marked by "*" are shown in section KU#2 in Figure 4-13.

are less than 100%, and the proportion of carbonate reported to have precipitated *in situ* represents the proportion of carbonate with *demonstrable* cement-like textures as opposed to an estimate of the amount of carbonate that was *interpreted* to have precipitated in place. Results show that from the base of the first microbialites to the first ash bed (40 m), a minimum of 35% of the rock precipitated as encrustations and void-filling cements, 30% of the rock consists of microcrystalline carbonate, and 40% of the rock is recrystallized to the extent that primary crystallographic textures were not preserved. Thirty percent of the void-filling cements and all of the calcite encrustations consist of herringbone calcite (15% of the rock) and precipitated contemporaneously with growth of the microbialites (Chapter 3). Preserved carbonate sand textures make up less than 1% of the microbialite assemblages and are not considered further. Microcrystalline carbonate is present only in areas with dense inclusions defining the microbial structures. Micritic beds, drapes, and geopedal void-fills are absent from the section, and there are no sedimentary features suggesting that the microcrystalline carbonate originally consisted of micritic sediment. Rather, the concentration of microcrystalline carbonate in organic-rich areas suggests that it precipitated in place as a microsparitic cement. Thus, of the 40 m analyzed, a minimum of 30% microcrystalline carbonate and 15% herringbone calcite precipitated in place contemporaneous with sedimentation, and an additional 30% of the rock consists of void-filling calcite that precipitated before lithostatic forces from burial were sufficient to compact even the most delicate void walls. An even larger proportion than this total of 65% of the rock probably precipitated as calcite cements and encrustations, but lacks the crystal textures required for possitive identification due to diagenetic recrystallization. Sections as far south as section HE contain similar proportions of marine cement. Thus, the *in situ* precipitation of calcite was an important rock-forming process in the deposition of the Gamohaan Formation.

Individual beds of microbialites and encrusting sea-floor precipitates can be identified in sections separated by the entire 140 x 50 km of good stratigraphic control. The most striking series of continuous beds consists of a two meter-thick interval containing plumose structures and beds of precipitates that show very little textural variation from section KU to section HE (Figures 4-3 and 4-12). The base of this interval consists of a layer of 35-65 cm tall plumose structures encrusted by a several cm-thick coating of herringbone calcite. The herringbone calcite is overlain by a second layer of 15-25 cm-tall plumose structures and then rolled-up microbial mat or massive dolostone that is variable along strike. The next bed is a 22-40 cm-thick bed of herringbone calcite with a 2 cm layer plumose structures in the middle. This 2 cm layer is continuous from section KU to HE (Figure 4-12). The herringbone calcite layer is overlain by a variable thickness of rolled-up mat and then another herringbone calcite bed. This upper herringbone calcite bed is variable along strike,

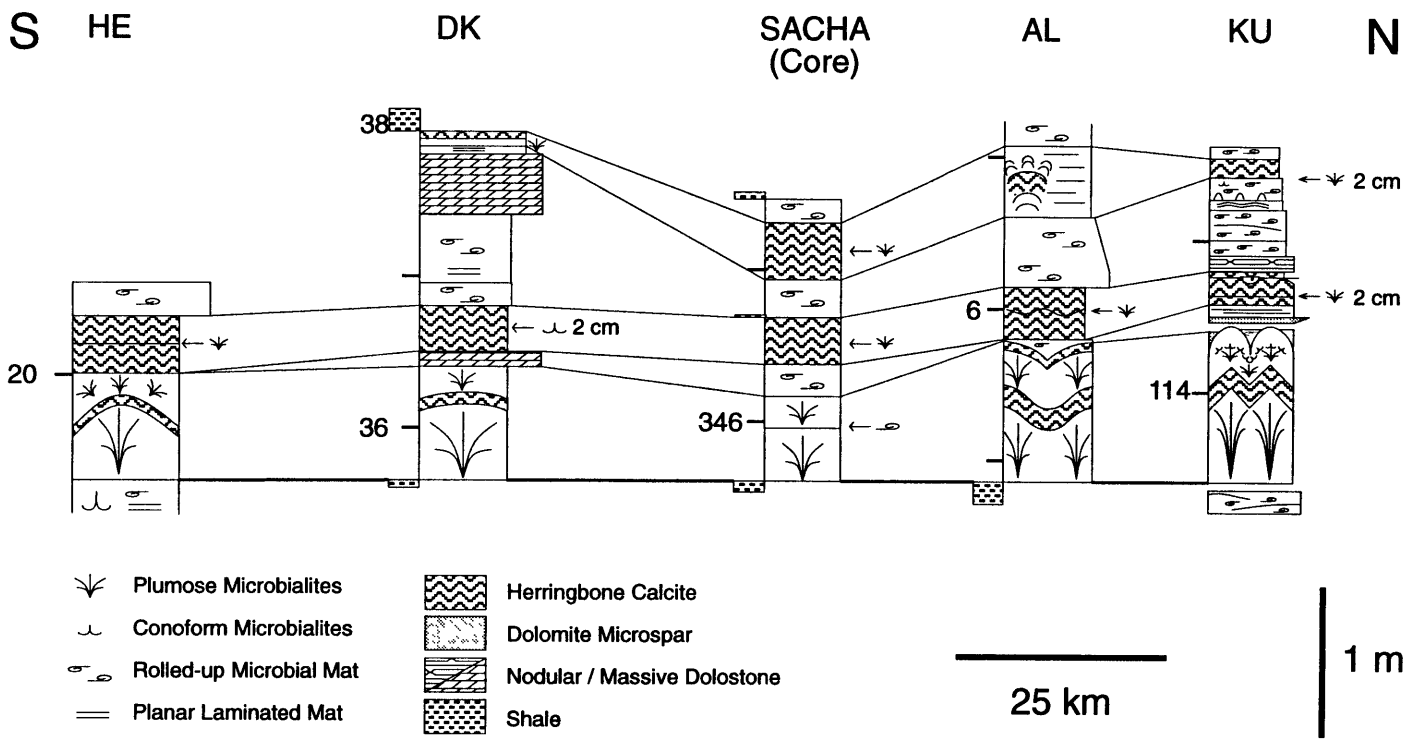


Figure 4-12: Details of stratigraphic columns from 5 sections through the Gamohaan Formation covering 140 x 50 km. Each of these sections was measured independently demonstrating the regional uniformity of the plumose structure and precipitated beds. For complete sections, see Appendix B.

but is recognizable in all sections where outcrop is present. This sequence of beds in unique and its uniformity in all sections demonstrates that depositional conditions were similar across large areas of the platform.

Other beds of *in situ* precipitated carbonate and of plumose structures are also laterally continuous from section KU to HE. For example, nine beds of plumose structures below the plumose-precipitate unit described above can be identified in all sections (Figure 4-13). Many of the thicker cuspate microbialite beds also are laterally continuous as demonstrated by 5 beds identified at section KU#1 that are traceable to core SACHA, 44 km away. Thinner cuspate microbialite beds are less continuous: 10 out of 13 (~75%) cuspate microbialite beds >10 cm thick are identifiable in sections KU#1 and KU #2, separated by 1 km, whereas only 10 out of 28 (~35%) cuspate microbialite beds <10 cm thick can be traced (Figure 4-13). Rare ~5 cm-thick cuspate microbialite beds are truncated within an outcrop suggesting either reworking prior to cementation or laterally discontinuous growth. None of the rolled-up laminae beds or units of irregular columnar microbialites are traceable, because these beds do not have distinguishing characteristics that can be identified and laminae disruption plays a larger role in their texture (Chapter 3).

Laterally continuous beds are less common above the 2 m-thick plumose-precipitate marker interval, but two distinctive laterally continuous beds deserve discussion. The first is a 10-30 cm thick dolostone bed (Figures 4-3 and 4-14). It is the only sucrosic dolomite in the Gamohaan Formation that is stratigraphically restricted to a single bed. It consists of two fenestral sucrosic dolomite layers separated by finely-laminated sucrosic dolomite. In the core SACHA, the lower fenestral bed contains organic inclusions suggestive of plumose structures although they are encased in dolomite rather than calcite. The plumose structure of the bed is not readily apparent in outcrop, but the fenestral fabric is consistent with plumose structures. Correlation of the dolostone bed at sections AL, KU, and SACHA is confirmed by the presence of an overlying calcite precipitate bed in all three localities. This precipitate bed, unlike those lower in the sections, consists of an encrustation of bladed calcite with 0.5-1.0 mm wide crystals that thins from 10-15 cm at section KU and AL, respectively, to 5 cm at core SACHA. The bladed texture of this encrustation is unique in the Gamohaan Formation, but has a texture similar to common Phanerozoic void-filling cements and to bladed calcite in voids in the microbialites.

In addition to the laterally continuous dolostone bed, a single laminated black chert bed is found in sections KU to HE. This chert is 10-15 cm thick and is the only finely-laminated black chert bed in the vicinity of the tuffaceous dolostone zone. The lateral correlation of the chert bed in various sections is confirmed by the presence of two laterally continuous ash beds, one above and one below the chert (Figure 4-3).

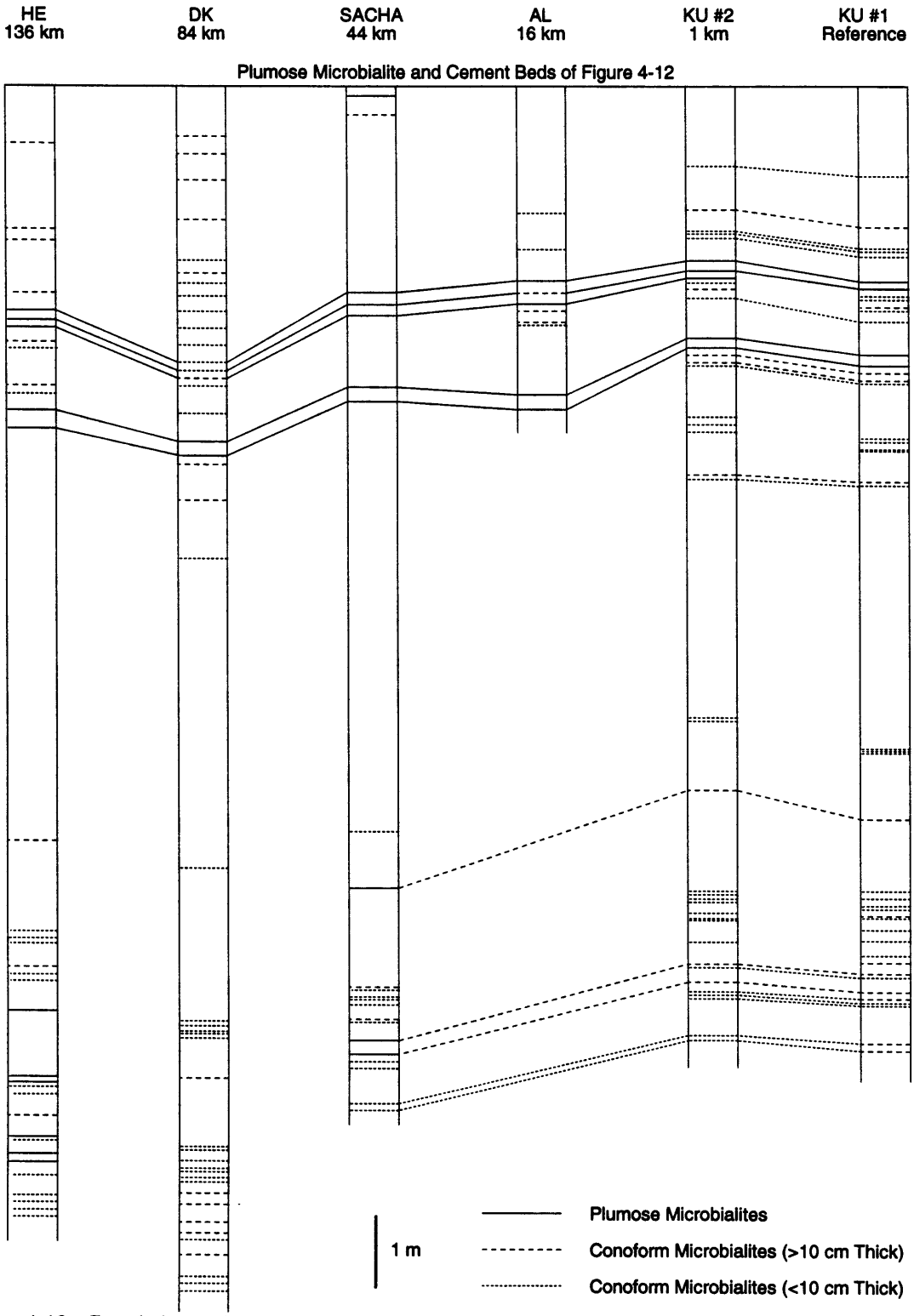


Figure 4-13: Correlation and distribution of laterally continuous beds below the plumose-precipitate beds shown in Figure 4-12. Section KU#1 is used as a reference and individual beds were identified in sections to the south. All plumose structure and cuspate microbialite beds are shown for each section. Correlations are based on the texture and thickness of each bed as well as the characteristics of overlying and underlying beds. See Figure 4-11 for an example of the detailed data on which the correlations are based.

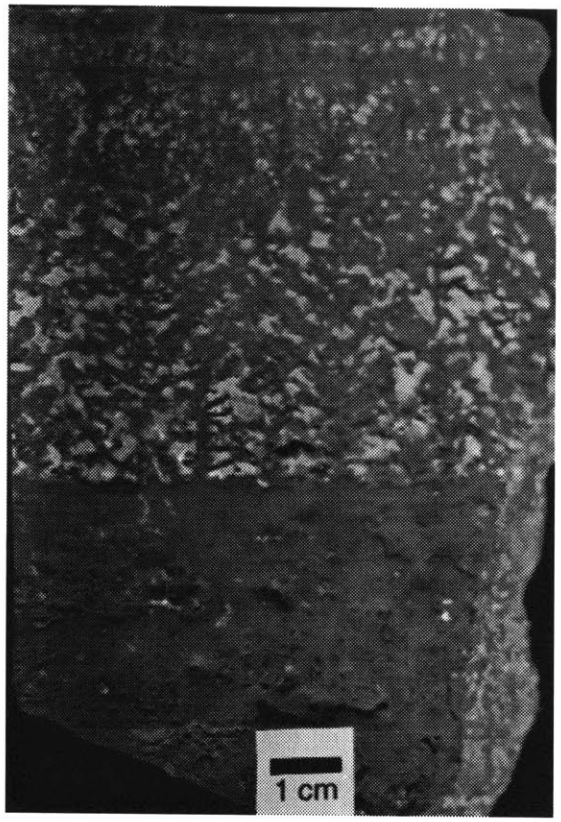


Figure 4-14: Hand sample of the laterally continuous dolomite bed in the Gamohaan Formation (marked "D" in Figure 4-3). The fenestral fabric is consistent with plumose structures as suggested by textures from core SACHA. Sample is from section KU.

**Implications**

The lateral continuity of beds suggests that regional chemical conditions were uniform across the preserved area of the Gamohaan Formation. Thus, the proportion of precipitates estimated at section KU reflects the proportion of precipitated carbonate for hundreds of square kilometers on the platform. The extent and large volume of precipitated carbonate suggest that deep subtidal marine water was highly supersaturated with respect to calcite. The presence of regionally maintained highly supersaturated seawater is necessary to account for the regional continuity of precipitated beds as well as the large volume of calcite cements: Neither microbial processes (see Chapter 3) nor ground water seeps (Beauchamp and Savard, 1992; Campbell, 1992; Gaillard, et al., 1992) can account for the regional continuity of cement-rich beds since they depend on localized shifts in chemistry. Regional control of carbonate precipitation is supported by the presence of the laterally continuous dolostone and chert beds. Regional dolomitization of a single 20 cm thick bed suggests a regional chemical change in depositional chemistry. For example, the original mineralogy of this bed may have been less stable and more suseptible to dolomitization than the surrounding beds. The laterally continuous chert bed is organic-rich and finely laminated suggesting that it either precipitated as a primary chert or that depositional chemistry promoted regional, early diagenetic replacement by chert. Thus, both beds record regional shifts in seawater chemistry that led to the precipitation of different minerals than the herringbone calcite typical of most of the Gamohaan Formation, and the chemical composition of regional seawater was probably the major control on mineral precipitation.

The lateral continuity of beds with specific microbialite morphologies suggests that regional conditions also affected microbialite growth. The continuity of individual beds as thin as 2 cm for >140 km requires a uniform growth environment, whereas vertical changes in microbialite textures require uniform changes in growth conditions across the platform. These controls were probably chemical in nature since there is no evidence of sensitive depth control on microbialite morphology. Either nutrient supply or the rate of carbonate precipitation could affect microbial communities, and thus, microbialite morphology.

### *Changes in Ocean Chemistry with Depth*

Chemical changes with depth in Archean seawater are documented by the gradual decrease in the abundance of *in situ* precipitated calcite and an increase of iron-rich sediments at the top of the Gamohaan Formation (Klein and Beukes, 1989). The upward decline in precipitated calcite reflects a general decline in the calcite saturation state of seawater with increasing depth. A similar decrease in carbonate saturation with depth is present in modern oceans. The depth at which modern seawater becomes undersaturated with re-

spect to calcite varies from 300-4000 m (Takahashi, 1975), and is almost always deeper than maximum depths for deposition of the Gamohaan Formation.

The change in saturation state in modern oceans is driven by several variables. The two most important are an increase in the partial pressure of $CO_2$ and a decrease in pH with depth and increasing age of the bottom water (Li, et al., 1969). Both of these changes are driven by the oxidation of organic detritus at depths (Li, et al., 1969) and are affected by the influx and oxidation rate of organic matter. Pressure increases and temperature decreases also tend to decrease the calcite saturation state with depth. The processes controlling changes in calcite saturation state with depth in Archean oceans may have been significantly different from those in modern oceans. First, the $CO_2$ increase in modern oceans may not have been as important in Archean oceans since the effects of oxidizing organic matter may have been significantly less with low oxygen concentrations in the deep oceans due to lower concentrations of oxygen, metal oxides (i.e., $Fe^{3+}$, $Mn^{3+}$, and $Mn^{4+}$), and possibly sulfate (Cameron, 1982). In addition, Logan, et al. (1995) suggest that prior to the evolution of organisms that produced fecal pellets at the beginning of the Cambrian Period, large amounts of organic matter were recycled in the upper mixed zone of the oceans. This would have the effect of reducing the rain of organic matter and limiting the buildup of oxidized compounds in the deep oceans (Logan, et al., 1995), both reducing the supply of $CO_2$ to deep seawater. A lack of organic matter in basinal iron-formations (i.e. Klein and Beukes, 1989; Beukes, et al., 1990) is consistent with limited pelagic rain of organic matter. Thus, any increases in $CO_2$ with depth in Archean oceans probably either were lower in amplitude or were caused by different organic decay mechanisms (see Froelich, et al., 1979). Instead, a decrease in saturation state could have been caused by other chemical gradients. In particular, an increase in $Fe^{2+}$ concentration with depth could affect calcite precipitation. As $Fe^{2+}$ concentration increases, siderite becomes supersaturated and would down calcite saturation as it precipitated (Chapter 6). The inhibiting effect of $Fe^{2+}$ on calcite precipitation would also reduce the precipitation rate of calcite and could enhance the change from calcite to siderite precipitation with depth (Chapter 6). Thus, increasing $Fe^{2+}$ concentration alone may cause siderite precipitation to replace calcite precipitation. A gradient in $Fe^{2+}$ concentration could be dynamically maintained by $O_2$ production in shallow platform environments and $O_2$ sinks in the deep oceans. Thus, this model does not require a stratified ocean. It is consistent, however, with ocean stratification supported by other chemical data (i.e. Klein and Beukes, 1989; Beukes, et al., 1990; Chapter 6).

## CONCLUSIONS

1. The Gamohaan and Frisco formations are correlative sequences that were deposited during a transgression that led to the drowning of the Campbellrand-Malmani carbonate platform. They are conformably overlain by the Kuruman and Penge iron-formations, respectively, and the change from limestone to iron-formation deposition was the result of continued deepening.

2. The microbialite assemblages that compose most of the Gamohaan and Frisco formations were deposited in deep subtidal environments either within or below the photic zone.

3. The abundance of marine precipitates, particularly herringbone calcite, that precipitated as encrustations on the sea floor and in primary voids in microbialites demonstrates that deep subtidal seawater was supersaturated with respect to Mg-calcite. The continuity of individual precipitated calcite beds, a dolostone bed, and a chert bed for 140 x 50 km suggests that mineral precipitation was controlled by regional seawater chemistry rather than local processes. Thus, the high abundance of calcite that precipitated from marine waters probably represents normal precipitation from ambient Archean seawater.

4. Stratigraphic data suggests that iron-formation and calcite precipitated simultaneously in the same basin. Precipitation of calcite in shallow water and siderite in deeper water can be explained by a gradient in $Fe^{2+}$ concentration with depth. As $Fe^{2+}$ concentration increases, siderite becomes supersaturated, and precipitation of siderite could drawn down $CO_3^{2-}$ concentration reducing calcite saturation. Thus, a transition to siderite-rich iron-formation deposition with depth may require only a gradient in $Fe^{2+}$ concentration.

## REFERENCES


Beauchamp, B. and M. Savard, 1992. Cretaceous chemosynthetic carbonate mounds in the Canadian Arctic. Palaios, v. 7, p. 434-450.

Beukes, N. J. and C. A. Smit, 1987. New evidence for thrusting in Griqualand West, South Africa: implications for stratigraphy and the age of red beds. South African Journal of Geology, v. 90, p. 378-394.

Beukes, N. J., 1980. Stratigrafie en litofasies van die Campbellrand-subgrop van die Proterofitiese Ghaapgroep, noord-Kaapland. Transactions of the Geological Society of South Africa, v. 83, p. 141-170.

Beukes, N. J., 1983. Paleoenvirnomental setting of iron-formations in the depositional basin of the Transvaal Supergroup, South Africa *in* Iron-formation: Facts and problems (A. F. Trendall and R. C. Morris, eds.). Elsevier, Amsterdam. p. 131-198.

Beukes, N. J., 1987. Facies relations, depositional environments and diagenesis in a major early Proterozoic stromatolitic carbonate platform to basinal sequence, Campbellrand Subgroup, Transvaal Supergroup, southern Africa. Sedimentary Geology, v. 54, p. 1-46.

Beukes, N. J., C. Klein, A. J. Kaufman and J. M. Hayes, 1990. Carbonate petrography, kerogen distribution, and carbon and oxygen isotope variations in an Early Proterozoic transition from limestone to iron-formation deposition, Transvaal Supergroup, South Africa. Economic Geology, v. 85, p. 663-689.

Button, A., 1973. The stratigraphic history of the Malmani dolomite in the eastern and north-eastern Transvaal. Transactions of the Geological Society of South Africa, v. 76, p. 229-247.

Button, A., 1976. Iron-formation as an end member in carbonate sedimentary cycles in the Transvaal Supergroup, South Africa. Economic Geology, v. 71, p. 193-201.

Cameron, E. M., 1982. Sulphate and sulphate reduction in early Precambrian oceans. Nature, v. 296, p. 145-148.

Campbell, K. A., 1992. Recognition of a Mio-Pliocene cold seep setting from the northeast Pacific convergent margin, Washington, U.S.A. Palaios, v. 7, p. 422-433.

Cook, H. E. and M. E. Taylor, 1977. Comparison of continental slope and shelf environments in the Upper Cambrian and lowest Ordovician of Nevada in Deep-Water Carbonate Environments (H. E. Cook and P. Enos, eds.). SEPM, Tulsa. 25, p. 51-82.

Davies, G. R., 1977. Turbidites, debris sheets, and truncation structures in Upper Paleozoic deep-water carbonates of the Sverdrup Basin, Arctic Archipelago *in* Deep-Water Carbonate Environments (H. E. Cook and P. Enos, eds.). SEPM, Tulsa. 25, p. 221-247.

Des Marais, D. J., 1985. Carbon exchange between the mantle and the crust, and its effect upon the atmosphere: today compared to Archean time *in* The Carbon Cycle and Atmospheric $CO_2$: Natural Variations Archean to Present (E. T. Sundquist and W. S. Broecker, eds.). American Geophysical Union, Washington. Geophysical Monograph 32, p. 602-611.

Froelich, P. N., G. P. Klinkhammer, M. L. Bender, N. A. Luedtke, G. R. Heath, D. Cullen, P. Dauphin, D. Hammond, B. Hartman and V. Maynard, 1979. Early oxidation of organic matter in pelagic sediments of the eastern equatorial Atlantic: suboxic diagenesis. Geochimica et Cosmochimica Acta, v. 43, p. 1075-1090.

Gaillard, C., M. Rio, Y. Rolin and M. Roux, 1992. Fossil chemosynthetic communities related to vents or seeps in sedimentary basins: The pseudobioherms of southeastern France compared to other world examples. Palaios, v. 7, p. 451-465.

Grotzinger, J. P. and J. F. Kasting, 1993. New constraints on Precambrian ocean composition. Journal of Geology, v. 101, p. 235-243.

Hälbich, I. W., D. Lamprecht, W. Altermann and U. E. Horstmann, 1992. A carbonate-banded iron formation transition in the Early Protorezoicum of South Africa. Journal of African Earth Sciences, v. 15, p. 217-236.

Hartzer, F. J., 1989. Stratigraphy, structure, and tectonic evolution of the Crocodile River Fragment. South African Journal of Geology, v. 92, p. 110-124.

Holland, H. D., 1984. The Chemical Evolution of the Atmosphere and Oceans. Princeton University Press, Princeton. 582 p.

Kempe, S. and E. T. Degens, 1985. An early soda ocean? Chemical Geology, v. 53, p. 95-108.

Kennedy, W. J. and R. E. Garrison, 1975. Morphology and genesis of nodular chalks and hardgrounds in the upper Cretaceous of southern England. Sedimentology, v. 22, p. 311-386.

Klein, C. and N. J. Beukes, 1989. Geochemistry and sedimentology of a facies transition from limestone to iron-formation deposition in the Early Proterozoic Transvaal Supergroup, South Africa. Economic Geology, v. 84, p. 1733-1742.

Li, T. H., T. Takahashi and W. S. Broecker, 1969. The degree of saturation of CaCO3 in the oceans. Journal of Geophysical Research, v. 74, p. 5507-5525.

Logan, G. A., J. M. Hayes, G. B. Hieshima and R. E. Summons, 1995. Terminal Proterozoic reorganization of biogeochemical cycles. Nature, v. 376, p. 53-56.

Marshall, H. G., J. C. G. Walker and W. R. Kuhn, 1988. Long-term climate change and the geochemical cycle of carbon. Journal of Geophysical Research, v. 93, p. 791-801.

Miyano, T. and N. J. Beukes, 1984. Phase relations of stilpnomelane, ferri-annite, and riebeckite in very low-grade metamorphosed iron-formations. Transactions of the Geological Society of South Africa, v. 87, p. 111-124.

Moller, N. K. and K. Kvingan, 1988. The genesis of nodular limestones in the Ordovician and Silurian of the Oslo region (Norway). Sedimentology, v. 35, p. 405-420.

Mullins, H. T., A. C. Neumann, R. J. Wilber and M. R. Boardman, 1980. Nodular carbonate sediment on Bahamian slopes; possible precursors to nodular limestones. Journal of Sedimentary Petrology, v. 50, p. 117-131.

Noble, J. P. A. and K. D. M. Howells, 1974. Early marine lithification of the nodular limestones in the Silurian of New Brunswick. Sedimentology, v. 21, p. 597-609.

Simonson, B. M., K. A. Schubel and S. W. Hassler, 1993. Carbonate sedimentology of the early Precambrian Hamersley Group of Western Australia. Precambrian Research, v. 60, p. 287-335.

Sumner, D. Y. and J. P. Grotzinger, in review a. Herringbone calcite. Journal of Sedimentary Research.

Sumner, D. Y. and J. P. Grotzinger, in review b. Was the carbonate saturation state of Archean seawater related to oxygen concentration? Geology.

Sumner, D. Y. and S. A. Bowring, in press. U-Pb geochronologic constraints on deposition of the Campbellrand Subgroup, Transvaal Supergroup, South Africa. Precambrian Research.

Takahashi, T., 1975. Carbonate chemistry of sea water and the calcite compensation depth in the oceans *in* Dissolution of Deep-sea Carbonates (W. V. Sliter, A. W. H. Bé and W. H. Berger, eds.). Cushman Foundation for Foraminiferal Research Special Publication No. 13, p. 11-26.

Van Schalkwyk, J. F. and N. J. Beukes, 1986. The sishen iron ore deposit, Griqualand West *in* Mineral Deposits of Southern Africa (C. R. Anhaeusser and S. Maske, eds.). Geological Society of South Africa, Johannesburg. p. 931-956.

Volk, T. and M. I. Hoffert, 1985. Ocean carbon pumps: Analysis of relative strengths and efficiencies in ocean-driven atmospheric $CO_2$ changes *in* The Carbon Cycle and Atmospheric $CO_2$: Natural Variations Archean to Present (E. T. Sundquist and W. S. Broecker, eds.). American Geophysical Union, Washington. Geophysical Monograph 32, p. 99-110.

Walker, J. C. G., 1983. Possible limits on the composition of the Archean ocean. Nature, v. 302, p. 518-520.

# CHAPTER 5: HERRINGBONE CALCITE


## ABSTRACT

Herringbone calcite is a previously undescribed carbonate cement and sea-floor precipitate that is common in Archean carbonates, but rare in Proterozoic and Phanerozoic rocks. It is abundant in the ~2520 Ma Campbellrand-Malmani platform, South Africa, where field relationships, such as erosional truncation of layers of herringbone calcite and interbedding of herringbone calcite with grainstones, demonstrate that it precipitated from ambient marine water. This interpretation is supported by depositional relationships in the >2.6 Ga Huntsman Limestone of the Bulawayo greenstone belt, Zimbabwe; the 2.6 Ga Carawine Dolomite, Australia; the 1.90 Ga Rocknest Formation and the 1.8-1.2 Ga Dismal Lakes Group, Canada; the Ordovician Porterfield carbonate buildup, Virginia, and various Silurian carbonate buildups in the mid-continent, United States. Each of these occurrences is associated with anaerobic depositional environments or organic-rich sediments.

Herringbone calcite consists of alternating light and dark crenulated bands; each light-dark pair is 0.5-1.0 mm thick. Microscopically, each pair of bands consists of a row of elongate crystals with their long axes aligned perpendicular to banding and along the growth direction of the cement. The bases of the crystals are optically unoriented, but upwards in each crystal, the optical c-axis rotates until it is perpendicular to crystal elongation. The tops of the elongate crystal are thus optically aligned and length slow. The light bands of herringbone calcite correspond to the optically oriented parts of the elongate crystals whereas the dark bands correspond to the optically unoriented, lower parts of the elongate crystals. Microspar crystals are also present in some dark bands. A Mg-calcite precursor for herringbone calcite, now preserved as low Mg calcite or dolomite, is supported by the presence of microdolomite inclusions and textural differences between herringbone calcite and textures interpreted as neomorphosed former aragonite or low Mg calcite.

Precipitation of herringbone calcite may be consistent with a diffusionally controlled growth model involving branching growth of fibrous crystals and the diffusion of a precipitation inhibitor away from the crystallization surface. Since herringbone calcite is associated with oxygen-depleted depositional environments, the inhibitor promoting precipitation of herringbone calcite may be present only in poorly oxygenated seawater. Thus, the stratigraphic distribution of herringbone calcite may be an important indicator of the abundance of oxygen in carbonate depositional environments through time.

## INTRODUCTION

The composition and crystallographic characteristics of carbonate minerals contain important information about the chemical environment in which they formed. Laboratory experiments and studies of modern carbonate-precipitating systems provide background information for the interpretation of specific relationships between microenvironmental chemistry and crystal morphology and mineralogy (e.g. Folk and Assereto, 1976; Folk, et al., 1985; Burton and Walter, 1987; Buczynski and Chafetz, 1991; Chafetz, et al., 1991). As workers tackle the causes of variations in crystal morphology and mineralogy, descriptions of various marine precipitates and their distributions have become an important tool for understanding changes in depositional environments and ocean chemistry though time (Sandberg, 1983, 1985; Wilkinson, et al., 1984, 1985; Given and Wilkinson, 1985, 1986). For example, distributions of marine precipitates in Precambrian carbonate platforms show systematic changes through time including both precipitated stromatolites (Grotzinger, 1989, 1990) and beds of sea-floor precipitates (Grotzinger and Kasting, 1993). Since both facies precipitated directly from seawater, their abundance and textural changes may reflect changes in carbonate chemistry through time. Specific textures in marine precipitates may also reflect variations in ocean chemistry. Of particular interest is herringbone calcite, a distinctive carbonate with a unique crenulate, mm-scale banding that is preserved during fabric-retentive neomorphic recrystallization. It differs from previously described calcite cement textures in the presence of ubiquitous mm-scale banding that cross-cuts growth banding and the length-slow optical orientation of elongate crystals (similar to "coconut-meat" calcite of Folk and Assereto, 1976). Herringbone calcite may be particularly well suited for tracing some aspects of carbonate chemistry through time because it has well-defined crystal properties that make it easily identifiable and its spatial and temporal distribution suggests that the texture of herringbone calcite may reflect a specific chemical environment.

Although herringbone calcite is not a well known carbonate cement morphology, it is present in rocks ranging in age from Archean to Eocene (Table 5-1). Occurrences have been published under the names "zebraic dolomite" (Kerans, 1982; Simonson, et al., 1993), "zebraic calcite" (Graber, 1984), and "chevron cement" (Lehmann, 1978; Savard and Bourque, 1989). We prefer the name herringbone calcite. While "zebraic dolomite" and "zebraic calcite" were used by others due to the apparent textural similarity between zebraic chalcedony and herringbone calcite (Kerans, 1982; Simonson, et al., 1993; Graber, 1984), the crystallographic cause of the texture in the two minerals is different. Herringbone calcite has mm-thick bands that are visible in hand sample as well as microscopically (Simonson, et al., 1993) while banding in zebraic chalcedony is purely an optic axis effect seen with

crossed polarizers and is not apparent in hand sample (Frondel, 1978). There is also potential for confusion between "zebraic dolomite" and "zebra dolomite", a late-stage diagenetic fabric consisting of alternating cm-scale layers of light and dark dolomite (Gary, et al., 1974). Similarly, the term "chevron" has been used to describe an evaporative halite morphology (Chipley and Kyser, 1994) with a texture different from herringbone calcite. "Herringbone calcite", however, has not been used for any other carbonate or associated mineralogical textures, and it reflects the texture of this calcite: In hand sample and thin section, the texture of herringbone calcite is akin to the zig-zag pattern characteristic of cloth with a herringbone weave. While the term "herringbone cement" may seem to offer a definition independent of mineralogy, its genetic connotations are misleading because, technically, herringbone calcite is not always a cement since it formed encrusting beds on the sea floor in addition to cement coatings that filled primary voids and bound loose sediment particles. Thus, we use "herringbone calcite" and when discussing specific cases of dolomite with the characteristics of herringbone calcite, we use the term "dolomitized herringbone calcite".

## FIELD RELATIONSHIPS

Depositional field relationships in carbonate deposits from three regions were studied: the Late Archean Campbellrand-Malmani platform, South Africa, the Late Archean Huntsman Limestone, Zimbabwe, and the Middle Ordovician Porterfield Buildup, Virginia.

Table 5-1: Known Occurrences of Herringbone Calcite

| Age | Location | Environment | Reference |
|---|---|---|---|
| ≥2.6 Ga | Huntsman Limestone, Bulawayo, Zimbabwe | subtidal | this study; Figure 5-4A |
| 2.93 Ga | Red Lake area, Uchi Greenstone Belt, Canada | shallow water | Hofmann, et al., 1985; Figure 5-6A |
| 2.6 Ga | Carawine Dolomite, Hamersley Basin, Australia | various | Simonson, et al., 1993; Figure 5-6B |
| 2.52 Ga | Cambellrand and Malmani Subgrps., South Africa | deep subtidal to peritidal | this study; Figures 5-2 and 5-3 |
| 1.90 Ga | Rocknest Fm., Northwest Territories, Canada | shelf slope | this study; Figure 5-6C |
| 1.8-1.2 Ga | Dismal Lakes Grp., Northwest Territories, Canada | deep subtidal | Kerans, 1982, 1988; Figure 5-6D |
| Cambrian | Cathedral Formation, Canadian Rocky Mountains | reef-flat | McIlreath and Aitken, 1976 * |
| Ordovician | Porterfield buildup, Virginia | deep subtidal | this study; Figure 5-4B |
| Silurian | Pipe Creek Jr., Thornton, Schoonmaker, and Delphi buildups, Indiana, Illinois, and Wisconsin | subtidal | Lehmann, 1978; Pray, pers. comm.; Figure 5-5 |
| Silurian | West Point Fm., Gaspé Basin, Canada | reef margin | Savard and Bourque, 1989 |
| Eocene | Gulf Coast | unknown | Graber, 1984 |

*called *Yoholaminities* and interpreted as a skeletal organism

In addition, Silurian reefs along the Cincinnati-Kankakee Arch, midwestern United States, contain herringbone calcite of probable synsedimentary origin (Lehmann, 1978; Lehmann and Simo, 1988). The field settings of other occurrences of herringbone calcite are also consistent with a marine origin. The geometric relationships between herringbone calcite and various other sedimentary features demonstrate that this distinctive carbonate is a primary marine precipitate. For example: Layers of herringbone calcite are truncated erosionally; it coats sea-floor topography isopachously; herringbone calcite fills shelter porosity and stromatactis-like voids; and it forms the microtexture of columnar and domal stromatolites.

### *Campbellrand-Malmani Platform*

Depositional constraints on the origin of herringbone calcite are best established in the Campbellrand-Malmani platform of the Transvaal Supergroup, South Africa. This 2520 Ma (Sumner and Bowring, in press) platform is the oldest extensive and well-preserved carbonate platform known. The platform geometry and lateral extent of the platform imply that deposition occurred in a marine setting and facies relationships suggest that deposition occurred in both restricted and open marine depositional environments (Chapter 2). Herringbone calcite is preserved in samples from depositional environments ranging from deep subtidal to peritidal, and invariably occurs as either a marine precipitate or a synsedimentary pore-filling cement (Figure 5-1).

Herringbone calcite is most abundant in deep subtidal, open marine lithofacies which contain very little carbonate sand and no siliciclastic detritus. The Gamohaan Formation, a transgressive deposit at the top of the Campbellrand-Malmani platform, was deposited during drowning of the platform and contains extensive deep subtidal deposits rich in herringbone calcite (Chapter 4). Three relationships in the Gamohaan Formation suggest that herringbone calcite precipitated from ambient marine water. First, it fills voids within and encrusts microbialites that consist of finely laminated mat (Figure 5-2; Chapters 3 and 4). It also forms decimeter-thick beds that are continuous for up to 140 x 50 km laterally as well as numerous thinner, less continuous beds. These beds are non-stromatolitic and isopachously coat topography on the tops of the underlying beds (Figure 5-3A). Third, herringbone calcite forms a volumetrically large part of the Gamohaan Formation (Chapter 4). The quantitative proportion of herringbone calcite was estimated for a representative section of the Gamohaan Formation by recording the composition of each bed and estimating the proportions of carbonate sand, microspar, herringbone calcite, and other carbonate cements. Results for a 40 m stratigraphic interval indicate that a minimum of 15% of the total rock precipitated *in situ* as herringbone calcite with an additional 20% of the rock consisting of

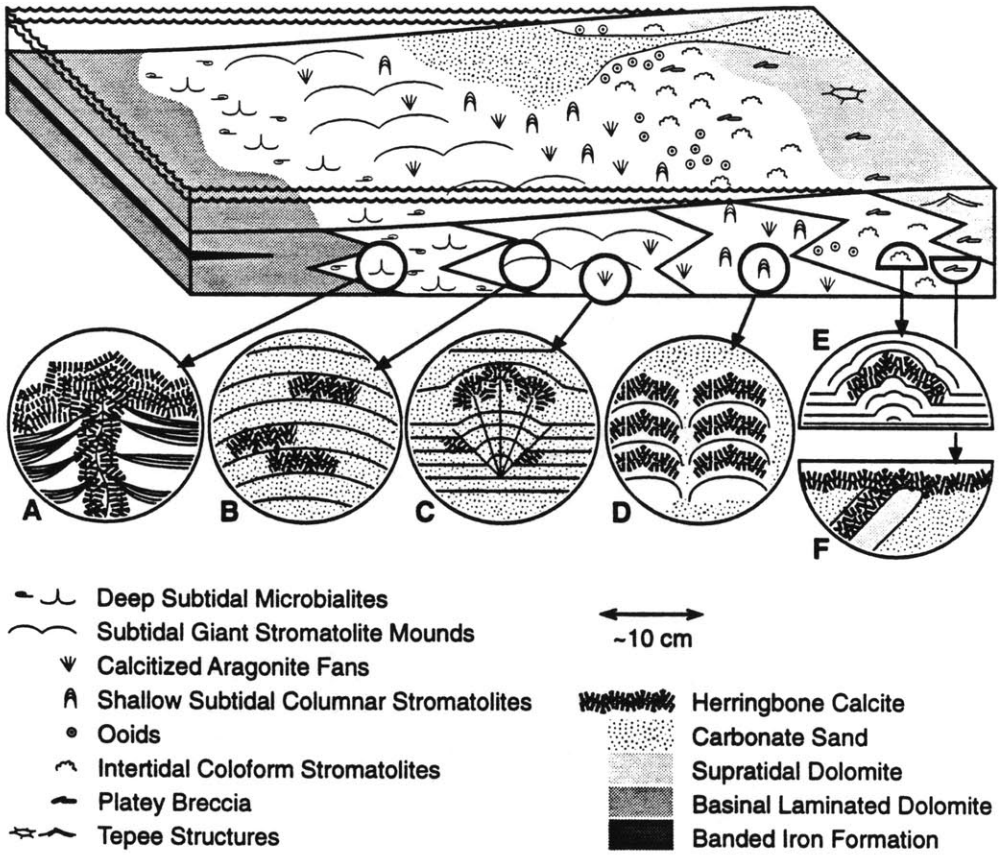


Figure 5-1: Block diagram representing ramp facies of the Campbellrand-Malmani platform showing the occurrences of herringbone calcite in different environments. The sketched view inside each circles is approximately 20 cm wide. A: Herringbone calcite is abundant in deep subtidal microbialite facies where it coats microbialites and forms centimeter- to decimeter-scale encrustations on the sea floor. The thin black lines represent preserved remnants of microbial mats (Figure 5-2). B: Herringbone calcite is present within giant subtidal stromatolite mounds. It is often poorly preserved and patchily distributed. C: Herringbone calcite coats crystal fans interpreted to have precipitated as aragonite, but now preserved as calcite (Figure 5-3B). Herringbone calcite also precipitated in shelter porosity under blades of the fans. D: Some shallow subtidal columnar stromatolites consist entirely of herringbone calcite (Figure 5-3B) while others contain only a few laminae of herringbone calcite. E: Peritidal coloform stromatolites contain rare laminae consisting of herringbone calcite. F: Layers of herringbone calcite in intertidal to supratidal settings are occasionally brecciated and redeposited. Subsequent encrustations of herringbone calcite coat the brecciated ends of the blocks or form layers concordant to bedding.

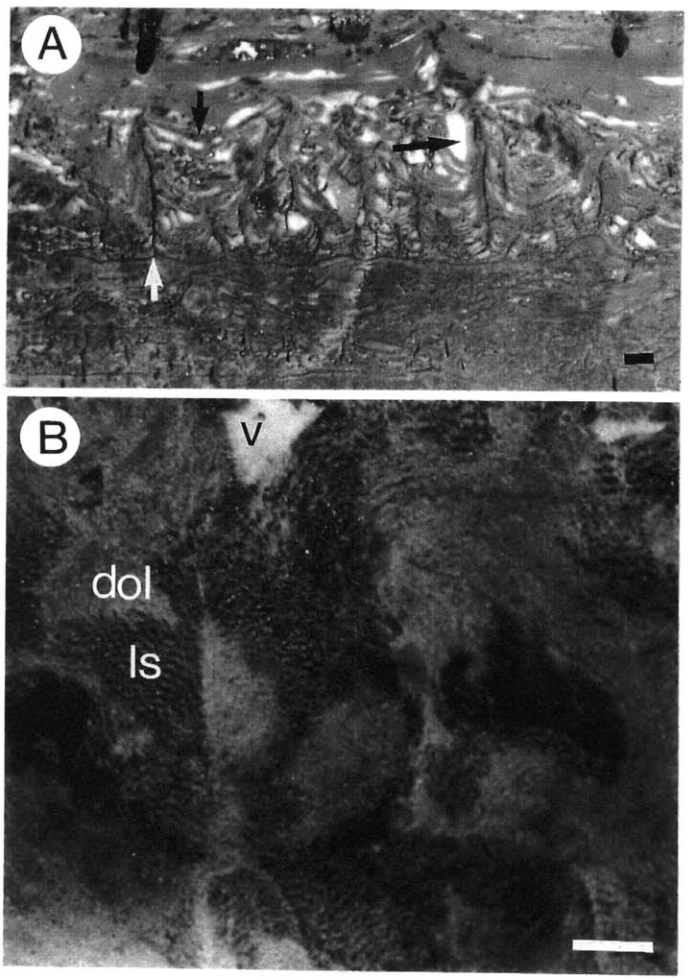


Figure 5-2: Herringbone calcite coating microbialites from the Gamohaan Formation. A) A conoform microbialite with dish-shaped voids filled with herringbone and bladed calcite. The white arrow indicates a central support that is draped by laminae interpreted to be the preserved remnants of microbial mats (short black arrow). The long black arrow points to a coating of herringbone calcite growing sideways off of a central support. It grades into bladed calcite (white) in the growth direction. Scale bar represents 1 cm. B) A herringbone calcite encrustation on a microbialite (not visible). This sample is partially dolomitized with one dolomitized region marked "dol" and one limestone region marked "ls". A void filled with bladed calcite is marked "v". The characteristic herringbone-like banding is better preserved in limestone than dolomite. Encrustations such as this one grew in all directions off of the microbialites. Scale bar represents 5 mm.

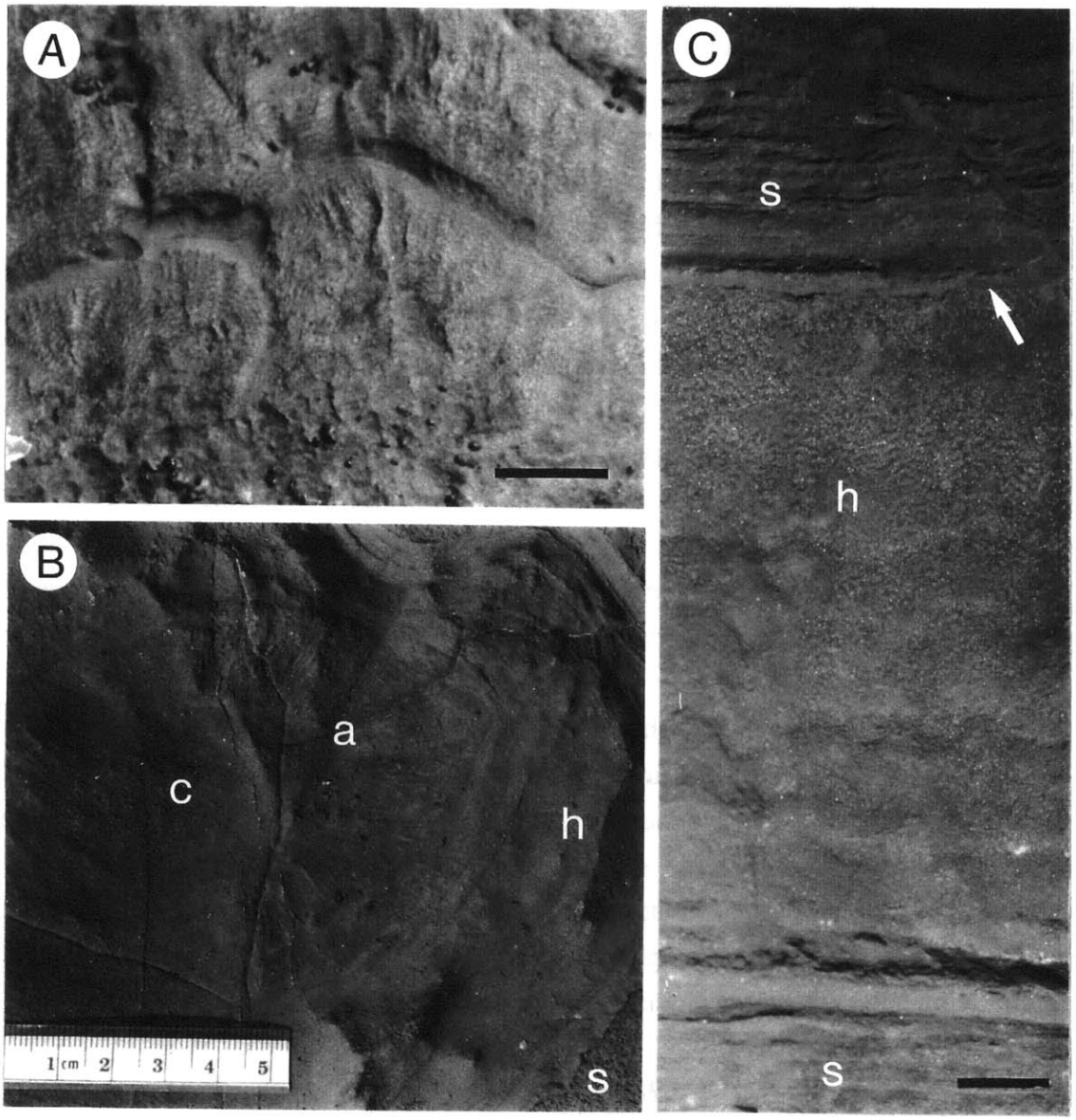


Figure 5-3: Herringbone calcite from the Campbellrand-Malmani platform. A) A 20 cm-thick herringbone calcite bed that is laterally continuous for 140 km. Note the domal structure that propagates upward in the bed due to a protuberance on the underlying bed. Scale bar represents 1 cm. B) Plan view of a column (c) consisting entirely of herringbone calcite with a calcitized aragonite fan (a) radiating off the side to the right. A subsequent encrustation of herringbone calcite (h) coats both the column and the fan. Sediment (s) filled the intra-column troughs after precipitation of the herringbone calcite encrustation. C) Partially dolomitized herringbone calcite (h) interbedded with dolomitic clastic carbonate (s). The transition from sediment to herringbone calcite is gradational while the contacts at the top of herringbone calcite layers are sharp (arrow) and occasionally scoured. Scale bar represents 5 mm.

other void-filling cements that precipitated after herringbone calcite. The large volume of cements indicate that precipitation of herringbone calcite was a synsedimentary process.

In open ramp and shelf margin carbonates, herringbone calcite is present as a constituent in giant elongate stromatolite mounds as well as columnar stromatolites, some of which consist entirely of herringbone calcite (Figures 5-1 and 5-3B). It also forms centimeter-thick layers that coat the tops of crystals in large calcitized aragonite fans which grew on the sea floor, and it occasionally fills shelter porosity within the fans (Figures 5-1 and 5-3B). Herringbone calcite is also repetitively interbedded with clastic carbonate on a centimeter scale showing a gradation from sediment to herringbone calcite and then a sharp, occasionally scoured contact with overlying carbonate sand (Figure 5-3C). In shallow subtidal to supratidal carbonates, herringbone calcite forms thin coatings on stromatolites, carbonate sand lenses, and intraclasts. In one instance, herringbone calcite precipitated on intraclasts that were later reworked, resulting in the truncation of herringbone calcite layers (Figure 5-1). Laterally discontinuous decimeter-thick beds of herringbone calcite are also present. In one locality, a paleo-channel was coated by herringbone calcite that created overhangs, and was then infilled with graded volcaniclastic sandstone containing accretionary lapilli at the base.

In addition to the relationships describe above, herringbone calcite always appears to have grown away from a specific depositional surface as a cement or encrustation and is not a later replacement phenomenon that cross-cuts primary sedimentary surfaces. These observations, combined with the abundant field evidence, demonstrate that herringbone calcite is a synsedimentary precipitate that grew in open deep subtidal to restricted peritidal marine environments during Campbellrand-Malmani platform time and is not a product of precipitation in an unusual microenvironment or of diagenetic alteration.

### *Huntsman Limestone*

Herringbone calcite is present in the ≥2.6 Ga Huntsman Limestone of the Bulawayo greenstone belt, Zimbabwe (Figure 5-4A). While limited exposure makes the stratigraphic setting of the Huntsman Limestone difficult to evaluate, depositional facies are very similar to those in deep subtidal facies of the Gamohaan Formation, South Africa. Cuspate microbialites are abundant, but herringbone calcite textures are rare within them, partially due to metamorphic recrystallization and penetrative deformation fabrics. Laterally continuous encrustations of herringbone calcite are present as coatings over mudstone layers. These crusts are commonly columnar with 2-5 cm diameters. Overlying beds of clastic carbonate drape the columns implying a synsedimentary origin for the herringbone calcite.

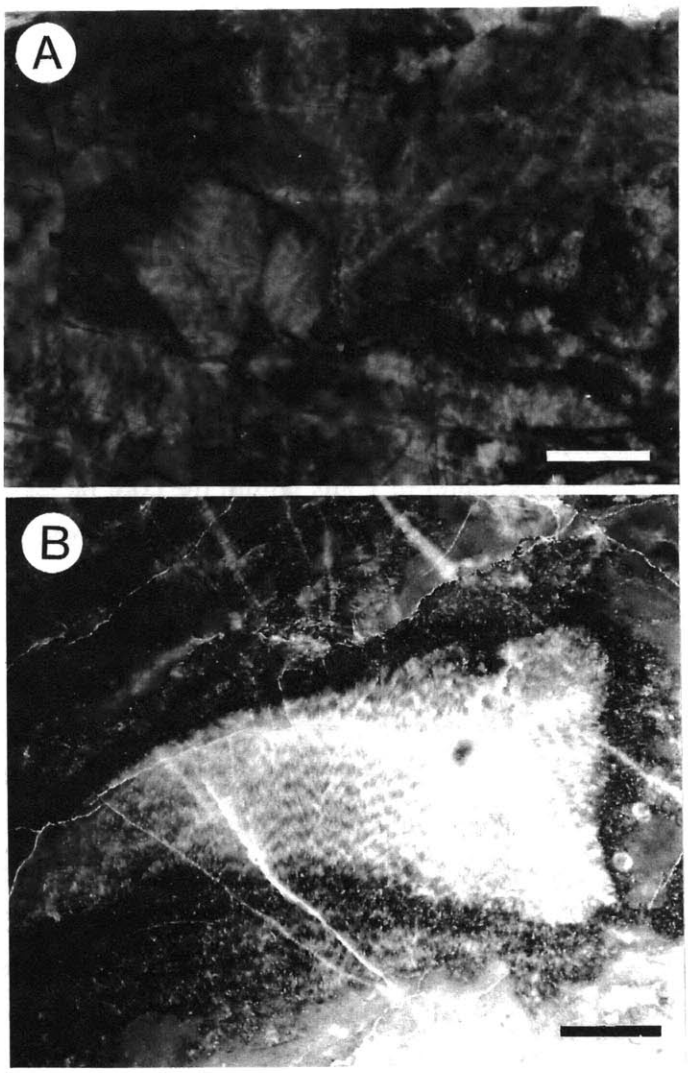


Figure 5-4: Herringbone calcite (polished and etched slabs). A) Dolomitized herringbone calcite from the Huntsman Limestone. Scale bar represents 5 mm. B) Herringbone calcite filling voids in the Porterfield buildup, Virginia. Scale bar represents 1 cm.

### *Porterfield Buildup*

Herringbone calcite is also found in a Middle Ordovician deep slope carbonate buildup exposed in Porterfield Quarry, southwest Virginia. The buildup was deposited during a marine transgression in a deep ramp setting surrounded by black shales and carbonates of the Botetourt Formation and anaerobic, non-fossiliferous Liberty Hall Formation (Read, 1982). The mound is approximately 20 km in diameter and reaches a maximum thickness of 250 m. Core facies of the mound consist of mudstone, wackestone, rare lenses and beds of packstone to grainstone, and up to 10% fibrous cements (Read, 1982), including herringbone calcite. Fossils, including bryozoans, pelmatozoans, tubules suggestive of lithistid sponges, rare crinoids and gastropods, and abundant calcified cyanobacteria and red algae, suggest a subtidal, open marine depositional environment, an interpretation supported by stratigraphic relationships (Read, 1980). The presence of calcifying cyanobacteria suggests that the mounds grew within the photic zone and rare cross stratified grainstone beds suggest that the mounds occasionally grew above wave base (Read, 1982). In contrast, lithofacies surrounding the mound are organic rich, fossil-poor, and lack evidence of photosynthetic cyanobacteria, suggesting that water depths surrounding the mounds were 30 m to more than 50 m (Read, 1982).

Herringbone calcite is found in voids within the core facies (Figure 5-4B). These cement-filled voids are 1-5 cm thick and 1-100 cm long in cross section. The tops and sides of voids are irregular with rounded sub-centimeter variability. Void floors are either similar to the sides or are smooth and planar due to deposition of calcitic internal sediment prior to cement infill like that in stromatactis cavities. The first generation of void-filling cement precipitated as either fibrous Mg-calcite or herringbone calcite. These cements do not occur in the same voids or within the same horizon in the mound. Fibrous and herringbone calcite coatings are often thicker on the tops of voids than on bases, possibly due to internal sediment deposition during cement growth. Cements are also overlain by internal sediment similar in appearance to that deposited prior to cement precipitation and Read (1982) reports open burrows in some of this second generation of internal sediment, indicating a marine origin. Dolomite silt partially filled remaining voids and coarse baroque dolomite forms the final void-occluding phase.

Several relationships suggest that herringbone calcite precipitated from marine or slightly altered marine waters in the Porterfield buildup. First, it grew in stromatactoid structures in the same position as typical marine fibrous Mg-calcite cements without the herringbone banding (e.g. Krebs, 1969; Davies, 1977). It also underlies internal sediment of probable marine origin. Cracks through crusts of fibrous cement are sometimes filled with internal sediment of probable marine origin. These relationships suggest a

synsedimentary origin for fibrous cements both with and without the herringbone banding.

### *Silurian Buildups*

Herringbone calcite is present in primary and synsedimentary voids in at least four buildups deposited during Silurian time in Illinois, Indiana, and Wisconsin (Lehmann 1978; Pray, pers. comm., 1993). They grew on the Wabash Platform over the Kankakee-Cincinnati arch between the deeper water Michigan, Illinois, and Appalachian basins. They consist of isolated buildups surrounded by argillaceous carbonate.

The Pipe Creek Jr. buildup formed within the Late Silurian Wabash Formation and contains minor amounts of herringbone calcite. The buildup has a minimum diameter of 1.8 km and a preserved height of 48 m with estimates of synsedimentary relief ranging from 90-200 m (Lehmann and Simo, 1988). The Pipe Creek Jr. buildup was deposited in a deep, quiet water environment as demonstrated by the lack of shallow water sedimentary structures and evidence for emergence. Preserved areas of the buildup do not show evidence of photosynthetic organisms. However, deposition above the photic zone, for at least the top of the buildup, is supported by the presence of *Renalcis*, a photosynthetic calcified cyanobacteria, in breccia clasts preserved on the buildup slope. Normal marine conditions are supported by diverse fauna and a lack of restricted environmental indicators (Lehmann and Simo, 1988). In contrast, interbuildup sediments consist of argillaceous micritic carbonate containing only limited *in situ* fauna suggesting high salinity, a cloudy water column, or anaerobic bottom waters which limited productivity and colonization (Lehmann, 1978).

Marine cements are very abundant in the preserved buildup flank facies; herringbone texture is present only in the largest pores and in fractures associated with sedimentary dikes (Lehmann, 1978). Fibrous cements are interpreted as marine in origin because 1) they are interbedded with pelloidal and marine skeletal internal sediment, 2) marine encrusters are contained within sedimentary dikes occluded by fibrous cement, 3) resedimented clasts contain fibrous cement, and 4) cement formed encrustations on the sea floor (Lehmann, 1978).

The Thornton buildup, also on the Wabash platform, is similar to the Pipe Creek Jr. buildup, and formed within the argillaceous Middle Silurian Racine Formation (McGovney, 1988). It has a diameter of 2.0-2.7 km and a maximum preserved thickness of 90 m. It was also deposited in a low energy marine environment. Fibrous cements are abundant in both buildup center and flank settings with herringbone calcite textures common in buildup core facies (Figure 5-5A; Lehmann, 1978). Fibrous and herringbone calcite cements are present in inter- and intra-particle voids, framework voids, and stromatactis voids (McGovney, 1988)

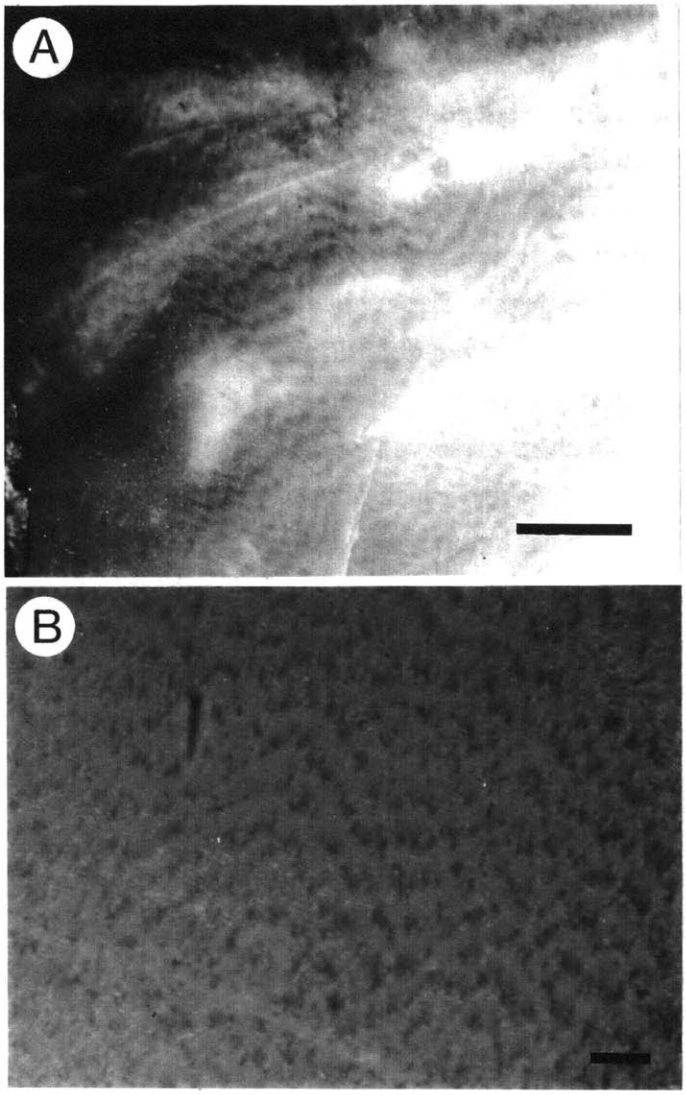


Figure 5-5: Dolomitized herringbone calcite from Silurian reefs in the mid continent, United States (samples courtesy of L. Pray). A) Polished slab from Thornton reef. Scale bar represents 5 mm. (Sample TT146X) B) Thin section in transmitted light from Schoonmaker reef. Scale bar represents 1 mm. (Sample SK-4)

and are interpreted as marine in origin based on texture of the fibrous cements and rare synsedimentary erosional truncation of cements. Two other Silurian buildups on the Wabash platform, the Schoonmaker (Wisconsin) and Delphi (Indiana) buildups, also contain herringbone calcite (Figure 5-5B; Lehmann, 1978; Pray, pers. comm., 1993).

### *Other Localities*

Herringbone calcite has been observed in a number of other deposits of various ages (Table 5-1). It is most abundant in Archean carbonates including the ~2930 Ma Uchi greenstone belt (Figure 5-6A; Hofmann, et al., 1985) and the ~2.6 Ga Carawine Dolomite, Hamersley Supergroup, Australia (Figure 5-6B; Simonson, et al., 1993). Simonson et al. (1993) interpret dolomitized herringbone calcite from the shallow water Carawine Dolomite as marine in origin based on its encrusting geometry and its presence as discrete layers in domal structures. Herringbone calcite is less abundant in Proterozoic carbonates. It is present in the 1.9 Ga Rocknest Formation, Canada, where it occurs in slope facies (Figure 5-6C; J. P. Grotzinger, unpublished data), and the Mesoproterozoic Dismal Lakes Group, Canada (Figure 5-6D; Kerans, 1982; Kerans and Donaldson, 1988), where herringbone calcite precipitated in association with sub-wave base stromatolites on an extensive platform. Although herringbone calcite is even less common in Phanerozoic carbonate accumulations, it has been observed in rocks as young as Eocene in age (Graber, 1984). Most Phanerozoic herringbone calcite precipitated in subtidal depositional environments, with the possible exception of that found in reef-flat facies of the Cambrian Cathedral Formation (McIlreath and Aitken, 1976). In each report of herringbone calcite, the favored interpretation is that it precipitated from marine water in voids or on depositional surfaces.

## PETROGRAPHIC DESCRIPTION

Samples and thin sections from the Campbellrand-Malmani platform, Huntsman Limestone, the Carawine Dolomite, Rocknest Formation, Dismal Lakes Group, Porterfield Buildup, and various Silurian buildups from the mid-continent have been studied to characterize the texture of herringbone calcite and its crystallographic properties.

The most distinctive characteristic of herringbone calcite is its 0.5-1.0 mm thick serrated banding (Table 5-2) defined by alternating light and dark layers that trend approximately perpendicular to the growth direction. In outcrop, this gives herringbone calcite a distinctive appearance with a shiny or silky texture in direct sunlight due to reflections from the light bands (Figures 5-2B and 5-3). Dark bands are dull in outcrop and weather recessively. Dolomitized herringbone calcite looks similar, but textural detail is often less well

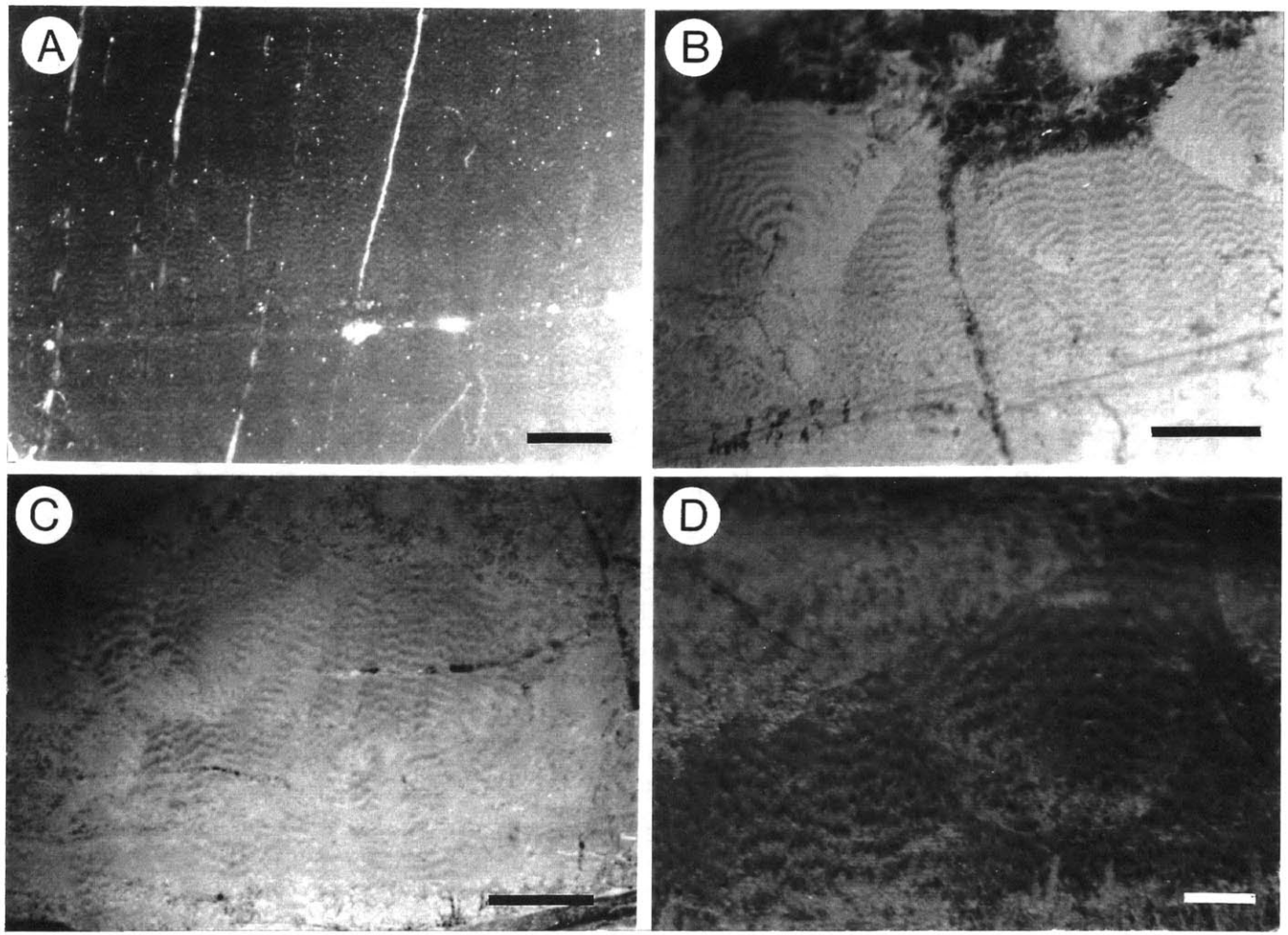


Figure 5-6: Herringbone calcite. A) Polished slab from the Red Lake area, Uchi greenstone belt. Scale bar represents 5 mm. (photograph courtesy of H. Hofmann) B) Dolomitized herringbone calcite in thin section in transmitted light from the Carawine Dolomite,. Scale bar represents 5 mm. (sample courtesy of B. Simonson) C) Dolomitized herringbone calcite in thin section in transmitted light from the Rocknest Formation. Scale bar represents 5 mm. D) Dolomitized herringbone calcite in thin section in transmitted light from the Dismal Lakes Group. Scale bar represents 2 mm. (sample courtesy of C. Kerans)

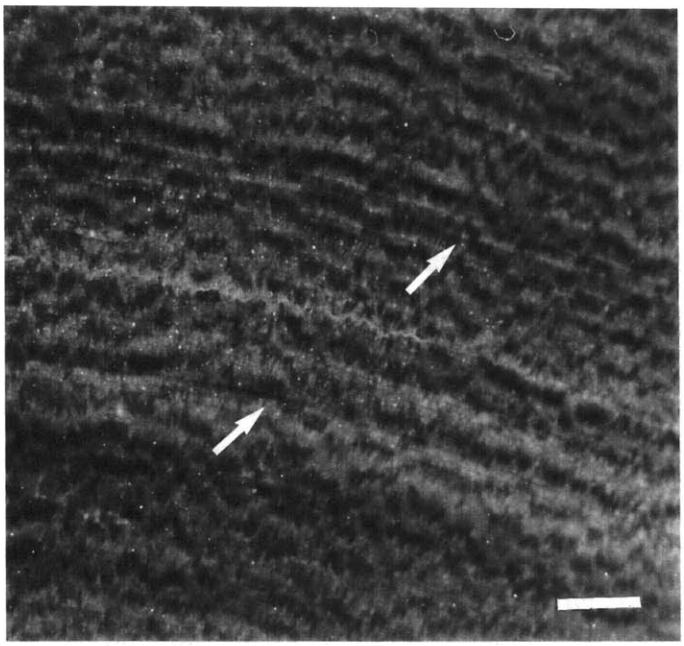

Figure 5-7: Polished and etched slab of herringbone calcite with trains of inclusions defining growth horizons (arrows) from the Gamohaan Formation. Note that growth horizons do not correspond with the serrate crystal banding. Sample is from the bed of herringbone calcite shown in Figure 5-3a. Scale bar represents 2 mm.

preserved (Figure 5-2B); light layers are grayish to red-brown and still have a sheen, particularly in strong sunlight. Intervening dark layers are typically red-brown in color. Extensive dolomitization produces an equigranular fabric with no remnants of the original texture.

In both handsample and thin section, herringbone banding shows millimeter-scale and sub-millimeter scale discontinuities and crenulations (Figure 5-7). Light bands bifurcate, join, and end causing 1-10 mm variations in relief along overlying bands. Similar variations are also created by doming of bands over lenses of slightly larger calcite crystals between bands. Relief in bands persists for up to a centimeter in overlying bands. On a sub-millimeter scale (0.5-0.8 mm; Table 5-2), light bands are crenulated and dull bands fill the intervening space. Some of the larger crenulations are inherited from one light band to the next so that successive bands have similar shapes. Small-scale irregularities are abundant enough, however, that bands separated by several millimeters have unrelated crenulations. The crenulations give herringbone calcite a zig-zag or herringbone-like texture and are one of its most distinctive attributes.

Microscopically, herringbone calcite consists of layers of ~500 x 100 μm crystals with their long axes aligned perpendicular to banding (Figures 5-8 and 5-9; Table 5-2). Intervening layers of microspar crystals are sometimes present (Figure 5-8B). The layers of elongate crystals are parallel to the macroscopic banding, but neither the bases nor the tops of the crystals are well aligned, and neighboring elongate crystals can be vertically offset from each other by as much as 80 μm. Boundaries between elongate crystals are interlocking and irregular. In transmitted light, they are indistinct (Figure 5-9A), whereas under crossed polarizers they are defined by sharp changes in birefringence color (Figures 5-9B and C). Extinction patterns in elongate crystals are complex. The c-axis at the base of a given crystal has a random orientation. In the growth direction of the crystal, however, the c-axis progressively rotates until it is oriented roughly perpendicular to crystal elongation

Figure 5-8: Herringbone calcite in thin section between crossed polarizers from the Gamohaan Formation. "l" marks layers corresponding to macroscopically light bands, "d" marks layers corresponding to macroscopically dull bands, and "v" marks voids filled with bladed calcite cements. Arrows in the lower left corner indicate the orientation of the polarizers. A) Radiating growth of herringbone calcite grading into void-filling bladed calcite on the right. Box outlines the field of view in B. Scale bar represents 500 μm. B) Herringbone calcite that grew from left to right and finally graded into bladed calcite. Note the alternation of dull and light bands. The arrow points to a zone in an elongate crystal where the c-axis is perpendicular to the thin section and thus remains extinct with rotation of the polarizers. This area does not contain microspar crystals which are common in dull bands in this thin section and is thus easy to distinguish from true dull bands. Scale bar represents 500 μm. C) One dull and parts of two light bands of herringbone calcite from the same sample shown in A and B. Note the microspar crystals (arrow) in the dull band as well as the presence of both extinct and non-extinct crystals. Extinction in the elongate crystals is variable. Scale bar represents 100 μm.

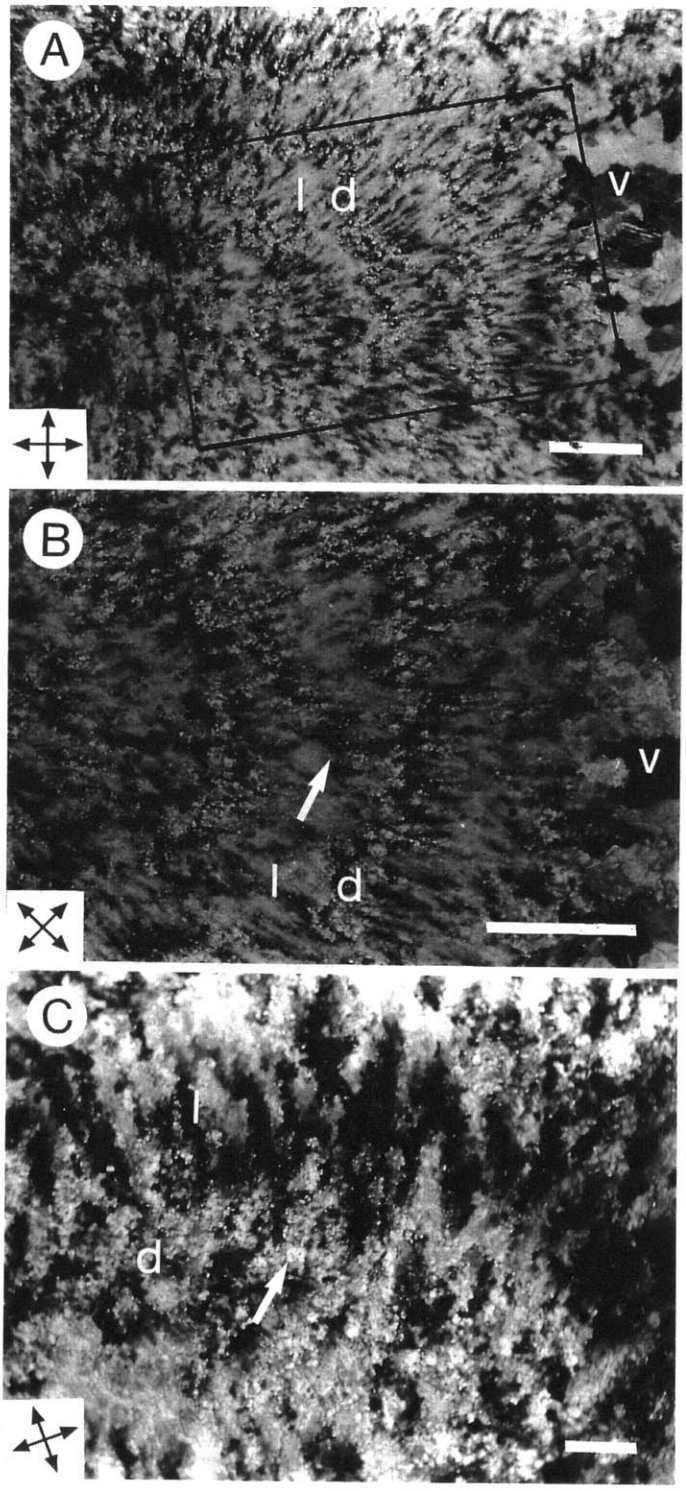
A
l d
v
B
v
l d
C
l
d

Table 5-2: Petrographic Properties of Herringbone Calcite

| | Mineralogy (c=calcite, d=dolomite) | Preservation (g=good, p=poor, v=very) | Macroscopic Banding Width | Amplitute of Band Variations | Dull Band Width | Microspar Crystal Size | Shiny Band Width | Elongate Crystal Length | Elongate Crystal Width | Undulose Extinction | C-axis Rotation Along Growth Direction | C-axis Rotation Around Elongate Axis | Microdolomite Inclusions | Trains of Inclusions |
|---|---|---|---|---|---|---|---|---|---|---|---|---|---|---|
| Campbellrand-Malmani | | | | | | | | | | | | | | |
| Deep Subtidal | c | vg | 730 | 630 | 150 | 30 | 560 | 540 | 70 | X | X | X | X | X |
| Shallow Subtidal | c d | g | 640 | 550 | 150 | 50 | 475 | 300 | 125 | X | X | | | X |
| Peritidal | d | p | 700 | 450 | 175 | 60 | 525 | 300 | 150 | X | X | | --- | |
| Huntsman Limestone | d | vp | 650 | | | | | | | | | | --- | |
| Carawine Dolomite | d | p | 580 | 375 | 125 | 50 | 450 | 150 | 75 | | | | --- | X |
| Rocknest Formation | d | p | 700 | 500 | 300 | 50 | 450 | 200 | 75 | X | X | | --- | |
| Dismal Lakes Group | d | p | 590 | 500 | 200 | 50 | 350 | 250 | 50 | | | | --- | |
| Porterfield Buildup | c | vg | 1000 | 1000 | 200 | none | 800 | 650 | 100 | X | X | X | X | |
| Thornton Buildup | d | vp | 930 | 800 | 500 | 100 | 450 | 100 | 100 | | | | --- | |
| Schoonmaker Buildup | d | p | 1000 | 800 | 400 | 75 | 600 | 100 | 75 | | | | --- | |

Numerical entries represent the average of multiple measurements and are in μm. "none" indicates that the microspar crystals are absent. "X" indicates that the features was observed. "---" indicates that all samples are dolomite and microdolomite inclusions are not expected. Blank entries indicate that the feature was not observed.

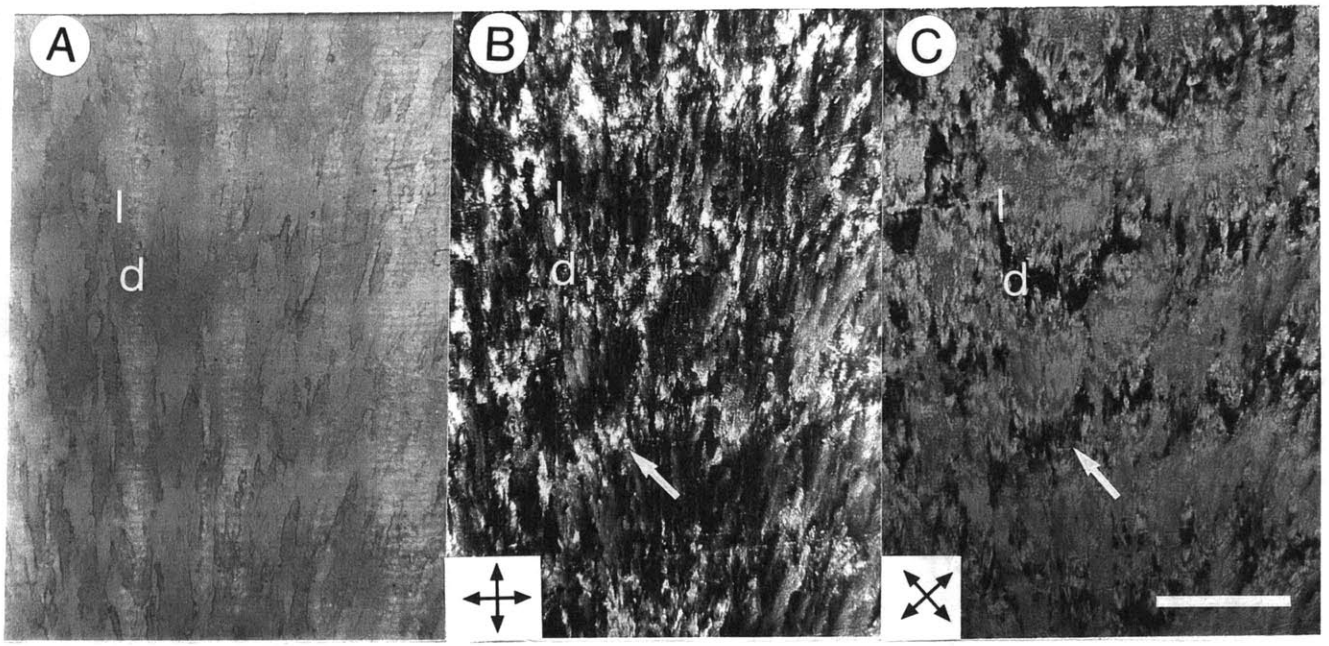


Figure 5-9: Herringbone calcite in thin section from the Porterfield build-up. "l" marks bands corresponding to macroscopically light bands and "d" marks layers corresponding to macroscopically dull bands. Microspar crystals are absent from the dull bands. Arrows in the lower left corner indicate the orientation of the polarizers. All three photographs are of the same view and the scale bar represents 500 μm. A) Plane light view of herringbone calcite showing planar crystal boundaries with small-scale irregularities. B and C) Herringbone calcite between crossed polarizers with the same view. The arrow indicates the same point in a dull band (d) in both photographs. Note that the crystals indicated transmit light with the polarizers perpendicular to the edges of the photograph and are extinct when the polarizers are rotated 45°. In contrast, the majority of the light bands (l) are extinct in b and transmit in c. This demonstrates the rotation in optic axes within the elongate crystals defining banding in samples without microspar as well as the nearly uniform optical orientation within light bands.

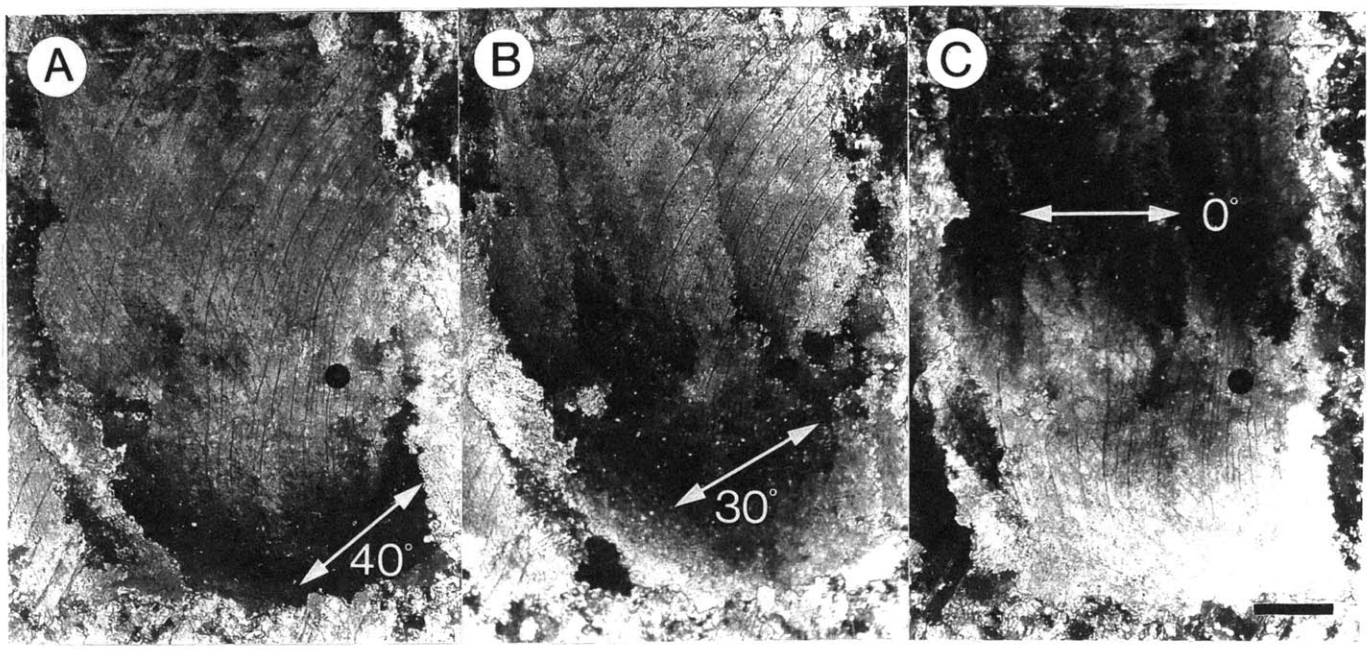


Figure 5-10: An unusually large elongate crystal in herringbone calcite from the Porterfield build-up, Virginia. All three photos show the same field of view with crossed polarizers and the scale bar represents 100 μm. Arrows in the lower left corner indicate the orientation of the polarizers. Although this crystal is exceptionally large, its extinction pattern is identical to that of the much smaller elongate crystals that compose the majority of herringbone calcite from the Porterfield build-up. The white arrows indicate the c-axis orientation of the extinct region within the crystal. In each case, the c-axis is oriented within 10° of the plane of the thin section as determined with a universal stage. Note that the c-axis migrates into the plane perpendicular to crystal elongation from the base to the top of the crystal.

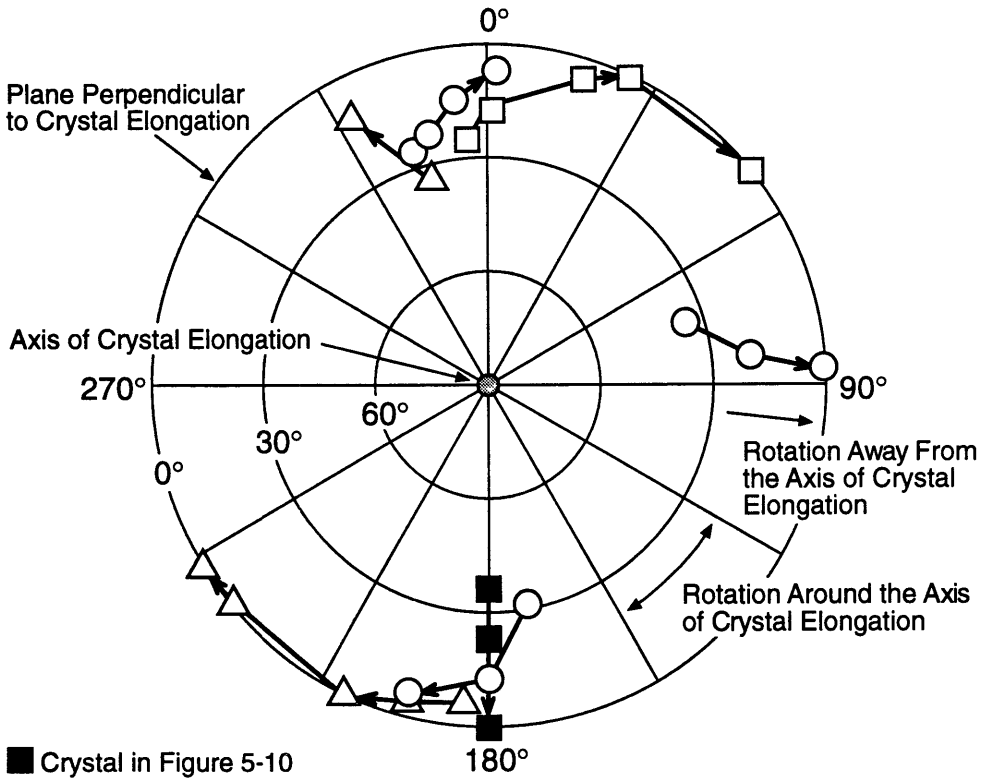


Figure 5-11: Polar plot of the change in c-axes of elongate crystals in herringbone calcite from Campbellrand-Malmani platform and the Porterfield buildup as determined with a universal stage. The axis of crystal elongation is aligned with the pole at the center of the plot. The outer circle represents the plane perpendicular to crystal elongation. Rotation of c-axes towards the plane perpendicular to crystal elongation is reflected by outward radial changes. Rotation of c-axes around the axis of crystal elongation is reflected by rotations around the pole at a constant radius. Each measurement is represented by a symbol and arrows connect measurements from the base to the top of a single crystal. Note that all crystals show a rotation of the c-axis towards the plane perpendicular to crystal elongation. The magnitude of this rotation depends on the initial angle of the c-axis and is often 30° or more. In addition, most crystals show rotation of the c-axis around the axis of crystal elongation. This rotation is most pronounced when the c-axis is nearly perpendicular to crystal elongation.

(Figures 5-10 and 5-11). Thus, the lower part of each crystal has undulatory extinction and the upper 1/3 to 2/3 of each crystal has unit extinction and is length slow. In addition to the rotation of the c-axis from a random to a length-slow orientation, many elongate crystals show an additional rotation of the c-axis around the direction of crystal elongation (Figure 5-11). Microspar crystals between the tops and bottoms of successive layers of elongate crystals (Figure 5-8B) are 30-100 μm equant crystals with unit extinction. They are optically unoriented. Better preserved samples contain smaller microspar crystals, and microspar crystals are absent from herringbone calcite in the Porterfield buildup (Figure 5-9).

Macroscopic light bands in herringbone calcite consist of the optically oriented tops of elongate crystals and are shiny in outcrop due to the parallel alignment and optical orientation of the crystals. Dark bands consist of overlapping tops and bottoms of elongate crystals and the microspar crystals where present (Figures 5-8 and 5-9). The bands are dark both in hand sample and in thin section under crossed polarizers because the bases of the elongate crystals and the microspar crystals are optically unoriented and some crystals are extinct at any given orientation of the polarizers (Figures 5-8, 5-9, and 5-10). Dark bands are not due to c-axis alignment perpendicular to the thin section (as suggested by Graber, 1984 and Simonson, et al., 1993). Universal stage c-axis orientation data indicate that the bases of the elongate crystals have random optic axis orientations and c-axes in dark bands are not universally perpendicular to the thin section (Figures 5-10 and 5-11). Some crystals do have a c-axis orientation perpendicular to the thin section (Figure 5-8B), but they do not correspond to macroscopic dark bands.

End on, herringbone calcite has a much different character (Figure 5-12). Banding is absent and the texture consists of patches of micritic crystals and cross sections of elongate crystals. Cross sections of elongate crystals are equant to slightly elongate with diameters ranging from 50 to 100 μm. They have poorly defined crystal boundaries and unit to undulatory extinction. Neighboring crystals often show similar elongation, but their optical orientations are variable over small areas. In transmitted light, wandering, subangular boundaries consist of distinct crystal boundaries with rare microspar crystals (Figure 5-12A). These boundaries usually separate 0.5 to 2 mm groups of optically oriented crystals with sharp extinction angle contrasts, but not all zones with highly contrasting extinction angles show distinct boundaries in transmitted light. Although these boundaries are present in all cross sectional views of herringbone calcite, they are interpreted as diagenetic in origin rather than as primary crystal boundaries due to their irregularity and discontinuity.

Herringbone calcite contains abundant anhedral, transparent inclusions that are probably fluid inclusions. These 1-3 μm inclusions are both dispersed throughout the crystals and concentrated along crystal boundaries. In well preserved thin sections and slabs of

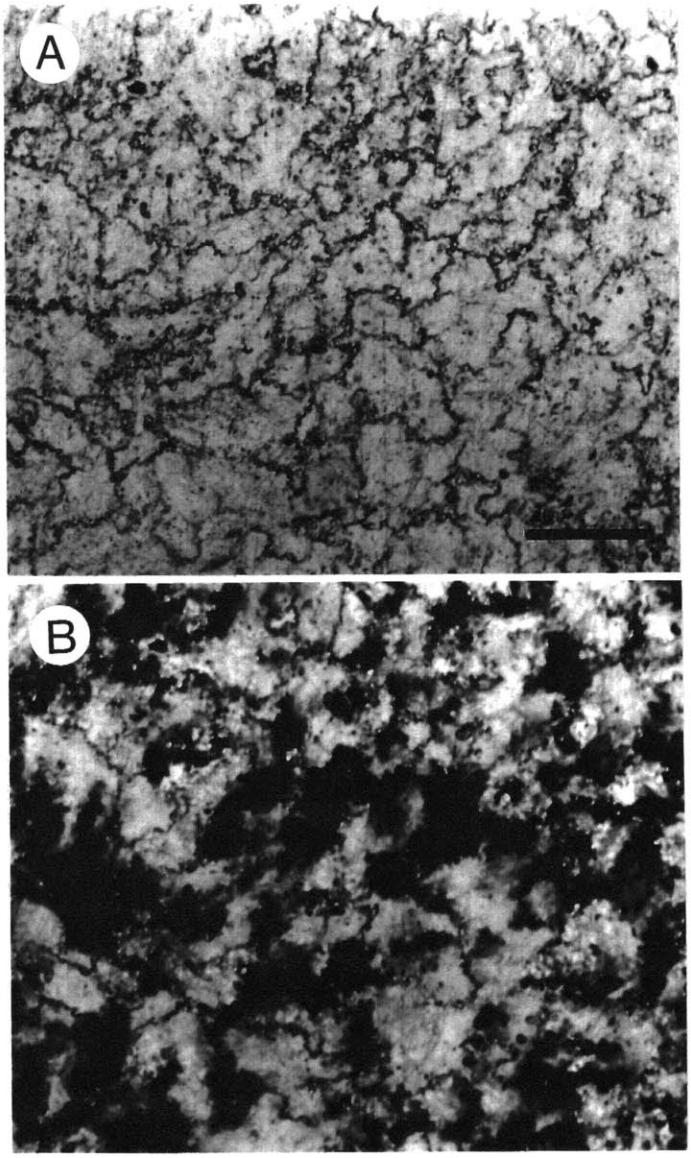


Figure 5-12: Thin section of herringbone calcite perpendicular to the growth direction from the Gamohaan Formation. Both photographs show the same field of view and the scale bar represents 200 μm. A) In transmitted light, irregular boundaries are visible. They do not close on themselves and crystal boundaries are indistinct. B) Between crossed polarizers, crystals show various optical orientations.

herringbone calcite, laterally continuous zones of fluid inclusions are aligned parallel to coated surfaces (Figure 5-7). They form ~0.1 mm inclusion-rich zones variably spaced from <1-3 mm apart. The distance between any given pair of inclusion trains is constant. Inclusion trains do not show any of the small-scale irregularities expressed by the light-dark crystal band boundaries: Although inclusion trains and banding are parallel on average, they do not correspond exactly and band boundaries cross back and forth across inclusion trains at irregular intervals (Figure 5-7). Inclusion trains do reflect some of the larger scale variations in light-dark banding as demonstrated by doming of both over underlying topography, but on a finer scale, the two do not correspond.

Other inclusions in herringbone calcite include 5-30 μm, clear inclusions that occasionally have one or more rhombic faces, but are more commonly anhedral (Figure 5-13). Etching in dilute acetic acid dissolved the calcite matrix, but not these inclusions suggesting that they consist of dolomite (Lohmann and Meyers, 1977). Electron microprobe analyses using the same analytical conditions described by Lohmann and Meyers (1977) demonstrate that the calcite matrix contains 0.66±0.09 mol % $MgCO_3$ (8 analyses) whereas the inclusions contain 43.0±1.8 mol % $MgCO_3$ (5 analyses), confirming the dolomite interpretation The microdolomite inclusions are in optical continuity with the host calcite and cleavage planes are continuous from the calcite into the dolomite (Figure 5-13A). These observations strongly suggest that the dolomite inclusions formed from the exsolution of Mg contained within the original calcite. Inferred bladed and blocky low Mg-calcite cement associated with the best preserved herringbone calcite cements do not contain microdolomite inclusions.

### *Alteration*

Herringbone calcite is often recognizable in both hand sample and thin section even when it has been extensively recrystallized or dolomitized. The distinctive herringbone banding persists through all but the most obliterative recrystallization, but the size and character of the component crystals change dramatically. With progressive alteration, microspar crystals become more common and increase in size (Figure 5-14A). Extinction patterns in elongate crystals become less undulatory with alteration; extinction jumps from one subcrystal to the next as opposed to showing smooth transitions. With more extensive alteration, all crystals show unit extinction, and, with stage rotation, extinction still moves vertically through the light bands by means of multiple crystals rather than a single undulatory crystal. Tops of bands typically retain the uniform optical orientation that produces the macroscopic herringbone calcite sheen. Extensive alteration results in equant crystals of uniform size preserving only hints of the original texture (Figure 5-14B). Often the her-

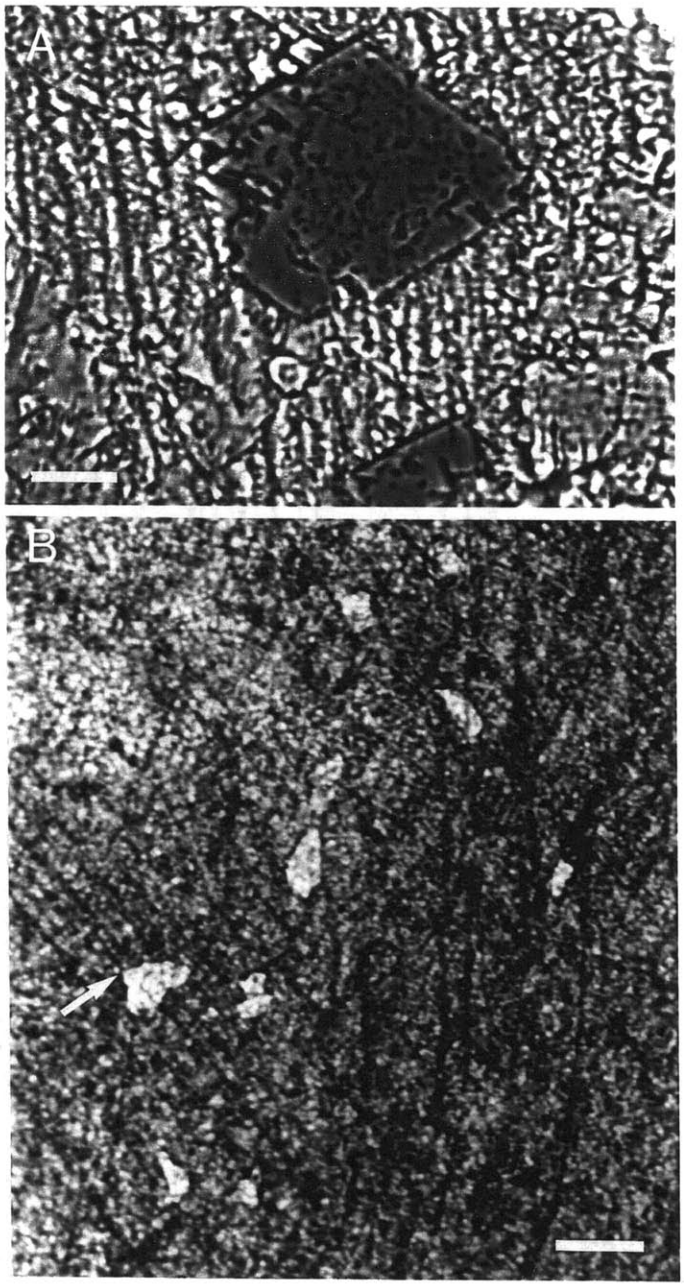


Figure 5-13: Microdolomite inclusions in herringbone calcite from the Porterfield buildup. A) Electron probe scanning image of a euhedral dolomite inclusion. The light background is calcite that was etched in dilute acetic acid. Scale bar represents 10 μm. B) Thin section of herringbone calcite etched with dilute acetic acid in transmitted light. Inclusions appear light against dark calcite because they were not etched by acetic acid. Note cleavage planes are continuous from the calcite into the dolomite inclusions (arrow). Scale bar represents 50 μm.

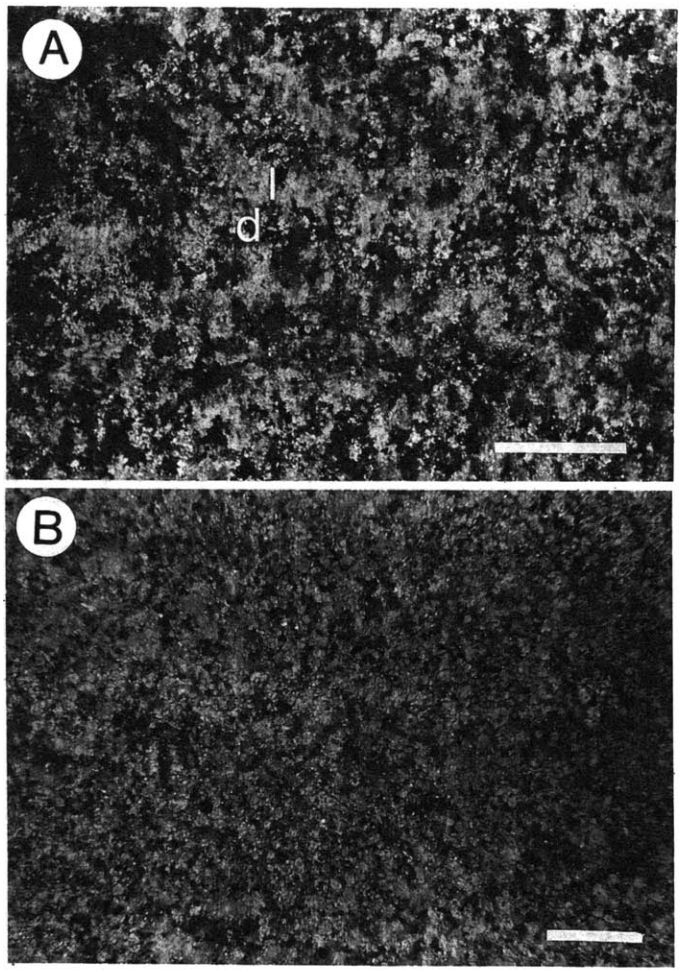


Figure 5-14: Altered herringbone calcite in thin section. Scale bars represent 200 μm. A) Poorly preserved herringbone calcite between crossed polarizers. Note that elongate crystals are still present and the characteristic alternation between light (l) and dull (d) bands are still visible. Undulose extinction is rare, however. B) Dolomitized herringbone calcite retaining few of the microscopic characteristics of herringbone calcite. The herringbone texture in this sample is visible in hand sample, but none of the characteristic microscopic properties are preserved.

ringbone calcite texture is still visible in hand sample even when it is extremely difficult to identify in thin section.

The textural degradation of herringbone calcite when it becomes dolomitized is much like that occurring during progressive recrystallization; crystal sizes coarsen and become more uniform in extinction. Dark bands, however, appear to be more susceptible to dolomitization. In partially dolomitized samples, dark bands are replaced more extensively than light bands. The same is true for samples partially replaced by chert.

## DISCUSSION

### *Original Mineralogy*

Herringbone calcite is interpreted to have precipitated as Mg-calcite rather than aragonite or low Mg calcite. Petrographically, it is distinct from neomorphosed aragonite textures which typically consist of equant to elongate crystals with unoriented optic axes and inclusions defining remnants of the original fibrous texture (Sandberg, 1975). In the Campbellrand-Malmani platform, herringbone calcite coats calcitized aragonite botryoids (Figure 5-3B), yet shows none of the characteristic aragonite replacement features, implying that herringbone calcite precipitated as low Mg calcite or Mg-calcite rather than aragonite. The presence of dolomite inclusions in optical continuity with the calcite suggests a Mg-calcite rather than a low Mg calcite primary mineralogy.

### *Crystallization Model*

#### Petrographic Constraints

Even though all studied samples of herringbone calcite are interpreted to have inverted from Mg-calcite to calcite and many have experienced more extensive recrystallization, several aspects of the herringbone calcite texture probably reflect crystal properties of the original precipitate. For example, unlike crystals in most diagenetic mosaics, the optic axes of the elongate crystals change systematically with respect to the growth direction defined by macroscopic relationships. This consistent relationship holds regardless of the orientation of the growth surface. In addition, recrystallization and dolomitization of herringbone calcite produce an increase in crystal uniformity: undulatory crystals are replaced by multiple equant crystals with more uniform extinction. Thus, it is proposed that elongate crystals with rotating c-axes have been the least altered texturally whereas crystals with more uniform optic axes are products of recrystallization. C-axes in the original precipi-

tates probably rotated much like those in the best preserved elongate crystals. Banding in herringbone calcite is probably also original because it is defined by the rotation of c-axes in addition to crystal layering. The microspar crystals in the dark bands may be the result of neomorphism of the bases of the elongate crystals or could represent a sporadically developed primary feature.

The smoothness and parallel arrangement of inclusion trains and their similarity to inclusion trains defining growth profiles in void filling cements (e.g. Schroeder, 1972; Roedder, 1994) suggest that they represent time horizons during cement precipitation. Since the crystal bands in herringbone calcite do not correspond to the trains of inclusions, they are not time lines. Therefore the nucleation of new elongate crystals in herringbone calcite is not caused by fluctuations in bulk water chemistry. The discontinuity of bands in herringbone calcite supports this interpretation because bands caused by temporal fluctuations are usually laterally continuous, particularly within a single void (Schroeder, 1972). Bands in herringbone calcite are not continuous implying that the banding is not caused by fluctuations in external conditions affecting carbonate precipitation. Models of herringbone calcite formation must therefore rely on local crystallization processes to produce banding without requiring external fluctuations in chemical conditions.

**Spherulitic Precipitation**

The geometry and optical characteristics of elongate crystals in herringbone calcite are consistent with a model of spherulitic crystal growth modified from Keith and Padden (1963). These authors described the crystallization of polymers and minerals from melts in terms of conditions promoting the two key requirements for spherulitic growth: 1) a fibrous growth habit and 2) noncrystallographic branching of fibers. The most important factor promoting both fibrous habit and branching is the presence of a chemical that is excluded from the crystal during crystallization and which adsorbs onto slowly growing crystal faces inhibiting continued growth.

Fibrous crystal morphology is promoted by the build-up of the inhibitor and depletion of growth components near the crystallization front (Keith and Padden, 1963). As a crystal grows, the concentration of impurities increases at the boundary between the crystal and solution due to its exclusion from the crystal (Figure 5-15). Conversely, the concentration of the growth components is depleted depressing the saturation state. Any projection in the crystal surface that grows beyond the average crystal surface sees both an increase in saturation and a decrease in the concentration of impurities. Thus, the projection has a faster growth rate than the average surface and extends farther into the fresh solution resulting in a fibrous crystal morphology. In general, this process promotes the preferential growth

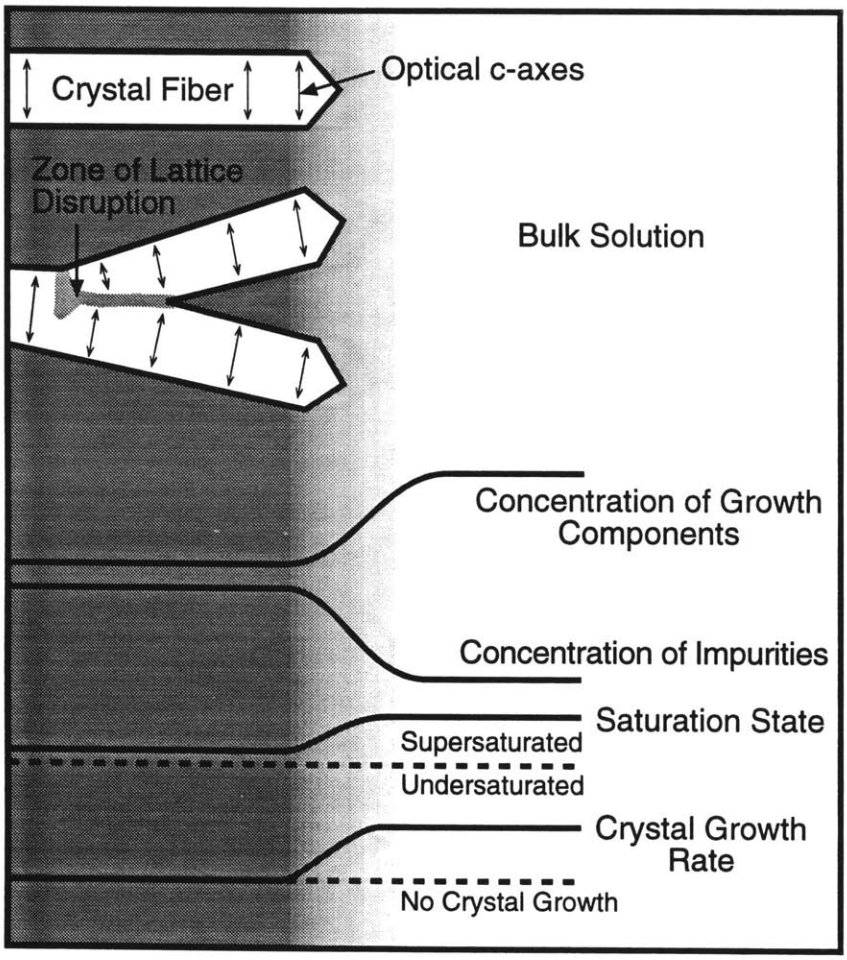


Figure 5-15: Model for spherulitic precipitation of branching fibrous crystals. Precipitation of a mineral changes local concentrations of crystal growth components which are depleted relative to the bulk solution, and impurities which are excluded from the crystal and thus enriched by precipitation. Precipitation driven depletion and enrichment of chemicals is balanced by diffusion of fresh solution to the site of precipitation creating a diffusion gradient. Precipitation rates within this gradient increase dramatically in the direction of bulk solution so that fibrous crystal morphologies are favored. If precipitation occurs on a convex surface, fibers diverge outwards and fibers branch to fill the intervening space. Branching is caused by misalignments in the crystal lattice which propagate into new branches given sufficient space between neighboring fibers. Each branch retains the original optical orientation relative to elongation (Keith and Padden, 1963).

of fibers over crystals with large faces.

The maximum diameter of fibers that see this enhanced growth depends on the width of a boundary layer defined by gradients in inhibitor and growth component concentrations at the crystallization surface. The wider a fiber is, the more its growth affects the local concentration gradients: increasing fiber width decreases the growth advantage. This negative feedback produces an effective maximum diameter for fiber growth. Keith and Padden (1963) estimate this diameter by analyzing the influence of each fibrous projection on the local concentration gradients. Their results indicate that the maximum fiber diameter is of the same order of magnitude as the thickness of the diffusion boundary layer between the crystal and bulk solution where crystallization influences the concentration of impurities and growth components. This means that steeper concentration gradients, i.e. thinner boundary layers, lead to finer fibers. Thus, the diffusion characteristics of the system determine the size of fibrous crystals.

The second characteristic of spherulitic growth, noncrystallographic branching, also requires the presence of an inhibitor. To obtain branching, individual fibers can not coalesce immediately after growth. In the Keith and Padden model, an inhibitor excluded from the crystal becomes concentrated between fibers where it adsorbs onto the surfaces of the fibers inhibiting widening of the fibers. This leaves room between neighboring fibers for new fibers to form. Keith and Padden (1963) propose that misalignments in the crystal axes of existing fibers can nucleate new fibers if the diameter of these misalignments is of the same order of magnitude as the diffusion boundary layer (Figure 5-15). In this model, the new fibers retain the crystallographic orientation of the original fiber relative to their elongation, but the crystal axes of the two new fibers diverge slightly resulting in the noncrystallographic branching of crystallographically oriented fibers (Figure 5-15). Thus, a fiber could initiate growth of a spherulitic crystal aggregate where all fibers radiate outward and have the same sense of elongation relative to their optic axes. This model for crystallization of spherulites, including both the cause of fibrous growth and noncrystallographic branching, is supported by experimental evidence for crystallization of polymers (Keith and Padden, 1963, 1964a and b) and plagioclase (Lofgren, 1974).

We propose that the elongate crystals in herringbone calcite may have grown through a similar process (Figure 5-16). Each elongate crystal represents a recrystallized aggregate of fibers that nucleated on an older fibrous aggregate or a microspar crystal. The initial fibers grew with a length slow elongation, but were not necessarily oriented perpendicular to the underlying surface due to the random orientation of crystal nuclei. As spherulitic growth progressed, neighboring spherulites grew together and only fibers with orientations closest to the macroscopic growth direction of the cement coating had space to grow. This

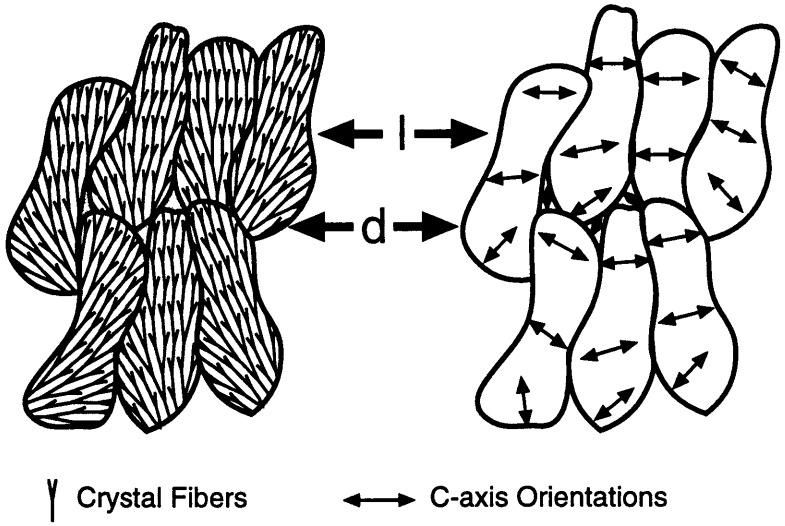


Figure 5-16: Illustration of the model for herringbone calcite precipitation proposed in the text. Each elongate crystal originally precipitated as a spherulitic aggregate of fibers. During inversion, the fibers coalesced to form single elongate crystals with rotating c-axes that reflect the original orientation of the fibers. The herringbone banding is due to the alternation of optically oriented and unoriented bands corresponding to the macroscopic light (l) and dull (d) bands respectively. Microspar crystals may or may not initially have been present in the dull bands.

produced a rotation in the average orientation of the fibers upward within the spherulite. Since noncrystallographic branching results in all fibers having the same optical elongation, the upper parts of the elongate crystals are length-slow matching the original fiber orientation. The observed rotation of the c-axes in neomorphic crystals that replaced the fiber aggregates is a relict of the orientation of the original fibers.

This model has some similarities to the split-crystal model proposed by Kendall (1985) for the growth of radiaxial fibrous calcite (RFC), but contains two important differences. First, in the model for RFC proposed by Kendall (1985), the fibers do not have a uniform optical orientation relative to their length. Instead, the fibers initially grow radiating outwards, but in optical continuity with an underlying crystal, so some fibers are length-slow while others are length-fast. In the model for herringbone calcite proposed here, all fibers are length-slow and retain this orientation throughout growth. Second, Kendall (1985) proposes that rotation of crystal axes in RFC is due to the bending of fibers during growth. This is mechanistically different from the selective growth of fibers with favorable orientations as proposed here. Although spherulitic fibers as described by Keith and Padden (1963) may appear curved due to the preferential growth of branches facing a given side, they consist of straight crystals that diverge slightly with branching (Figures 5-15 and 5-16). The misalignment in the crystal lattice producing branching in spherulites probably requires different conditions than the progressive bending of fibers presumably due to inclusion of impurities in the crystal lattice. These two differences make the spherulitic crystallization model proposed here mechanistically different from that proposed by Kendall (1985) for RFC.

The rotation of the c-axis around the axis of elongation in addition to upwards in the elongate crystals (Figure 5-11) can be explained by a rotation of the c-axis in the individual fibers of the spherulites similar to that observed in quartz fibers (Frondel, 1978; Wang and Merino, 1990). Quartz fibers commonly show twisting of the c-axis around the axis of fiber elongation, a characteristic of zebraic chalcedony. This banding is superficially similar to that in herringbone calcite when viewed between crossed polarizers (Kerans, 1982; Graber, 1984; Simonson, et al., 1993), but the banding in zebraic chalcedony is due to rotation of the c-axis within the plane perpendicular to growth direction and is purely an optical effect; it does not contain bands of crystals like those in herringbone calcite. There is, however, similar twisting of the c-axis in herringbone calcite in addition to the crystal banding, and this twisting may be similar to that in many quartz fibers. Wang and Merino (1990) proposed that the twisting in quartz fibers is due to the incorporation of $Al^{3+}$ into the $SiO_2$ crystal lattice. A similar process may cause twisting of the calcite fibers in herringbone calcite: the inhibitor promoting spherulitic growth also may cause twisting of individual

fibers when small amounts become incorporated into the crystal lattice. When the fiber aggregates are neomorphically replaced by elongate crystals, the rotation in axes is preserved.

**Herringbone Banding**

While the spherulitic crystallization model adequately explains the change in the optical orientation of the elongate crystals, it does not account for the 0.5-1.0 mm-scale herringbone banding (Table 5-2) which is one of its defining attributes. This banding may also have a diffusion origin. The impurities excluded during calcite crystallization may have built up with time. If diffusion of the inhibitor away from the crystallization front was slow relative to the growth rate, it may have become concentrated enough to prohibit precipitation all together. The inhibitor would have adsorbed to the surface of the crystals making the nucleation of new crystals necessary for continued growth. When crystallization ceased, the buildup of the inhibitor also stopped and diffusion reduced the concentrations at the crystal surface. Subsequently, nucleation occurred, but the newly nucleated crystals did not have the same optical orientation as the underlying crystals due to the adsorption of the inhibitor onto the old surface. Thus, the base of the new band did not have a uniform optical orientation. As new crystals grew, the inhibitor began to build up again promoting spherulitic growth and leading to the preferential growth of fibers oriented parallel to the growth direction. Repetition of this process would lead to multiple bands of elongate crystals as seen in herringbone calcite.

This mechanism is consistent with the observation that crystal banding does not correspond to trains of inclusions defining growth horizons. The concentration of the inhibitor could have built up in the diffusion boundary layer at different places along the crystallization front at different times due to local variations in precipitation rates. Crystal growth would have terminated where inhibitor concentrations were high while continuing in places where concentrations were lower. Thus, differences in inhibitor concentrations along the crystallization front could have produced variations in the crystal texture along a single growth horizon, and the crystal bands in herringbone calcite could crosscut growth horizons.

**Diffusion Rates**

One problem with applying diffusion models to herringbone calcite precipitation is that the diffusion rates in the solutions from which it precipitated are unknown and it is difficult to determine whether diffusion could have been slow enough for both the spherulitic and banding models to be realistic. This is especially difficult for the mm-scale of

banding in herringbone calcite. Wang and Merino (1990) propose a diffusion model for banding of quartz fibers in agates of roughly the same scale. Based on their numerical simulations of crystallization, however, the concentration of silica must be high enough that it required crystallization from a silica gel. The high viscosity of gels decreases chemical diffusion rates and promotes diffusionally controlled crystallization. Although Hofmann et al. (1985) suggested that herringbone calcite may have precipitated from a gel, carbonate gels are rare due to the high solubility of calcium carbonate minerals and the numerous inhibitors to carbonate nucleation in seawater. "Gel-like calcium carbonate" can be produced in laboratory settings (e.g. Brooks, et al., 1950), but it requires high saturation states and conditions in the experiments do not mimic natural systems. Thus, the presence of a viscous gel cannot be called apon to help lower diffusion rates. Diffusion rates of impurities and growth rates of the cements are both currently unconstrained, but may be of the proper relative magnitude in some natural carbonate precipitating systems to allow spherulitic crystallization and diffusionally derived crystal banding in the environments where herringbone calcite precipitated.

### *Distribution and Implications*

The stratigraphic distribution of herringbone calcite suggests that it precipitated in a specific chemical environment. The abundance of herringbone calcite in Archean carbonates both in the number of occurrences and the range of environments is impressive when compared to the limited occurrences in younger deposits (Table 5-1). This is especially striking when also considering the limited preservation of Archean relative to younger carbonates. In younger occurrences, herringbone calcite is both less common and restricted to carbonate buildups, many isolated from other carbonates and surrounded by organic-rich sediments. An association between precipitation of herringbone calcite and disaerobic seawater is supported by the abundance of herringbone calcite in Archean shallow marine environments when global atmospheric and oceanic oxygen concentrations were much lower than at present (e.g. Holland, 1984 and references therein), and by its absence from younger, oxygenated shallow environments. Furthermore, Archean carbonates in general contain higher concentrations of manganese and iron as compared to Proterozoic and Phanerozoic carbonates (Veizer, et al., 1989, 1990, 1992) suggesting that lower oxygen levels are reflected in trace elemental distributions in Archean carbonates. In the Phanerozoic carbonate buildups (e.g. the Porterfield, Pipe Creek Jr., and Thornton buildups), the buildups themselves were oxygenated as demonstrated by the diverse fauna, but they are surrounded by anaerobic sediments. In these examples herringbone calcite occurs in voids, suggesting that it could have precipitated from marine water that was depleted in oxygen due to decay

of the surrounding organic-rich sediments. An interpretation that herringbone calcite precipitated from modified seawater is supported by cathodoluminescence of samples from the Porterfield buildup; micritic sediment is non-cathodoluminescent implying precipitation from low manganese waters, while both fibrous and herringbone calcite are brightly luminescent implying higher manganese concentrations (Hemming, et al., 1989). Since manganese is insoluble in waters with more than $10^{-13}$ atm oxygen (Holland, 1984), it suggests that the water the marine cements precipitated from was oxygen-depleted relative to ambient marine water. Alternatively, the marine cements could have recrystallized under reducing conditions while associated micritic sediment did not.

The association between herringbone calcite and oxygen-depleted water suggests that the impurities possibly leading to spherulitic growth and crystal banding in herringbone calcite may be related to the oxidation state of the water it precipitated from. Two obvious candidates include $Mn^{2+}$ and $Fe^{2+}$ both of which kinetically inhibit calcite precipitation (Dromgoole and Walter, 1990a and b). $Mn^{2+}$ and $Fe^{2+}$ adsorb more strongly and are incorporated more frequently on slowly growing crystal faces than on rapidly growing ones (Mucci, 1988; Dromgoole and Walter, 1990a). This behavior is consistent with the role of inhibitors in spherulitic crystallization where growth is allowed at rapidly growing fiber tips, but inhibited on the sides of fibers.

## CONCLUSIONS

1. Herringbone calcite precipitated in marine environments, both in voids as a cement and, in Archean carbonate platforms, as sea-floor encrustations forming beds up to 20 cm thick that extend laterally for up to 140 km. Its abundance and environmental distribution are progressively more limited in younger rocks; it is preserved in deep subtidal to peritidal environments in Archean carbonates, but usually only in subtidal settings in Proterozoic and Phanerozoic carbonates.

2. Detailed petrographic observations of Precambrian and Phanerozoic marine cements indicate that the distinctive texture of herringbone calcite is due to the rotation of optic axes within successive bands of elongate crystals. The bases of the elongate crystals are optically unoriented and may be associated with microspar. They correspond to macroscopic dark bands. The tops of the crystals are optically oriented and correspond to macroscopic light bands. The repetitive nucleation of new elongate crystals creates the characteristic herringbone calcite banding.

3. The proposed model for the precipitation of herringbone calcite involves three components. First, the rotation of crystal axes within elongate crystals from a random

orientation at the base to length-slow at the top may be due to neomorphic replacement of an initially spherulitic fibrous crystal aggregate whose growth was promoted by slow diffusion of a chemical that inhibited calcite precipitation. Second, the rotation of the c-axis around the axis of elongation of the crystals may be due to the twisting of individual fibers in the original spherulites (now replaced by the elongate crystals) due to dislocations produced by the incorporation of small amounts of the inhibitor into the crystal lattice. Third, the banding produced by the nucleation of successive layers of elongate crystals may be due to a self-regulating mechanism involving build-up of the inhibitor to levels that prohibited further growth; new crystals nucleated only after the concentration of the inhibitor decreased to a critical level.

4. The inhibitor causing the herringbone calcite texture may be related to low oxygen concentrations. In Phanerozoic occurrences, herringbone calcite is associated with organic-rich sediments suggesting that it precipitated from oxygen-depleted marine water. Since normal, open marine depositional environments of Archean age characteristically had low oxygen concentrations, it is proposed that the presence of an inhibitor, such as Fe or Mn, associated with anaerobic marine water may have promoted growth of herringbone calcite. If the association of herringbone calcite and oxygen-depleted water can be confirmed and the cause of banding can be attributed to a trace element or chemical in seawater with low oxygen concentrations, herringbone calcite may be a useful petrographic indicator for depositional chemistry. Its stratigraphic distribution would then be an important indicator of the oxidation state of carbonate depositional environments through time.

## ADDITIONAL ACKNOWLEDGMENTS

I would like to thank Mario Coniglio, Jay Gregg, and Bruce Wilkinson for providing helpful reviews of the manuscript submitted to Journal of Sedimentary Research, much of which is included here. Thanks also go to Fred Read for accommodation and help during field work in Virginia. Samples of herringbone calcite were generously provided by Lloyd Pray (Silurian buildup samples), Bruce Simonson (Carawine Dolomite samples), and Charley Kerans (Dismal Lakes Group samples). Hans Hofmann provided the photograph of herringbone calcite from the Uchi greenstone belt, and Bob Folk provided information on the Holocene Gulf Coast occurrence.

## REFERENCES

Brooks, R., L. M. Clark and E. F. Thurston, 1950. Calcium carbonate and its hydrates. Philosophical Transactions of the Royal Society of London, v. 243, p. 145-167.

Buczynski, C. and H. S. Chafetz, 1991. Habit of bacterially induced precipitates of calcium carbonate and the

influence of medium viscosity on mineralogy. Journal of Sedimentary Petrology, v. 61, p. 226-233.
Burton, E. A. and L. M. Walter, 1987. Relative precipitation rates of aragonite and Mg calcite from seawater: Temperature or carbonate ion control? Geology, v. 15, p. 111-114.
Chafetz, H. S., P. F. Rush and N. M. Utech, 1991. Microenvironmental controls on mineralogy and habit of CaCO3 precipitates: an example from an active travertine system. Sedimentology, v. 38, p. 107-126.
Chipley, D. and T. K. Kyser, 1994. The sedimentological significance of chevron halite: A reappraisal *in* Sedimentology and Geochemistry of Mondern and Ancient Saline Lakes (R. W. Renaut and W. M. Last, eds.). SEPM Special Publication No. 50, p. 307-313.
Davies, G. R., 1977. Former magnesian calcite and aragonite submarine cements in upper Paleozoic reefs of the Canadian Arctic: A summary. Geology, v. 5, p. 11-15.
Dromgoole, E. L. and L. M. Walter, 1990a. Iron and manganese incorporation into calcite: Effects of growth kinetics, temperature and solution chemistry. Chemical Geology, v. 81, p. 311-336.
Dromgoole, E. L. and L. M. Walter, 1990b. Inhibition of calcite growth rates by Mn2+ in CaCl2 solutions at 10, 25, and 50°C. Geochimica et Cosmochimica Acta, v. 54, p. 2991-3000.
Folk, R. L. and R. Assereto, 1976. Comparative fabrics of length-slow and length-fast calcite and calcitized aragonite in a Holocene speleothem, Carlsbad Caverns, New Mexico. Journal of Sedimentary Petrology, v. 46, p. 486-496.
Folk, R. L., H. S. Chafetz and P. A. Tiezzi, 1985. Bizarre forms of depositional and diagenetic calcite in hot-spring travertines, central Italy *in* Carbonate Cements (N. Schneidermann and P. M. Harris, eds.). S. E. P. M., Tulsa. 36, p. 349-369.
Frondel, C., 1978. Characters of quartz fibers. American Mineralogist, v. 63, p. 17-27.
Gary, M., R. J. McAfee and C. L. Wolf, 1974, Glossary of Geology: Washington, American Geological Institute, 805 p.
Given, R. K. and B. H. Wilkinson, 1985. Kinetic control of morphology, composition, and mineralogy of abiotic sedimentary carbonates. Journal of Sedimentary Petrology, v. 55, p. 109-119.
Graber, E. R., 1984. Diagenesis of Eocene Gulf Coast Carbonates: Paradoxes in the Feculent Weches (Masters Thesis). University of Texas at Austin.
Grotzinger, J. P., 1989. Facies and evolution of Precambrian carbonate depositional systems: emergence of the modern platform archetype *in* Controls on Carbonate Platform and Basin Development (P. D. Crevello, J. L. Wilson, J. F. Sarg and J. F. Read, eds.). Society of Economic Paleontologists and Mineralogists, Special Publication 44, p. 79-106.
Grotzinger, J. P., 1990. Geochemical model for Proterozoic stromatolite decline. American Journal of Science, v. 290-1, p. 80-103.
Grotzinger, J. P. and J. F. Kasting, 1993. New constraints on Precambrian ocean composition. Journal of Geology, v. 101, p. 235-243.
Hemming, N. G., W. J. Meyers and J. C. Grams, 1989. Cathodoluminescence in diagenetic calcites: the roles of Fe and Mn as deduced from electron probe and spectrophotometric measurements. Journal of Sedimentary Petrology, v. 59, p. 404-411.
Hofmann, H. J., P. C. Thurston and H. Wallace, 1985. Archean Stromatolites from Uchi greenstone belt, Northwestern Ontario *in* Evolution of Archean Supracrustal Sequences (L. D. Ayres, P. C. Thurston, K. D. Card and W. Weber, eds.). Geological Association of Canada Special Paper 28, p. 1125-132.
Holland, H. D., 1984. The Chemical Evolution of the Atmosphere and Oceans. Princeton University Press, Princeton. 582 p.
Keith, H. D. and F. J. Padden, 1963. A phenomenological theory of spherulitic crystallization. Journal of Applied Physics, v. 34, p. 2409-2421.
Keith, H. D. and F. J. Padden, 1964a. Spherulitic crystallization from the melt. I. Fractionation and impurity segregation and their influence on crystalline morphology. Journal of Applied Physics, v. 35, p. 1270-1285.
Keith, H. D. and F. J. Padden, 1964b. Spherulitic crystallization from the melt. II. Influence of fractionation and impurity segregation on the kinetics of crystallization. Journal of Applied Physics, v. 35, p. 1286-1296.
Kendall, A. C., 1985. Radiaxial fibrous calcite: A reappraisal *in* Carbonate Cements (N. Schneidermann and P. M. Harris, eds.). S.E.P.M., Special Publication No. 36, Tulsa. p. 59-78.

Kerans, C., 1982. Sedimentology and Stratigraphy of the Dismal Lakes Group (Doctoral Thesis). Carleton University.

Kerans, C. and J. A. Donaldson, 1988. Deepwater conical stromatolite reef, Sulky Formation (Dismal Lakes Group), Middle Proterozoic, N. W. T. *in* Reefs, Canada and adjacent area (H. H. J. Geldsetzer, N. P. James and G. E. Tebbutt, eds.). Canadian Society of Petroleum Geologists, Calgary. Memoir 13, p. 81-88.

Krebs, W., 1969. Early void-filling cementation in Devonian fore-reef limestones (Germany). Sedimentology, v. 12, p. 279-299.

Lehmann, P. J., 1978. Deposition, Porosity Evolution and Diagenesis of the Pipe Creek Jr. Reef (Silurian), Grant County, Indiana (Masters Thesis). University of Wisconsin - Madison.

Lehmann, P. J. and A. Simo, 1988. Depositional facies and diagenesis of the Pipe Creek Jr. reef, Silurian, Great Lakes region, Indiana *in* Reefs: Canada and Adjacent Areas (H. H. J. Geldsetzer, N. P. James and G. E. Tebbutt, eds.). Canadian Society of Petroleum Geologists, Calgary. Memoir 13, p. 319-329.

Lofgren, G., 1974. An experimental study of plagioclase crystal morphology: Isothermal crystallization. American Journal of Science, v. 274, p. 243-273.

Lohmann, K. C. and W. J. Meyers, 1977. Microdolomite inclusions in cloudy prismatic calcites: A proposed criterion for former high-magnesium calcites. Journal of Sedimentary Petrology, v. 47, p. 1078-1088.

McGovney, J. E., 1988. Thornton reef, Silurian, northeastern Illinois *in* Reefs: Canada and Adjacent Areas (H. H. J. Geldsetzer, N. P. James and G. E. Tebbutt, eds.). Canadian Society of Petroleum Geologists, Calgary. Memoir 13, p. 330-338.

McIlreath, I. and J. D. Aitken, 1976. *Yoholaminites* (Middle Cambrian), problematical calcareous sediment-stabilizing organism. Program with Abstracts, Geological Association of Canada, Annual Meeting, v. 1, p. 84.

Mucci, A., 1988. Manganese uptake during calcite precipitation from seawater: Conditions leading to the formation of a pseudokutnahorite. Geochimica et Cosmochimica Acta, v. 52, p. 1859-1868.

Read, J. F., 1980. Carbonate ramp-to-basin transitions and foreland basin evolution, Middle Ordovician, Virginia Appalachians. American Association of Petroleum Geologists Bulletin, v. 64, p. 1575-1612.

Read, J. F., 1982. Geometry, facies, and development of Middle Ordovician carbonate buildups, Viginia Appalachians. American Association of Petroleum Geologists Bulletin, v. 66, p. 189-209.

Roedder, E., 1994. Fluid Inclusions. Mineralogical Society of America, Washington, v. 12, 644 p.

Sandberg, P. A., 1975. New interpretations of Great Salt Lake ooids and of ancient non-skeletal carbonate mineralogy. Sedimentology, v. 22, p. 497-537.

Sandberg, P. A., 1983. An oscillating trend in Phanerozoic non-skeletal carbonate mineralogy. Nature, v. 305, p. 19-22.

Sandberg, P. A., 1985. Nonskeletal aragonite and pCO2 in the Phanerozoic and Proterozoic *in* The carbon cycle and atmospheric CO2: Natural variations Archean to Present (E. T. Sundquist and W. S. Broecker, eds.). American Geophysical Union, Washington. Geophysical Monograph 32, p. 585-594.

Savard, M. and P-A. Bourque, 1989. Diagenetic evolution of a Late Silurian reef platform, Gaspé Basin, Quebec, based on cathodoluminescence petrography. Canadian Journal of Earth Sciences, v. 26, p. 791-806.

Schroeder, J. H., 1972. Fabrics and sequences of submarine carbonate cements in Holocene Bermuda cup reefs. Geologische Rundschau, v. 61, p. 708-730.

Simonson, B. M., K. A. Schubel and S. W. Hassler, 1993. Carbonate sedimentology of the early Precambrian Hamersley Group of Western Australia. Precambrian Research, v. 60, p. 287-335.

Sumner, D. Y. and S. A. Bowring, in press. U-Pb geochronologic constraints on deposition of the Campbellrand Subgroup, Transvaal Supergroup, South Africa. Precambrian Research.

Veizer, J., J. Hoefs, D. R. Lowe and P. C. Thurston, 1989. Geochemistry of Precambrian carbonates: II. Archean greenstone belts and Archean seawater. Geochimica et Cosmochimica Acta, v. 53, p. 859-871.

Veizer, J., R. N. Clayton, R. W. Hinton, V. vonBrunn, T. R. Mason, S. G. Buck and J. Hoefs, 1990. Geochemistry of Precambrian carbonates: III. Shelf seas and non-marine environments of the Archean.

Geochimica et Cosmochimica Acta, v. 54, p. 2717-2729.
Veizer, J., R. N. Clayton and R. W. Hinton, 1992. Geochemistry of Precambrian carbonates: IV. Early Paleoproterozoic (2.25±0.25 Ga) seawater. Geochimica et Cosmochimica Acta, v. 56, p. 875-885.
Wang, Y. and E. Merino, 1990. Self-organizational origin of agates: Banding, fiber twisting, composition, and dynamic crystallization model. Geochimica et Cosmochimica Acta, v. 54, p. 1627-1638.
Wilkinson, B. W. and R. K. Given, 1986. Secular variation in abiotic marine carbonates: Constraints on Phanerozoic atmospheric carbon dioxide contents and oceanic Mg/Ca ratios. Journal of Geology, v. 94, p. 321-333.
Wilkinson, B. H., C. Buczynski and R. M. Owen, 1984. Chemical control of carbonate phases; implications from Upper Pennsylvanian calcite-aragonite ooids of southeastern Kansas. Journal of Sedimentary Petrology, v. 54, p. 932-947.
Wilkinson, B. H., R. M. Owen and A. R. Carroll, 1985. Submarine hydrothermal weathering, global eustasy, and carbonate polymorphism in Phanerozoic marine oolites. Journal of Sedimentary Petrology, v. 55, p. 171-183.

# CHAPTER 6: CARBONATE CHEMISTRY AND ARCHEAN SEAWATER


## ABSTRACT

New observations of textures in Archean carbonates suggest that seawater contained a calcite precipitation inhibitor that was absent in younger seawater. Inhibitors reduce crystallization rates and crystal nuclei formation leading to kinetic maintenance of supersaturated solutions. Inhibitors also affect carbonate textures by limiting micrite precipitation and promoting growth of older carbonate crystals on the sea floor. $Fe^{2+}$, a strong calcite precipitation inhibitor, is thought to have been present at relatively high concentrations in Archean seawater because oxygen concentrations were low. It may have promoted the *in situ* precipitation of thick beds of carbonate on the sea floor and inhibited micrite precipitation in Archean oceans. The rise in oxygen concentration at 2.2-1.8 Ga led to the removal of $Fe^{2+}$ from seawater and resulted in a shift from Archean facies, which often include precipitated beds, to Proterozoic facies which contain more micritic sediment and fewer precipitated beds.

The concentration of $Fe^{2+}$ in Archean oceans probably varied with depth since surface ocean and atmospheric oxygen concentrations were higher than deep ocean concentrations. In an ocean where $Fe^{2+}$ concentration increases with depth, siderite precipitation could replace calcite precipitation at deeper levels due to increasing siderite saturation. This would lead to the simultaneous deposition of siderite facies iron-formation in basinal environments and calcite precipitates in shallow environments. The inhibition of calcite precipitation by $Fe^{2+}$ would enhance the depth sensitivity of calcite versus siderite precipitation.


## INTRODUCTION

The rise in free oxygen concentration between 2.2 and 1.8 Ga produced one of the most dramatic chemical changes in the history of the Earth's oceans and atmosphere (Berkner and Marshal, 1965; Cloud, 1972; Garrels, et al., 1973; Holland, 1984; Kasting, 1991). This change from anaerobic to oxidized depositional environments profoundly affected the chemistry of sedimentary rocks and the sedimentary cycling of iron. For example, temporal distributions of iron-formations and red beds reflect the oxidation state of seawater and meteoric water respectively (e.g. Garrels, et al., 1973; Holland, 1984). Here, it is proposed that certain aspects of secular variation in the texture of carbonate rocks also reflect changes in the oxidation state of specific depositional environments.

Carbonate mineralogy and textures reflect the chemical, biological, and physical

aspects of their depositional environment. The best documented changes in carbonate rocks are related to the evolution of life, i.e., the early Cambrian radiation of carbonate-secreting metazoans and the diversification of foraminifera near the end of the Jurassic period. These two events altered the modes of carbonate precipitation and the distribution of carbonate accumulation. The evolution of the first carbonate-secreting organisms at the end of the Neoproterozoic Era changed the dominant mechanism of carbonate precipitation and led to the accumulation of coarse, biologically-produced carbonate grains in quiet water carbonates (Knoll, et al., 1993a). The evolution of foraminifera and other carbonate-secreting planktonic organisms provided an efficient mechanism for depositing carbonate in ocean basins as well as on continental shelves. This led to the accumulation of deep sea carbonate deposits that were subducted rather than stored on continental margins, changing the cycling of carbonates between crustal and atmospheric-oceanic reservoirs (Boss and Wilkinson, 1991).

Similarly dramatic change in the record of carbonate precipitation is recorded in Precambrian rocks. Grotzinger and Kasting (1993) document a decline across the Archean-Proterozoic boundary in the abundance of decimeter-thick beds of calcite and neomorphosed aragonite that precipitated from ambient seawater. Within the Proterozoic Eon, there is also a decline in microdigitate stromatolites which consist of fibrous cement crusts that precipitated in restricted tidal flat settings (Grotzinger, 1989; Grotzinger and Kasting, 1993). The abundance and diversity of subtidal, precipitated stromatolites, particularly conoform stromatolites, decline within the Mesoproterozoic Era (Walter and Heys, 1985; Grotzinger, 1990). In contrast to the trend in sea-floor precipitates, thick accumulations of micrite are abundant in Neoproterozoic carbonates (Knoll and Swett, 1990), present in older Proterozoic carbonates (Sami and James, 1994), and rare in Archean carbonates (Grotzinger, 1989). Previously, these changes in carbonate texture were either not addressed in models of Archean seawater (e.g. Walker, 1983; Holland, 1984) or were ascribed to a decline in carbonate saturation state from very supersaturated Archean seawater to less supersaturated Neoproterozoic seawater (e.g. Monty, 1973; Grotzinger, 1989, 1990; Knoll and Swett, 1990; Grotzinger and Kasting, 1993). Data presented in Chapters 2-5 provide a basis for addressing mechanisms for maintaining high saturation states and the causes of textural changes through time. These data suggest that a calcite precipitation inhibitor present in oxygen-depleted seawater played an important role in maintaining the high supersaturation of seawater and determining the texture of precipitated carbonate. In addition, stratigraphic evidence from the Transvaal (Beukes, 1983; Beukes, 1987; Klein and Beukes, 1989; Beukes, et al., 1990; Chapter 4) and the Hamersley basins (Simonson, 1992) suggests that deep-water iron-formation precipitation was contemporaneous with shallow-water carbonate pre-

cipitation. Insights into the role of inhibitors in carbonate chemistry also suggest a possible cause for variations in the mineralogy of precipitates with depth.

## ARCHEAN CARBONATES

The abundance of sea-floor encrusting carbonate and the lack of micrite are striking in the 2521±3 Ma (Sumner and Bowring, in press; Appendix A) Gamohaan Formation (Chapters 3 and 4). The Gamohaan Formation contains 40 m of deep subtidal carbonates with abundant bladed and herringbone calcite that precipitated as marine cement in primary voids and as encrusting beds on the sea floor (Sumner and Grotzinger, in review; Chapters 3, 4, and 5). Individual herringbone calcite beds are laterally continuous for more than 3,500 $km^2$. Facies analysis and integration of the composition of all beds >5 cm thick demonstrates that more than 45% of this 40 m section of the Gamohaan Formation precipitated from seawater directly on the sea floor as beds and void-filling cements (Chapter 4). The abundance of these precipitates demonstrates that ambient seawater was supersaturated with respect to calcite. The supersaturated state of late Archean seawater in general is confirmed by an abundance of aragonite pseudomorphs in shallow water carbonates throughout the Campbellrand-Malmani carbonate platform (Chapter 2) as well as in various other late Archean carbonate deposits (e.g. Martin, et al., 1980; Grotzinger, et al., 1993; Simonson, et al., 1993).

Despite the extraordinary abundance of sea-floor and void-filling precipitated carbonate, fine-grained carbonate sediments are not present in the Gamohaan Formation: micritic beds, drapes, and geopedal void-fills are absent (Chapter 4). The delicate nature of the microbialites coated by cements in the Gamohaan Formation, the absence of any tractionally deposited sediment, and the absence of scoured beds indicate that the depositional environment was unaffected by strong currents that may have transported micrite to other sites. Any micrite that precipitated in the overlying water column should have accumulated in the Gamohaan Formation. Thus, the lack of fine sediment suggests that micrite precipitation was rare to absent despite strong evidence for the supersaturation of the oceans at that time.

Archean carbonates also contain abundant herringbone calcite. Herringbone calcite has a distinctive texture consisting of mm-scale serrated layers of elongate crystals with sweeping extinction (Sumner and Grotzinger, in review; Chapter 5). The extinction pattern suggests that each elongate crystal initially precipitated as a spherulitic aggregate of fibers, and a crystallization model for herringbone calcite suggests that an inhibitor to calcite precipitation promoted spherulitic growth (Chapter 5). Since herringbone calcite is abundant

in Archean carbonates when atmospheric and oceanic oxygen concentrations were negligible in most depositional environments (Kasting, 1991) and only locally present in younger deposits where it is usually associated with organic-rich, anaerobic sediments, the inhibitor that produces the herringbone calcite texture may be present only in seawater with low oxygen concentrations (Figure 6-1; Sumner and Grotzinger, in review; Chapter 5). The decline in the abundance of bedded cements roughly coincides with the decline in herringbone-textured calcite and the rise of free oxygen (Figure 6-1), and may also be related to the presence of an inhibitor in oxygen-depleted seawater.

## PRECIPITATION INHIBITORS

The inhibition of calcite precipitation by several ions and molecules in seawater and during diagenesis has been known for decades (e.g. Weyl, 1967; Berner, 1975; Meyer, 1984; Busenberg and Plummer, 1985; Burton and Walter, 1990; Dromgoole and Walter, 1990a, b). For example, $Mg^{2+}$ is one of the major kinetic inhibitors thought to maintain calcite supersaturation of modern surface seawater (Weyl, 1967; Berner, 1975). Inhibitors help maintain the supersaturation of seawater by reducing carbonate precipitation rates and thus, the rate of removal of $Ca^{2+}$ and $CO_3^{2-}$ from seawater. The saturation state of seawater increases until the effects of the inhibitors are overcome and the removal of $Ca^{2+}$ and $CO_3^{2-}$ as calcium carbonate balances the influx of these ions. Thus, by reducing precipitation rates, inhibitors kinetically maintain highly saturated solutions and provide a mechanism for sustaining supersaturated modern and ancient seawater.

Inhibitors to precipitation also reduce the rate of new crystal nucleation. For a crystal nucleus to form in a solution, a cluster of appropriate molecules must form and exceed a minimum size, $R_c$ (Ohara and Reid, 1973; Kittel and Kroemer, 1980). If the size of the cluster is less than $R_c$, it will tend to dissolve. If the size of the cluster is larger than $R_c$, it will tend to grow and form a new crystal. At a given solution saturation, temperature, and pressure, the most important factor affecting the critical cluster size is the surface free energy ($\sigma$) of the cluster since $R_c \propto \sigma$ (Kittel and Kroemer, 1980). The presence of impurities that adsorb onto the clusters increases the critical size for crystal nucleation by increasing the surface free energy (Ohara and Reid, 1973). Since large clusters are less likely to form than small ones, the rate of crystal nucleation decreases as the inhibitor concentration increases. Thus, a calcite precipitation inhibitor in seawater could significantly reduce the precipitation of micrite in the water column if it significantly increased the surface free energy (Figure 6-2). Precipitation would preferentially occur on existing crystals producing a deposit of a small number of relatively large crystals. The beds of herringbone calcite

and botryoidal aragonite pseudomorphs that commonly occur in Archean carbonates are interpreted to record the preferential growth of existing crystals over the nucleation of new crystals (i.e. micrite precipitation).

Inhibitors can also influence the morphology of individual crystals. Preferential adsorption of an inhibitor onto certain crystal faces can promote the growth of other faces, changing crystal habit (Ohara and Reid, 1973). Fibrous and spherulitic crystal morphologies also can be promoted by some inhibitors to crystallization (Keith and Padden, 1963), and herringbone calcite may be an example of a carbonate texture, preserved in the sedimentary record, that documents the role of an inhibitor in carbonate precipitation and a

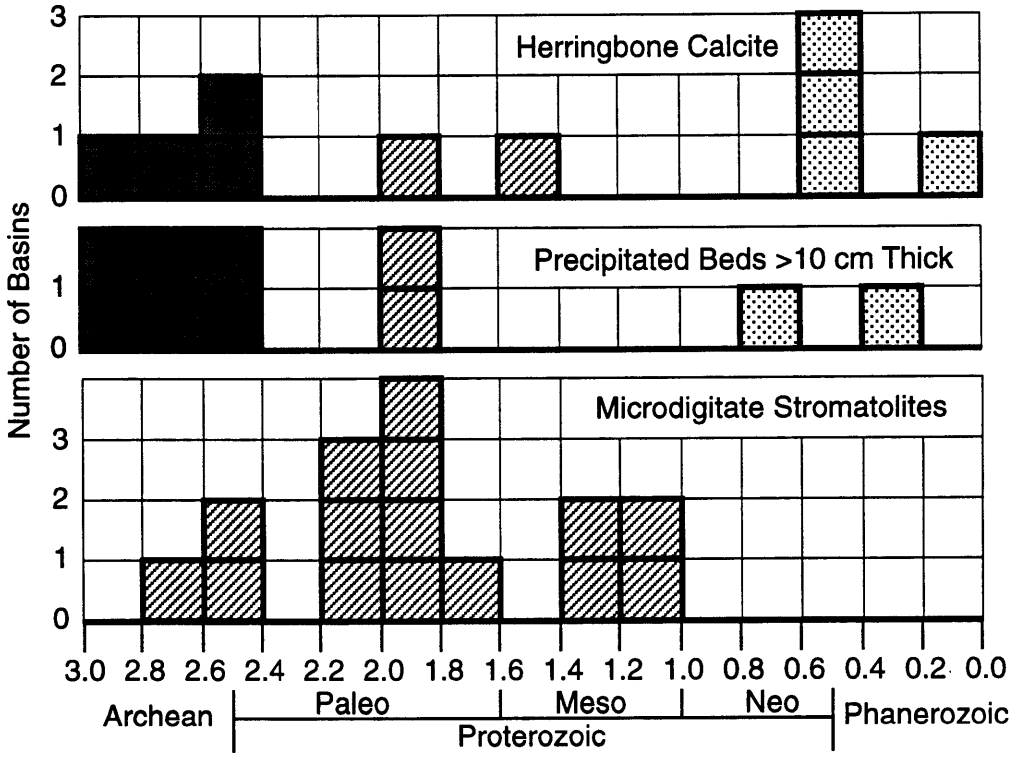


Figure 6-1: The temporal distribution of precipitated carbonates. Occurrences are binned into 200 m.y. increments to account for errors in ages of the basins. Bin width is held constant through time to facilitate comparison. Each basin is considered a single occurrence even if the precipitated texture is abundant and occurs within several formations or members within the basin. Dark gray squares represent basins where the precipitated texture is abundant in diverse depositional environments, hatched squares represent basins where the texture is abundant in only a limited number of environments, and stippled squares represent basins where the texture is present, but nowhere abundant. Note the decline in abundance and distribution of herringbone calcite and thick precipitated beds between 2.4 and 2.0 Ga. Microdigitate stromatolites do not show this decline, suggesting that they were unaffected by changes in the $Fe^{2+}$ concentration in seawater. Occurrences of microdigitate stromatolites and precipitated beds are after Grotzinger (1989) with two additional microdigitate stromatolites occurrences from Knoll, et al. (1993b) and Kah and Knoll (in review) and an additional precipitated bed occurrence from Schmidt (1977). Occurrences of herringbone calcite are after Sumner and Grotzinger (in review).

secular variation in its concentration (Sumner and Grotzinger, in review; Chapter 5).

The presence of herringbone calcite in oxygen-depleted environments suggests that $Fe^{2+}$ or $Mn^{2+}$ may be an important inhibitor to calcite precipitation in Archean seawater; experimental results indicate both cations inhibit calcite precipitation. Meyer (1984) studied calcite precipitation rates in the presence of 34 anionic molecules (including $SO_4^{2-}$ and $PO_4^{3-}$), cations (including $Fe^{2+}$, $Mn^{2+}$, $Sr^{2+}$, and $Mg^{2+}$), and organic molecules. Of these, $Fe^{2+}$ was shown to be the strongest inhibitor to calcite precipitation. Dromgoole and Walter (1990a, b) also report that $Fe^{2+}$ is a very strong calcite precipitation inhibitor even at solution concentrations of <20 μmol/l.

Geological evidence indicates that $Fe^{2+}$ was present in carbonate precipitating Archean seawater: Iron-formations are common in sedimentary sequences prior to ~1.8 Ga suggesting that an oceanic source of $Fe^{2+}$ was present (Holland, 1984; Kasting, 1991), and Ewers (1983) suggests that a minimum iron concentration of >100 μmol/l is required for deposition of iron-formation, well above the concentration of iron necessary to inhibit calcite precipitation in laboratory experiments. Carbonate deposits are commonly associated with these iron-formations implying that at least some $Fe^{2+}$ could have been present in many carbonate precipitating environments (Beukes, et al., 1990; Simonson, et al., 1993; Chapter 4). In the Campbellrand-Malmani platform, iron concentrations in carbonate increase with increasing depositional depth and its proximity to iron-formations (Beukes, 1987; Klein and Beukes, 1989), and Veizer, et al. (1989) have documented higher iron concentrations in Archean calcite (2300 ppm) than in Proterozoic and Phanerozoic calcite. Dromgoole and Walter (1990a) found that only ≤2200 ppm iron (0.4 mol% $FeCO_3$) was incorporated into calcite even when precipitation rates were significantly reduced by the presence of $Fe^{2+}$. This suggests that $Fe^{2+}$ may have played an important role as an inhibitor

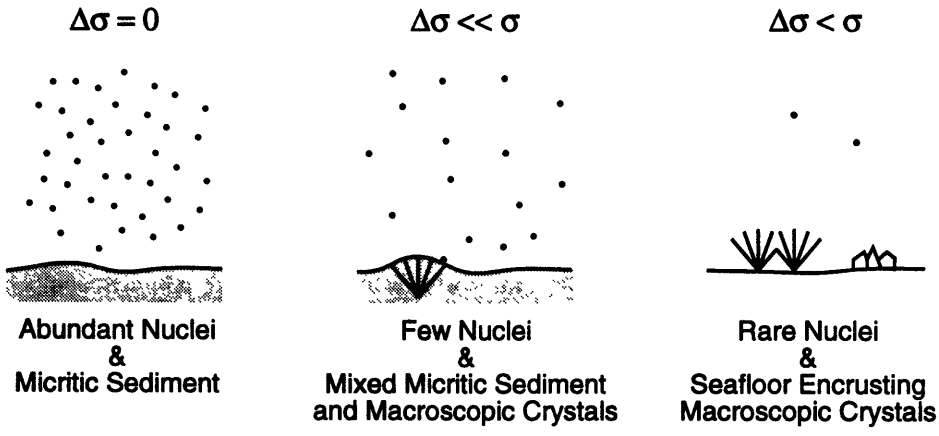


Figure 6-2: The effect of increases in surface free energy on carbonate nucleation and the textural changes in carbonate sediments.

even where only small concentrations are preserved in the crystals. Unfortunately, diagenetic recrystallization often increases the iron concentration of marine cements (Dickson, 1966) complicating interpretations of primary iron concentrations. Data are consistent, however, with high $Fe^{2+}$ concentrations in Archean seawater.

Other known inhibitors are unlikely to have played as important a role as $Fe^{2+}$ in Archean calcite precipitation. $Mn^{2+}$, another inhibitor, is abundant in oxygen-depleted seawater and inhibits carbonate precipitation, but it probably did not play a more important role than $Fe^{2+}$ in Archean calcite precipitation, because it is significantly less effective as an inhibitor than $Fe^{2+}$ (Meyer, 1984; Dromgoole and Walter, 1990a, b). It may have played a role in textural changes after $Fe^{2+}$ was removed from seawater, however, because it becomes insoluble at higher oxygen concentrations than iron (Holland, 1984). Secular variations in oceanic $Mg^{2+}$ concentration are controlled by the balance between crustal erosion and sea floor hydrothermal alteration (Edmond, et al., 1979), but the relative importance of these processes is unknown for Archean seawater so its concentration is unconstrained. However, $Mg^{2+}$ is also much less effective as an inhibitor to calcite precipitation than $Fe^{2+}$ (Meyer, 1984). Both $SO_4^{2-}$ and $PO_4^{3-}$ concentrations were probably lower prior to the Paleoproterozoic rise in oxygen (Cameron, 1982; Holland, 1984; Knoll, 1984) and are weak inhibitors compared to $Fe^{2+}$ (Meyer, 1984). Organic compounds are also less effective (Meyer, 1984), and there are no data to support an increase in their effectiveness in oxygen-depleted seawater.

## IMPLICATIONS FOR PRECAMBRIAN CARBONATES

### *Carbonate Textures*

Several significant changes in Precambrian carbonate textures can be attributed to changes in $Fe^{2+}$ concentration given that $Fe^{2+}$ probably was present in Archean oceans due to low oxygen concentrations and that $Fe^{2+}$ inhibits calcite precipitation even at very low concentrations. First, as the $Fe^{2+}$ concentration declined with the rise in oxygen partial pressure, herringbone calcite became less abundant and only precipitated in environments where oxygen was locally depleted and $Fe^{3+}$ was reduced to $Fe^{2+}$. Second, the presence of decimeter-thick precipitated beds in Archean carbonates may be due to the inhibiting effects of $Fe^{2+}$ on nucleation of new calcite crystals, promoting the growth of existing crystals on the sea floor over micrite precipitation in the water column. As the $Fe^{2+}$ concentration decreased, nucleation of new calcite crystals became more rapid and carbonate textures shifted from large to small crystals. Although the abundance of micrite in some Proterozoic

carbonates (e.g. Knoll and Swett, 1990; Sami and James, 1994) may be due in part to the evolution of pelagic organisms that induced micrite precipitation, the lack of micrite in the Archean Gamohaan Formation requires the presence of a substance that inhibited spontaneous precipitation of both calcite and aragonite from supersaturated seawater.

### *Stromatolite Microtextures*

Changes in stromatolite microtexture may also reflect this trend in carbonate morphology. The microtextures of stromatolites have changed through time, and these changes generally are attributed to changes in the constituent microbial communities (e.g. Komar, 1989; Cloud and Semikhatov, 1969; Gebelein, 1974; Walter and Heys, 1985; Semikhatov and Raaben, 1993; Grey, 1994). Although the character of organic remnants of microtextures are likely to reflect the composition and degradation of microbial communities (Semikhatov, et al., 1979), primary (non-diagenetic) carbonate textures depend on the modes of stromatolite accretion (Grotzinger, 1990). For precipitated stromatolites, the chemistry of their depositional environment may strongly affect the morphology of constituent carbonate crystals and thus microtextures. Even if precipitation of carbonate in stromatolites was induced by microbial processes, crystal growth would have been affected by external conditions such as the presence of inhibitors. For example, if $Fe^{2+}$ is present within the mat, the inhibiting effect would promote growth of larger crystals and limit nucleation of abundant micritic crystals. Thus, $Fe^{2+}$ could affect the microtexture of stromatolites, and a change in ocean chemistry could result in a change in stromatolite microtexture without requiring evolution of the microbial communities (Monty, 1973; Grotzinger, 1990).

Long-term trends in stromatolite distributions may reflect long-term changes in ocean chemistry. The decline of conoform stromatolites, interpreted to have formed predominantly through the precipitation of carbonate rather than trapping-and-binding of sediment, has been attributed to the evolution of grazing metazoans (e.g. Walter and Heys, 1985 and references therein) or the rise of benthic seaweeds (Knoll and Swett, 1990), whereas others have attributed it to chemical changes, usually a decrease in calcite supersaturation or atmospheric $CO_2$ (Monty, 1973; Grotzinger, 1990). One possible chemical mechanism for the decline is suggested here: a shift of abiotic precipitation style from large to small crystals due to a decrease in the concentration of precipitation inhibitors would be mimicked by the microtexture of precipitated stromatolites. In addition, an increase in micritic precipitation would reduce the number of depositional environments with low particulate carbonate influx, a requirement for growth of precipitated stromatolites (Grotzinger, 1990). This would lead to a greater abundance of trapped-and-bound than precipitated stromatolites. Thus, as suggested by Grotzinger (1990), the decline in precipitated stromatolites may be the result

of chemical changes in seawater rather than evolution and extinction of mat-forming or grazing organisms. Since precipitated stromatolites were abundant until ~1 Ga (Walter and Heys, 1985), a decrease in $Fe^{2+}$ concentration cannot account for their decline, and additional chemical and/or biological changes are necessary to explain some textural variations in Proterozoic stromatolites.

Changes in ocean chemistry besides a decline in $Fe^{2+}$ concentration are supported by the distribution of microdigitate stromatolites and their decline after the establishment of permanently oxidizing surface environments (Figure 6-1). Microdigitate stromatolites consist of small botryoidal aragonite pseudomorphs that usually precipitated in restricted to evaporitic, tidal-flat settings (Grotzinger and Read, 1983) where the saturation state of seawater was probably elevated due to extensive evaporation. Since the decline in microdigitate stromatolites occurs after 1.8 Ga (Figure 6-1), it probably is related to a general decline in the calcium carbonate saturation state of seawater during Proterozoic time (Grotzinger, 1990; Grotzinger and Kasting, 1993) or to the change in concentration of an inhibitor besides $Fe^{2+}$.

These observations have important implications for the use of stromatolites as "fossils" for stratigraphic correlations. If changes in stromatolite microtexture are due to changes in chemistry rather than the evolution of microbial communities, one cannot assume a unidirectional evolution of stromatolite microtextures. Unlike organisms whose morphology continually evolves, identical chemical conditions can occur at many different times and places throughout the history of the earth. Some coarse correlations between units based on stromatolite morphology and microtexture may still have some validity, however, since chemical conditions promoting specific textures can be regionally controlled (e.g. Chapter 4). This provides a reasonable alternative explanation for the success of interbasinal correlations based on stromatolite microtextures (e.g. Cloud and Semikhatov, 1969; Preiss, 1976; Semikhatov, 1976; Semikhatov and Raaben, 1993; Grey, 1994). Although regional correlations may prove tenable, global chemical conditions probably vary too much to allow refined stromatolite-based correlations.

### *Siderite Versus Calcite Deposition*

In addition to affecting the texture of precipitated calcite, $Fe^{2+}$ may have played an important role in changes of mineralogy with depth in Archean oceans. Abundant stratigraphic data demonstrate that carbonate and iron-formation deposition occurred simultaneously in different environments (e.g. Beukes, 1983b; Klein and Beukes, 1989; Simonson, 1992; Chapters 2 and 4). In particular, calcite is succeeded by siderite and then oxide facies iron-formation with increasing depth (Klein and Beukes, 1989; Beukes, et al., 1990; Carrigan

and Cameron, 1991; Morris, 1993). Since siderite is less soluble than calcite, an increase in $Fe^{2+}$ concentration with depth could cause a mineralogic change in precipitates with depth.

The solubility product ($k_i$) of a mineral is defined as the product of the activities of the reactants over the activities of the products at equilibrium. Solute activities are often approximately equal to solute concentrations, and the activity of solids equals one. Thus, for siderite

$$FeCO_3 = Fe^{2+} + CO_3^{2-}, \tag{1}$$

$$k_{sid} = [Fe^{2+}][CO_3^{2-}] = 10^{-9.5} \tag{2}$$

at 25°C and 1 atm (Bruno, et al., 1992), and for calcite

$$CaCO_3 = Ca^{2+} + CO_3^{2-}, \tag{3}$$

$$k_{cal} = [Ca^{2+}][CO_3^{2-}] = 10^{-8.5} \tag{4}$$

(Morse and Mackenzie, 1990, p. 23). In a solution where both calcite and siderite are saturated, the $CO_3^{2-}$ concentration in equations (2) and (4) will be equal and

$$[CO_3^{2-}] = \frac{k_{cal}}{[Ca^{2+}]} = \frac{k_{sid}}{[Fe^{2+}]} \tag{5}$$

and

$$[Fe^{2+}] = \frac{k_{sid}}{k_{cal}}[Ca^{2+}] = 10^{-1}[Ca^{2+}]. \tag{6}$$

If the solution is not in equilibrium, and the saturation state of calcite ($\Omega_{cal}$) or siderite ($\Omega_{sid}$) is not equal to one,

$$[CO_3^{2-}] = \frac{\Omega_{cal}k_{cal}}{[Ca^{2+}]} = \frac{\Omega_{sid}k_{sid}}{[Fe^{2+}]} \tag{7}$$

and

$$[Fe^{2+}] = \frac{\Omega_{sid}k_{sid}}{\Omega_{cal}k_{cal}}[Ca^{2+}] = 10^{-1}\frac{\Omega_{sid}}{\Omega_{cal}}[Ca^{2+}]. \tag{8}$$

Once the solution becomes supersaturated with respect to siderite, it begins to precipitate drawing down $CO_3^{2-}$ concentration and causing a decline in calcite saturation (Figure 6-3). Thus, an increase in $Fe^{2+}$ concentration with depth could lead to siderite precipitation and calcite undersaturation. Since the main source of $O_2$ is photosynthesis on shallow platforms, and the main sink for $O_2$ is reduced ions in the oceans (Holland, 1984), a gradient in $O_2$ concentration is expected from the platform to deep ocean water. Thus, $Fe^{2+}$ concentration should increase with depth, and siderite precipitation could replace calcite precipitation.

This model does not require an inhibiting effect of $Fe^{2+}$ on calcite precipitation, but an inhibition of calcite precipitation by $Fe^{2+}$ would kinetically limit calcite precipitation to higher depths than those where seawater became supersaturated with respect to siderite and undersaturated with respect to calcite (Figure 6-3). Meyer (1984) found a 20-80% reduction in calcite precipitation rates with $Fe^{2+}$ concentrations of $1x10^{-2}$ to $6x10^{-2}$ µmol/l. These concentrations are much lower than those at which siderite becomes supersaturated except at very elevated $CO_3^{2-}$ concentrations. His experiments were performed at exceedingly high calcite saturation states (~250 times supersaturated; Meyer, 1984), but Dromgoole and Walter (1990a) also documented inhibiting effects with $Fe^{2+}$ concentrations of 20 µmol/l at calcite saturation states of less than 10 times supersaturated and below siderite saturation. Thus, it is likely that $Fe^{2+}$ in seawater inhibited calcite precipitation at shallower depths than those where siderite reached saturation suggesting that a zone of little calcite and no siderite precipitation would be present between zones of calcite and siderite accumulation. A shale-rich zone is observed in the transition from calcite-rich to siderite-rich sediments at the top of the Gamohaan Formation (Klein and Beukes, 1989; Beukes, et al., 1990; Chapter

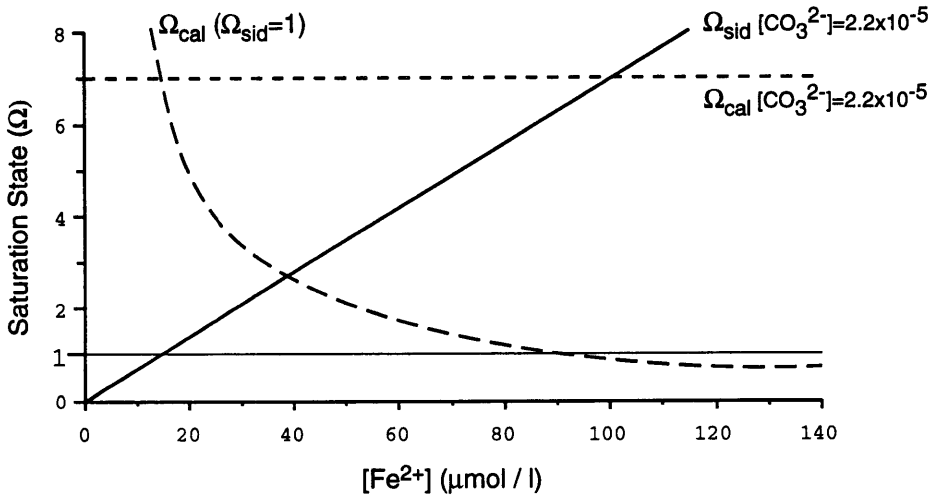


Figure 6-3: Diagram illustrating the equilibrium effects of increasing $[Fe^{2+}]$ on calcite saturation ($\Omega_{cal}$). For the purposes of illustration, surface seawater is assumed to have $[Ca^{2+}]=10^{-3}$ mol/l (value of modern seawater; Morse and Mckenzie, 1990, p. 18), $[CO_3^{2-}]=2.2x10^{-5}$ mol/l for $\Omega_{cal}=7$, and $[Fe^{2+}]=0$ mol/l. $\Omega_{cal}=7$ for model surface water (short dashed line) and W=1 are plotted for reference. The solid line represents siderite saturation ($\Omega_{sid}$) with increasing $[Fe^{2+}]$ assuming no siderite precipitation and constant $[CO_3^{2-}]$. The long dash represents $\Omega_{cal}$ if $\Omega_{sid}=1$ is maintained by decreasing $[CO_3^{2-}]$ with increasing $[Fe^{2+}]$. Thus, an increase in $[Fe^{2+}]$ with depth resulting in siderite precipitation may lead to calcite undersaturation, ignoring kinetic effects and all other changes with depth. The influence of increasing $[Fe^{2+}]$ is enhanced by the inhibiting effect of $[Fe^{2+}]$ on calcite precipitation. Dromgoole and Walter (1990a and b) observed significant inhibiting effects at $[Fe^{2+}]\leq 20$ µmol/l. Ewers (1983) suggests that $[Fe^{2+}]>100$ µmol/l may have been necessary in seawater for oxide-facies iron-formation deposition.

4), as well as in other iron-formations (e.g. Carrigan and Cameron, 1991; Morris, 1993), and may have accumulated above the depth at which siderite became saturated and below the depth at which calcite precipitation was effectively stopped by increasing $Fe^{2+}$ concentration. Thus, increasing $Fe^{2+}$ concentrations with depth alone can cause a change from limestone deposition to siderite facies iron-formation deposition. Since this model only depends on a gradient in $Fe^{2+}$ concentration which could be dynamically maintained, it does not require a stratified ocean. It is consistent, however, with ocean stratification supported by other chemical data (e.g. Klein and Beukes, 1989; Beukes, et al., 1990).

Although this model illustrates a possible mechanism for transitions from calcite to siderite precipitation with depth, it uses poorly constrained solubility constants for siderite, assumes ambient conditions of 25°C and 1 atm, does not account for changes in solubility constants or pH with depth, and ignores kinetic effects beyond the implicit assumption that surface seawater is supersaturated with respect to calcite. More data are needed to test the applicability of this model.

## CONCLUSIONS

The presence of calcite precipitation inhibitors helped maintain the calcium carbonate supersaturation of Archean and Proterozoic seawater and affected the texture of carbonate precipitates. In particular, experimental data show that $Fe^{2+}$ strongly inhibits calcite precipitation, and geological evidence suggests that $Fe^{2+}$ was present in seawater prior to 2.2-1.8 Ga. Thus, $Fe^{2+}$ may account for the predominance of precipitated sea-floor carbonates over micrite precipitation in the water column during Archean time. The rise in oxygen partial pressure and corresponding decline in seawater $Fe^{2+}$ concentration changed the kinetics of carbonate deposition allowing more micrite precipitation and reducing the likelihood that sea-floor encrusting precipitates would form. A reduction in $Fe^{2+}$ concentration would also cause a decrease in calcite supersaturation since $Fe^{2+}$ dramatically reduces calcite precipitation rates.

In addition to affecting calcite morphology and saturation state, an increase in $Fe^{2+}$ concentration with depth in Archean oceans could cause siderite precipitation and calcite undersaturation. This change could be driven by an oxygen gradient between an oxygen-producing shallow platform and an anoxic deep ocean that acted as an oxygen sink. This gradient could be dynamically maintained on an earth with low surface oxygen concentrations and does not require a stratified ocean.

The importance of $Fe^{2+}$ in carbonate textural changes and the depositional environments for calcite versus siderite precipitation can be tested in several ways. Further docu-

mentation of the distribution of herringbone calcite, particularly in Phanerozoic carbonates, will provide constraints on the chemical conditions promoting herringbone calcite precipitation. Second, the paucity of micrite in Archean rocks predicts that aragonite nucleation was also inhibited. No experimental data currently are available on the influence of $Fe^{2+}$ and $Mn^{2+}$ on aragonite precipitation. A better understanding of the inhibition of calcite and aragonite precipitation is essential to thoroughly evaluate models for secular variations in carbonate textures. Better characterization of the low temperature chemistry of siderite is also necessary to evaluate the role of changing $Fe^{2+}$ concentrations on the precipitation of siderite as opposed to calcite. Finally, detailed stratigraphic and petrographic studies of Archean and Proterozoic carbonate platforms and associated iron-formations that specifically address the modes and mechanisms of mineral precipitation will provide an essential geological framework for testing models of seawater chemistry.

## REFERENCES


Berkner, L. V. and L. C. Marshall, 1965. On the origin and rise of oxygen concentration in the Earth's atmosphere. Journal of the Atmospheric Sciences, v. 22, p. 225-261.

Berner, R. A., 1975. The role of magnesium in the crystal growth of calcite and aragonite from seawater. Geochimica et Cosmochimica Acta, v. 39, p. 489-504.

Beukes, N. J., 1983. Paleoenvirnomental setting of iron-formations in the depositional basin of the Transvaal Supergroup, South Africa *in* Iron-formation: Facts and problems (A. F. Trendall and R. C. Morris, eds.). Elsevier, Amsterdam. p. 131-198.

Beukes, N. J., 1987. Facies relations, depositional environments and diagenesis in a major early Proterozoic stromatolitic carbonate platform to basinal sequence, Campbellrand Subgroup, Transvaal Supergroup, southern Africa. Sedimentary Geology, v. 54, p. 1-46.

Beukes, N. J., C. Klein, A. J. Kaufman and J. M. Hayes, 1990. Carbonate petrography, kerogen distribution, and carbon and oxygen isotope variations in an Early Proterozoic transition from limestone to iron-formation deposition, Transvaal Supergroup, South Africa. Economic Geology, v. 85, p. 663-689.

Boss, S. K. and B. H. Wilkinson, 1991. Planktongenic/eustatic control on cratonic/oceanic carbonate accumulation. Journal of Geology, v. 99, p. 497-513.

Bruno, J., P. Wersin and W. Stufmm, 1992. On the influence of carbonate in mineral dissolution: II. The solubility of $FeCO_3$ (s) at 25°C and 1 atm total pressure. Geochimica et Cosmochimica Acta, v. 56, p. 1149-1155.

Burton, E. A. and L. M. Walter, 1990. The role of pH in phosphate inhibition of calcite and aragonite precipitation rates in seawater. Geochimica et Cosmochimica Acta, v. 54, p. 797-808.

Busenberg, E. and L. N. Plummer, 1985. Kinetic and thermodynamic factors controlling the distribution of $SO_4^{2-}$ and $Na^+$ in calcites and aragonites. Geochimica et Cosmochimica Acta, v. 49, p. 713-725.

Cameron, E. M., 1982. Sulphate and sulphate reduction in early Precambrian oceans. Nature, v. 296, p. 145-148.

Carrigan, W. J. and E. M. Cameron, 1991. Petrological and stable isotope studies of carbonate and sulfide minerals from the Gunflint Formation, Ontario: evidence for the origin of early Proterozoic itonformation. Precambrian Research, v. 52, p. 347-380.

Cloud, P., 1972. A working model of the primitive Earth. American Journal of Science, v. 272, p. 537-548.

Cloud, P. E. and M. A. Semikhatov, 1969. Proterozoic stromatolite zonation. American Journal of Science, v. 267, p. 1017-1061.

Dickson, J. A. D., 1966. Carbonate identification and genesis as revealed by staining. Journal of Sedimentary Petrology, v. 36, p. 491-505.

Dromgoole, E. L. and L. M. Walter, 1990a. Iron and manganese incorporation into calcite: Effects of growth kinetics, temperature and solution chemistry. Chemical Geology, v. 81, p. 311-336.

Dromgoole, E. L. and L. M. Walter, 1990b. Inhibition of calcite growth rates by $Mn^{2+}$ in $CaCl_2$ solutions at 10, 25, and 50°C. Geochimica et Cosmochimica Acta, v. 54, p. 2991-3000.

Edmond, J. M., C. Measures, B. Mangum, B. Grant, F. R. Sclater, R. Collier, A. Hudson, L. I. Gordon and J. B. Corliss, 1979. On the formation of metal-rich deposits at ridge crests. Earth and Planetary Science Letters, v. 46, p. 19-30.

Ewers, W. E., 1983. Chemical factors in the deposition and diagenesis of banded iron-formation *in* Iron-formation Facts and Problems (A. F. Trendall and R. C. Morris, eds.). Elsevier, Amsterdam. p. 491-512.

Garrels, R. M., E. A. J. Perry and F. T. Mackenzie, 1973. Genesis of Precambrian iron-formations and the development of atmospheric oxygen. Economic Geology, v. 68, p. 1173-1179.

Gebelein, C. D., 1974. Biologic control of stromatolite microstructure: Implications for Precambrian time stratigraphy. American Journal of Science, v. 274, p. 575-598.

Grey, K., 1994. Stromatolites from the Paleoproterozoic Earaheedy Group, Earaheedy Basin, Western Australia. Alcheringa, v. 18, p. 187-218.

Grotzinger, J. P., 1989. Facies and evolution of Precambrian carbonate depositional systems: emergence of the modern platform archetype *in* Controls on Carbonate Platform and Basin Development (P. D. Crevello, J. L. Wilson, J. F. Sarg and J. F. Read, eds.). Society of Economic Paleontologists and Mineralogists, Special Publication 44, p. 79-106.

Grotzinger, J. P., 1990. Geochemical model for Proterozoic stromatolite decline. American Journal of Science, v. 290-1, p. 80-103.

Grotzinger, J. P. and J. F. Kasting, 1993. New constraints on Precambrian ocean composition. Journal of Geology, v. 101, p. 235-243.

Grotzinger, J. P. and J. F. Read, 1983. Evidence for primary aragonite precipitation, lower Proterozoic (1.9 Ga) dolomite, Wopmay orogen, northwest Canada. Geology, v. 11, p. 710-713.

Grotzinger, J. P., D. Y. Sumner and N. J. Beukes, 1993, Archean carbonate sedimentation in an active extensional basin, Belingwe Greenstone Belt, Zimbabwe. GSA Annual Meeting, Abstracts, v. 25, p. A64.

Holland, H. D., 1984. The Chemical Evolution of the Atmosphere and Oceans. Princeton University Press, Princeton. 582 p.

Kah, L. C. and A. H. Knoll, in review. Microbenthic distribution in Proterozoic tidal flats: Environmental and taphanomic considerations. Geology.

Kasting, J. F., 1991. Box models for the evolution of atmospheric oxygen: an update. Palaeogeography, Palaeoclimatology , Palaeoecololgy , v. 97, p. 125-131.

Keith, H. D. and F. J. Padden, 1963. A phenomenological theory of spherulitic crystallization. Journal of Applied Physics, v. 34, p. 2409-2421.

Kittel, C. and H. Kroemer, 1980. Thermal Physics. Freeman and Company, New York. 473 p.

Klein, C. and N. J. Beukes, 1989. Geochemistry and sedimentology of a facies transition from limestone to iron-formation deposition in the Early Proterozoic Transvaal Supergroup, South Africa. Economic Geology, v. 84, p. 1733-1742.

Knoll, A. H., 1984. The Archean/Proterozoic transition: A sedimentary and paleobiological perspective *in* Patterns of Change in Earth Evolution (H. D. Holland and A. F. Trendall, eds.). Springer-Verlag, Berlin. p. 221-242.

Knoll, A. H. and K. Swett, 1990. Carbonate deposition during the later Proterozoic Era: an example from Spitsbergen. American Journal of Science, v. 290-A, p. 104-132.

Knoll, A. H., I. J. Fairchild and K. Swett, 1993a. Calcified microbes in Neoproterozoic carbonates: Implications for our understanding of the Proterozoic/Cambrian transition. Palaios, v. 8, p. 512-525.

Knoll, A. H., J. P. Grotzinger and V. N. Sergeev, 1993b, Carbonate precipitation in stratiform and domal structures from the Mesoproterozoic Kotuikan Formation, northern Siberia. Geological Society of America, Abstracts with Programs, v. 25, p. A-357.

Martin, A., E. G. Nisbet and M. J. Bickle, 1980. Archean stromatolites of the Belingwe Greenstone Belt, Zimbabwe (Rhodesia). Precambrian Research, v. 13, p. 337-362.

Meyer, H. J., 1984. The influence of impurities on the growth rate of calcite. Journal of Crystal Growth, v. 66, p. 639-646.

Monty, C. L. V., 1973. Precambrian background and Phanerozoic history of stromatolitic communities, an overview. Annales de la Société Géologique de Belgique, v. 96, p. 585-624.

Morris, R. C., 1993. Genetic modelling for banded iron-formation of the Hamersley Group, Pilbara Craton, Western Australia. Precambrian Research, v. 60, p. 243-286.

Morse, J. W. and F. T. Mackenzie, 1990. Geocheimstry of Sedimentary Carbonates. Elsevier, New York. 707 p.

Ohara, M. and R. C. Reid, 1973. Modeling Crystal Growth Rates from Solution. Prentice-Hall Inc., Englewood Cliffs, NJ. 272 p.

Preiss, W. V., 1976. Intercontinental correlations *in* Stromatolites (M. R. Walter, ed.). Elsevier, New York. p. 359-370.

Sami, T. T. and N. P. James, 1994. Peritidal carbonate platform growth and cyclicity in an early Proterozoic foreland basin, Upper Pethei Group, northwest Canada. Journal of Sedimentary Research, v. B64, p. 111-131.

Schmidt, V., 1977. Inorganic and organic reef growth and subsequent diagenesis in the Permian Capitan Reef Complex, Guadalupe Mountains, Texas, New Mexico *in* Uper Guadalupian Facies, Permian Reef Complex, Guadalupe Mountains New Mexico and West Texas: 1977 Field Conference Guidebook (M. E. Hileman and J. J. Mazzullo, eds.). S.E.P.M., Permian Basin Section. Publication 77-16, p. 93-131.

Semikhatov, M. A., 1976. Experience in stromatolite studies in the U.S.S.R. *in* Stromatolites (M. R. Walter, ed.). Elsevier, New York. p. 337-358.

Semikhatov, M. A. and M. E. Raaben, 1993. Dynamics of the taxonomic diversity of Riphean and Vendian stromatolites in northern Eurasia. Stratigraphy and Geological Correlation, v. 1, p. 133-141.

Semikhatov, M. A., C. D. Gebelein, P. Cloud, S. M. Awramik and W. C. Benmore, 1979. Stromatolite morphogenesis—progress and problems. Canadian Journal of Earth Science, v. 16, p. 992-1015.

Simonson, B. M., 1992, Sea level control on the deposition of large banded iron formations: Sedimentological evidence from the Hamersley Group, Western Australia. Geological Society of America, Annual Meeting, v. 24, p. 138.

Simonson, B. M., K. A. Schubel and S. W. Hassler, 1993. Carbonate sedimentology of the early Precambrian Hamersley Group of Western Australia. Precambrian Research, v. 60, p. 287-335.

Sumner, D. Y. and S. A. Bowring, in press. U-Pb geochronologic constraints on deposition of the Campbellrand Subgroup, Transvaal Supergroup, South Africa. Precambrian Research.

Sumner, D. Y. and J. P. Grotzinger, in review. Herringbone calcite. Journal of Sedimentary Research.

Veizer, J., J. Hoefs, D. R. Lowe and P. C. Thurston, 1989. Geochemistry of Precambrian carbonates: II. Archean greenstone belts and Archean seawater. Geochimica et Cosmochimica Acta, v. 53, p. 859-871.

Walker, J. C. G., 1983. Possible limits on the composition of the Archean ocean. Nature, v. 302, p. 518-520.

Walter, M. R. and G. R. Heys, 1985. Links between the rise of the metazoa and the decline of stromatolites. Precambrian Research, v. 29, p. 149-174.

Weyl, P. K., 1967. The solution behavior of carbonate materials in sea water. Studies in Tropical Oceanography, University of Miami, v. 5, p. 178-228.

# APPENDIX A

(Accepted for Publication in Precambrian Research)

# U-PB GEOCHRONOLOGIC CONSTRAINTS ON DEPOSITION OF THE CAMPBELLRAND SUBGROUP, TRANSVAAL SUPERGROUP, SOUTH AFRICA

Dawn Y. Sumner and Samuel A. Bowring
Department of Earth, Atmospheric, and Planetary Sciences,
Massachusetts Institute of Technology, Cambridge, MA 02139 U.S.A.

## ABSTRACT

A volcanic ash bed that crops out 40-50 m below the contact between the Campbellrand Subgroup and the Kuruman Iron Formation, Transvaal Supergroup, South Africa, yields an U-Pb zircon age of 2521±3 Ma. This new age demonstrates that the Campbellrand-Malmani carbonate platform was deposited during late Archean time, and is the oldest extensively preserved carbonate platform known. In addition, the age constrains deposition of the Kuruman, Griquatown, and Penge iron-formations to latest Archean to earliest Paleoproterozoic time. Although a previously reported Pb-Pb age of 2557±49 Ma for dolomites at the base of the Campbellrand Subgroup is broadly consistent with this U-Pb zircon age, new Pb-isotopic data for carbonate cements and massive sulfides lie along the same Pb-Pb array as the dolomites. This relationship implies that the "isochron" is the result of post depositional resetting of the U-Pb system in dolomite by fluids responsible for sulfide mineralization, and that the age which corresponds to its slope has no geological significance.

## INTRODUCTION

The Kaapvaal Craton, South Africa, contains an extensive record of Archean to Paleoproterozoic platform sedimentation. Deposition of cratonic cover sequences including siliciclastic, chemical, and volcanic sediments began at about 3.0 Ga (Tankard et al., 1982). These sediments include the auriferous Witwatersrand Supergroup, the oldest extensively preserved carbonate platform known, large volumes of iron-formation, and red bed deposits. The chemical and physical charateristics of these and other deposits on the Kaapvaal craton can provide important constraints on late Archean and Proterozoic sedi-

mentary environments. For example, establishing the timing of carbonate deposits and the textures within them can help constrain variations in Archean and Paleoproterozoic carbonate facies and possible long term changes in ocean chemistry (Grotzinger, 1989; Grotzinger and Kasting, 1993). Iron-formations and red bed deposits contain important information on oxygen concentrations in both the oceans and atmosphere. Temporal comparisons of oxidation states in various sedimentary environments will lead to a better understanding of early ocean stratification (Simonson, 1985, Beukes, et al., 1990) and global changes in oxygen concentration (Holland, 1984).

Kaapvaal cratonic stratigraphy is poorly dated in absolute time, however, hindering the improvement of Archean to Paleoproterozoic sedimentation models as well as development of inter-regional lithostratigraphic correlations. In order to better constrain the depositional ages of Kaapvaal cratonic sediments, we present U-Pb geochronology of an ash bed interlayered with sedimentary rocks, and examine the possibility of obtaining geologically meaningful ages of carbonate rocks using Pb-Pb dating.

**Stratigraphic Framework and Previous Geochronological Constraints**

Archean basement of the Kaapvaal craton consists of granitoids, gneisses, and greenstone belts (Tankard et al., 1982) that are overlain by the siliciclastic and volcanic Dominion Group dated at 3074±6 Ma (U-Pb, zircon; Armstrong et al., 1991). The Witwatersrand Supergroup overlies the Dominion Group and contains detrital zircons ranging in age from 3.33-2.89 Ga (Barton et al., 1989; Robb et al., 1990). The Witwatersrand Supergroup is in turn overlain by the Ventersdorp Supergroup, a succession of volcanic and other sediments. Reported ages for the Ventersdorp Supergroup range from ~2.2 Ga (Rb-Sr and Pb-Pb whole rock; Armstrong et al., 1986), to 2643±80 Ma (U-Pb zircon upper intercept; Van Niekerk and Burger, 1978), to 2709±4 Ma and 2714±8 Ma (U-Pb zircon ion probe; Armstrong et al. 1991). Armstrong et al. (1991) suggest that the 2.2 Ga ages reflect an episode of regional metamorphism.

The Transvaal Supergroup unconformably overlies the Ventersdorp Supergroup and older granitic and greenstone basement. It is preserved over much of the northern and western Kaapvaal Craton and is largely undeformed. Locally, metamorphic grades reach hornblende-hornfels facies adjacent to the Bushveld Complex, but most of the supergroup is below the zeolite grade of metamorphism (Saggerson and Turner, 1992). Structural disruption of preserved strata is limited to gentle warping over most of the craton with locally steeper dips around the Bushveld Complex. Along the western boundary of the Kaapvaal craton intense folds and faults in the Keis Belt and Dooringberg Fault Zone (Fig. 2; Stowe, 1986; Beukes and Smit, 1987) truncate sedimentary facies demonstrating that deposition

continued beyond this boundary during Transvaal time (Beukes, 1987). The rest of the outcrop and subsurface patterns of the Transvaal Supergroup are due to erosion along younger unconformities and do not reflect original depositional extents.

The Transvaal Supergroup consists of a thick succession of sandstone, shale, limestone/dolostone, iron-formation, and volcanic rocks (Fig. 1). The base of the Transvaal Supergroup in the Transvaal Province is marked by 0-2 km thick sequence of quartz arenite and shale forming the Wolkberg and Buffalo Springs groups. Isopach maps reveal large thickness variations in these basal siliciclastics related to paleotopography and differential subsidence across the Transvaal Province (Button, 1973a). The Wolkberg and Buffalo Springs groups are overlain by the fluvial to shallow marine Black Reef Quartzite (Button, 1973a; Tyler, 1979). In the Cape Province, the base of the Transvaal Supergroup is marked by the mixed siliciclastic and carbonate rocks of the Schmidtsdrif Subgroup.

The Schmidtsdrif Subgroup and Black Reef Quartzite grade conformably into the carbonate platform of the Campbellrand and Malmani subgroups respectively (Beukes, 1987; Button, 1973a). The 500-1700 m thick carbonate platform contains almost no siliciclastic detritus (Beukes, 1987; Button, 1973b). The Malmani Subgroup consists mostly of peritidal deposits while the correlative Campbellrand Subgroup contains both peritidal and subtidal facies. A small area of basinal carbonates, shales, and iron-formation is preserved near

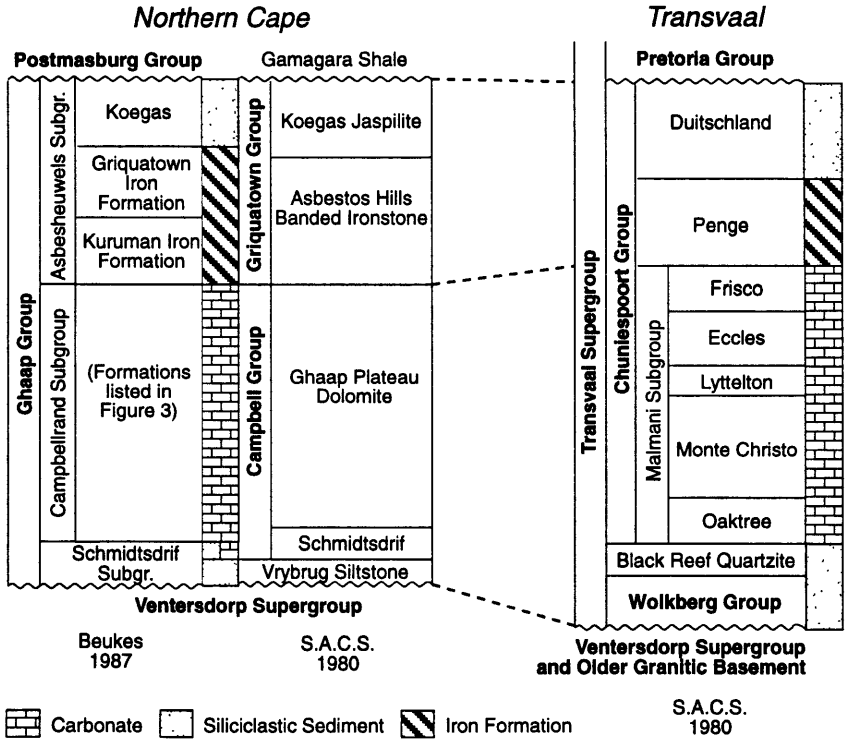


Figure 1: Stratigraphic summary of the Transvaal Supergroup in the Cape and Transvaal Provinces.

Prieska in the far southwestern corner of outcrop area (Figs. 2 and 3; Beukes, 1987). The platform had a ramp geometry during its early development and, after a transgressive event at the top of the Reivilo Formation, the platform developed a rimmed margin (Fig. 3; Beukes, 1987). The Gamohaan and Frisco formations were deposited during a major transgression that marked the end of carbonate deposition.

The Gamohaan Formation is dominated by a variety of deep subtidal microbialites consisting of very thin microbial films entombed in calcite with marine cement textures. In rare instances, individual microbialite and associated cement beds are continuous for >100 km (Sumner, unpublished data). Siliciclastic detritus is absent from the Gamohaan Formation except for a volcanic ash-rich zone in which the dated ash bed is preserved. Two of the ash beds in this zone are continuous for at least 80 km and represent airfall tuffs that accumulated subaqueously. They grade upward from fine sand to very fine silt, are green to black in color, and outcrop resistantly. Other ash beds have similar characteristics, but are not laterally continuous and show sedimentary structures such as current ripples that suggest reworking of tuffaceous sediment by subaqueous density currents. Carbonates adjacent to ash beds typically show silica replacement and concretionary banding.

Forty to fifty meters above the tuffaceous zone, the Gamohaan Formation is conformably overlain by deep water, microbanded iron-formation of the Kuruman Iron Forma-

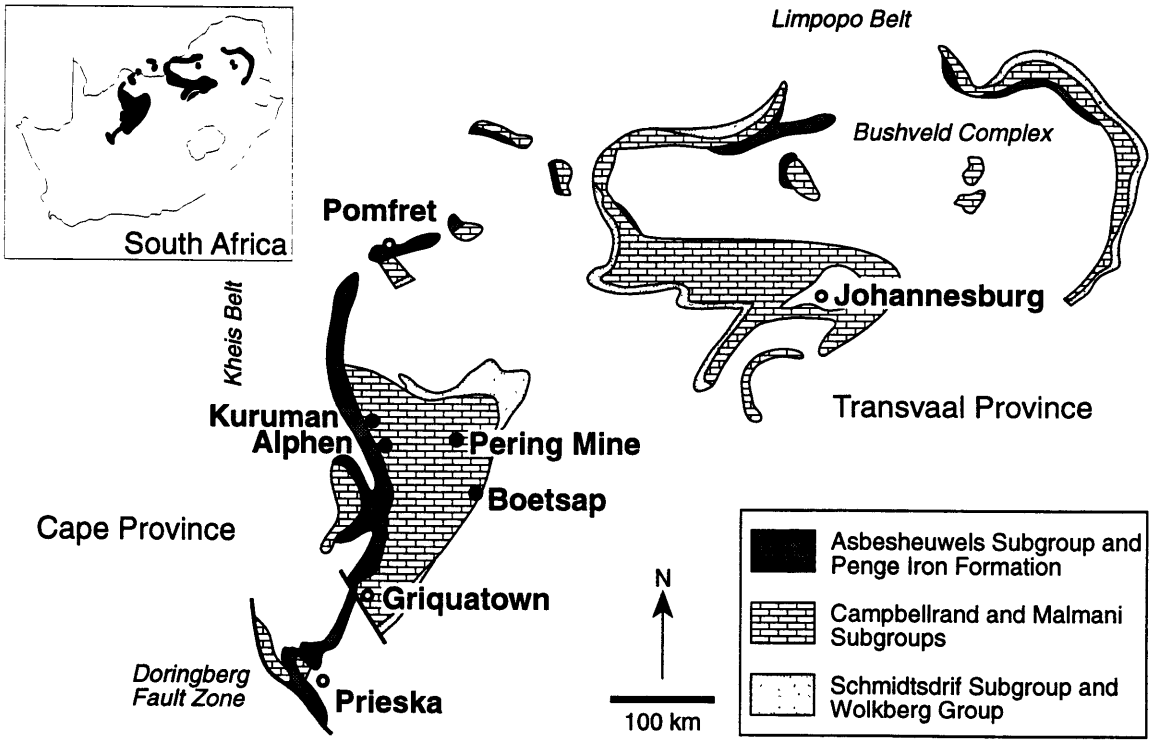


Figure 2: Map of lower Transvaal Supergroup outcrop.

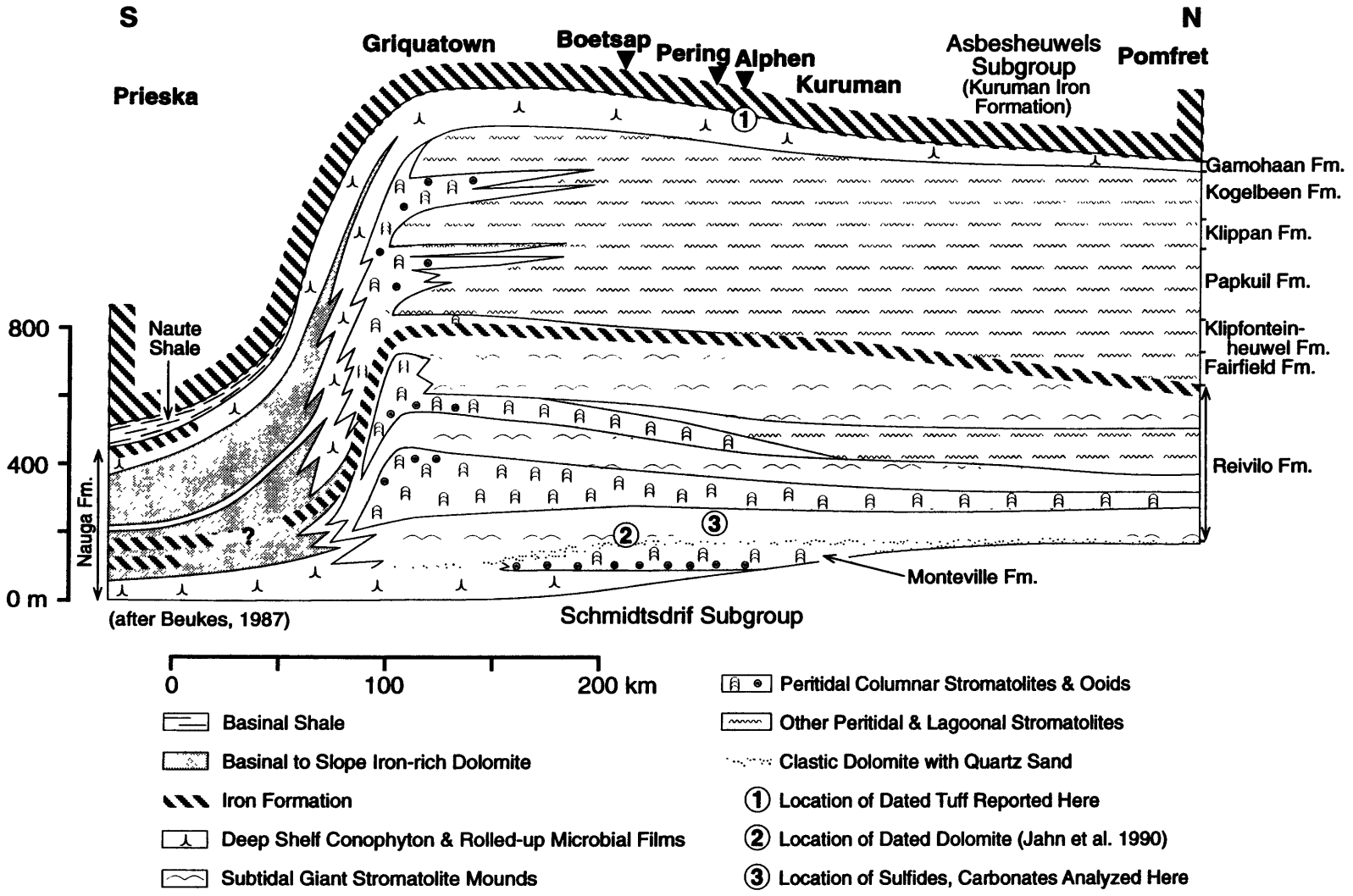


Figure 3: Cross section of the Campbellrand Subgroup showing sample locations.

tion (Beukes, 1984) which is in turn overlain by the Griquatown Iron Formation. The Griquatown Iron Formation consists of various clastic-textured iron-formation lithotypes deposited in a shallow epeiric sea or a fresh water lake (Beukes, 1984). It is overlain by remnants of a siliciclastic delta, the Koegas Formation. The Penge Iron Formation, conformably overlying the Frisco Formation in the Transvaal Province is correlative with and lithologically similar to the Kuruman Iron Formation and probably formed on a stable shelf below wave base (Beukes, 1973). It is unconformably overlain by a mixed carbonate and siliciclastic unit, the Duitschland Formation. The Duitschland and Koegas formations were deeply eroded prior to deposition of the Pretoria and Postmasburg groups. The unconformity beneath the Pretoria Group truncates the iron-formation and carbonates down to basement in the southeastern Transvaal Province, removing at least 2 km of sediment (Button, 1973b).

A variety of Pb-Pb and Rb-Sr whole rock isotopic data from rocks of the Transvaal Supergroup indicate ages of ~2.2 Ga (e.g. Burger and Coertze, 1975; Hunter and Hamilton, 1978; Walraven et al., 1990). In contrast to this, Jahn et al. (1990) report a Pb-Pb dolomite age of 2557±49 Ma near the base of the Campbellrand-Malmani platform and Barton et al. (1994) report an U-Pb zircon age of 2552±11 Ma for basinal carbonates temporally equivalent to the platform. Trendall et al. (1990) report an U-Pb zircon age of 2432±31 Ma for the base of the Griquatown Iron Formation (these authors placed the dated ash bed within the Kuruman Iron Formation, but the samples were collected by N. J. Beukes near the base of the Griquatown Iron Formation (pers. comm., 1994)). These dates suggest a late Archean to earliest Paleoproterozoic age for the lower Transvaal Supergroup. The minimum age of the Transvaal Supergroup is constrained by the ~2060 Ma Bushveld complex which intrudes it (Walraven et al., 1990).

## METHODS

Zircons were separated from samples using standard techniques of crushing, and density and magnetic separation. Inclusion free, colorless zircons were selected for analysis and were air-abraded to remove the outer portion of the grains which are prone to Pb-loss (Krogh, 1982), and then acid washed in 4N $HNO_3$. The zircons were spiked with a mixed $^{205}Pb$-$^{233}U$-$^{235}U$ tracer solution before dissolution in HF + $HNO_3$ in teflon bombs at 220° C for 48 hours. Lead and U were separated from the resulting solution using anion exchange chemistry modified after Krogh (1973). Total procedural blanks during the course of these analyses were 2.0-3.5 pg for Pb, and less than 1 pg for U. Lead was loaded on single rhenium filaments with silica gel and phosphoric acid. Isotopes of Pb were measured with a VG Sector-54 thermal ionization mass spectrometer using a Daly detector in

ion-counting mode. An ion-beam between 0.5 and 1.5 X $10^{-13}$ amps was maintained for $^{206}Pb$ during data acquisition. Uranium was loaded with phosphoric acid and colloidal graphite on rhenium filaments and was measured as metal ions in static mode by utilizing three Faraday collectors and an average $^{235}U$ ion beam intensity of 2.5 X $10^{-13}$ amps. Errors in $^{238}U/^{206}Pb$, $^{235}U/^{207}Pb$, and $^{207}Pb/^{206}Pb$ were estimated using the method of Ludwig (1988), and all age uncertainties are quoted at the 2s confidence level.

Carbonate, quartz, and sulfide samples for Pb-isotopic analysis were crushed to coarse sand size, washed in distilled water, and picked for purity. They were weighed and dissolved in HF (quartz), HCl (carbonates), or $HNO_3$ (sulfides). All samples except galena were spiked with a mixed $^{205}Pb$-$^{233}U$-$^{235}U$ tracer solution. Lead was isolated using standard HBr anion exchange chemistry. Isotopic compositions were determined in static mode using Faraday collectors. Uncertainty associated with fractionation corrections is assumed to be 0.05% error/amu difference in mass for $2\sigma$.

## RESULTS

### *U-Pb Zircon Geolchronology*

Samples for U-Pb zircon analysis were collected from a laterally continuous, fine grained, dark green-gray airfall tuff in the upper Gamohaan Formation at Alphen farm, 16 km south of the town of Kuruman (27°35' S 23°25' E; Figs. 2 and 3). No sedimentary structures are apparent within the 15-20 cm thick bed. Extracted zircons consisted of <100x100x70 μm euhedral crystals without apparent inherited cores. Four fractions consisting of 1 or 2 zircons each were analyzed. The zircons are characterized by relatively high common Pb contents (Table 1) as well as opaque inclusions. They define a chord on a concordia diagram with an upper intercept of 2521±3 Ma and a lower intercept of 502±129 Ma with an MSWD of 0.12. We interpret the upper intercept as the age of the ash bed with non-concordant samples showing evidence for Pb-loss.

### *Carbonate and Sulfide Pb-Isotopic Data*

In this study we measured Pb isotopes of various minerals in a Pb-Zn deposit at Pering Mine (Figs. 2 and 3) and compared them to isotopic results from nearby dolomite published by Jahn et al. (1990) in order to evaluate the data obtained by these authors. Pering Mine is located at a site of Pb-Zn mineralization in the Reivilo Formation near the base of the Campbellrand-Malmani platform (Figs. 2 and 3). Mineralization consists of subhorizontal stratiform lenses and subvertical breccia zones with about 18 Mt of ore grad-

Table 1: U-Pb Zircon Analytical Data

| Fraction | Weight (mg) | U (ppm) | Pb (ppm) | $^{206}Pb^{*1}/^{204}Pb$ | $^{208}Pb^{1}/^{206}Pb$ | $^{206}Pb^{1}/^{238}U$ | $^{207}Pb^{1}/^{235}U$ | $^{207}Pb^{1}/^{206}Pb$ | Age (Ma) $^{206}Pb/^{238}U$ | Age (Ma) $^{207}Pb/^{235}U$ | Age (Ma) $^{207}Pb/^{206}Pb$ | Corr. Coef. | Common Pb (pg) |
|---|---|---|---|---|---|---|---|---|---|---|---|---|---|
| P1 | 0.0033 | 145 | 75 | 1588 | 0.139 | 0.460 (1) | 10.50 (3) | 0.1654 (2) | 2440.5 | 2479.6 | 2511.9 | 0.935 | 11.8 |
| P2 | 0.0022 | 106 | 56 | 11,222 | 0.141 | 0.470 (2) | 10.76 (6) | 0.1659 (1) | 2485.6 | 2502.9 | 2517.0 | 0.989 | 4.0 |
| P4 | 0.0024 | 141 | 77 | 345 | 0.152 | 0.477 (2) | 10.94 (4) | 0.1662 (3) | 2515.6 | 2517.8 | 2519.6 | 0.878 | 30.4 |
| P13 | 0.0030 | 306 | 160 | 1041 | 0.154 | 0.4592 (7) | 10.47 (2) | 0.1653 (1) | 1435.8 | 2477.0 | 2511.0 | 0.868 | 26.1 |

[1]Corrected for blank and common lead. Estimated blank lead is 3.5 pg for each sample. Numbers in paranthases represent 2s error in the last digit.

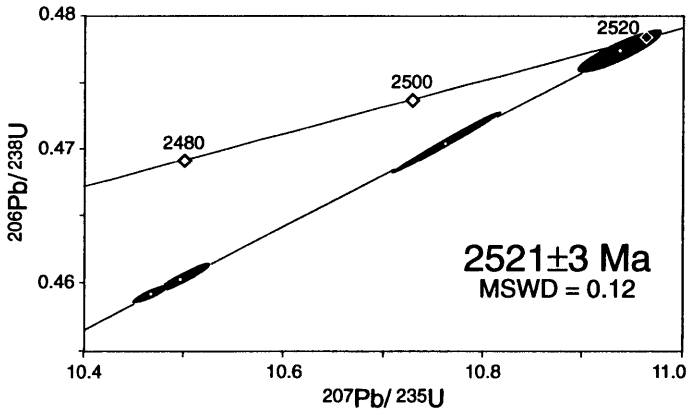


Figure 4: Concordia plot for analysed zircons from Alphen farm. Error elipses represent 2σ analytical errors.

ing 3.6% Zn and 0.6% Pb in the form of sphalerite and galena (Wheatley et al., 1986). In addition, dolomite, calcite, quartz, pyrite, and chalcopyrite precipitated from the mineralizing fluids. Lead-isotopic data were collected from calcite, dolomite, quartz, galena, and chalcopyrite, all of which precipitated directly from the mineralizing fluid and should not reflect mixing between host rock and fluid compositions unless the Pb concentration in the host carbonates was high enough to influence the Pb-isotopic composition of the bulk fluid.

Galena, chalcopyrite, and quartz all have similar isotopic ratios (Fig. 6; Table 2) and are similar to those reported for Pering sulfides by Duane et al. (1991). Most dolomite and calcite samples also have similar Pb-isotopic compositions while dolomite P4 and calcite P12 contain more radiogenic Pb-isotopic ratios. The similarity of Pb-isotopic ratios of most carbonates to galena values is not due to obvious galena contamination of the samples. All carbonate samples were carefully picked under both transmitted and reflected light and do not contain opaque mineral inclusions larger than a few microns. The high Pb concentrations in most samples, however, suggest that the carbonates contain Pb-rich fluid inclusions, <~3 μm galena inclusions, or abundant Pb in the crystal lattice, each of which implies interaction with, or precipitation from, a fluid with high Pb concentration. Three samples contain ≤2 ppm Pb (Table 2), and while two of these show more radiogenic Pb-isotopic signatures than the galena samples (dolomite P4 and calcite P12), calcite P10 has a galena-like Pb-isotopic signature and only contains 0.44 ppm Pb. This suggests that the uniformity of Pb-isotopic ratios is due to low U-Pb ratios in the fluid as well as to high Pb concentrations.

Differences in Pb-isotopic composition of samples dolomite P4 and calcite P12 may

Table 2: Pering Mine Pb-Isotopic Data

| Mineral (sample) | $\frac{^{206}Pb}{^{204}Pb}$ [1] | $\frac{^{207}Pb}{^{204}Pb}$ [1] | $\frac{^{208}Pb}{^{204}Pb}$ [1] | Pb (ppm) |
|---|---|---|---|---|
| galena (P4) | 13.49 (1) | 14.58 (2) | 33.29 (7) | - |
| galena (P10) | 13.47 (1) | 14.54 (2) | 33.21 (7) | - |
| chalcopyrite (P1a) [2] | 13.46 (1) | 14.56 (2) | 33.25 (7) | 66,480 |
| chalcopyrite (P1b) [2] | 13.46 (1) | 14.52 (2) | 33.11 (7) | 8,148 |
| quartz (P4) | 13.46 (1) | 14.51 (2) | 33.10 (7) | 12.38 |
| dolomite (P0) | 13.50 (1) | 14.54 (2) | 33.12 (7) | 349.4 |
| dolomite (P4) | 16.73 (2) | 15.16 (2) | 36.45 (7) | 0.41 |
| dolomite (P8) | 13.52 (1) | 14.55 (2) | 33.14 (7) | 1,351 |
| calcite (P9) | 13.49 (1) | 14.52 (2) | 33.10 (7) | 8.61 |
| calcite (P10) | 13.73 (1) | 14.50 (2) | 33.29 (7) | 0.44 |
| calcite (P12) | 18.14 (2) | 15.55 (2) | 38.05 (8) | 2.06 |

[1] Numbers in parentheses represent 2s error in the last decimal place. [2] May contain galena inclusions.

be due to precipitation from a fluid with a different isotopic composition than other dolomite and calcite samples, later alteration of these two samples, or natural evolution of an initial Pb-isotopic composition by decay of U and Th. The difference is probably not due to precipitation from a fluid with a different initial Pb-isotopic composition because both dolomite and calcite samples contain Pb-isotopic signatures identical to galena samples and all dolomite samples are petrographically similar to each other as are all calcite samples. Post-crystallization alteration cannot be ruled out, but galena closely associated with the carbonates would probably have dominated the Pb-isotopic signature of any later diagenetic fluids. If post-crystallization alteration did occur, the displacement of the Pb-isotopic signatures of the calcite and dolomite samples towards more radiogenic values than the galena is probably due to decay of U and Th. The most likely scenario is that the Pb-isotopic compositions of the two samples reflect evolution of an initial Pb-isotopic ratio similar to that of galena samples ensuing from decay of U and Th.

## DISCUSSION

Although the Pb-Pb dolomite "age" reported by Jahn et al. (1990) is broadly consistent with the U-Pb zircon age for the volcanic ash, our zircon data provide an important constraint on the age the Campbellrand-Malmani carbonate platform and overlying iron-formation, as well as on correlations between the Hamersley and Transvaal basins. After discussing the implications of this age, we will investigate the significance of their "isochron" in light of our new data.

### *Age of the Transvaal Supergroup*

A U-Pb zircon age of 2521±3 Ma for the Gamohaan Formation confirms that the Campbellrand and Malmani subgroups and underlying siliciclastics were deposited during late Archean time as suggested by Jahn et al. (1990) and Barton et al. (1994). The Penge, Kuruman, and Griquatown iron-formations conformably overlie the carbonates and the new age is consistent with their deposition during earliest Paleoproterozoic time as suggested by Trendall et al. (1990). A significant unconformity separates the iron-formations from the Postmasburg and Pretoria groups which could be much younger. Up to 2 km of iron-formation and carbonate were eroded prior to deposition of the Pretoria and Postmasburg groups (Button, 1973b) suggesting a significant break in the sedimentary record. While Rb-Sr ages of ~2.2 Ga (Burger and Coertze, 1975; Hunter and Hamilton, 1978; Walraven et al., 1990) from the Pretoria and Postmasburg groups support a younger age, these may reflect metamorphic overprints, especially since similar ages have also been reported for the

Ventersdorp Supergroup which is now considered to be 2709±4 Ma and older (Armstrong et al., 1991).

### *Correlations between the Transvaal and Hamersley Basins*

The Transvaal Supergroup is similar to the Hamersley Group of Western Australia in tectonic setting, stratigraphy, and age (Trendall et al., 1990; Button, 1976). Similar developmental histories of the two basins lead to speculation that they represent different

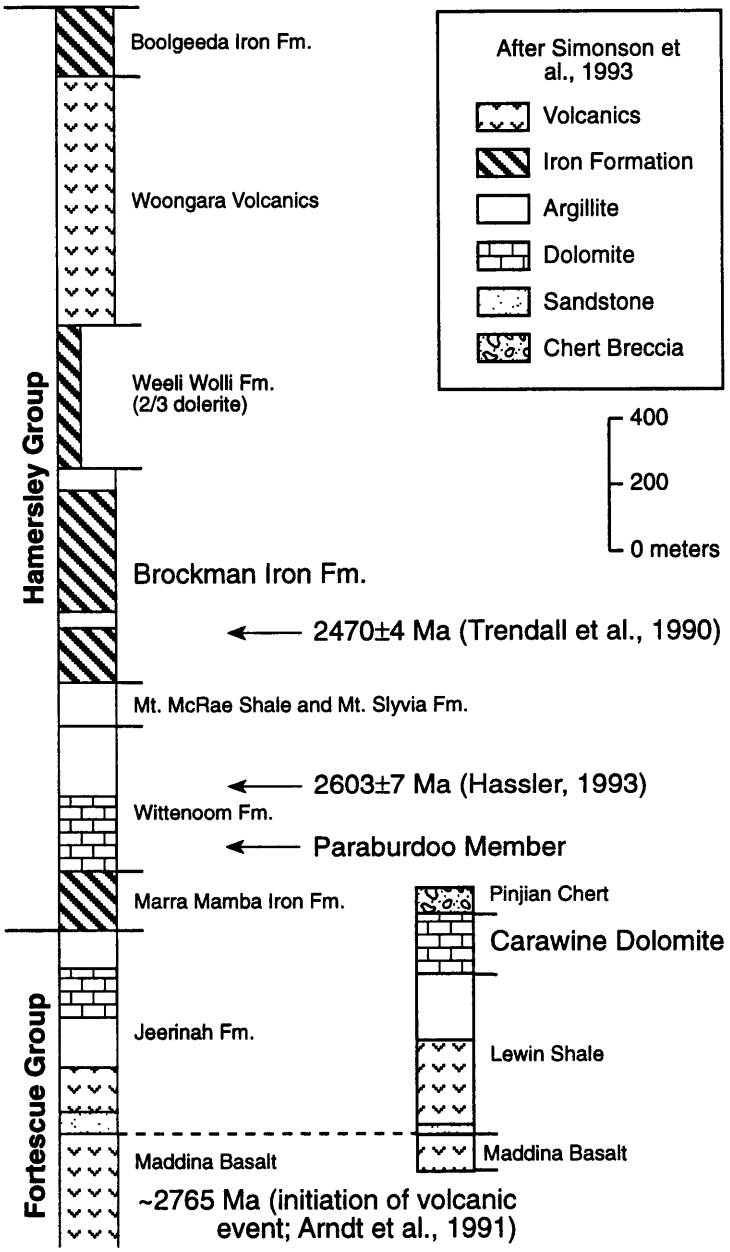


Figure 5: Summary of Hamersley Basin stratigraphy with available age constraints.

parts of a single depositional basin. Both basins contain an extensive volcanic sequence deposited immediately before 2.7 Ga, overlain by mixed siliciclastic and carbonate sediments (Fig. 5). These grade upward into a thick carbonate, iron-formation, and shale unit which is overlain by another mixed siliciclastic and volcanic sequence.

Even though the general evolution and fill of the two basins are similar, specific correlations between the chemical sedimentary units are difficult. Basinal environments are preferentially preserved in the Hamersley basin (Simonson et al., 1993) whereas platform sediments are most abundant in the Transvaal basin. Although the Paraburdoo Member of the Wittenoom Formation is lithologically similar to basinal carbonates of the Campbellrand-Malmani platform, correlations between the two are not consistent with available age constraints. Hassler (1993) sites an U-Pb age of 2603±7 Ma for zircons from a quartz-rich ash bed just above the Paraburdoo Member (Fig. 5) whereas we obtained an age of 2521±3 Ma for the upper Campbellrand-Malmani platform. With deposition of the Campbellrand-Malmani platform culminating 80 Ma after deposition of the Paraburdoo Member, temporal overlap between the two units is only possible if accumulation rates for the Campbellrand-Malmani platform were <~10m/m.y or a major unrecognized diastem is present within the section. Instead, argillites with minor carbonate between the Paraburdoo Member and the Brockman Iron Formation could be temporally equivalent to the Campbellrand-Malmani platform. Correlation between the Campbellrand-Malmani platform carbonates and the Carawine Dolomite may be possible, but neither the age of the Carawine Dolomite nor its stratigraphy is well enough constrained to support or refute any correlation. Correlations between the Brockman Iron Formation and the Kuruman Iron Formation are broadly consistent with the age constraints of 2470±4 Ma for the Brockman Iron Formation, 2432±31 Ma for the lowermost Griquatown Iron Formation (Trendall et al., 1990), and 2521±3 Ma for the carbonates which conformably underlie the Kuruman Iron Formation. Current age constraints do not, however, demonstrate synchronous deposition. While sedimentation in the Transvaal and Hamersley basins may be roughly contemporaneous, many more precise ages throughout both basins are essential to establishing any correlations between them.

## Carbonate Pb-Isotopic Signatures

Lead-isotopic signatures have been extensively used to trace mineralizing fluids in carbonate hosted Pb-Zn deposits (e.g. Clay, 1986; Gunnesch et al., 1990; Thompson and Beaty, 1990) as well as to obtain age information on carbonate deposition and alteration (e.g. Jahn et al., 1990; Moorbath et al., 1987; Bowring et al., 1989; Smith et al., 1991, Smith et al., 1994). Interpretations of the significance of Pb-isotopic trends often depend on addi-

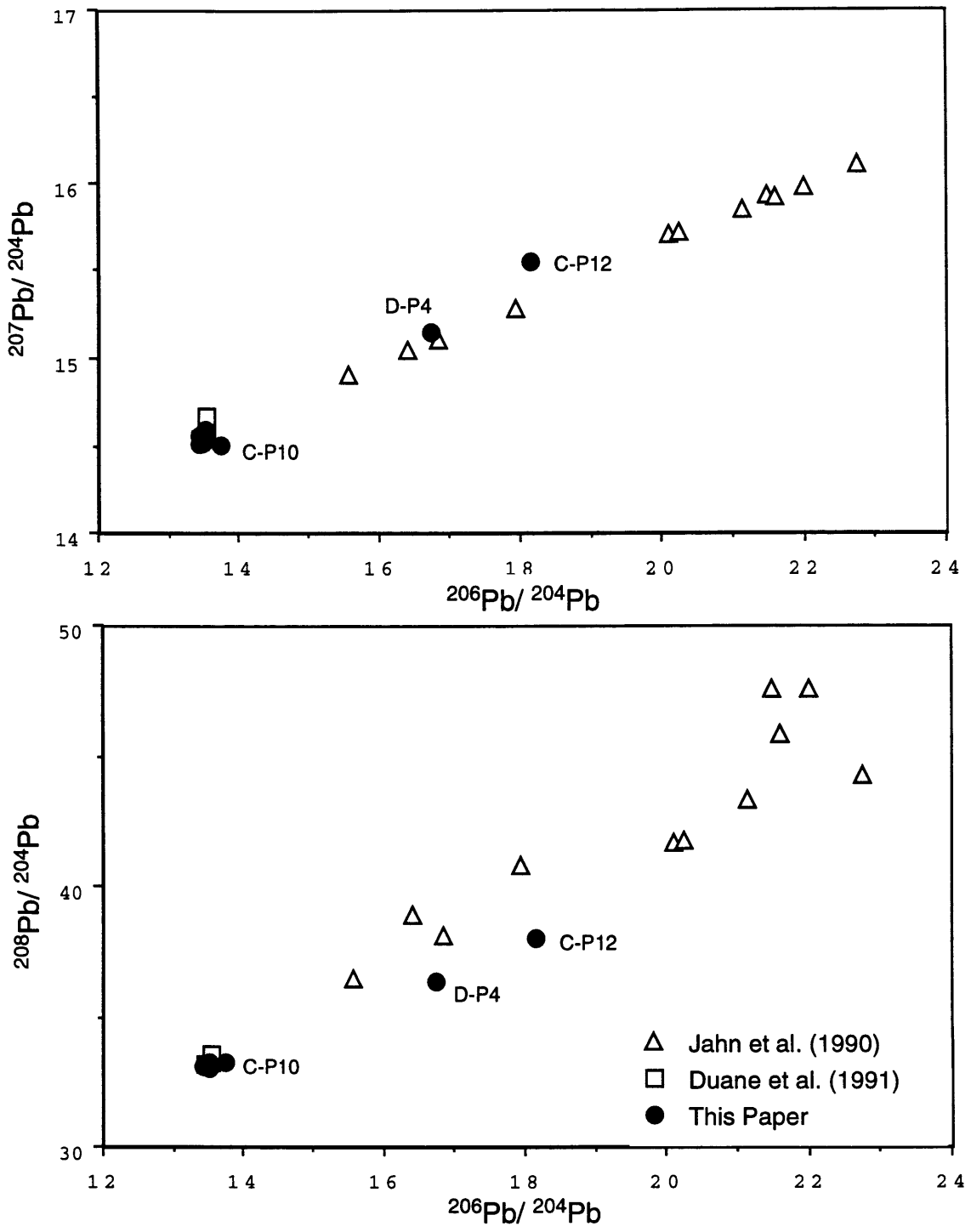


Figure 6: Lead isotope data from sulfides, dolomite, and calcite plotted with dolomite data from Jahn et al. (1990) and sulfide data from Duane et al. (1991). Sample numbers are labled for three points and correspond to numbers in Table 2 (C=calcite, D=dolomite). $2\sigma$ fractionation errors are smaller than symbols for data presented here and from Jahn et al. (1990). Duane et al. (1991) report only analytical errors which are also smaller than the symbols.

tional age constraints, assumptions about the extent of diagenesis, and evaluation of the extent of mixing between Pb reservoirs. These problems are magnified in carbonate rocks for several reasons. Carbonates are easily altered by diagenetic fluids and Pb is a minor element in calcite and dolomite with concentrations typically <1 ppm Pb. Diagenetic brines often contain >10 ppm Pb (Anderson, 1978; Svenjensky, 1981). Thus a small amount of fluid can alter the Pb-isotopic signature and decrease the U/Pb ratio of a large volume of carbonate rock. It is thus essential to critically evaluate diagenetic influences when evaluating the significance of carbonate Pb-isotopic results.

Pering Mine sulfide and carbonate Pb-isotopic data provide an interesting perspective on the isotopic alteration of samples analyzed by Jahn et al. (1990). Their dolomite samples were collected at Boetsap, 65 km south of Pering Mine and at the same to slightly lower stratigraphic levels. Lead-isotopic data from Pering Mine lie at the less radiogenic end of data published by Jahn et al. (1990) on both $^{207}Pb/^{204}Pb$ vs. $^{206}Pb/^{204}Pb$ and $^{208}Pb/^{204}Pb$ vs. $^{206}Pb/^{204}Pb$ diagrams. The relationship between these data sets as well as the proximity of the two areas suggests that dolomites at Boetsap were altered by the fluids that produced the Pering mineral deposits. Thus, the slope of the array presented by Jahn et al. (1990) probably does not represent the depositional age of the carbonates. It may not provide a minimum age constraint either since the slope of the array is poorly defined with an MSWD of 10 (Jahn et al., 1990), demonstrating that the scatter in the data is much greater than analytical errors. In addition, the array consists of two groups of data. The more radiogenic group of seven analyses from a single sample gives a slope of 0.1518 which yields an "age" of ~2.36 Ga. The less radiogenic group of four analyses from three samples gives a slope of 0.1608 yielding an "age" of ~2.46 Ga. The fact that both subgroups produce younger ages than the data set as a whole suggests that the age reported by Jahn et al. (1990) is an artifact of mixing and alteration processes and does not provide reliable minimum estimates of the depositional age of the Campbellrand Subgroup or the timing of Pering mineralization. Therefore, we do not consider their "age" a reliable constraint on deposition of the Campbellrand Subgroup.

## CONCLUSIONS

An age of 2521±3 Ma for the top of the Campbellrand Subgroup demonstrates that deposition of the extensive carbonate platform of the Transvaal Supergroup occurred in Archean time while the overlying iron-formation is latest Archean to Paleoproterozoic in age. While this age also demonstrates that the Hamersely and Transvaal basins are broadly time equivalent, additional precise age constraints in both basins are required to evaluate

lithological correlations.

Lead-isotopic results from Pering Mine sulfides and carbonates suggest that mineralization at Pering Mine and U- and Pb-isotopic resetting at Boetsap occurred during the same fluid migration. In addition, they imply that the data reported by Jahn et al. (1990) do not represent a depositional age. These results emphasize the need to carefully evaluate Pb-isotopic data from carbonates in terms of diagenetic processes.

## ACKNOWLEDGMENTS

This work was supported by a National Science Foundation Graduate Fellowship and the Gretchen L. Blechsmidt Research Grant, Geological Society of America, to DYS and by NASA Grant #NAGW-2795 to John P. Grotzinger at Massachusetts Institute of Technology. The authors also wish to thank Paul Hoffman, Jay Kaufman, and Antje Danielson for reviewing the manuscript and Nic Beukes for field support.

## REFERENCES

Anderson, G. M., 1978. Basinal brines and Mississippi Valley-type ore deposits. Episodes, 1978: 15-19.

Armstrong, R. A., Compston, W., Retief, E. A. and Wilke, N. J., 1986. Ages and isotopic evolution of the Ventersdorp volcanics. Extended Abstract, Geocongress 1986, Geological Society of South Africa, 89-92.

Armstrong, R. A., Compston, W., Retief, E. A., Williams, I. S. and Welke, H. J., 1991. Zircon ion microprobe studies bearing on the age and evolution of the Witwatersrand triad. Precambrian Research, 53: 243-266.

Barton, E. S., Compston, W., Williams, I. S., Bristow, J. W., Hallbauer, D. K. and Smith, C. B., 1989. Provenance ages for the Witwatersrand Supergroup and the Ventersdorp Contact Reef: Constraints from ion microprobe U-Pb ages of detrital zircons. Economic Geology, 84: 2012-2019.

Barton, E. S., Altermann, W., Williams, I. S. and Smith, C. B., 1994. U-Pb zircon age for a tuff in the Campbell Group, Griqualand West Sequence, South Africa: Implication for Early Proterozoic rock accumulation rates. Geology, 22: 343-346.

Beukes, N. J., 1973. Precambrian iron-formations of southern Africa. Economic Geology, 68: 960-1004.

Beukes, N. J., 1984. Sedimentology of the Kuruman and Griquatown iron formations, Transvaal Supergroup, Griqualand West, South Africa. Precambrian Research, 24: 47-84.

Beukes, N. J., 1987. Facies relations, depositional environments and diagenesis in a major early Proterozoic stromatolitic carbonate platform to basinal sequence, Campbellrand Subgroup, Transvaal Supergroup, southern Africa. Sedimentary Geology, 54: 1-46.

Beukes, N. J. and Smit, C. A., 1987. New evidence for thrusting in Griqualand West, South Africa: implications for stratigraphy and the age of red beds. South African Journal of Geology, 90: 378-394.

Beukes, N. J., Klein, C., Kaufman, A. J. and Hayes, J. M., 1990. Carbonate petrography, kerogen distribution, and carbon and oxygen isotope variations in an Early Proterozoic transition from limestone to iron-formation deposition, Transvaal Supergroup, South Africa. Economic Geology, 85: 663-689.

Bowring, S. A., Housh, T. B., Heatherington, A. L., and Grotzinger, J. P. 1989. U-Pb isotopic analysis of carbonate cements, early Proterozoic Rocknest Formation: Evidence for differential element mobility during diagenesis. Program with Abstracts, Geological Association of Canada and Mineralogical Association of Canada, 14:78.

Burger, A. J. and Coertze, F. J., 1975. Age determinations-April 1972 to March 1974. Annals of the Geological Survey of South Africa, 10: 135-141.

Button, A., 1973a. The depositional history of the Wolkberg proto-basin, Transvaal. Transactions of the Geological Society of South Africa, 76: 15-25.
Button, A., 1973b. The stratigraphic history of the Malmani dolomite in the eastern and north-eastern Transvaal. Transactions of the Geological Society of South Africa, 76: 229-247.
Button, A., 1976. Transvaal and Hamersley basins — review of basin development and mineral deposits. Minerals Science Engineering, 8: 262-293.
Clay, A. N., 1986. The stratigraphy of the Malmani Dolomite Subgroup in the Carletonville area, Transvaal: Genetic implications for lead-zinc mineralization. In: C. R. Anhaeusser and S. Maske (editors), Mineral Deposits of Southern Africa. Geological Society of South Africa, 853-860.
Duane, M. J., Kruger, F. J., Roberts, P. J. and Smith, G. B., 1991. Pb and Sr isotope and origin of Proterozoic base metal (fluorite) and gold deposits, Transvaal Sequence, South Africa. Economic Geology, 86: 1491-1505.
Grotzinger, J. P., 1989. Facies and evolution of Precambrian carbonate depositional systems: emergence of the modern platform archetype. In: P. D. Crevello, J. L. Wilson, J. F. Sarg and J. F. Read (editors), Controls on Carbonate Platform and Basin Development. Society of Economic Paleontologists and Mineralogists, Special Publication 44: 79-106.
Grotzinger, J. P. and Kasting, J. F., 1993. New constraints on Precambrian ocean composition. Journal of Geology, 101: 235-243.
Gunnesch, K. A., Baumann, A. and Gunnesch, M., 1990. Lead isotope variations across the central Peruvian Andes. Economic Geology, 85: 1384-1401.
Hassler, S. W., 1993. Depositional history of the Main Tuff Interval of the Wittenoom Formation, late Archean-early Proterozoic Hamersley Group, Western Australia. Precambrian Research, 60: 337-359.
Holland, H. D., 1984. The chemical evolution of the atmosphere and oceans, Princeton, Princeton University Press, 582 pp.
Hunter, D. R. and Hamilton, P. J., 1978. The Bushveld Complex. In: D. H. Tarling (editor), Evolution of the Earth's Crust. Academic Press, London, 107-173.
Jahn, B., Bertrand-Sarfati, J., Morin, N. and Mace, J., 1990. Direct dating of stromatolitic carbonates from the Schmidtsdrif Formation (Transvaal Dolomite), South Africa, with implications on the age of the Ventersdorp Supergroup. Geology, 18: 1211-1214.
Krogh, T. E., 1973. A low-contamination method for hydrothermal decomposition of zircon and extraction of U and Pb for isotopic age determinations. Geochimica et Cosmochimica Acta, 37: 485-494.
Krogh, T. E., 1982. Improved accuracy of U-Pb zircon ages by creation of more concordant systems using an air abrasion technique. Geochimica et Cosmochimica Acta, 45: 637-649.
Ludwig, K. R., 1988. Isoplot for MS-DOS: A plotting and regression program for radiogenic-isotope data, for IBM-PC compatible computers. Open File Report, U. S. Geological Survey, 88-557: 39 pp.
Moorbath, S., Taylor, P. N., Orpen, J. L., Treloar, P. and Wilson, J. F., 1987. First direct radiometric dating of Archaean stromatolitic limestone. Nature, 326: 865-867.
Robb, L. J., Davis, D. W. and Kamo, S. L., 1990. U-Pb ages on single detrital zircon grains from the Witwatersrand basin, South Africa: Constraints on the age of sedimentation and on the evolution of granites adjacent to the basin. Journal of Geology, 98: 311-328.
S. A. C. S. (South African Committee for Stratigraphy), 1980. Stratigraphy of South Africa. Part 1. (Comp. by L. E. Kent) Lithostratigraphy of the Republic of South Africa, South West Africa/Namibia and the Republics of Bophuthatswana, Transkei and Venda, Handbook of the Geological Survey of South Africa, 690 pp.
Saggerson, E. P. and Turner, L. M., 1992. Metamorphic map of the republics of South Africa, Transkei, Boputhatswana, Venda, and Ciskei and the kingdoms of Lesotho and Swaziland. Department of Mineral and Energy affairs, Geological Survey of South Africa.
Simonson, B. M., 1985. Sedimentological constraints on the origins of Precambrian iron-formations. Geological Society of America Bulletin, 96: 244-252.
Simonson, B. M., Schubel, K. A. and Hassler, S. W., 1993. Carbonate sedimentology of the early Precambrian Hamersley Group of Western Australia. Precambrian Research, 60: 287-335.
Smith, P. E., Farquhar, R. M. and Hancock, R. G., 1991. Direct radiometric age determination of carbonate diagenesis using U-Pb in secondary calcite. Earth and Planetary Science Letters, 105: 474-491.
Smith, P. E., Brand, U. and Farquhar, R. M., 1994. U-Pb systematics and alteration trends of Pennsylvanian-

aged aragonite and calcite. Geochimica et Cosmochimica Acta, 48: 313-322.
Stowe, C. W., 1986. Synthesis and interpretation of structures along the north-eastern boundary of the Namaqua tectonic province, South Africa. Transactions of the Geological Society of South Africa, 89: 185-198.
Svenjensky, D. A., 1981. The origin of a Mississippi Valley-type deposit in the Viburnum Trend, southeast Missouri. Economic Geology, 76: 1848-1872.
Tankard, A. J., Jackson, M. P. A., Eriksson, K. A., Hobday, D. K., Hunter, D. R. and Minter, W. E. L., 1982. Crustal Evolution of Southern Africa, New York, Springer-Verlag, 523 pp.
Trendall, A. F., Compston, W., Williams, I. S., Armstrong, R. A., Arndt, N. T., McNaughton, N. J., Nelson, D. R., Barley, M. E., Beukes, N. J., de Laeter, J. R., Retief, E. A., and Thorne, A. M., 1990. Precise zircon U-Pb chronological comparison of the volcano-sedimentary sequences of the Kaapvaal and Pilbara cratons between about 3.1 and 2.4 Ga. In: J. E. Glover and S. E. Ho (Editors), Extended Abstracts Volume, 3rd International Archean Symposium, p. 81-83.
Thompson, T. B. and Beaty, D. W., 1990. Geology and the origin of ore deposits in the Leadville district, Colorado: Part II. Oxygen, hydrogen, carbon, sulfur, and lead isotope data and development of a genetic model. Economic Geology Monograph, 7: 156-179.
Tyler, N., 1979. The stratigraphy of the early-Proterozoic Buffalo Springs Group in the Thabazimbi area, west-central Transvaal. Transactions of the Geological Society of South Africa, 82: 215-226.
Van Niekerk, C. B. and Burger, A. J., 1978. A new age for the Ventersdorp acidic lavas. Transactions of the Geological Society of South Africa, 81: 155-163.
Walraven, F., Armstrong, R. A. and Kruger, F. J., 1990. A chronostratigraphic framework for the north-central Kaapvaal craton, the Bushveld Complex and the Vredefort structure. Tectonophysics, 171: 23-48.
Wheatley, C. J. V., Whitfield, G. G., Kenny, K. J. and Birch, A., 1986. The Pering carbonate-hosted zinc-lead deposit, Griqualand West. In: C. R. Anhaeusser and S. Maske (editors), Mineral Deposits of Southern Africa. Geological Society of South Africa, Johannesburg, 867-874.

## APPENDIX B: STRATIGRAPHIC SECTIONS

### *Gamohaan Formation*

### Sections AL and AL#2

Location: Alphen Farm, 16 km south of Kuruman along road R31 towards Danielskuil. Sections located on slopes to west of road.

Stratigraphic Range: Lower Gamohaan Formation to base of Kuruman Iron Formation. Section AL#2 (starting on Page 236) was measured 400 m from Section Al, and the base of Section AL#2 corresponds to meter 14 in Section AL.

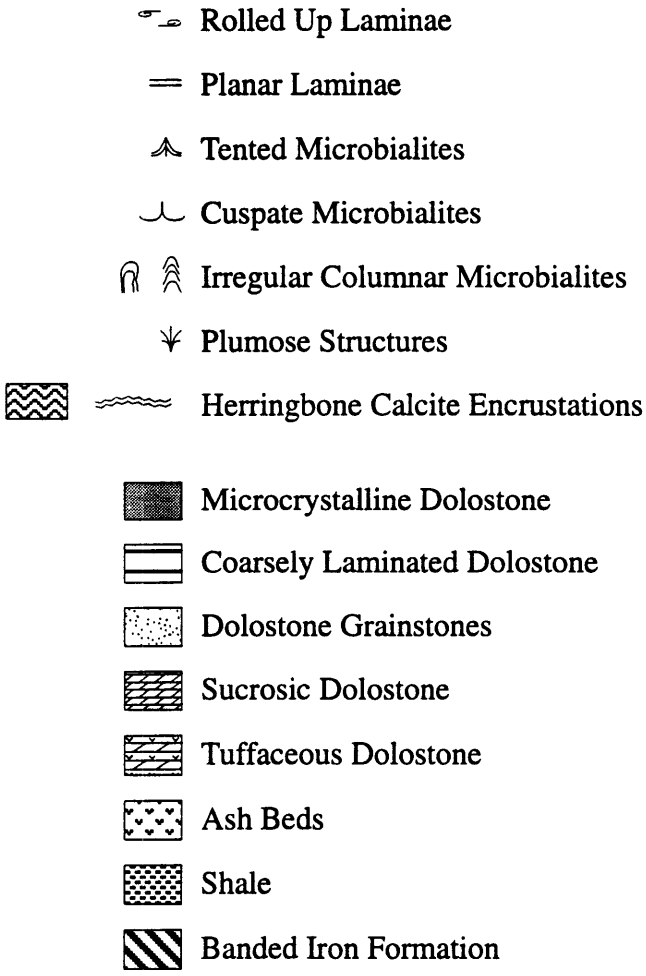

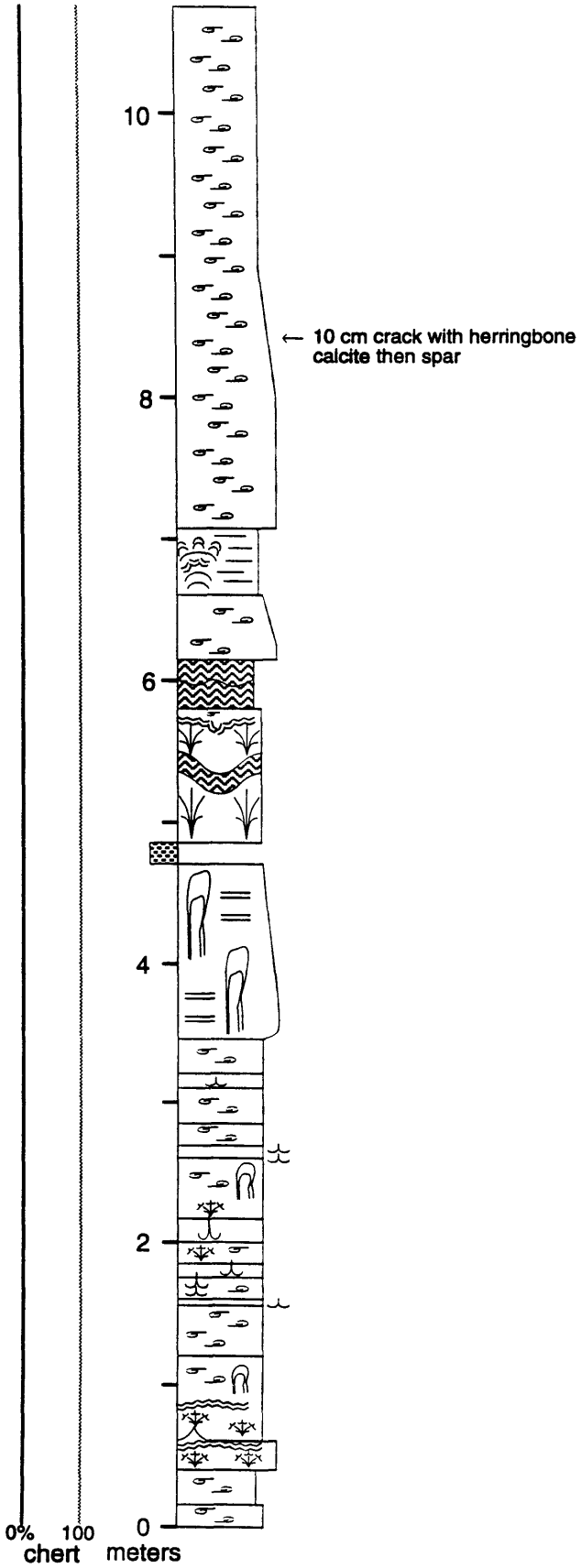
10
8
6
4
2
0
← 10 cm crack with herringbone calcite then spar
0%
100
chert
meters

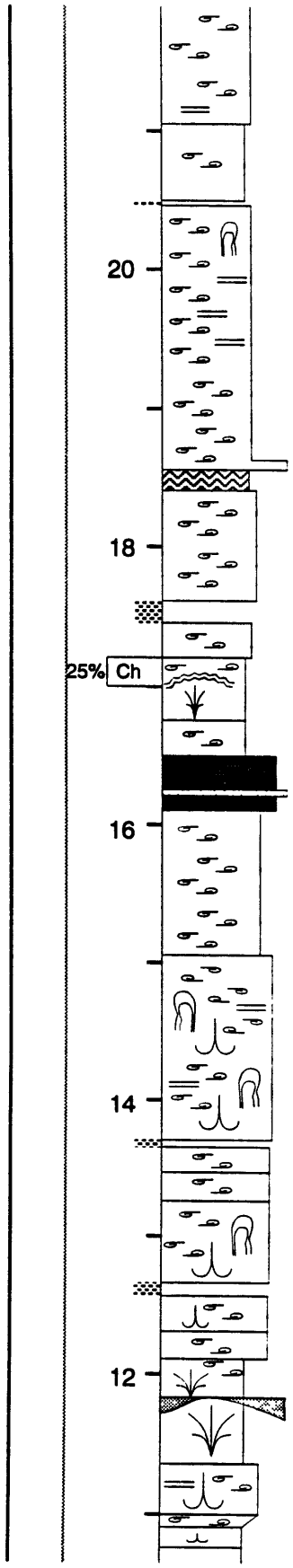
20
18
25%
Ch
16
14
12

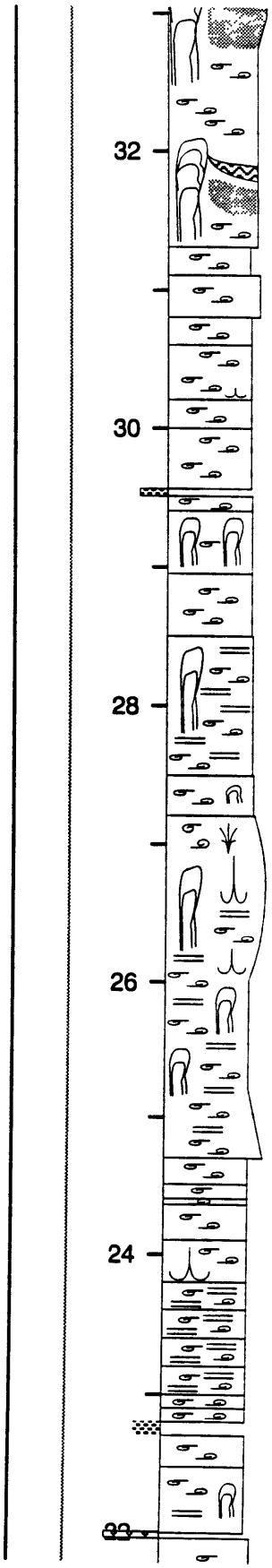
32
30
28
26
24

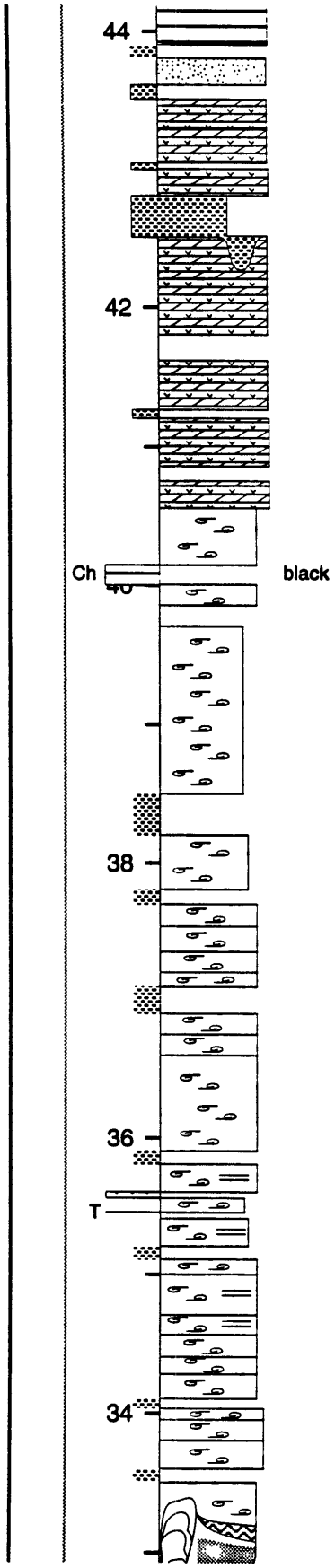
44
42
Ch
black
40
38
36
T
34

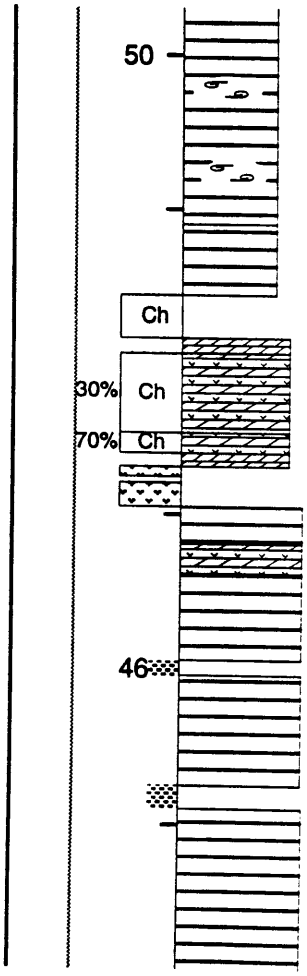
50
Ch
30%
Ch
70%
Ch
46

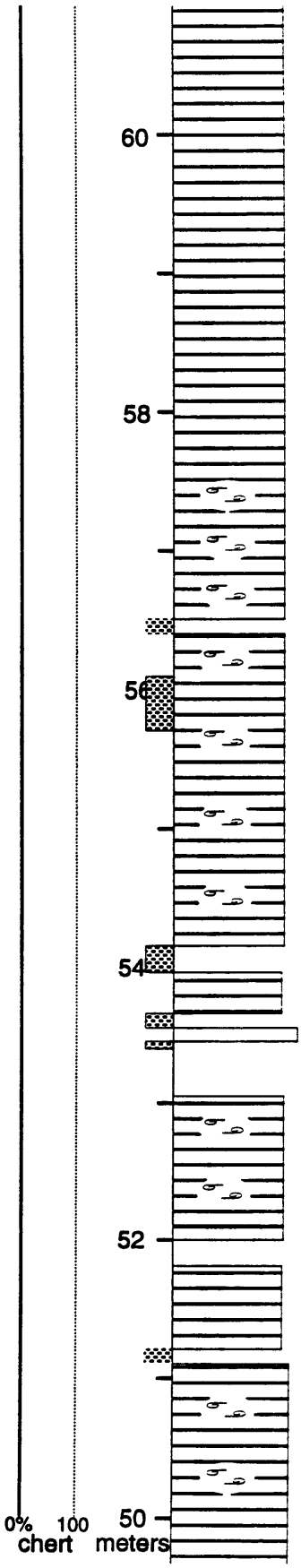
60
58
56
54
52
50
0%
100
chert
meters

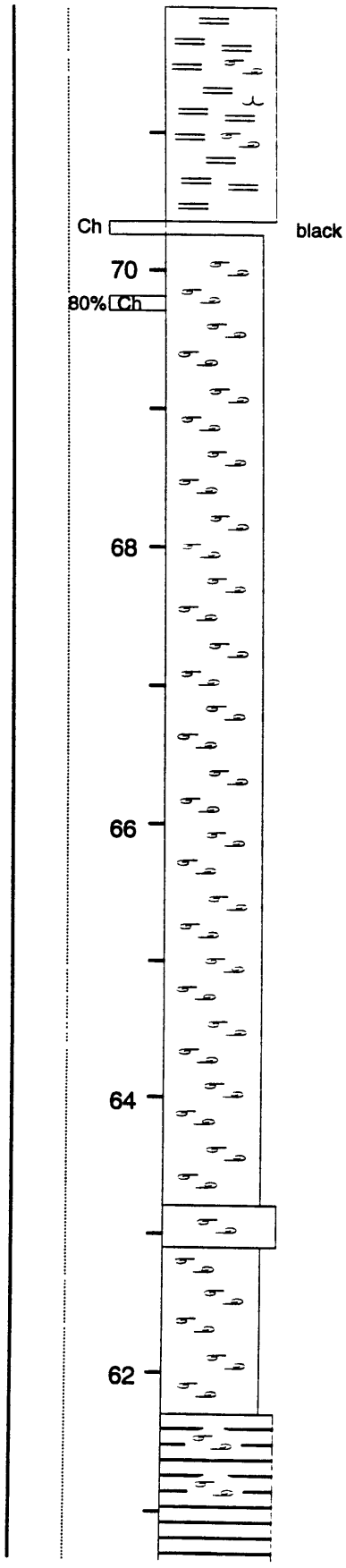
Ch
black
70
80% Ch
68
66
64
62

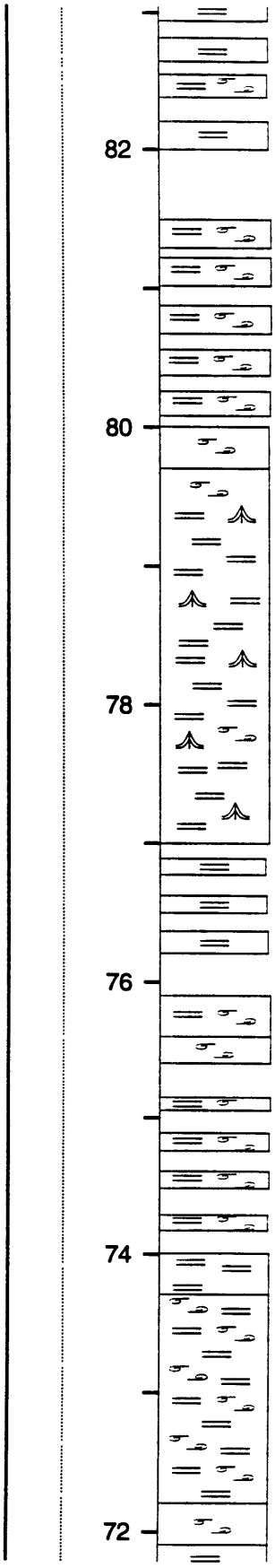
82
80
78
76
74
72

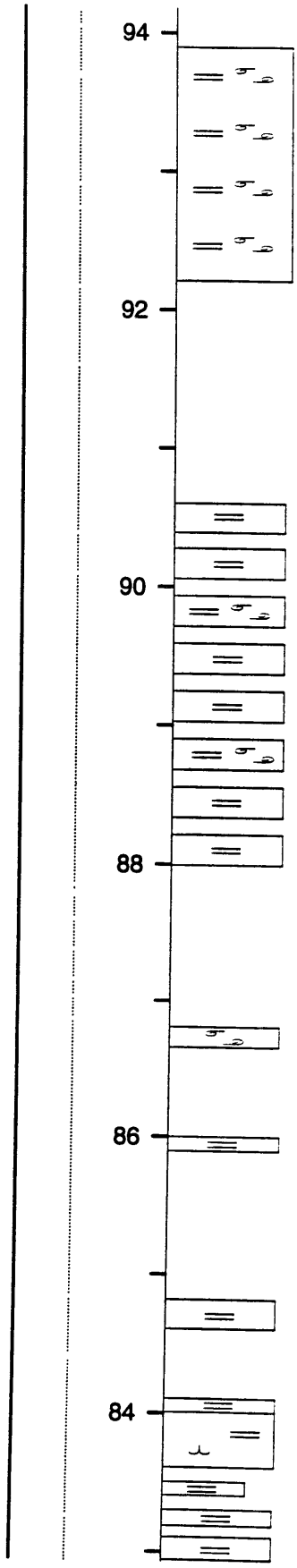
94
92
90
88
86
84

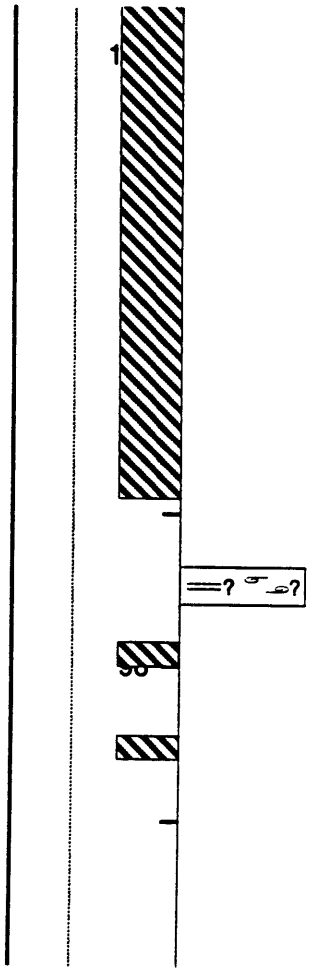
1
=?

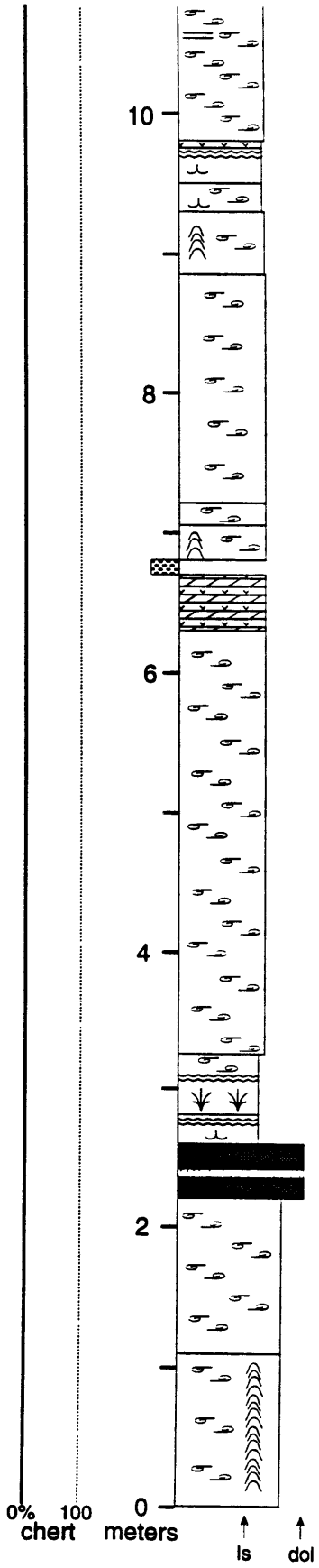
10
8
6
4
2
0
0%
100
chert
meters
ls
dol

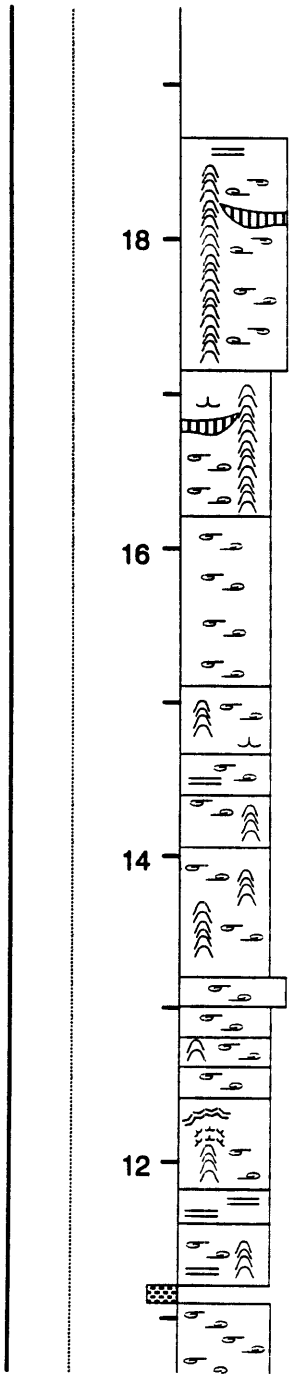
18
16
14
12

## Core BD2

Location: 5 km south of Griquatown. Core owned by Shell Minerals South Africa and stored at Pering Mine near Reivilo.

Stratigraphic Range: Slope deposits immediately below the Kuruman Iron Formation. Probably correlative to the Gamohaan Formation..

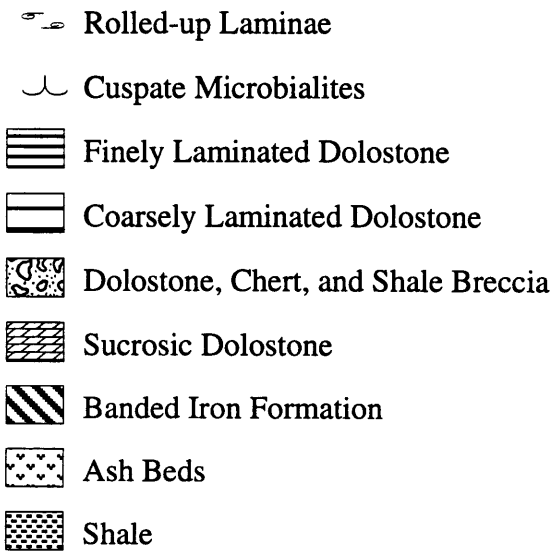

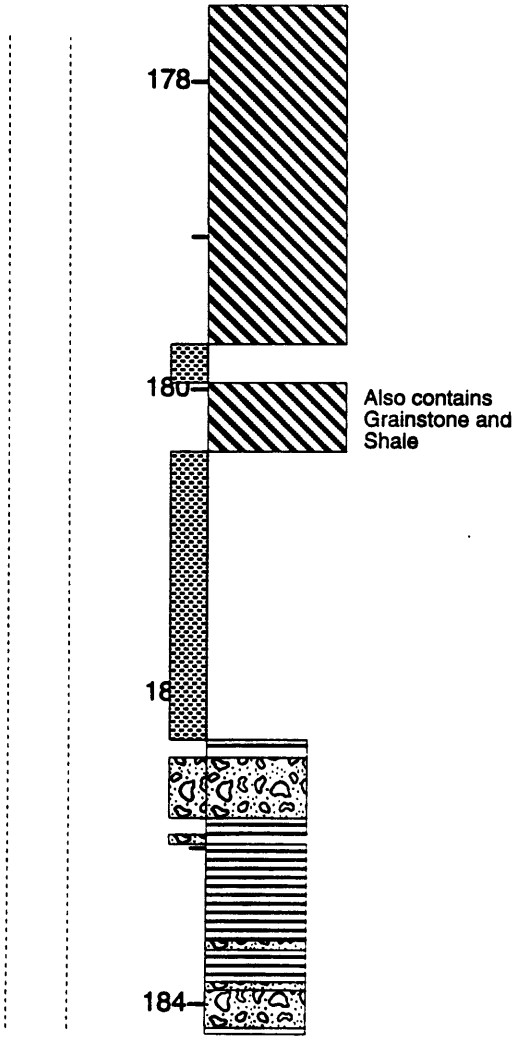
178
180
Also contains
Grainstone and
Shale
184

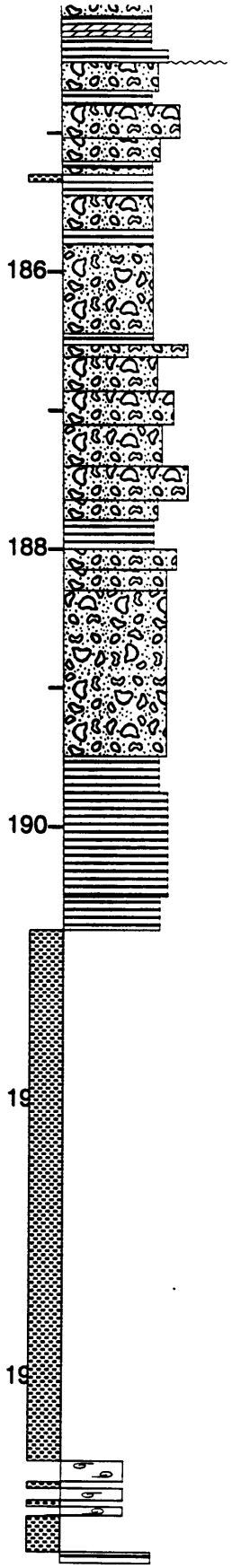
186
188
190

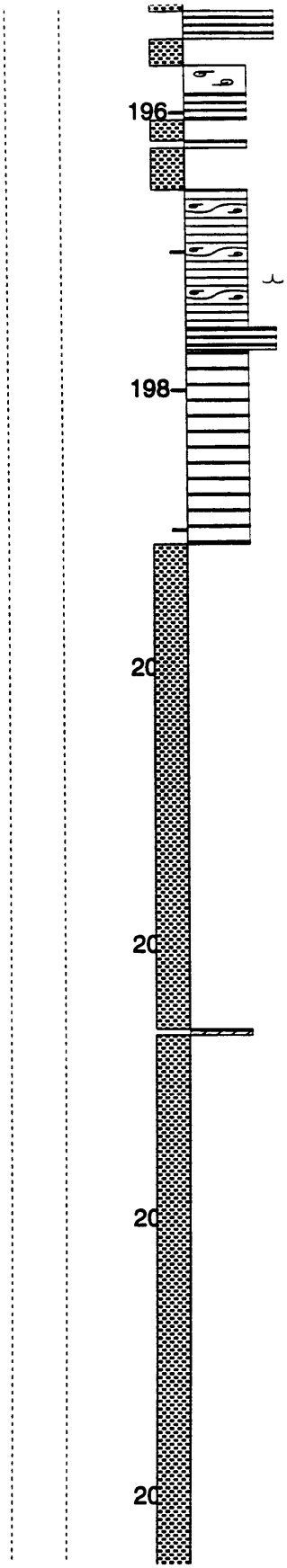
196
198
20
20
20
20

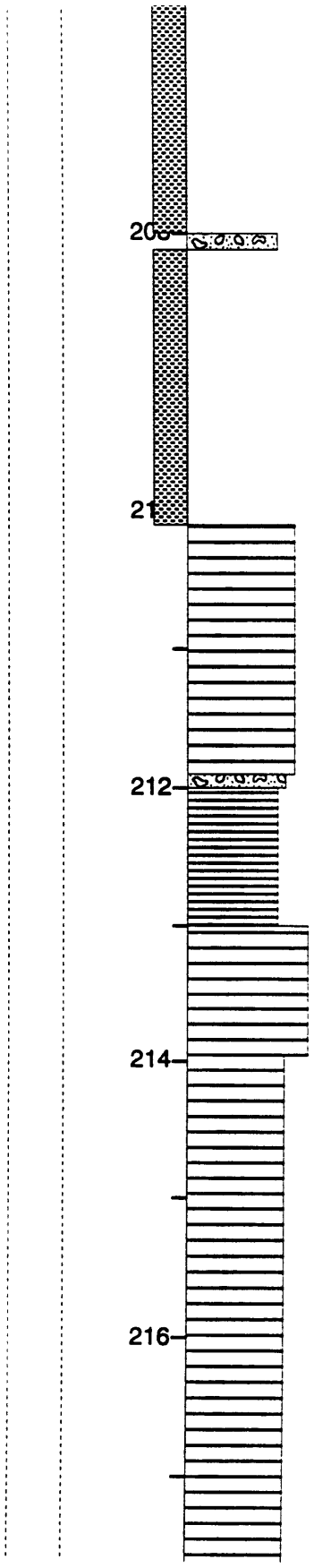
210
212
214
216

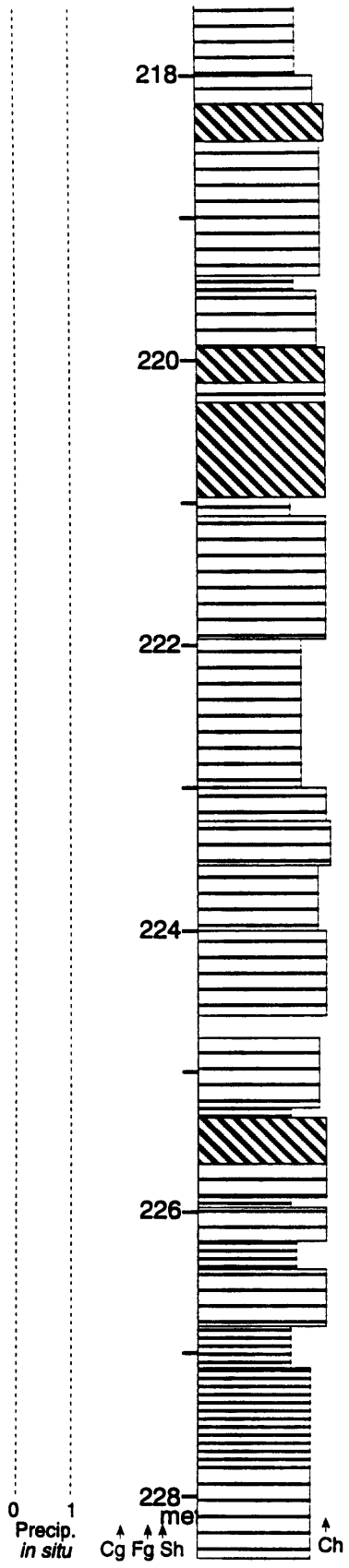
218
220
222
224
226
228
0
1
Precip.
in situ
Cg
Fg
Sh
me
Ch

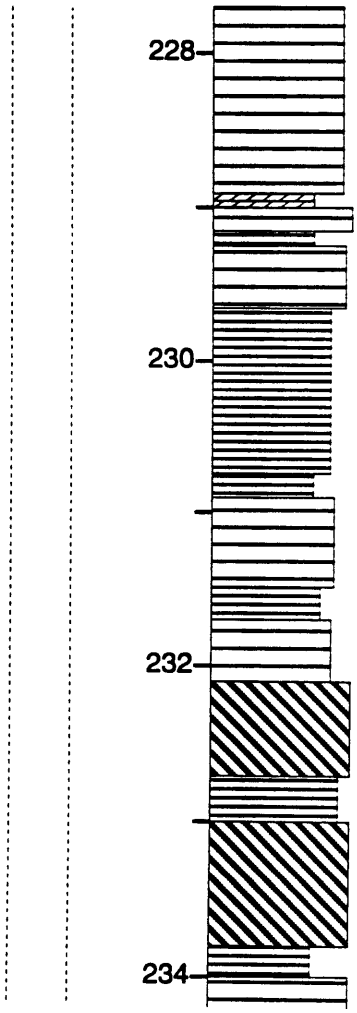
228
230
232
234

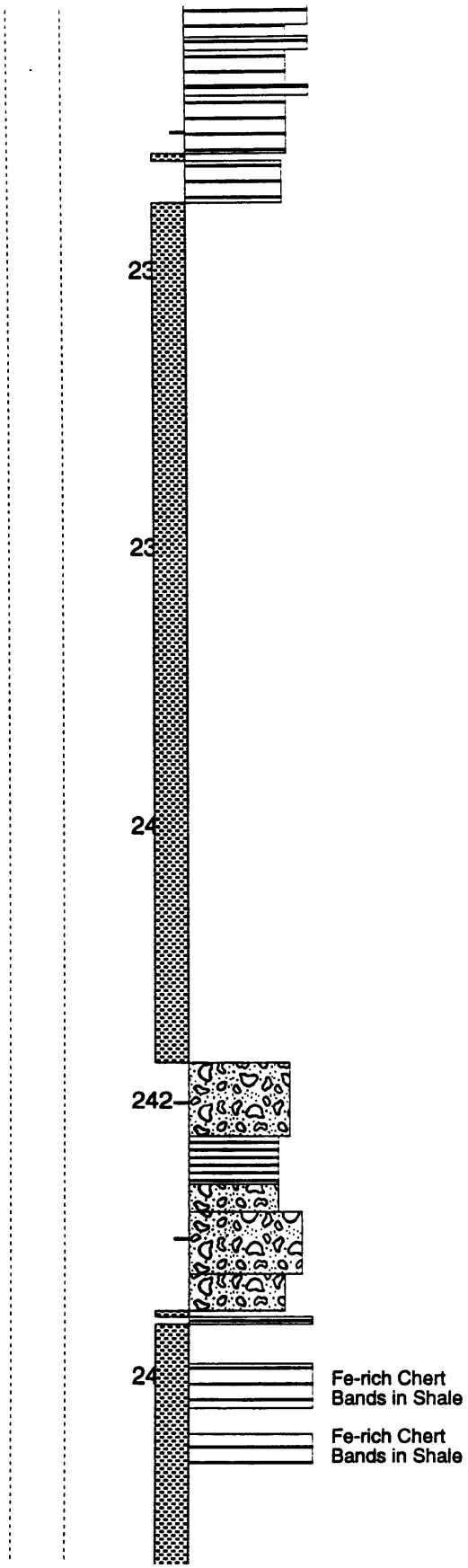
23
23
24
242
24
Fe-rich Chert
Bands in Shale
Fe-rich Chert
Bands in Shale

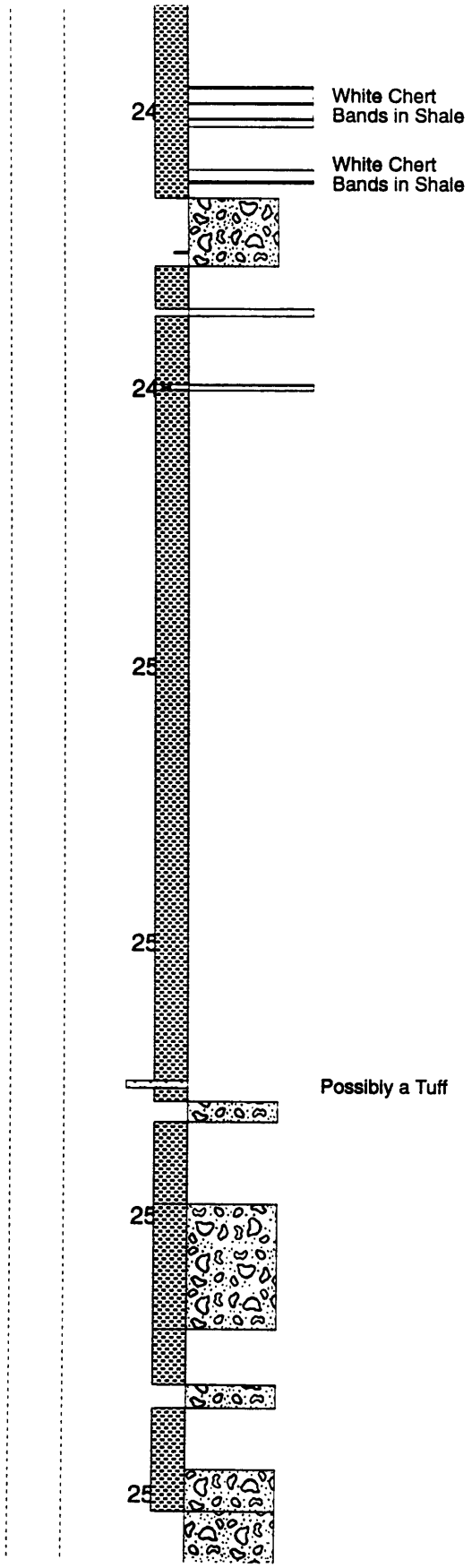
White Chert
Bands in Shale
White Chert
Bands in Shale
Possibly a Tuff

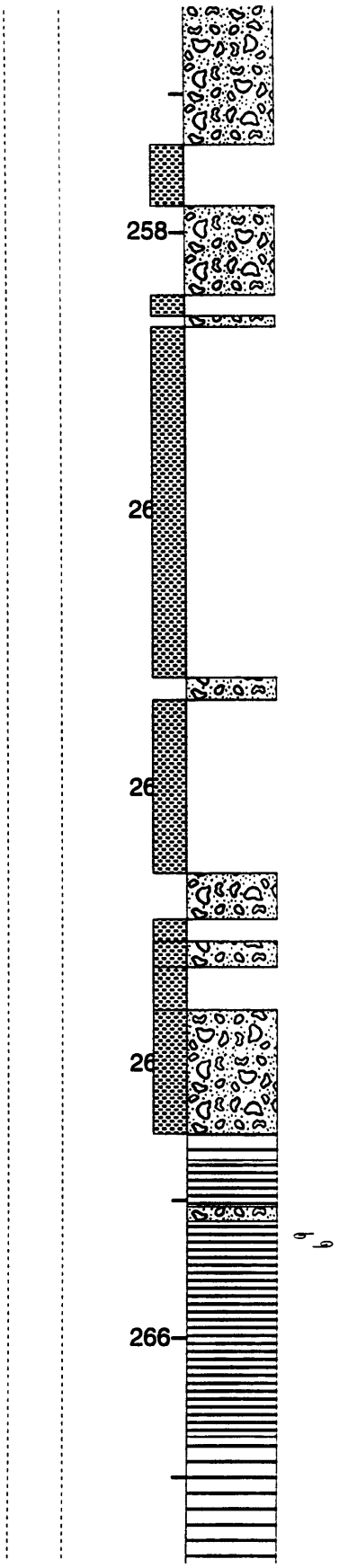


Fig. 9

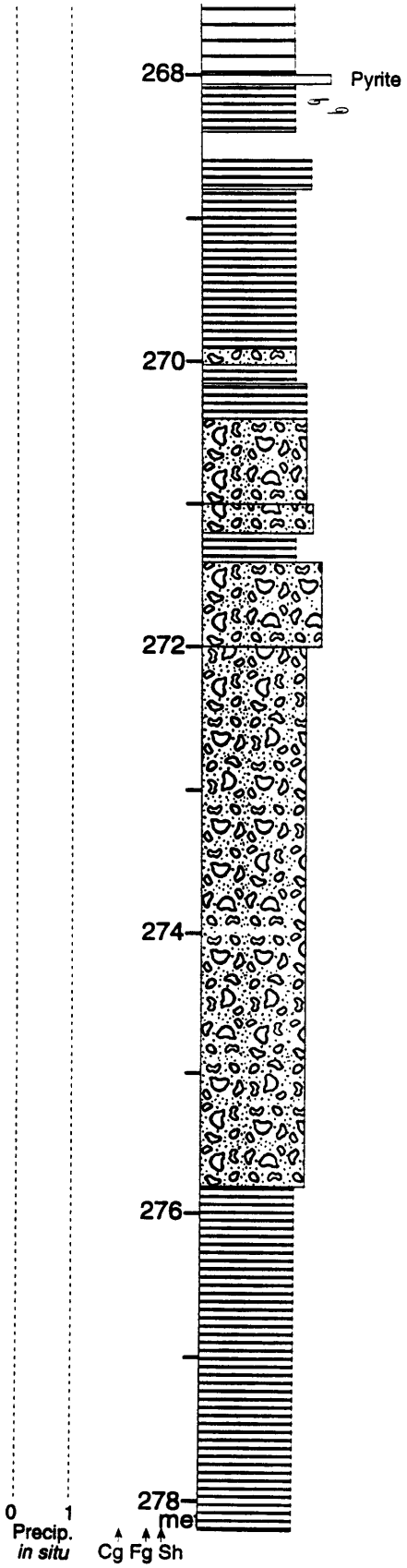
268
Pyrite
270
272
274
276
278
me
0
1
Precip.
in situ
Cg Fg Sh

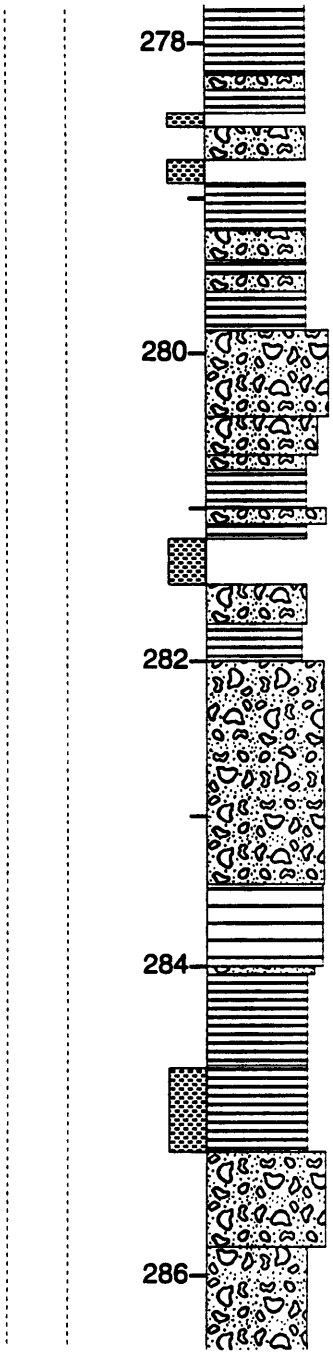
278
280
282
284
286

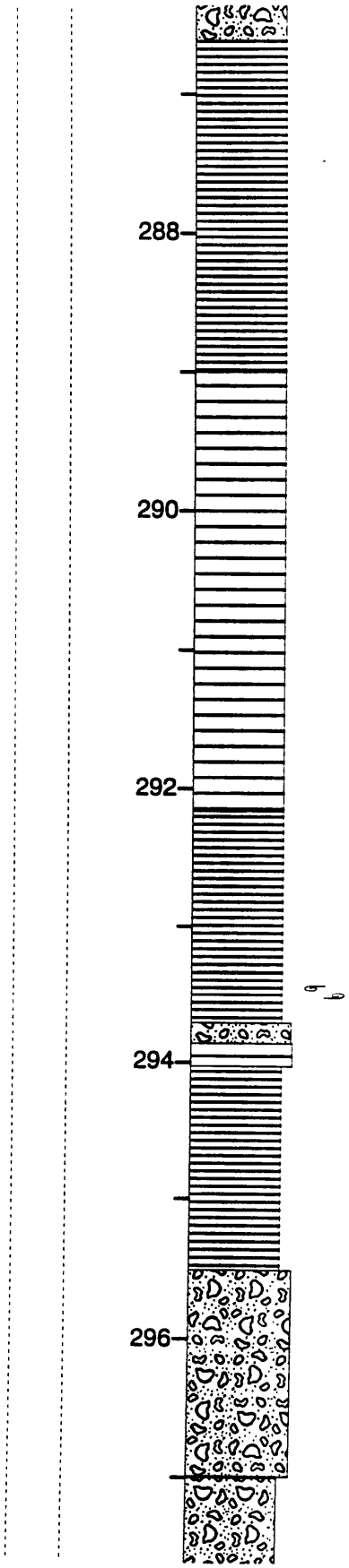
288
290
292
294
296

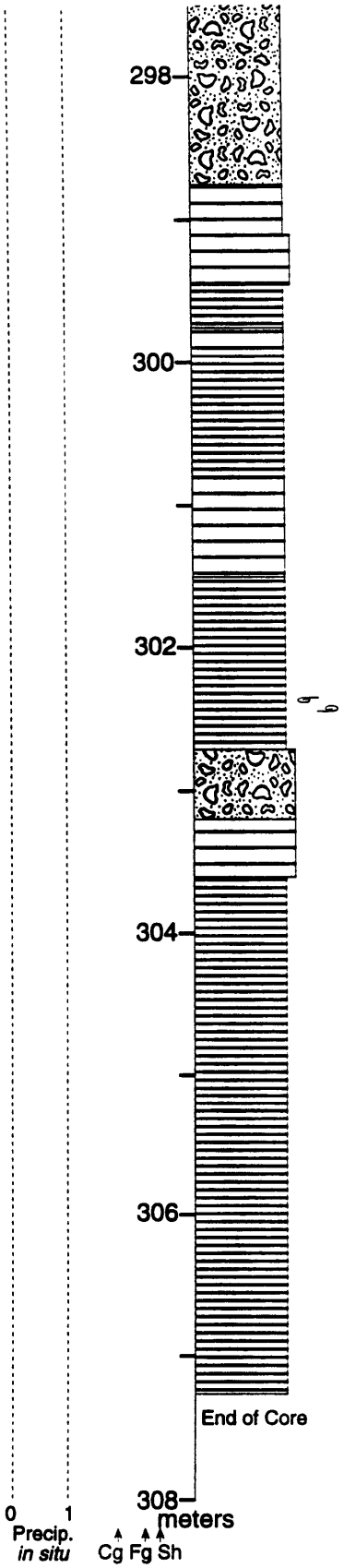
298
300
302
304
306
308
End of Core
meters
0
1
Precip.
in situ
Cg
Fg
Sh

## Section DK

Location: 3 km north of Danielskuil along road R31 towards Kuruman. Section is located on slope to west of road and just south of quarrie..

Stratigraphic Range: Top of the Kogelbeen Formation to base of Kuruman Iron Formation. This section is presented in two parts. The black chert at base of the second section is the same as the chert at 77.5 m of the first section.

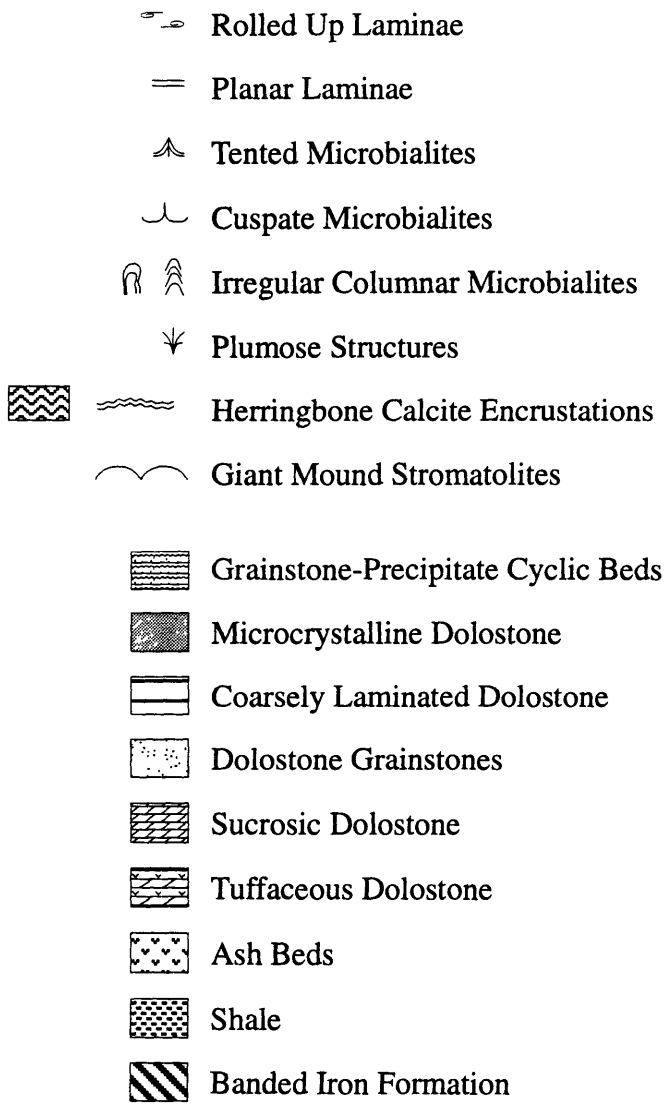

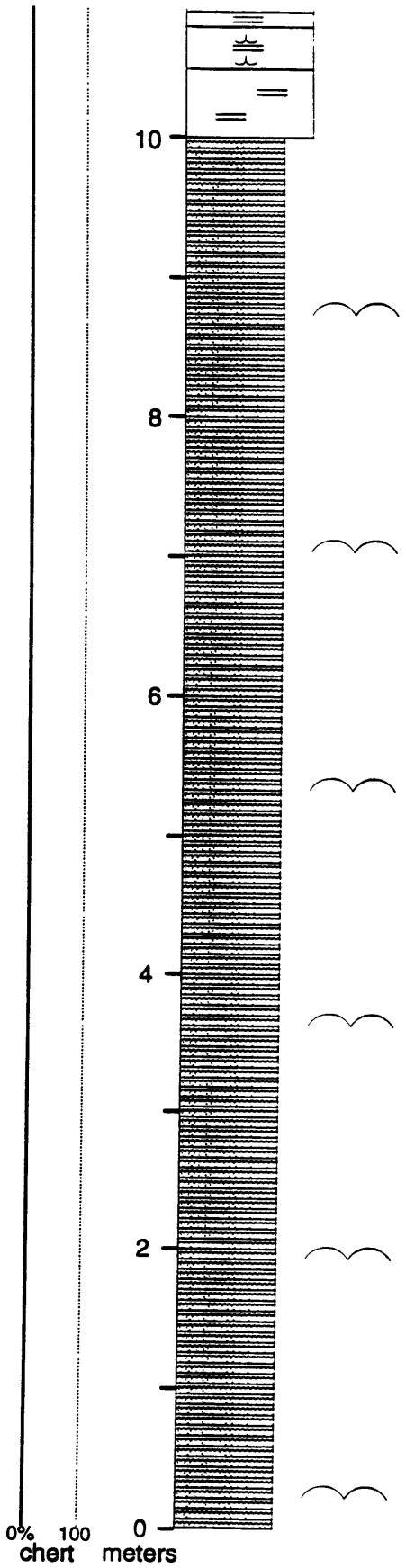
10
8
6
4
2
0
0%
100
chert
meters

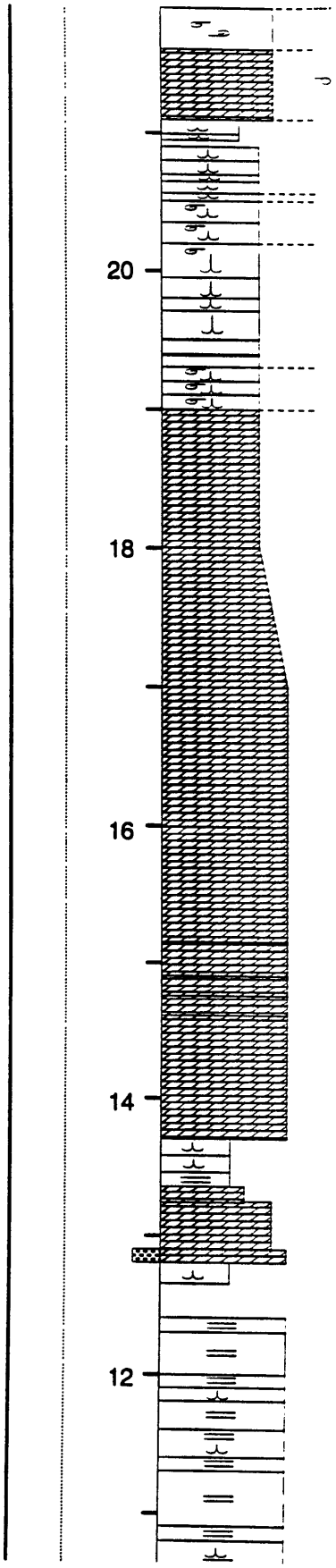
20
18
16
14
12

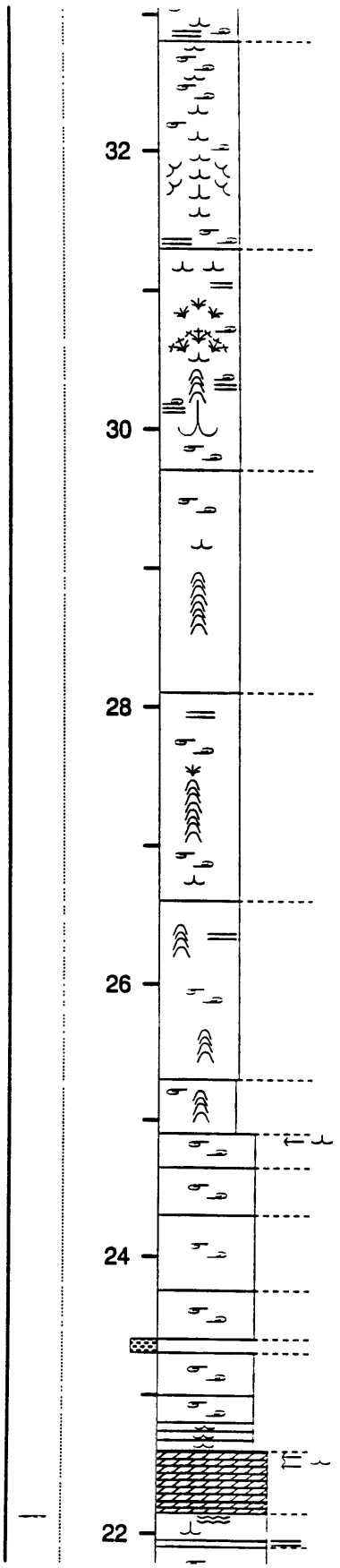
32
30
28
26
24
22

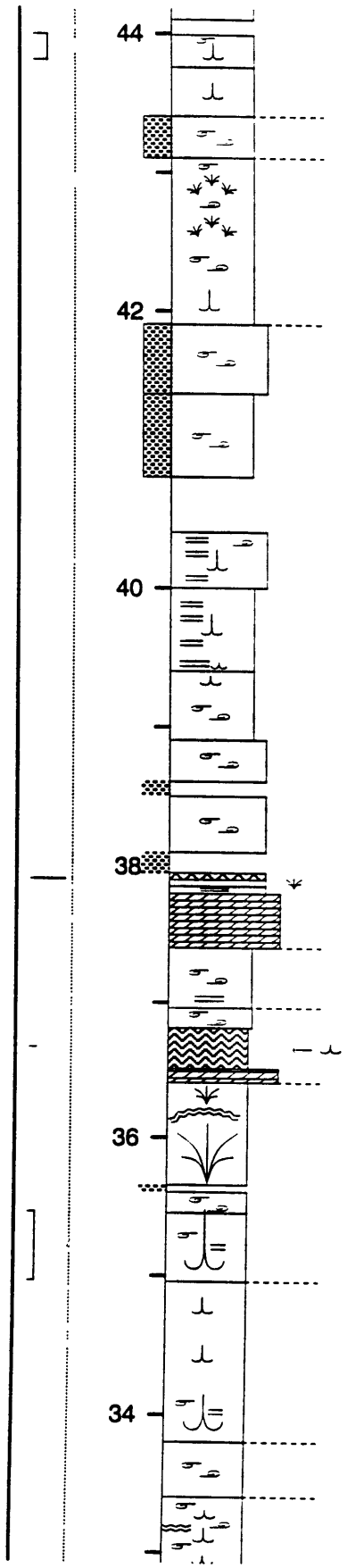
44
42
40
38
36
34

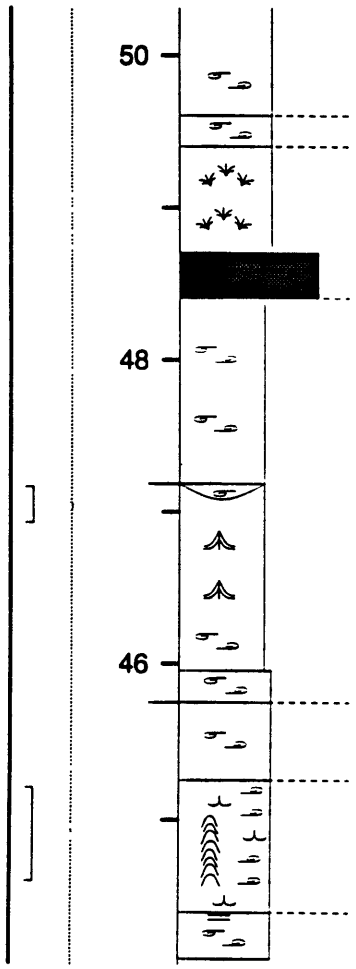
50
48
46

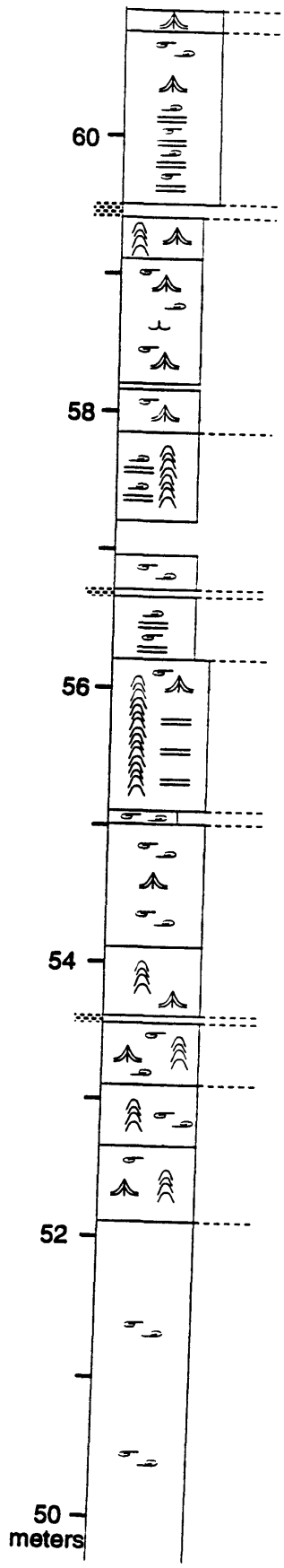
60
58
56
54
52
50
meters

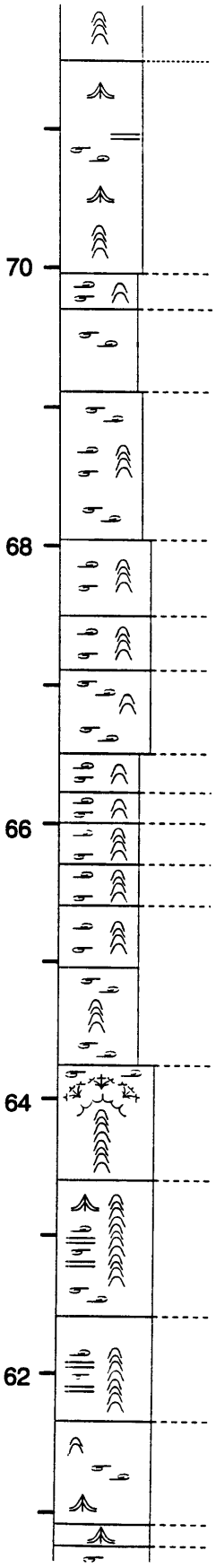
70
68
66
64
62

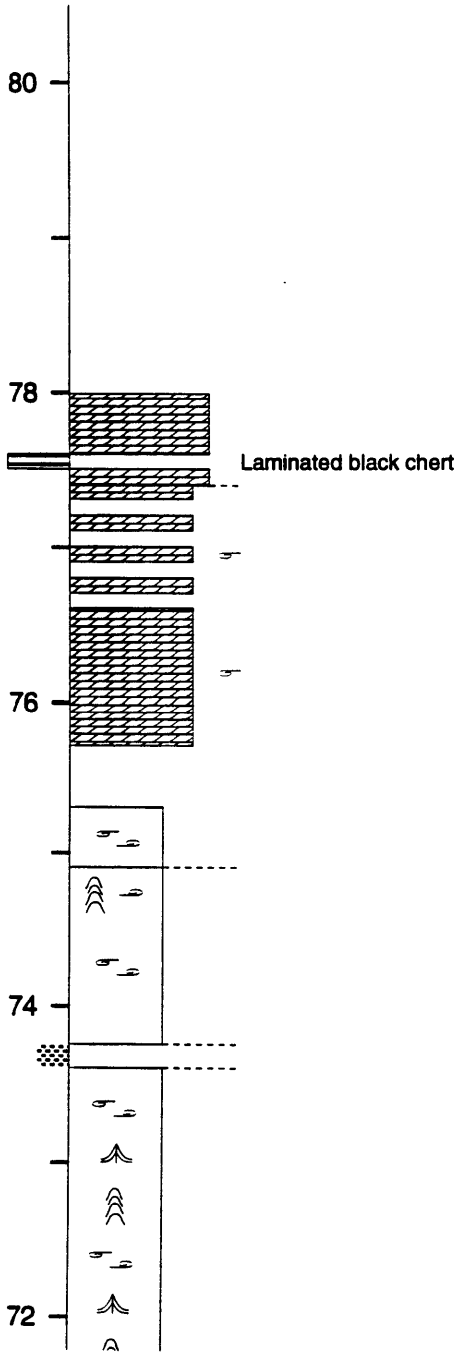
80
78
Laminated black chert
76
74
72

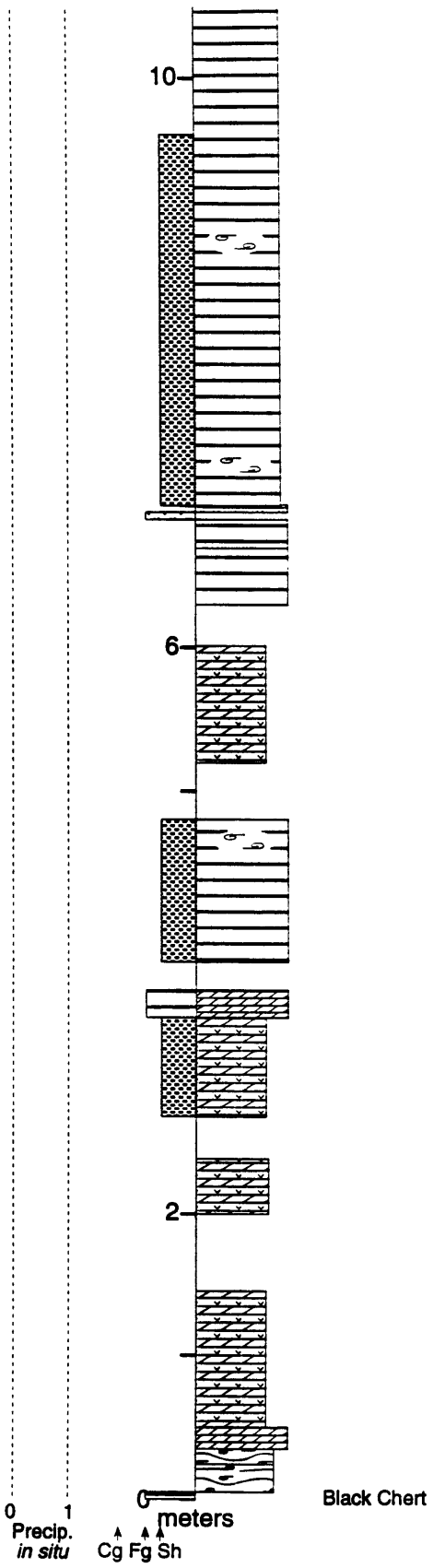
10
6
2
0
Black Chert
0 1
meters
Precip.
in situ
Cg Fg Sh

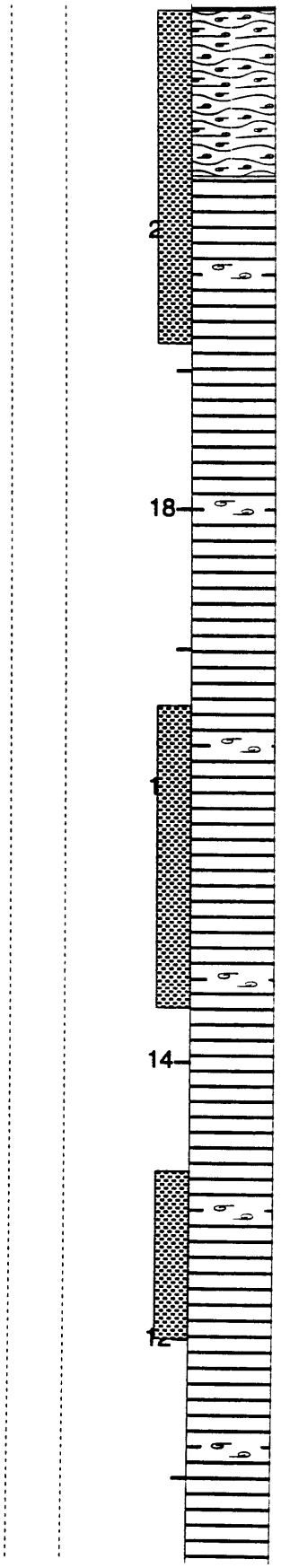
2
18
1
14
12

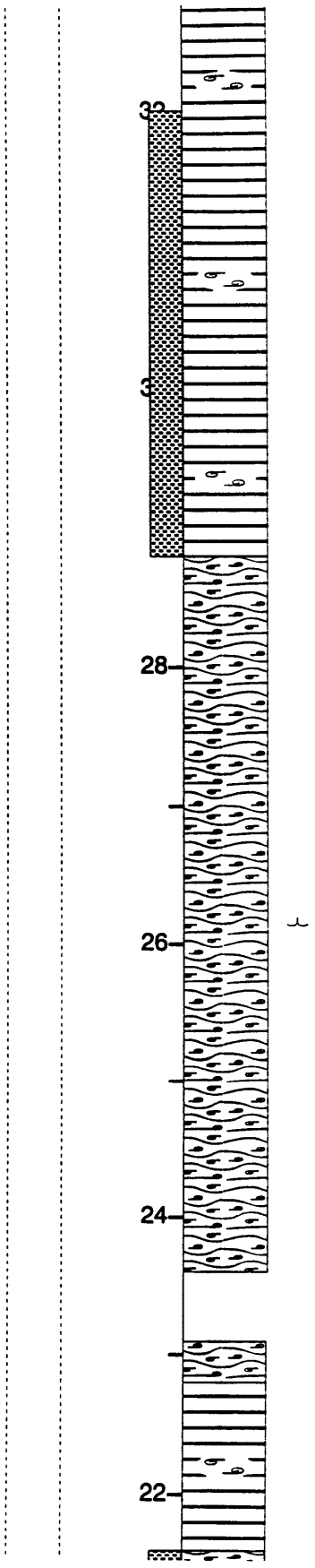
33
3
28
26
24
22

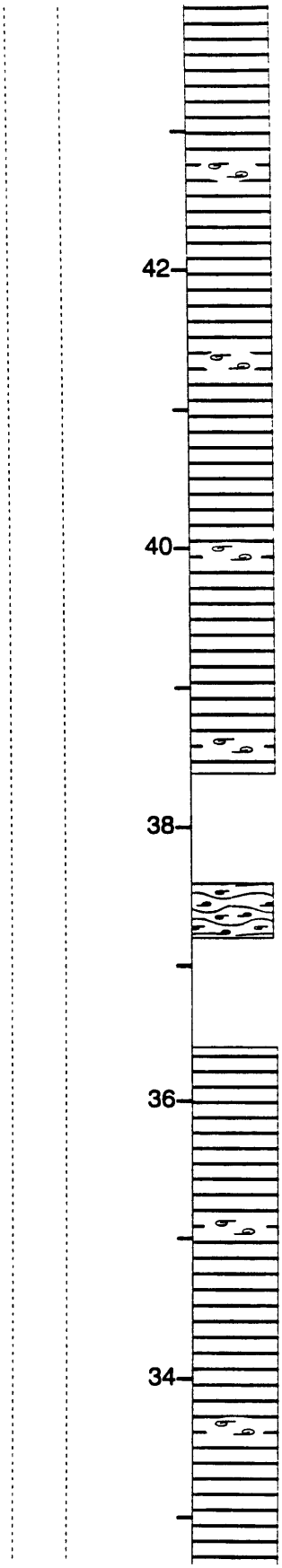
42
40
38
36
34

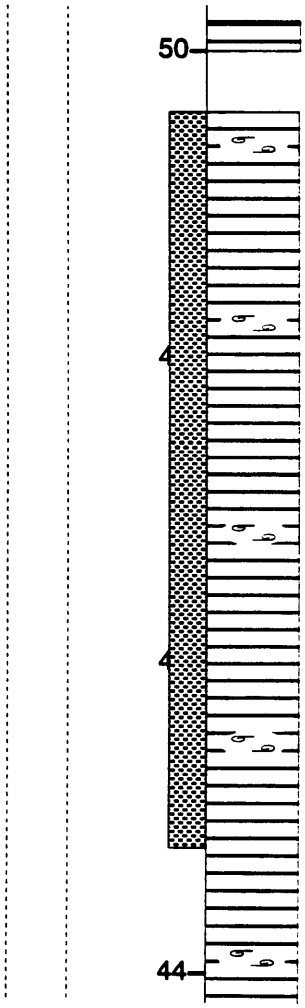
50
4
4
44

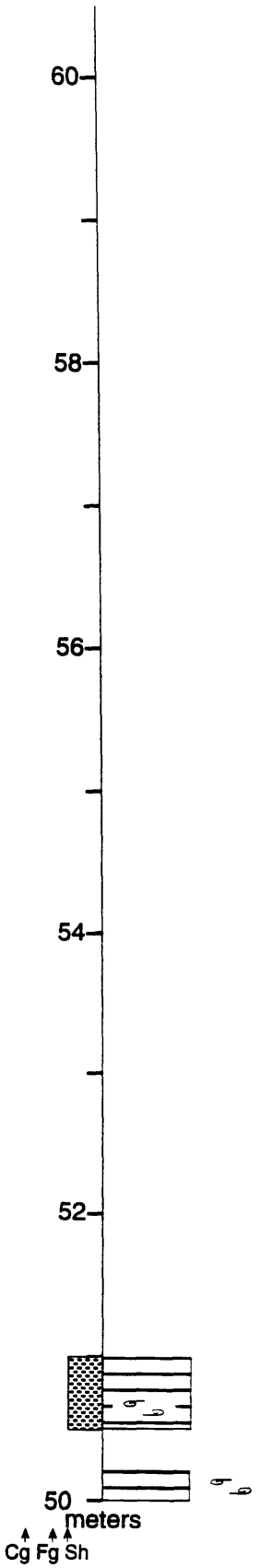
60
58
56
54
52
50
meters
Cg Fg Sh

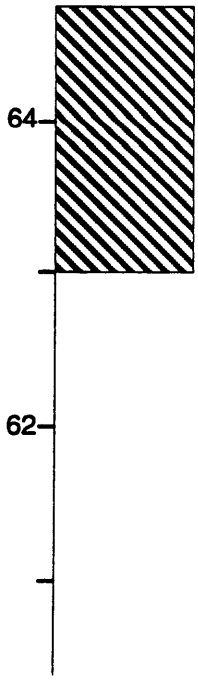
64
62

## Section HE

Location: On Hopefield Estates Farm near Kogelbeen Caves, off of the gravel road leading northeast out of Griquatowt and connecting to road R385.

Stratigraphic Range: Near the base of the Gamohaan Formation to base of Kuruman Iron Formation. This section is presented in three parts. The stratigraphic thicknesses between the three sections are unconstrained but less than 15 m is missing between each.

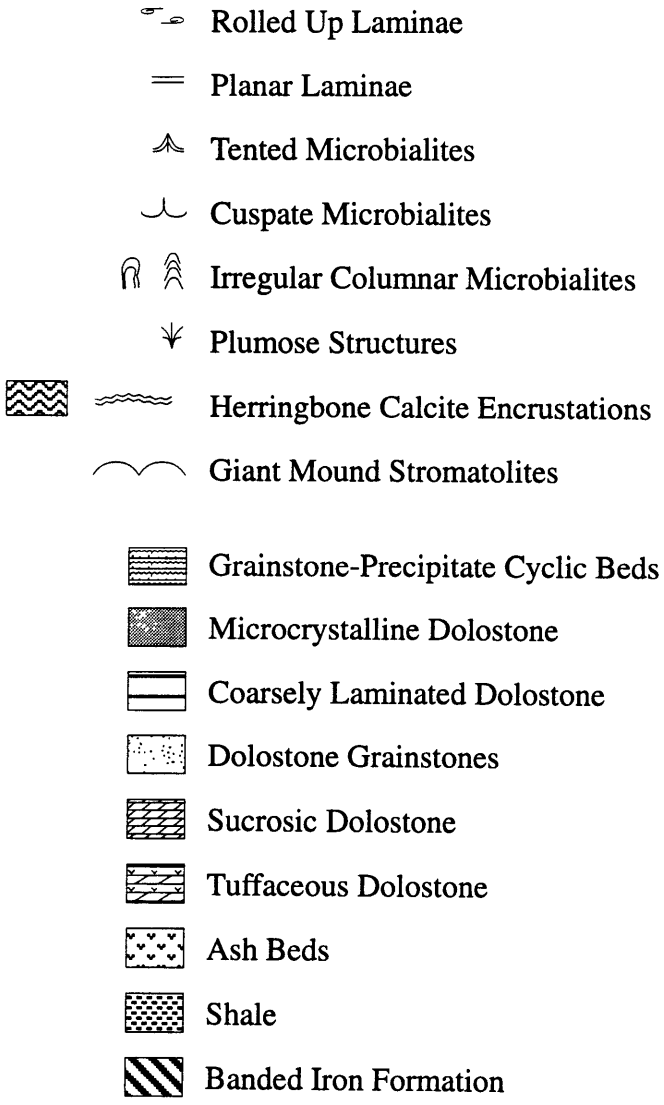

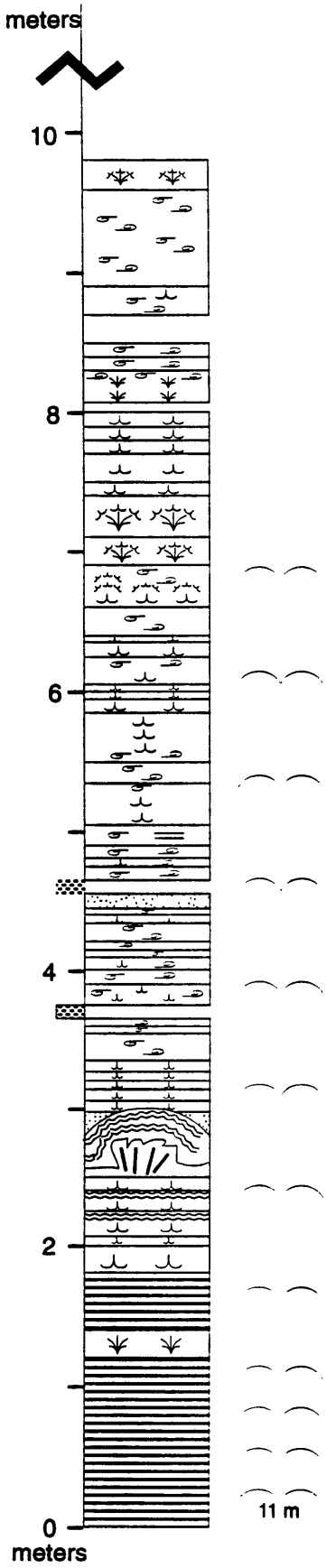
meters
10
8
6
4
2
0
meters
11 m

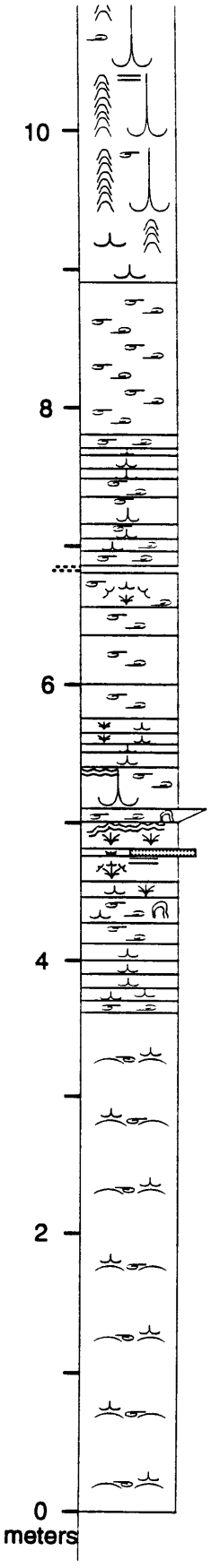
10
8
6
4
2
0
meters

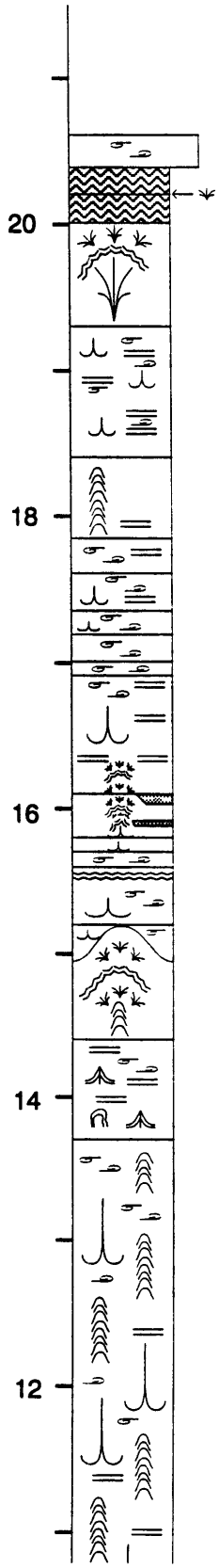
20
18
16
14
12

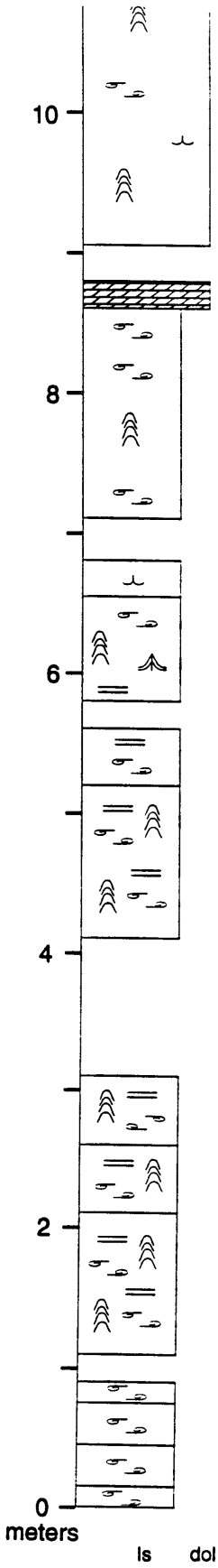
10
8
6
4
2
0
meters
ls
dol

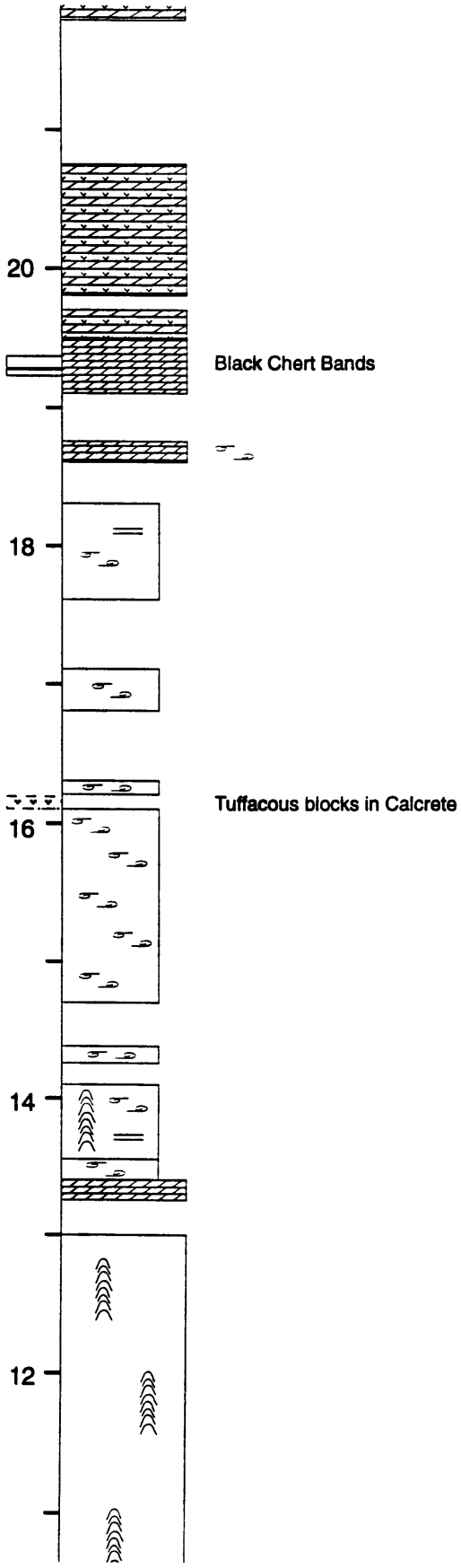
20
Black Chert Bands
18
Tuffacous blocks in Calcrete
16
14
12

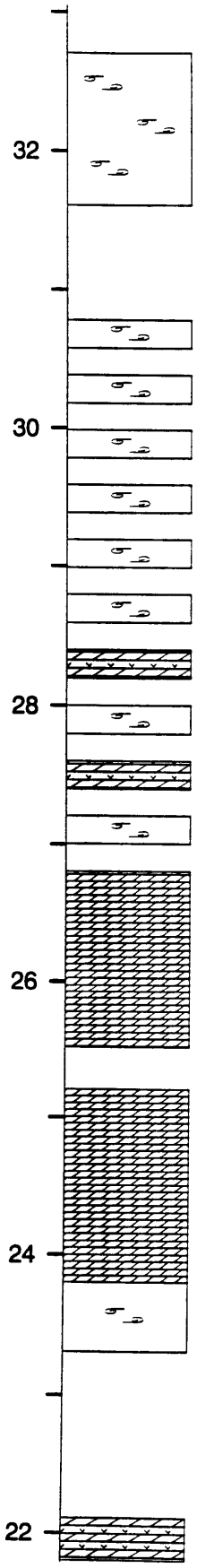
32
30
28
26
24
22

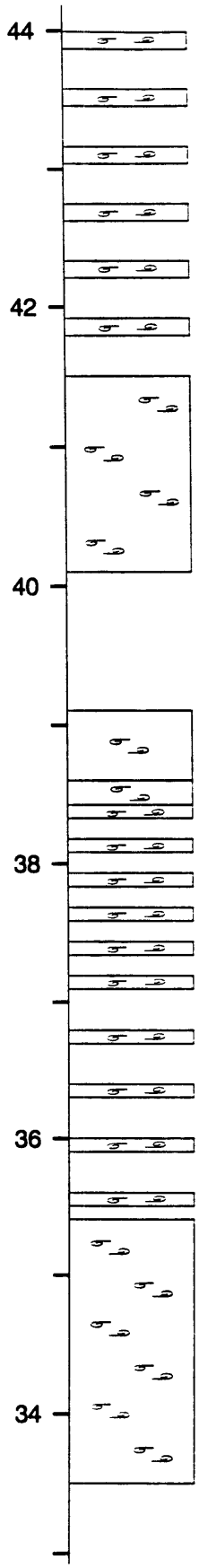
44
42
40
38
36
34

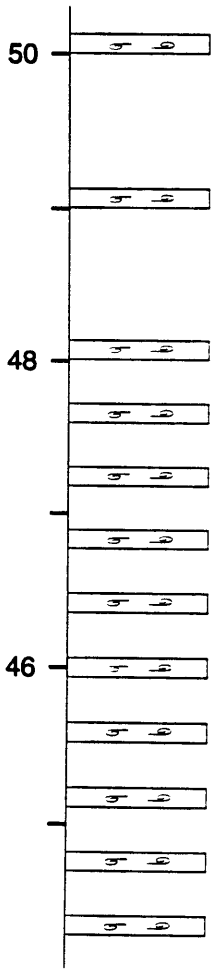
50
48
46

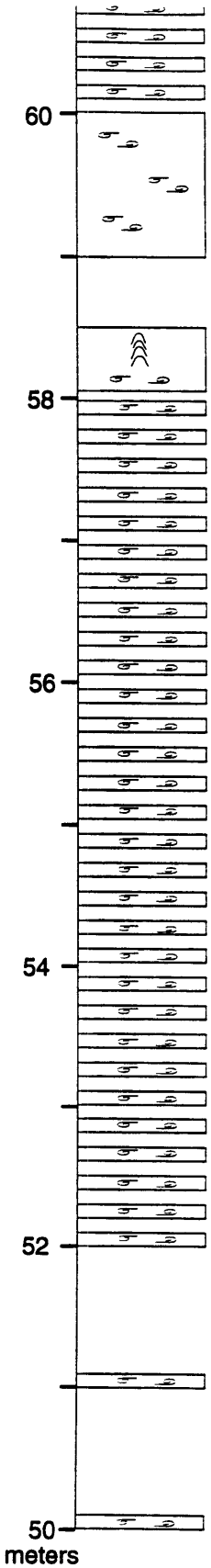
60
58
56
54
52
50
meters

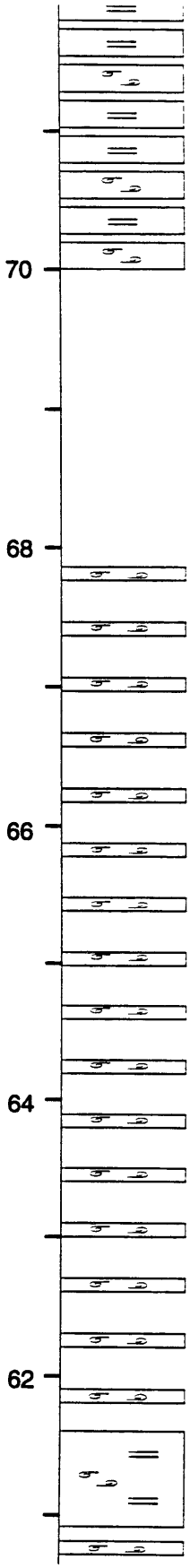
70
68
66
64
62

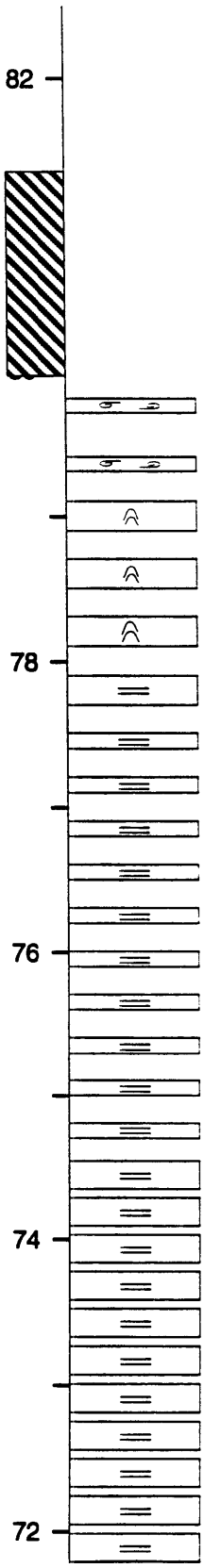
82
78
76
74
72

## Sections KU and KU#2

Location: 10 km west of Kuruman along road R31 towards Hotazel.. Section is located on a pointed hill and neighboring slope south of the road.

Stratigraphic Range: Within the Kogelbeen Formation to base of Kuruman Iron Formation. Section KU#2 is 1 km south of section KU and the base of section KU#2 corresponds to 100.0 m of section KU.

Notes: The column labeld "Spacing (cm)" shows the average spacing of draping laminae (thicker line) and the average spacing of supports (thinner line) in microbialites. The column labled "Herringbone, Other Precip." represents the ratio between cements with a herringbone calcite texture and bladed calcite. The proportion of "Micrite" corresponds to the proportion of microcrystalline calcite and dolomite and NOT to carbonate mud. All estimates of the proportion of components represent the proportion preserved in the rock, not interpretaions of the proportion of the rock that originally had the texture.

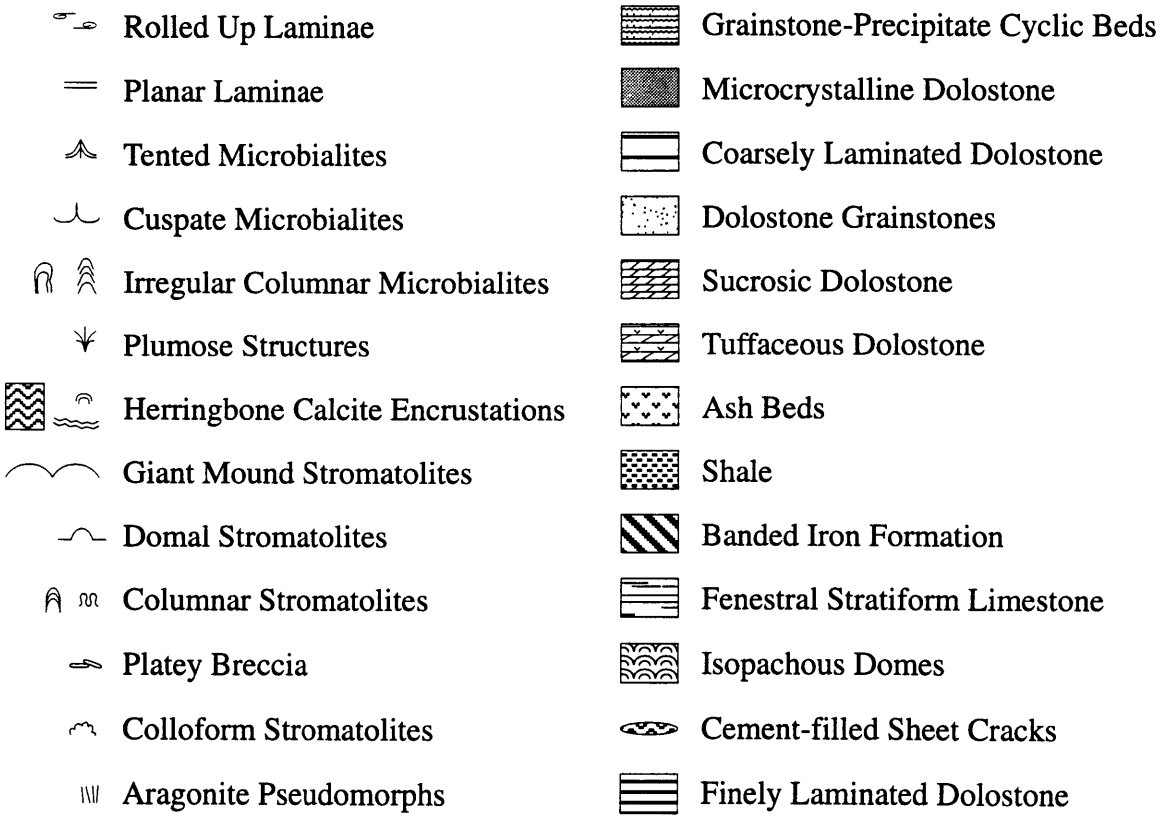

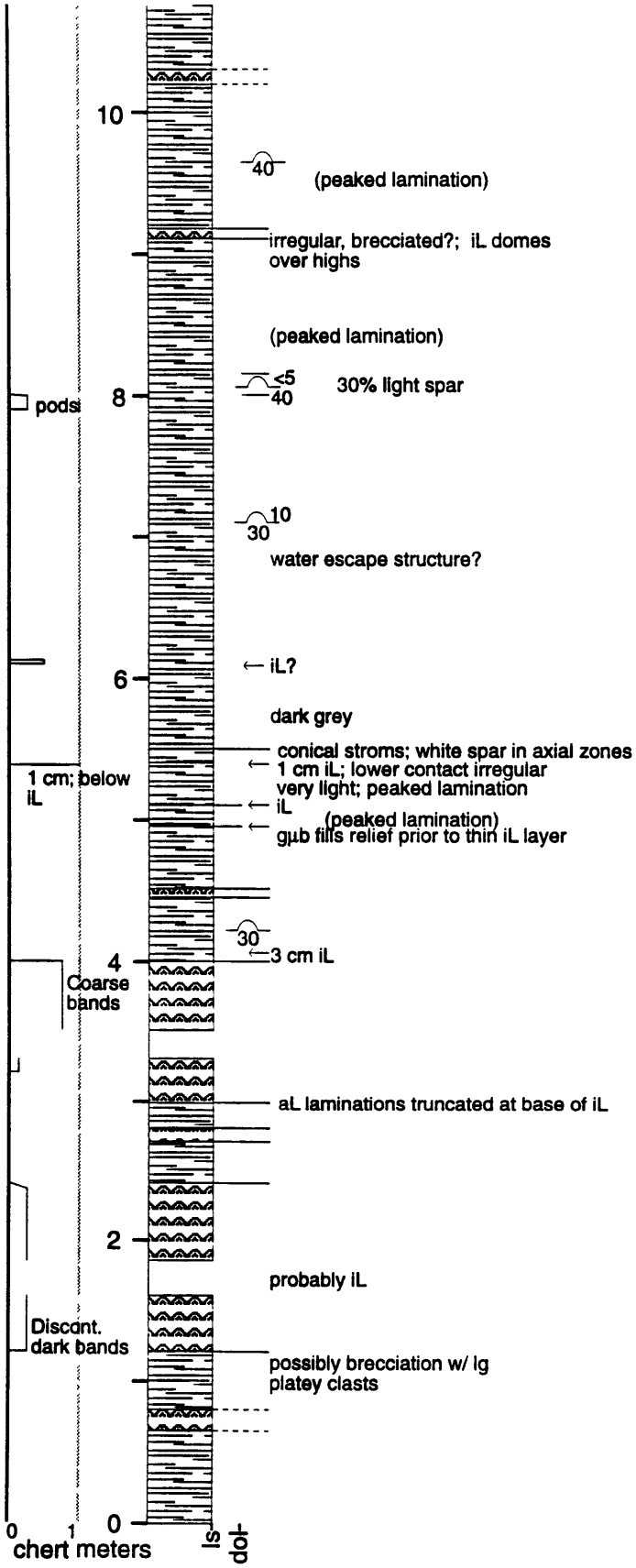
10
40
(peaked lamination)
irregular, brecciated?; iL domes over highs
(peaked lamination)
<5
40
30% light spar
pods
8
10
30
water escape structure?
← iL?
6
dark grey
conical stroms; white spar in axial zones
← 1 cm iL; lower contact irregular
very light; peaked lamination
1 cm; below iL
← iL
(peaked lamination)
← gμb fills relief prior to thin iL layer
30
4
← 3 cm iL
Coarse bands
aL laminations truncated at base of iL
2
probably iL
Discont. dark bands
possibly brecciation w/ lg platey clasts
0
0
1
chert meters
ss
dol

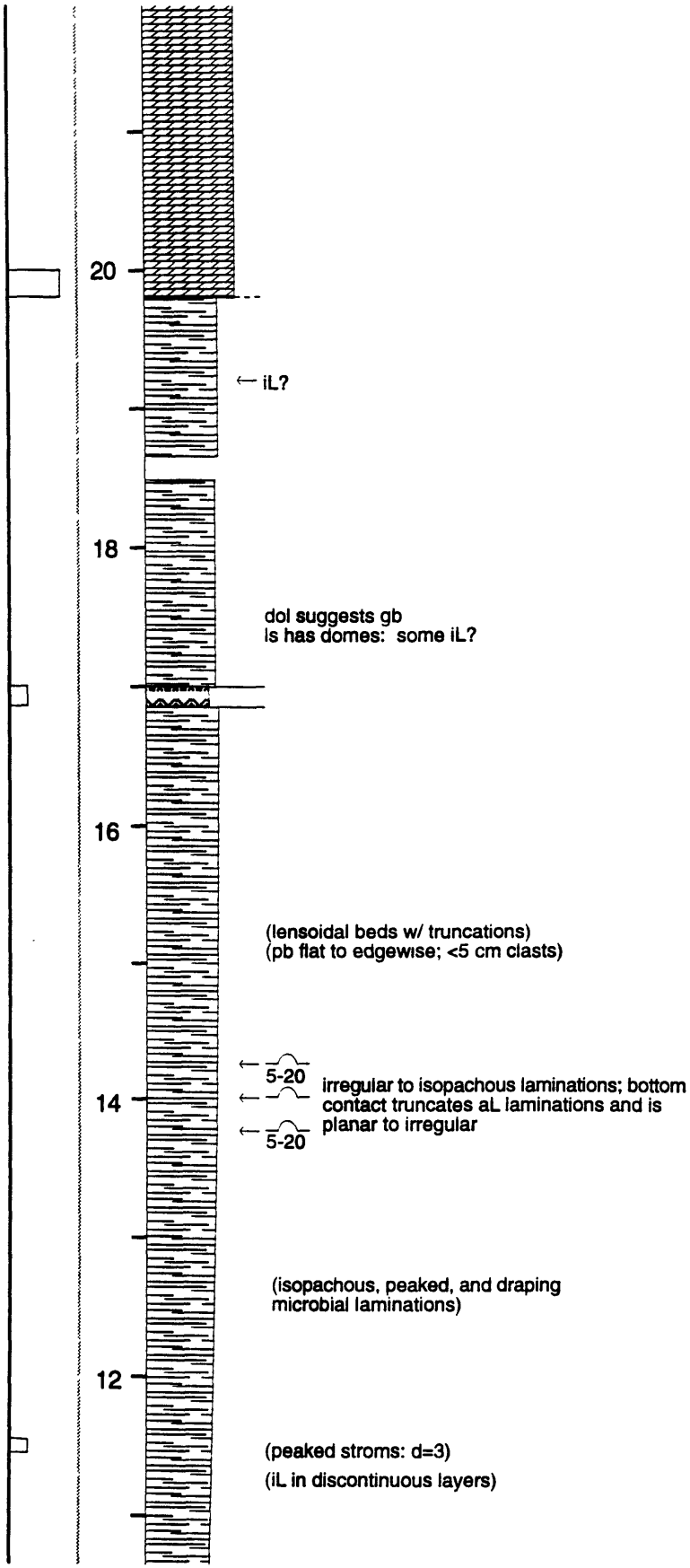
20
18
16
14
12
← iL?
dol suggests gb
ls has domes: some iL?
(lensoidal beds w/ truncations)
(pb flat to edgewise; <5 cm clasts)
← 5-20
← 5-20
irregular to isopachous laminations; bottom contact truncates aL laminations and is planar to irregular
(isopachous, peaked, and draping microbial laminations)
(peaked stroms: d=3)
(iL in discontinuous layers)

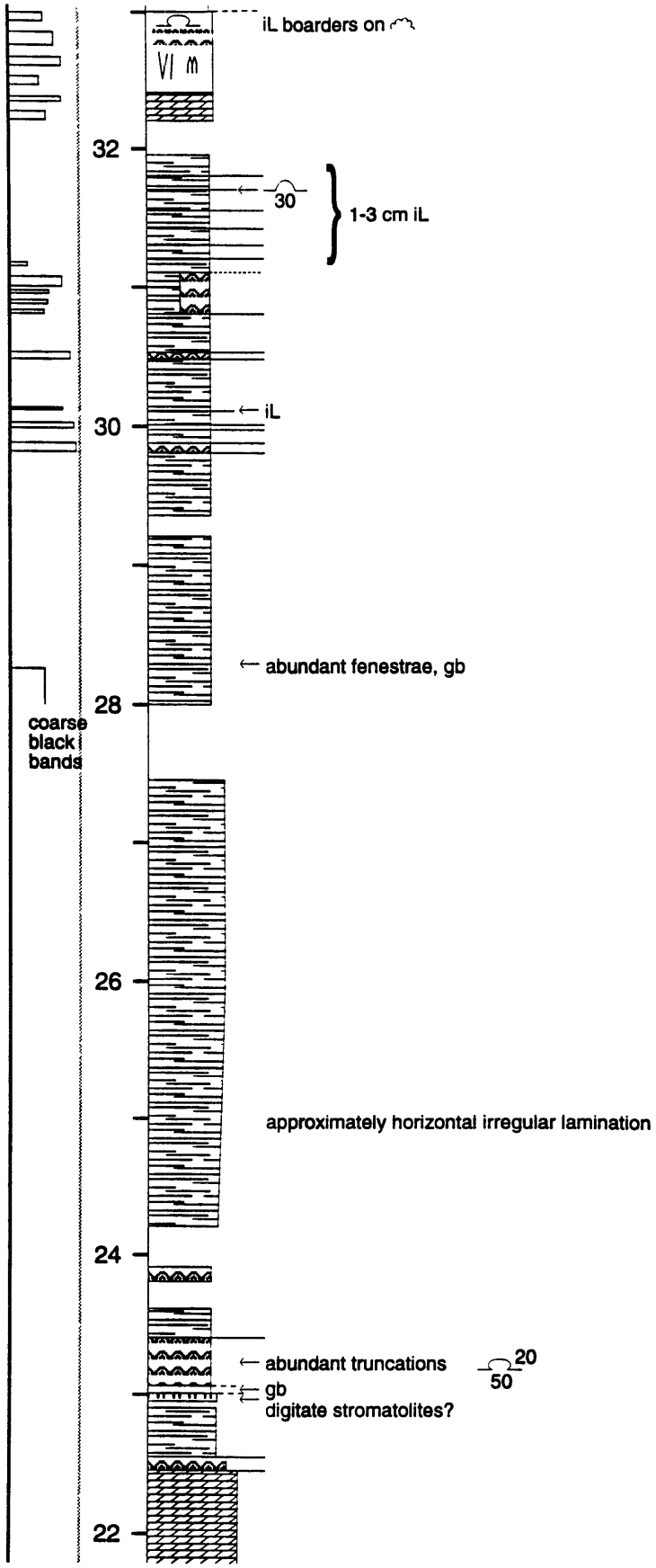
iL boarders on
VI m
32
30
1-3 cm iL
iL
30
abundant fenestrae, gb
28
coarse black bands
26
approximately horizontal irregular lamination
24
abundant truncations
20
50
gb
digitate stromatolites?
22

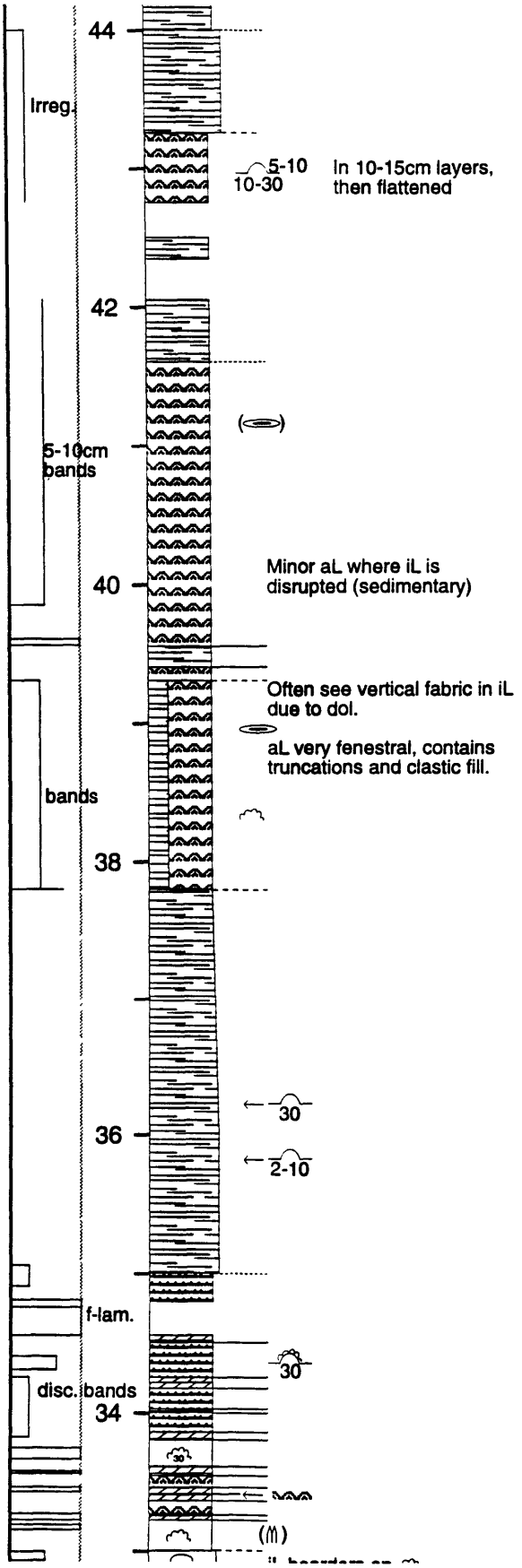
44
Irreg.
5-10
10-30
In 10-15cm layers,
then flattened
42
5-10cm
bands
Minor aL where iL is
disrupted (sedimentary)
40
Often see vertical fabric in iL
due to dol.
aL very fenestral, contains
truncations and clastic fill.
bands
38
30
36
2-10
f-lam.
30
disc. bands
34

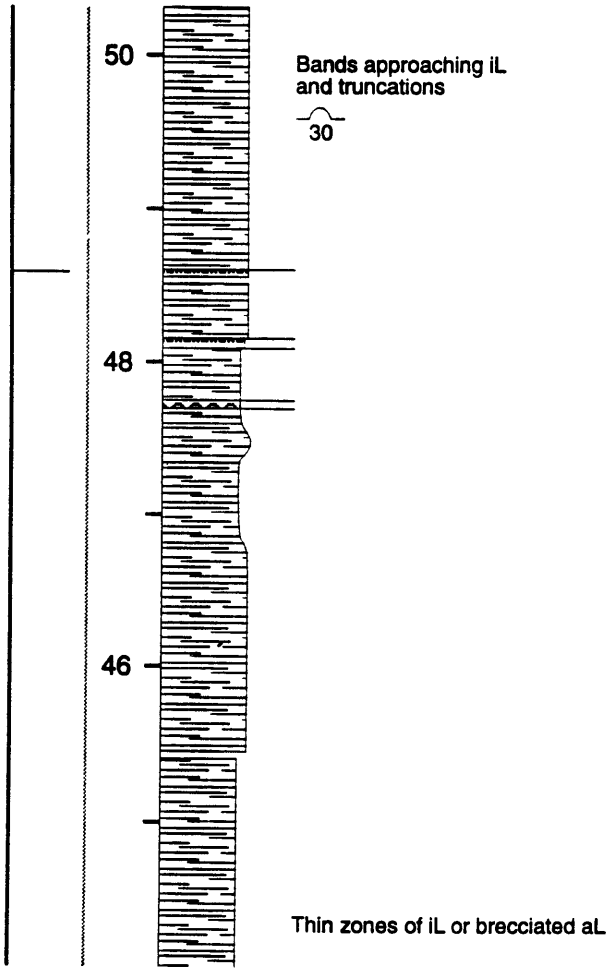
50
48
46
Bands approaching iL and truncations
30
Thin zones of iL or brecciated aL

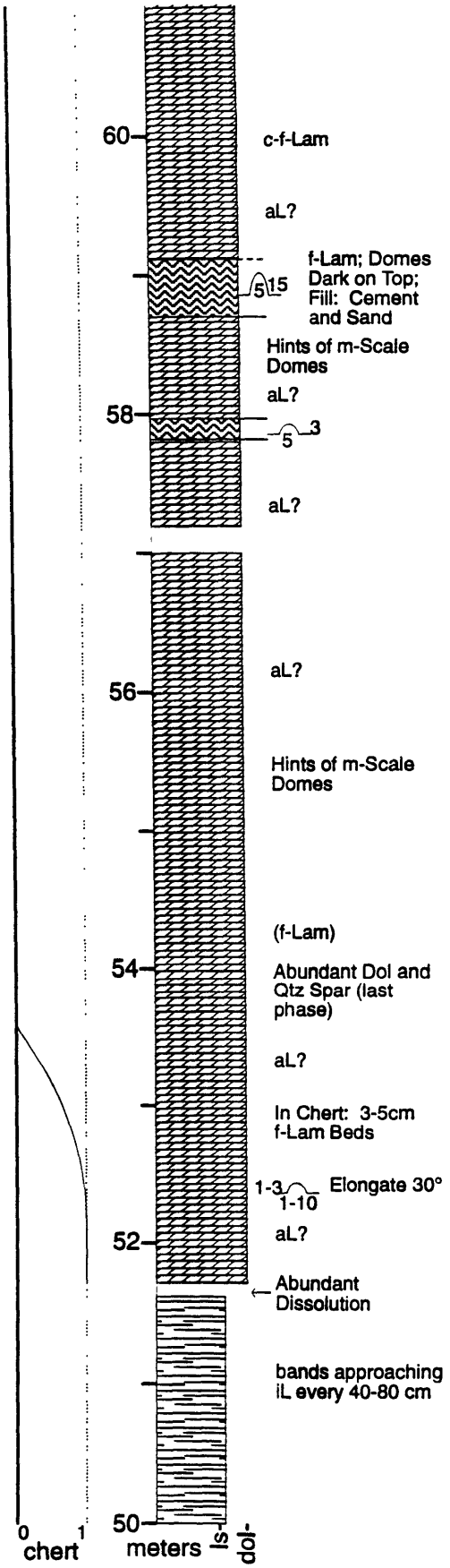
60
c-f-Lam
aL?
f-Lam; Domes
Dark on Top;
Fill: Cement
and Sand
5
15
Hints of m-Scale
Domes
aL?
58
5
3
aL?
aL?
56
Hints of m-Scale
Domes
(f-Lam)
54
Abundant Dol and
Qtz Spar (last
phase)
aL?
In Chert: 3-5cm
f-Lam Beds
1-3
1-10
Elongate 30°
aL?
52
Abundant
Dissolution
bands approaching
iL every 40-80 cm
50
0
chert
1
meters
ls
dol

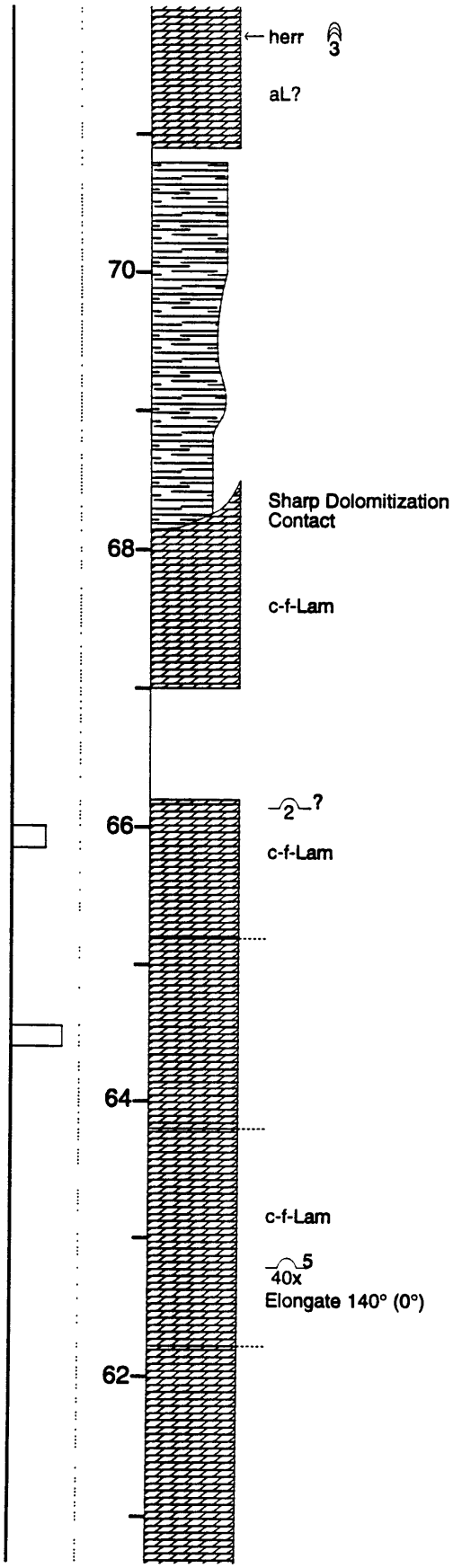
← herr
3
aL?
70
Sharp Dolomitization
Contact
68
c-f-Lam
2
?
66
c-f-Lam
64
c-f-Lam
5
40x
Elongate 140° (0°)
62

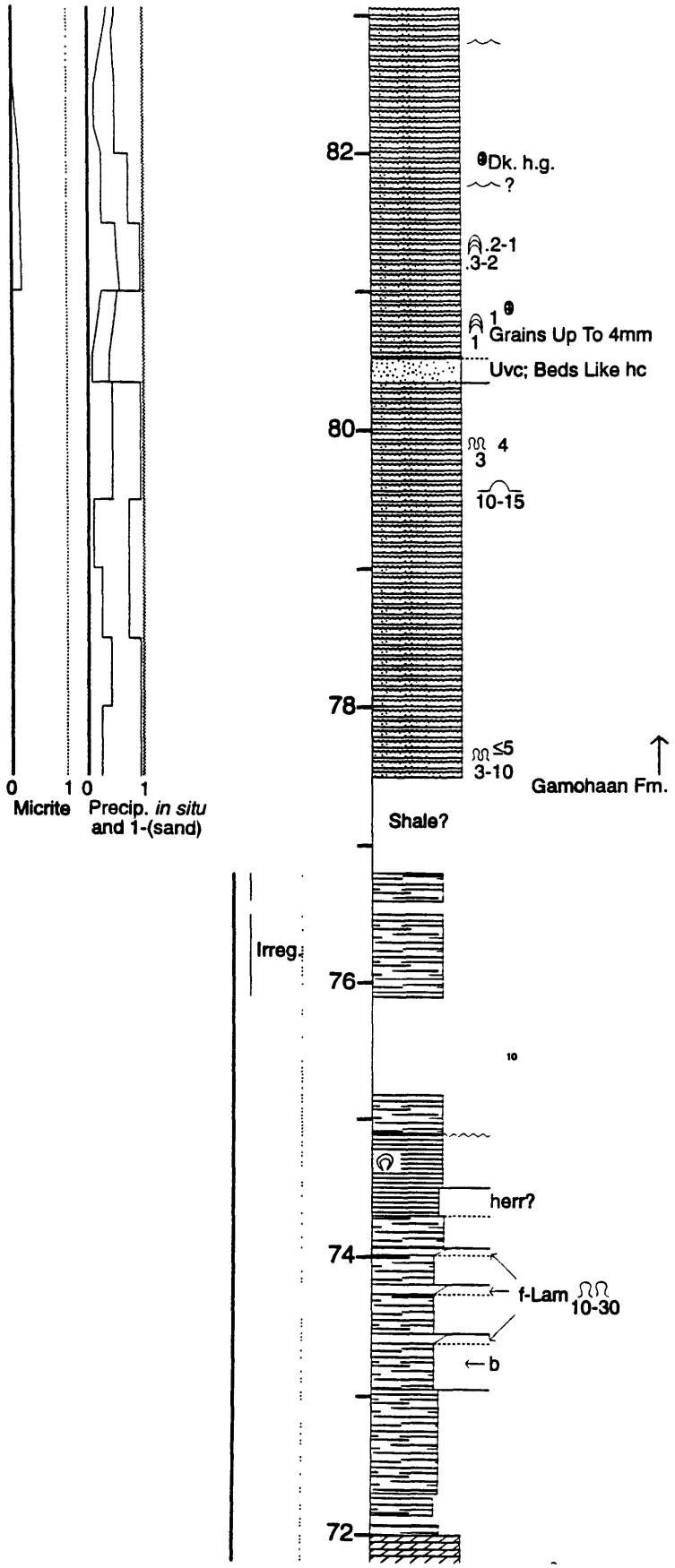
0 1 0 1
Micrite
Precip. in situ and 1-(sand)
82
80
78
76
74
72
Dk. h.g.
?
.2-1
3-2
1
1
Grains Up To 4mm
Uvc; Beds Like hc
4
3
10-15
≤5
3-10
Gamohaan Fm.
Shale?
Irreg.
herr?
f-Lam
10-30
b

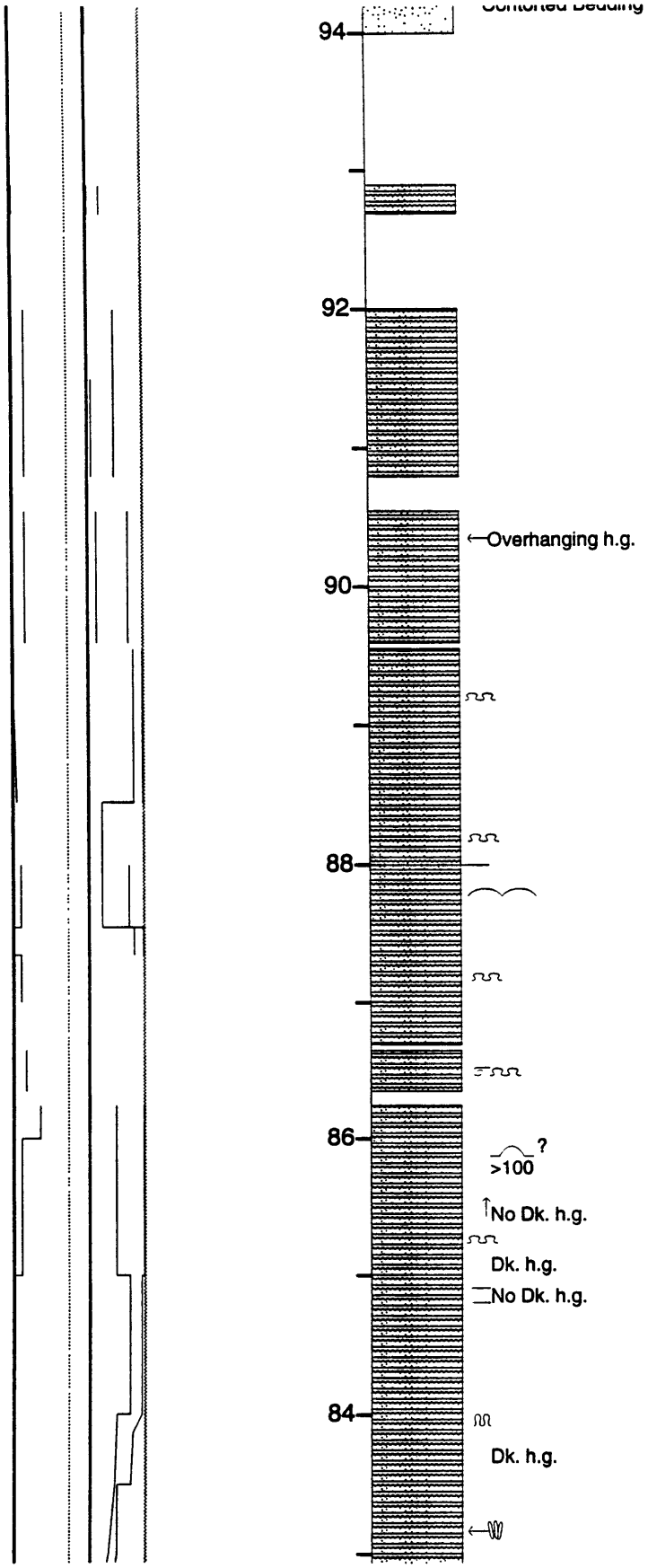
94
92
90
88
86
84
←Overhanging h.g.
?
>100
No Dk. h.g.
Dk. h.g.
No Dk. h.g.
Dk. h.g.

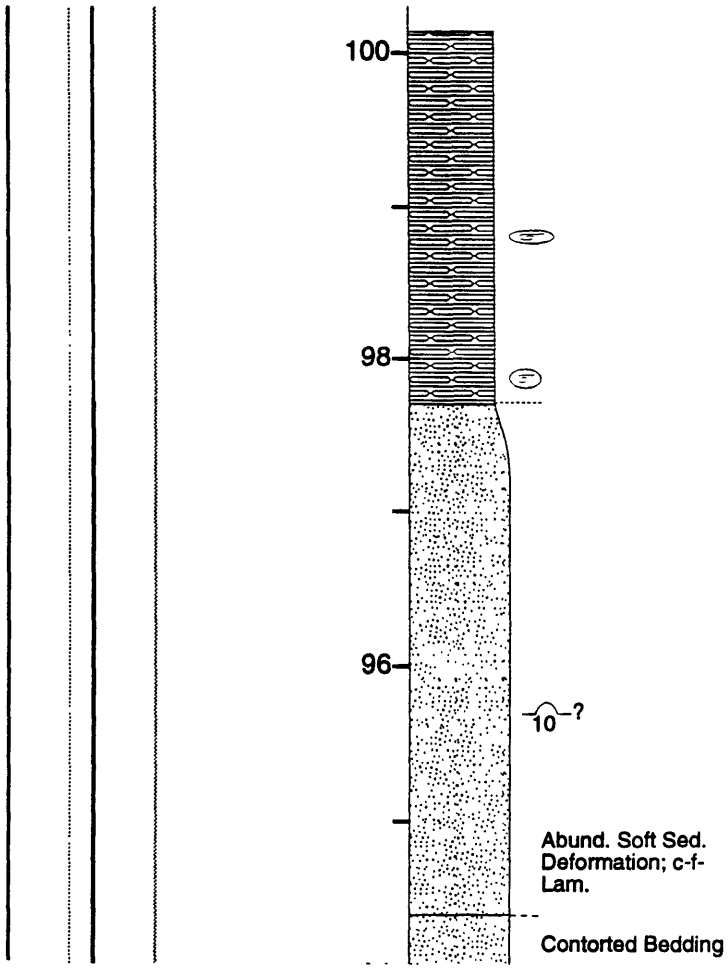
100
98
96
10
?
Abund. Soft Sed. Deformation; c-f-Lam.
Contorted Bedding

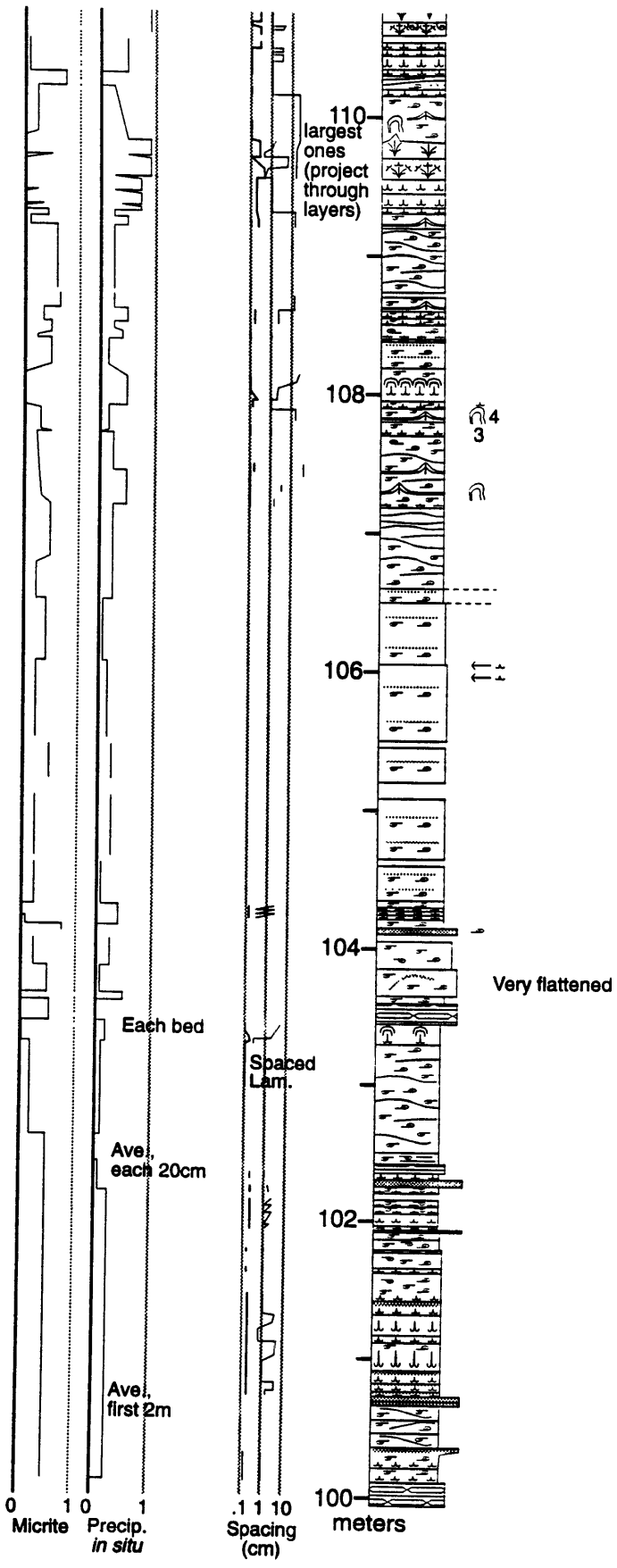
110
largest ones (project through layers)
108
4
3
106
104
Very flattened
Each bed
Spaced Lam.
Ave., each 20cm
102
Ave., first 2m
100
meters
0 1
Micrite
0 1
Precip. in situ
.1 1 10
Spacing (cm)

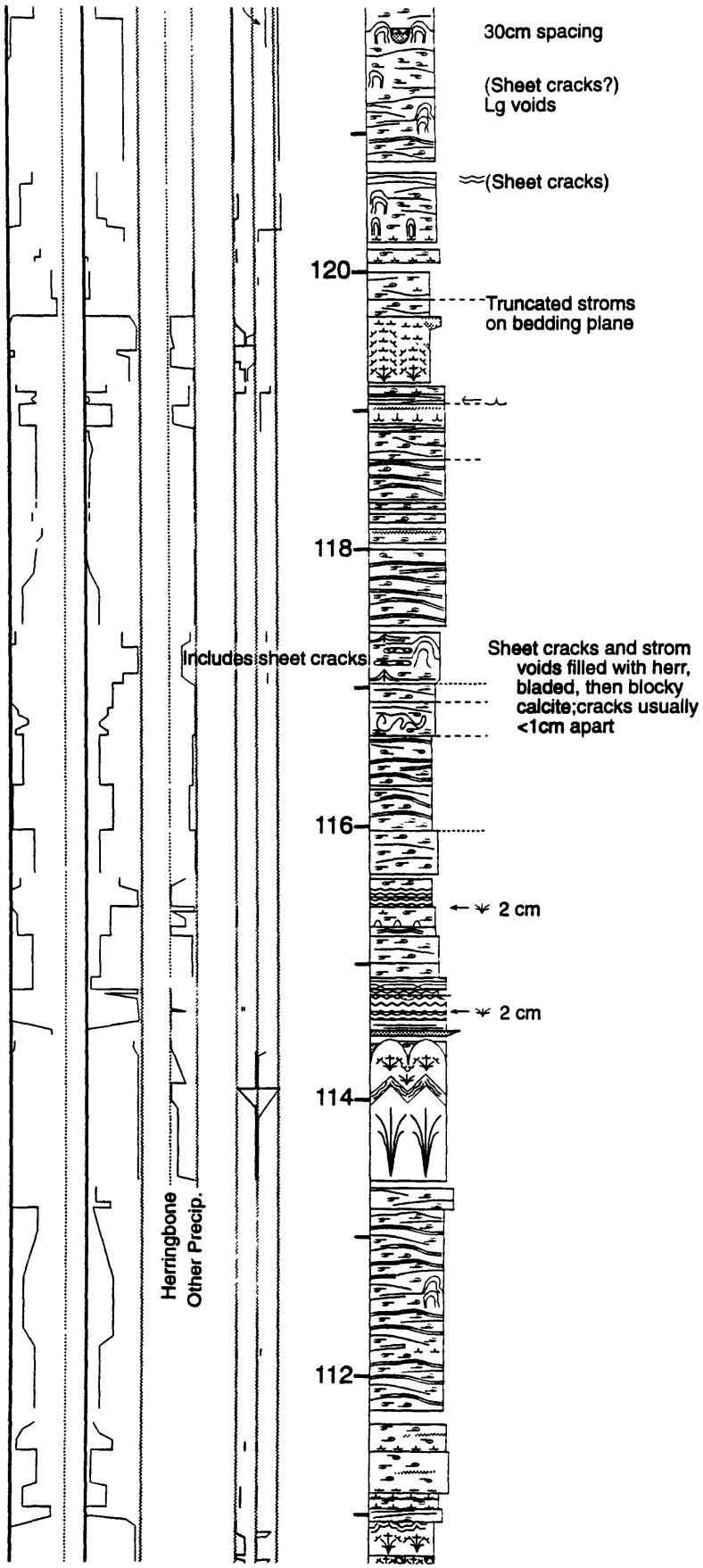
30cm spacing
(Sheet cracks?)
Lg voids
(Sheet cracks)
120
Truncated stroms
on bedding plane
118
Includes sheet cracks
Sheet cracks and strom
voids filled with herr,
bladed, then blocky
calcite;cracks usually
<1cm apart
116
2 cm
2 cm
114
112
Herringbone
Other Precip.

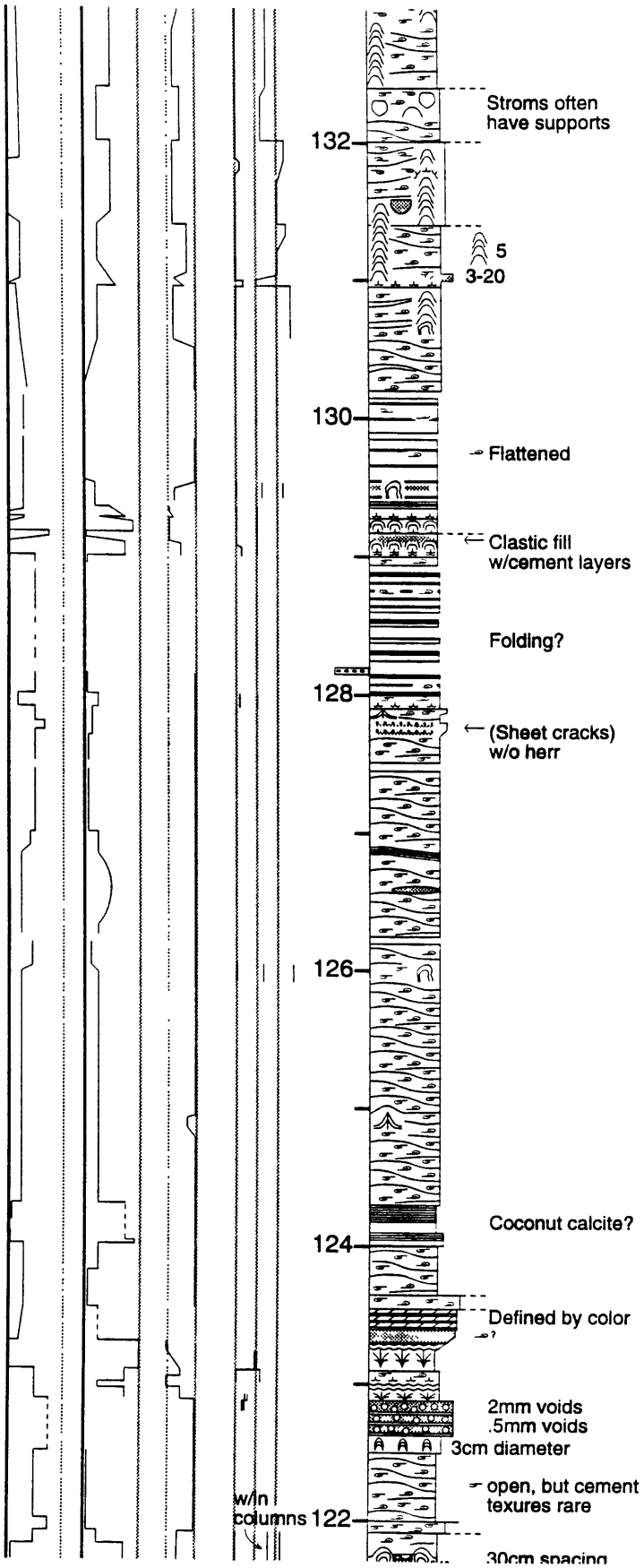
Stroms often
have supports
132
5
3-20
130
Flattened
Clastic fill
w/cement layers
Folding?
128
(Sheet cracks)
w/o herr
126
Coconut calcite?
124
Defined by color
2mm voids
.5mm voids
3cm diameter
open, but cement
texures rare
w/in
columns
122
30cm spacing

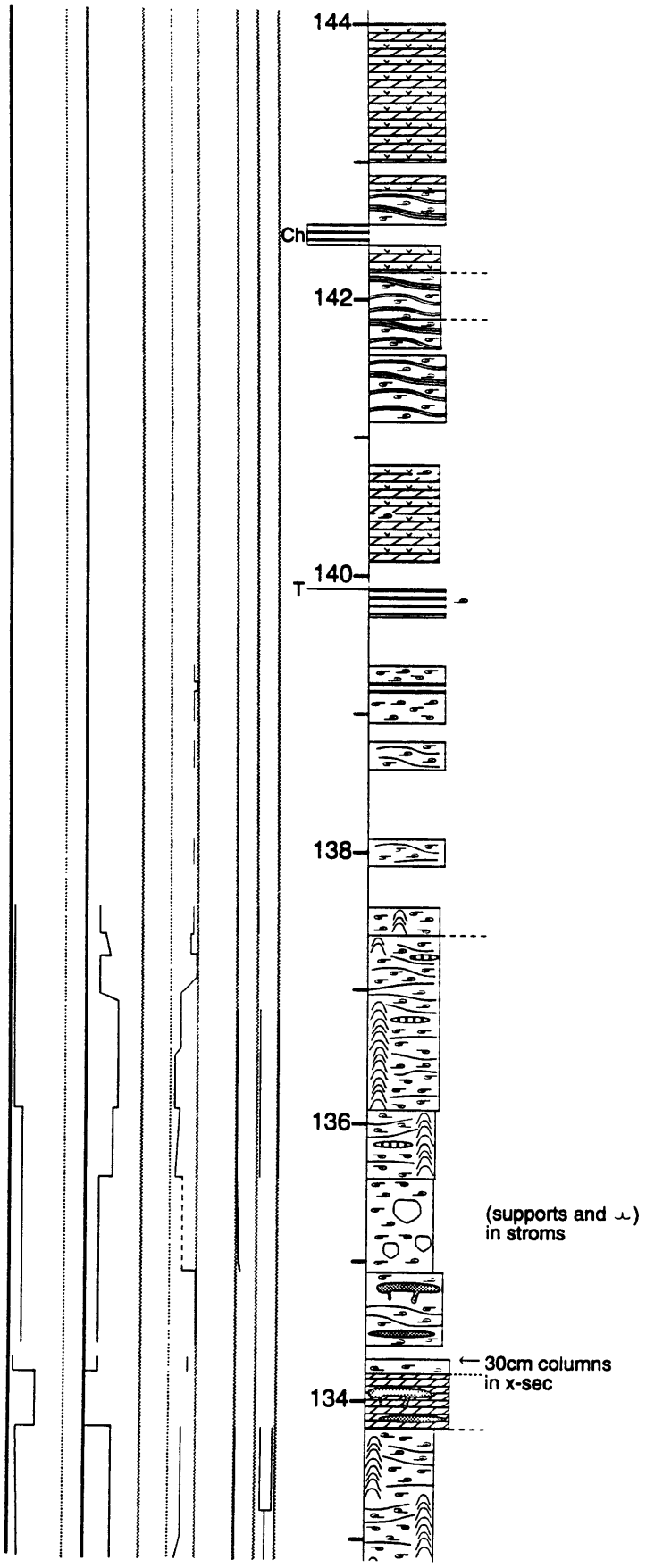
144
Ch
142
140
T
138
136
(supports and ⌒)
in stroms
30cm columns
in x-sec
134

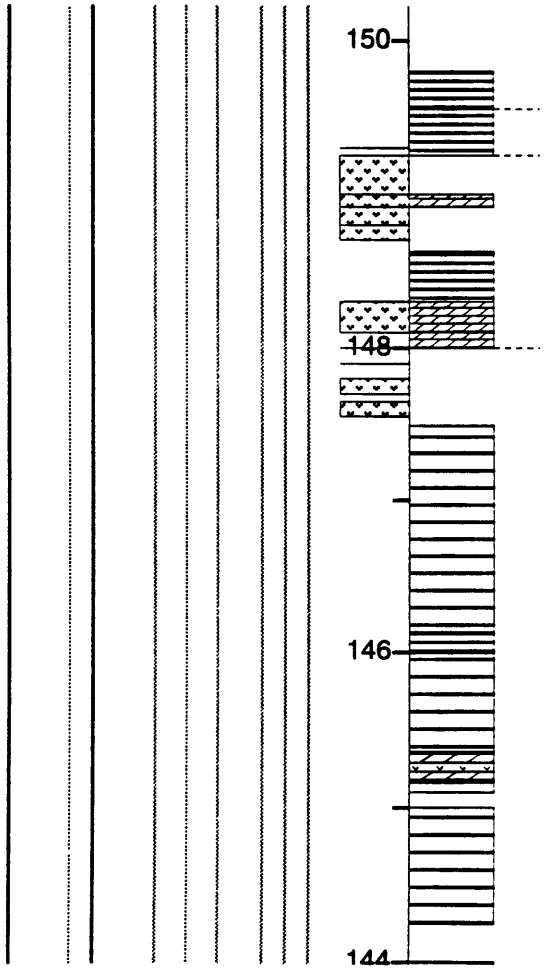
150
148
146
144

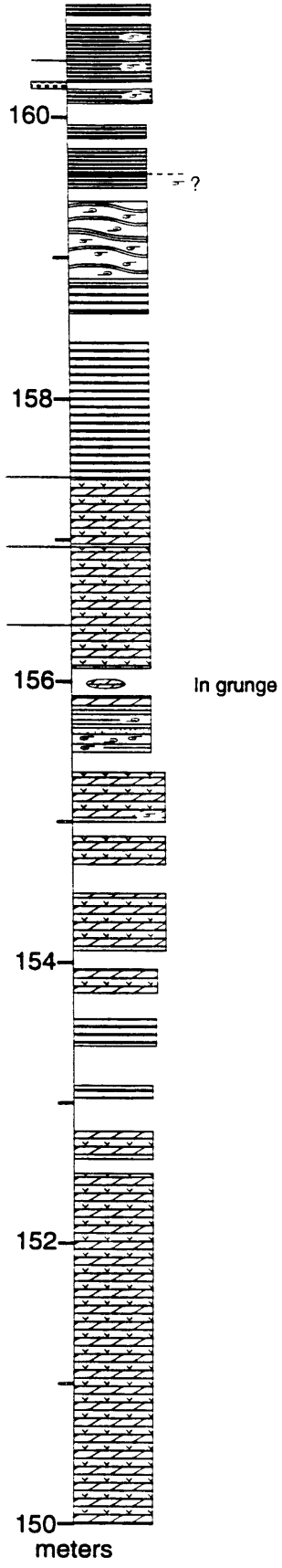
160
?
158
156
In grunge
154
152
150
meters

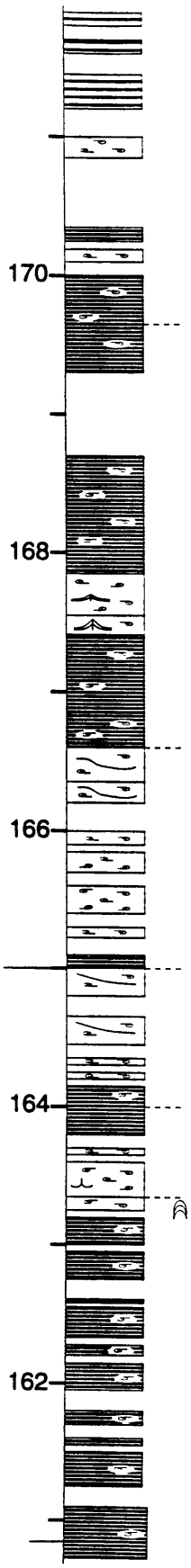
170
168
166
164
162

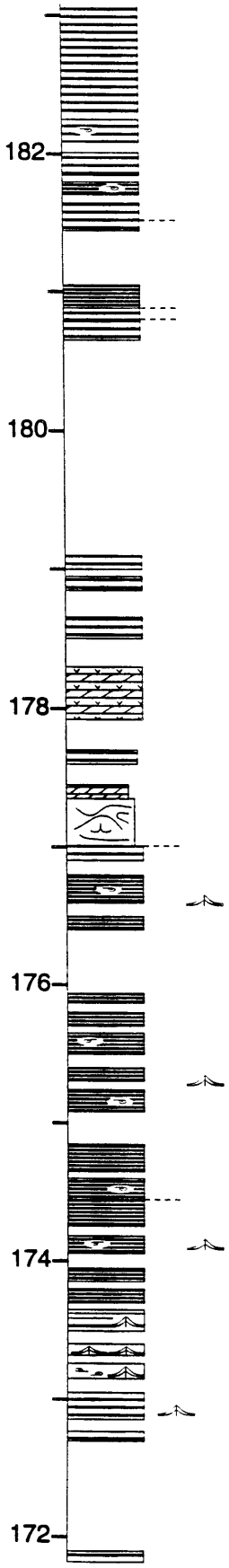
182
180
178
176
174
172

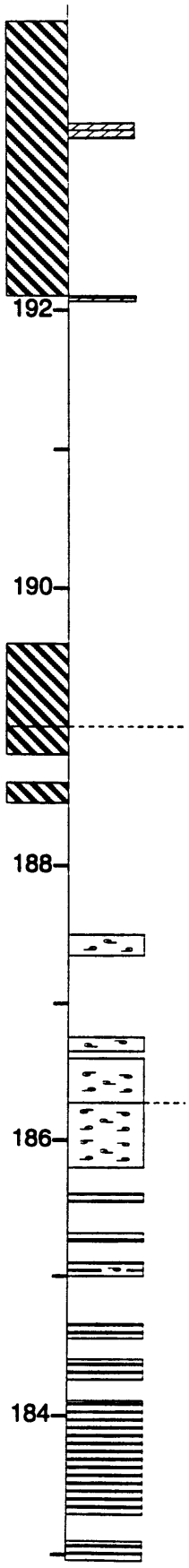
192
190
188
186
184

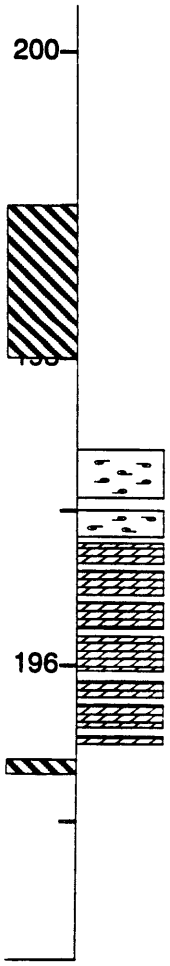
200
196

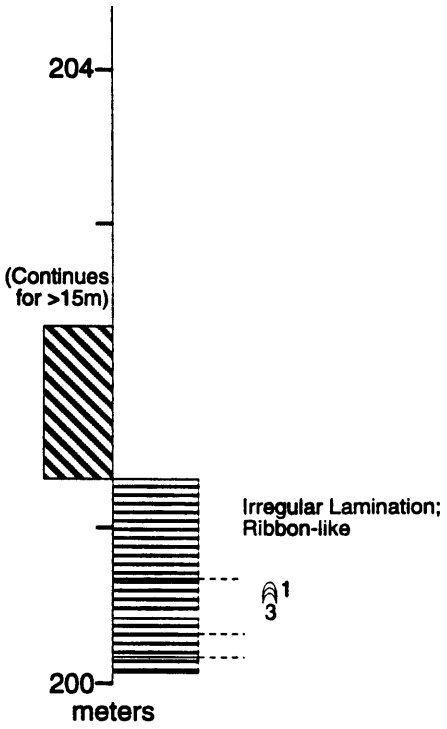
204
(Continues
for >15m)
Irregular Lamination;
Ribbon-like
1
3
200
meters

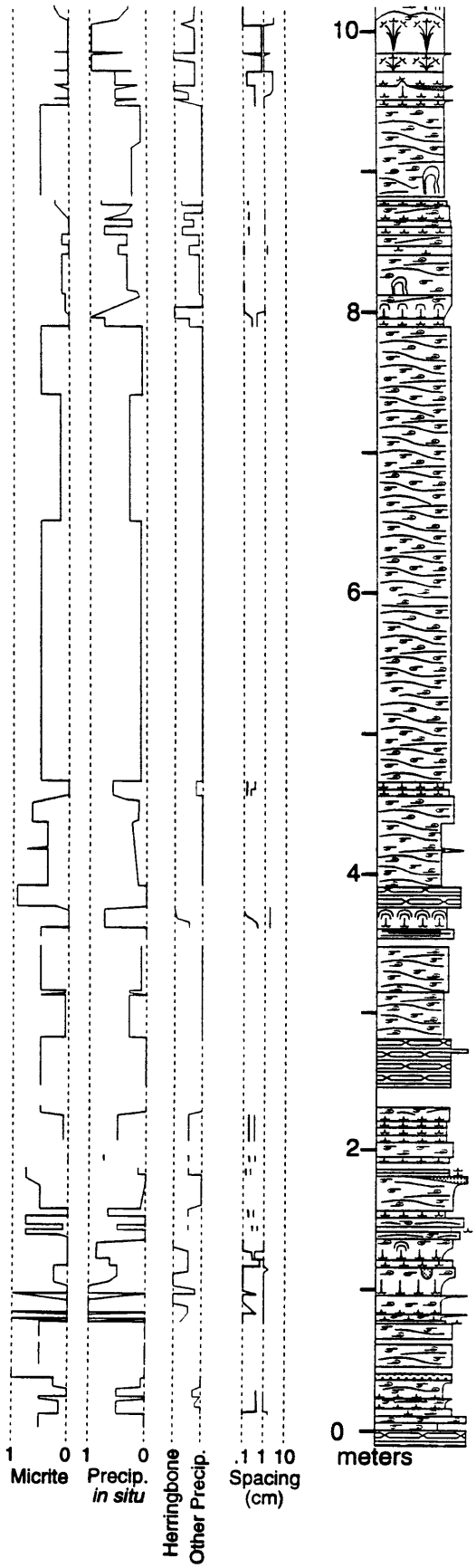
10
8
6
4
2
0
meters
1 0
Micrite
1 0
Precip.
in situ
Herringbone
Other Precip.
.1 1 10
Spacing
(cm)

14
12

## Section PM

Location: 5 km east of Pomfret along the gravel roadtowards Senlac.. Section is located north of the road.

Stratigraphic Range: Upper Gamohaan Formation to base of Kuruman Iron Formation. This section is presented in two parts separated by an unknown stratigraphic distance.

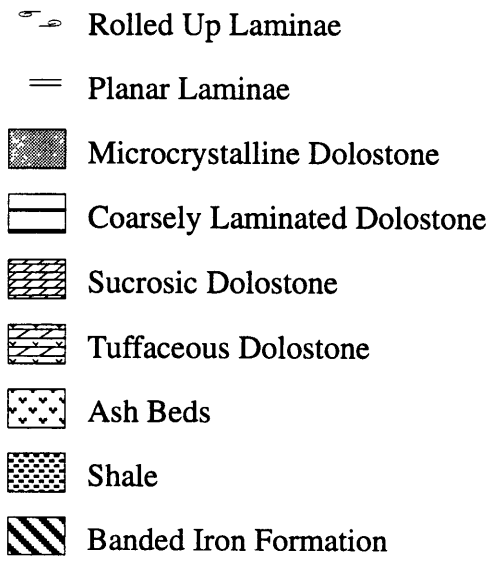

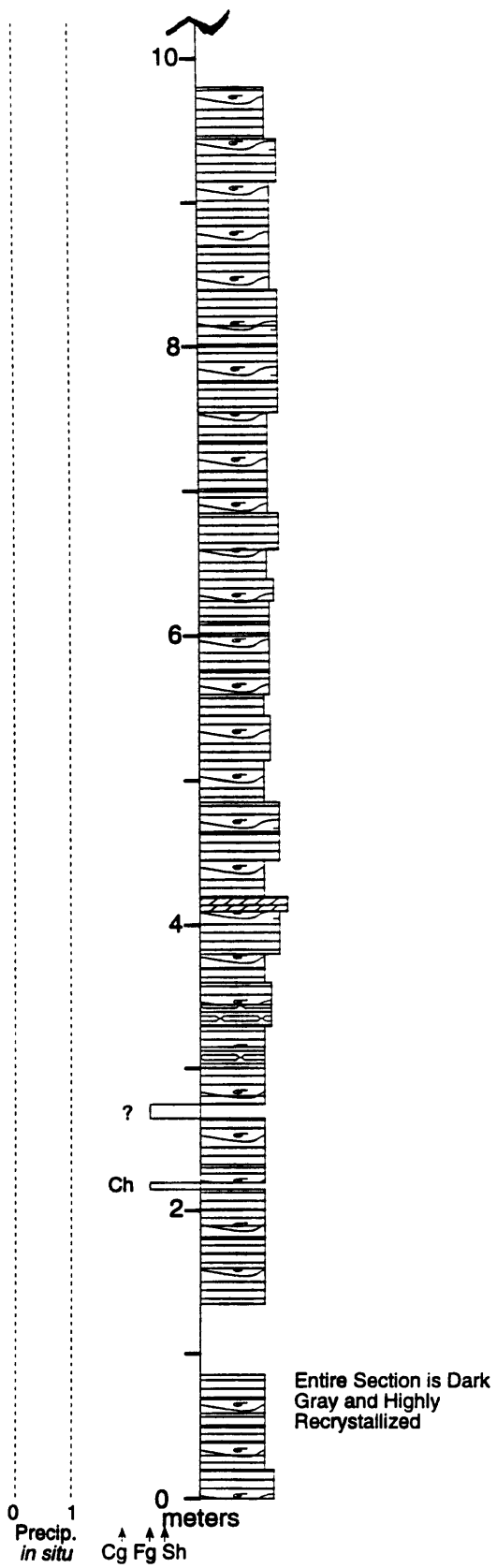
10
8
6
4
?
Ch
2
0
meters
0
1
Precip.
in situ
Cg Fg Sh
Entire Section is Dark
Gray and Highly
Recrystallized

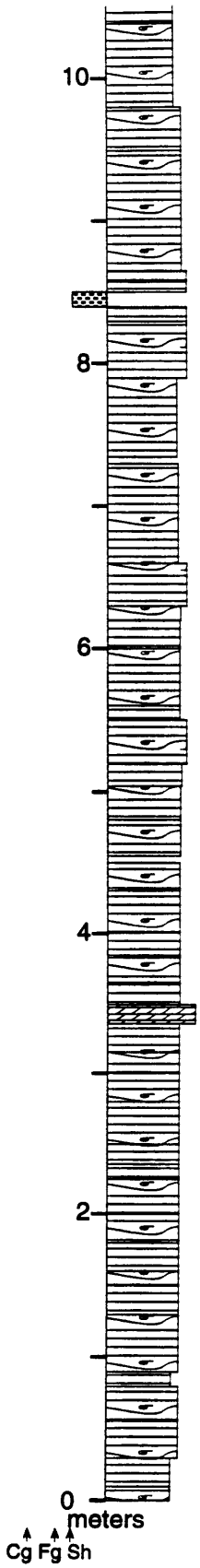
10
8
6
4
2
0
meters
Cg Fg Sh

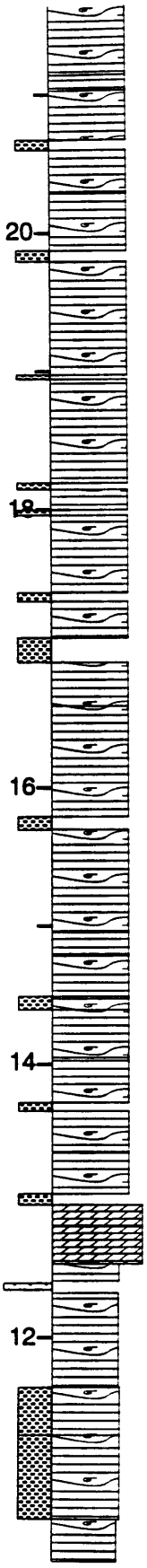
20
18
16
14
12

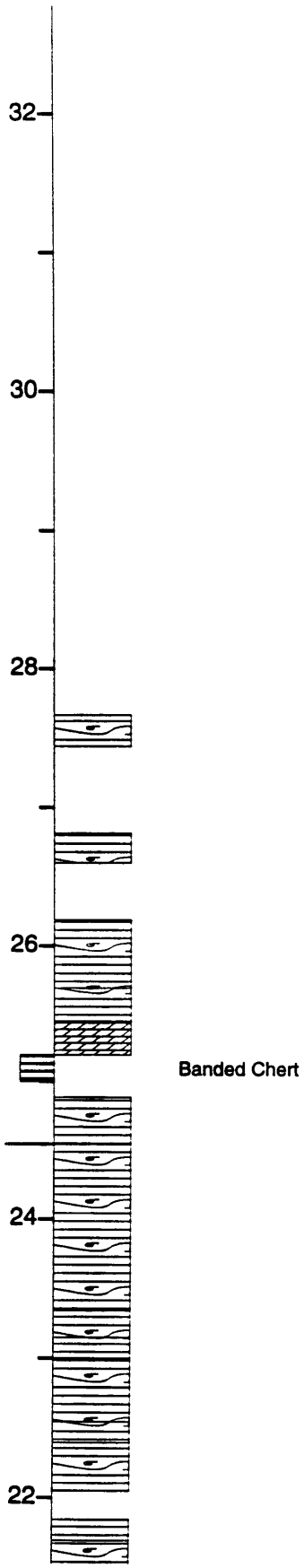
32
30
28
26
Banded Chert
24
22

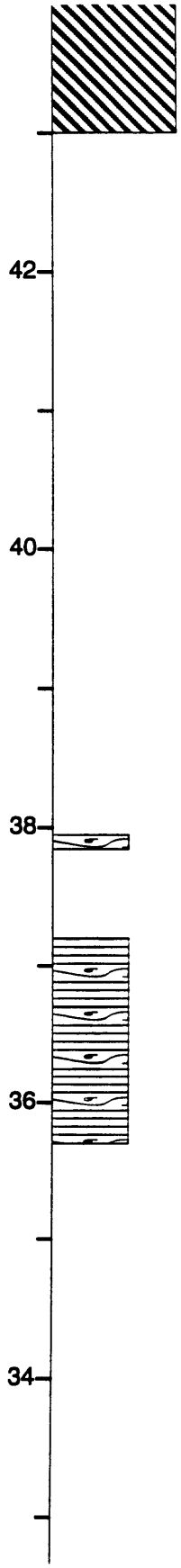
42
40
38
36
34

## Core SACHA g

Location: Sacha Farm, northwest of Shishen. Core owned by the Geological Survey of South Africa and stored in the facility in Uppington.

Stratigraphic Range: Top of the Kogelbeen Formation to mid-Gamohaan Formation. The upper contact of the Gamohaan Formation in the core is an unconformity overlain by Paleozoic glacial till of the Dwyka formation. The core continues downward through the entire platform.

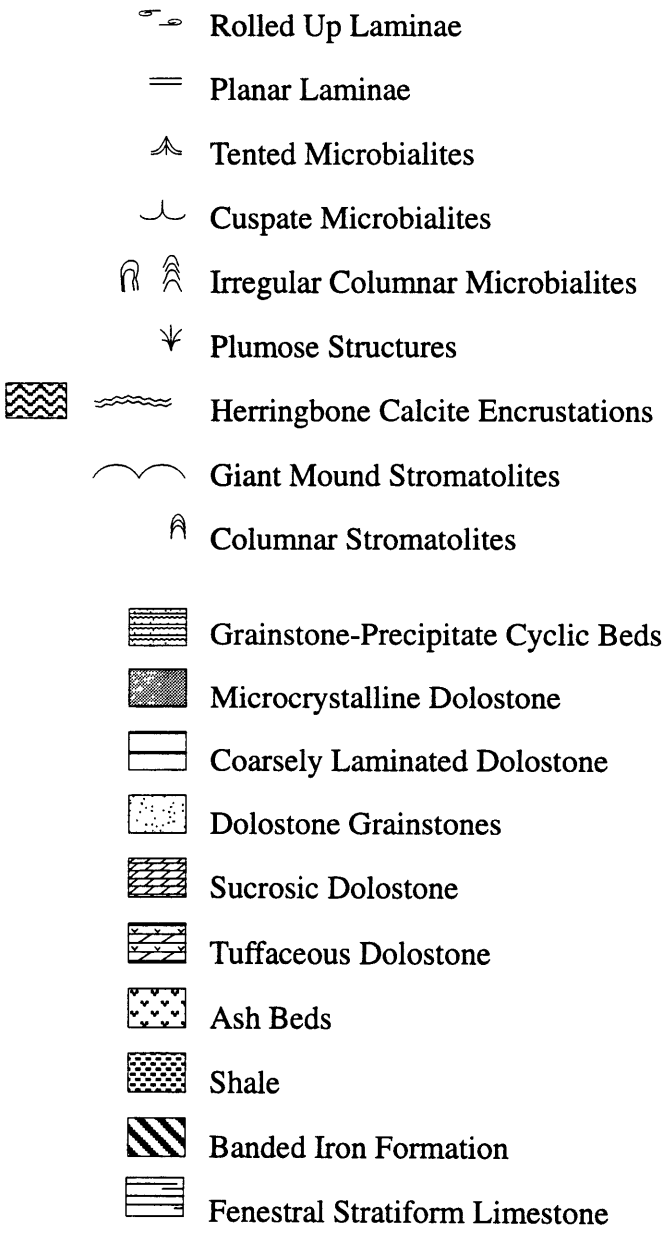

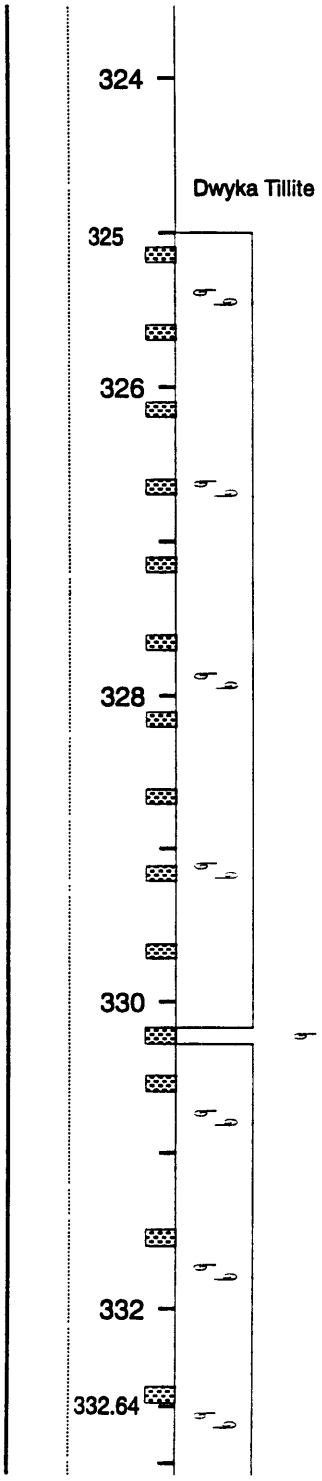
324
Dwyka Tillite
325
326
328
330
332
332.64

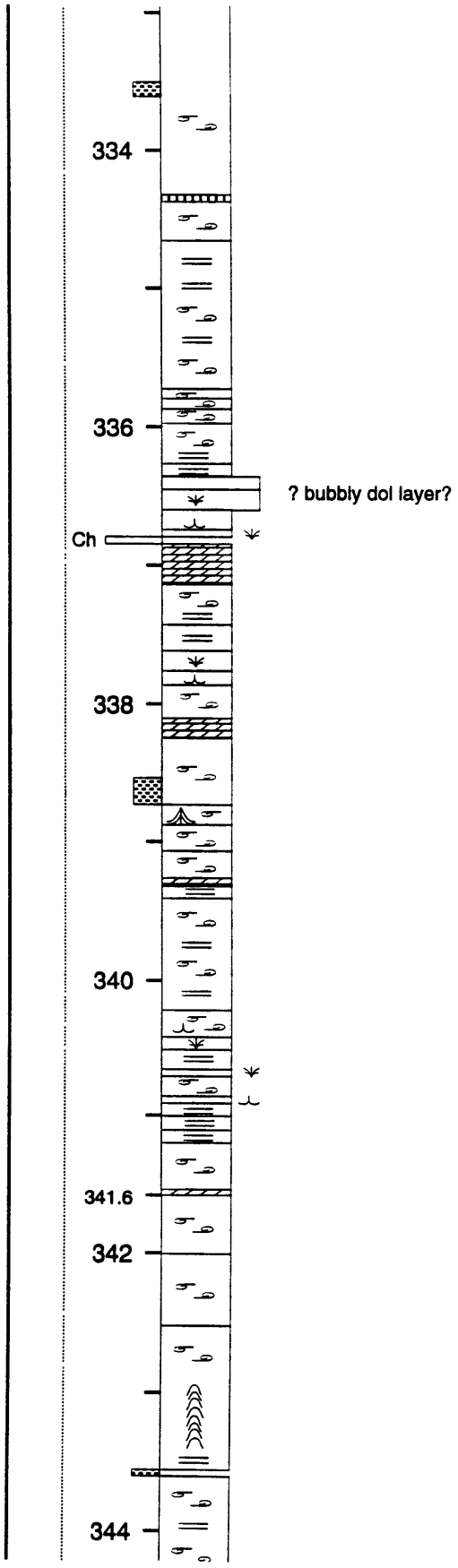
334
336
? bubbly dol layer?
Ch
338
340
341.6
342
344

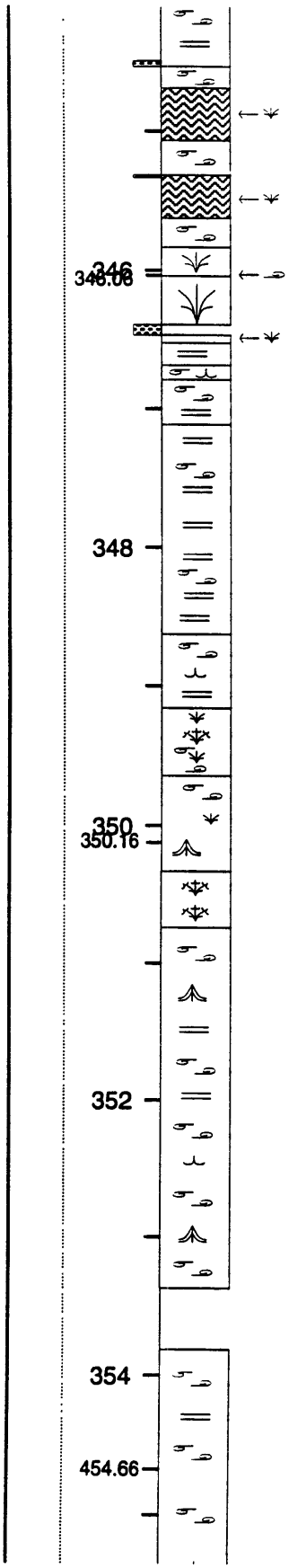
346
348.08
348
350
350.16
352
354
454.66

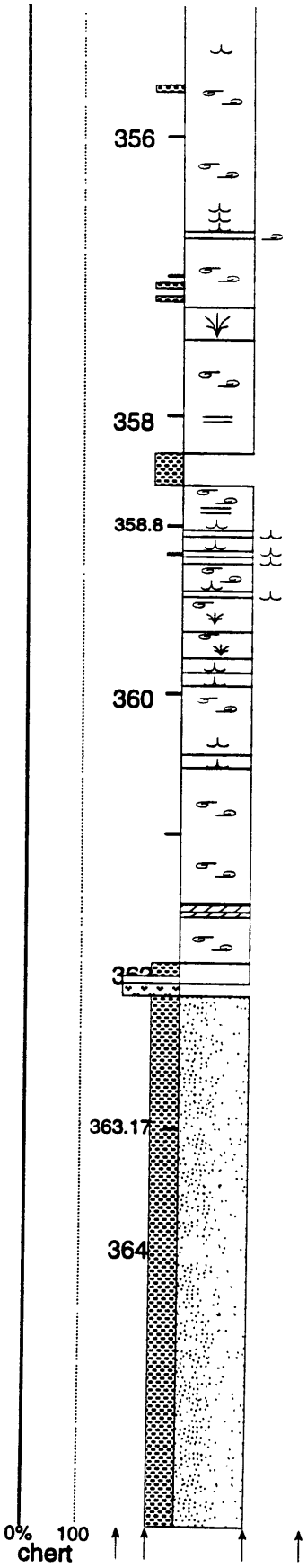
356
358
358.8
360
363.17
364
0%
100
chert

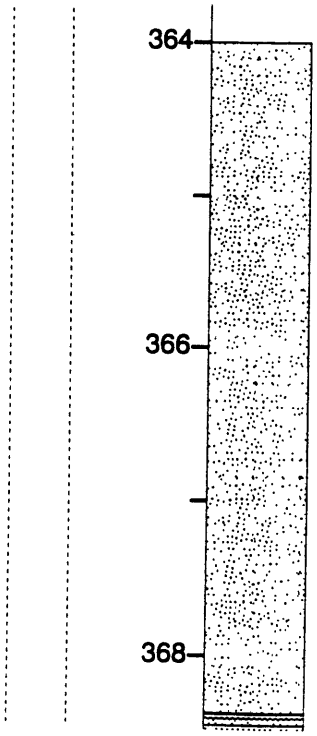
364
366
368

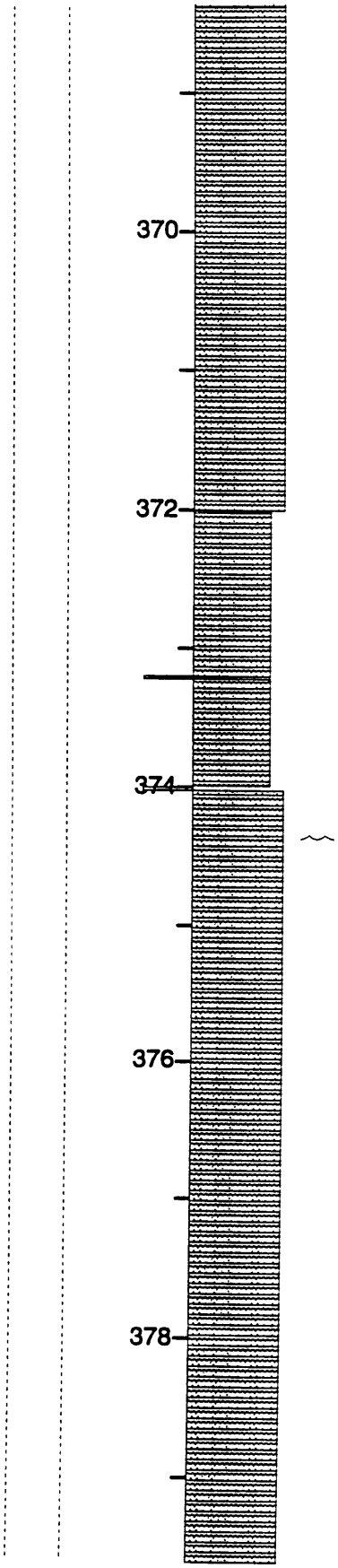
370
372
374
376
378

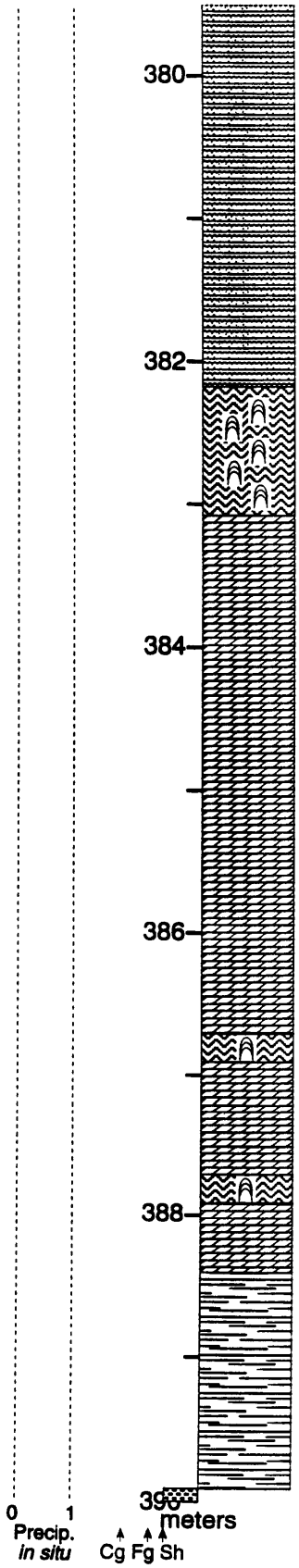
380
382
384
386
388
390
meters
0
1
Precip.
in situ
Cg Fg Sh

## Section AE f

Location: Top of mountain 5 km southwest of Strijdom Tunnel on road R36 near Abel Erasmus Pass.

Stratigraphic Range: Upper Kogelbeen Formation to upper Gamohaan Formation. This section continues from section AE and 65 m in section AE f corresponds to 986 m in section AE. (The lower 50 m of AE f were drafed with section AE.) Siliciclastic facies are plotted to the left and carbonate facies are plotted to the right of the section.

Rolled Up Laminae
Planar Laminae
Tented Microbialites
Cuspate Microbialites
Irregular Columnar Microbialites
Plumose Structures
Herringbone Calcite Encrustations
Giant Mound Stromatolites
Domal Stromatolites
Columnar Stromatolites
Platey Breccia
Colloform Stromatolites
Aragonite Pseudomorphs
Low Angle and Tabular X-strat
Ripple Cross Stratification
Ooids

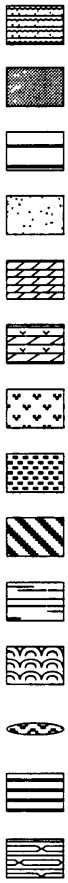

Grainstone-Precipitate Cyclic Beds
Microcrystalline Dolostone
Coarsely Laminated Dol/Quartz
Grainstones/Quartz Sandstone
Sucrosic Dolostone
Tuffaceous Dolostone
Ash Beds
Shale
Banded Iron Formation
Fenestral Stratiform Limestone
Isopachous Domes
Cement-filled Sheet Cracks
Finely Laminated Dolostone
Nodular Dolostone

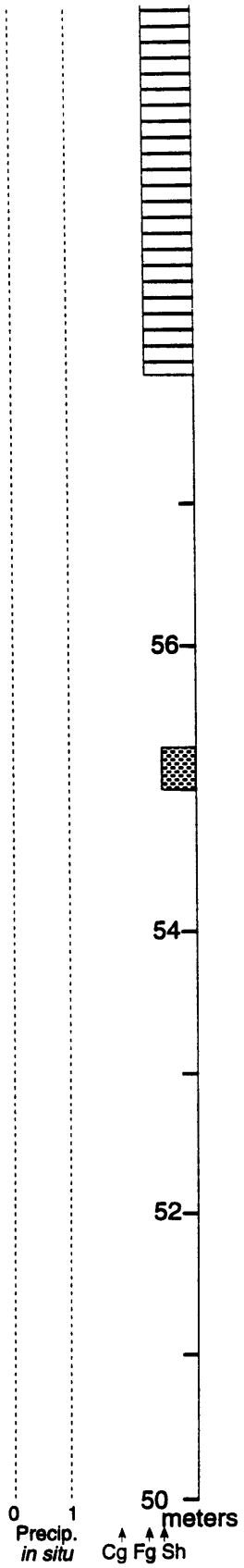
56
54
52
50
meters
0
1
Precip.
in situ
Cg
Fg
Sh

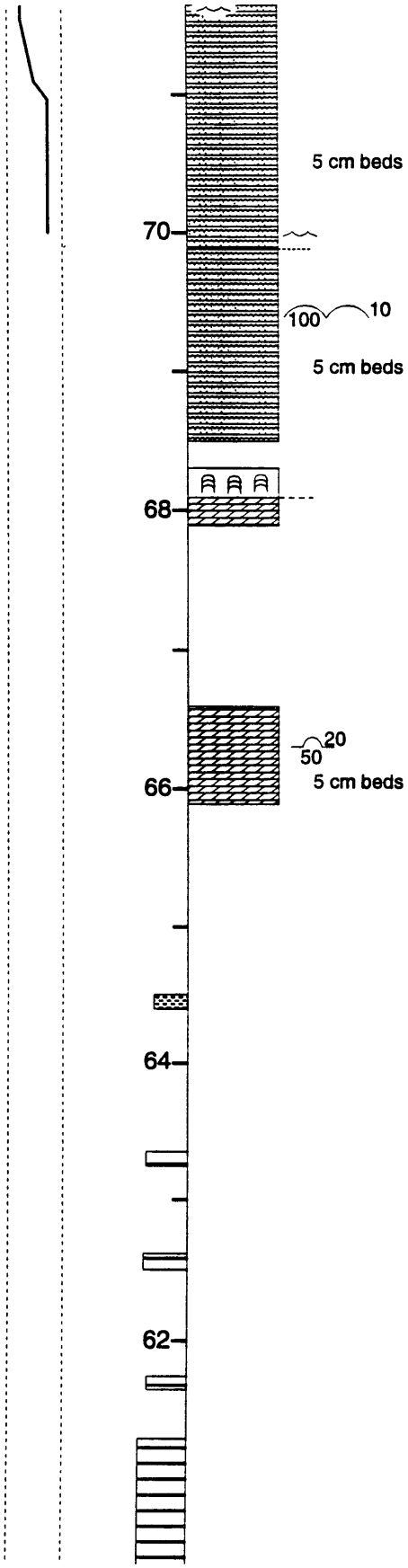
5 cm beds
70
100
10
5 cm beds
68
20
50
66
5 cm beds
64
62

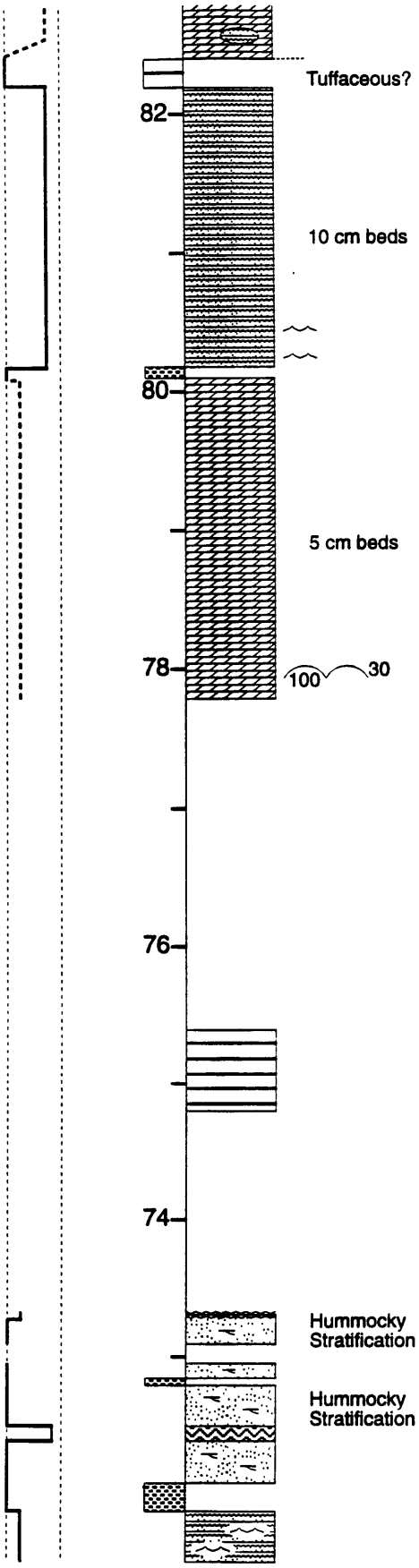
Tuffaceous?
82
10 cm beds
80
5 cm beds
78
100
30
76
74
Hummocky Stratification
Hummocky Stratification

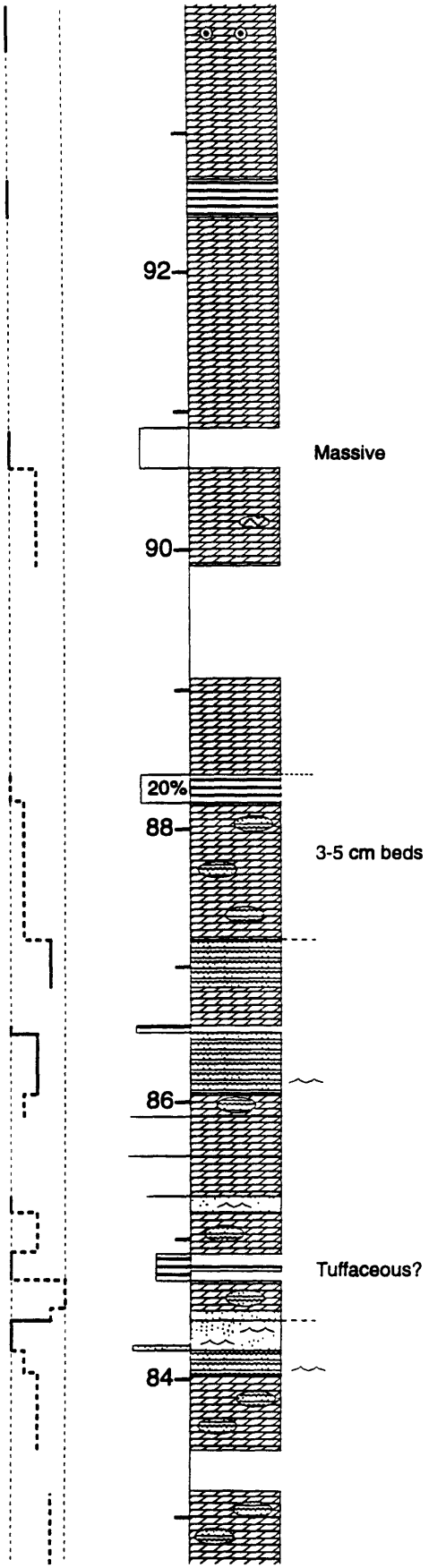
92
Massive
90
20%
88
3-5 cm beds
86
Tuffaceous?
84

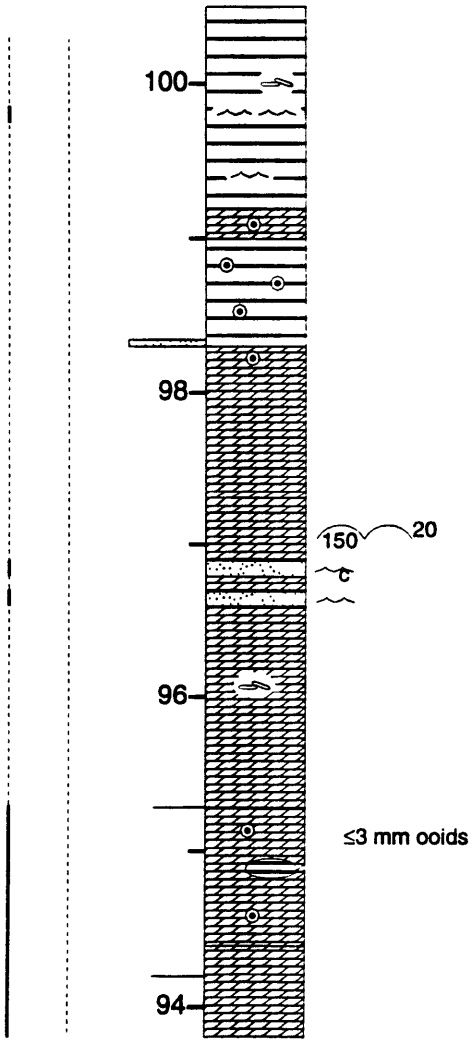
100
98
96
94
150
20
C
≤3 mm ooids

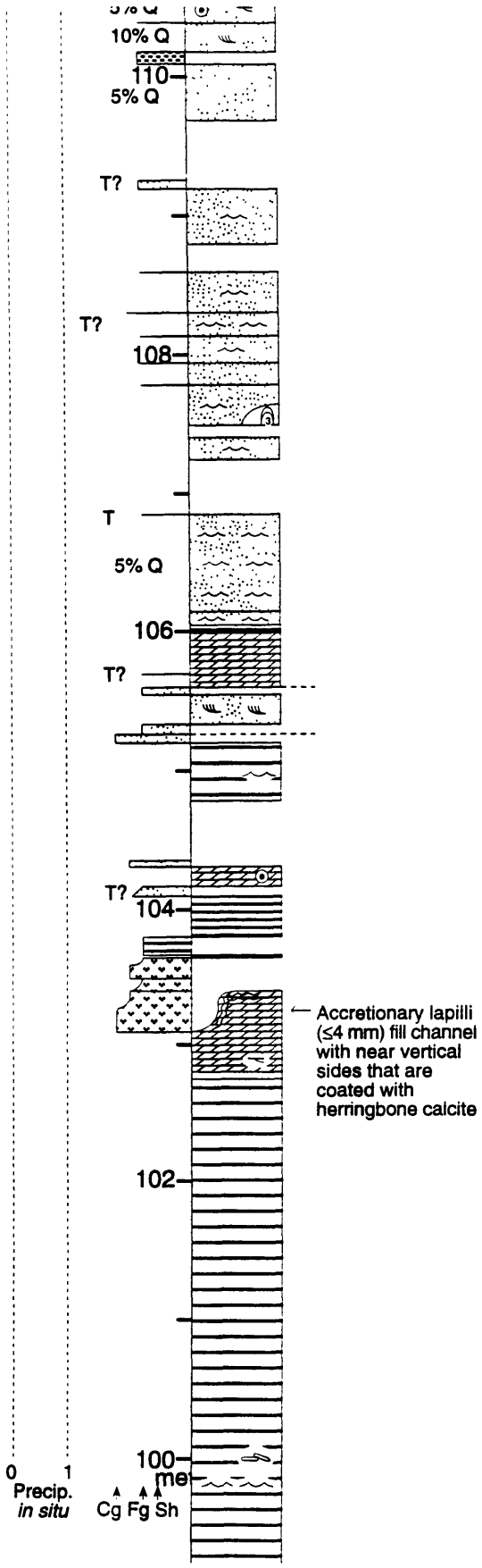
10% Q
110
5% Q
T?
T?
108
T
5% Q
106
T?
T?
104
Accretionary lapilli (≤4 mm) fill channel with near vertical sides that are coated with herringbone calcite
102
100
me
0
1
Precip.
in situ
Cg Fg Sh

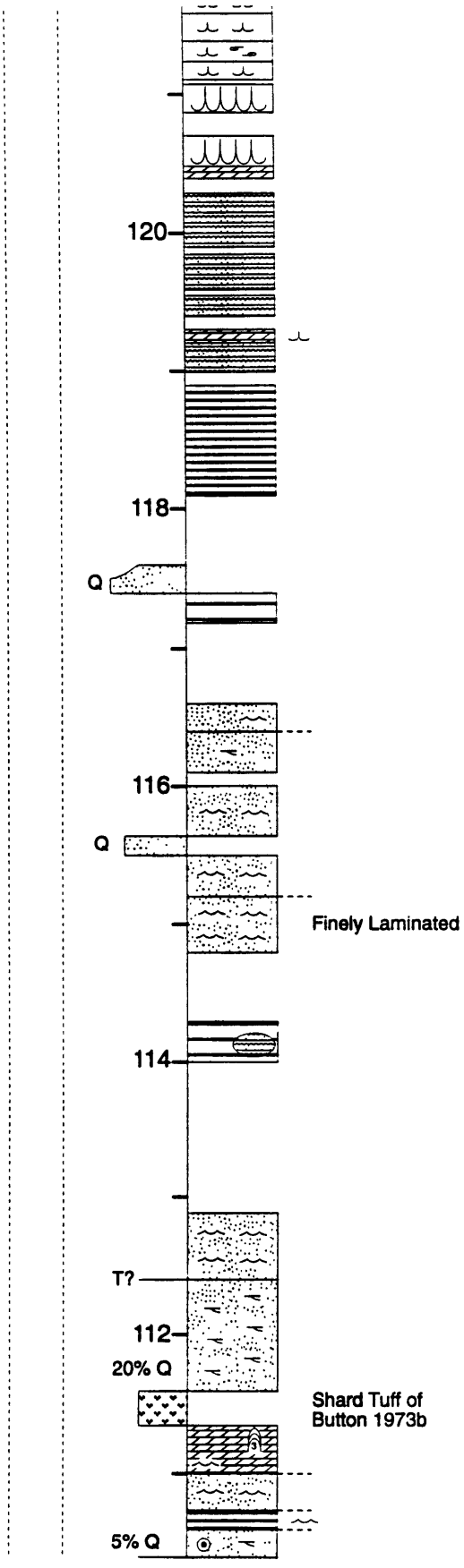
120
118
Q
116
Q
Finely Laminated
114
T?
112
20% Q
Shard Tuff of
Button 1973b
5% Q

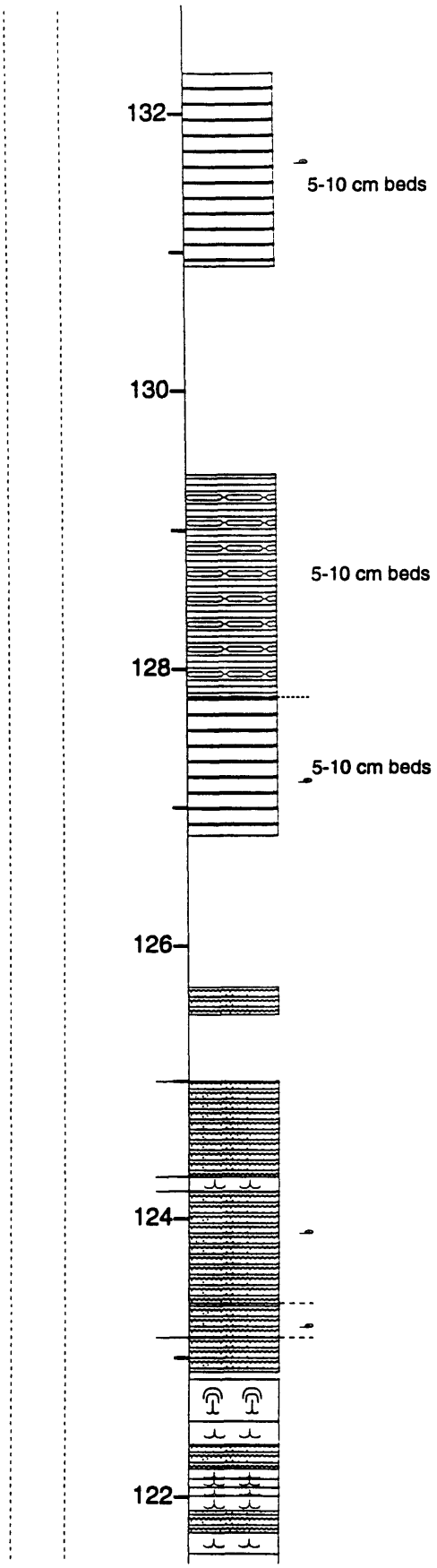
132
5-10 cm beds
130
5-10 cm beds
128
5-10 cm beds
126
124
122

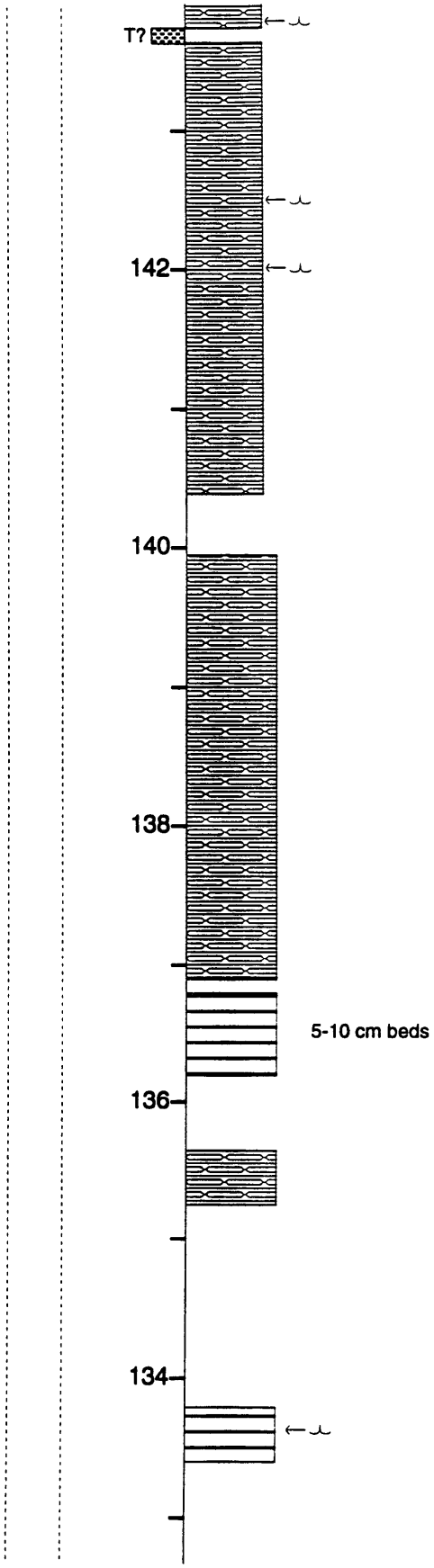
T?
142
140
138
5-10 cm beds
136
134

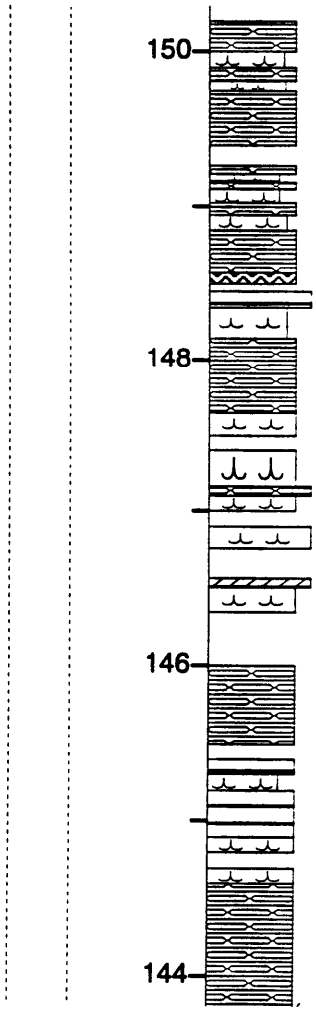
150
148
146
144

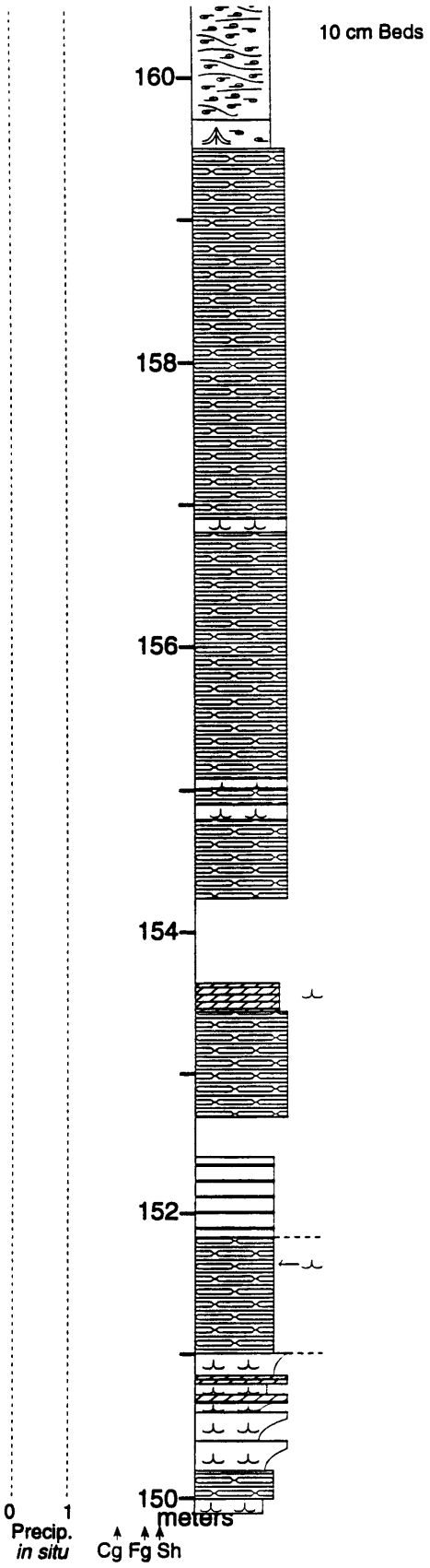
10 cm Beds
160
158
156
154
152
150
meters
0
1
Precip.
in situ
Cg
Fg
Sh

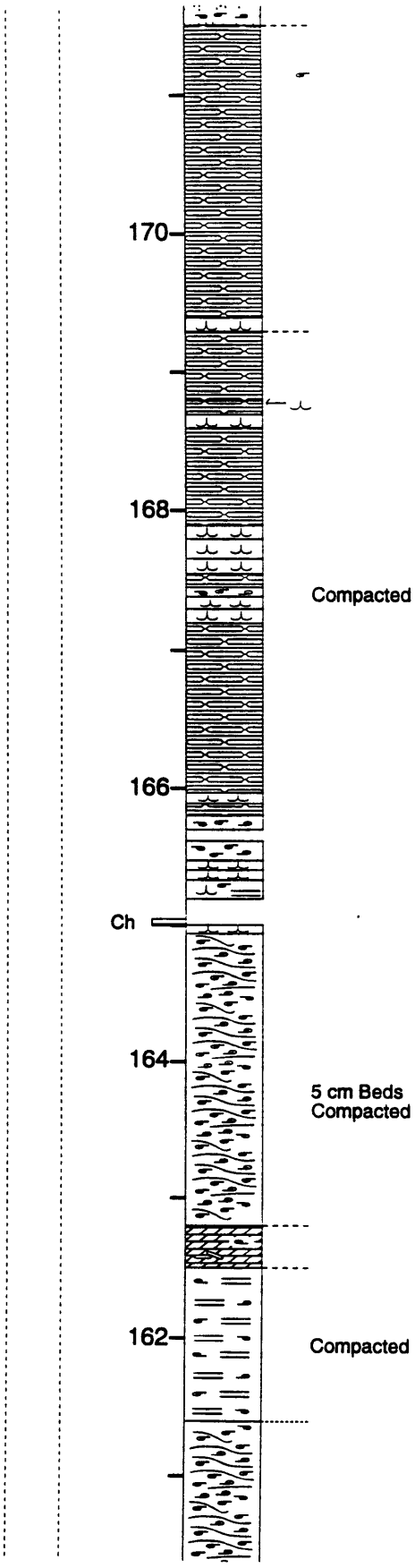
170
168
Compacted
166
Ch
164
5 cm Beds
Compacted
162
Compacted

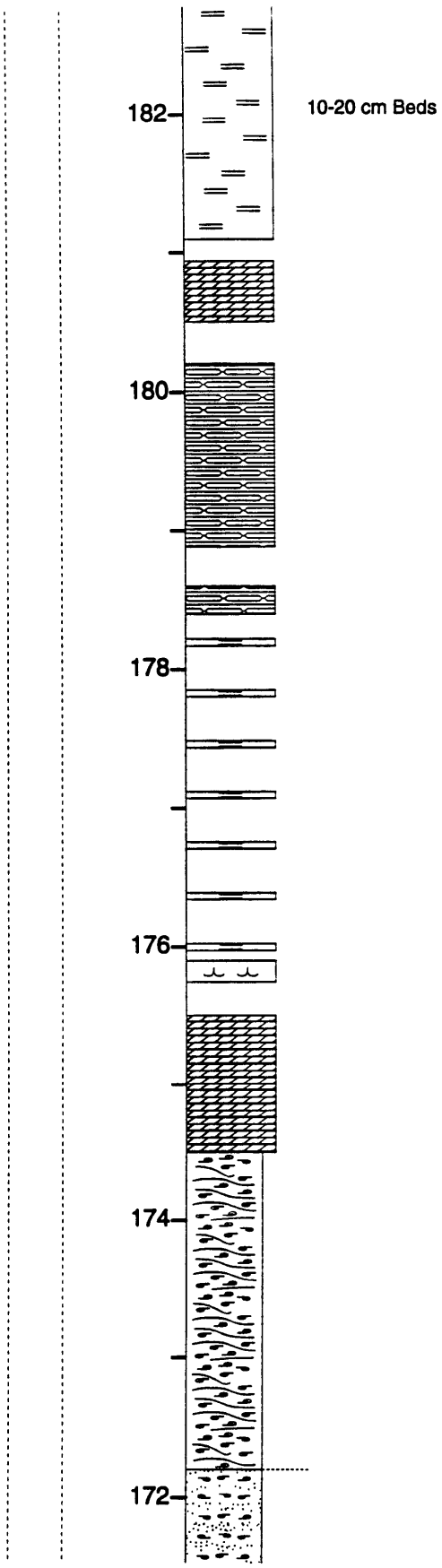
182
180
178
176
174
172
10-20 cm Beds

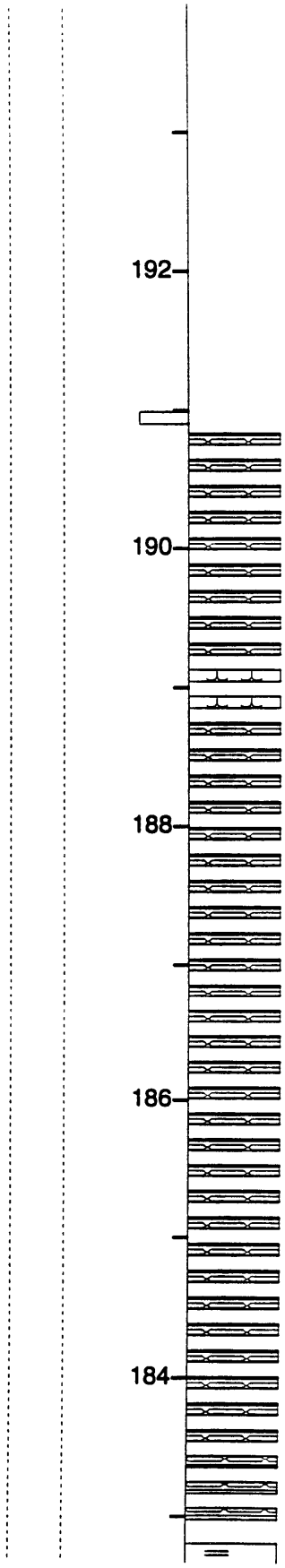
192
190
188
186
184

**Core BH74**

Location: Zeerust area. Stored at Rand Afrikaans University.

Stratigraphic Range: Middle of the Frisco Formation.

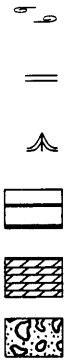

Rolled Up Laminae

Planar Laminae

Tented Microbialites

Coarsely Laminated Dolostone

Sucrosic Dolostone

Brecciated Dolostone (post sedimentary)

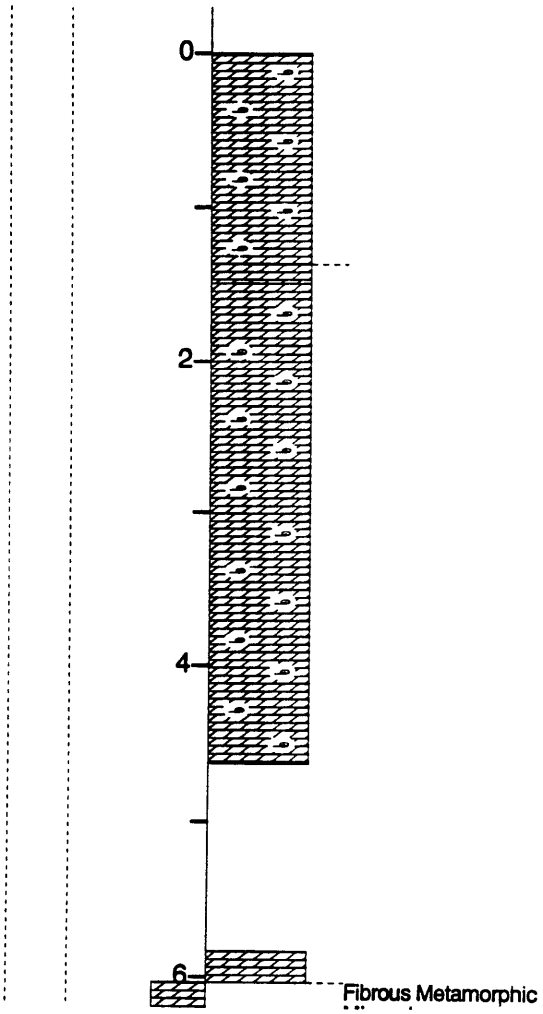
0
2
4
6
Fibrous Metamorphic

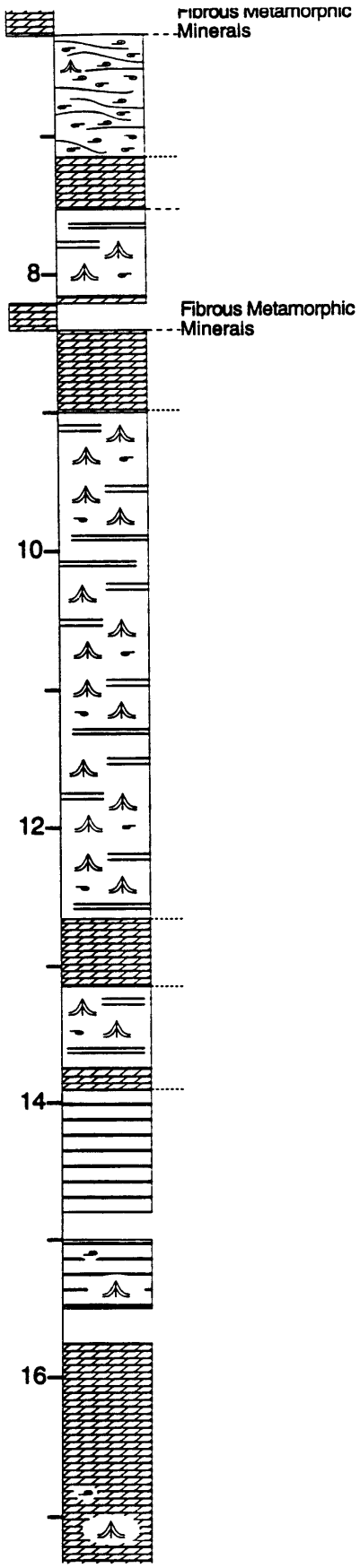
Fibrous Metamorphic Minerals
8
Fibrous Metamorphic Minerals
10
12
14
16

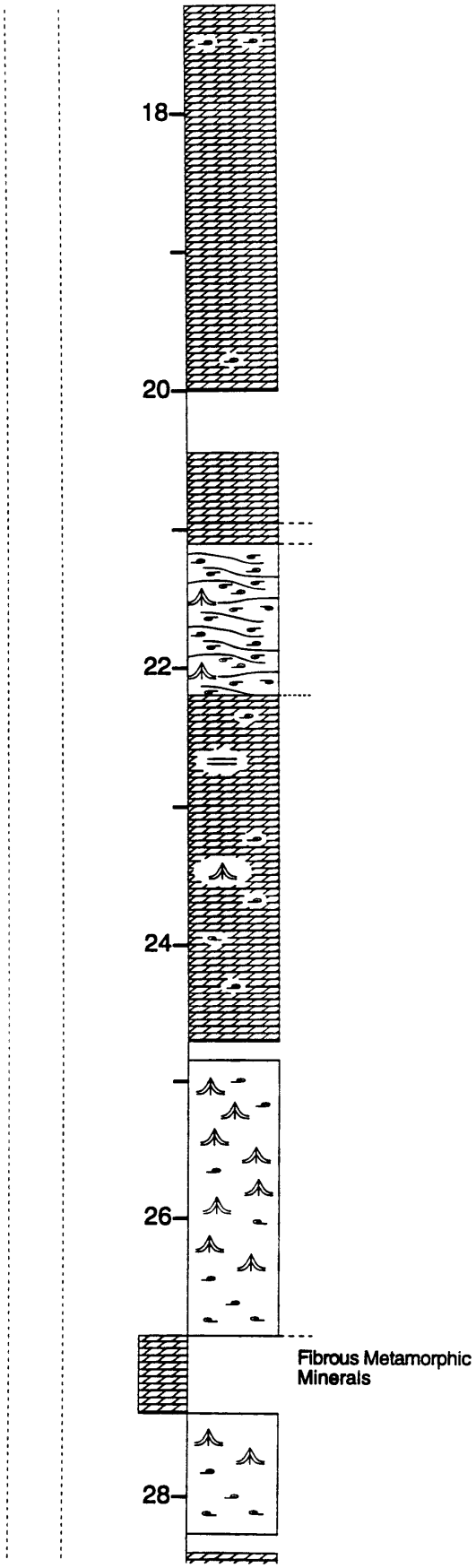
18
20
22
24
26
28
Fibrous Metamorphic
Minerals

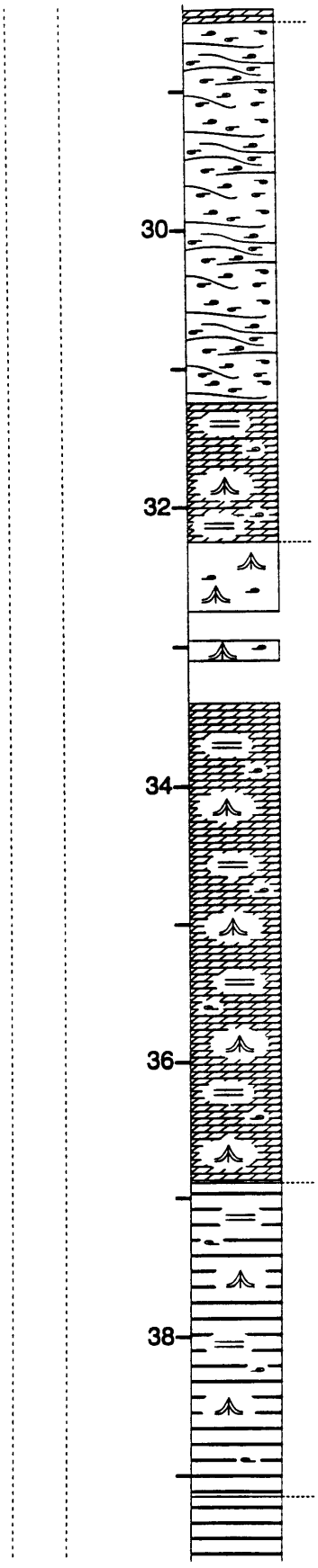
30
32
34
36
38

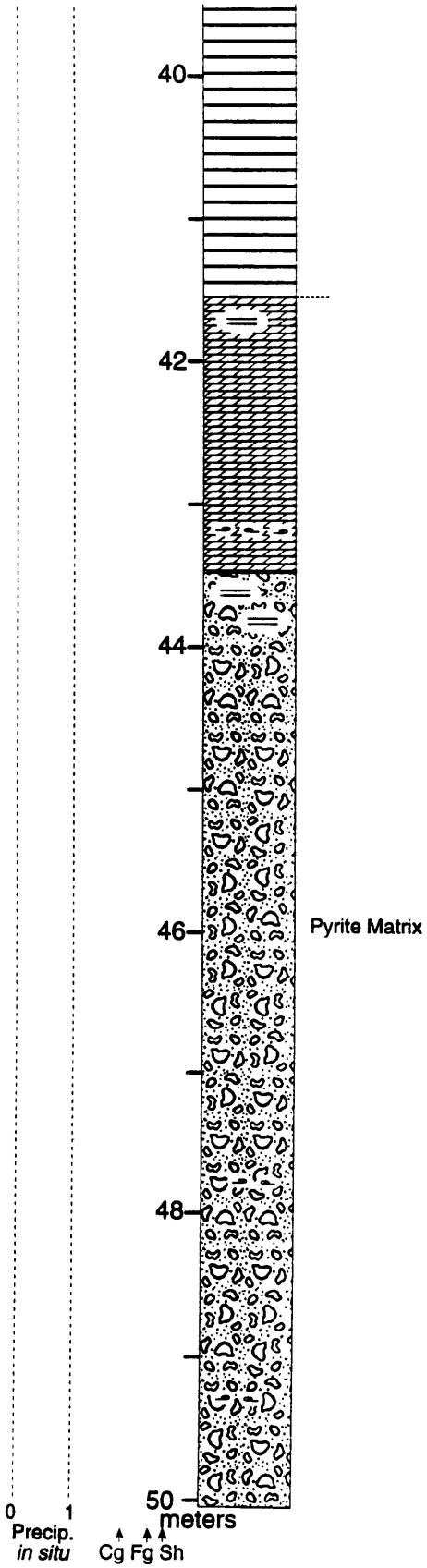
40
42
44
46
48
50
meters
Pyrite Matrix
0
1
Precip.
in situ
Cg Fg Sh

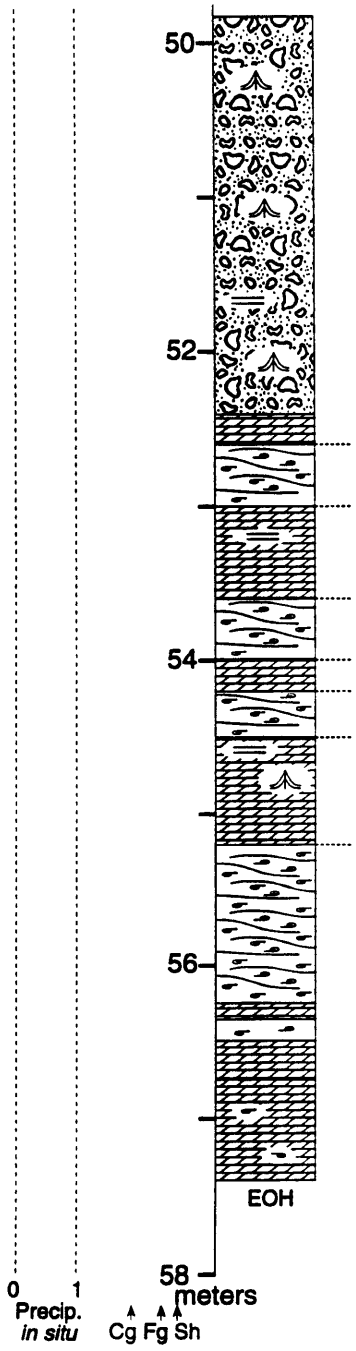
50
52
54
56
EOH
58
meters
0
1
Precip.
in situ
Cg Fg Sh

## Section DI

Location: 1 km north of Dinokana on far side of ridge.

Stratigraphic Range: Mid-Frisco Formation to base of Penge Iron Formation.

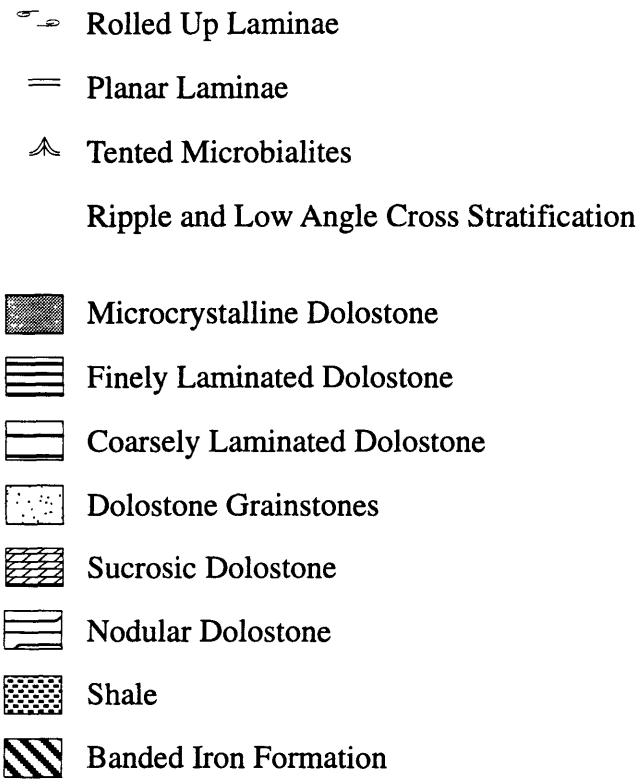

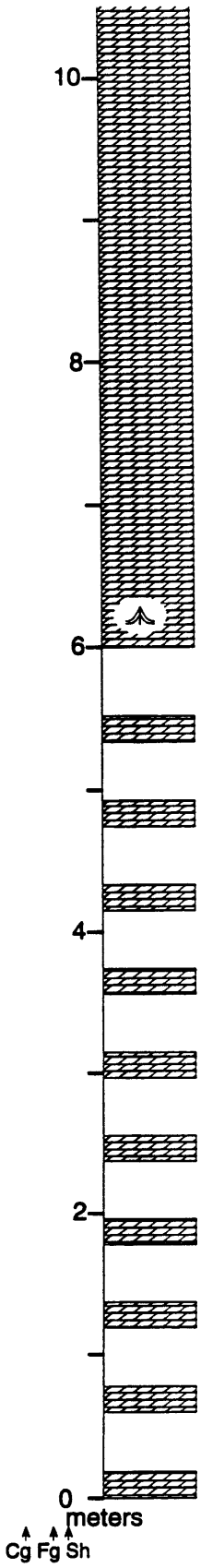
10
8
6
4
2
0
meters
Cg Fg Sh

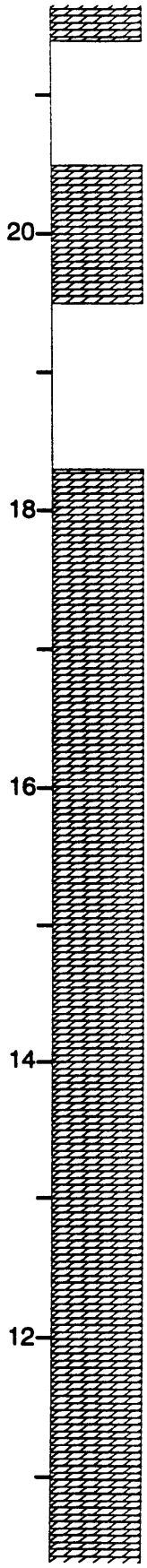
20
18
16
14
12

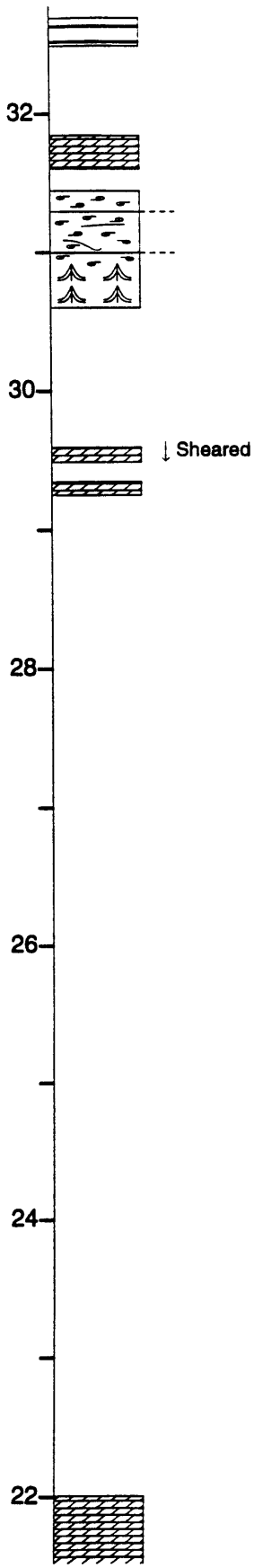
32
30
Sheared
28
26
24
22

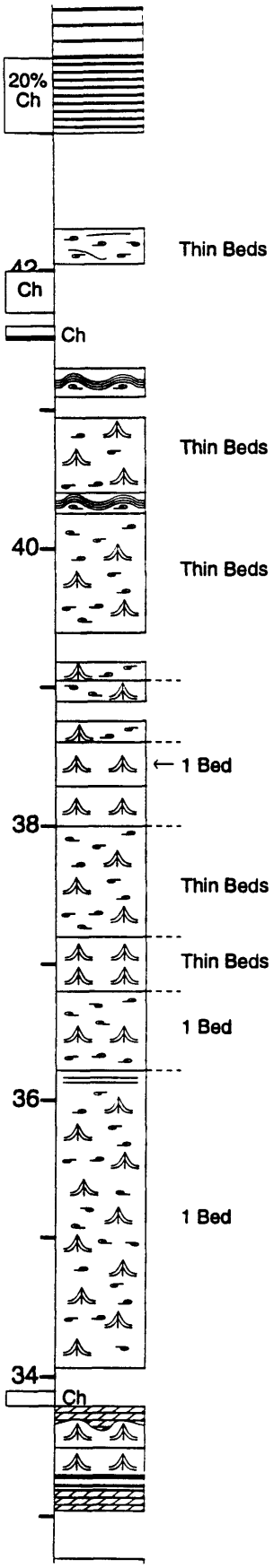
20%
Ch
Thin Beds
42
Ch
Ch
Thin Beds
40
Thin Beds
← 1 Bed
38
Thin Beds
Thin Beds
1 Bed
36
1 Bed
34
Ch

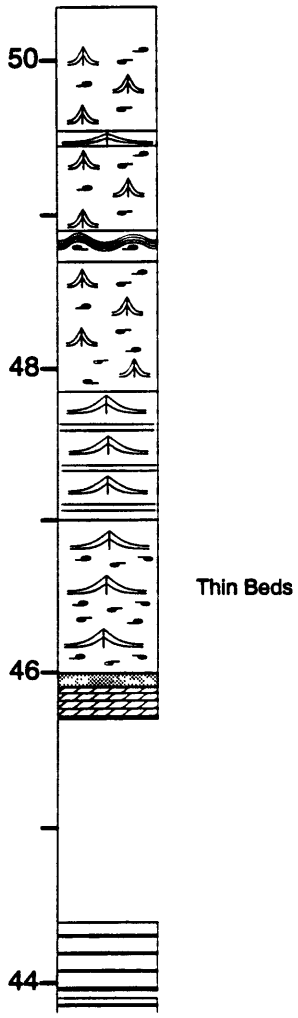
50
48
46
44
Thin Beds

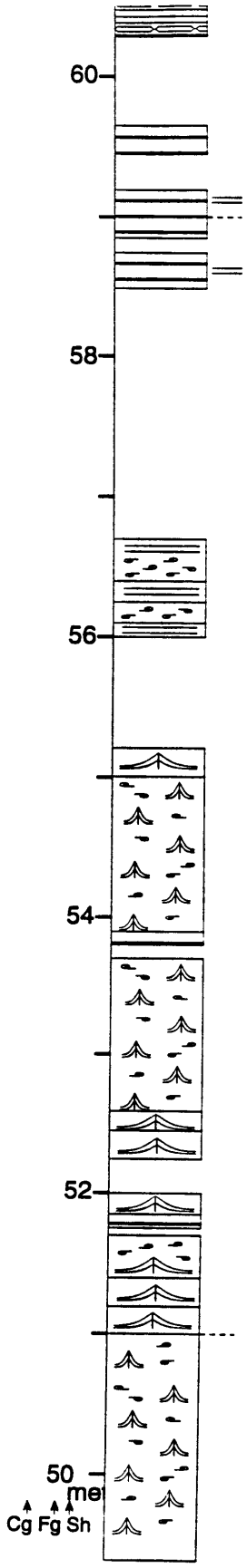
60
58
56
54
52
50
me
Cg Fg Sh

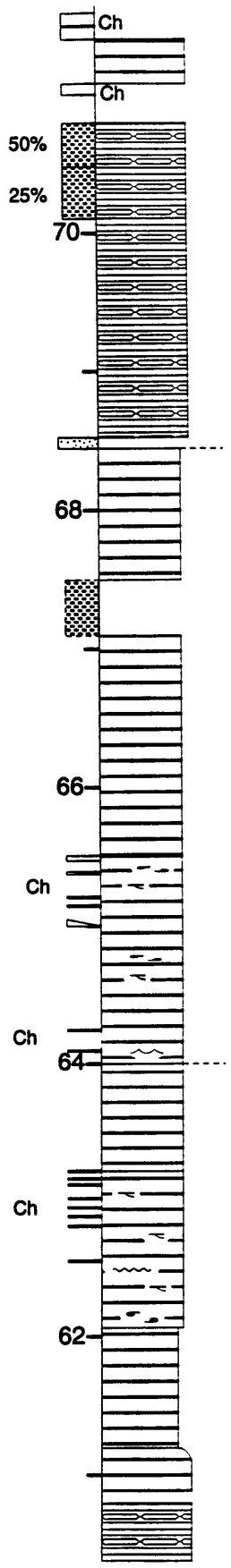
Ch
Ch
50%
25%
70
68
66
Ch
Ch
64
Ch
62

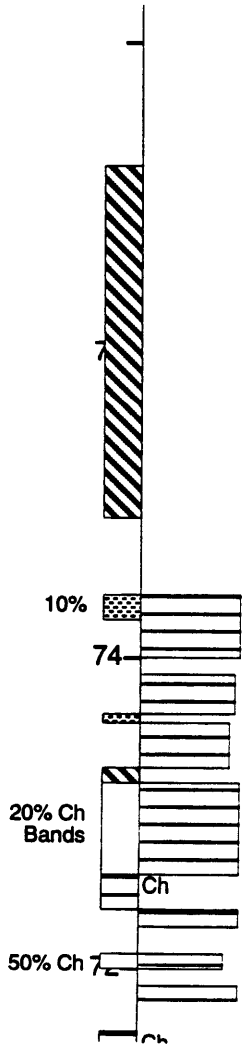
10%
74
20% Ch
Bands
Ch
50% Ch 7

## Section EC

Location: 10 km north of Echo Caves trun-off along road R36 towards Abel Erasmus Pass. Section in on the west side of the road starting at the road-cut containg shales and siltstones and continution up the slope and towards the south.

Stratigraphic Range: Base of Frisco Formation to upper Frisco Formation.

Notes: Large arrows mark the bases of cycles. Siliciclastic facies are plotted to the left of the column and carbonate facies are plotted to the right.

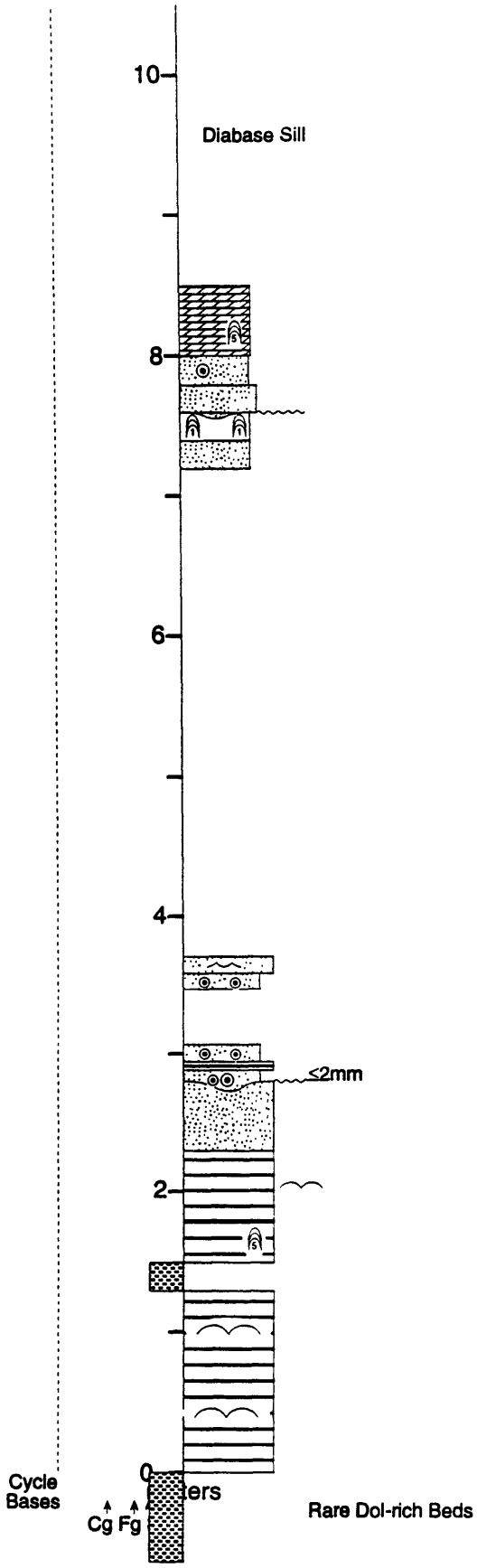
10
Diabase Sill
8
6
4
≤2mm
2
0
Cycle Bases
Cg Fg
Rare Dol-rich Beds

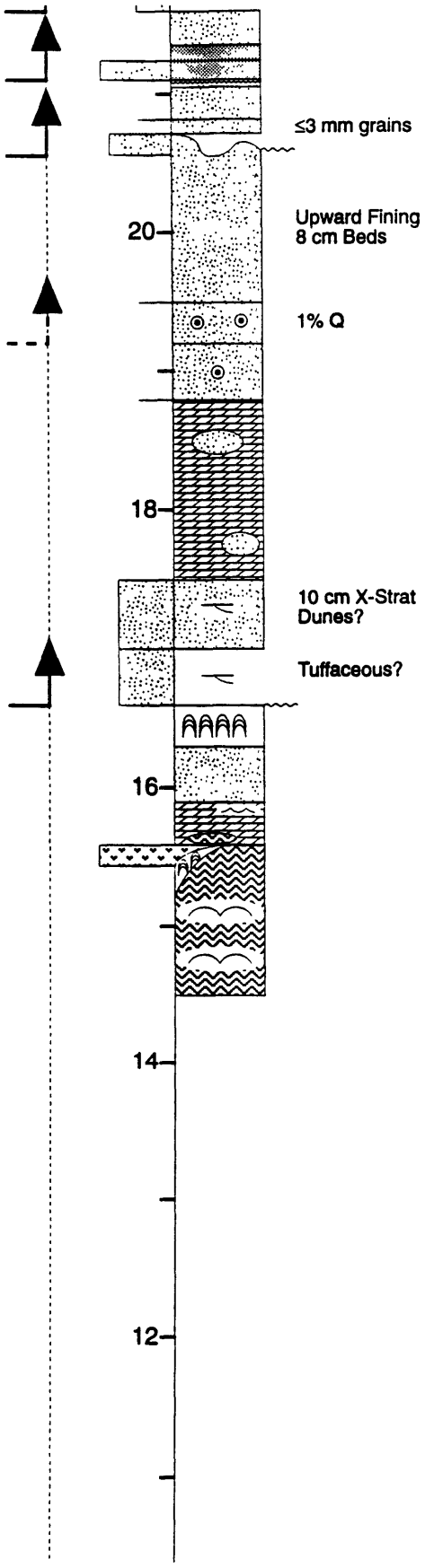
≤3 mm grains
Upward Fining
8 cm Beds
1% Q
10 cm X-Strat
Dunes?
Tuffaceous?
20
18
16
14
12

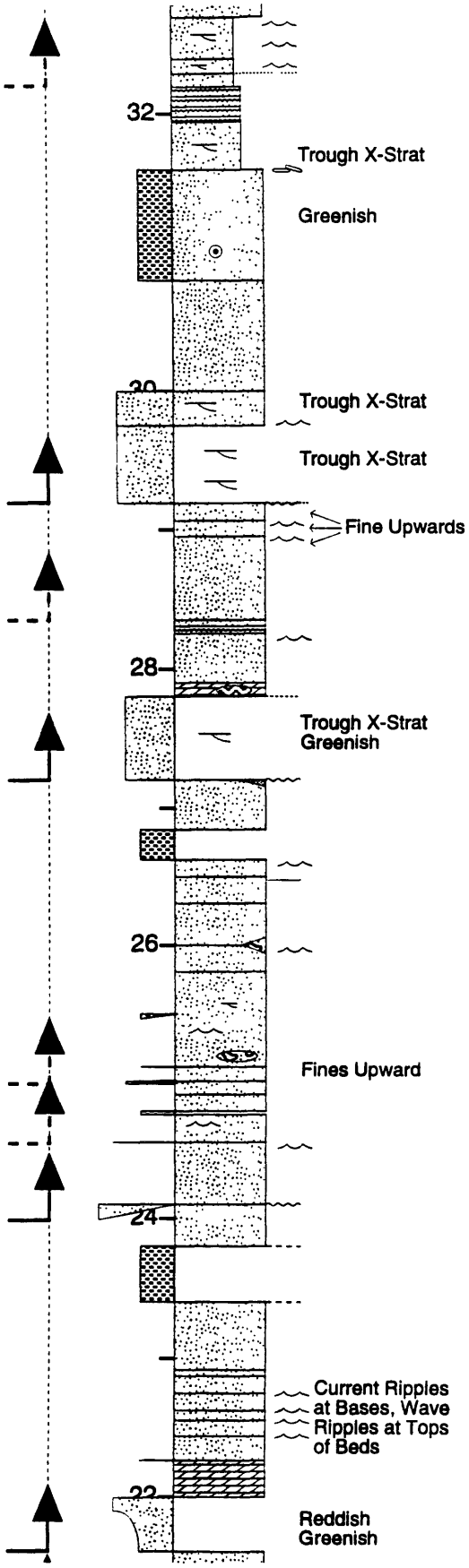
32
Trough X-Strat
Greenish
30
Trough X-Strat
Trough X-Strat
Fine Upwards
28
Trough X-Strat
Greenish
26
Fines Upward
24
Current Ripples
at Bases, Wave
Ripples at Tops
of Beds
22
Reddish
Greenish

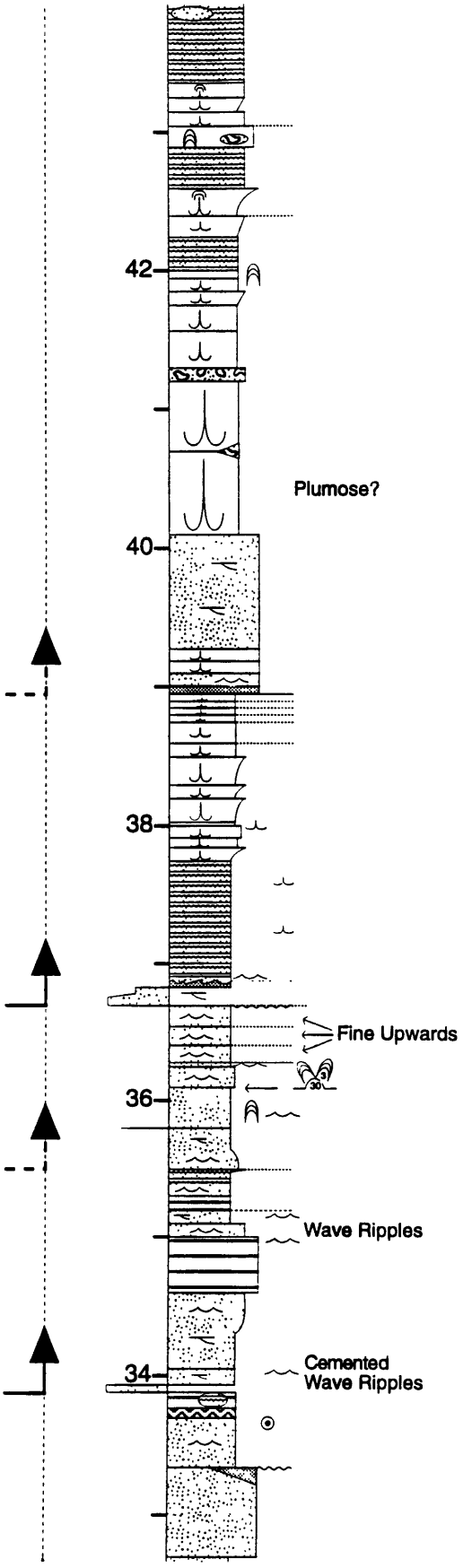
42
Plumose?
40
38
Fine Upwards
36
Wave Ripples
34
Cemented
Wave Ripples

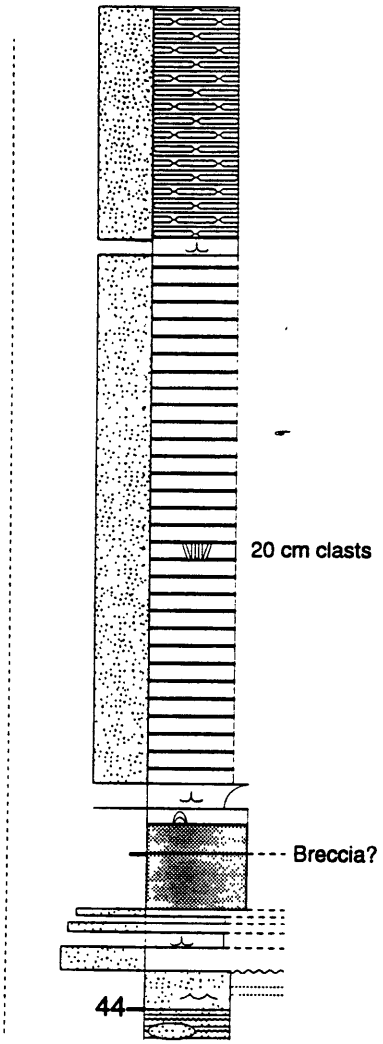
20 cm clasts
Breccia?
44

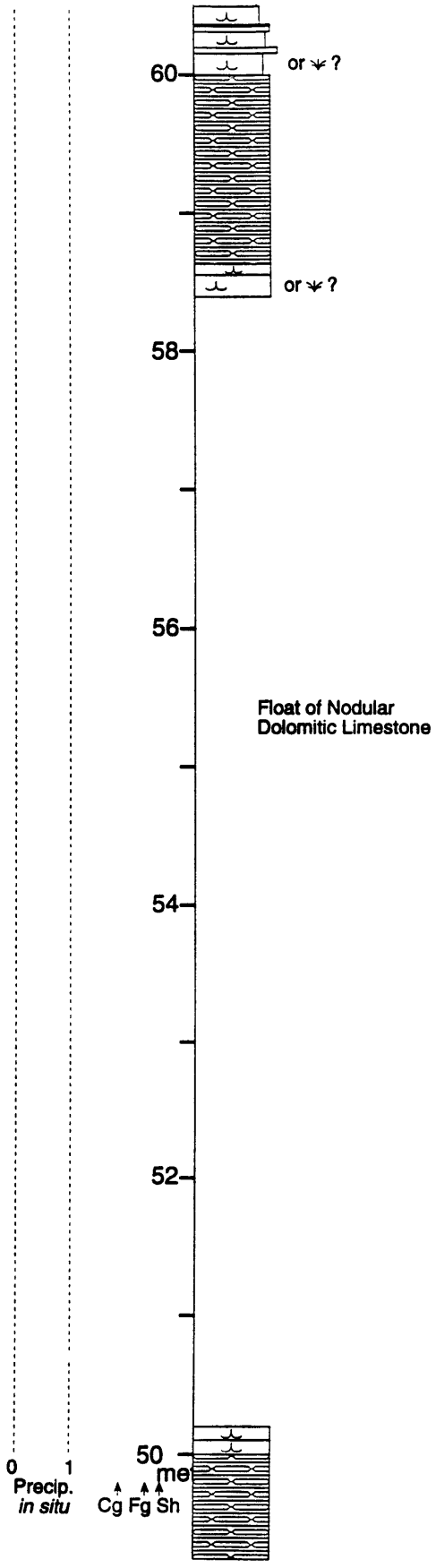
or ⊻ ?
60
or ⊻ ?
58
56
Float of Nodular
Dolomitic Limestone
54
52
50
0
1
Precip.
in situ
Cg Fg Sh
me

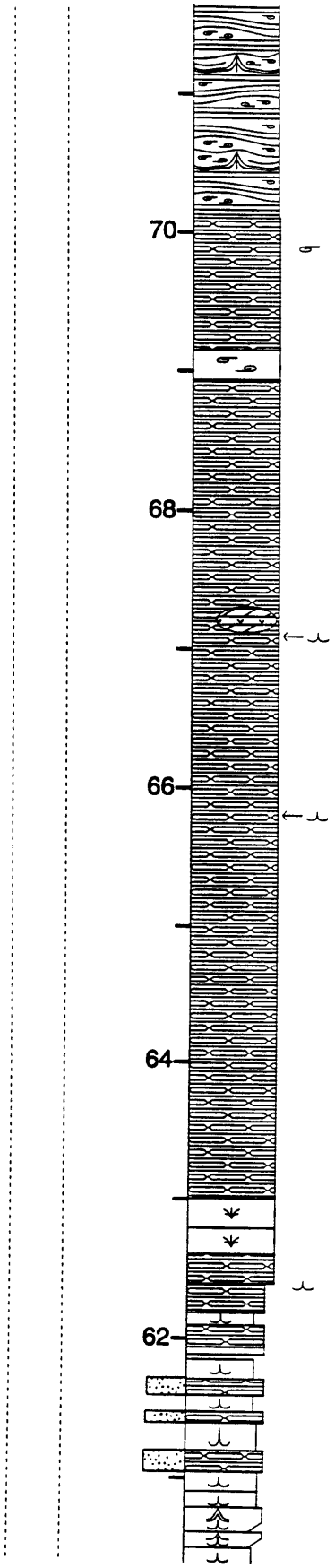
70
68
66
64
62

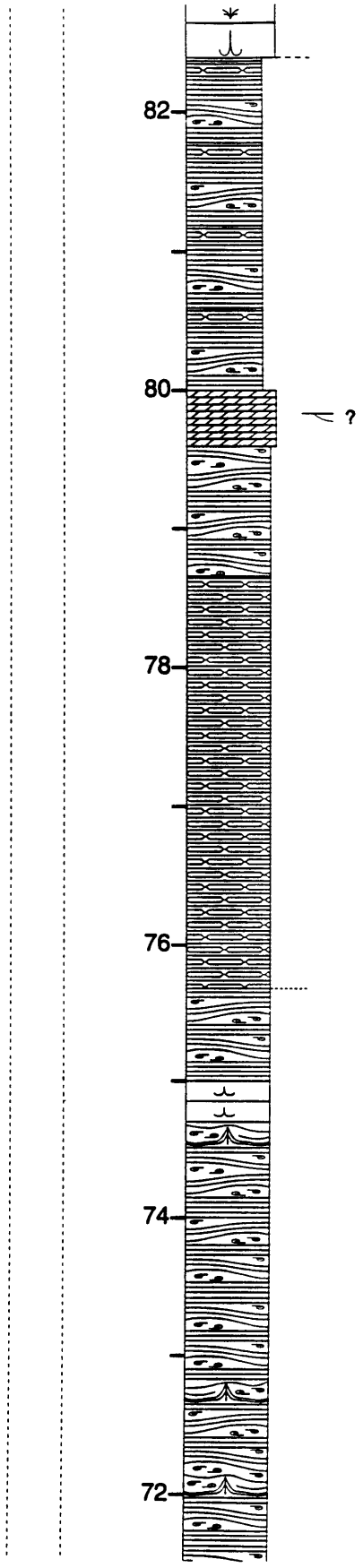
82
80
?
78
76
74
72

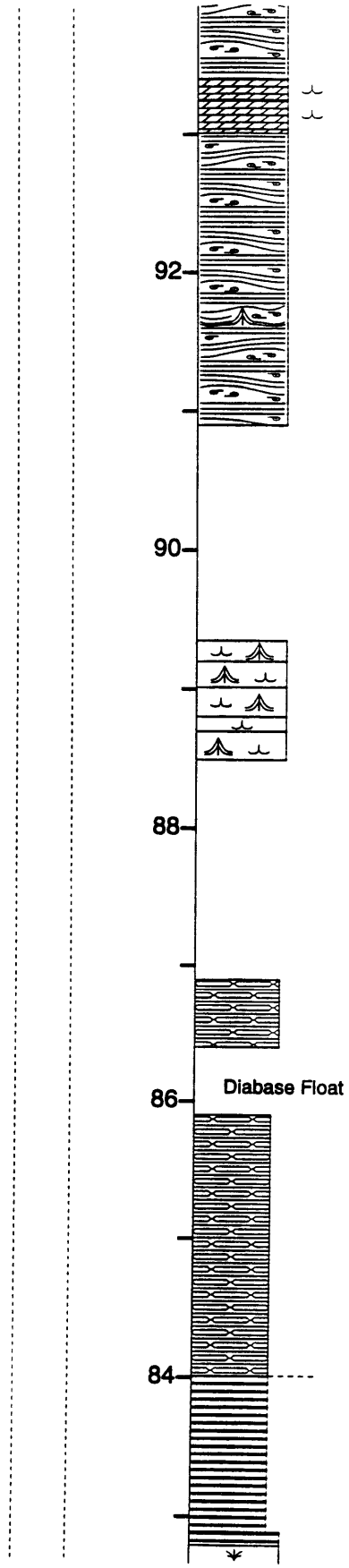
92
90
88
86
Diabase Float
84

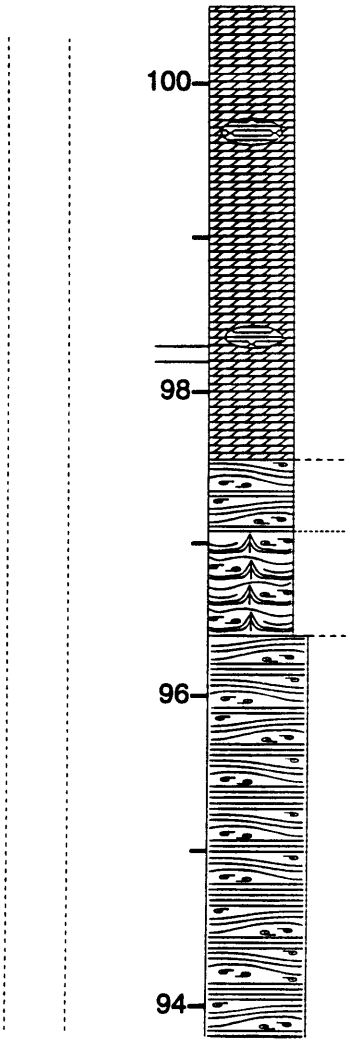
100
98
96
94

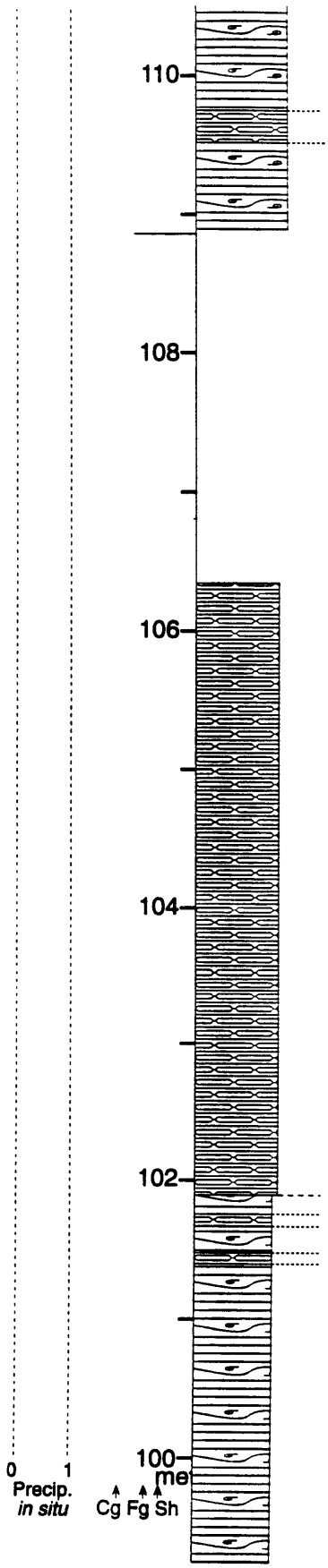
110
108
106
104
102
100
me
0
1
Precip.
in situ
Cg Fg Sh

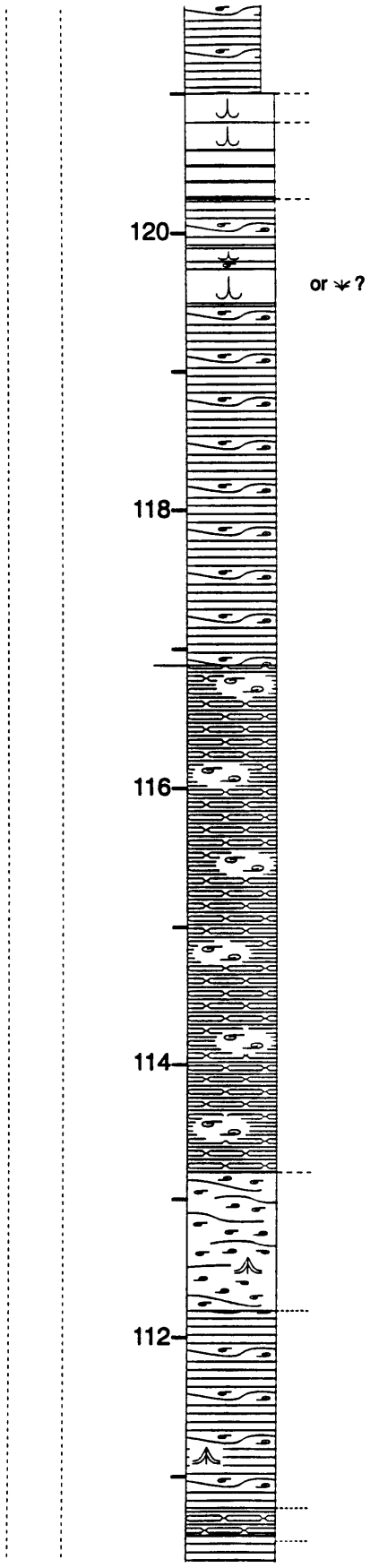
120
or ⊻ ?
118
116
114
112

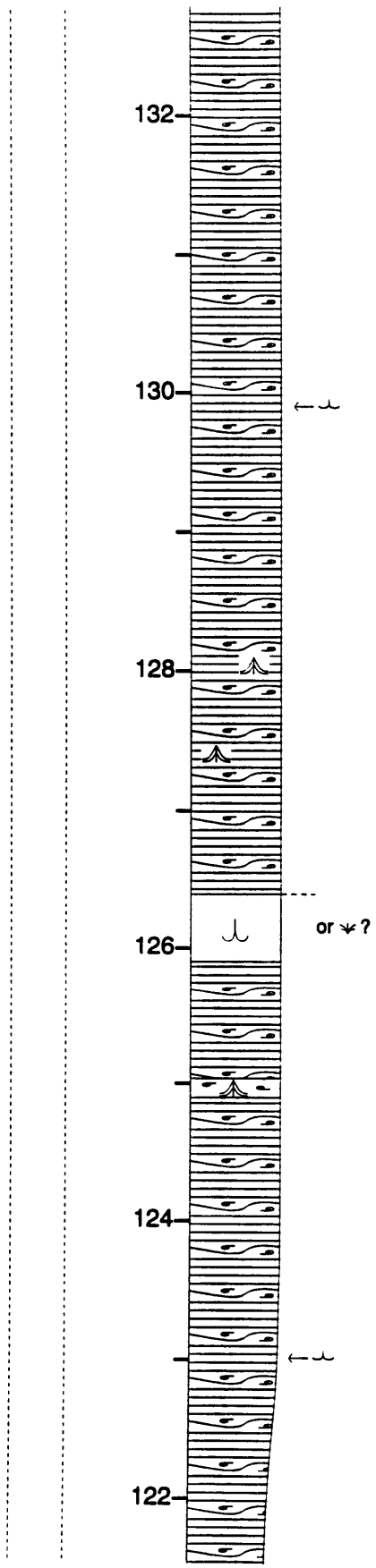
132
130
128
126
124
122
or ?

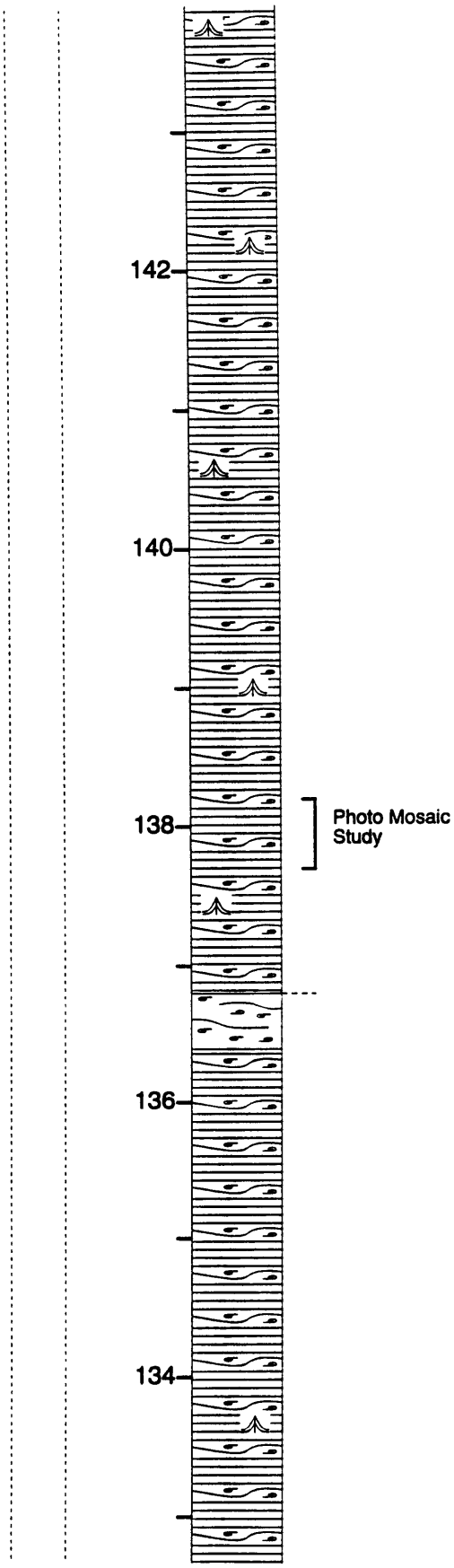
142
140
138
136
134
Photo Mosaic
Study

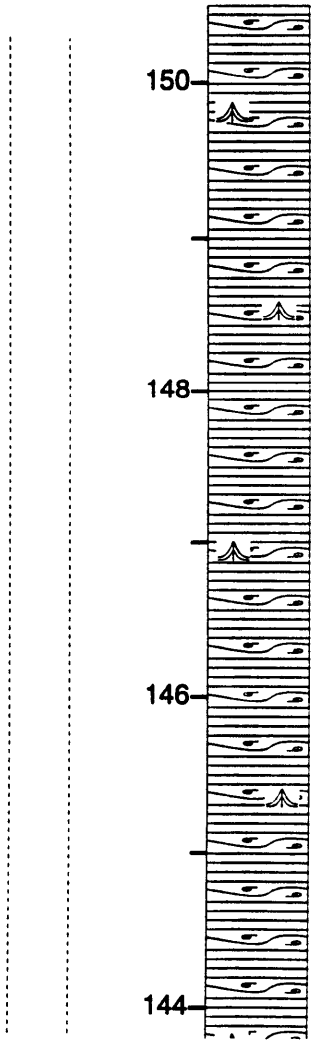
150
148
146
144

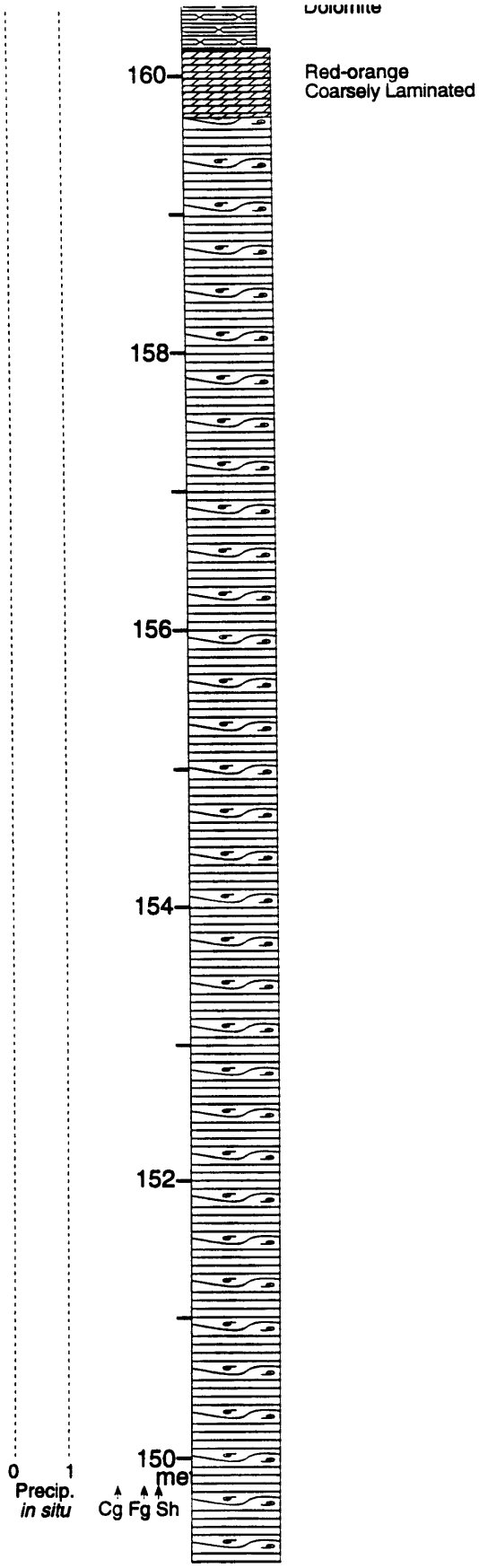
Dolomite
Red-orange
Coarsely Laminated
160
158
156
154
152
150
me
0
1
Precip.
in situ
Cg Fg Sh

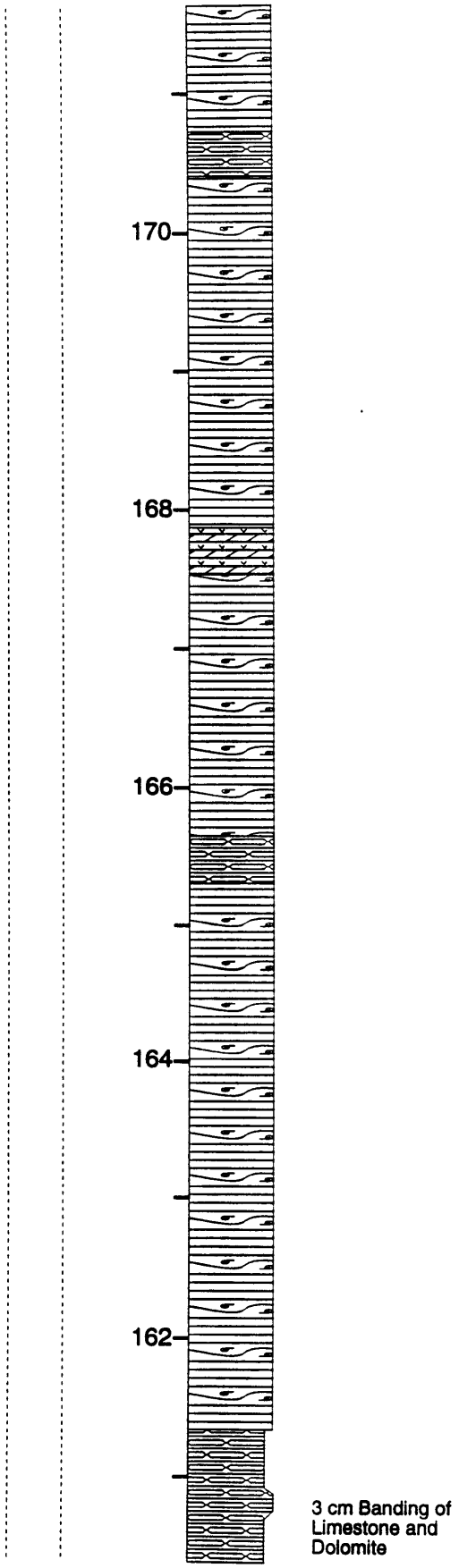
170
168
166
164
162
3 cm Banding of
Limestone and
Dolomite

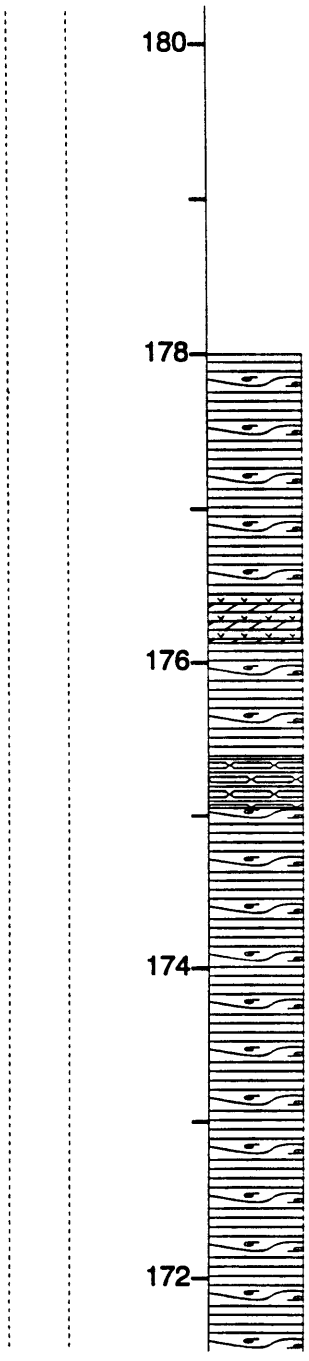
180
178
176
174
172

## Section MA

Location: On Makapan Farm, near Nuwe Smitsdorp east of road N1 between Potgietersrus and Pietersburg.

Stratigraphic Range: Base of Frisco Formation to mid-Frisco Formation.

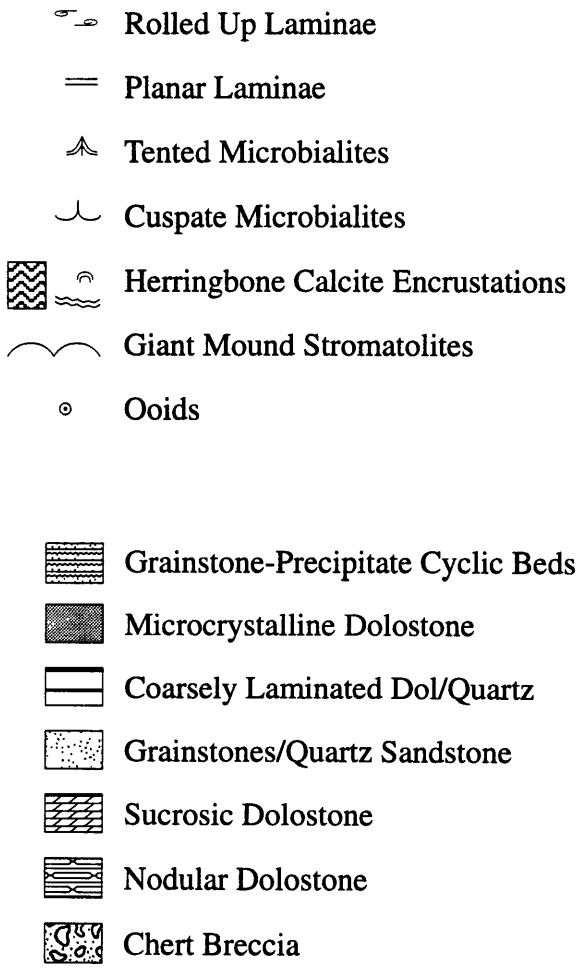

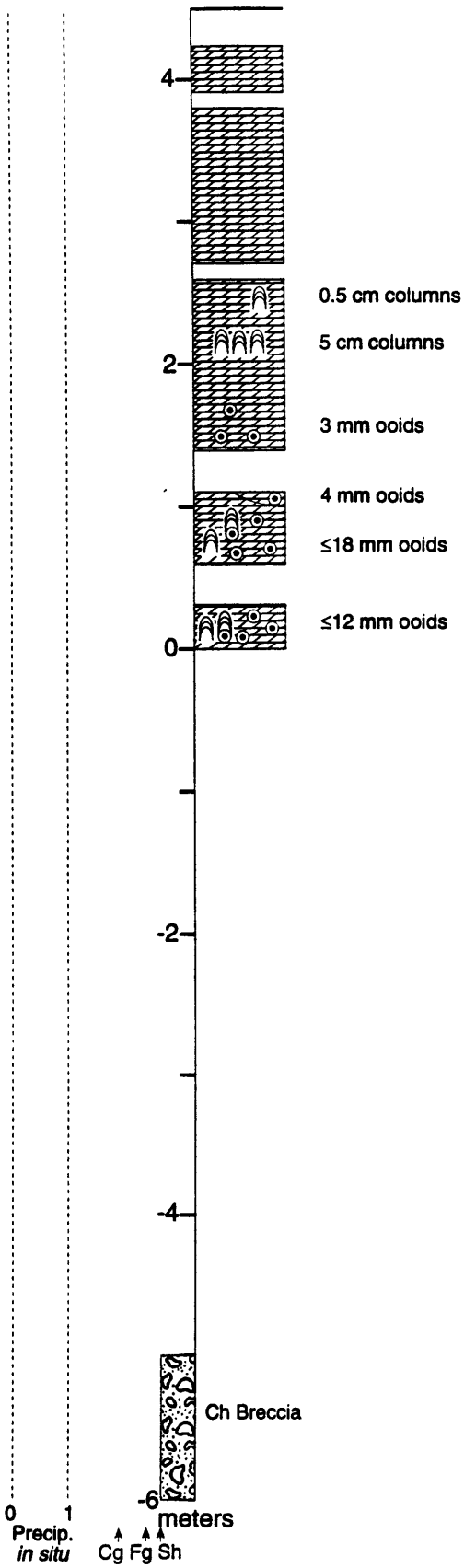
4
2
0
-2
-4
-6
0.5 cm columns
5 cm columns
3 mm ooids
4 mm ooids
≤18 mm ooids
≤12 mm ooids
Ch Breccia
0
1
meters
Precip.
in situ
Cg Fg Sh

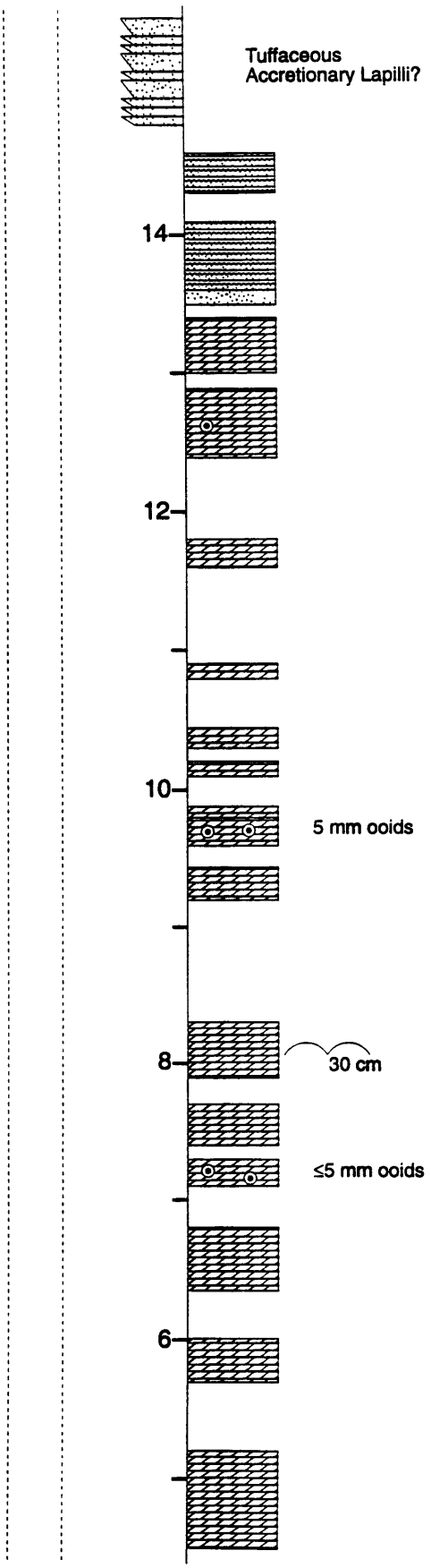
Tuffaceous
Accretionary Lapilli?
14
12
10
5 mm ooids
8
30 cm
≤5 mm ooids
6

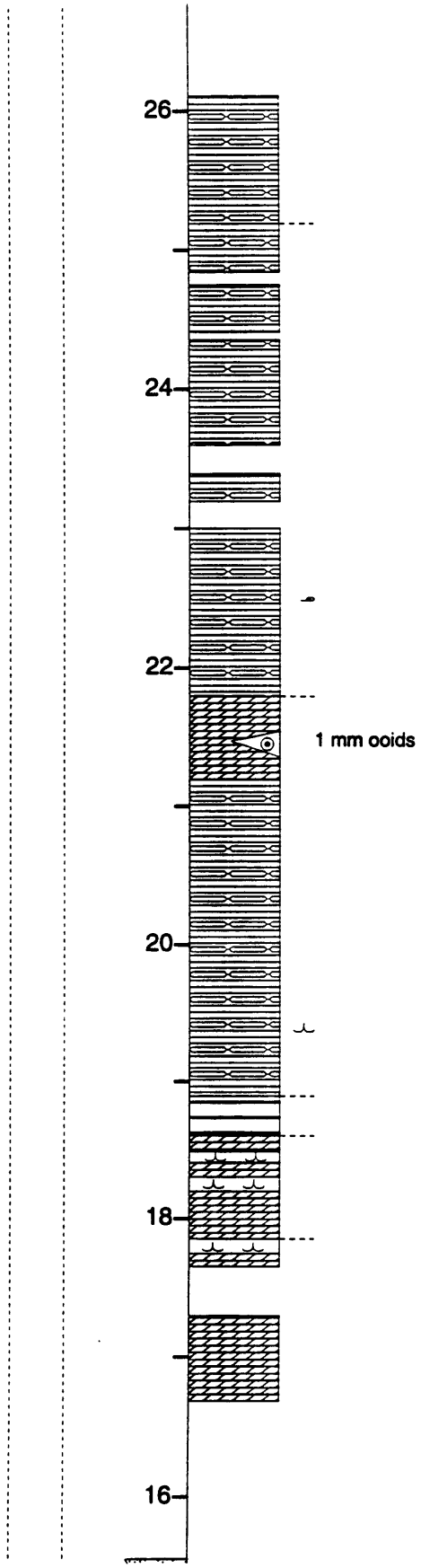
26
24
22
1 mm ooids
20
18
16

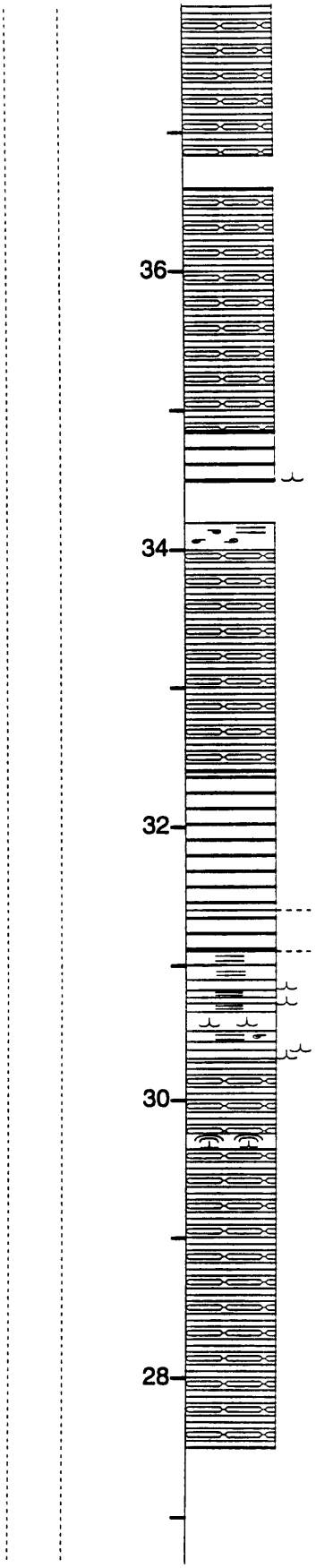
36
34
32
30
28

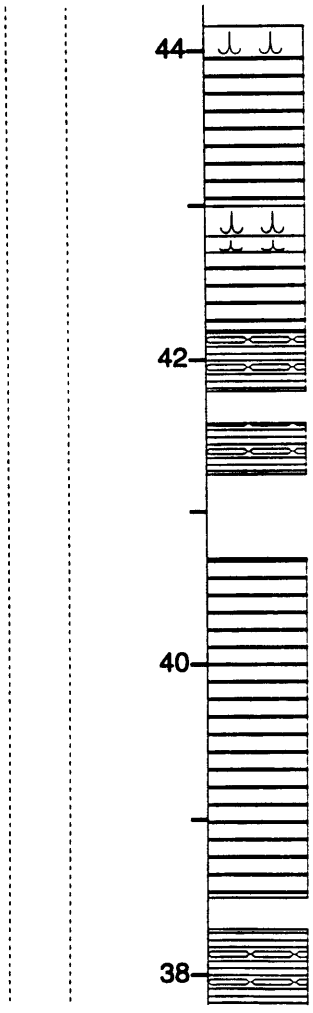
44
42
40
38

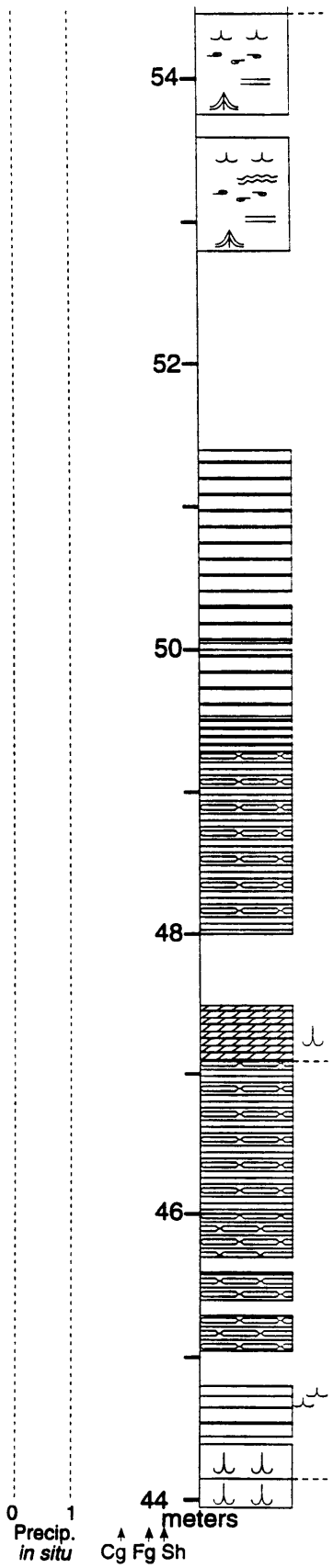
54
52
50
48
46
44
meters
0
1
Precip.
in situ
Cg Fg Sh

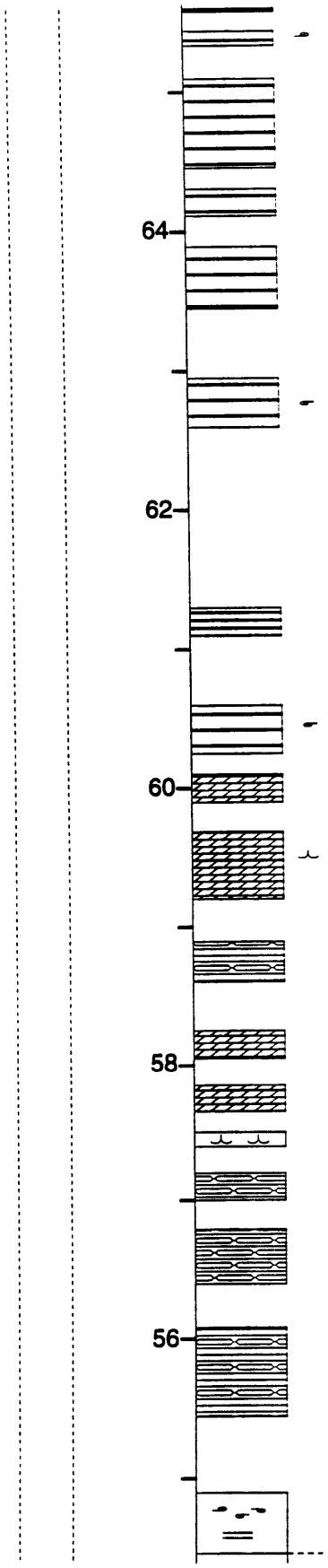
64
62
60
58
56

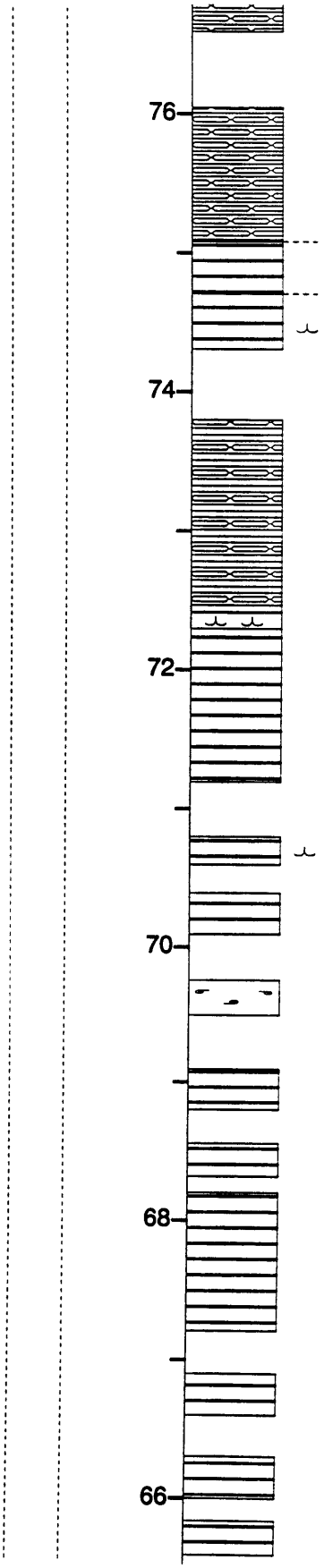
76
74
72
70
68
66

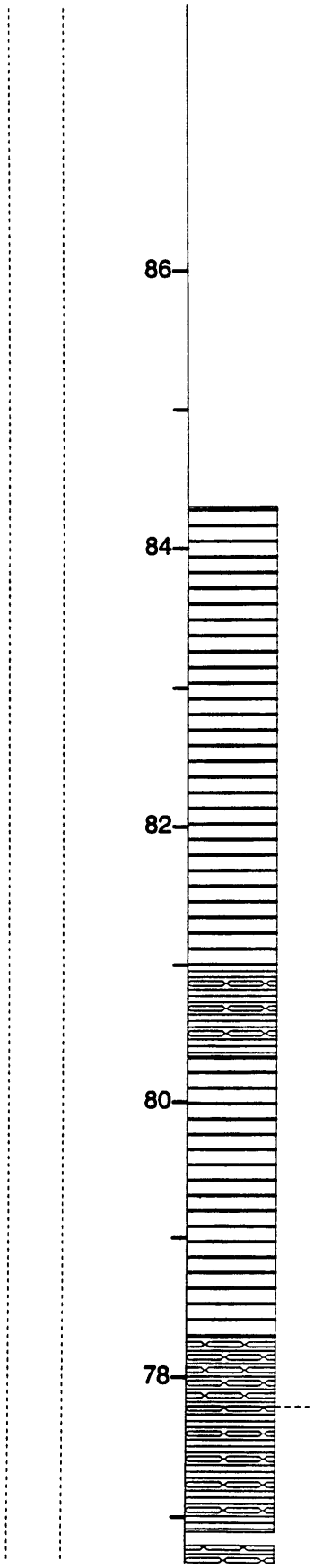
86
84
82
80
78

## Section Rd f

Location: Rotterdam Farm, northwest of Thabazimbi.

Stratigraphic Range: Top of Eccles Formation to base of the Penge Iron Formation. The base of the Frisco Formation is at 4 m and corresponds to 1190 m in section RD.

Notes: Siliciclastic facies are plotted to the left of the column and carbonate facies are plotted to the right.

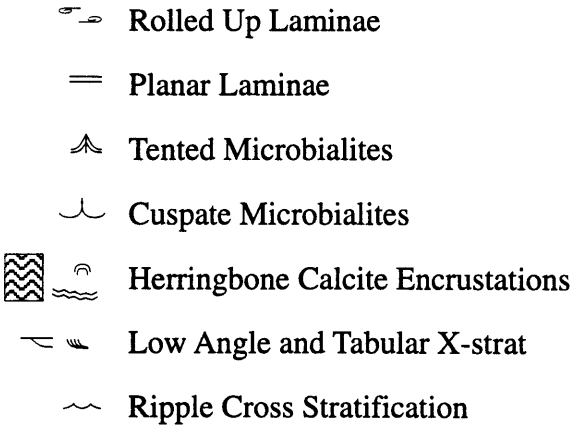


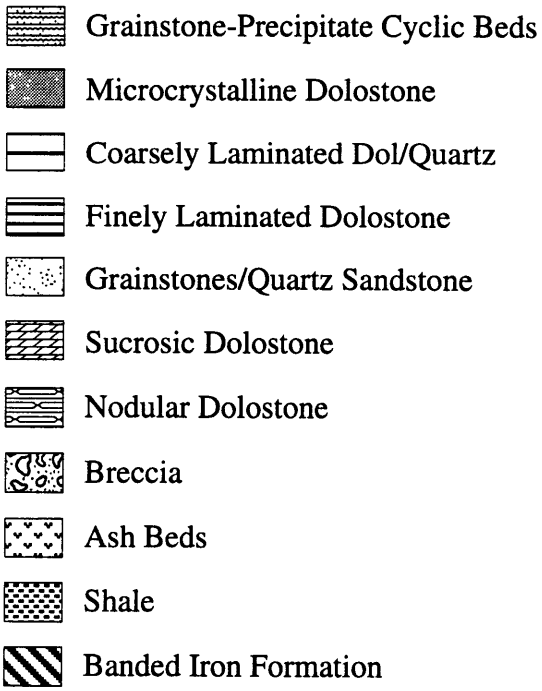

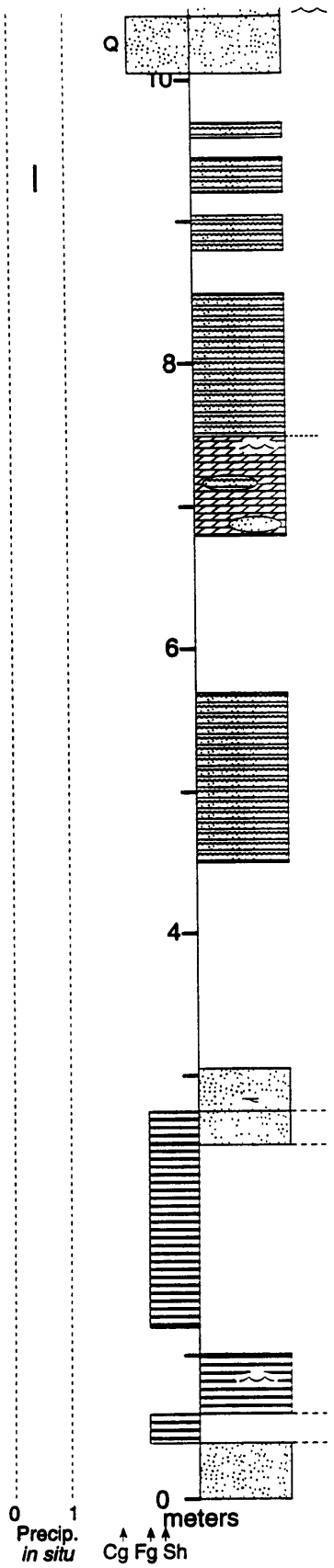
Q
10
8
6
4
0
meters
0
1
Precip.
in situ
Cg Fg Sh

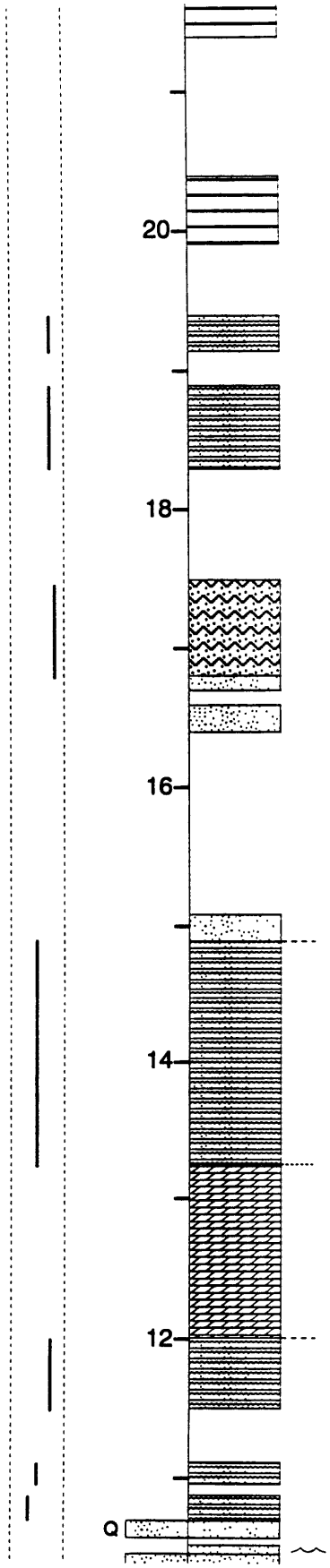
20
18
16
14
12
Q

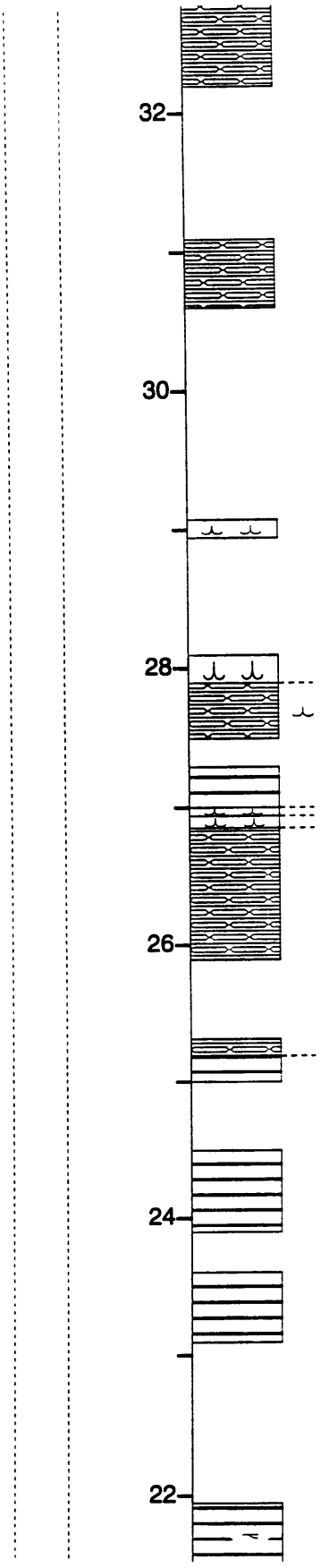
32
30
28
26
24
22

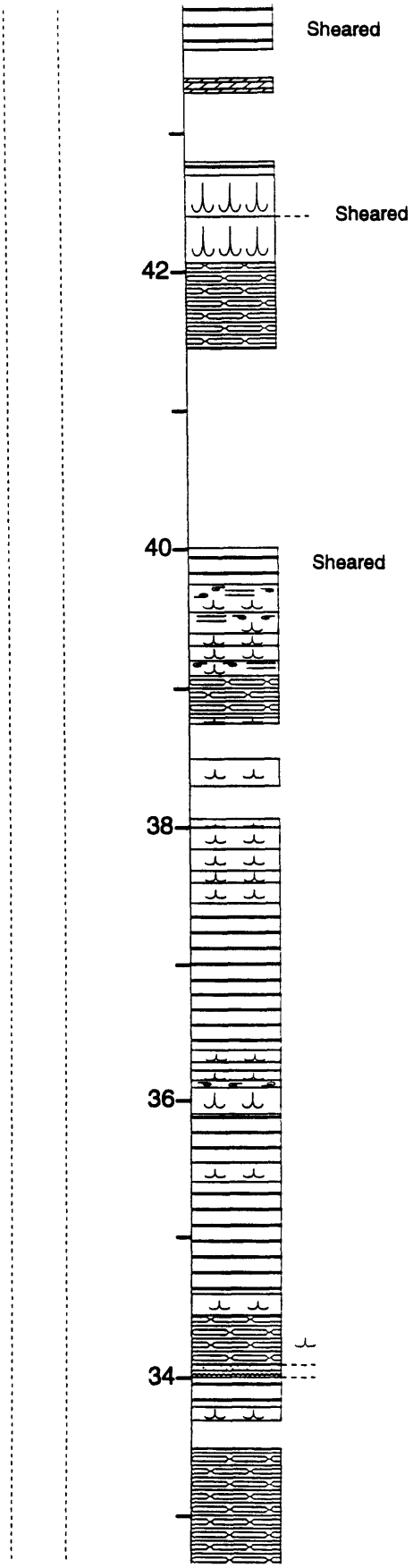
Sheared
Sheared
42
40
Sheared
38
36
34

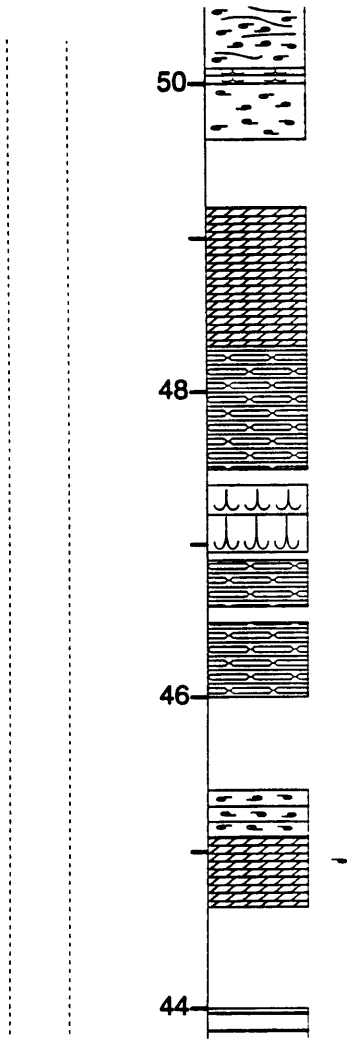
50
48
46
44

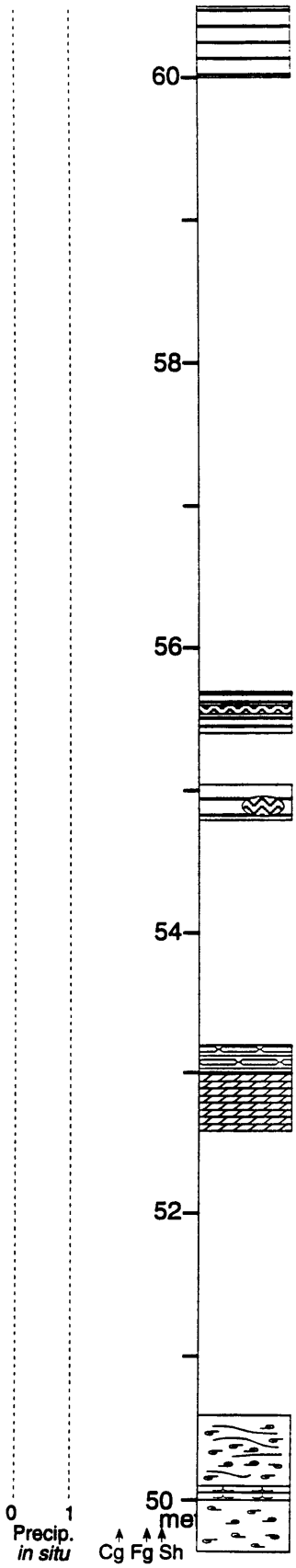
60
58
56
54
52
50
0
1
Precip.
in situ
Cg Fg Sh

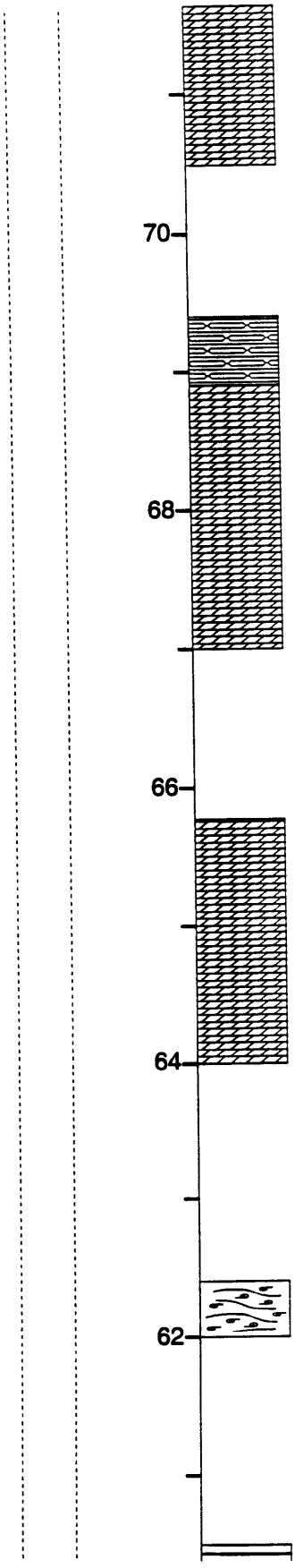
70
68
66
64
62

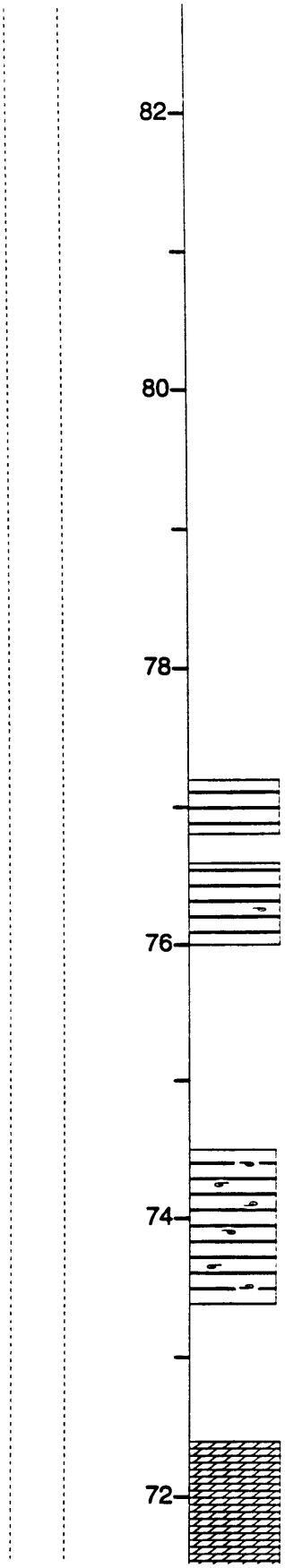
82
80
78
76
74
72

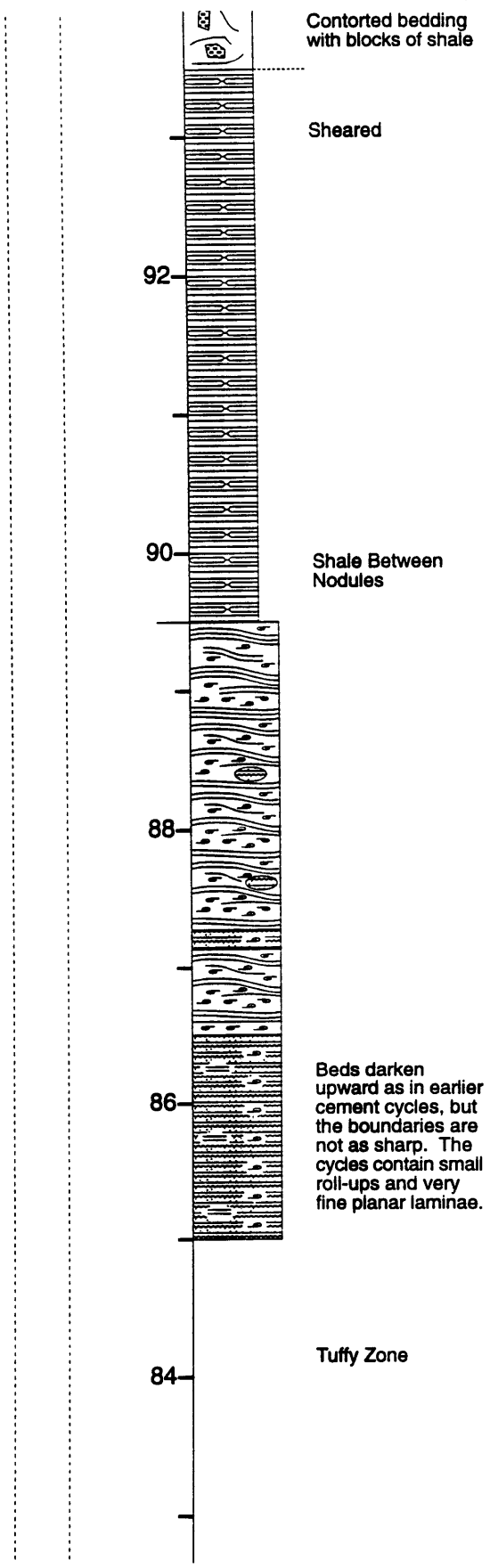
Contorted bedding with blocks of shale
Sheared
92
90
Shale Between Nodules
88
Beds darken upward as in earlier cement cycles, but the boundaries are not as sharp. The cycles contain small roll-ups and very fine planar laminae.
86
Tuffy Zone
84

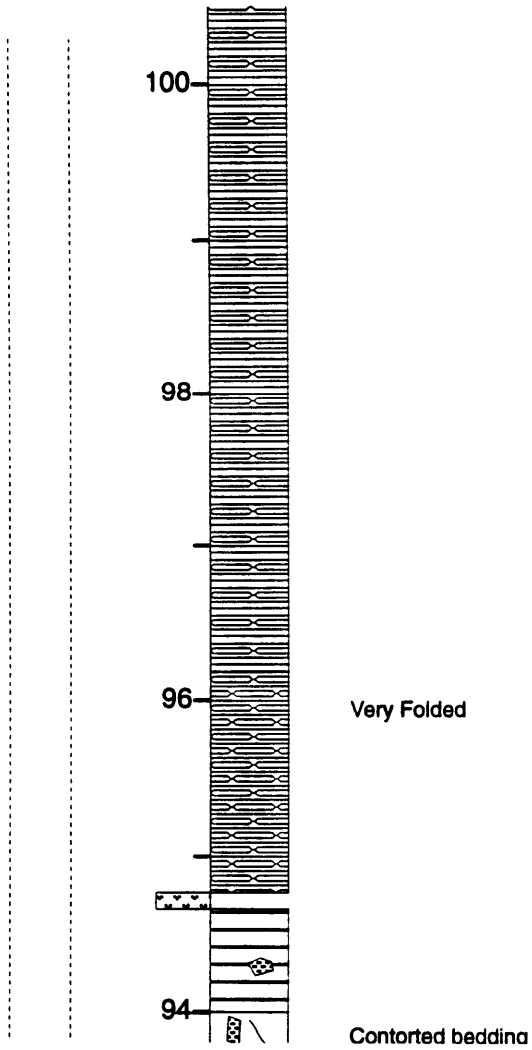
100
98
96
94
Very Folded
Contorted bedding

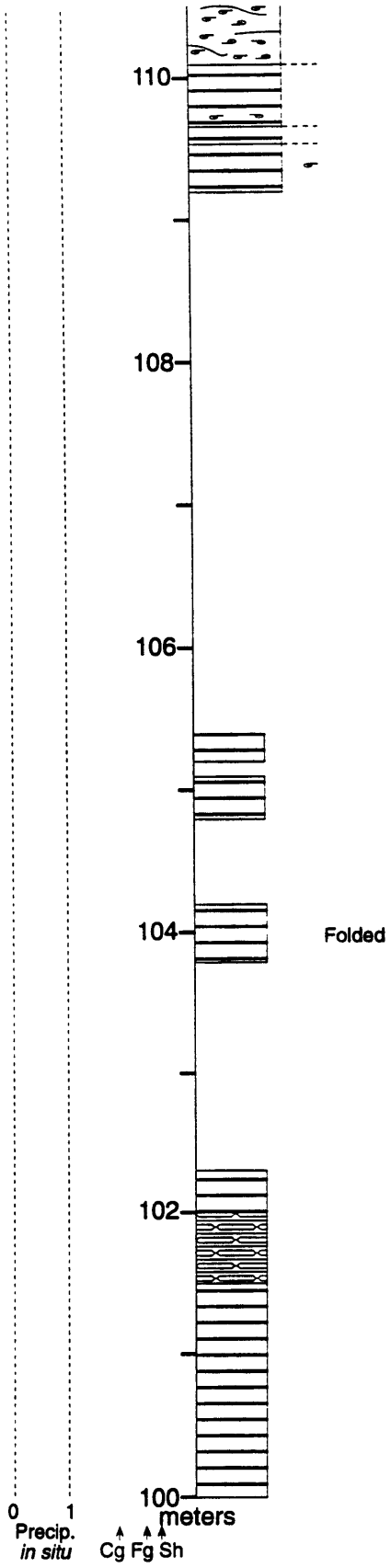
110
108
106
104
102
100
Folded
0
1
Precip.
in situ
Cg Fg Sh
meters

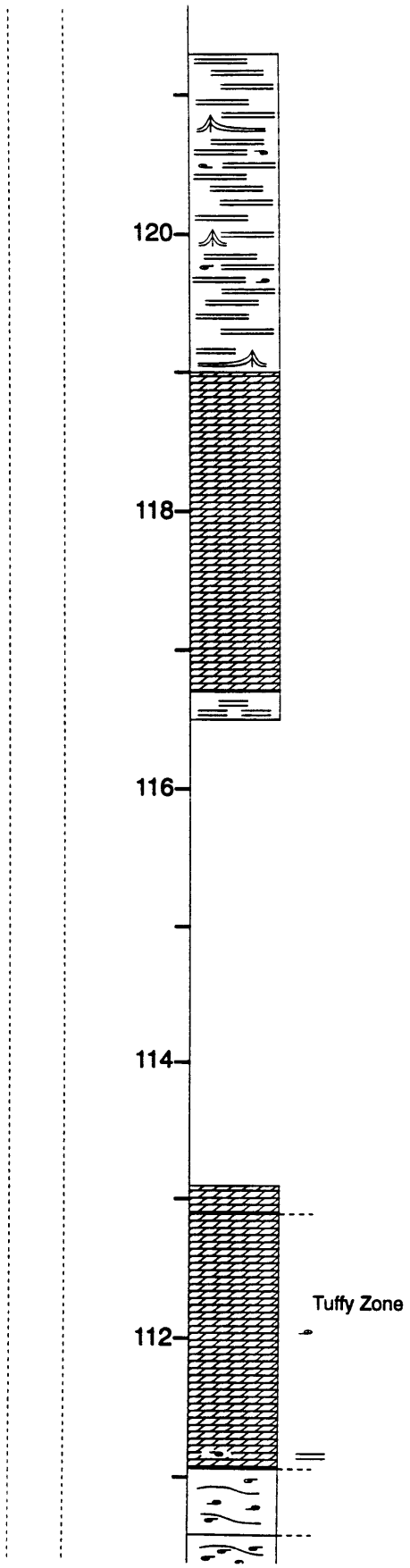
120
118
116
114
112
Tuffy Zone

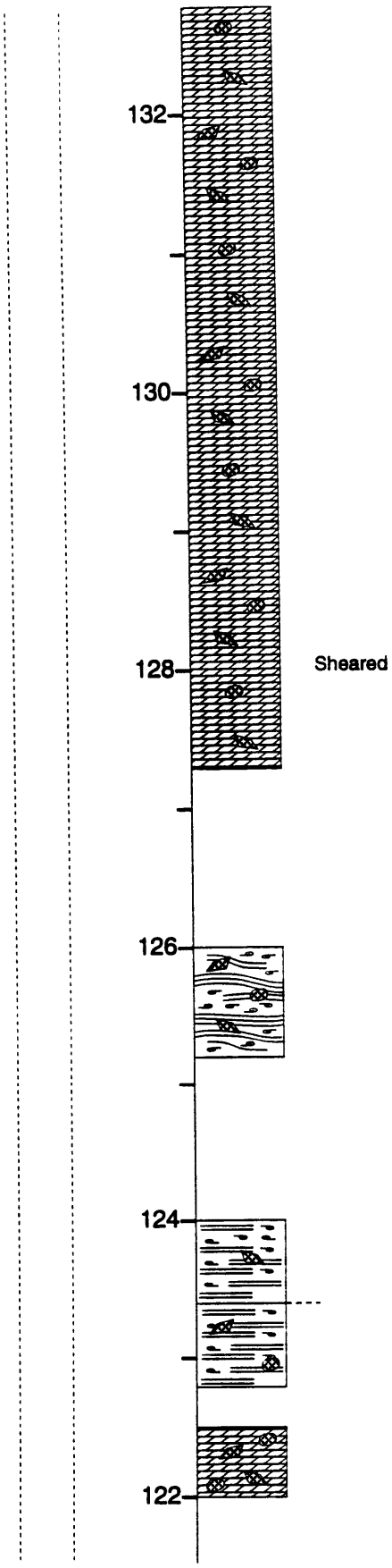
132
130
128
Sheared
126
124
122

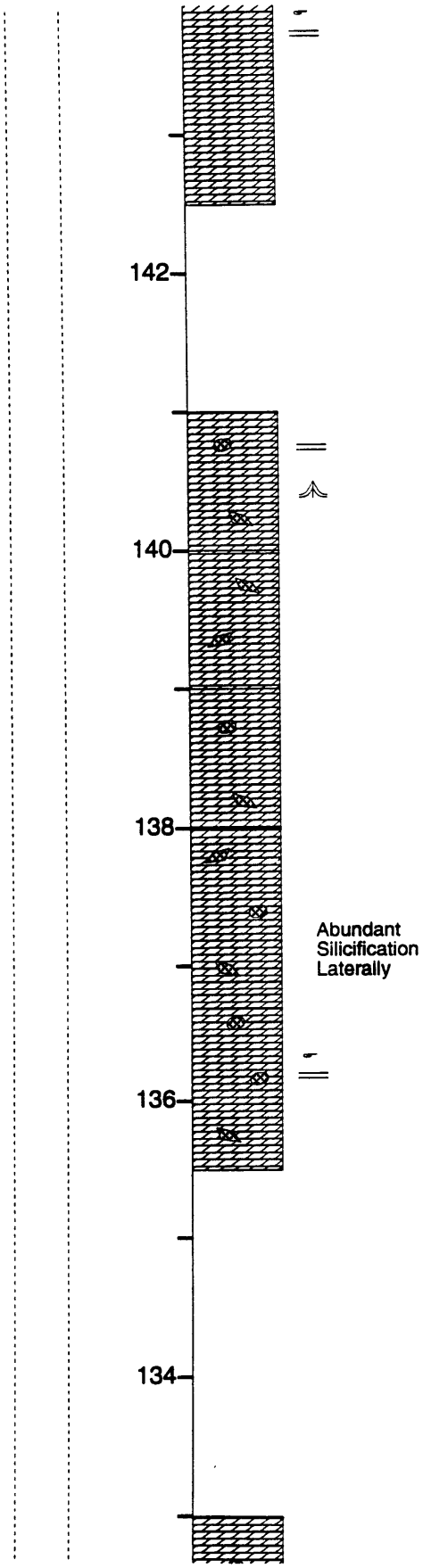
142
140
138
Abundant
Silicification
Laterally
136
134

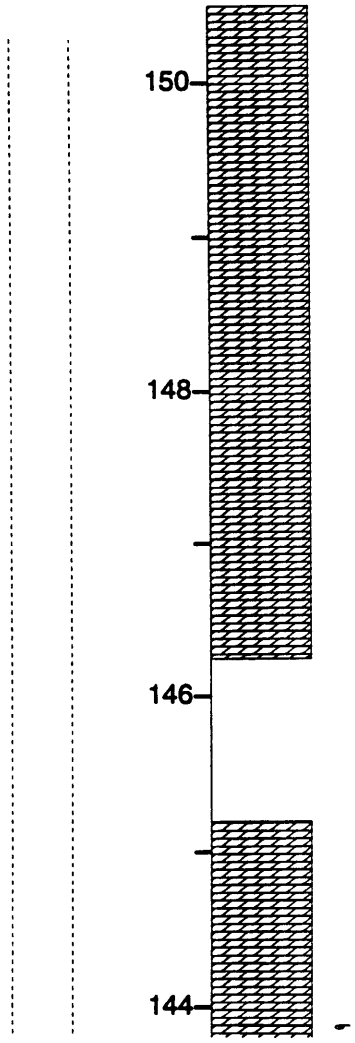
150
148
146
144

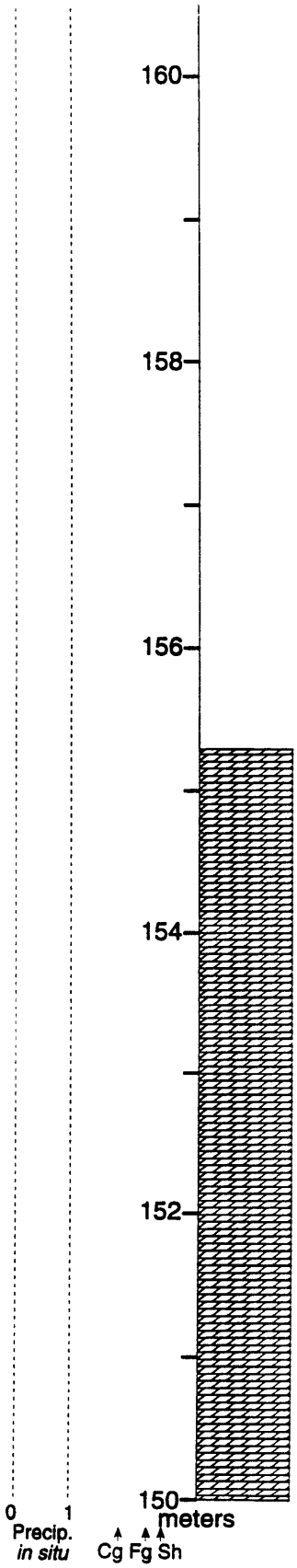
160
158
156
154
152
150
meters
0
1
Precip.
in situ
Cg Fg Sh

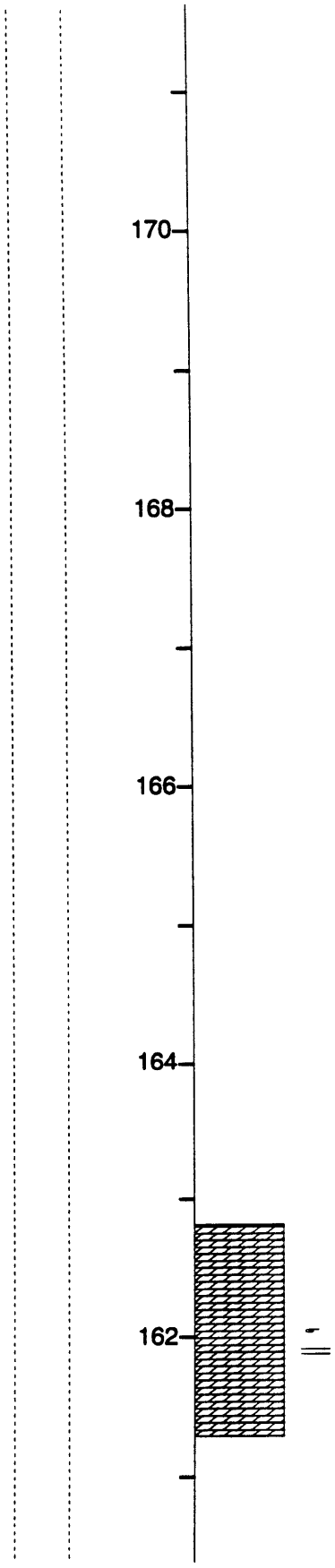
170
168
166
164
162

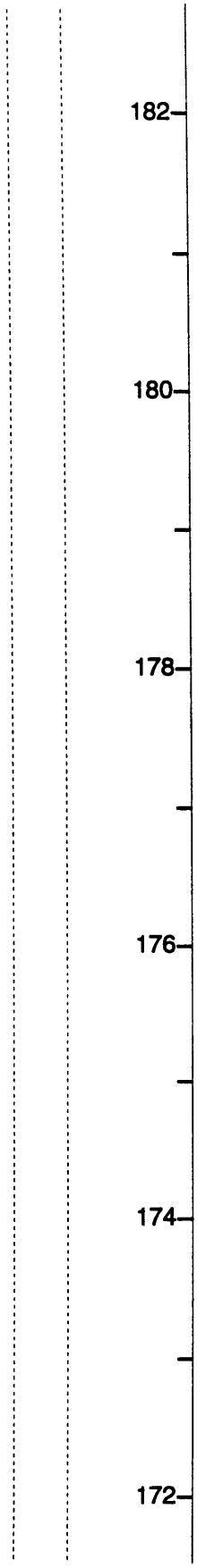
182
180
178
176
174
172

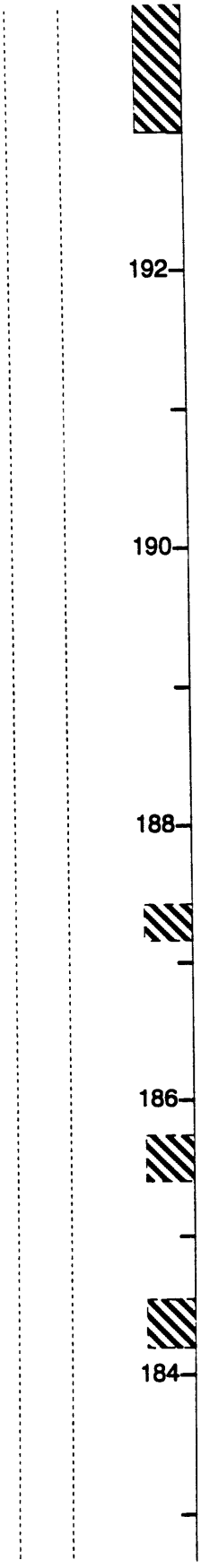
192
190
188
186
184

## General Facies

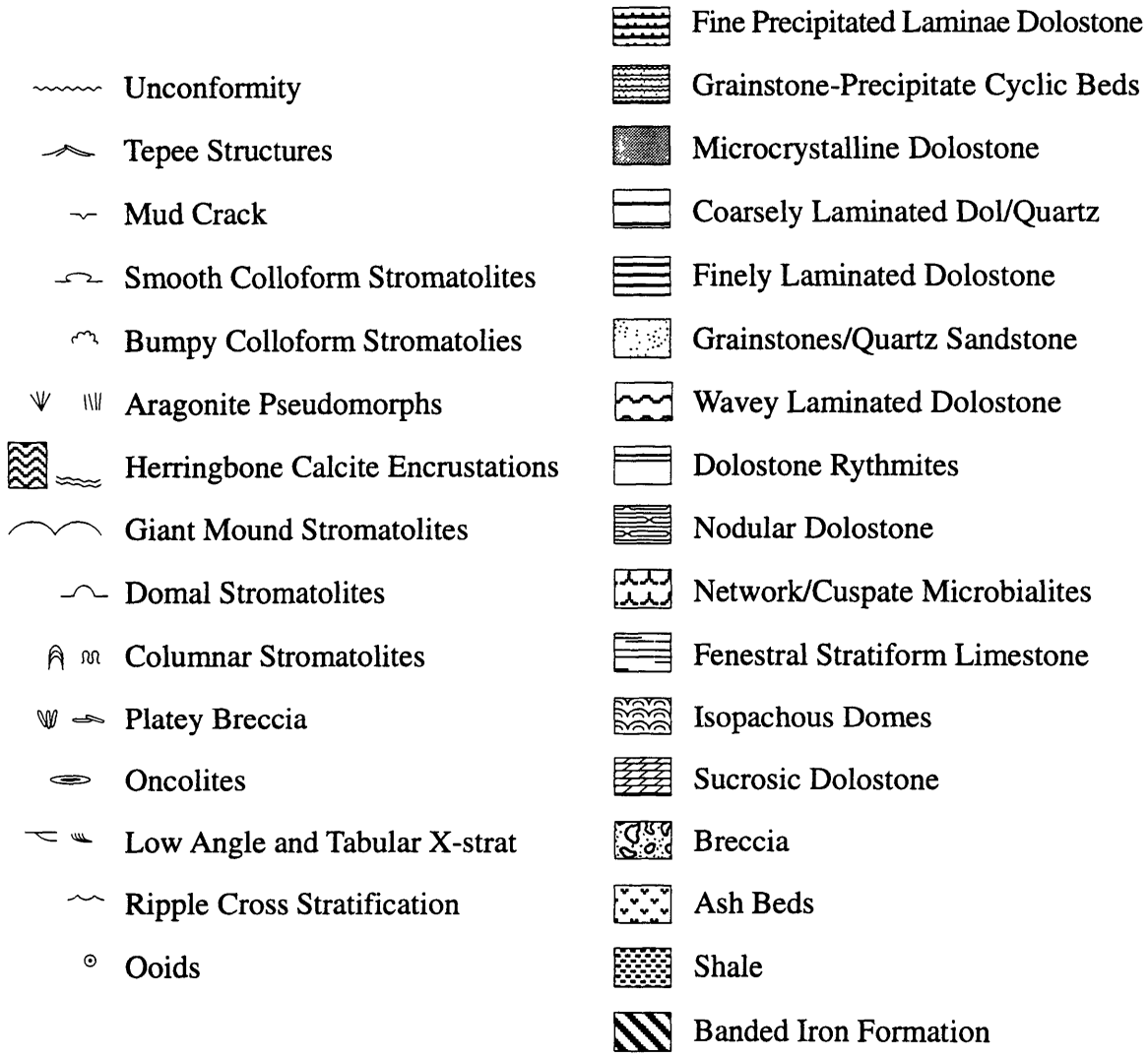

## Section AE

Location: Top of mountain 5 km southwest of Strijdom Tunnel on road R36 near Abel Erasmus Pass.

Stratigraphic Range: Top of the Black Reef Quartzite to the base of the Frisco Formation.

Additional Facies


Finely Laminated Dolostone


Coarsely Laminated Dolostone


Massive Dolostone

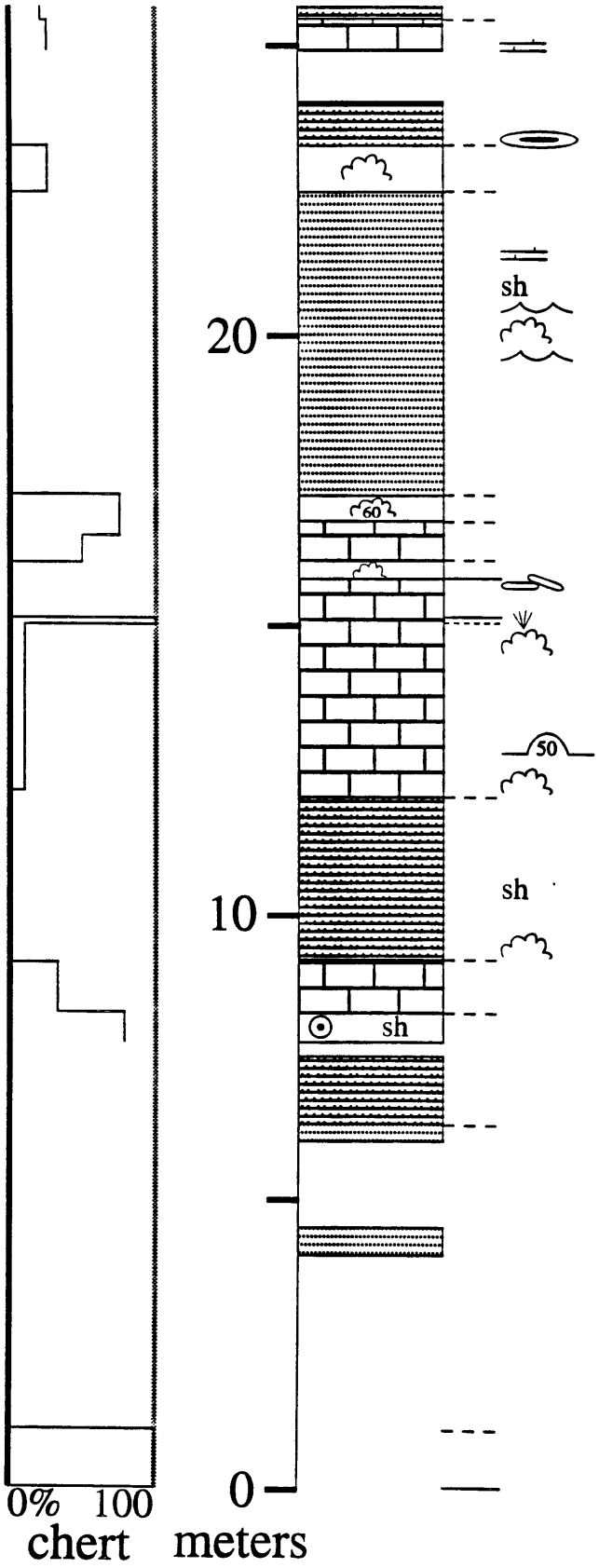
sh
20
60
50
sh
10
sh
0
0% 100
chert
meters

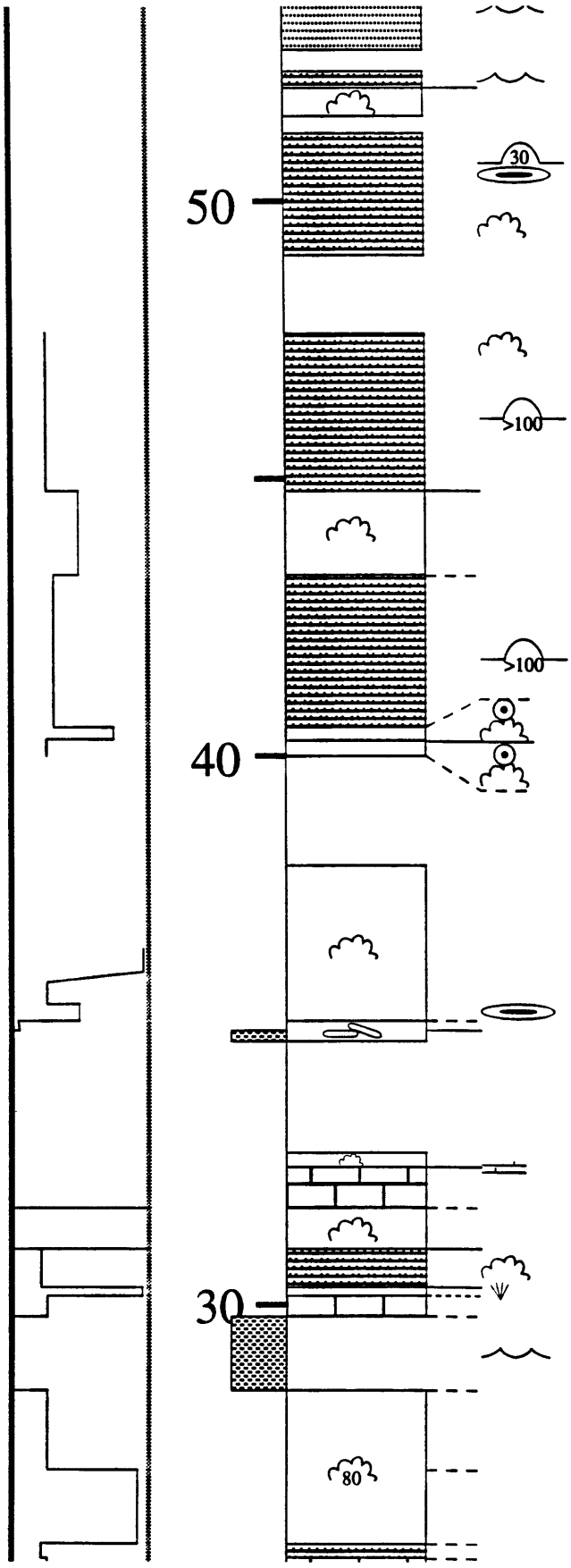
50
30
>100
>100
40
30
80

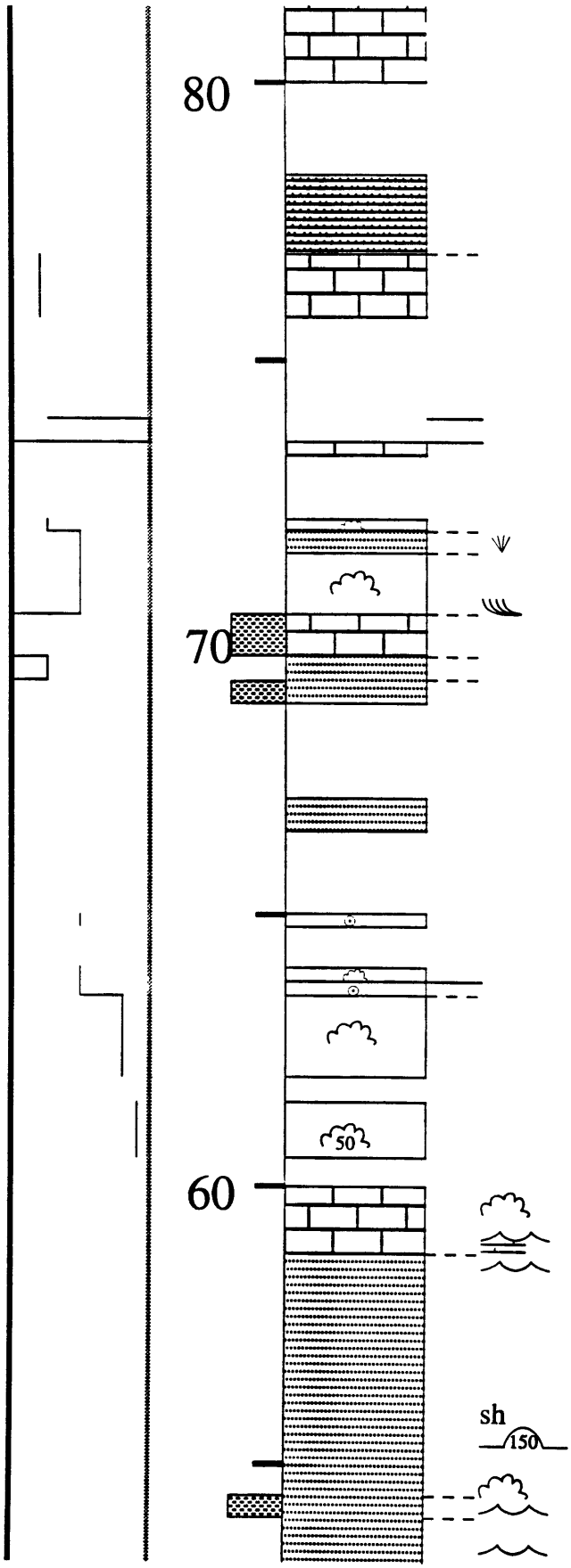
80
70
50
60
sh
150

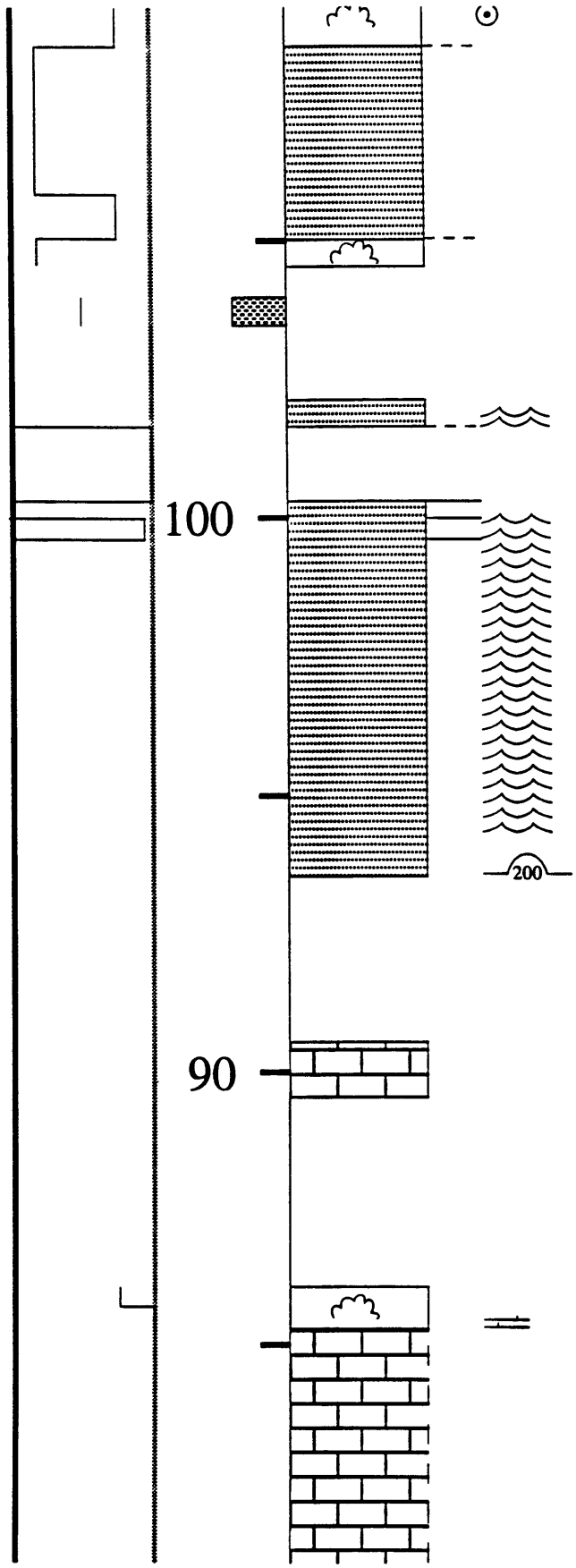
100
200
90

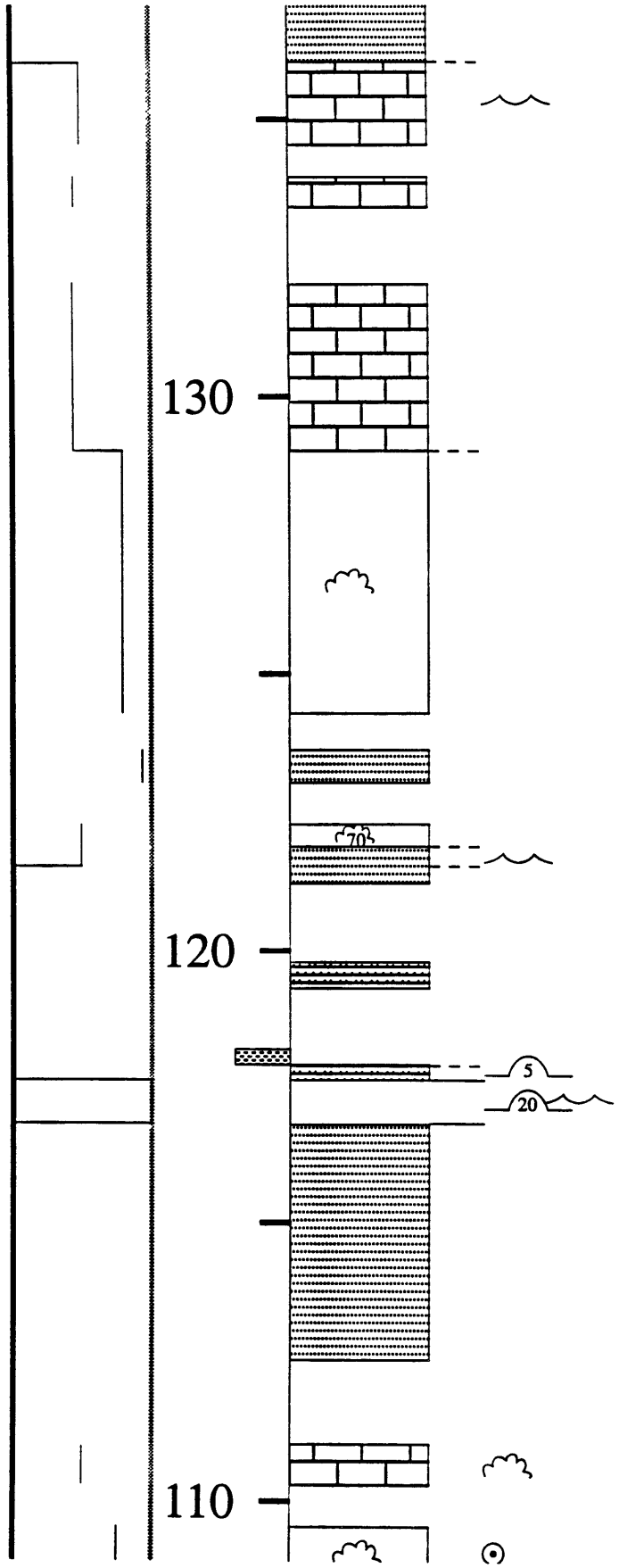
130
120
110
70
5
20

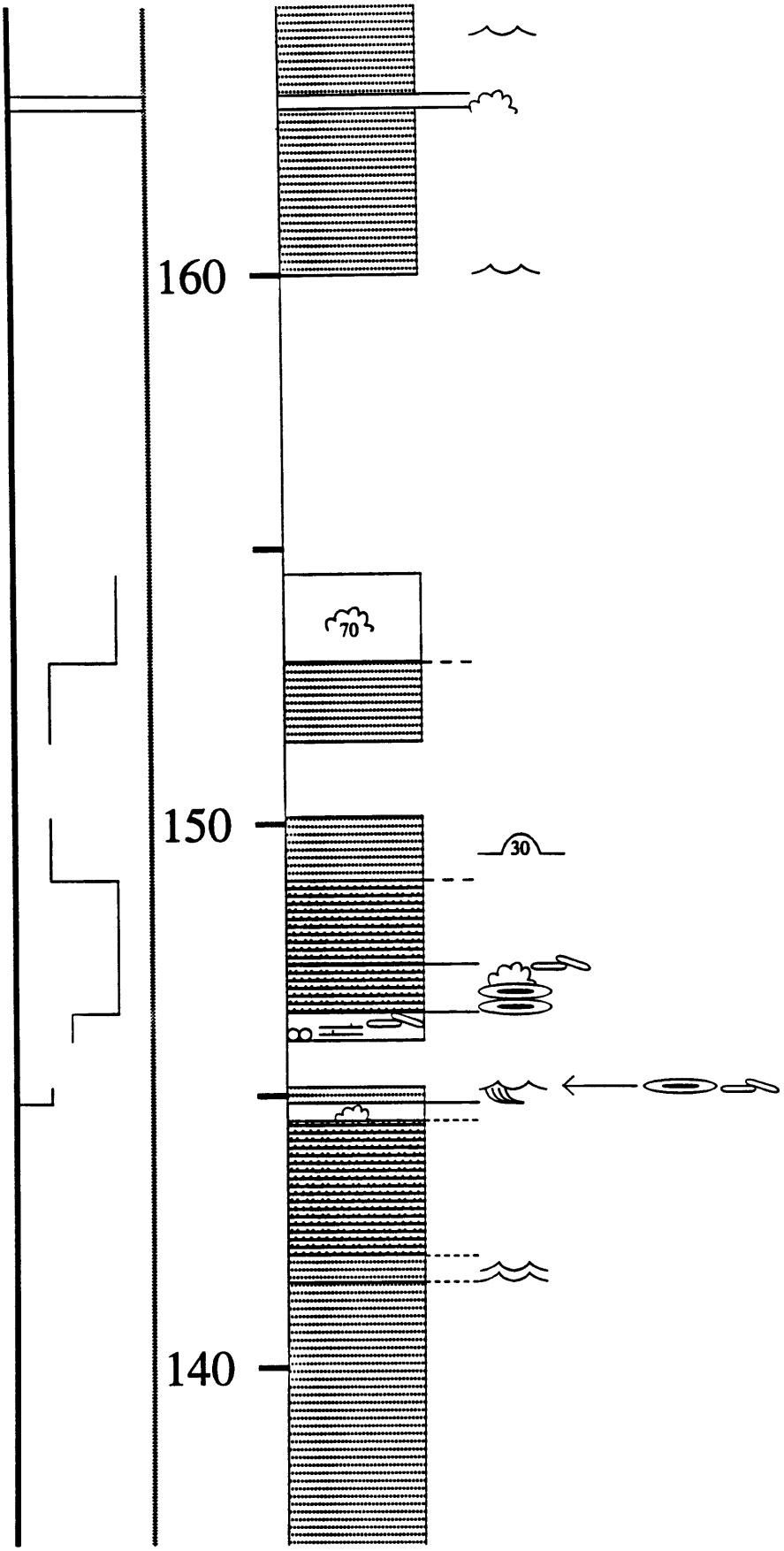
160
70
150
30
140

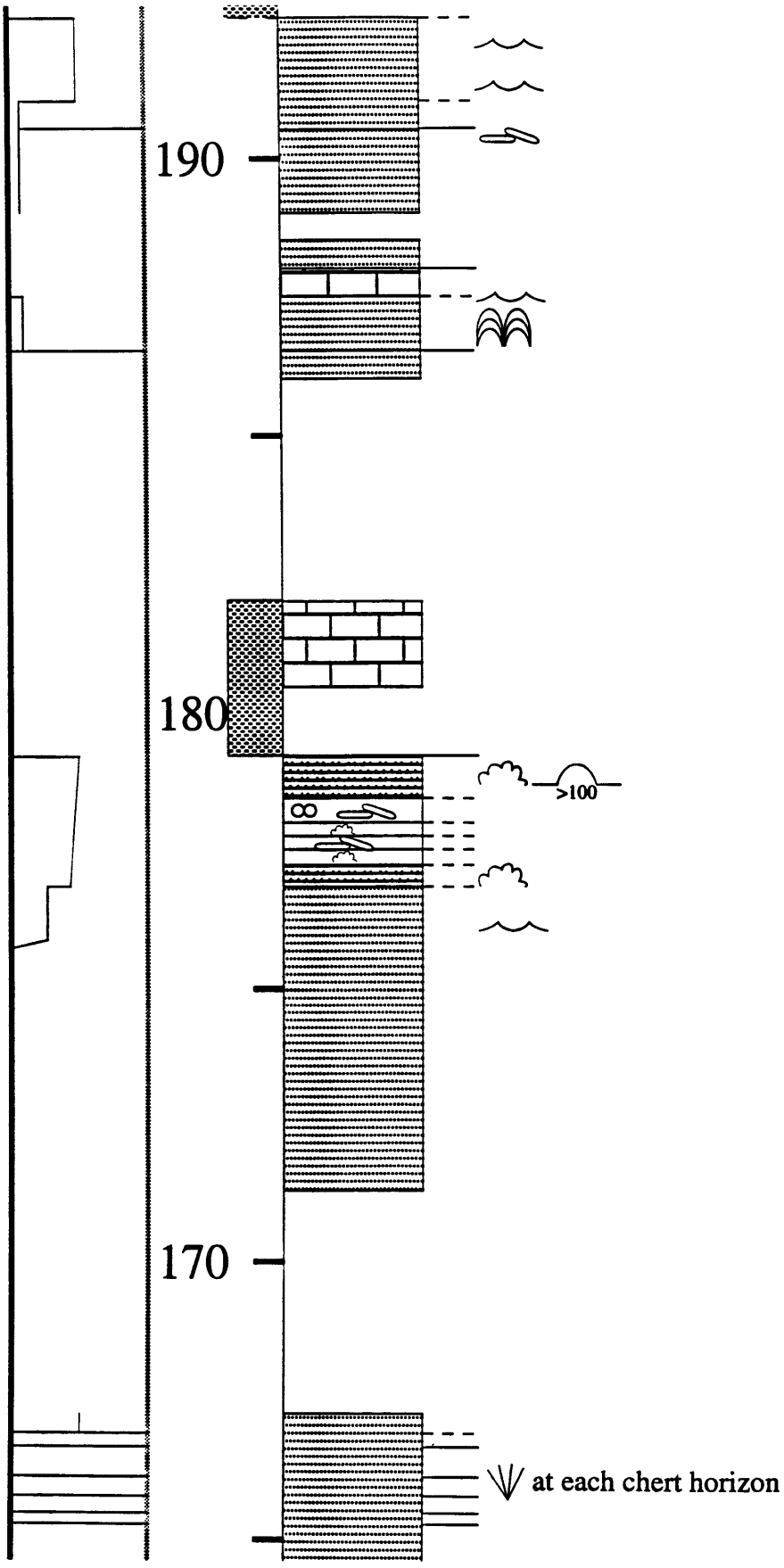
190
180
170
>100
at each chert horizon

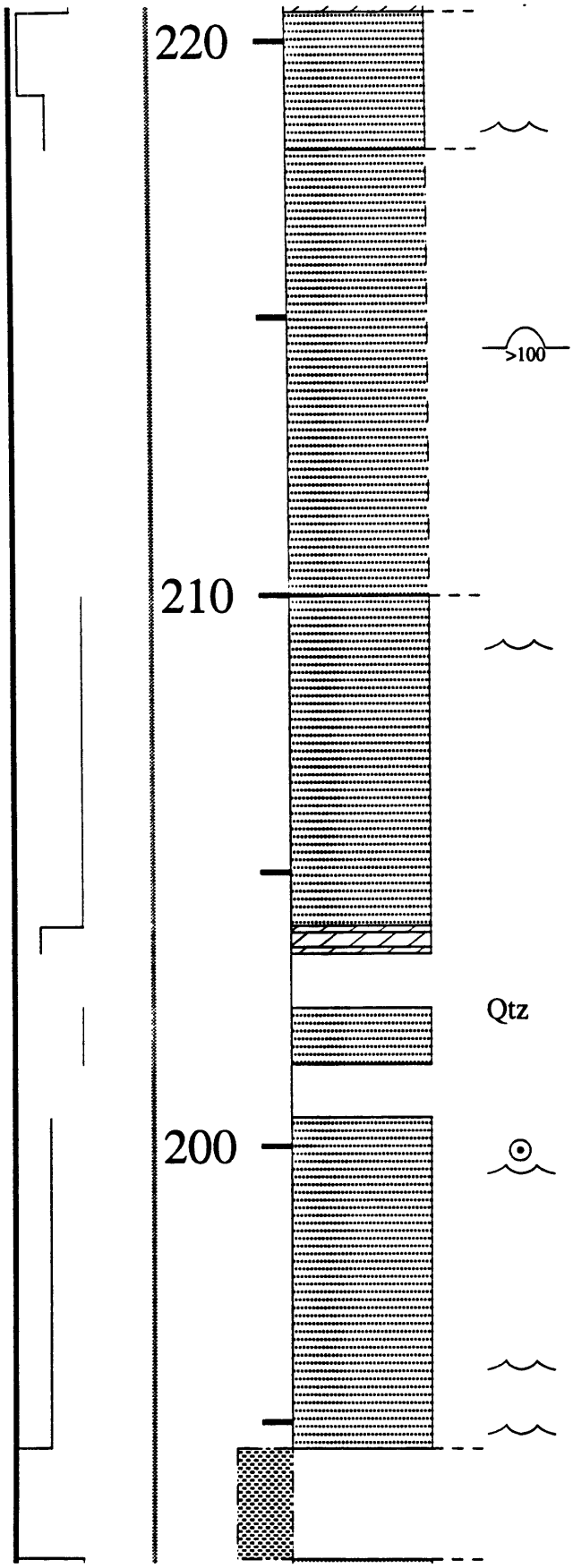
220
>100
210
Qtz
200

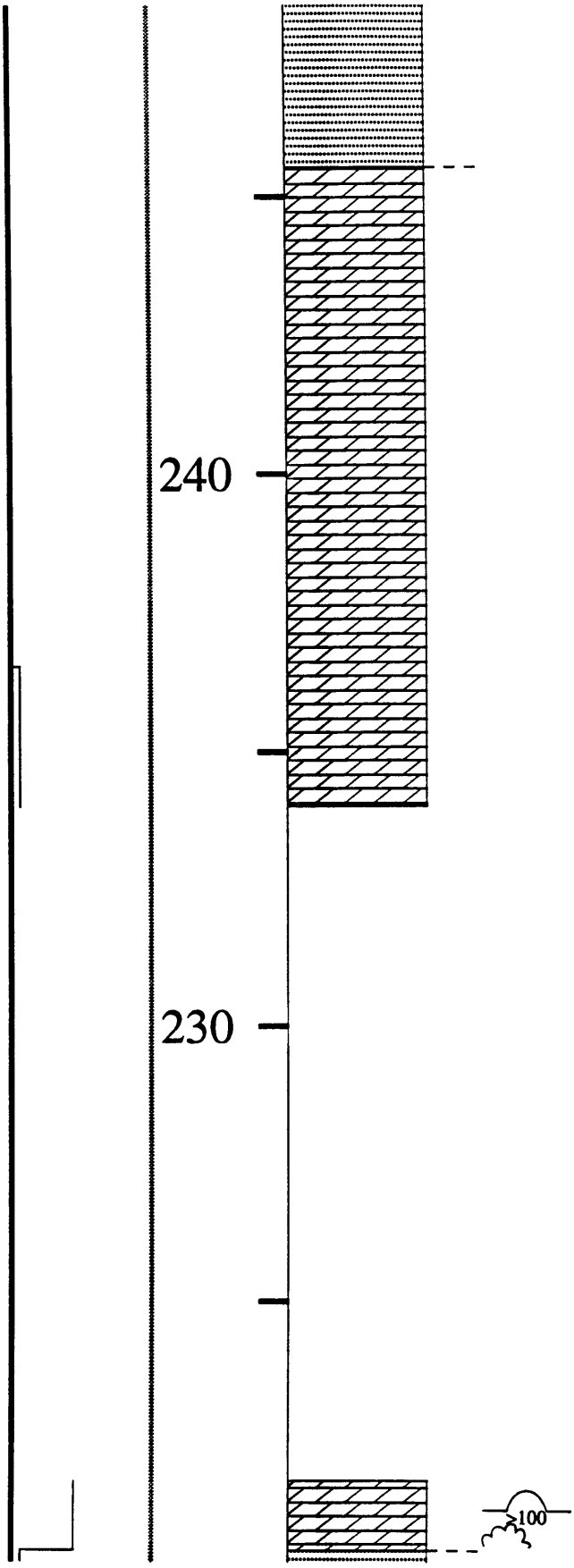
240
230
100

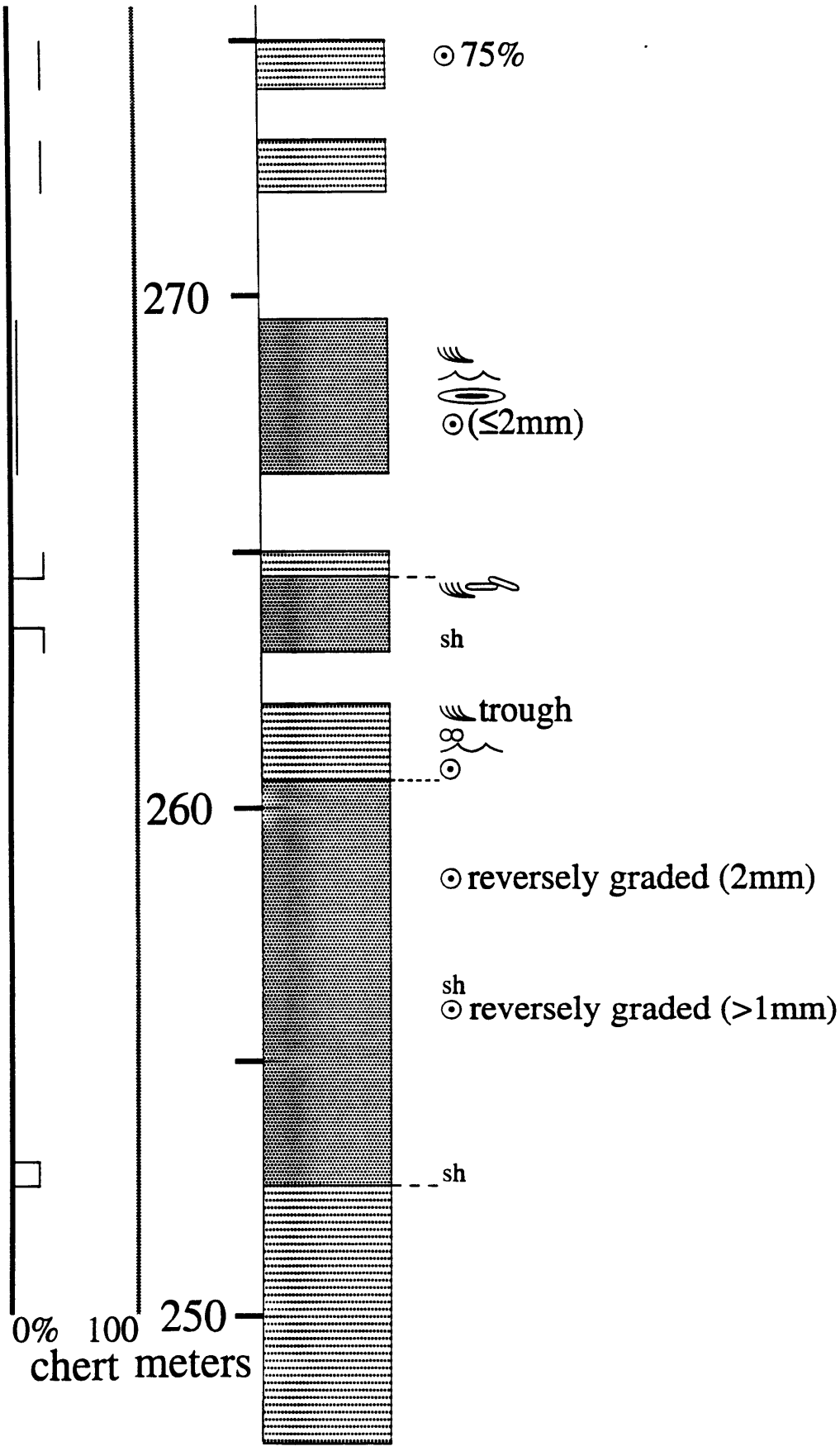
⊙75%
270
⊙(≤2mm)
sh
trough
260
⊙reversely graded (2mm)
sh
⊙reversely graded (>1mm)
sh
0% 100
250
chert meters

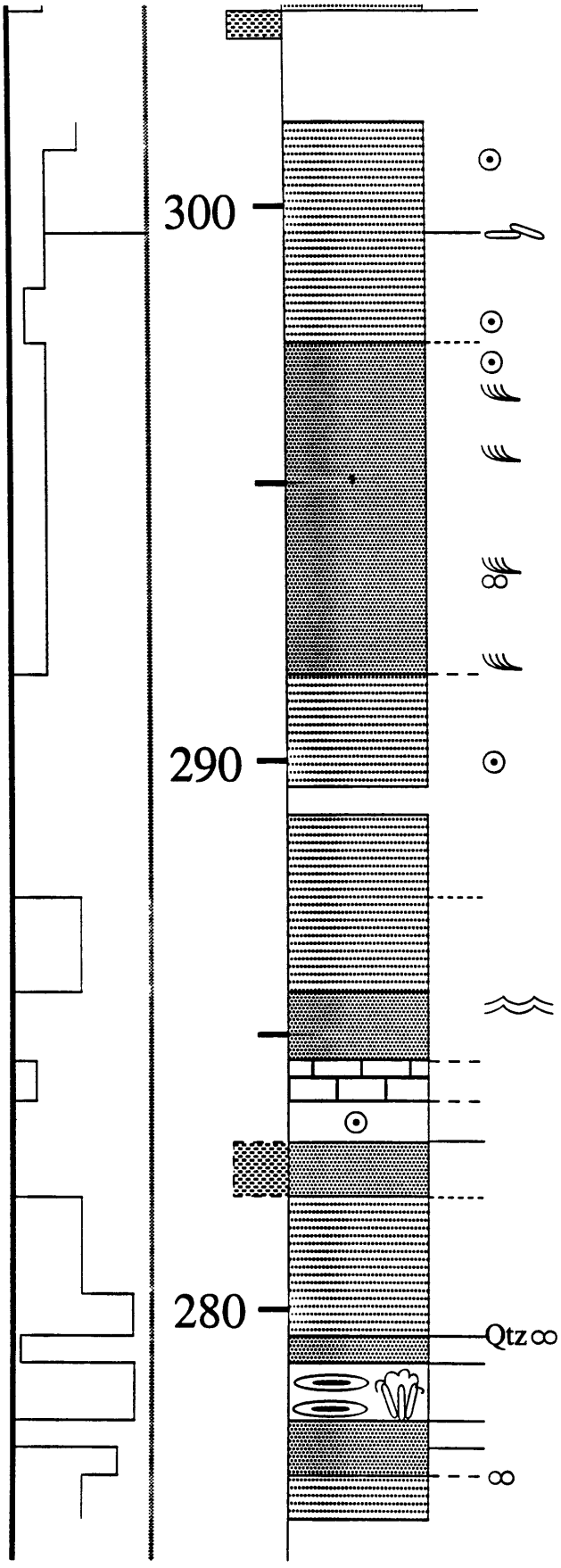
300
290
280
Qtz∞
∞

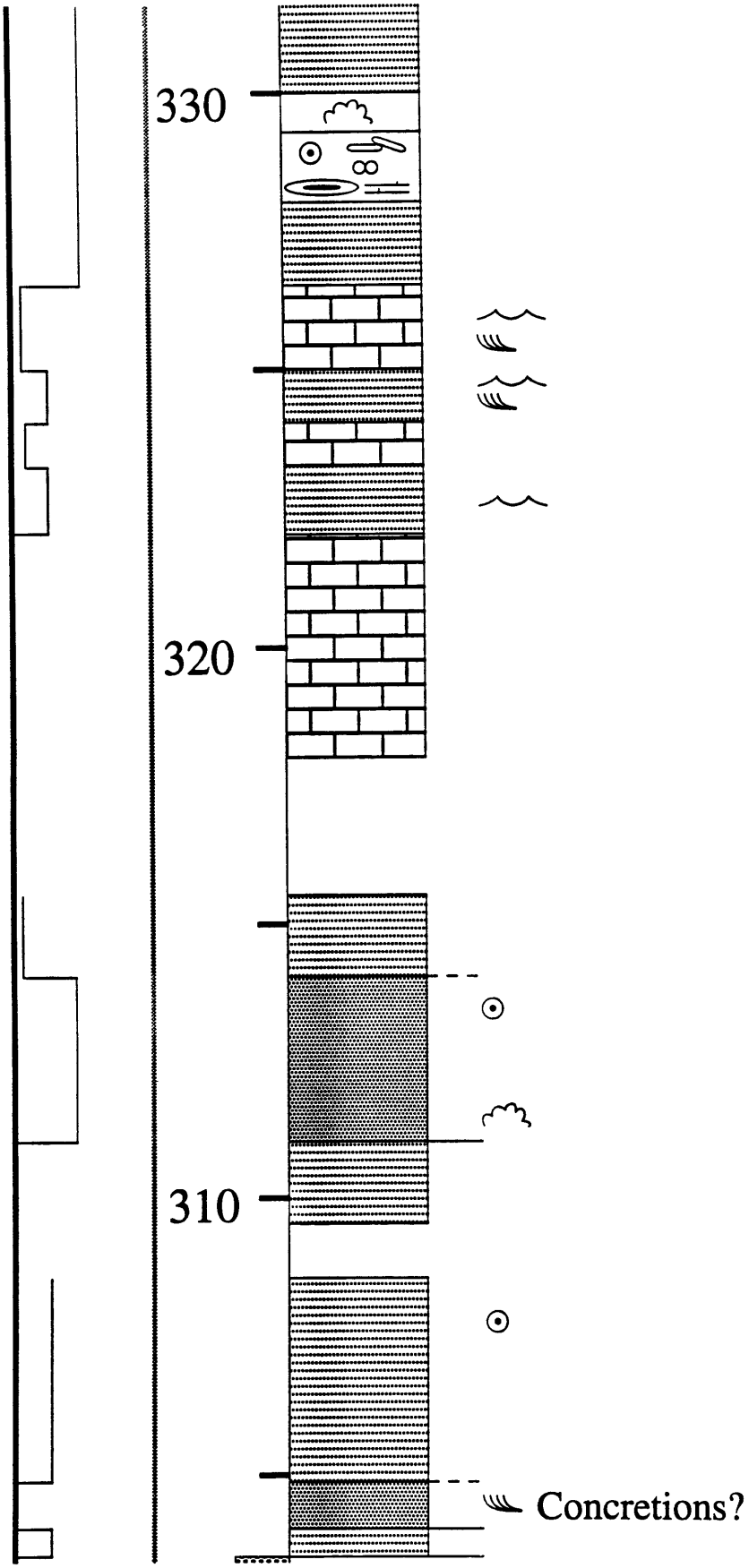
330
320
310
Concretions?

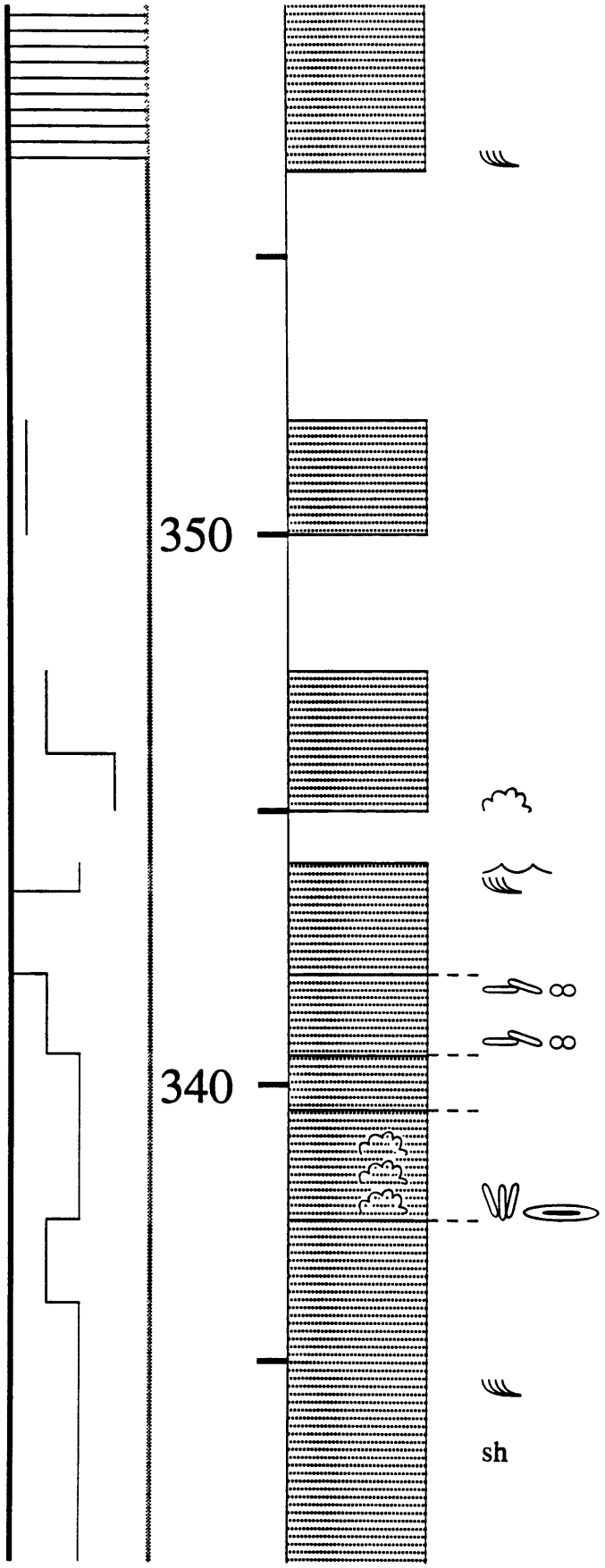
350
340
sh

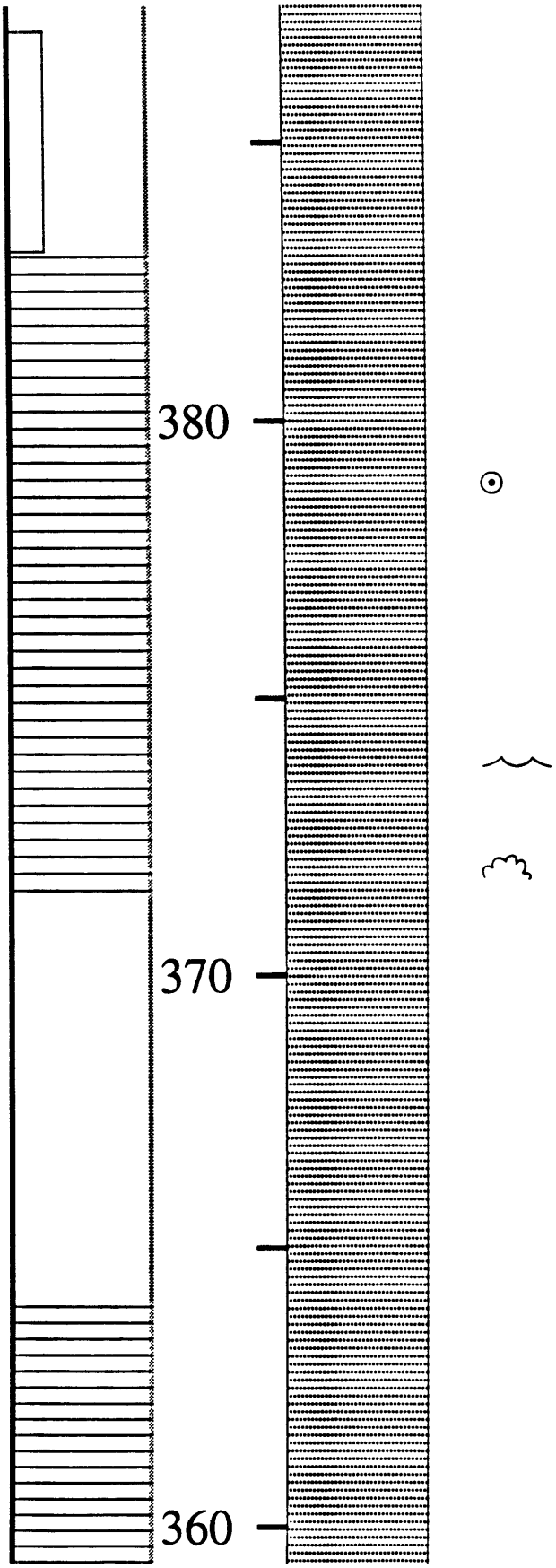
380
370
360

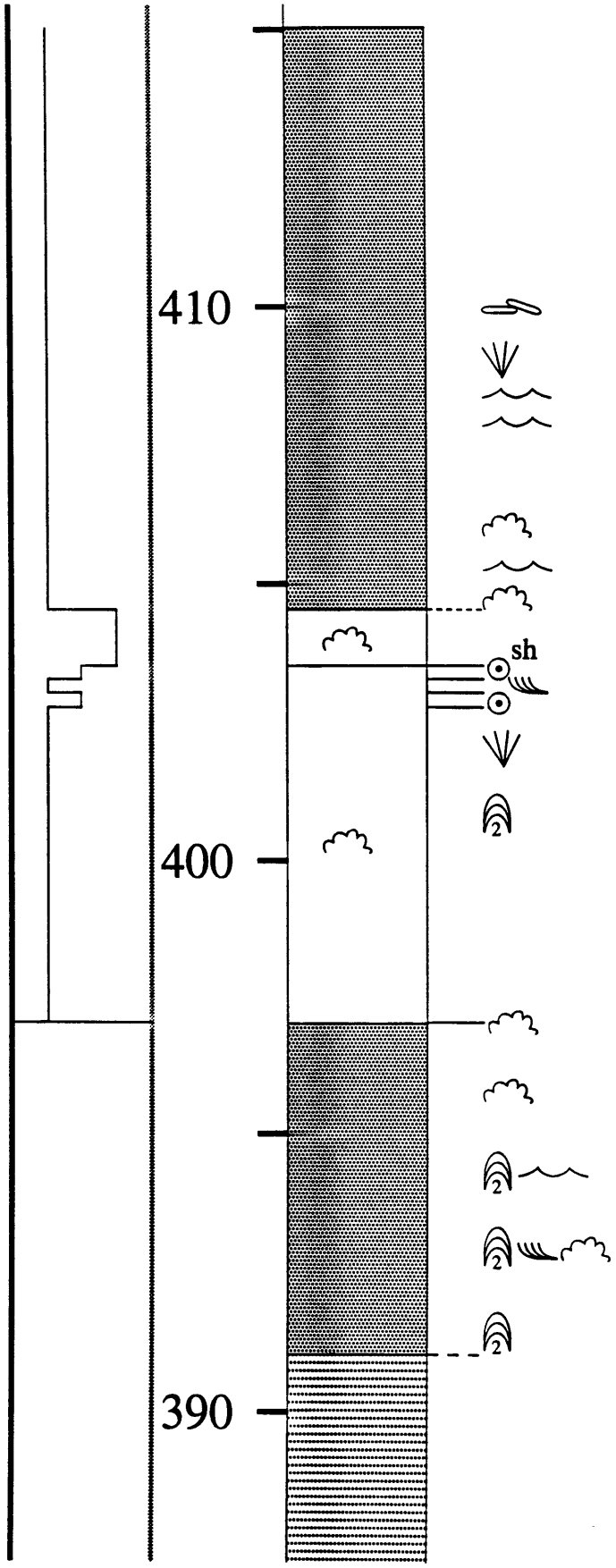
410
400
390
sh
2
2
2
2

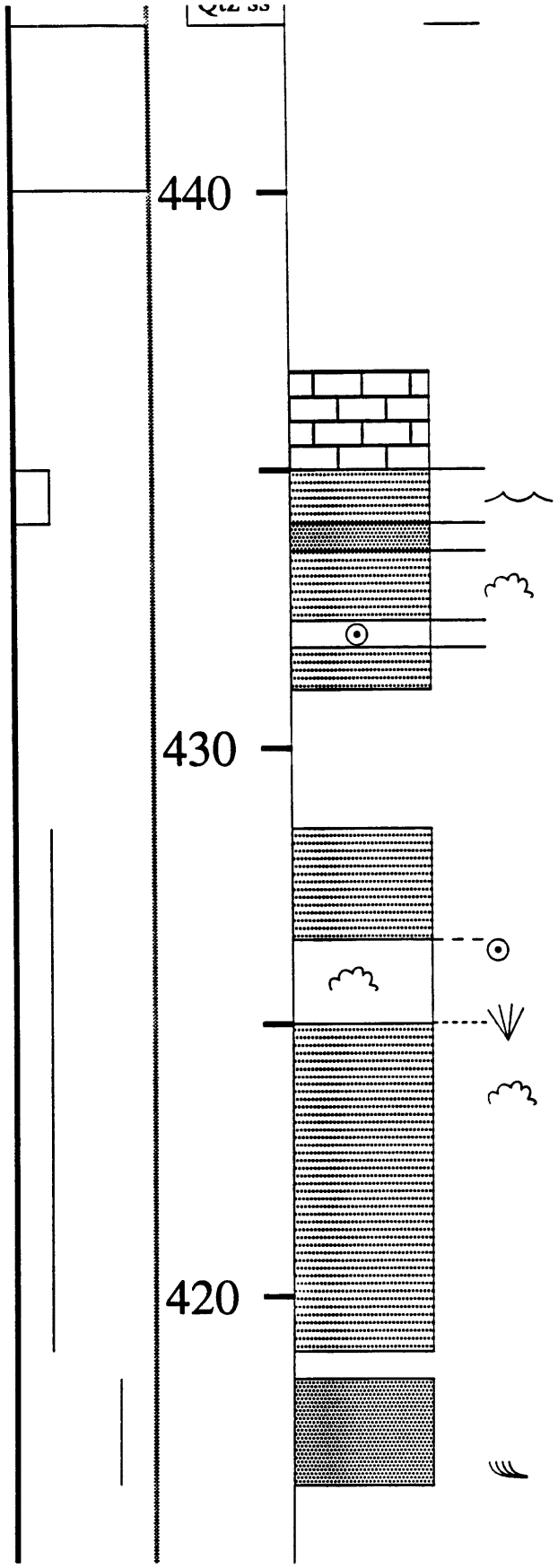
440
430
420

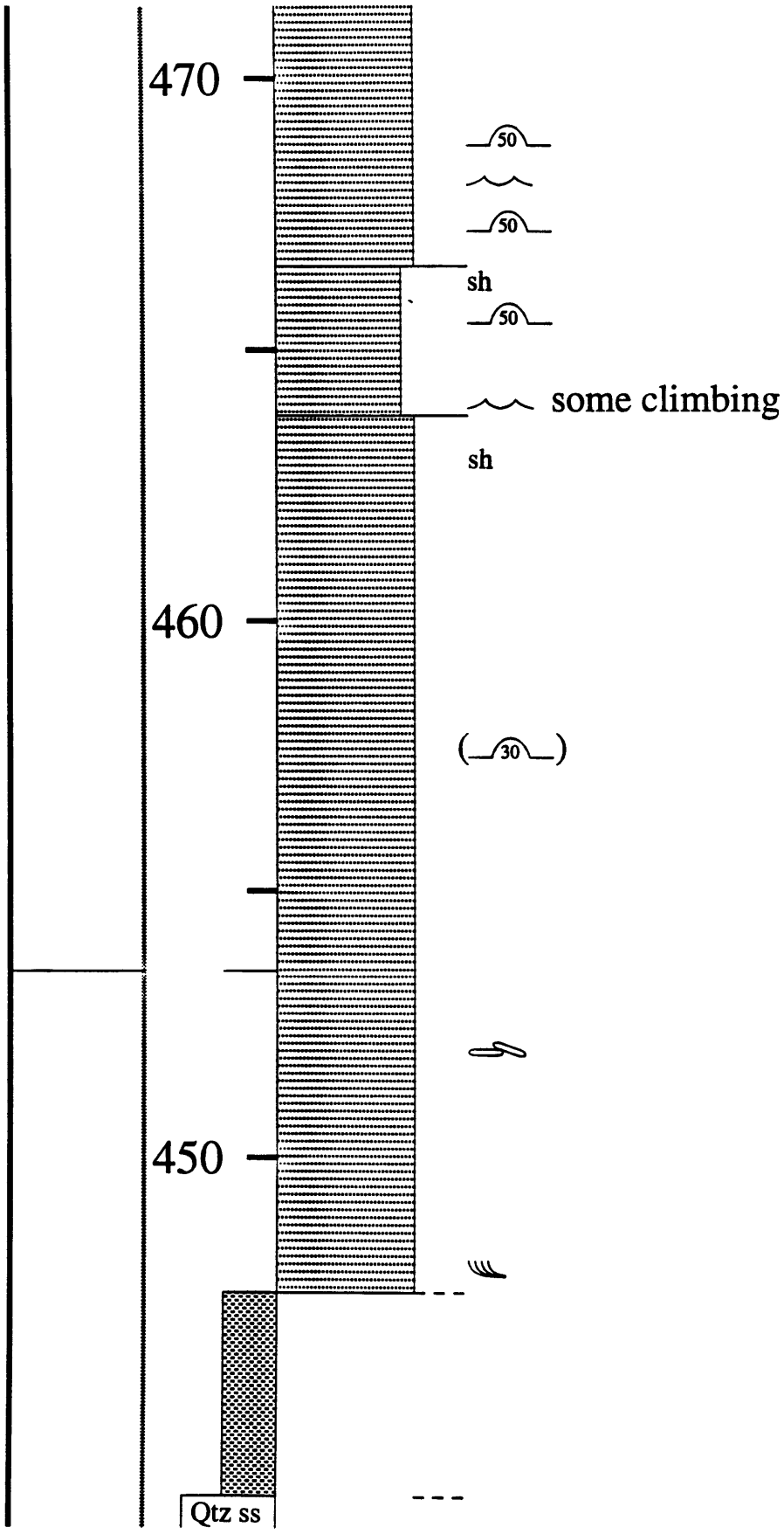
470
460
450
50
50
sh
50
some climbing
sh
30
Qtz ss

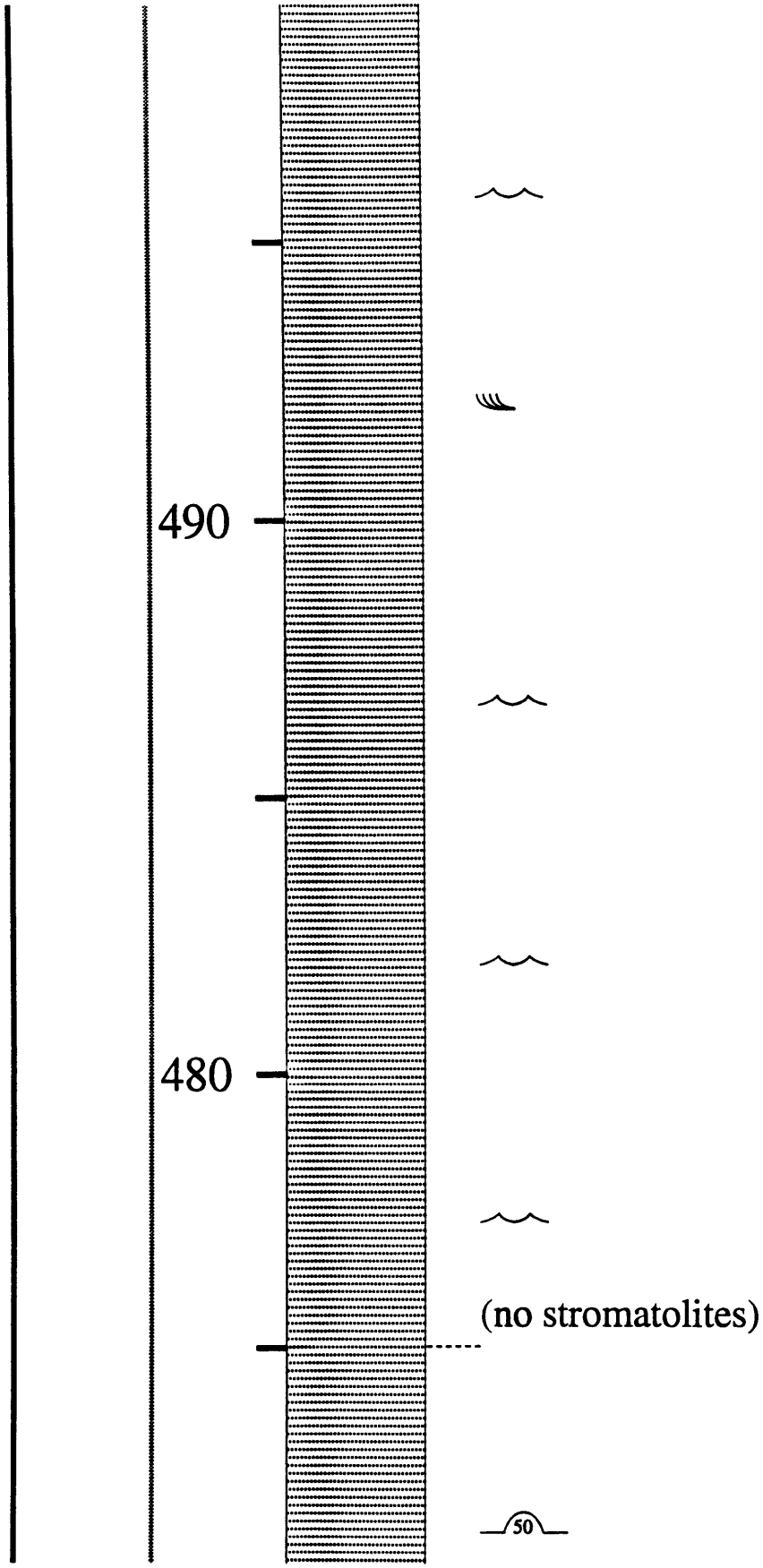
490
480
(no stromatolites)
50

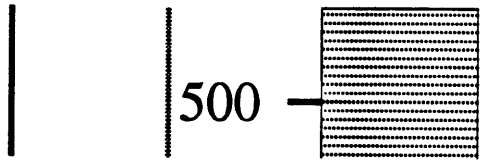
500

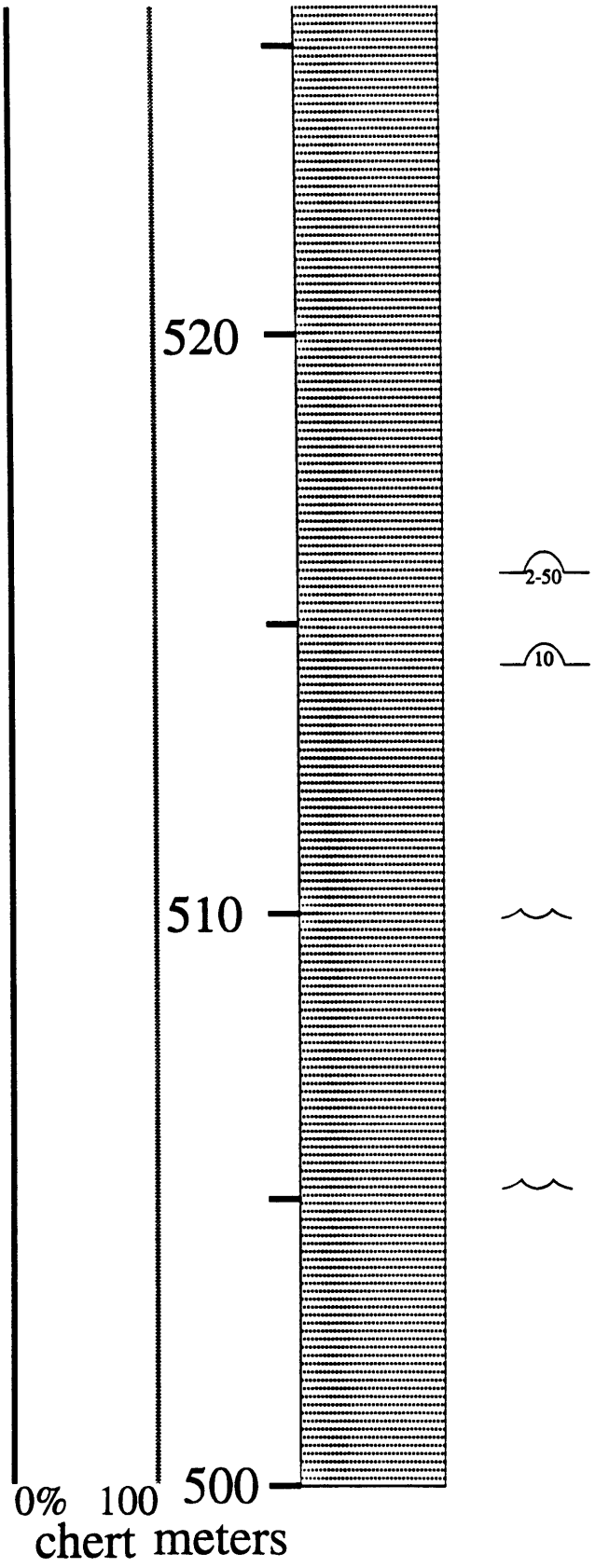
520
510
500
2-50
10
0%
100
chert meters

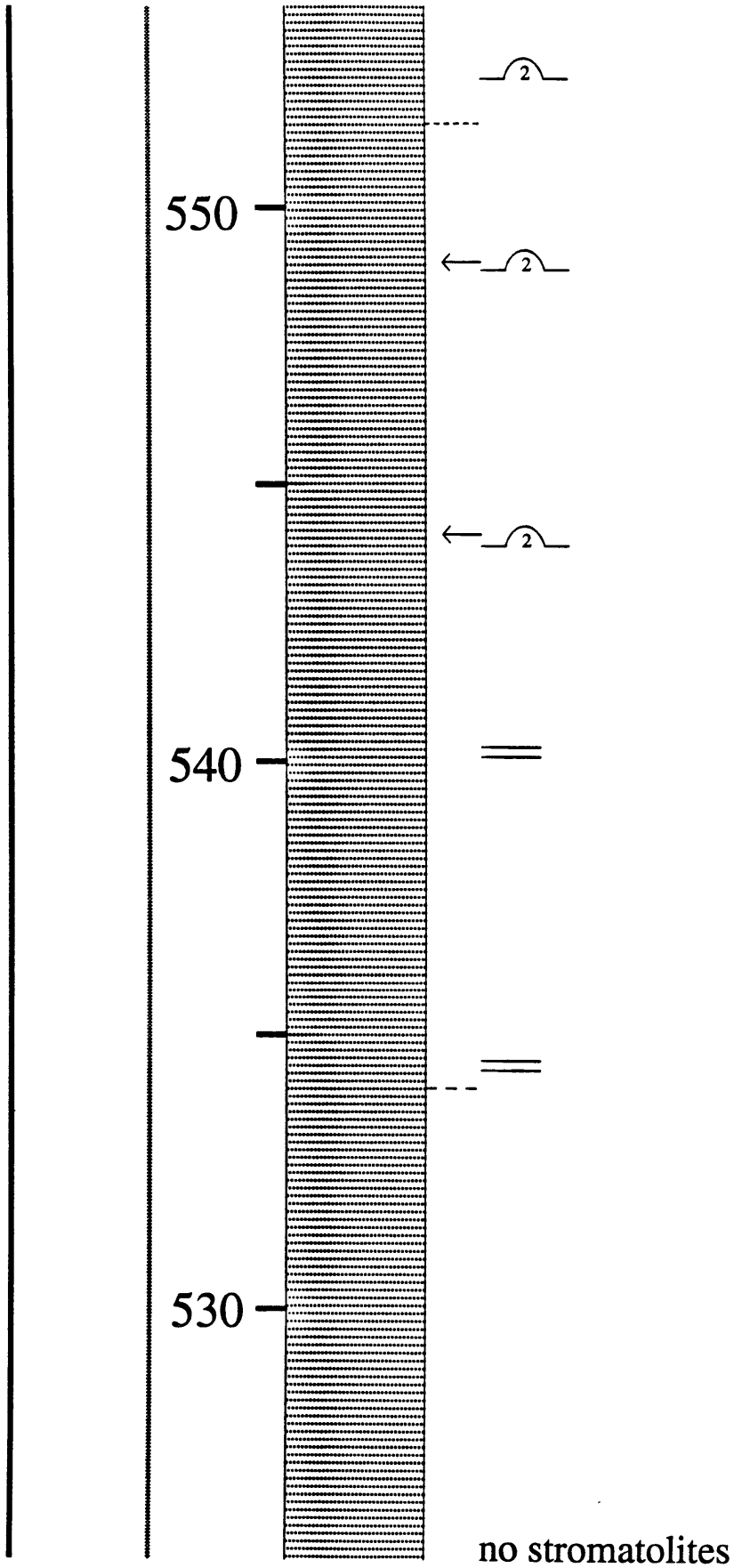
550
540
530
2
2
2
no stromatolites

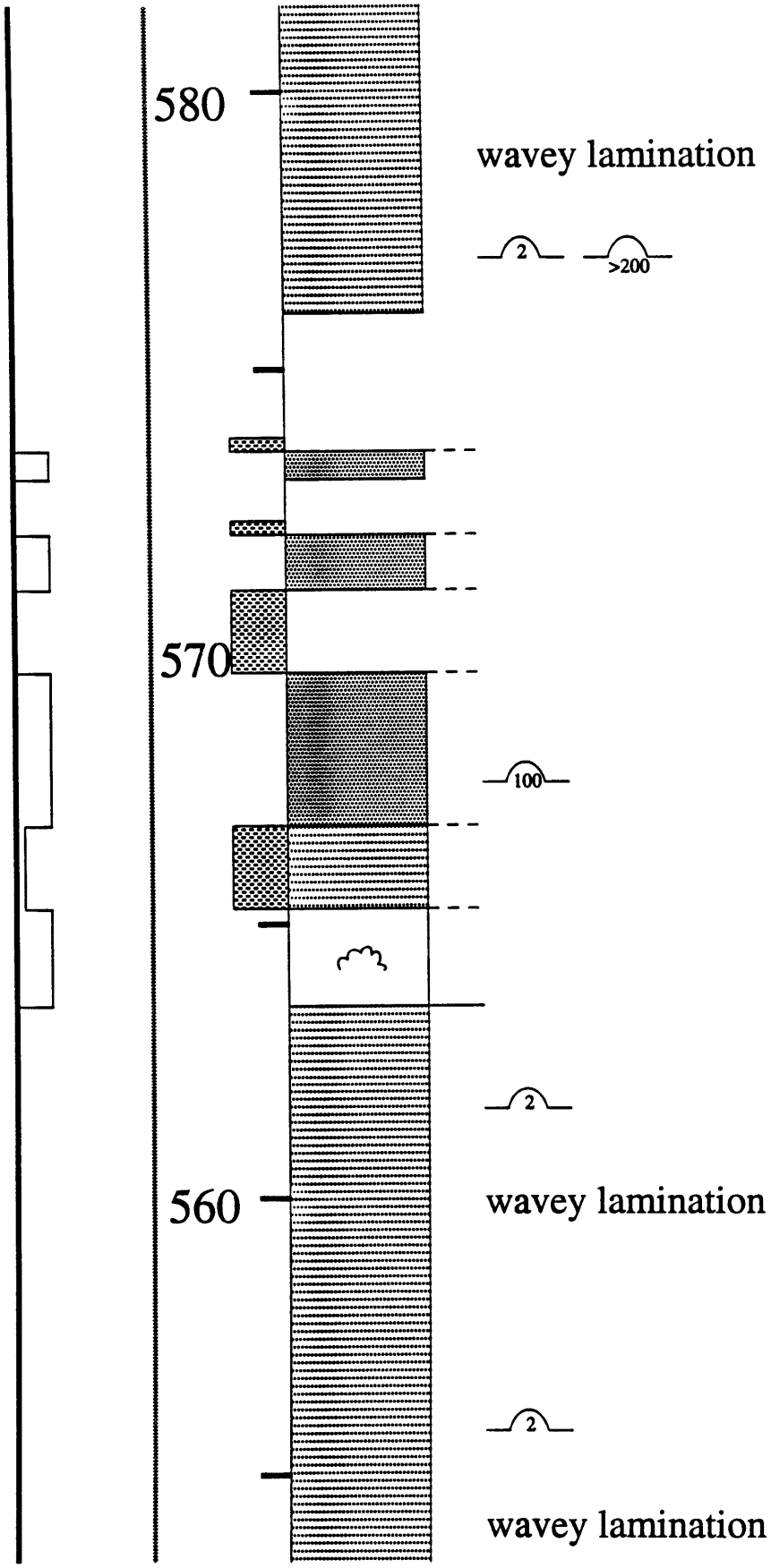
580
wavey lamination
2
>200
570
100
2
560
wavey lamination
2
wavey lamination

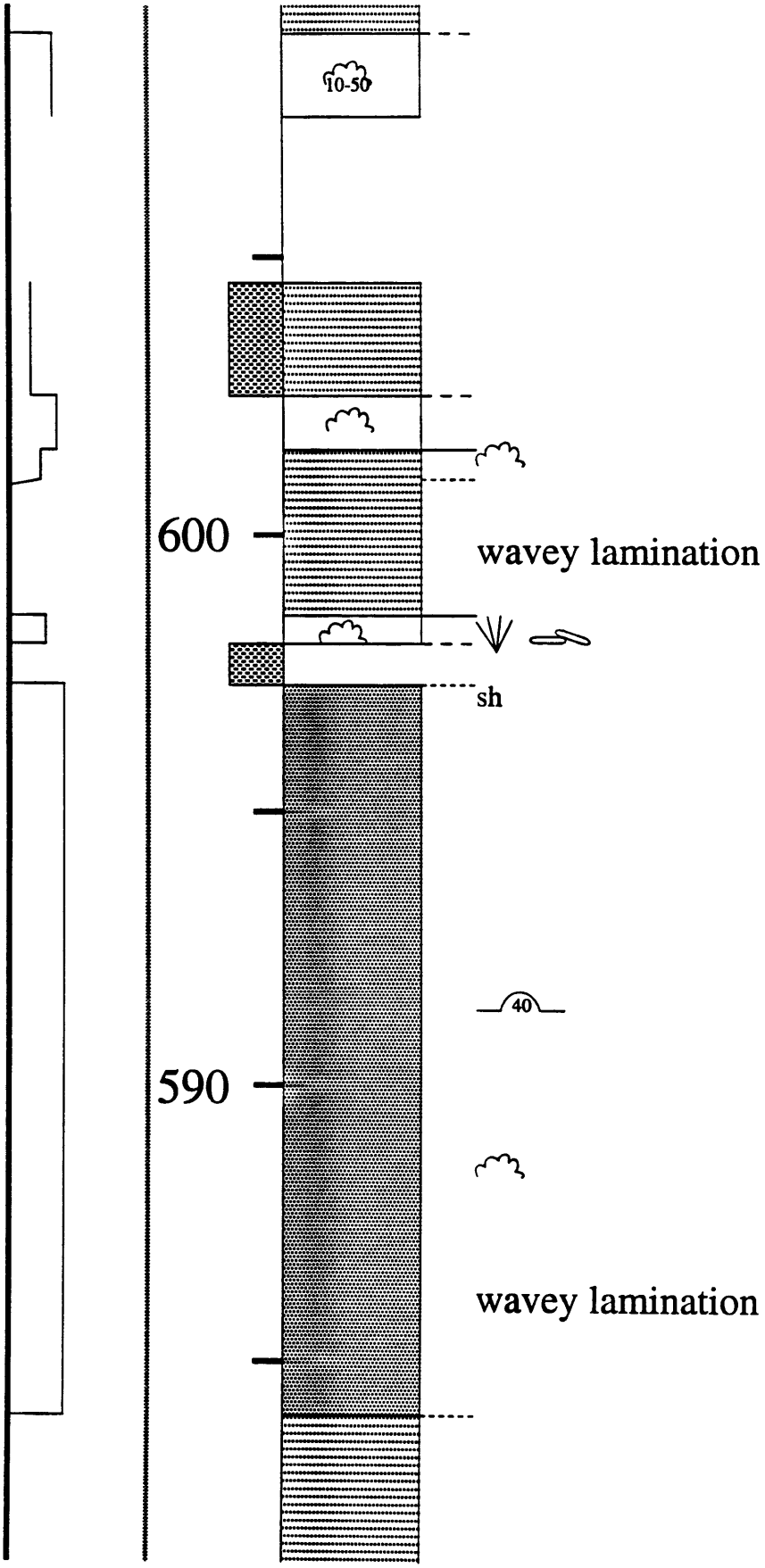
10-50
600
wavey lamination
sh
40
590
wavey lamination

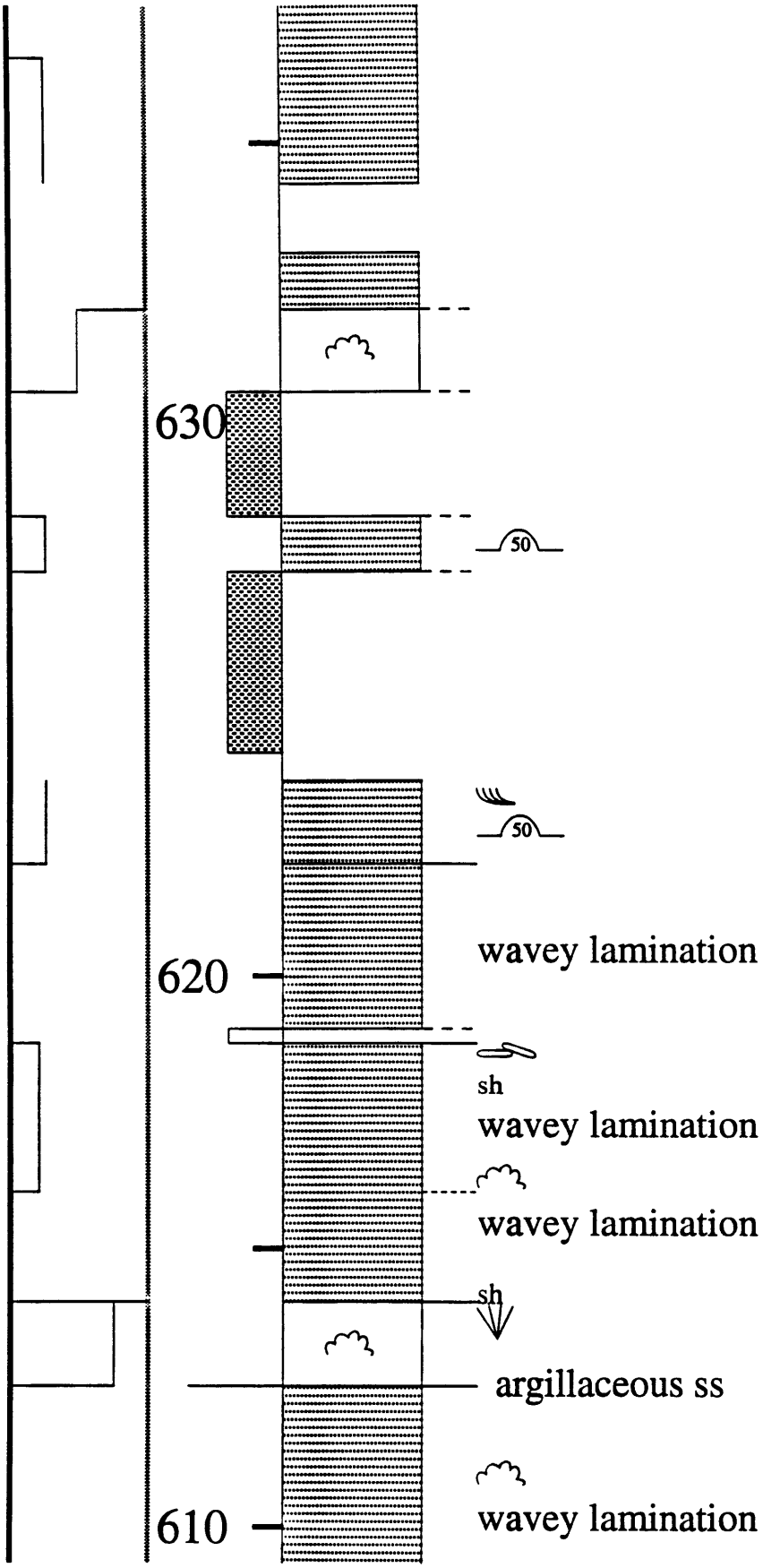
630
50
50
620
wavey lamination
sh
wavey lamination
wavey lamination
sh
argillaceous ss
610
wavey lamination

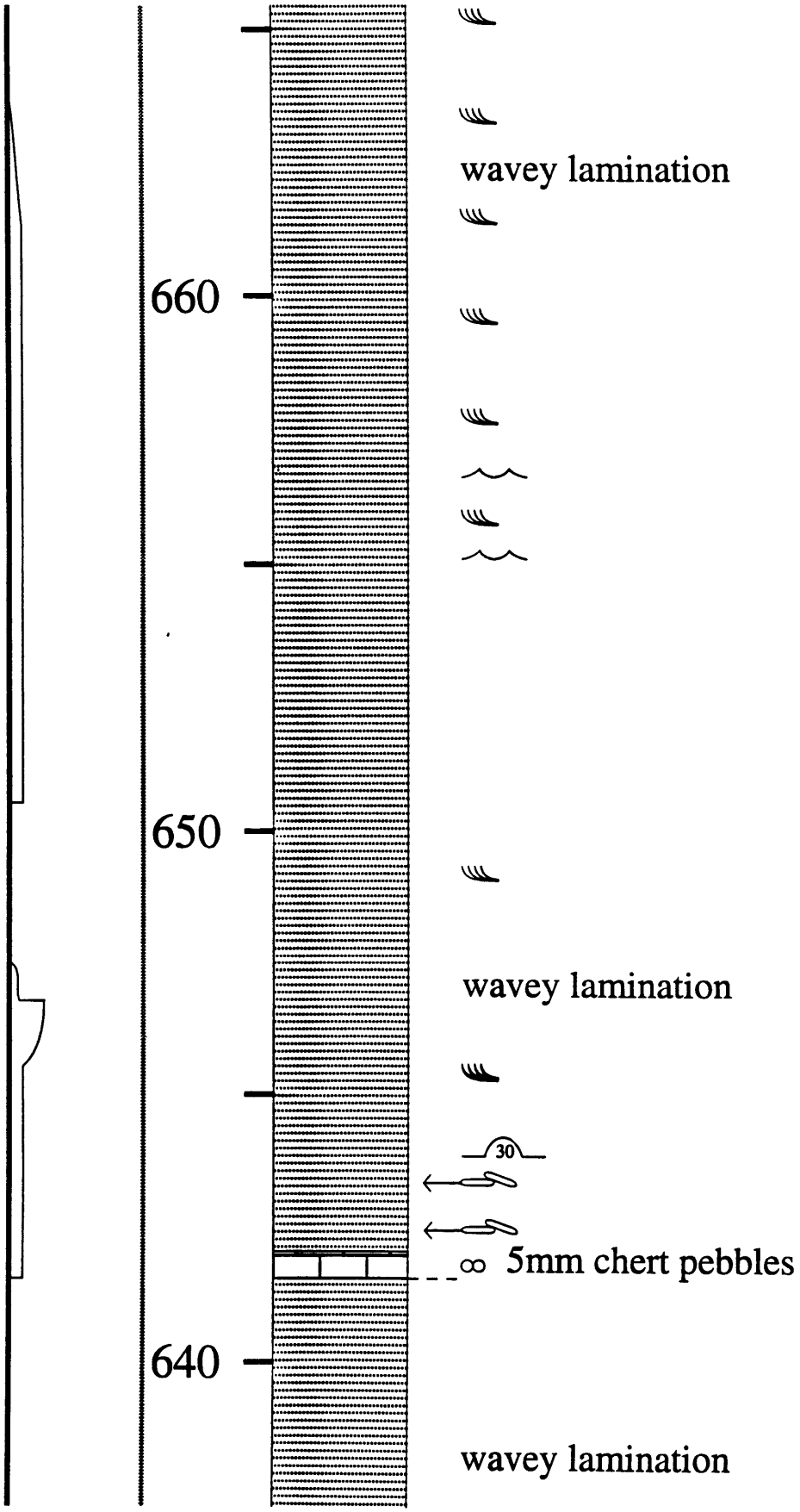
660
650
640
wavey lamination
wavey lamination
wavey lamination
30
∞ 5mm chert pebbles

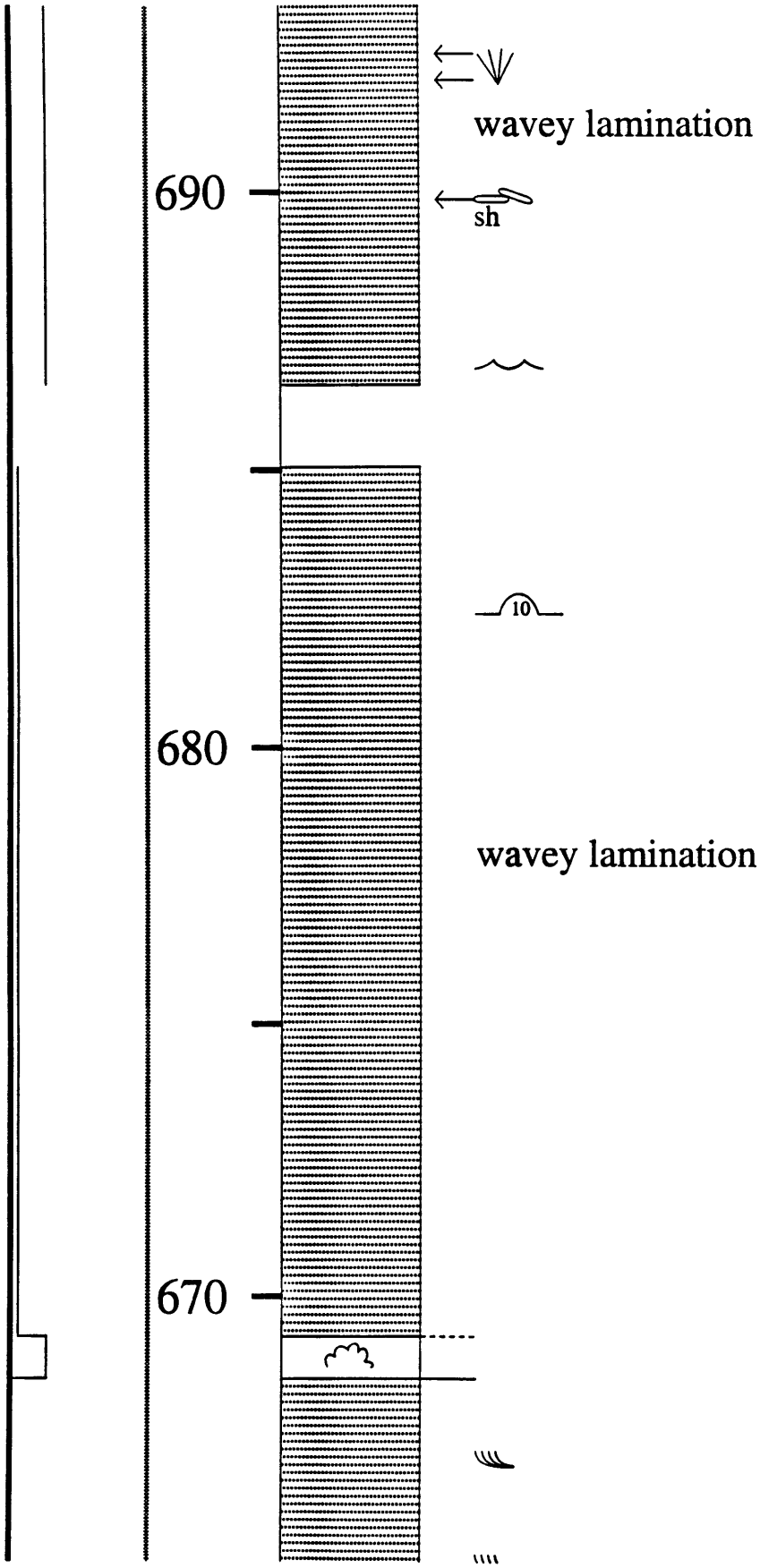
wavey lamination
690
sh
10
680
wavey lamination
670

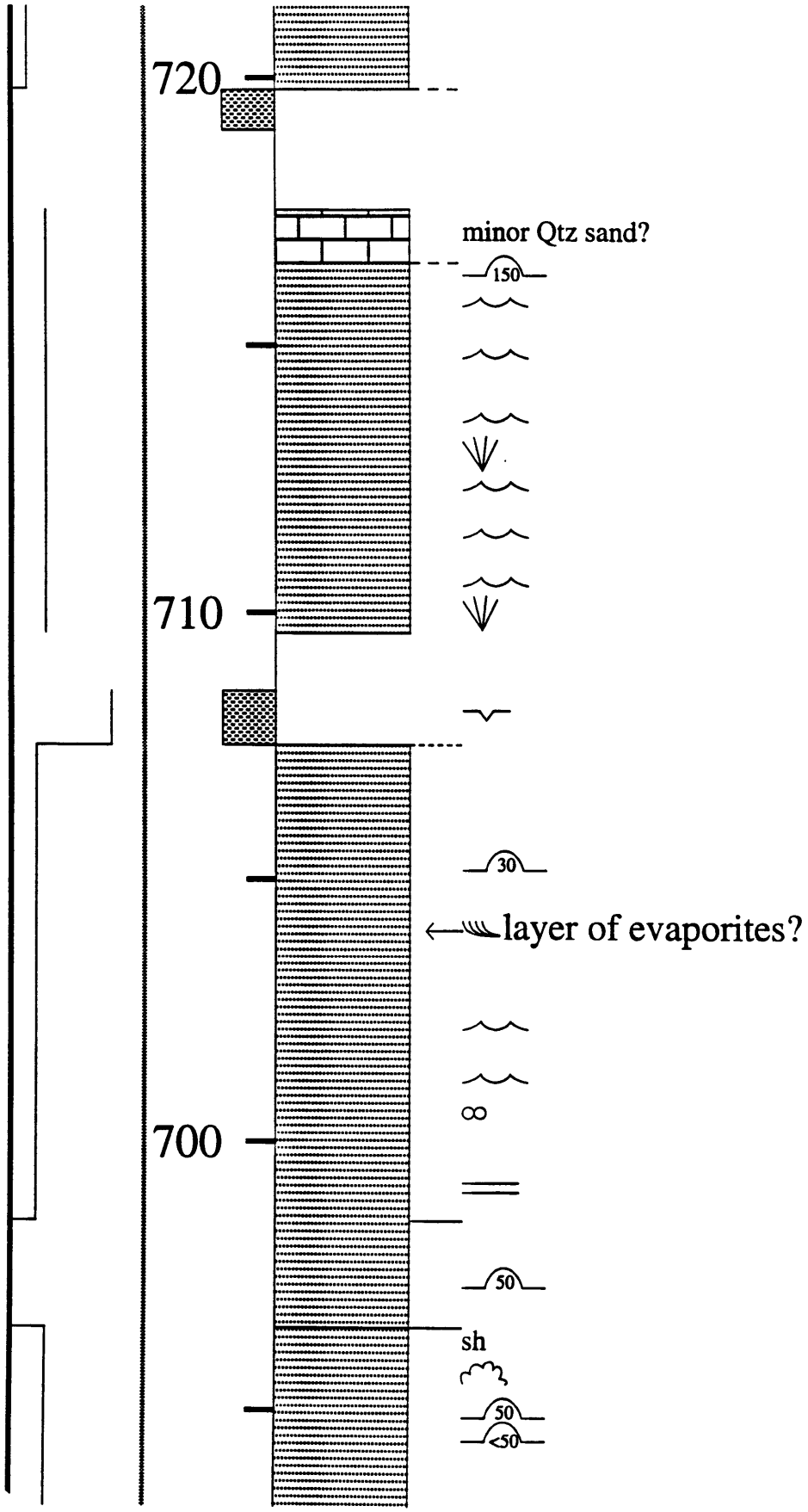
720
minor Qtz sand?
150
710
30
layer of evaporites?
700
50
sh
50
50

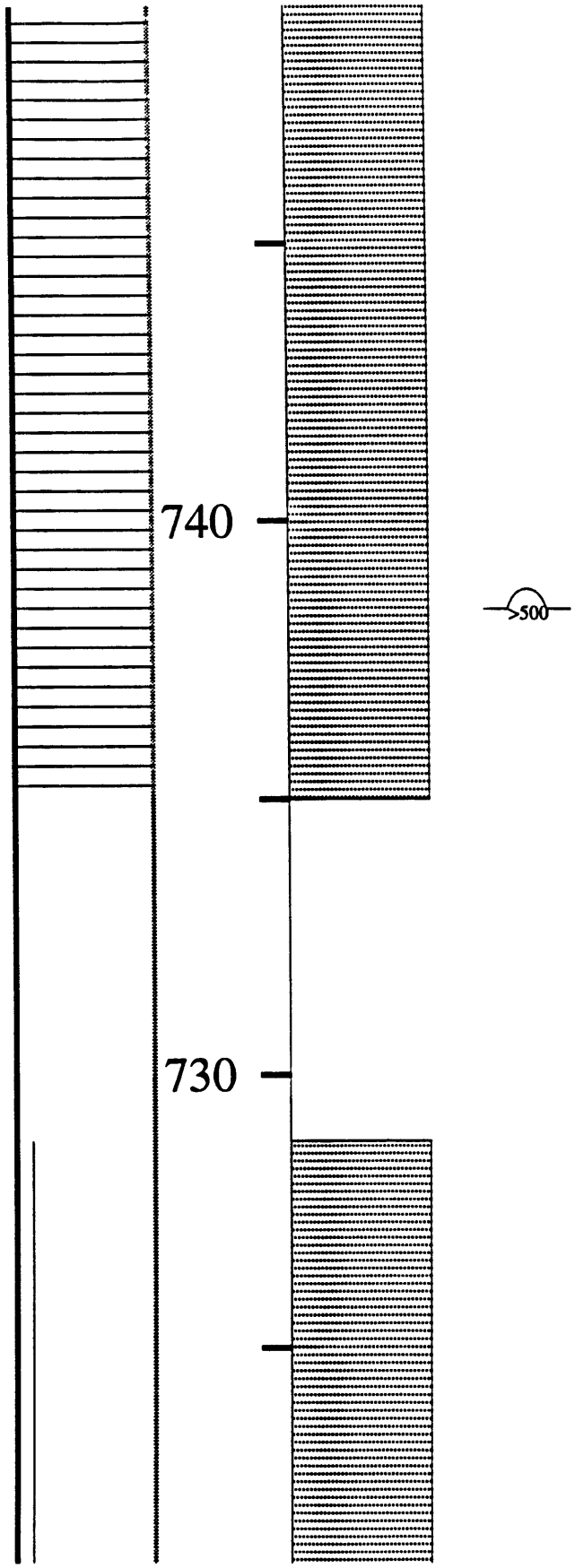
740
500
730

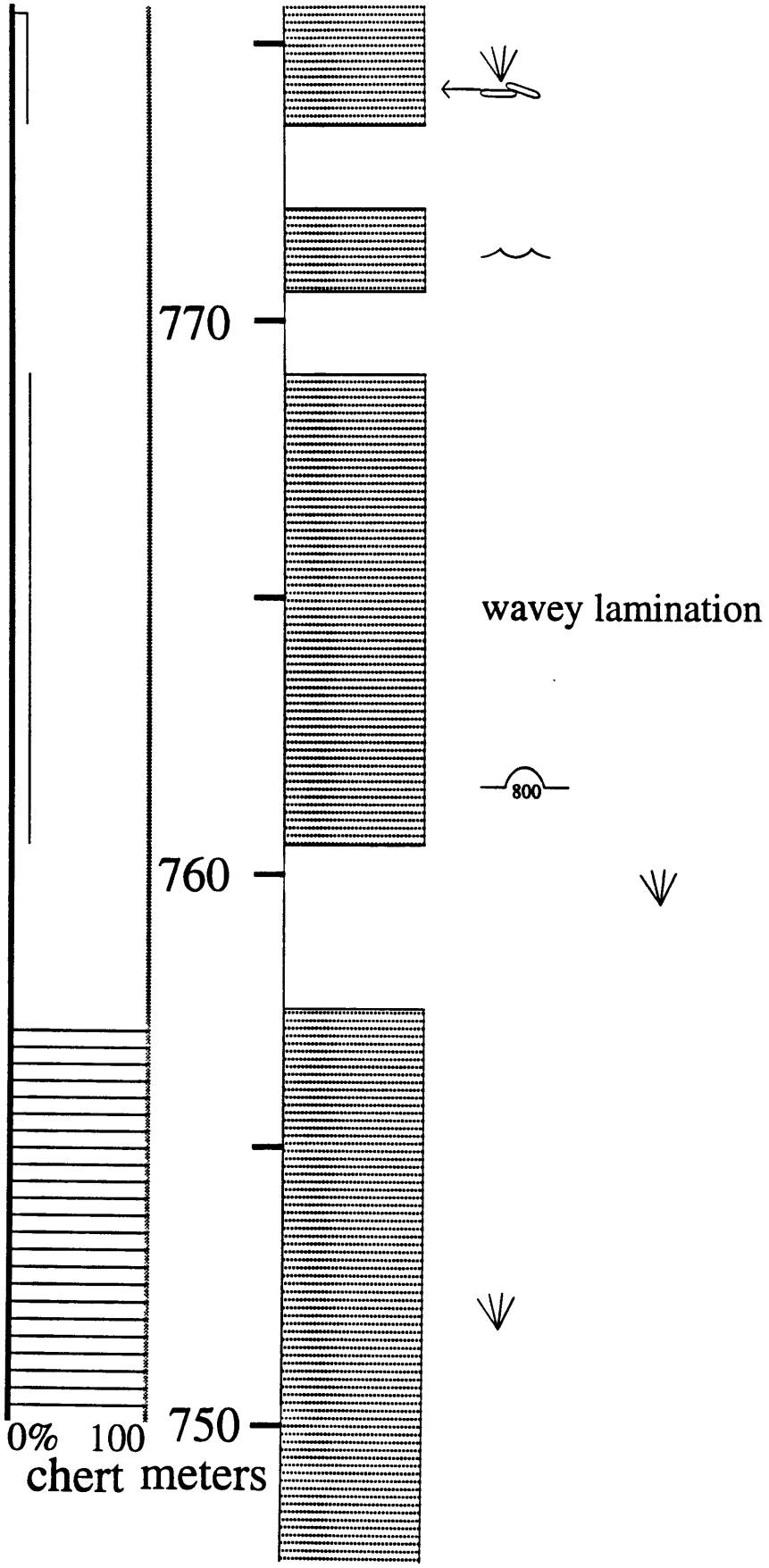
770
760
750
wavey lamination
800
0%
100
chert meters

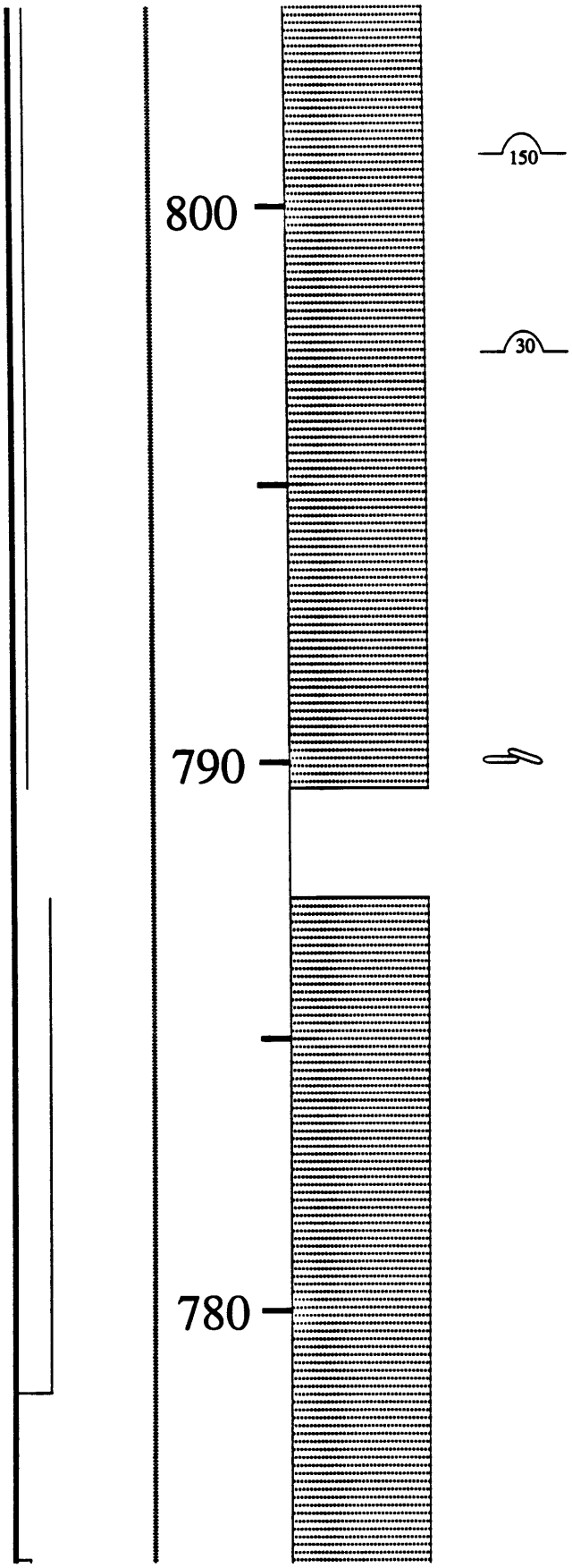
150
800
30
790
780

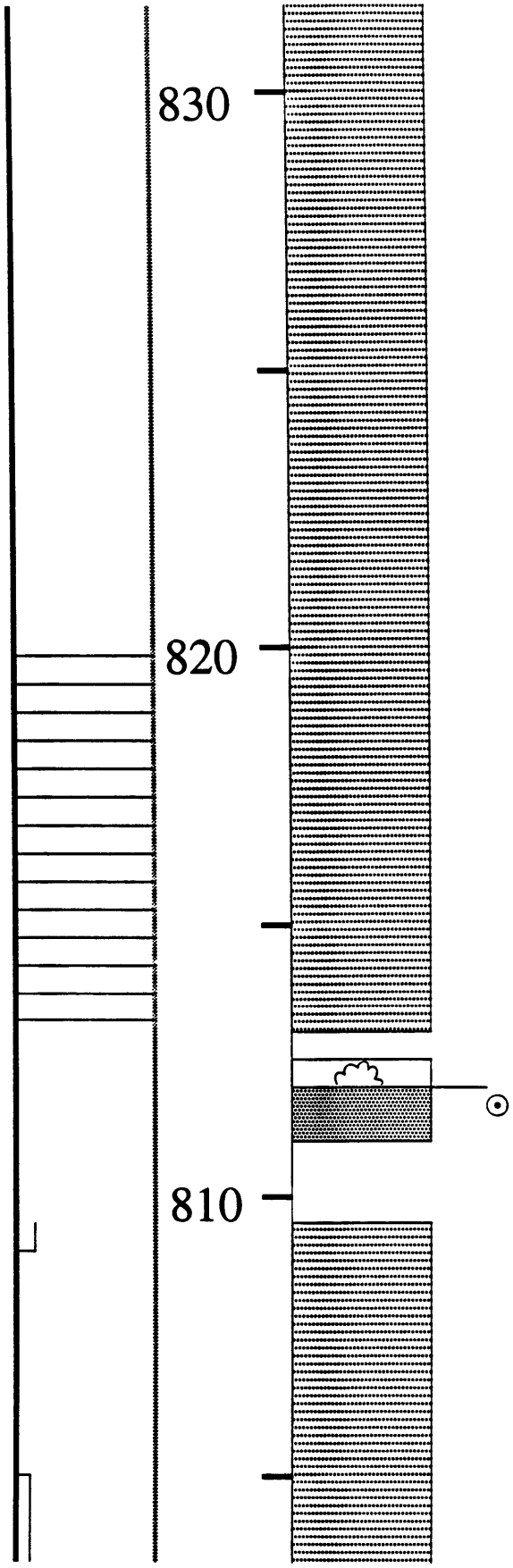
830
820
810

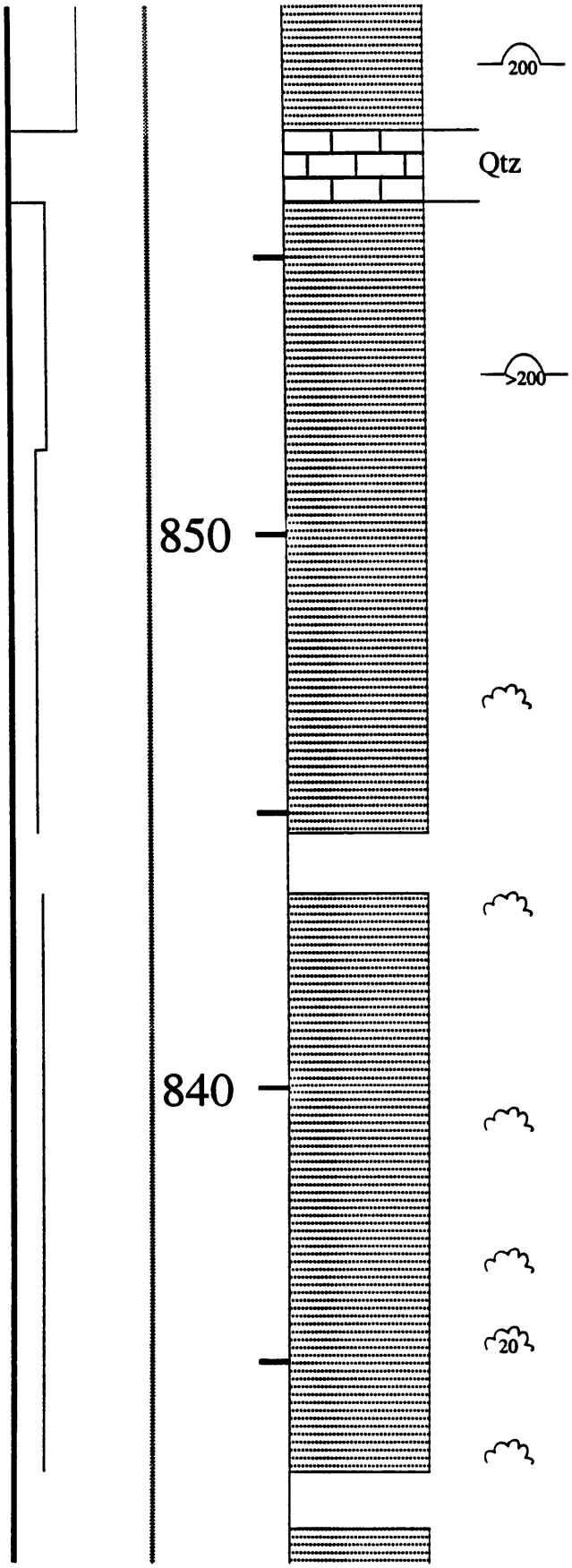
200
Qtz
>200
850
840
20

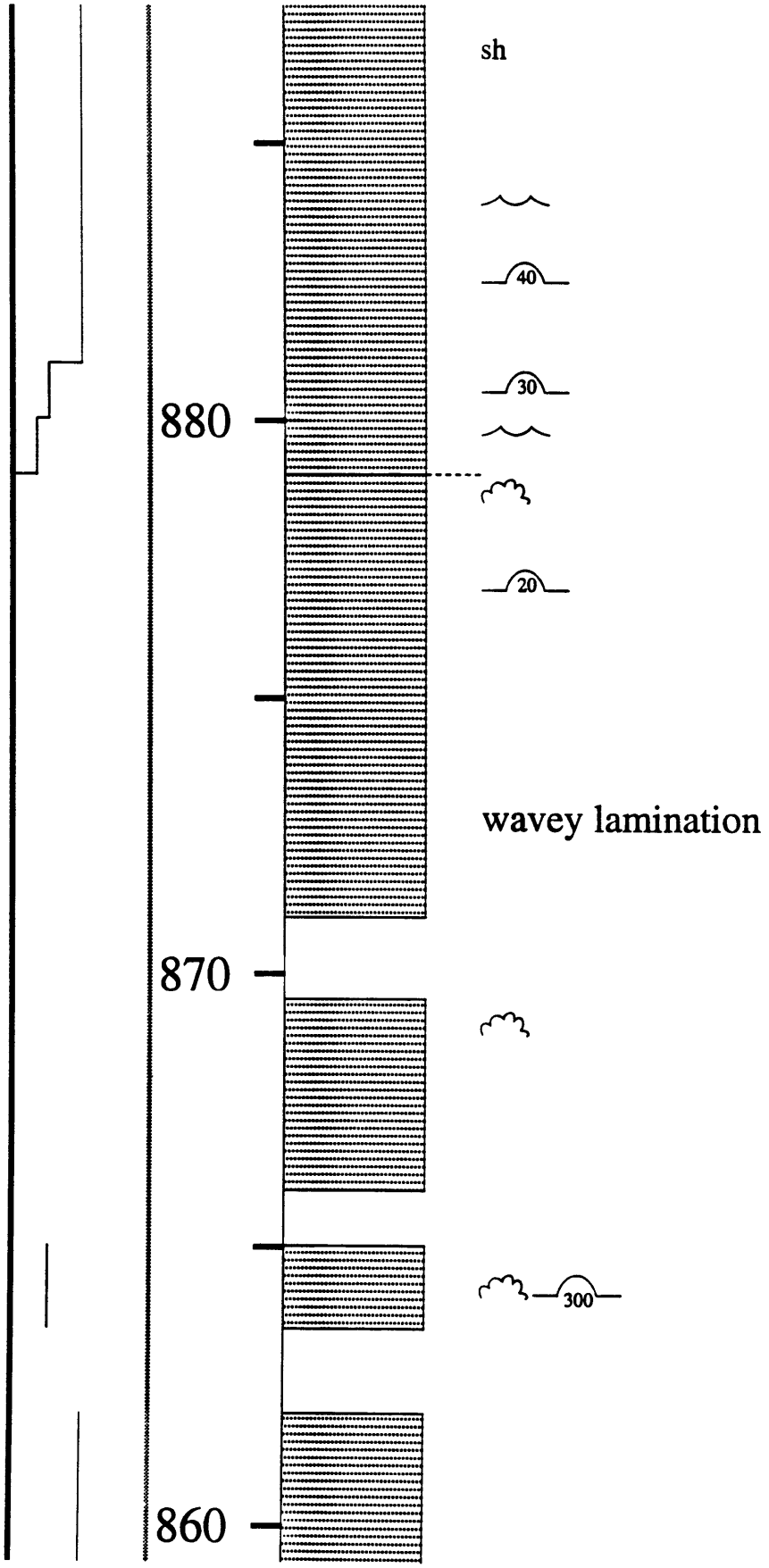
sh
40
30
880
20
wavey lamination
870
300
860

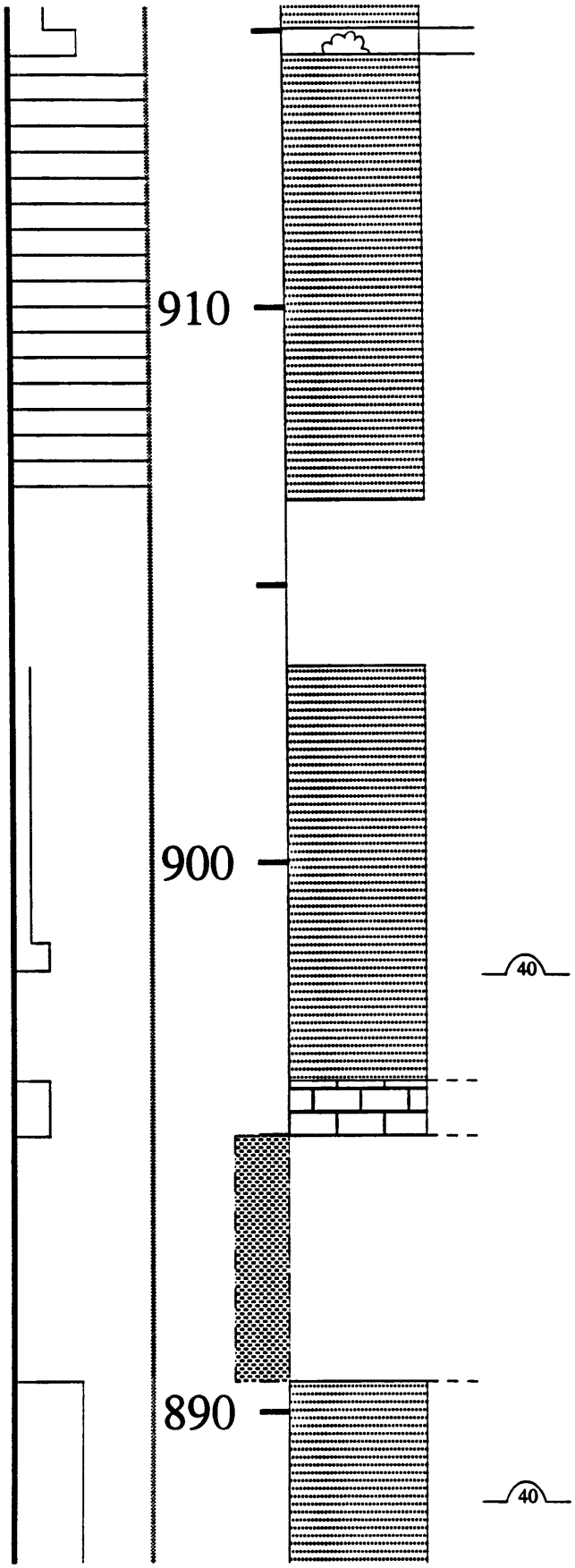
910
900
40
890
40

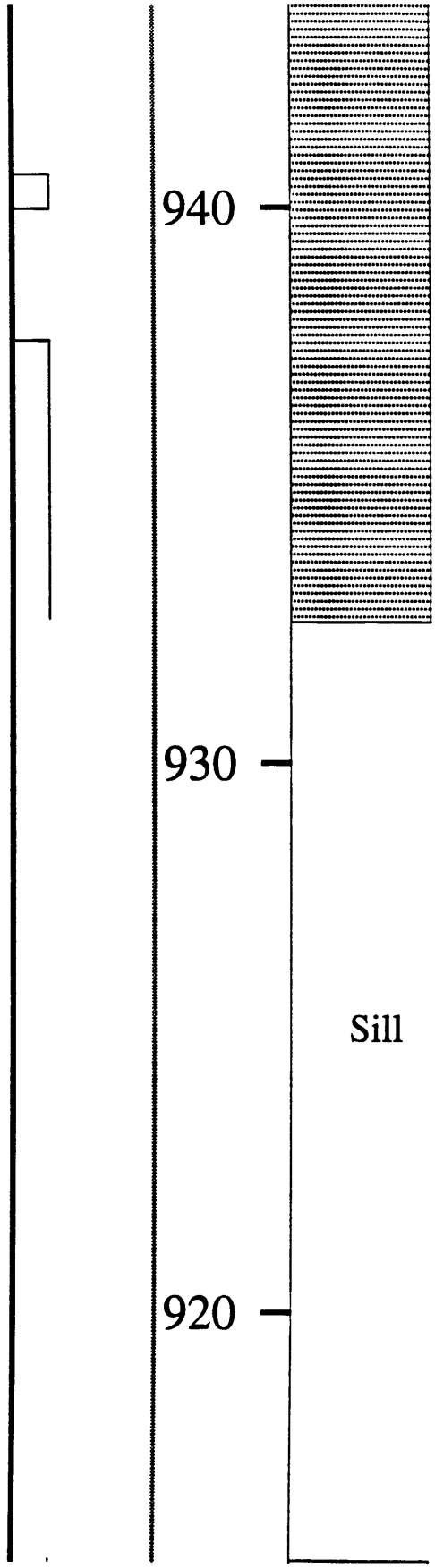
940
930
Sill
920

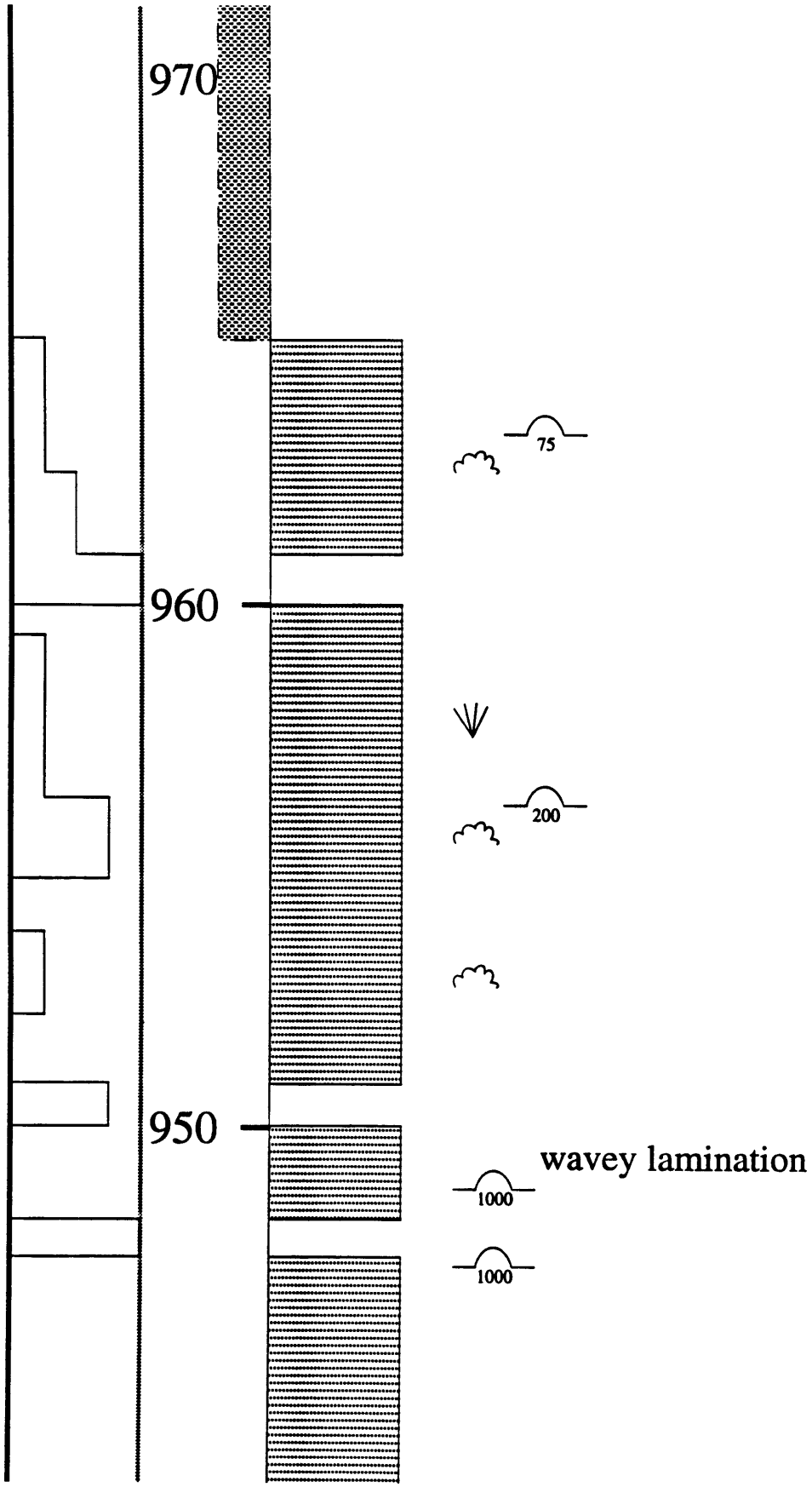
970
960
950
75
200
wavey lamination
1000
1000

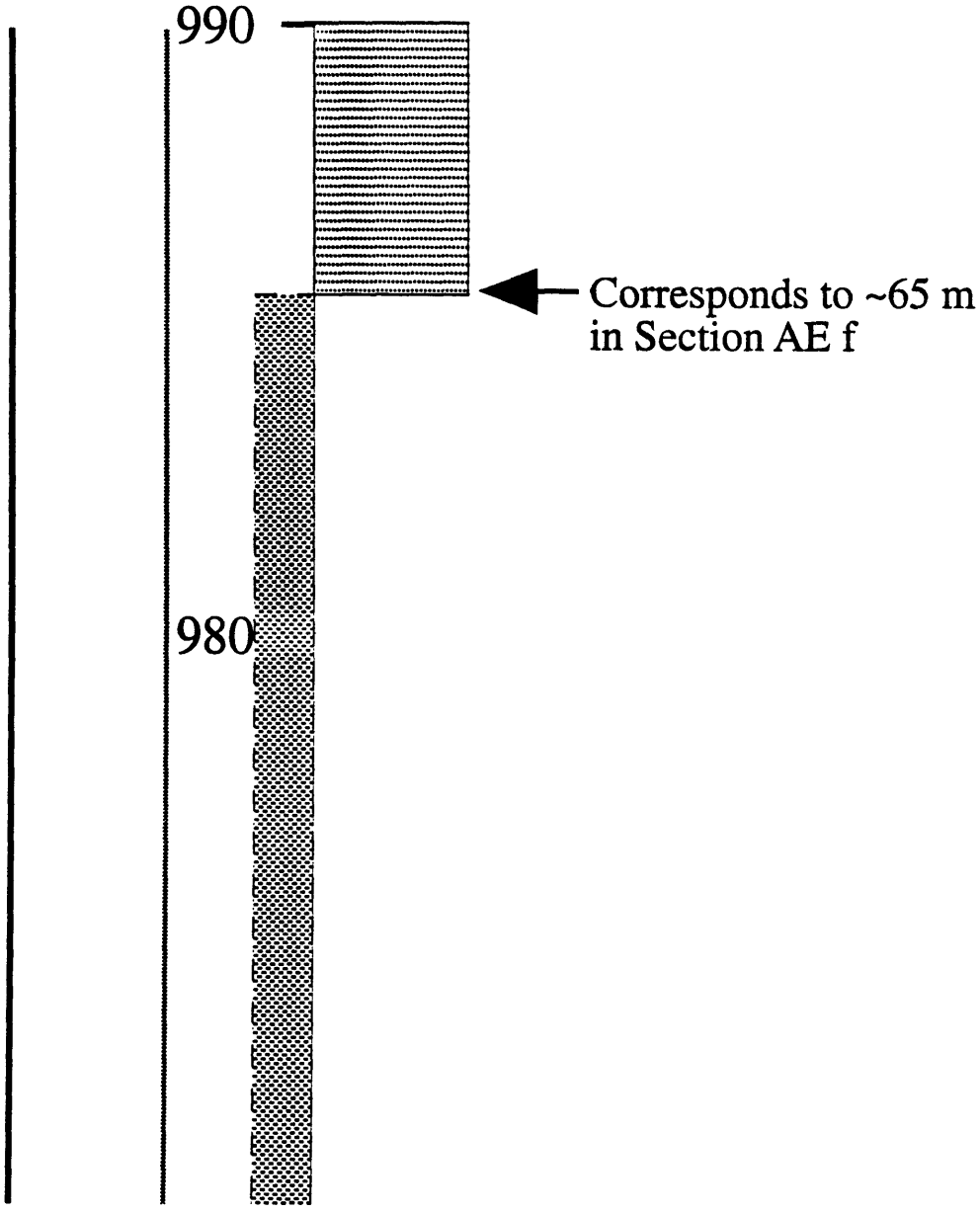
990
980
Corresponds to ~65 m
in Section AE f

## Section BT

Location: Dry falls in Hol River northwest of Boetsap.

Stratigraphic Range: Upper Monteville Formation to mid-Reivilo Formation. The upper section begisn approximately 35 m about the top of the lower section.

Notes: Stromatolites in the drafted section approximate stromatolite geometry in the rocks.

Additional Facies


Irregular, Trapped-and bound Domal Stromatolites


Boetsap-style Lamination


Precipitate-rich Boetsap-style Lamination

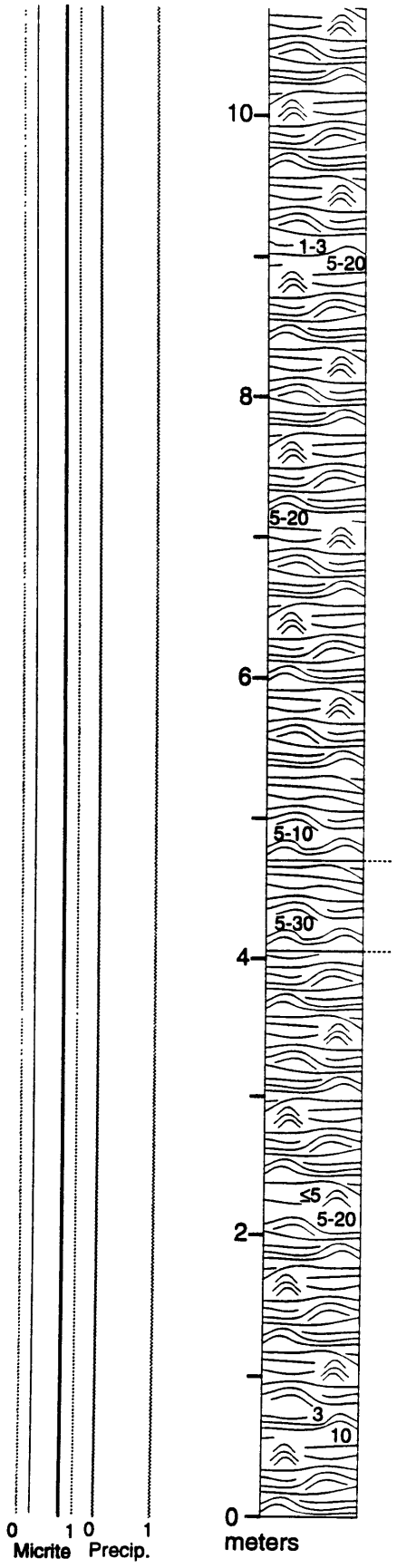
10
1-3
5-20
8
5-20
6
5-10
5-30
4
≤5
5-20
2
3
10
0
meters
0
1
0
1
Micrite
Precip.

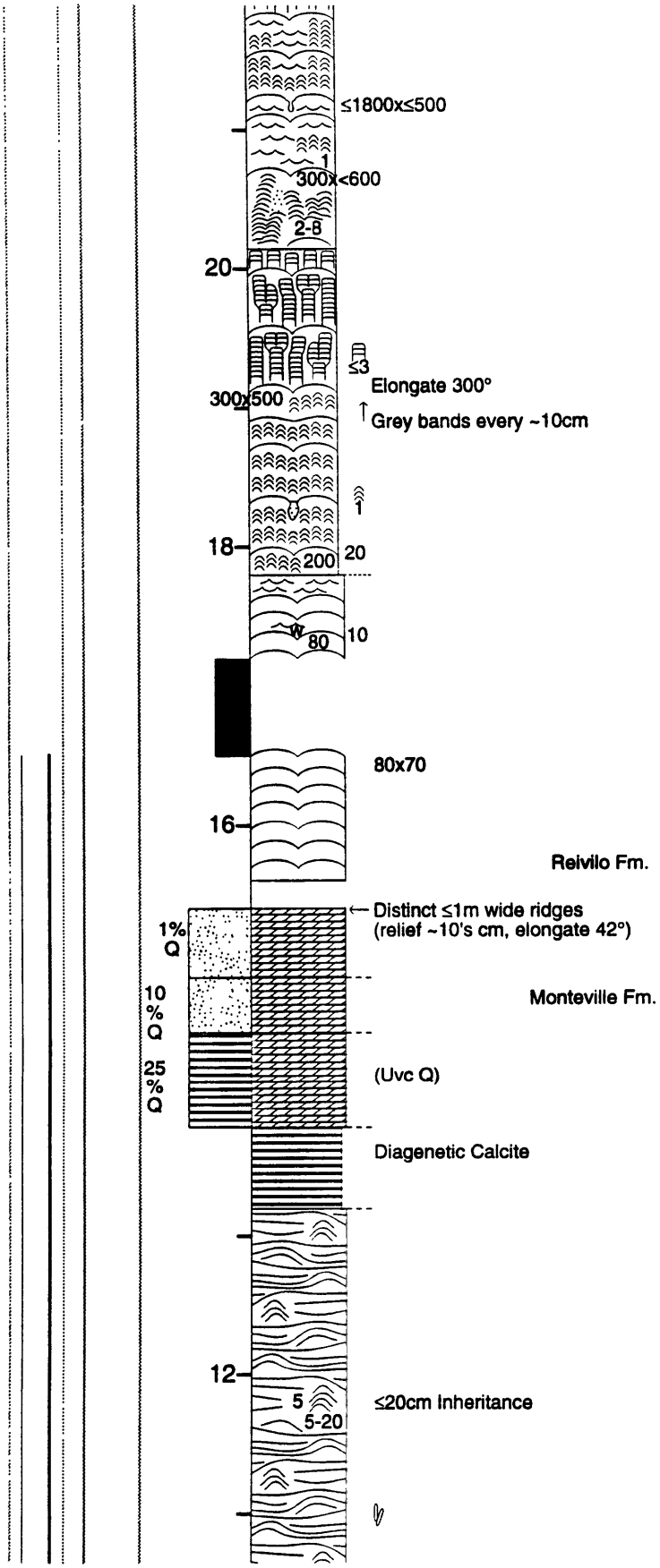
≤1800x≤500
1
300x<600
2-8
20
≤3
Elongate 300°
300x500
Grey bands every ~10cm
1
18
200
20
80
10
80x70
16
Reivilo Fm.
Distinct ≤1m wide ridges
(relief ~10's cm, elongate 42°)
1%
Q
10
%
Q
Monteville Fm.
25
%
Q
(Uvc Q)
Diagenetic Calcite
12
5
5-20
≤20cm Inheritance

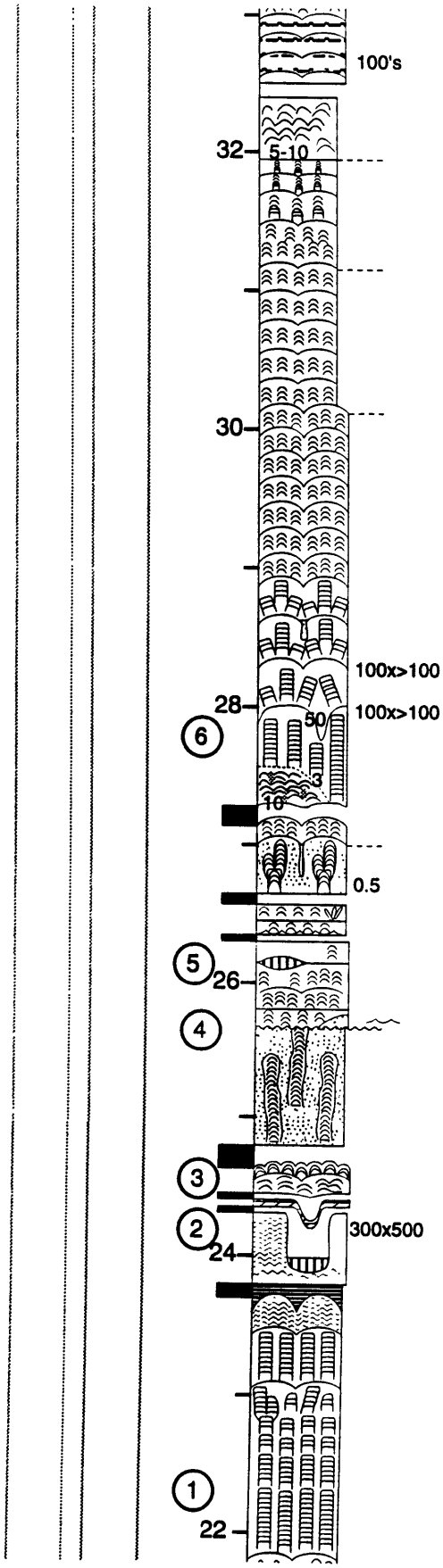
100's
32
5-10
30
100x>100
28
100x>100
50
6
3
10
0.5
5
26
4
3
2
300x500
24
1
22

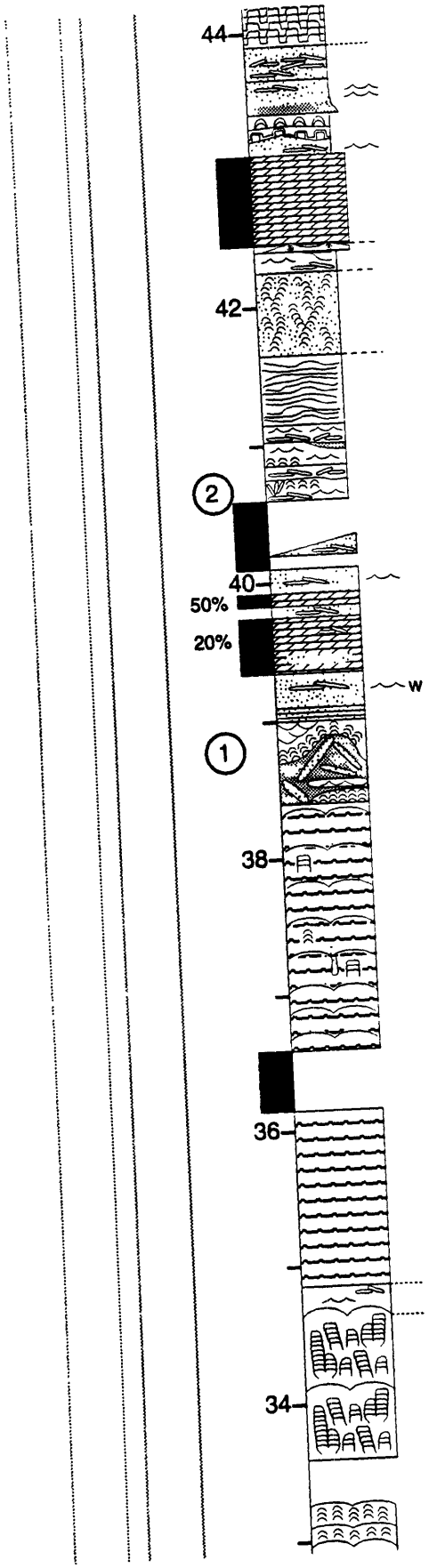
44
42
2
40
50%
20%
W
1
38
36
34

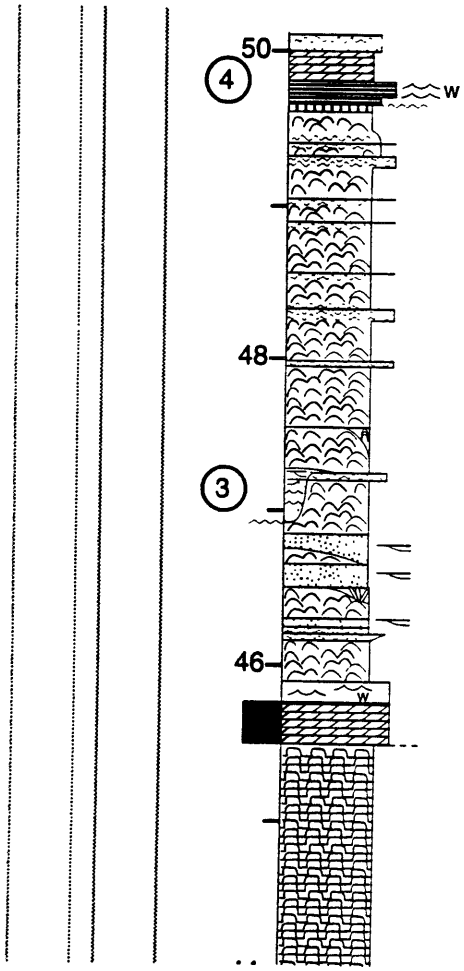
50
4
w
48
3
46
w

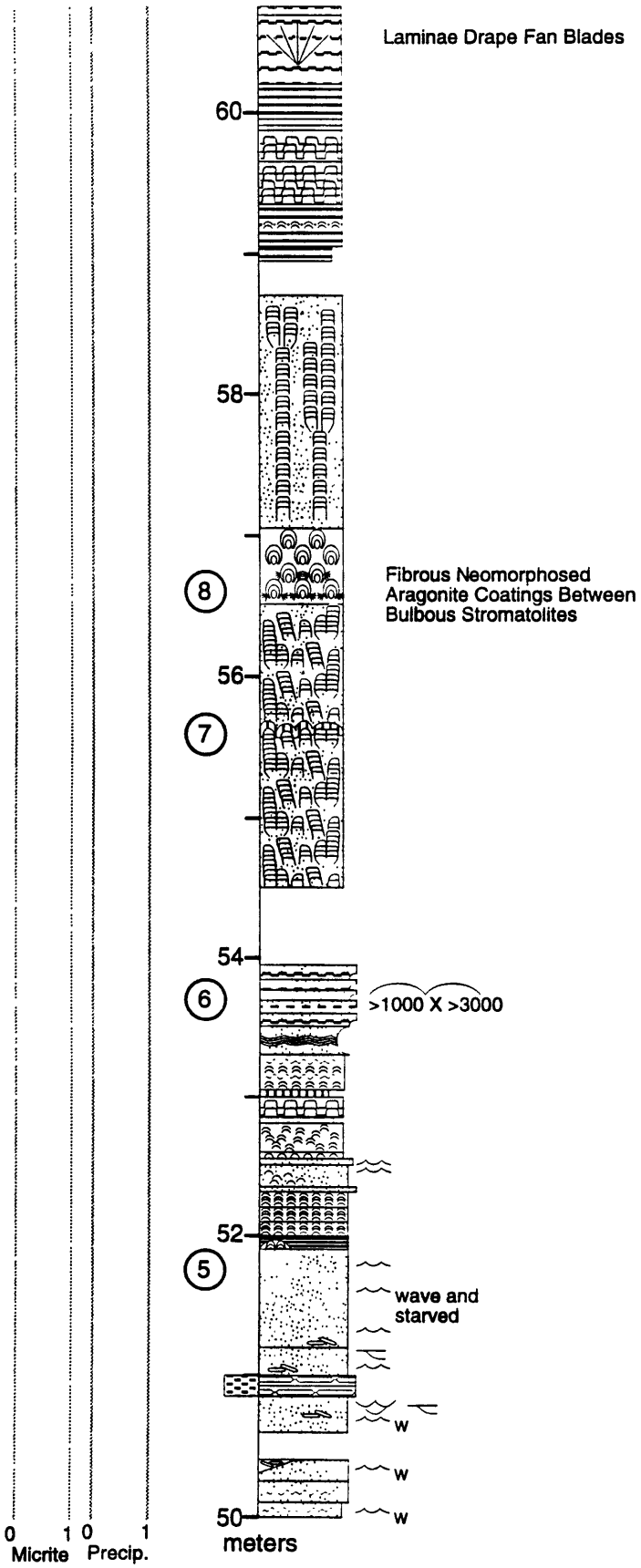
Laminae Drape Fan Blades
60
58
8
Fibrous Neomorphosed
Aragonite Coatings Between
Bulbous Stromatolites
56
7
54
6
>1000 X >3000
52
5
wave and
starved
w
w
w
50
meters
0 1 0 1
Micrite Precip.

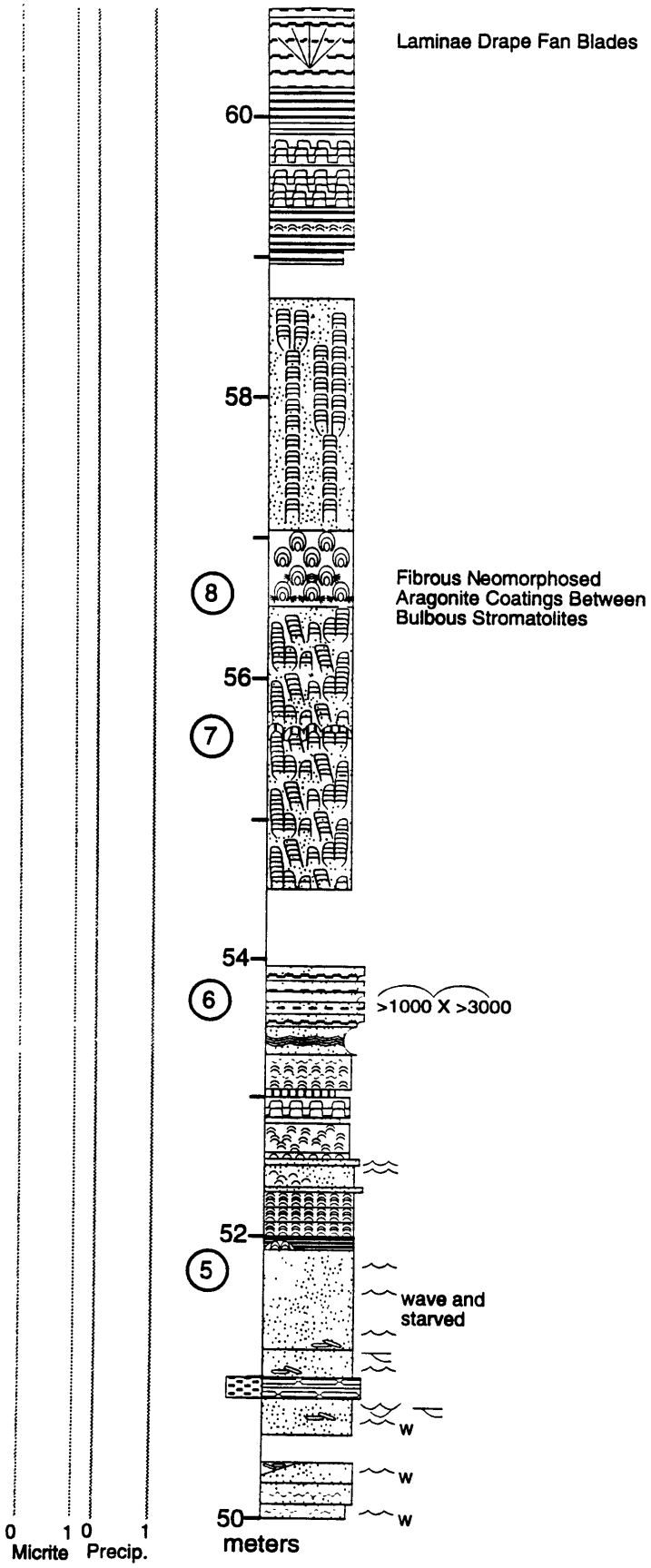
Laminae Drape Fan Blades
60
58
8
Fibrous Neomorphosed
Aragonite Coatings Between
Bulbous Stromatolites
56
7
54
6
>1000 X >3000
52
5
wave and
starved
w
w
w
50
meters
0
1
0
1
Micrite
Precip.

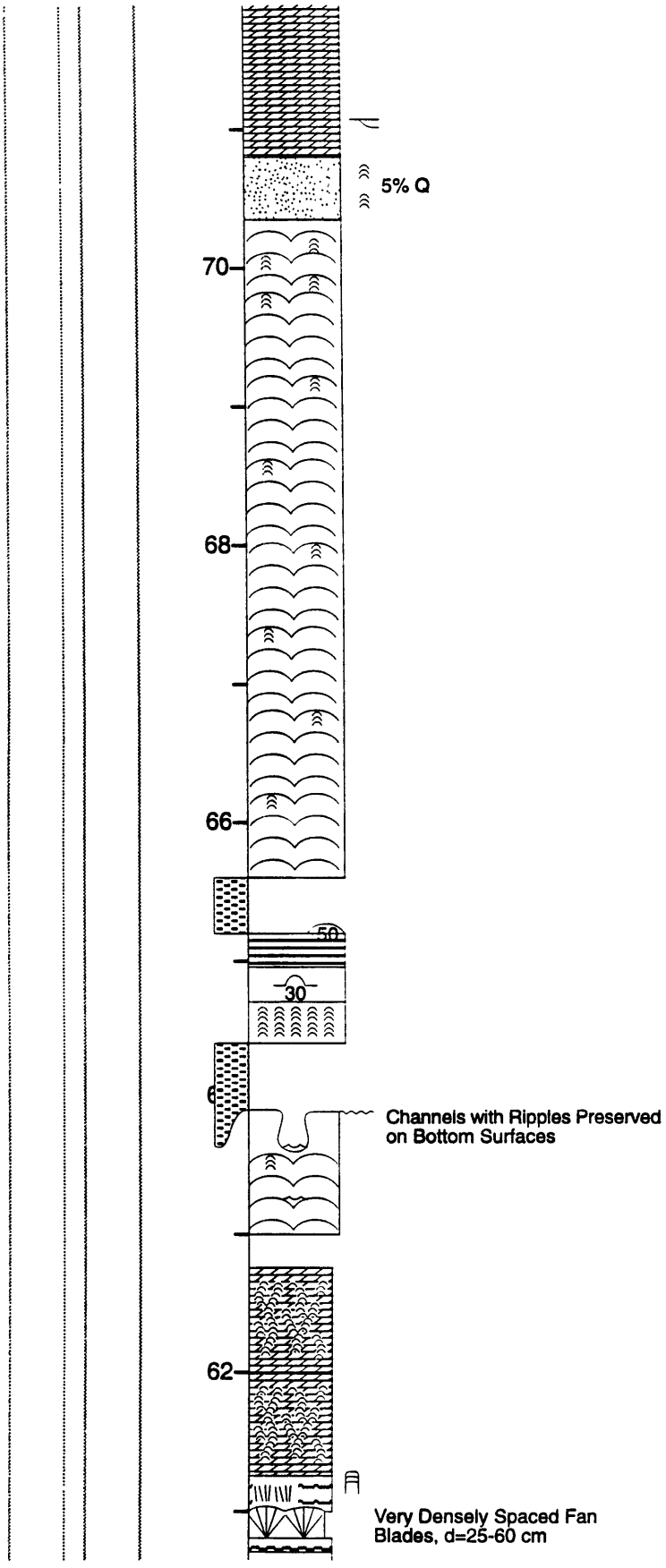
5% Q
70
68
66
50
30
Channels with Ripples Preserved
on Bottom Surfaces
62
Very Densely Spaced Fan
Blades, d=25-60 cm

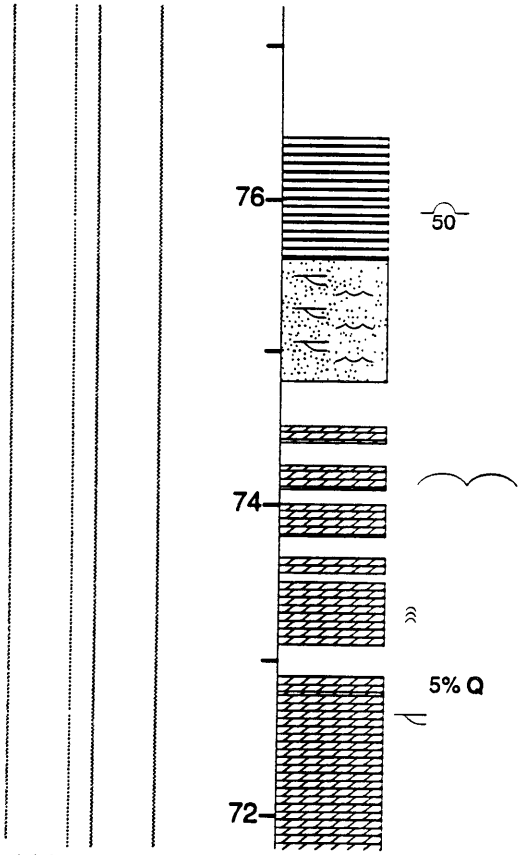
76
50
74
5% Q
72

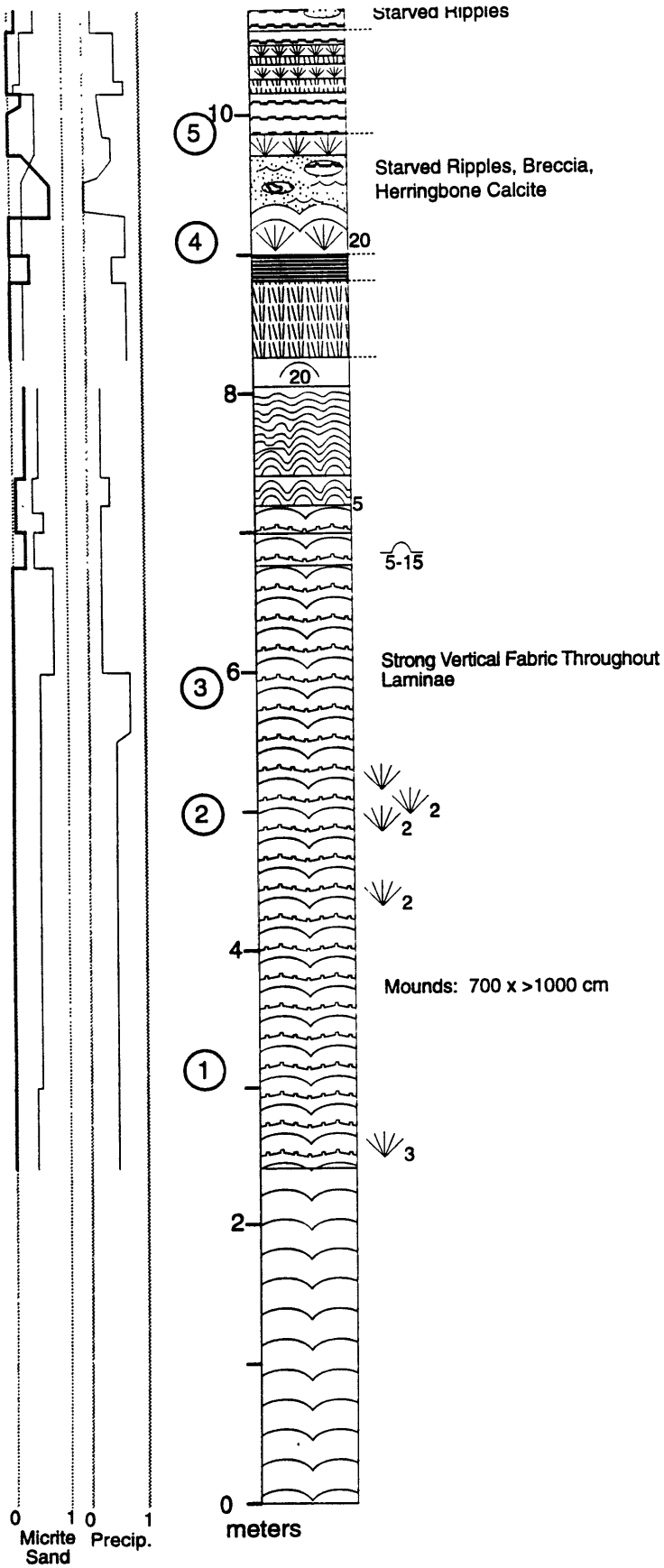
Starved Ripples
Starved Ripples, Breccia,
Herringbone Calcite
Strong Vertical Fabric Throughout
Laminae
Mounds: 700 x >1000 cm
5-15
20
5
2
3
10
8
6
4
2
0
0 1 0 1
Micrite Sand
Precip.
meters

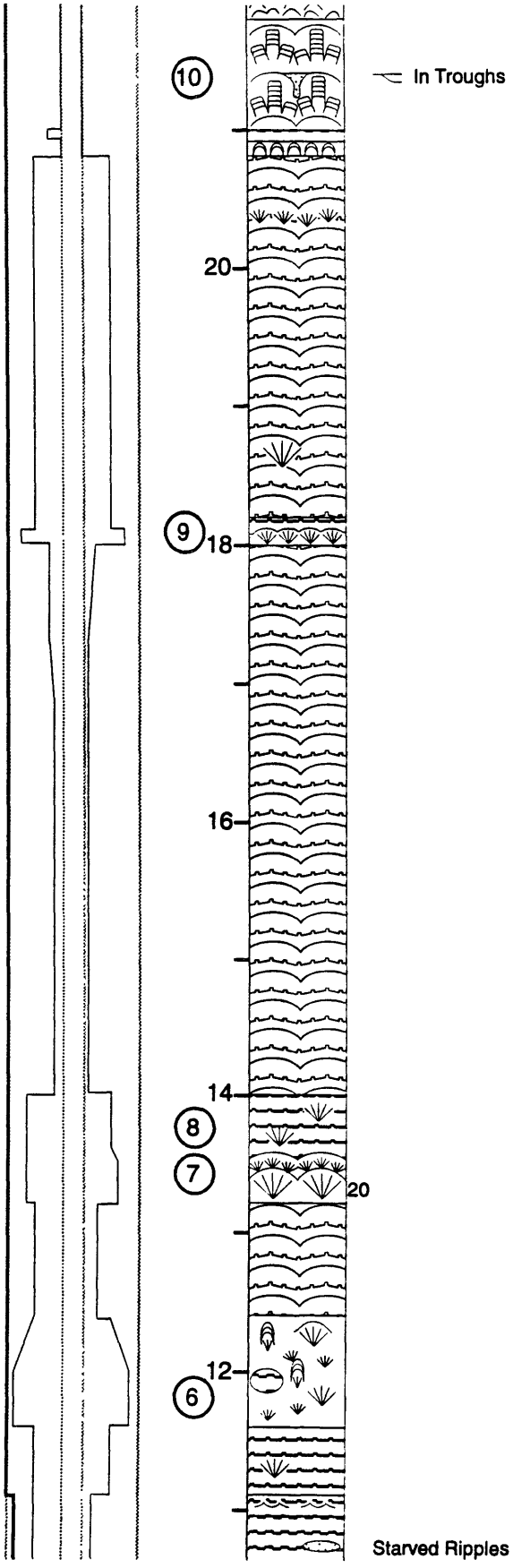
10
In Troughs
20
9
18
16
14
8
7
20
12
6
Starved Ripples

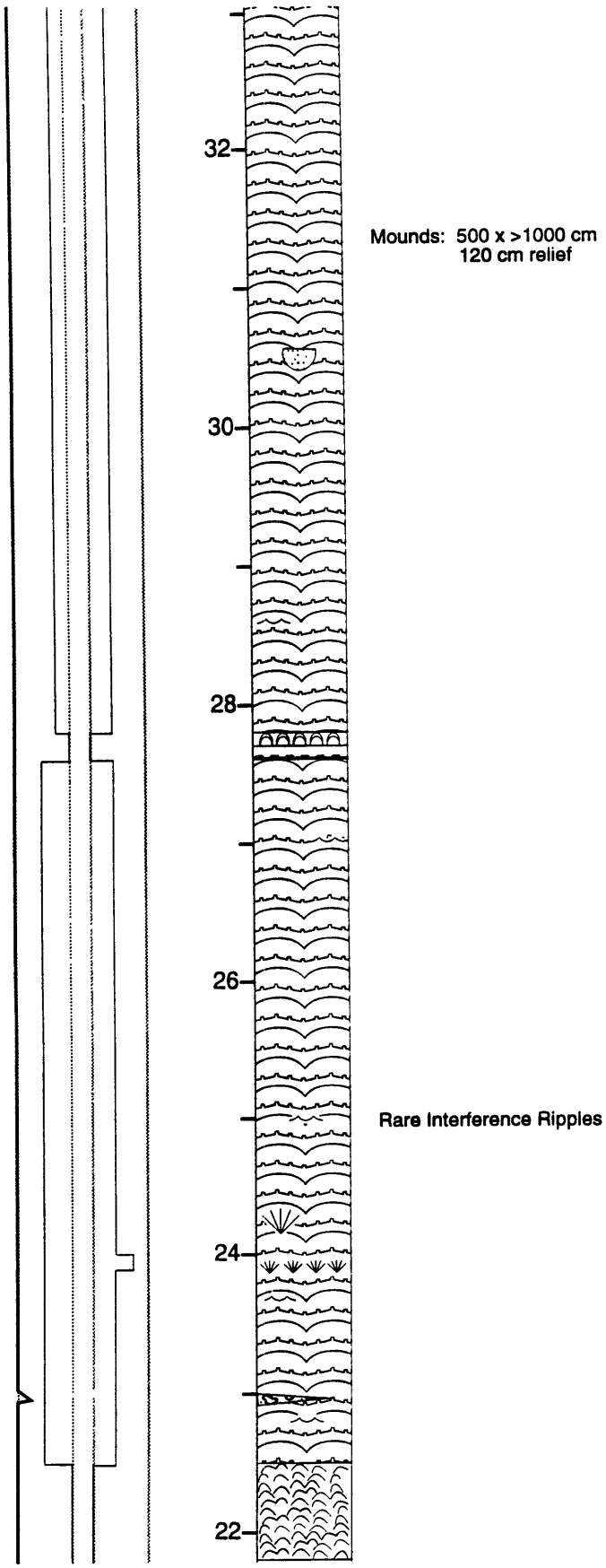
32
30
28
26
24
22
Mounds: 500 x >1000 cm
120 cm relief
Rare Interference Ripples

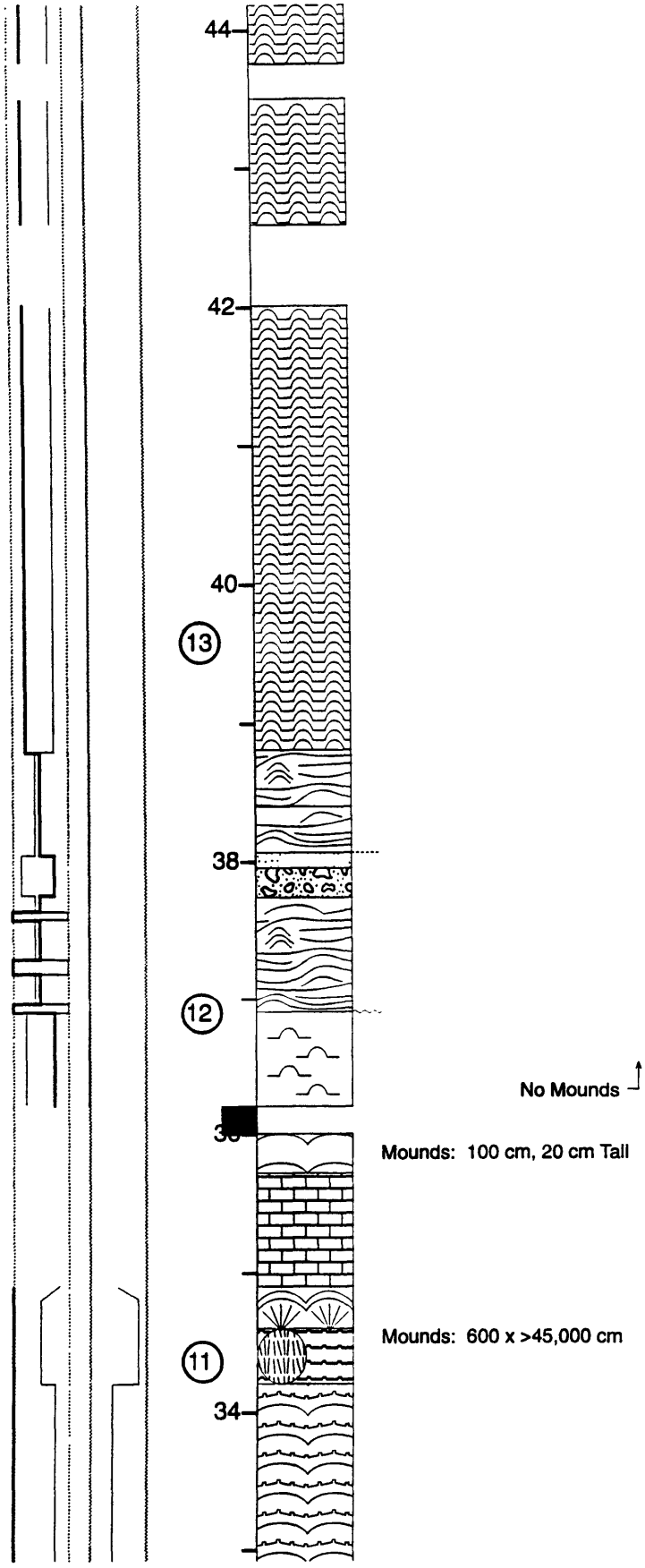
44
42
40
13
38
12
No Mounds
Mounds: 100 cm, 20 cm Tall
11
Mounds: 600 x >45,000 cm
34

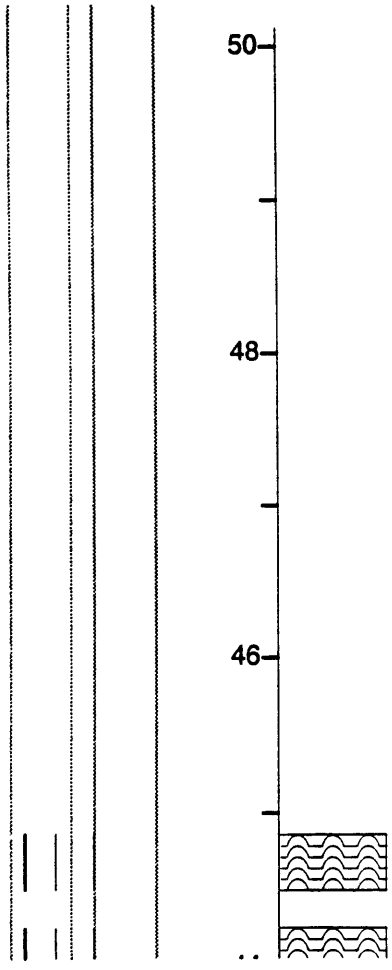
50
48
46

## Core ELF1

Location: Farm west of Johannesburg. Core belongs to Goldfields and is stored at their Carltonville facility.

Stratigraphic Range: Black Reef Quartzite to mid-Eccles Formation.

Additional Facies

 Herringbone Calcite-cemented Grainstone

 Small Columnar Stromatolites

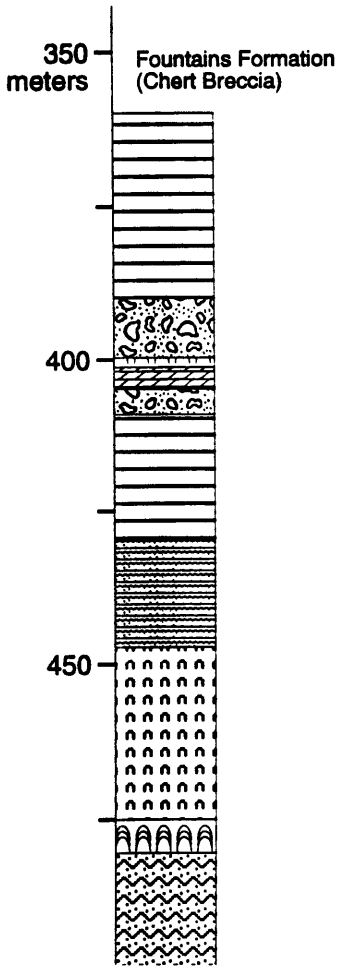
350
meters
Fountains Formation
(Chert Breccia)
400
450

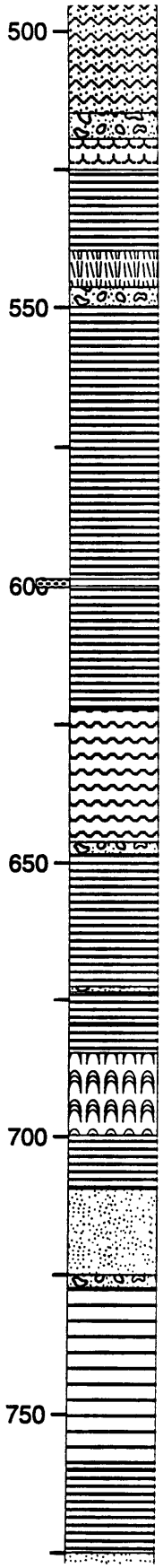
500
550
600
650
700
750

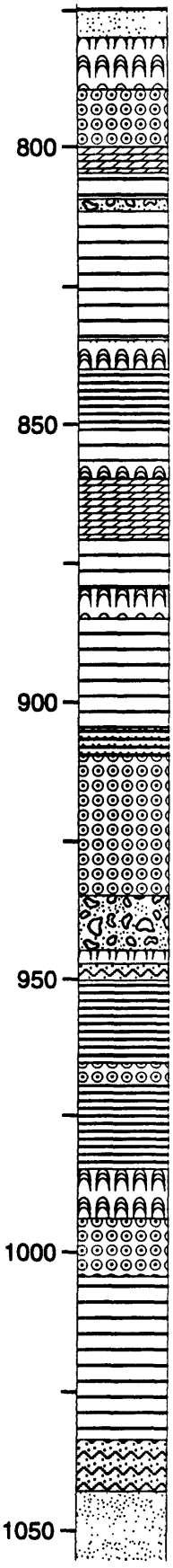
800
850
900
950
1000
1050

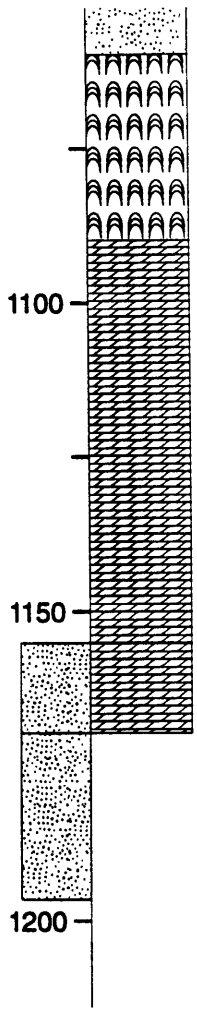
1100
1150
1200

## Section KN

Location: Klein Naute Farm on the northeast bank of the Orange River betwen Philippois and Luckhoff.

Stratigraphic Range: Mid- Nauga Formation to lower Naute Shale.

Additional Facies

⊥ Cuspate Microbialites

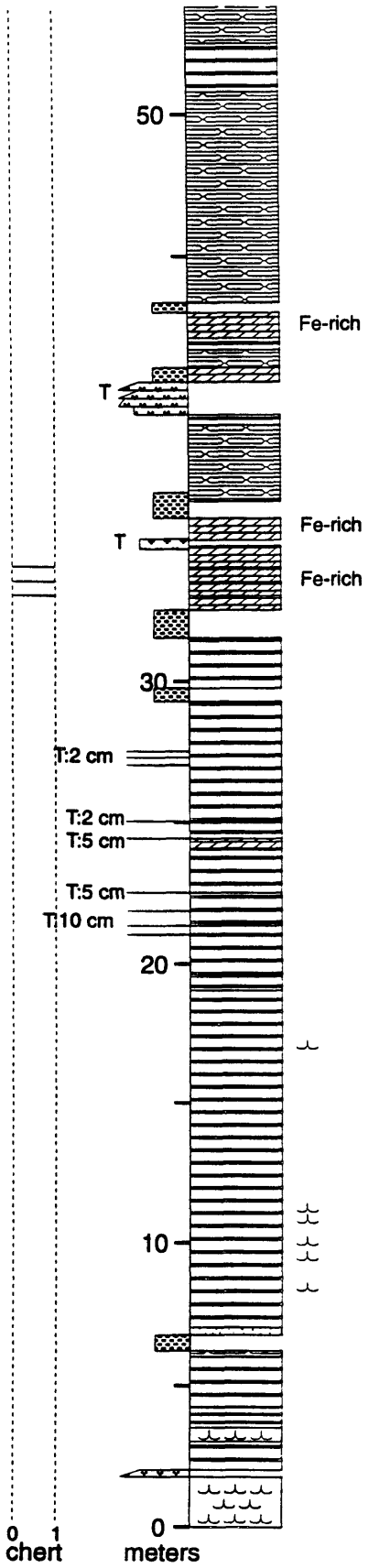
50
Fe-rich
T
Fe-rich
T
Fe-rich
30
T:2 cm
T:2 cm
T:5 cm
T:5 cm
T:10 cm
20
10
0
0 1
chert
meters

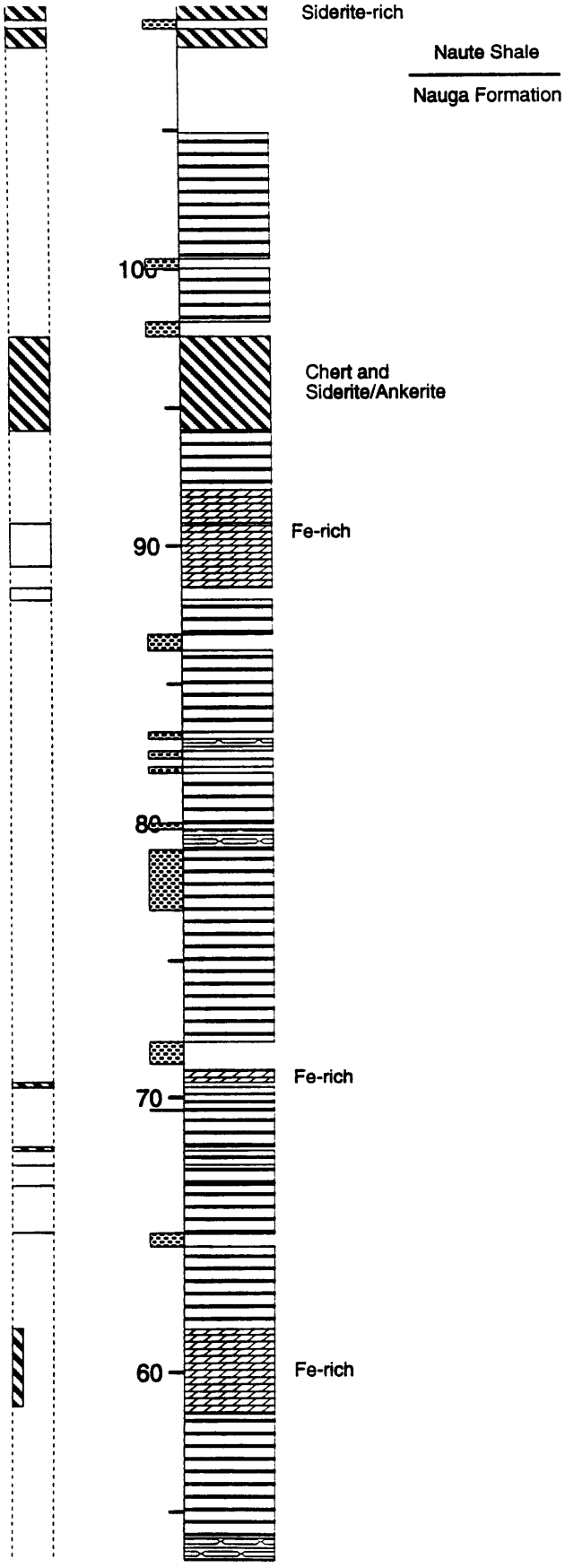
Siderite-rich
Naute Shale
Nauga Formation
100
Chert and
Siderite/Ankerite
Fe-rich
90
80
Fe-rich
70
Fe-rich
60

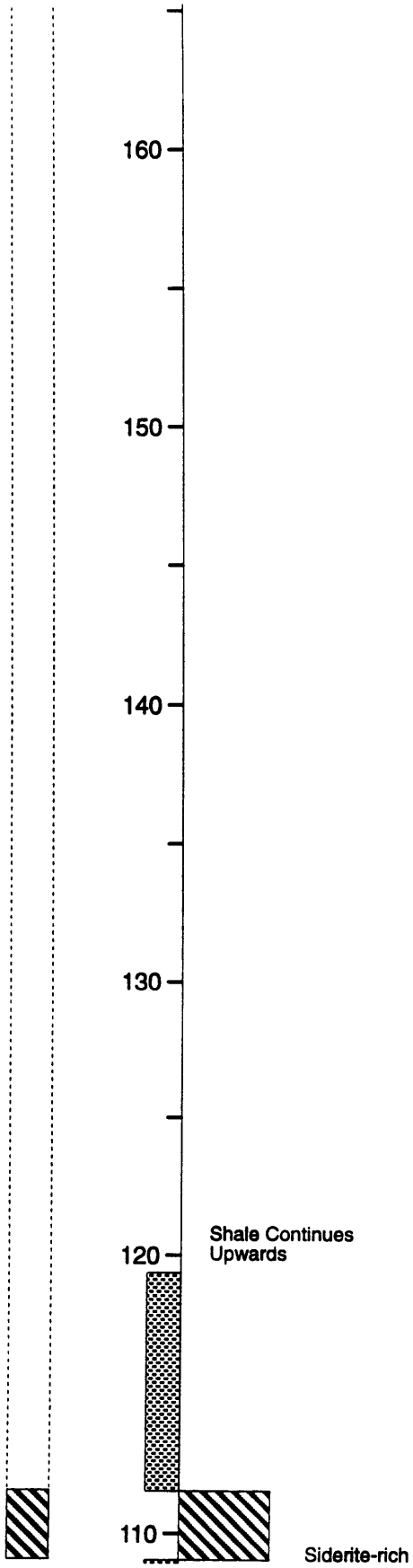
160
150
140
130
120
110
Shale Continues
Upwards
Siderite-rich

## Section MV

Location: Monteville Farm along gravel road between Schmidtsdrif and Papkuil.

Stratigraphic Range: Upper Monteville Formation to lower Reivilo Formation.

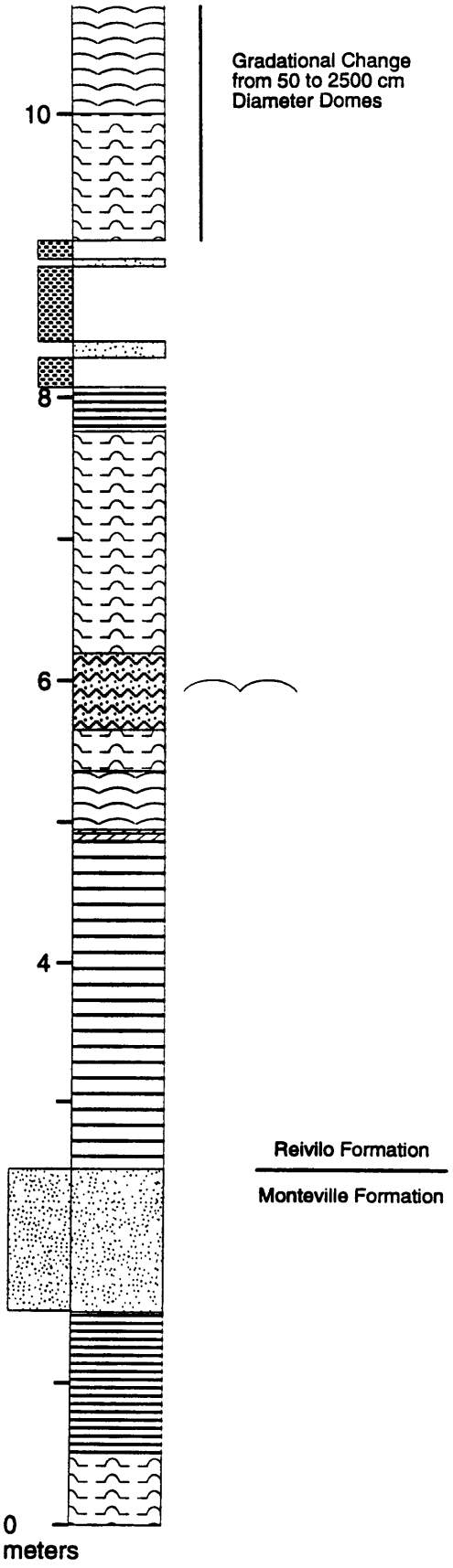
Gradational Change
from 50 to 2500 cm
Diameter Domes
10
8
6
4
0
meters
Reivilo Formation
Monteville Formation

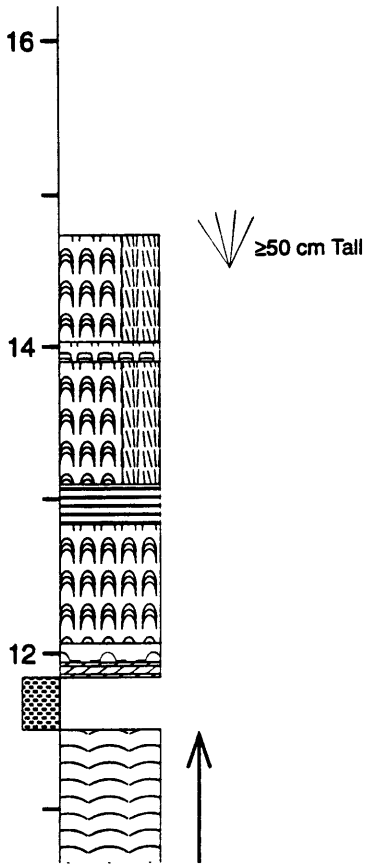
16
14
12
≥50 cm Tall

## Section NA

Location: Nauga Farm north of road R32 between Prieska and Marydale.

Stratigraphic Range: Within Nauga Formation

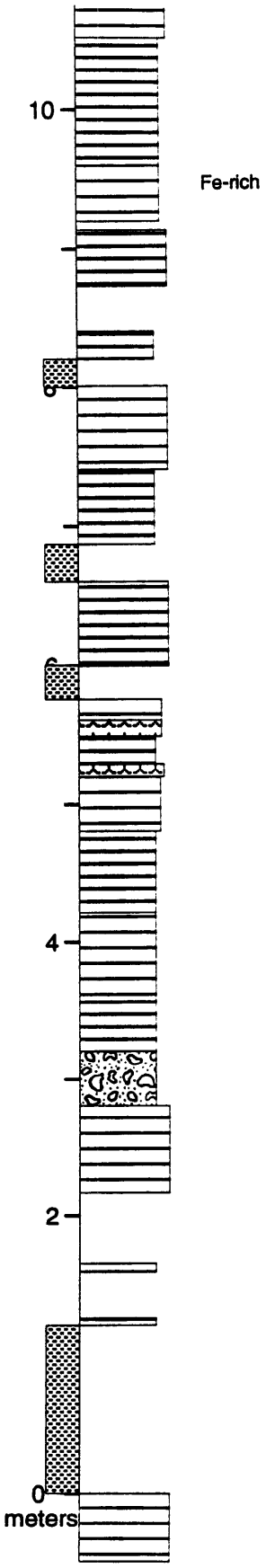
10
Fe-rich
8
6
4
2
0
meters

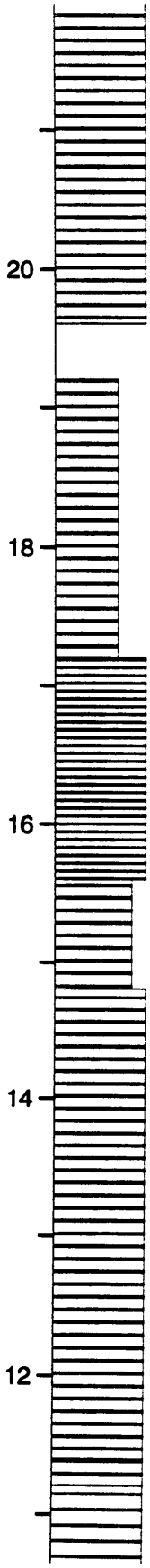
20
18
16
14
12

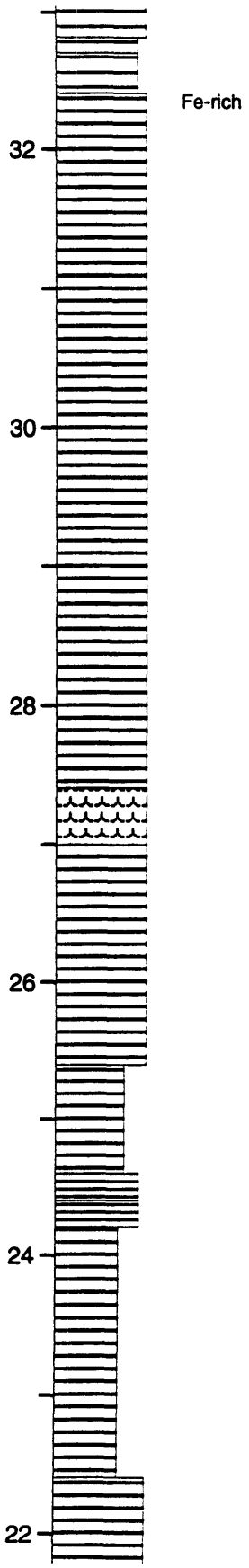
Fe-rich
32
30
28
26
24
22

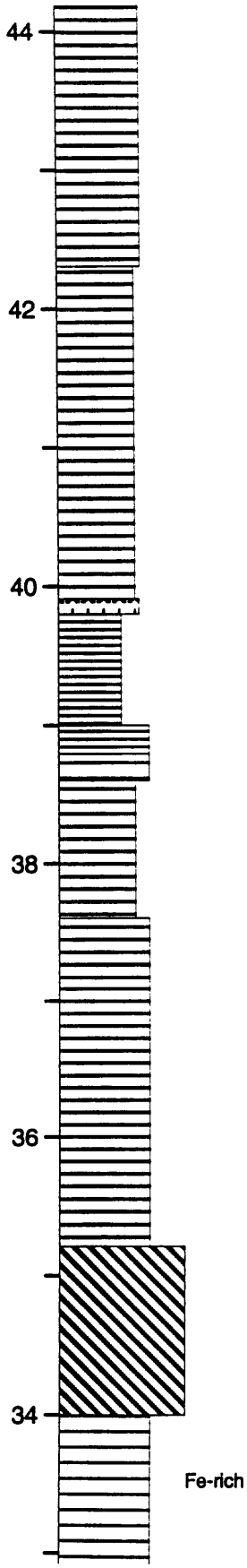
44
42
40
38
36
34
Fe-rich

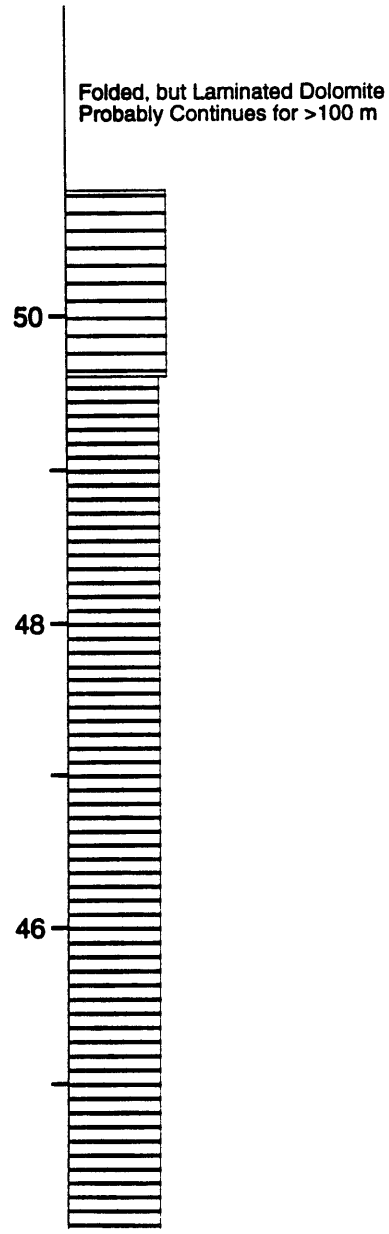
Folded, but Laminated Dolomite
Probably Continues for >100 m
50
48
46

## Sections RA and RA#2

Location: Ranger farm on south side of the gravel road leaving east from Koegas towards the Prieska-Niekerkshoop road (R386).

Stratigraphic Range: Slope equivalents to the Reivilo Formation. Section RA#2 is a more detailed log of the upper part of section RA a kilometer to the west. The iron-formation at 172 m in RA and 44 m in RA#2 is the Kamden Member at the top of the Reivilo Formation.

Additional Facies

 Rhythmites with Crinkled (Microbial?)Laminae

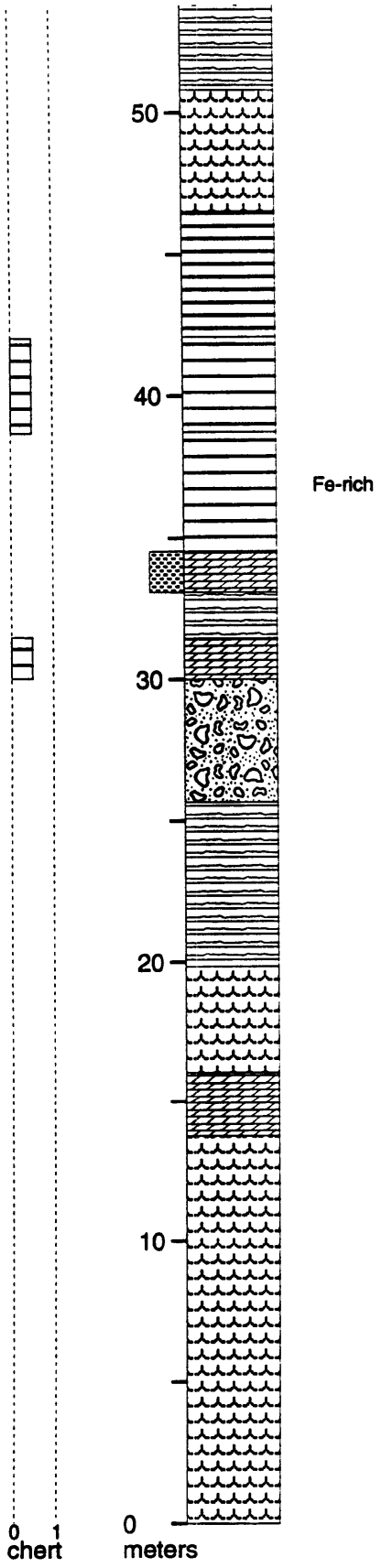
50
40
30
20
10
0
Fe-rich
0
1
chert
meters

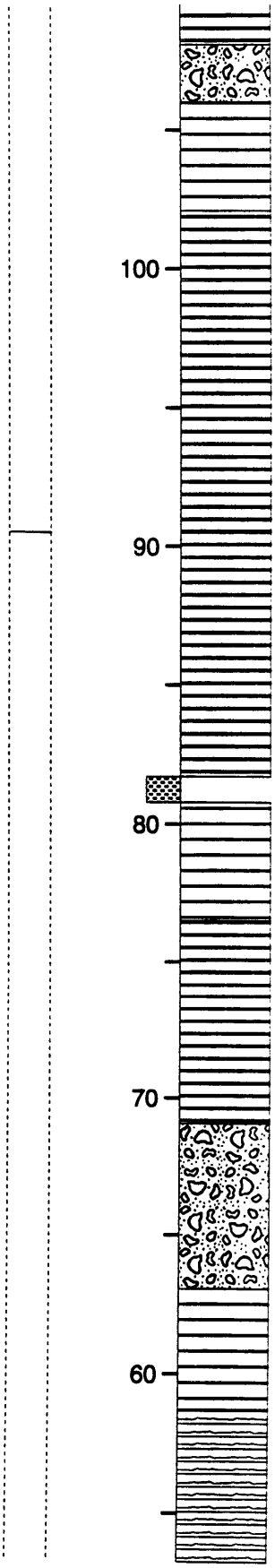
100
90
80
70
60

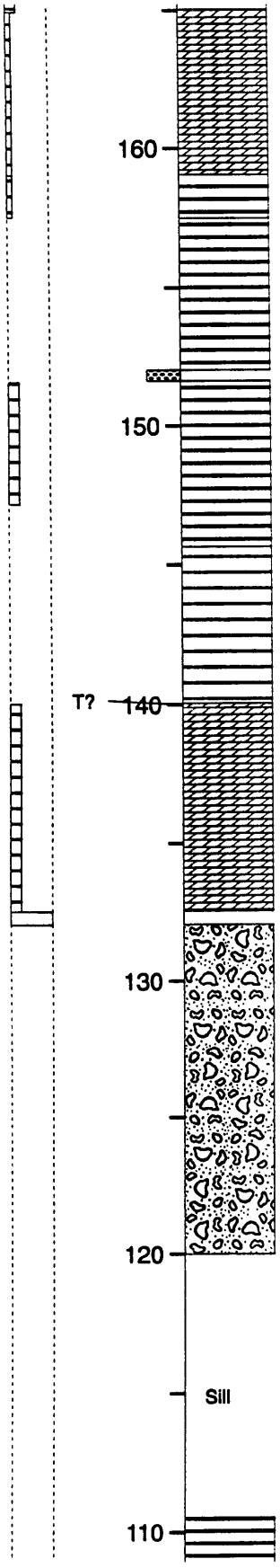
160
150
T?
140
130
120
Sill
110

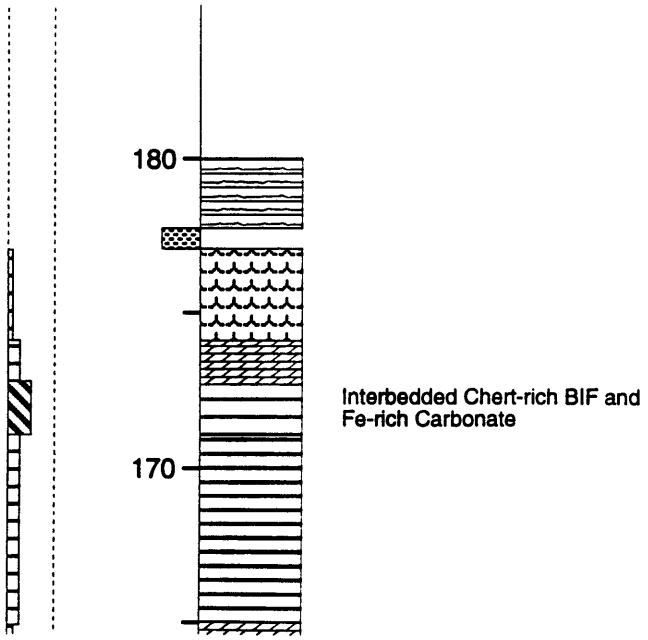
180
170
Interbedded Chert-rich BIF and
Fe-rich Carbonate

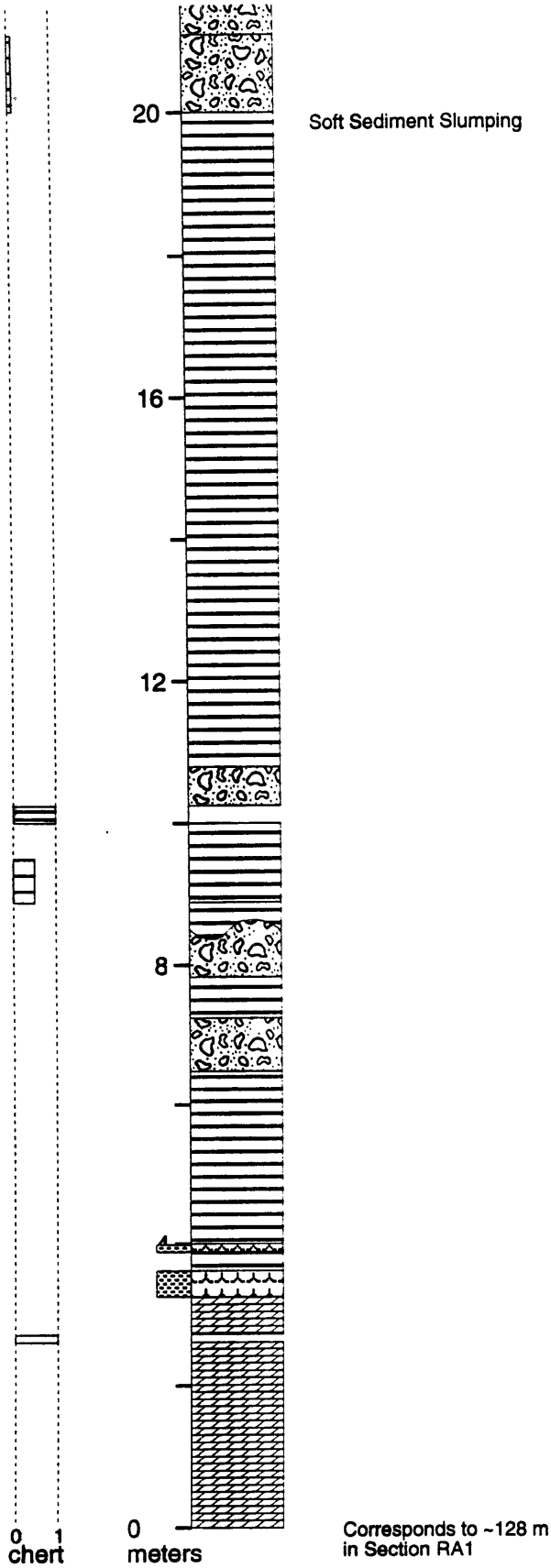
20
16
12
8
4
0
Soft Sediment Slumping
0 1
chert
meters
Corresponds to ~128 m
in Section RA1

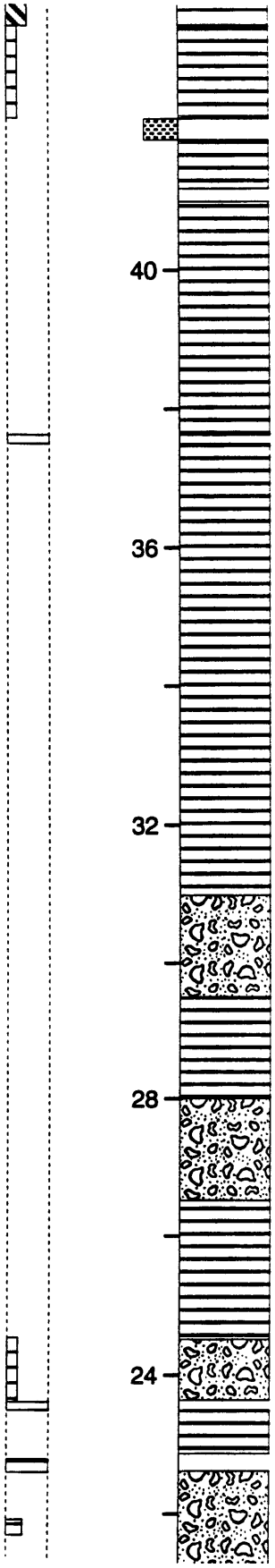
40
36
32
28
24

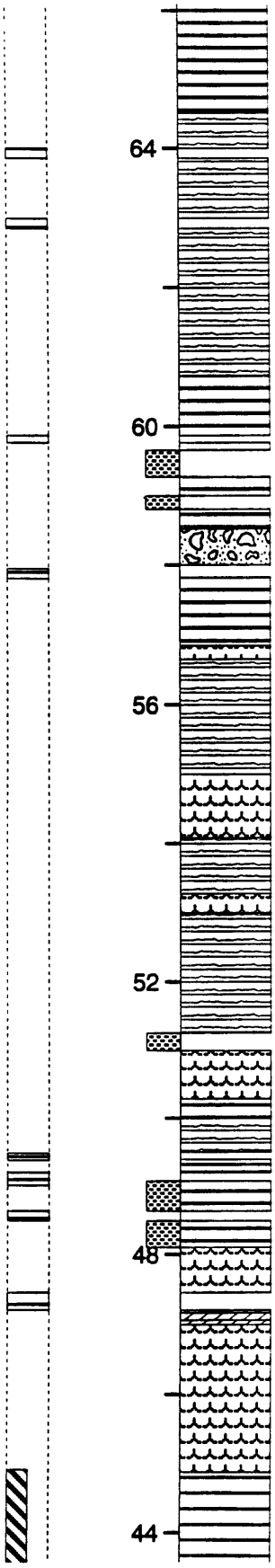


Interbedded Chert-rich
Iron-formation and Iron-rich
Carbonate

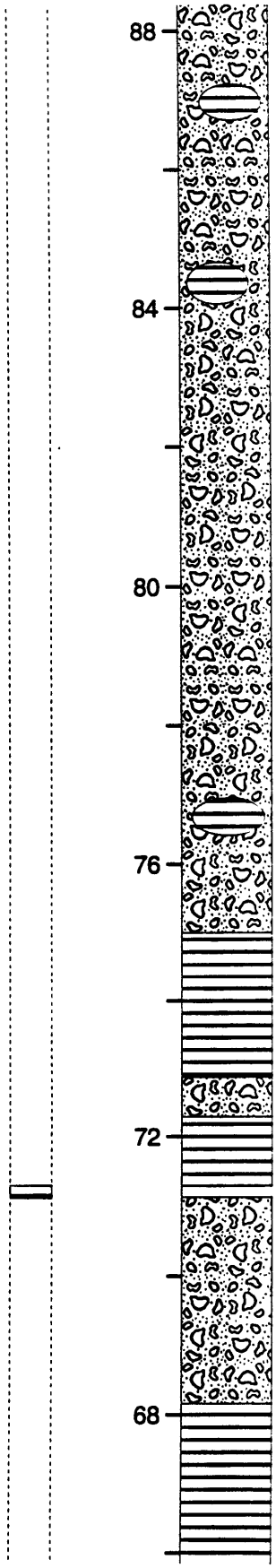


Soft Sediment Slumping and Folding

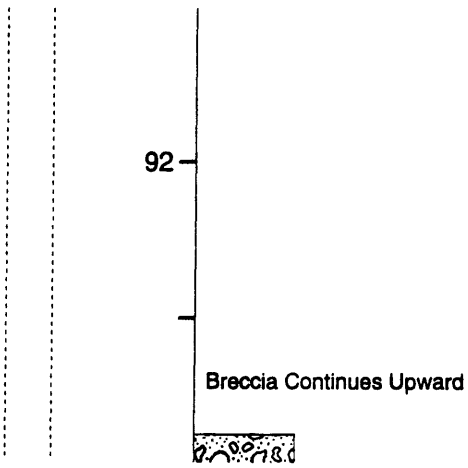
92
Breccia Continues Upward

## Section RD

Location: Rotterdam Farm, northwest of Thabazimbi.

Stratigraphic Range: Top of the Black Reef Quartzite to base of the Frisco Formation

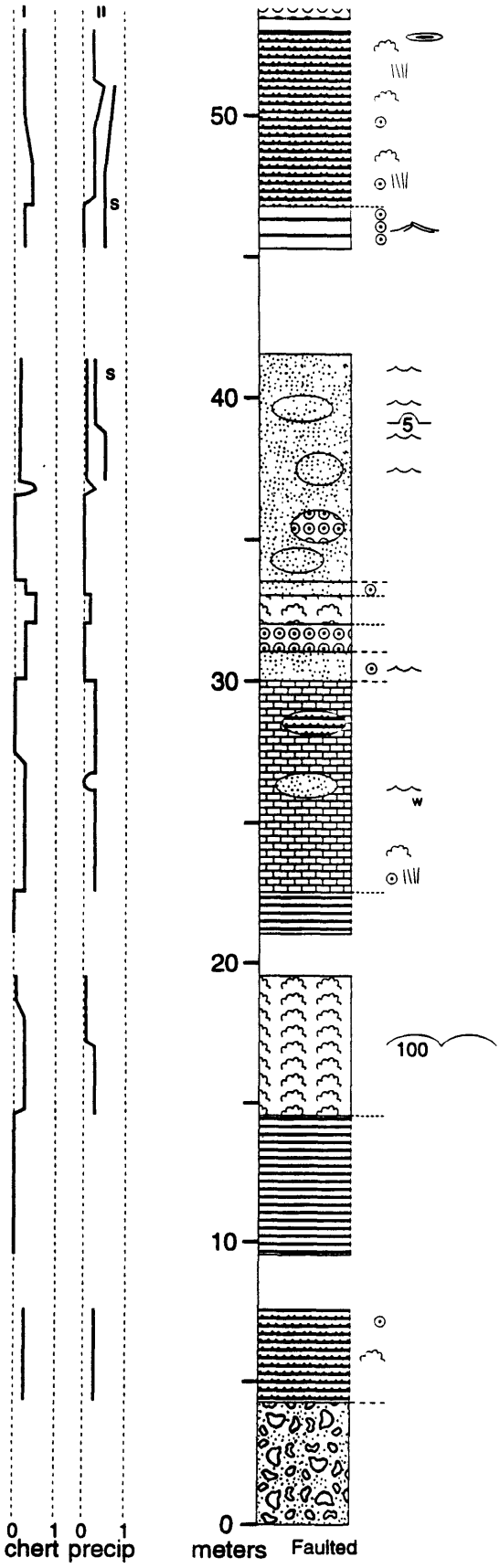
I
II
s
s
50
40
30
20
10
0
5
w
100
0 1 0 1
chert precip
meters
Faulted

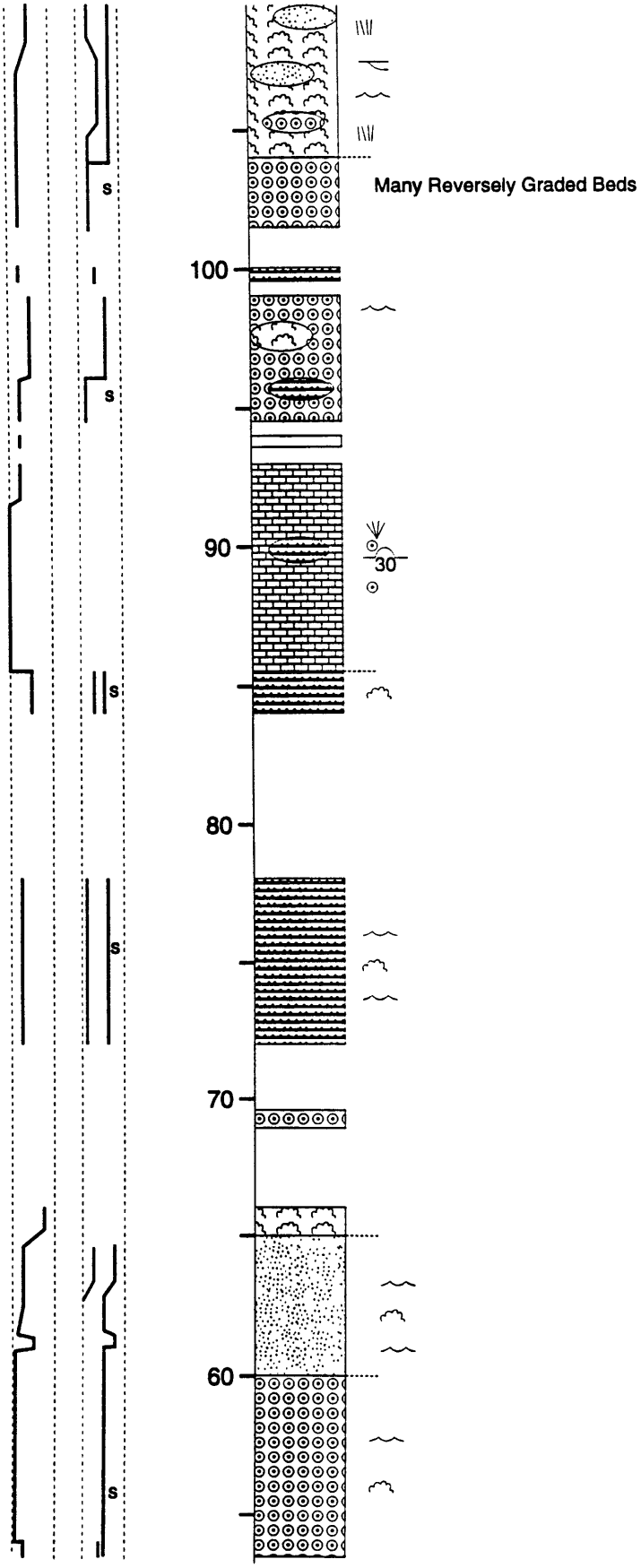
Many Reversely Graded Beds
100
90
80
70
60
30
s
s
s
s
s

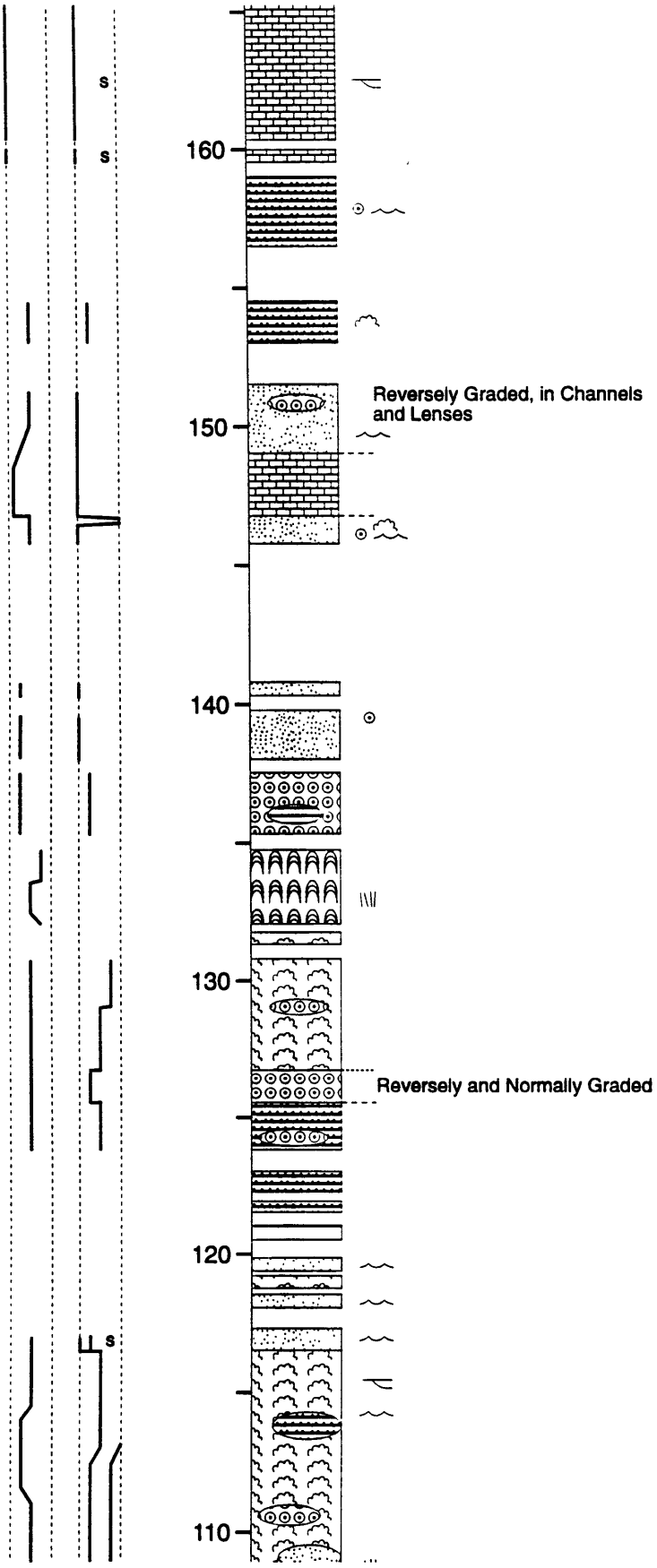
s
s
160
150
140
130
120
s
110
Reversely Graded, in Channels and Lenses
Reversely and Normally Graded

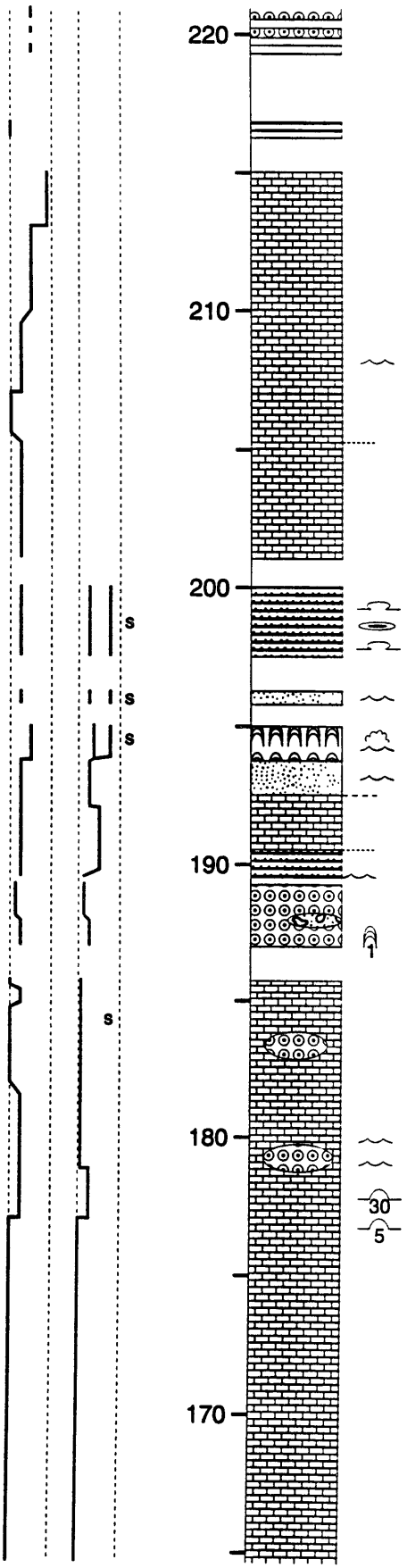
220
210
200
190
180
170
s
s
s
s
1
30
5

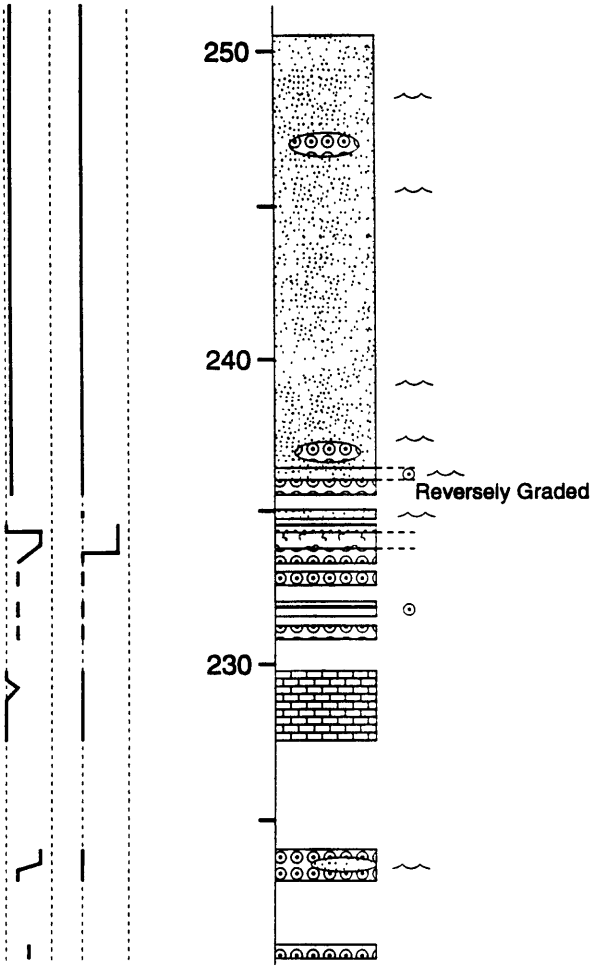
250
240
230
Reversely Graded

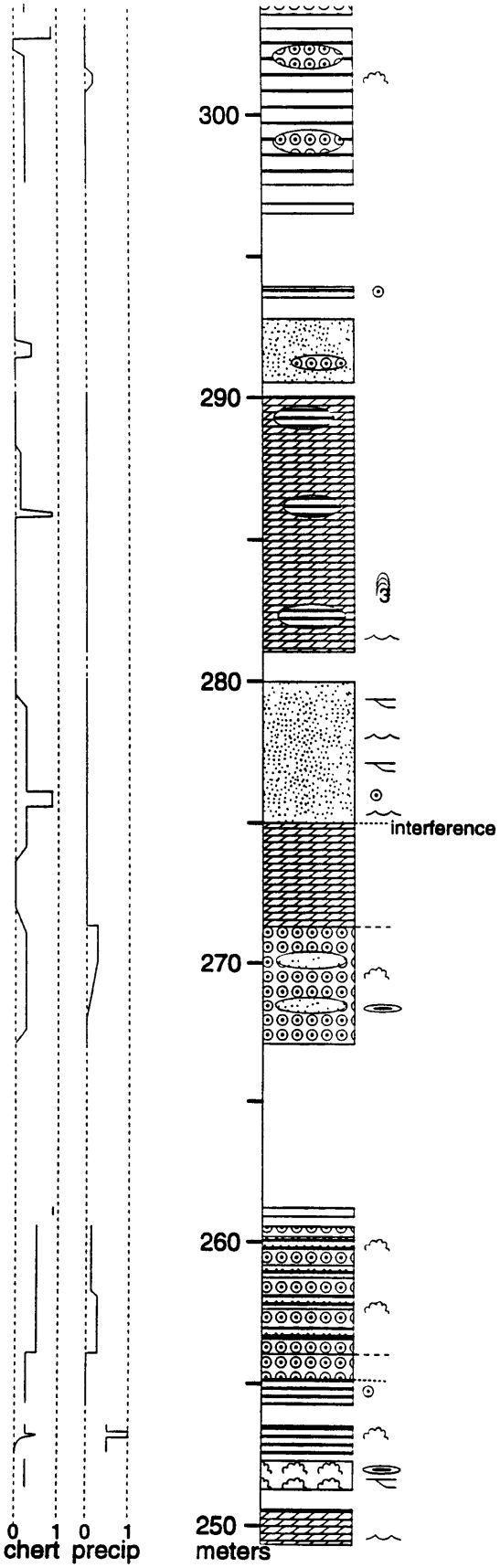
300
290
280
270
260
250
interference
0 1 0 1
chert precip
meters

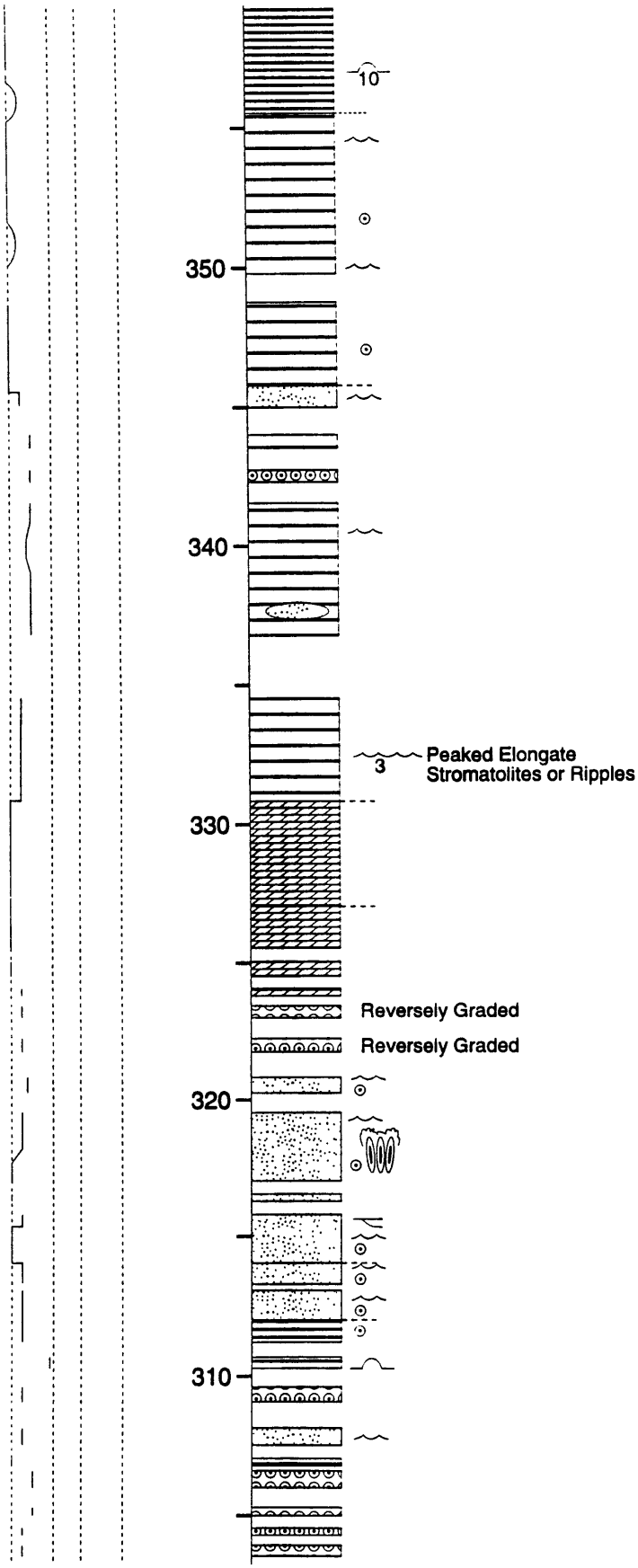
10
350
340
3
Peaked Elongate
Stromatolites or Ripples
330
Reversely Graded
Reversely Graded
320
310

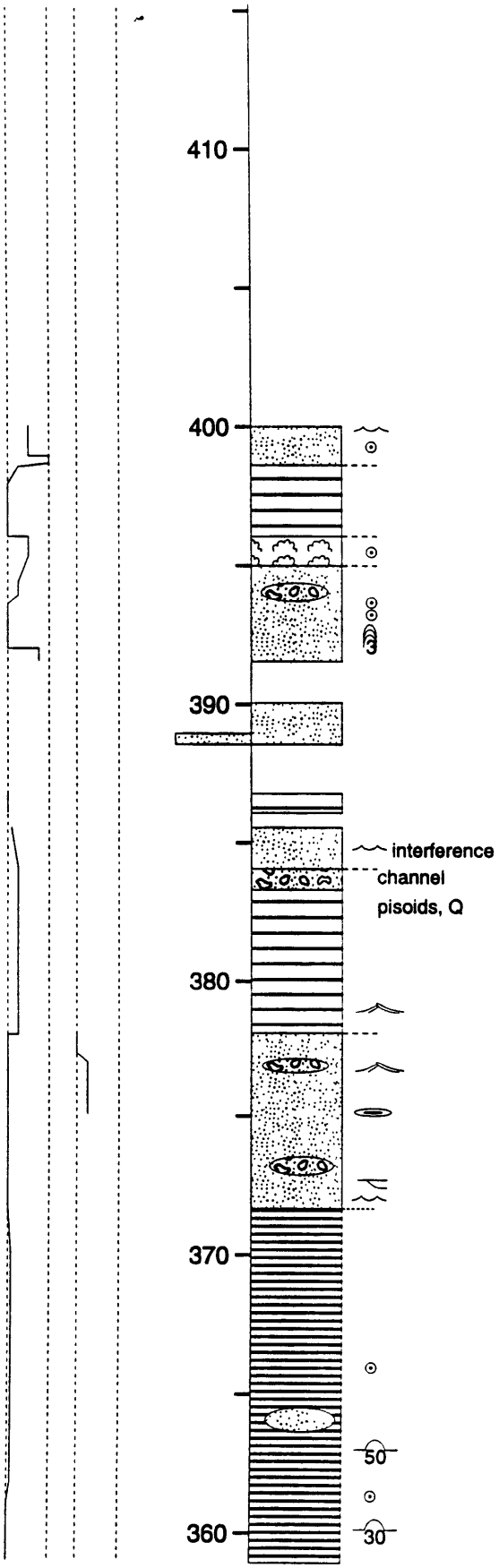
410
400
390
380
370
360
interference
channel
pisoids, Q
3
50
30

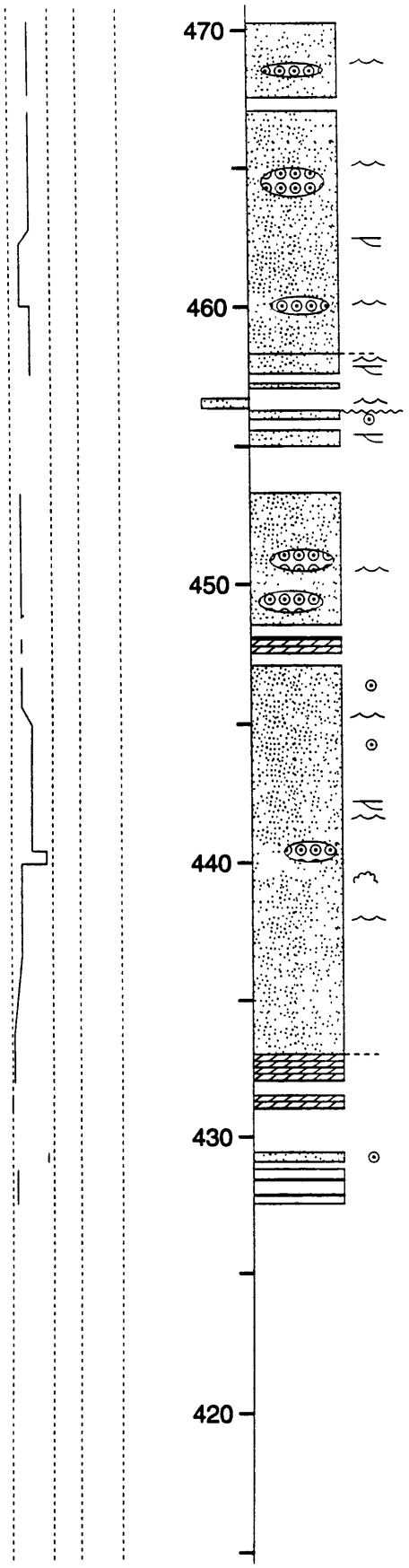
470
460
450
440
430
420

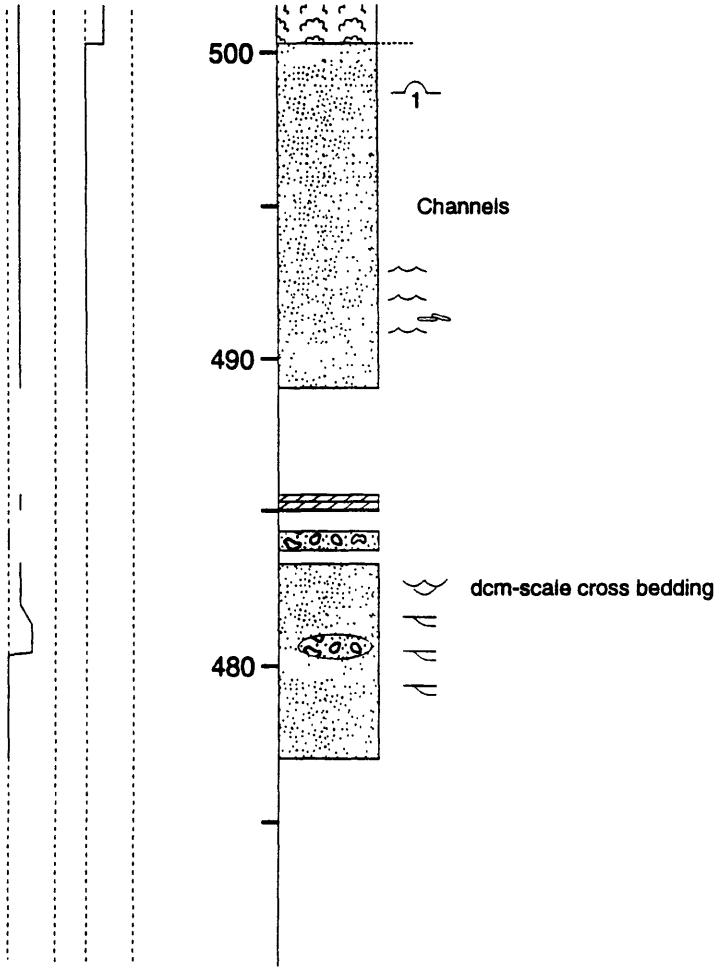
500
490
480
1
Channels
dcm-scale cross bedding

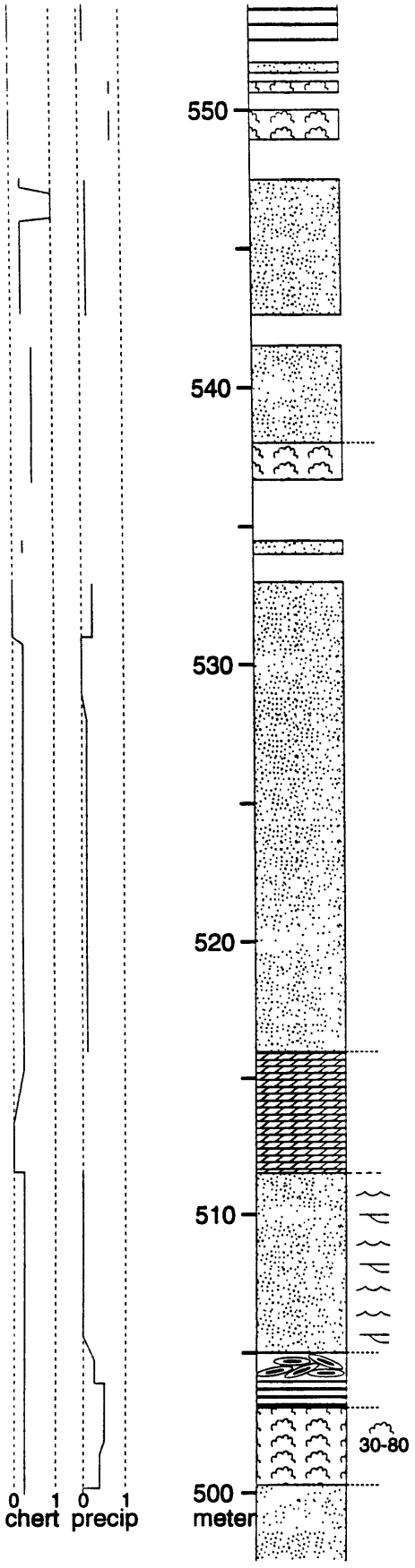
550
540
530
520
510
500
30-80
0 1 0 1
chert precip
meter

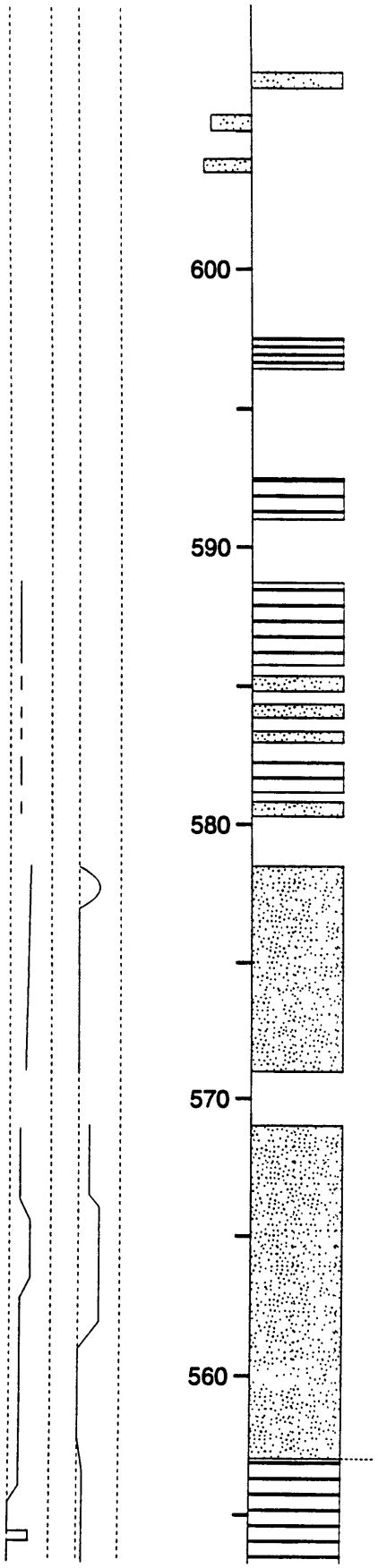
600
590
580
570
560

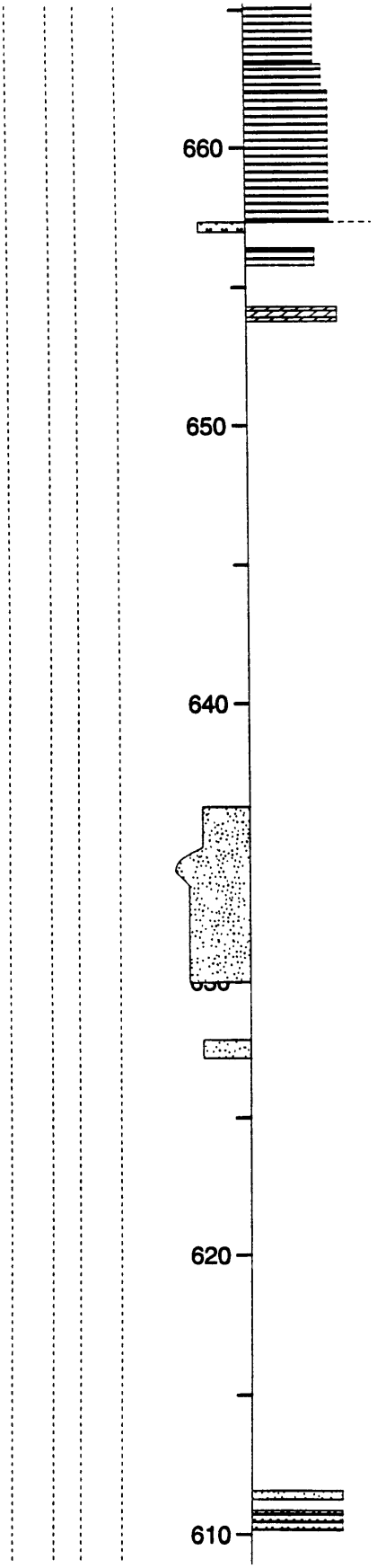
660
650
640
620
610

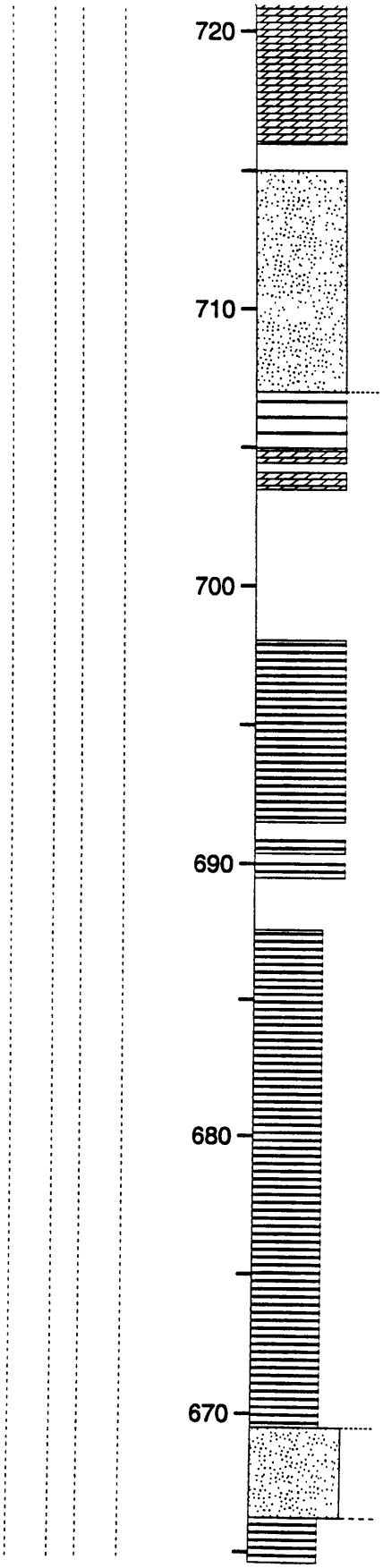
720
710
700
690
680
670

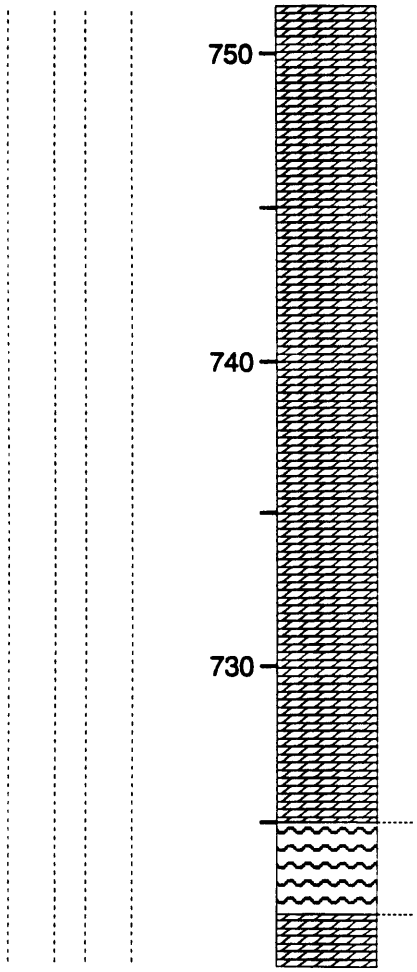
750
740
730

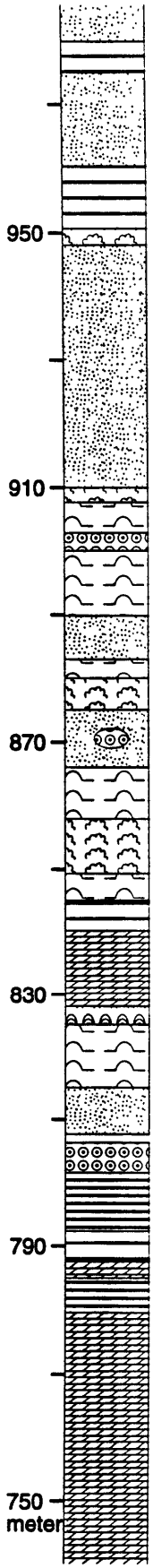


Note Change in Scale

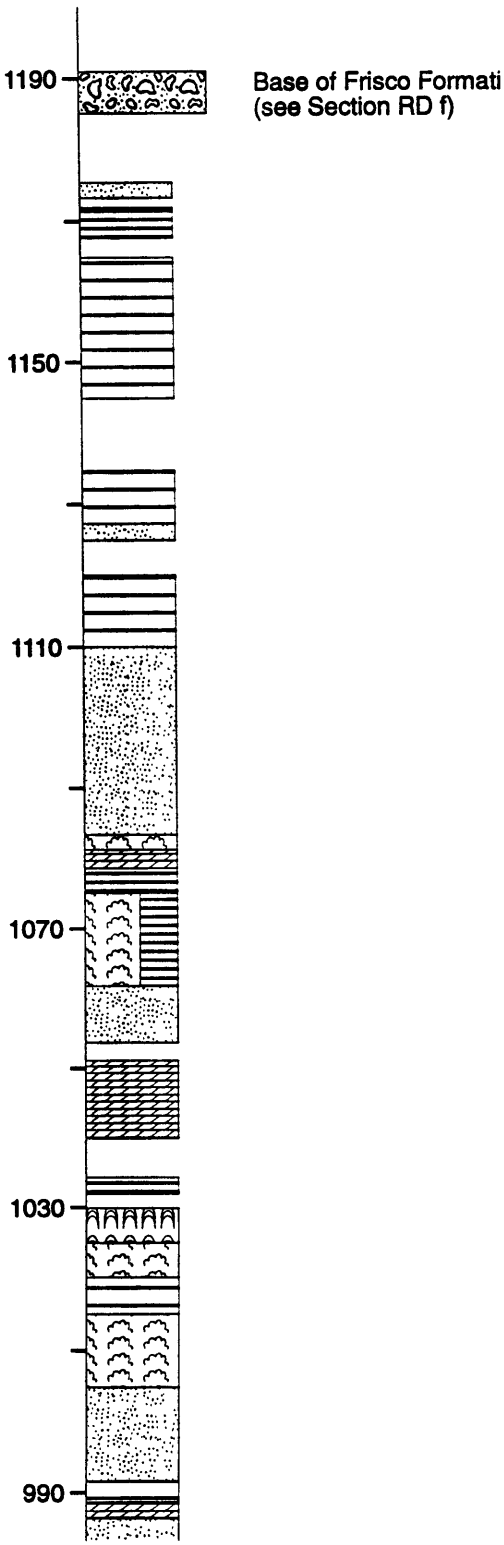
1190
Base of Frisco Formati
(see Section RD f)
1150
1110
1070
1030
990

## Section SC

Location: Road cuts along cut-off road between roads N4 and R37 just east of Sudwalla Caves.

Stratigraphic Range: Monte Christo Formation to base of the Lyttelton Formation.

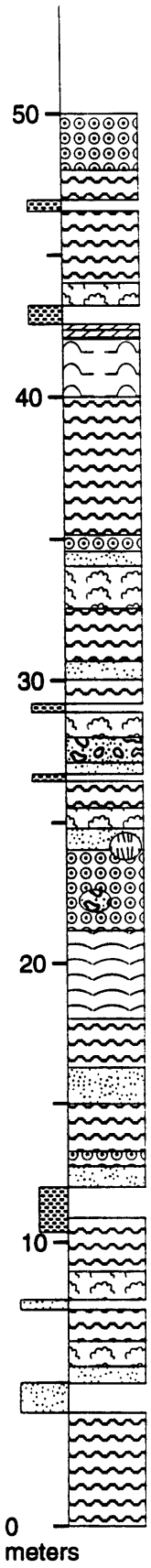
50
40
30
20
10
0
meters

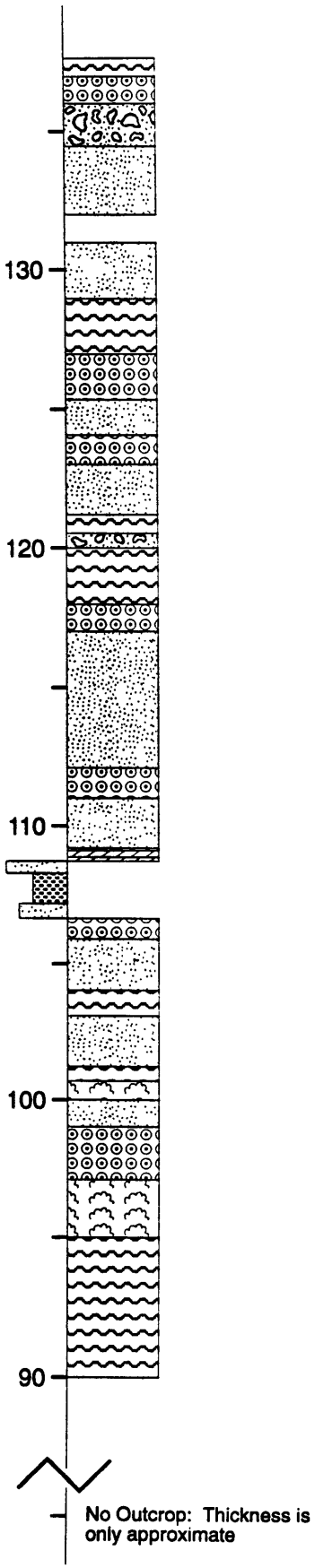
130
120
110
100
90
No Outcrop: Thickness is only approximate

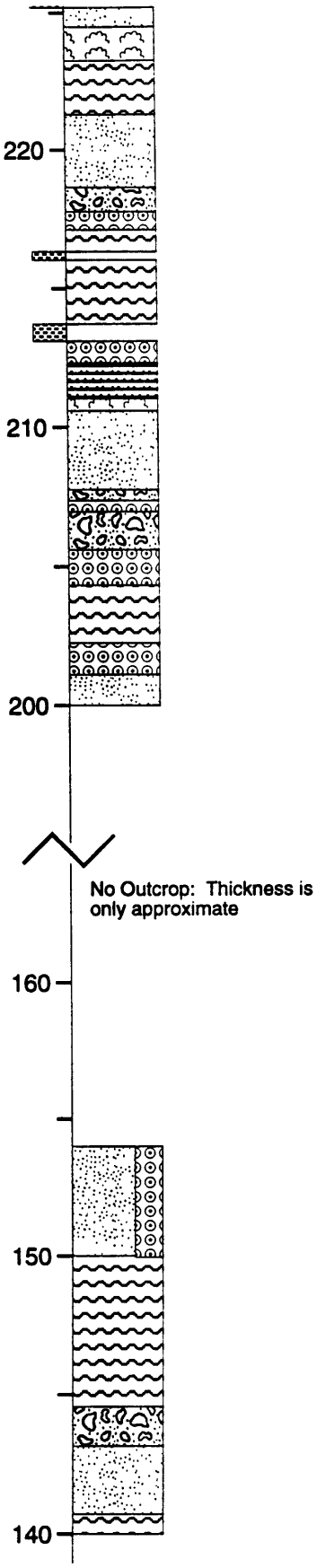
220
210
200
No Outcrop: Thickness is only approximate
160
150
140

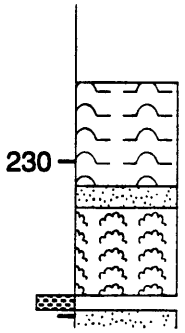
230

## Core SG1

Location: Core from the Sasolburg area. Owned by Goldfields and stored at their Carletonville facility.

Stratigraphic Range: Top of the Venterdorp Supergroup to the Eccles Formation.

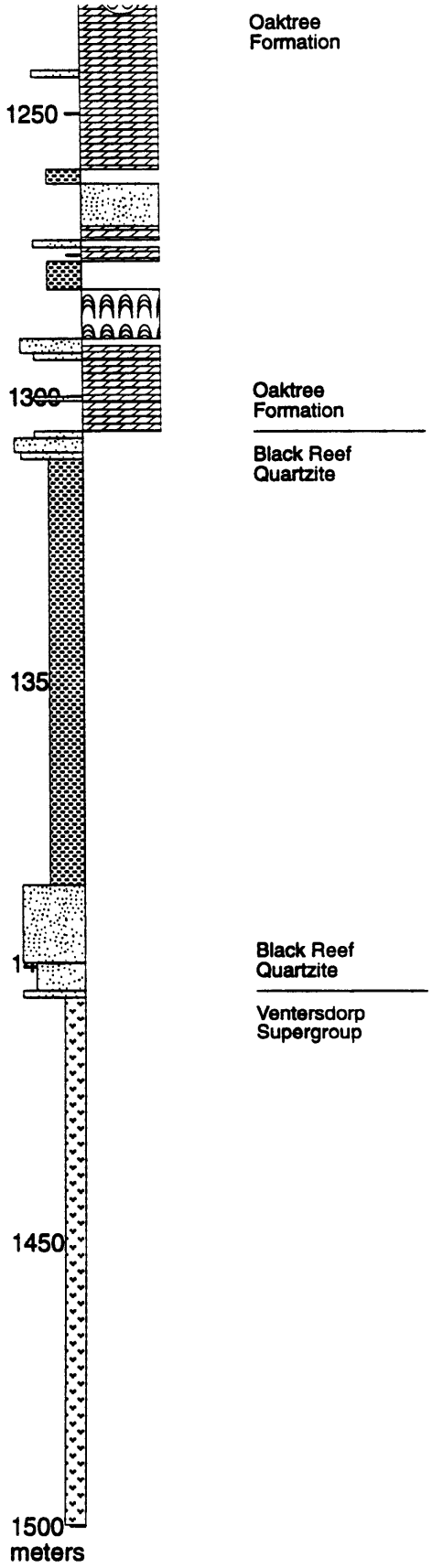
Oaktree
Formation
1250
1300
Oaktree
Formation
Black Reef
Quartzite
135
1
Black Reef
Quartzite
Ventersdorp
Supergroup
1450
1500
meters

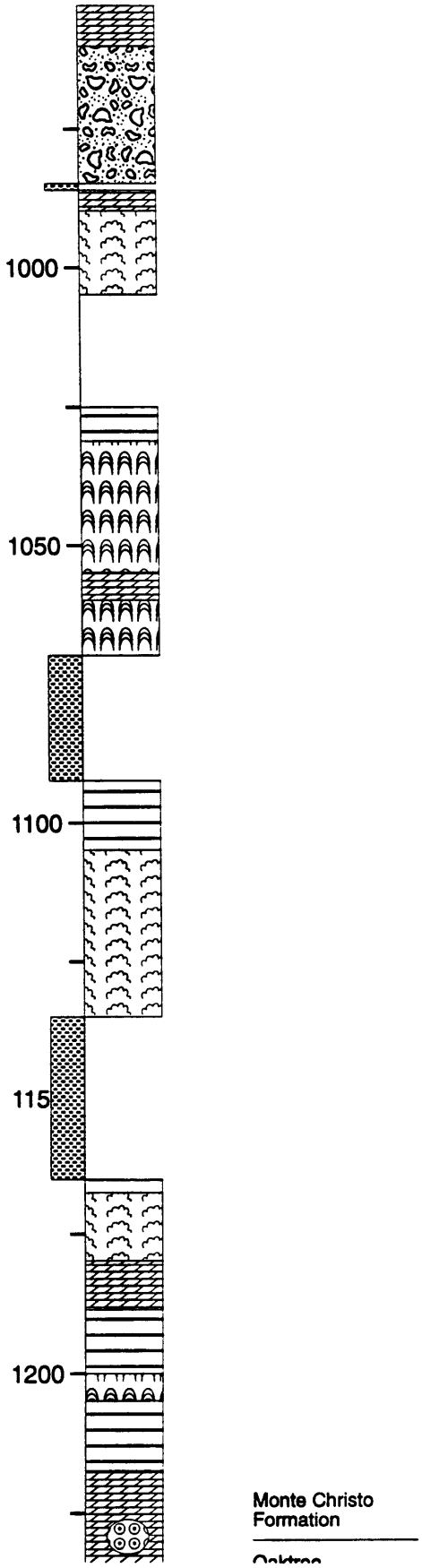
1000
1050
1100
115
1200
Monte Christo
Formation

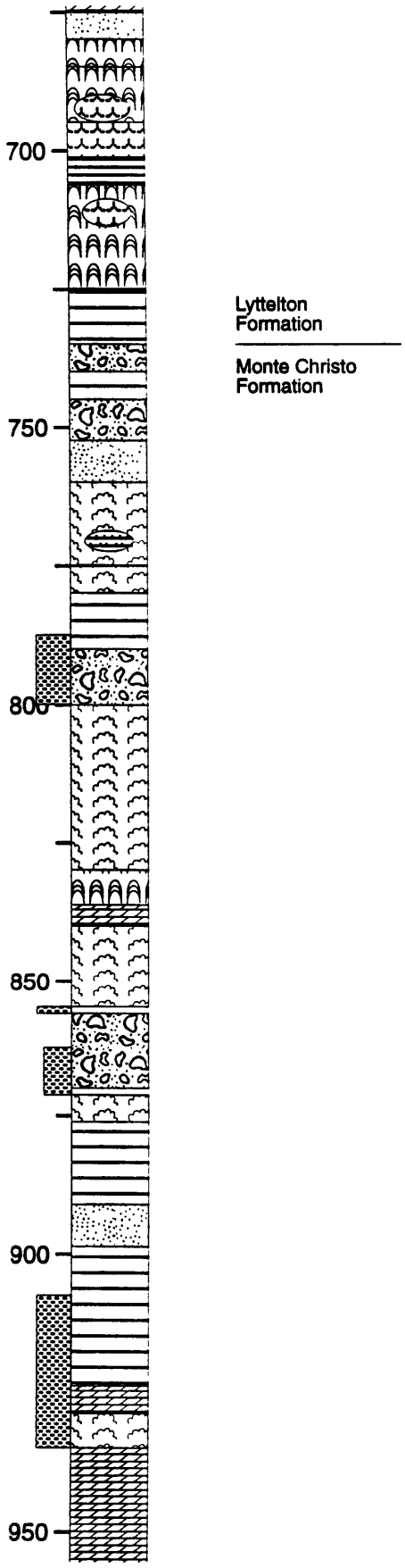
700
750
800
850
900
950
Lyttelton Formation
Monte Christo Formation

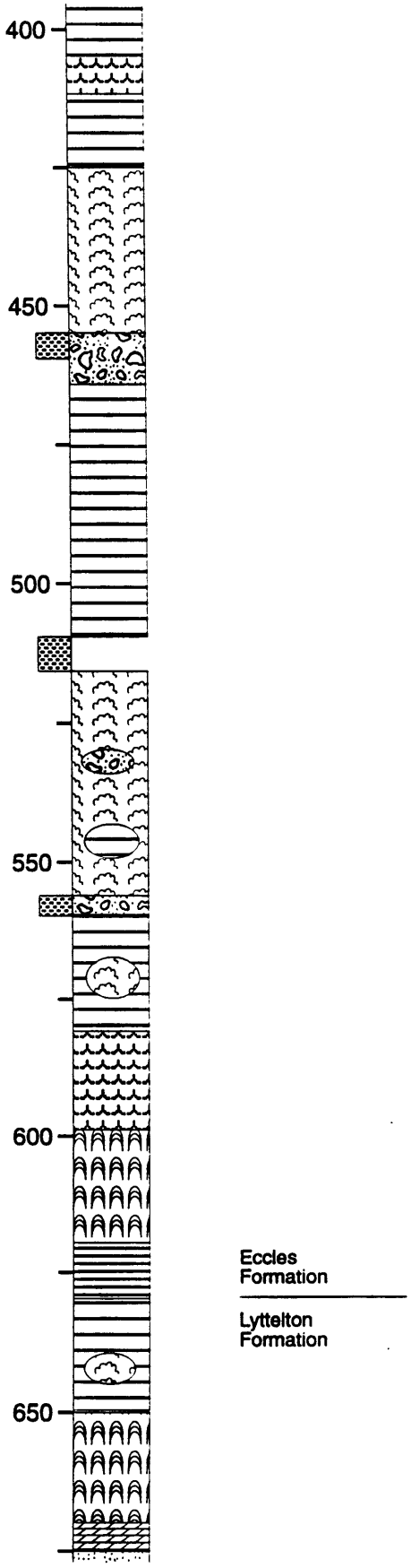
400
450
500
550
600
650
Eccles Formation
Lyttelton Formation

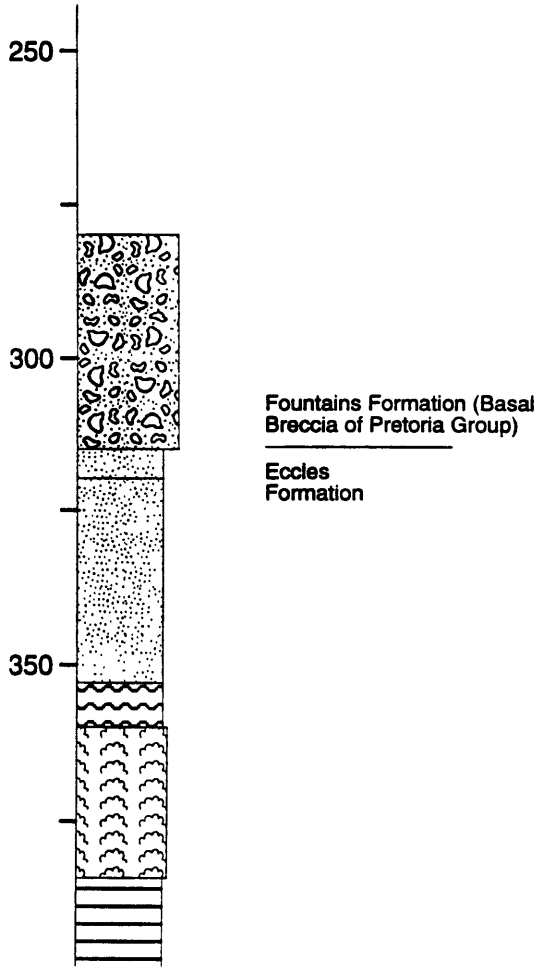
250
300
350
Fountains Formation (Basal Breccia of Pretoria Group)
Eccles Formation

## Core SK1

Location: Core from the Reivilo area. Owned by Shell Minerals South Africa and stored at Pering Mine.

Stratigraphic Range: Base of the Monteville Formation to mid-Reivilo Formation.

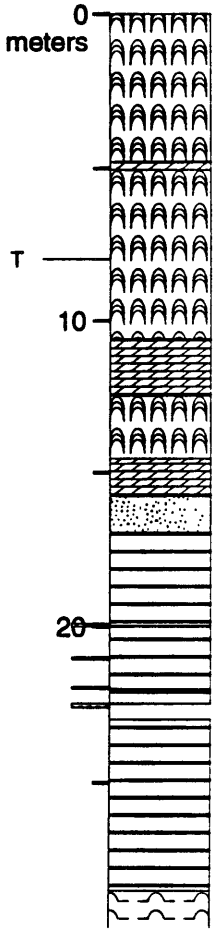
0
meters
T
10
20

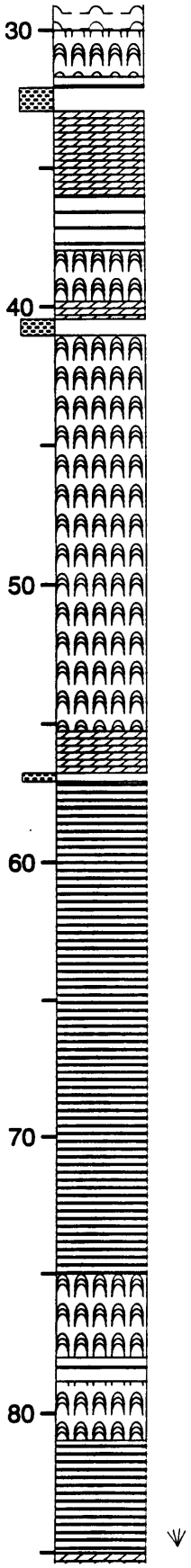
30
40
50
60
70
80

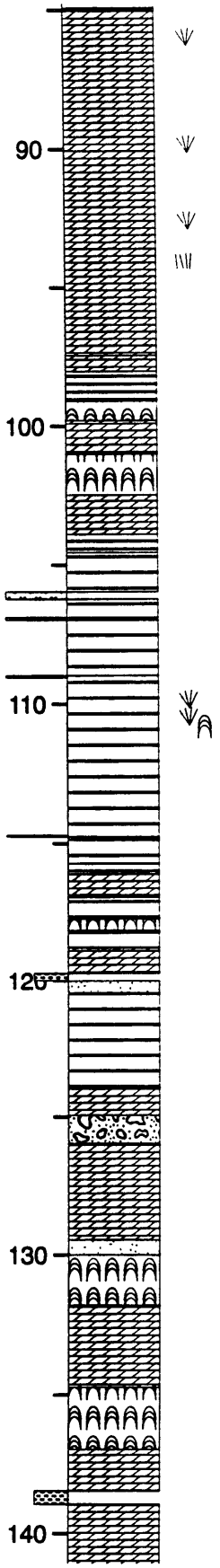
90
100
110
120
130
140

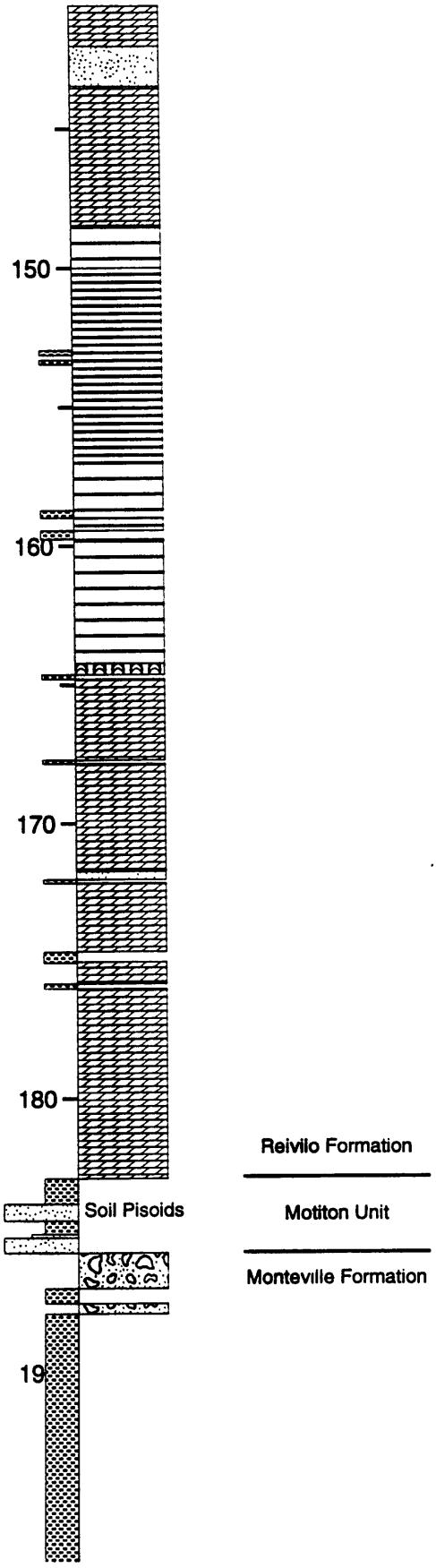
150
160
170
180
19
Soil Pisoids
Reivilo Formation
Motiton Unit
Monteville Formation

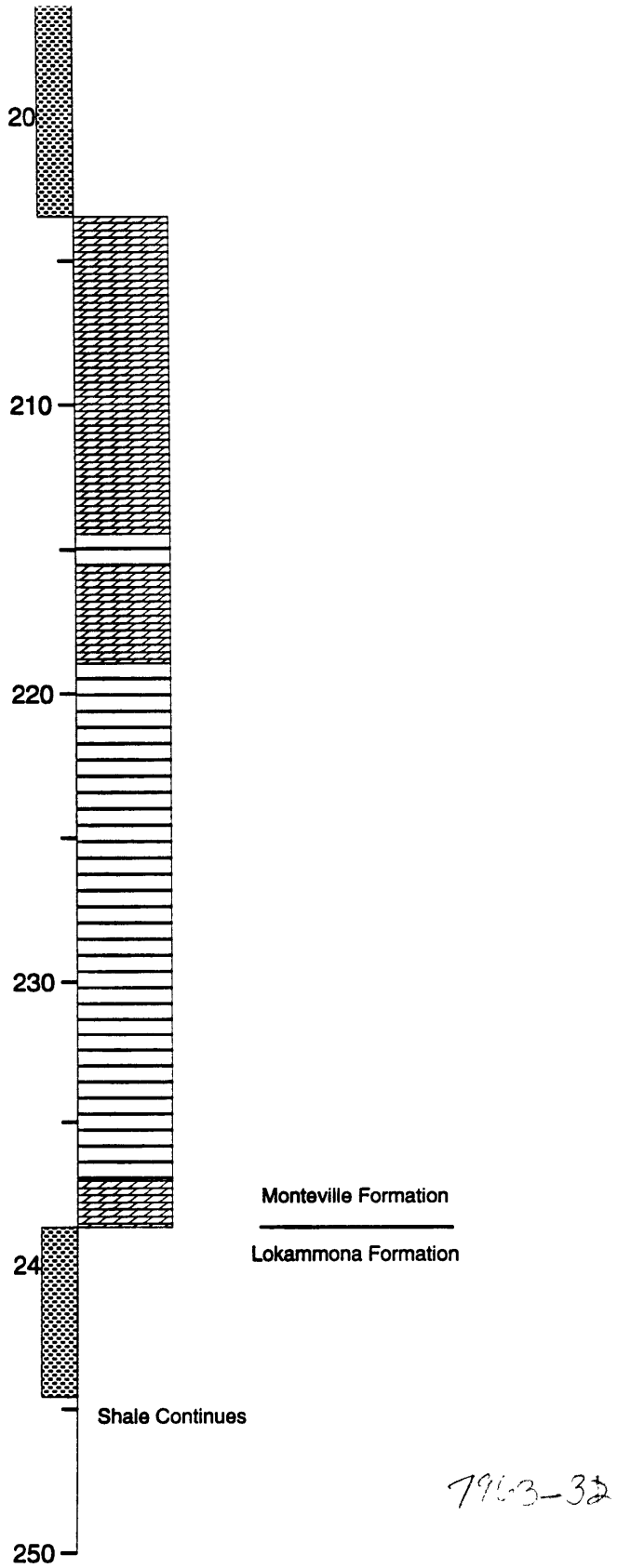
20
210
220
230
24
250
Monteville Formation
Lokammona Formation
Shale Continues

7963-32